Hydrology of mediterranean catchments

Antoine Allam

THÈSE POUR OBTENIR LE GRADE DE DOCTEUR DE MONTPELLIER SUPAGRO ET L'UNIVERSITE SAINT-JOSEPH DE BEYROUTH

En Sciences de l'Eau
École doctorale GAIA – Biodiversité, Agriculture, Alimentation, Environnement, Terre, Eau

Portée par

Unité de recherche 1221 – LISAH
Laboratoire d'Etude des Interactions entre Sol-Agrosystème-Hydrosystème

En Eau et Environnement
École Doctorale EDSIT – Sciences, Ingénierie et Technologie

Portée par

Centre de recherche – CREEN
Centre Régional de l'Eau et de l'Environnement

Hydrologie des Bassins Versants Méditerranéens

Présentée par Antoine ALLAM

Le 10 Novembre 2020

Sous la direction de Roger MOUSSA et Wajdi NAJEM

Devant le jury composé de

Marie-George TOURNOUD, Professeur, Université de Montpellier, Montpellier	**Présidente**
Vazken ANDREASSIAN, ICPEF, INRAE, UR HYCAR, Antony	**Rapporteur**
Rabi MOHTAR, Professeur et Doyen, Texas A&M University, Etats-Unis et AUB, Liban	**Rapporteur**
Mehrez ZRIBI, Directeur de recherche, CNRS, UMR CESBIO, Toulouse	**Examinateur**
Jérôme LATRON, Chercheur, IDAEA – CSIC, Barcelone, Espagne	**Examinateur**
Wajdi NAJEM, Professeur, CREEN – ESIB – USJ, Beyrouth, Liban	**Directeur de Thèse**
Roger MOUSSA, Directeur de recherche, INRAE, UMR LISAH, Montpellier	**Directeur de Thèse**
Christophe CUDENNEC, Professeur, Institut Agro, UMR SAS, Rennes	**Invité**
Claude BOCQUILLON, Professeur émérite, Université de Montpellier, Montpellier	**Invité**

UNIVERSITÉ DE MONTPELLIER

Montpellier SupAgro

USJ 145 ans 1875-2020 Université Saint-Joseph de Beyrouth جامعة القدّيس يوسف في بيروت

[This page was left intentionally blank]

THESIS TO OBTAIN THE GRADE OF DOCTOR FROM MONTPELLIER SUPAGRO AND SAINT-JOSEPH UNIVERSITY OF BEYROUTH

Water Sciences
Doctoral School GAIA– Biodiversity, Agriculture, Alimentation, Environment, Earth, Water

By

Research unit 1221 – LISAH
Soil-Agrosystem-Hydrosystem interaction lab

Water and Environment
Doctoral School EDSIT – Sciences, Engineering and Technology

By

Research center – CREEN
Regional Centre of Water and Environment

Hydrology of Mediterranean Catchments

Presented by Antoine ALLAM

10 November 2020

Under the direction of Roger MOUSSA et Wajdi NAJEM

In front of the jury composed of

Marie-George TOURNOUD, Professor, Montpellier University, Montpellier	**President**
Vazken ANDREASSIAN, ICPEF, INRAE, UR HYCAR, Antony	**Reporter**
Rabi MOHTAR, Professor and Dean, Texas A&M University, USA and AUB, Lebanon	**Reporter**
Mehrez ZRIBI, Research director, CNRS, UMR CESBIO, Toulouse	**Examiner**
Jérôme LATRON, Researcher, IDAEA – CSIC, Barcelona, Spain	**Examiner**
Wajdi NAJEM, Professor, CREEN – ESIB – USJ, Beirut, Lebanon	**Thesis Director**
Roger MOUSSA, Research director, INRAE, UMR LISAH, Montpellier	**Thesis Director**
Christophe CUDENNEC, Professor, Institut Agro, UMR SAS, Rennes	**Guest**
Claude BOCQUILLON, Emeritus Professor, Montpellier University, Montpellier	**Guest**

UNIVERSITÉ DE MONTPELLIER

Montpellier SupAgro

USJ 145 ans 1875-2020 Université Saint-Joseph de Beyrouth جامعة القدّيس يوسف في بيروت

[This page was left intentionally blank]

ACKNOWLEDGEMENT

I am grateful for all the pleasant encounters along my journey, all the support, advice, and help I received, but like every journey, even a thesis comes to an end.

I specially thank Professor Wajdi Najem for trusting my will to carry out this thesis and the wisdom of his advice, Doctor Roger Moussa for his patience, time, and tirelessness in shaping my research skills, Professor Claude Bocquillon and the abundance of ideas which he never spared.

Doctor Flavie Cernesson, Doctor Jérôme Latron, and Professor François Colin for taking part of the annual monitoring committee along the thesis period.

Doctor Jérôme Molenat and Jean-Stephane Bailly for receiving me at LISAH, Montpellier SupAgro, Doctors Armand Crabit, Camille Jourdan, and Martin Le-Mesnil and all my colleagues and staff at LISAH for easing my stay at Montpellier.

Doctor Cynthia Andraos, my colleague at CREEN, for the time we spent and will spend discussing hydrology.

Doctor Manal Moussalem for her continuous support and care along this journey,

Laurent Drapeau from IRD, which encounter in Laqlouq and during field visits rekindled my desire for research,

Fr. Samir which long discussions at Laqlouq monastery unpuzzled my mind and soul,

Stephany Achkouty and the precision of her illustrations of Mediterranean sceneries,

Parents and siblings, who never ceased cheering me, each in his special own way,

New and old friends and the thousand shots we had and will have!

Thank you!

[This page was left intentionally blank]

TABLE OF CONTENTS

LIST OF FIGURES

LIST OF TABLES

LIST OF VARIABLE AND ACRONYMS

A	Area of Catchment
BA	Bare Areas
BFImax	River type coefficient (the long-term ratio of baseflow to total streamflow)
CC	Climatic Class
CCA	Canonical Correlation Analysis
CMA	Cultivated and managed areas
DH5	90-days High Flow index
Dj	Degree Day Decomposition according to the need for habitat heating
DL5	90-days Low Flow index
E, ET	Evapotranspiration
E_p, ET_p	Potential Evapotranspiration
FH1	High Flow frequency index
FL1	Low Flow frequency index
G	Rain intensity.
GHG	Greenhouse Gas
H	Horton Index H=V/W
H	Average annual heat flow from the land surface into the atmosphere,
HC	Hydrological Class
HI	Hydrological indices
I_{Arid}	Aridity Index, Annual evapotranspiration over annual precipitation I_{Arid} = PET/P
I_{Decal}	Time Lag Index Time lag between the coldest and most humid month
I_{Hor}	Horizontal Inertia Index, Dispersion of monthly rainfall compared to the annual average
I_{Hypso}	Hypsometric index, ratio of Z_{Mean} and Z_{Med}
IPCC	International Panel for Climate Change
I_S	Seasonality Index
K_B	Sivapalan nondimensional water balance metric - Baseflow fraction
K_E	L'vovich water balance metric – Evaporation coefficient, K_E = E/W
K_H	Sivapalan nondimensional water balance metric – Horton index
K_R	Sivapalan nondimensional water balance metric - Runoff fraction
K_R	L'vovich water balance metric - Runoff coefficient, K_R = R/P
K_r	Ponce et Shetty water balance metric – Runoff coefficient
K'_r	Ponce et Shetty water balance metric – Runoff gain
K'_{rp}	Ponce et Shetty water balance metric – Runoff gain peak

K_u	Ponce et Shetty water balance metric – Baseflow coefficient
K'_u	Ponce et Shetty water balance metric – Baseflow gain
K'_{up}	Ponce et Shetty water balance metric – Baseflow gain peak
K_U	L'vovich water balance metric – Baseflow coefficient, $K_U = U/W$
K_V	Sivapalan nondimensional water balance metric - Vaporisation fraction
K_W	L'vovich water balance metric – Wetting coefficient, $K_W = W/P$
L	Latent heat of evaporation
LargEq	Equivalent rectangle width
Leptosols	Type of very shallow soil over hard rock or highly calcareous material
LongEq	Equivalent rectangle length
Luvisols	Type of soil in temperate climates, generally fertile used for agriculture
N	Mean duration between 2 successive showers.
$P_{25\%}$	Rain value exceeded 25% of the time
$P_{75\%}$	Rain value exceeded 75% of the time
P	Annual Precipitation
P	Catchment Perimeter
$\overline{P}$	Mean precipitation
$\widetilde{P}$	Scaled precipitation
P_a	Average precipitation
PC	Physiographic Class
PCA	Principal Components Analysis
PCI	Physio climatic indices
P_i	Monthly precipitation
P_{Karst}	Percentage of Karst Cover
P_m	Monthly annual precipitation
P_{rt}	Runoff threshold precipitation
PUB	Prediction on Ungauged Basins
P_{ut}	Baseflow threshold precipitation
Q	Runoff
Q_d	Direct runoff
Q_T	Total runoff (baseflow + direct runoff)
Rn	Average annual net radiative heat flux from the atmosphere to the land surface
RCM	Regional Climate Models
RCP	Radiative Concentration Pathway

S	Surface or quick flow
$\overline{S}$	Mean quick flow
S*	Nondimensional quick flow
S_A	Catchment Average Slope
S_AWC	Sub soil Available Water Capacity
SC_COD	Shrub Cover, closed-open, deciduous
SHC	Sparse herbaceous or sparse shrub cover
$SP_{1.5}$	Number of months exceeding the average monthly precipitation by 1.5 times
$SP_{1.7}$	Number of months exceeding the average monthly precipitation by 1.7 times
SP_2	Number of months exceeding the average monthly precipitation by 2 times
S_{PET}	Threshold Index Number of month where precipitation P exceeds evapotranspiration PET, (PET calculated using Turc (1961) formula)
$ST_{1.2}$	Number of months exceeding the average temperature by 1.2 times
$ST_{1.2}$	Number of months exceeding the average temperature by 1.2 times
STm	Mean temperature Index Number of months exceeding the Mediterranean monthly average temperature Tm 16.4 °C
T_1	Average duration of non-rain episodes
T_2	Average duration of rainy episodes
$T_{25\%}$	Temperature value exceeded 25% of the time
$T_{75\%}$	Temperature value exceeded 75% of the time
T_AWC	Topsoil Available Water Capacity
Tc	Concentration time
TC_BDC	Tree Cover, broadleaved, deciduous, closed
TC_MLT	Tree Cover, mixed leaf type
TC_NLE	Tree Cover, needle-leaved, evergreen
U	Underground Flow, baseflow
$\overline{U}$	Mean Baseflow
U*	Nondimensional baseflow
V	Vaporisation (or Evapotranspiration in some reports symbolised as E)
$\overline{V}$	Mean Vaporisation
V*	Non dimensional Vaporisation
$\widetilde{V}$	Scaled vaporisation
V_{HF1}, V_{HF2}	Physioclimatic Variate for High Flows
V_i	Physioclimatic canonical variates

V_{LF1}, V_{LF2}	Physioclimatic Variate for Low Flows
V_p	potential Vaporisation
V_{WB1} V_{WB2}	Physioclimatic Variate for Water Balance
W	Wetting, humidification
$\overline{W}$	Mean Wetting
$\widetilde{W}$	Scaled wetting
W*	Non dimensional Wetting
W_{HF1}, W_{HF2}	Hydrological Variate for High Flows
W_i	Hydrological canonical covariates
W_{LF1}, W_{LF2}	Hydrological Variate for High Flows
W_p	potential Wetting
W_{WB1} W_{WB2}	Hydrological Variate for Water Balance
Z_{Max}	Catchment Maximum Altitude
Z_{Mean}	Catchment Mean Altitude
Z_{Med}	Catchment Median Altitude
Z_{Range}	Catchment Altitude Range (Maximum - Minimum)
ZS_{Mean}	Mean Snow Cover altitude when it exceeds 1 month per year
$\Delta T1$	Temperature lag between the coldest and warmest months
$\Delta T2$	Temperature lag between the coldest and warmest three consecutive months
λ_i	Correlation
λ_s	initial abstraction coefficient of surface runoff
λ_u	initial abstraction coefficients of baseflow
ρ_Q	Total flow elasticity
ρ_U	Slow flow elasticity
ρ_S	Quick flow elasticity
φ	Aridity index

[This page was left intentionally blank]

FRENCH SUMMARY

Introduction

La Méditerranée, ses zones côtières et son environnement marin sont les régions les plus sensibles aux changements démographiques et climatiques ce qui pose des défis sur la gestion des ressources en eau et les recherches en hydrologie. Les ressources en eau, habituellement disponibles dans cette région, sont plus que jamais exposées continuellement aux besoins croissants de l'agriculture, l'industrie, le tourisme, le développement urbain et démographique afin d'améliorer les normes de vie; en plus, elles sont exposées à l'évolution climatique affectant principalement les ressources en eau douce.

Les ressources en eau en Méditerranée sont inégalement distribuées et donc constituent un défi socio-politique sérieux face aux besoins en croissance. Cette distribution inégale pourrait être causée par la morphologie très fragmentée avec 3681 bassins versants de différentes tailles où 35% sont de taille moyenne comprise entre 100 km^2 et 3000 km^2. Les problèmes de gestion de l'eau au niveau des petites et moyennes divisions administratives exigent nécessairement de nouvelles mesures pour bénéficier de petits bassins, puisque les ressources des grands bassins sont déjà réservées aux zones cultivées et aménagés couvrant 30% de la Méditerranée.

Ces défis ont amené les pays du pourtour méditerranéen en 1976 à adopter la Convention de Barcelone pour la protection des ressources marines, à lancer le Plan Bleu en 1977, un centre d'activités régionales du Plan d'Action pour la Méditerranée (PAM), et à initier plusieurs programmes de recherche sur les ressources en eau méditerranéennes comme MEDFRIEND en 1991, MEDHYCOS en 1995, SEMIDE en 1996 et dernièrement HyMeX en 2007.

La Méditerranée a prouvé être la plus convenable parmi les destinations touristiques en attirant 410 millions de touristes en 2018 contre 160 millions seulement en 1995 avec une croissance annuelle moyenne de 4,2% depuis 20 ans (Organisation Mondiale du Tourisme, 2019), toutefois, cette région subit de graves répercussions depuis quelques décennies à cause du changement climatique. Dans une étude basée sur un modèle d'impact physique, Ciscar et al., (2011) a détaillé les impacts attendus du changement climatique sur l'agriculture, les inondations, les systèmes côtiers et les activités touristiques en 2080. Tandis que le changement de rendement agricole devrait diminuer de -27 % en Europe du Sud, l'activité touristique devrait diminuer de -4% en Europe du Sud mais augmenter de 17% en Europe centrale. Dans une autre étude, Milano et al. (2013) souligne la tendance croissante du stress hydrologique actuel que connaissent les pays du pourtour méditerranéen, surtout ceux du Sud et de l'Est, en attendant une baisse de 30 à 50% des ressources en eau douce et l'estimation qu'une dizaine de pays de l'Est et du Sud de la Méditerranée seront en dessous du niveau de rareté, généralement estimé à 1000 mètres cubes disponibles par an et par habitant.

Les impacts climatiques et anthropiques nécessitent des mesures d'adaptation et d'atténuation urgentes et des politiques de gestion de l'eau qui devraient être davantage basées sur la recherche régionale en approfondissant les connaissances sur la variabilité spatiale et temporelle des ressources hydrologiques dans toute la Méditerranée, d'où l'importance de cette thèse qualifiée comme travail pionnier dans le sens de la collecte d'une base de données physioclimatiques couvrant l'ensemble de la Méditerranée et d'un ensemble de données hydrologiques de 55 bassins versants de 15 pays méditerranéens.

Cette thèse présente une étude complète qui vise à caractériser les bassins versants méditerranéens, d'un point de vue climatique, physiographique et hydrologique. Puisqu'il existe un grand intérêt et avantage à partager les connaissances pour la gestion durable des ressources en eau entre les pays développés, principalement dans le Nord, et les pays sous-développés dans le Sud, une quête pour comprendre le comportement hydrologique actuel et futur des bassins versants méditerranéens a été lancée à travers l'analyse de la similarité et de la variabilité hydrologiques des bassins versants méditerranéens. Ainsi, une approche en quatre objectifs a été adoptée.

Le premier consiste à rassembler une base de données hydrologique comprenant la délimitation des bassins versants, les données climatologiques et hydrométriques et toutes les caractéristiques physiographiques.

Le deuxième, à établir une nouvelle classification climatique pour l'hydrologie basée sur des indices climatiques spécifiques à la Méditerranée tels que la saisonnalité des précipitations et l'aridité qui jouent un rôle important dans les mécanismes hydrologiques des bassins versants méditerranéens et l'intermittence des écoulements. Cette classification est utile pour la projection de scénarios futurs et le suivi d'applications hydrologiques (gestion des ressources en eau, inondations, sécheresses, etc.) et écohydrologiques telles que la culture méditerranéenne de l'olivier et d'autres pratiques environnementales.

Le troisième, à effectuer une classification physiographique de tous les bassins versants méditerranéens en fonction des indices physiographiques de relief, d'occupation du sol etc. pour mettre en évidence la variabilité méditerranéenne. Cette classification permettra de découvrir l'interaction physioclimatique (microclimats, répartition de la couverture végétale, etc.) dans le cadre de l'auto-organisation de la végétation avec le climat telle que proposée par Horton (1933), et son rôle dans la formation de l'hydrologie et des régimes d'écoulement méditerranéens.

Le quatrième, à effectuer une analyse approfondie du bilan hydrique de 55 bassins versants méditerranéens selon les différents modèles fonctionnels du bilan tels avancés par L'vovich (1979) et élaborés par Ponce & Shetty (1995a, 1995b) et Sivapalan et al., (2011) pour vérifier la variabilité hydrologique et la similarité entre tous les bassins versants et entre les mêmes classes climatiques et / ou physiographiques. L'analyse

de la variabilité hydrologique aidera à définir de meilleurs plans de gestion pour les bassins versants méditerranéens afin d'adapter et d'atténuer l'impact attendu du changement, exprimé par l'augmentation de la température, le décalage saisonnier.

Le climat méditerranéen est connu pour sa saisonnalité et l'alternance d'hivers humides et d'étés secs (Köppen, 1936) qui conditionnent les régimes d'écoulement des rivières, la couverture terrestre, l'agriculture et par conséquent tout plan de gestion des ressources en eau. La caractéristique la plus notable du climat méditerranéen est le caractère saisonnier des précipitations et de l'alternance entre les saisons courtes humides, 3 à 6 mois accompagnés par temps froid et les pluies torrentielles et les inondations, et les saisons en quelque sorte plus sèches, 6 à 9 mois accompagnés de temps chaud et les sécheresses sévères.

La région méditerranéenne partage plusieurs traits physiographiques qui pourraient être observés, les formations karstiques élevées et exposées, datant de la période Messénienne de 5,96 à 5,33 Ma lorsque le niveau de la mer a baissé d'une façon spectaculaire (Audra et al., 2004; Krijgsman et al., 1999). Des paysages karstiques sont observés au Mont Liban, en Syrie, sur la côte turque d'Adana à Antalya, dans les pays des Balkans, au centre de l'Italie, à la Côte d'Azur et à l'est de l'Espagne (Chen et al., 2017). D'autre part, les zones cultivées et aménagés couvrent 30% de la Méditerranée, et l'olivier, vu partout dans la région, est considéré comme l'un de ses emblématique bioindicateurs principalement pour la commodité de son climat, comme cycle de reproduction d'olive et l'intensité de floraison est influencé par la température saisonnière et la disponibilité de l'eau (Moreno, 2014 ; Fraga et al., 2019).

La similarité hydrologique entre bassins devrait être jugée en fonction de paramètres spécifiques prenant en compte la complexité des facteurs environnementaux affectant la réponse du bassin versant (Wagener et al., 2007). Haines et al., (1988) ont classé les régimes fluviaux du monde par basés uniquement sur les débits moyens mensuels, et ainsi les régimes méditerranéens ont été classés dans 3 des 15 groupes en identifiant toutefois une relation claire Köppen du climat méditerranéen. Les fleuves méditerranéens ont été classés aussi en 6 régimes d'écoulement par Oueslati et al., (2015) sur la base des indices hydrologiques de de Richter et al., (1996) et de quelques caractéristiques physiques des bassins, une autre classification de 300 bassins italiens a été réalisée par Di Prinzio et al., (2011) en utilisant des cartes d'auto-organisation. Cependant, à notre connaissance, aucune étude méditerranéenne n'a abordé une classification climatique et physiographique avant d'évaluer la similarité hydrologique. La méta-analyse des caractéristiques de la réponse hydrologique des bassins versants méditerranéens, Merheb et al., (2016) a mis en évidence le manque d'études multidisciplinaires utilisant des bases de données multinationales au niveau de la région et qui jusqu'à présent étaient encore légèrement abordées dans la littérature en tant qu'entité hydrologique. Ce manque d'études est principalement dû à la diversité géopolitique avec 23 pays limitrophes et plus de 15 langues officielles différentes.

Par conséquence, une homogénéité climatique, physiographique et hydrologique a été détectée mais non confirmée encore à travers la Méditerranée. Toutefois, une hydrologie spécifique méditerranéenne est loin d'être définit encore et nécessite des recherches supplémentaires pour déterminer la relation entre les indices climatiques et physiographiques d'une part et les processus hydrologiques de l'autre et qui reste faiblement pris en compte.

Chapitre 1 – Etat de l'Art

Le Chapitre 1 présente une revue bibliographique sur la Méditerranée et la modélisation fonctionnelle initialement abordée avec le bilan thermique de Budyko (1974), le modèle de partitionnement du bilan hydrologique de L'vovich (1979), le modèle conceptuel de Ponce et Shetty (1995a, 1995b) et sa formulation non dimensionnelle de Sivapalan et al., (2011). Le chapitre aborde également la classification hydrologique et l'analyse de similarité.

Chapitre 2 – Base de données Méditerranéenne

Le Chapitre 2 présente un aperçu des bases de données rassemblées pour cette étude en commençant par la délimitation de tous les bassins versants situés à l'intérieur de la limite hydrologique ; Les données climatiques dérivées de la base de données maillée WorldClim-2 et l'ensemble des stations climatiques pour la classification climatique au Chapitre 3; les caractéristiques physiographiques dérivées d'ensembles de données mondiales de topographie, géologie, couverture terrestre, lithologie, sol, neige et karst pour une classification physiographique au Chapitre 4; et les données hydrométriques de 55 bassins versants servant d'échantillon pour une caractérisation ultérieure du bilan hydrologique au Chapitre 5. Malgré le travail étendu effectué pour la collecte de données, qui a nécessité des communications directes par courrier et par téléphone, avec plusieurs services hydrologiques de différents pays (Grèce, Turquie, Espagne, etc.), il était impossible d'obtenir des données de débit de bassin versant égyptien ou libyen. En outre, il était aussi très difficile de trouver des séries concomitantes pour les 55 bassins versants, d'où la première source d'incertitude. Une deuxième source réside dans l'influence des projets de gestion existants que nous avons essayé de réduire au minimum en sélectionnant bassins versants peu influencés. Une liste des paramètres, indices et autres abréviations est élaborée au début, avant ce résumé.

Chapitre 3 – Caractérisation climatique

Le Chapitre 3 présente une nouvelle classification climatique à des fins hydrologiques basée sur des indices climatiques spécifiques à la Méditerranée principalement l'indice de saisonnalité des précipitations I_S et l'indice d'aridité I_{Arid}. Cette classification serait utile pour le suivi de la gestion des ressources en eau, les inondations et les étiages, pour le suivi des activités écohydrologiques et l'agriculture méditerranéenne comme l'olivier et pour d'autres pratiques environnementales.

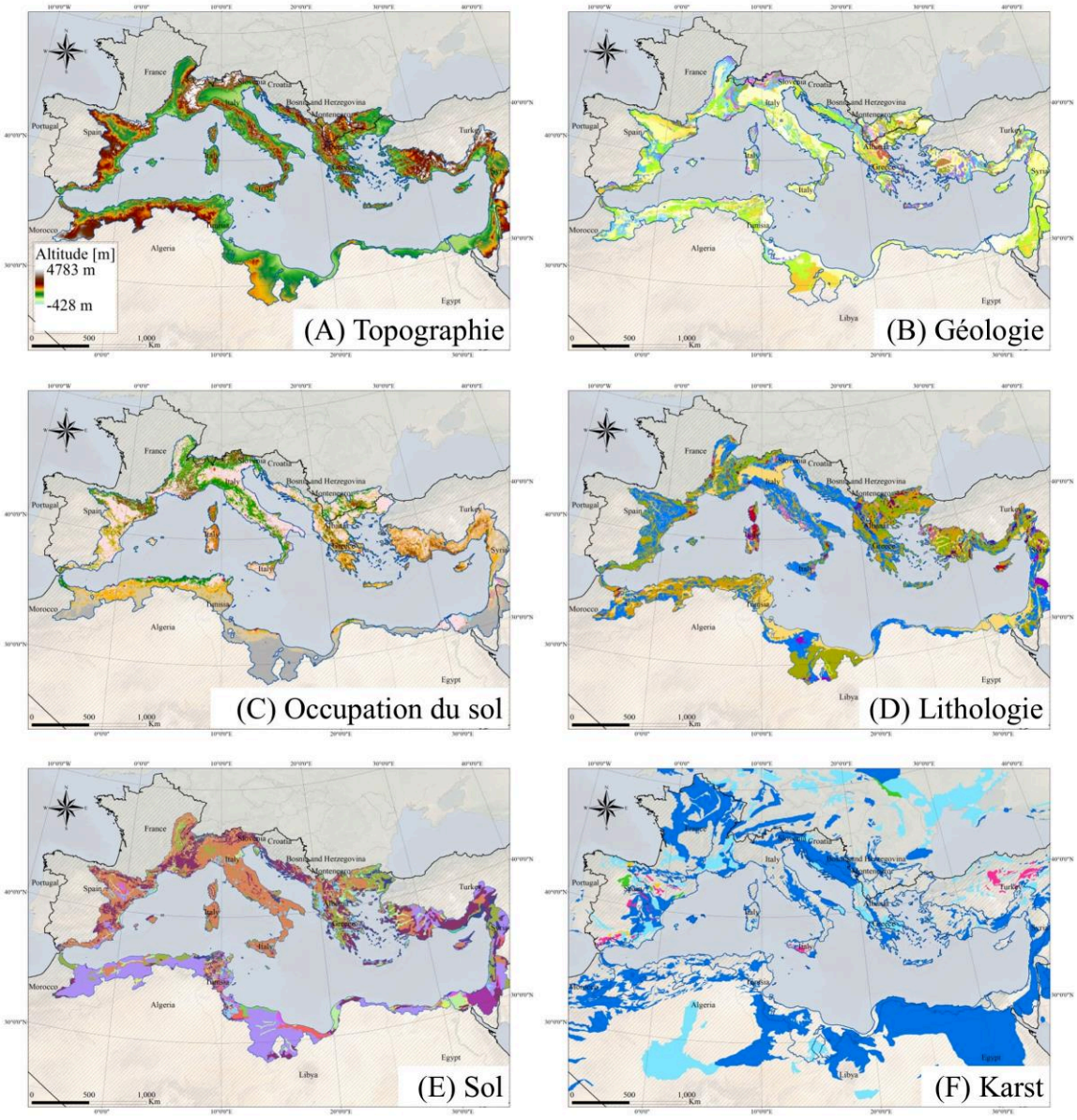

Figure a: Caractéristiques physiographiques de la région Méditerranéenne à l'intérieur de la limite hydrologique, dérivée d'un ensemble de cartes globales: (a) topographie, (b) géologie, (c) couverture du sol, (d) lithologie, (e) sol et (f) karst.

La démarche proposée comporte une Analyse en Composantes Principales pour réduire le nombre d'indices et ne considérer que les plus contributaires, une classification en K-moyennes pour distribuer les stations en un certain nombre de classes, ici 5 et finalement la construction d'un arbre de décision à partir des distances aux noyaux des classes climatiques pour déterminer si un lieu quelconque possède ou non un climat méditerranéen et à quel type appartient-il. La classification a été établie sur des données spatialisées à haute résolution WorldClim-2 à 1-km pour la période de référence 1970-2000 et vérifiée pour 144 stations sur 30 à 120 ans, à pas de temps mensuels. Cette classification montre que la distribution en 5 classes coïncide avec une distribution géographique en Méditerranée allant de CC1 au Sud avec le climat le plus sec et saisonnier vers CC5 au Nord le moins saisonnier et plus humide. L'analyse de la connexité interclasse montre que l'évolution du climat se fait de façon continue, puisqu'une même station peut appartenir à plusieurs classes adjacentes.

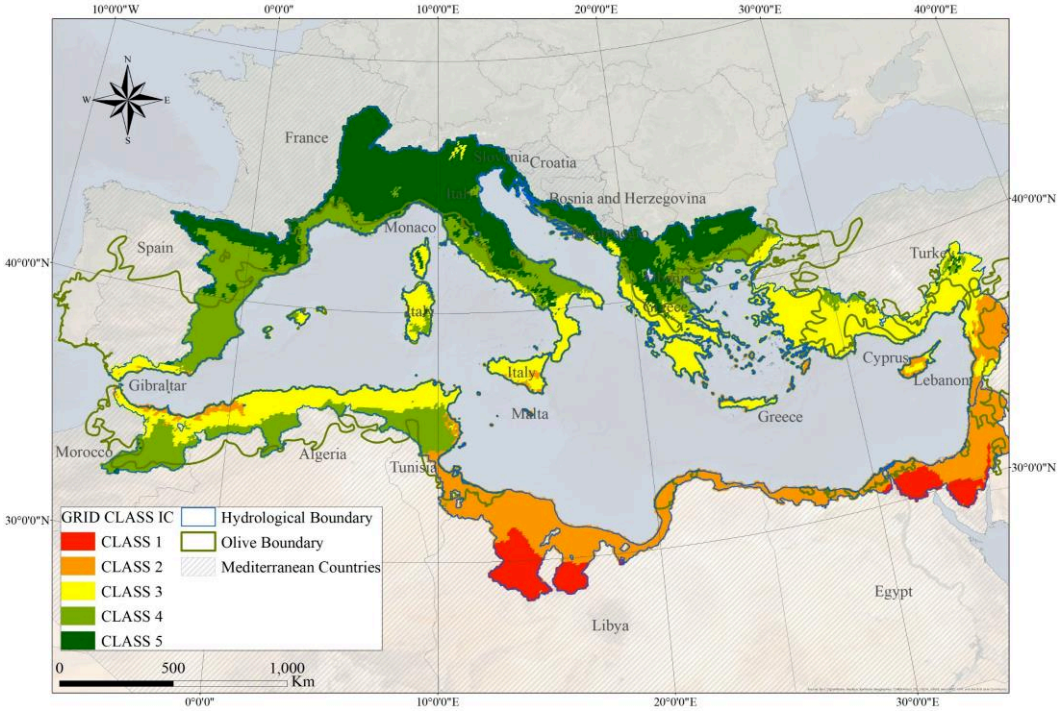

Figure b: Classification climatique de Méditerranée basée sur les données mensuelles de WorldClim-2.

La projection des données historiques avec les modèles régionaux climatiques MED-CORDEX RCM ALADIN et CCLM à des résolutions de 12 km et 50 km simulées suivant les scénarios RCP 4.5 et 8.5 pour la période 2070-2100 ont servi à évaluer l'impact du changement climatique sur la classification climatique en superposant les changements projetés sur la classification de référence de 1970-2000. RCM ALADIN et CCLM ont indiqué une évolution de la région méditerranéenne vers le climat aride. Les classes situées au Nord évoluent lentement vers des classes côtières modérées ce qui pourrait affecter les régimes hydrologiques en raison des saisons humides plus courtes et des fontes précoces des neiges.

Chapitre 4 – Caractérisation physiographique

Le Chapitre 4 met en évidence la diversité des bassins méditerranéens à travers une classification physiographique de l'ensemble des bassins versants basée sur des indices de forme et relief (A, I_{Hypso}, S_A, Z_{MEAN} …), d'occupation du sol (CMA, P_{Karst}, SC_COD, TC_BDC) et indices pédologiques (T_AWC, Leptosols, …). Cette classification devrait exposer l'interaction physioclimatique exprimée par les microclimats, la distribution et variabilité de la couverture végétale. La démarche proposée comporte une analyse en composantes principales pour réduire le nombre d'indices et ne considérer que les plus contributaires et une classification en K-moyennes pour les répartir en classes. Le nombre de classes a été fixé à 10 selon la méthode du coude. Cette classification fourni un aperçu unique sur la physiographie des bassins versants méditerranéens.

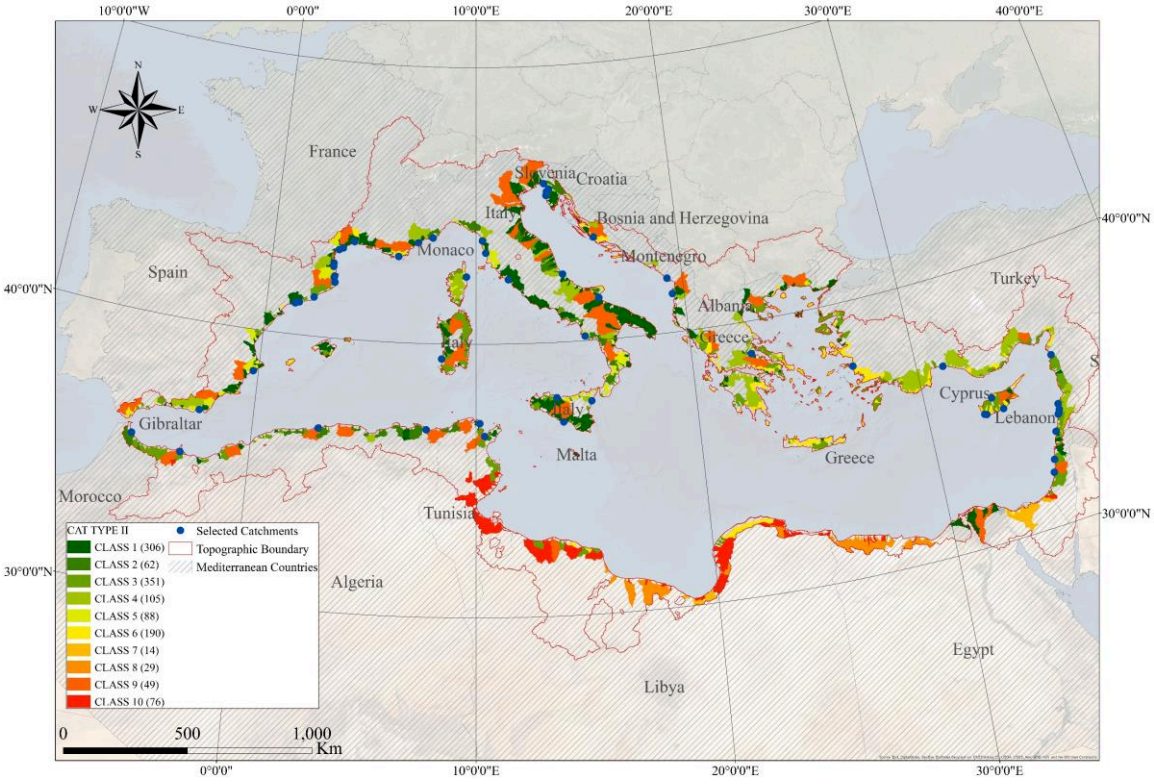

Figure c: Classification physiographique des bassins Méditerranéens de type II (entre 100 and 3000 km²).

L'analyse des caractéristiques physiographiques, principalement le relief, avec les caractéristiques climatiques locales, révèle l'existence d'une variabilité microclimatique masquée par l'homogénéité macro-climatique. Cette variabilité microclimatique est la raison principale derrière la variabilité naturelle de la couverture végétale.

Chapitre 5 – Caractérisation hydrologique

Le Chapitre 5 caractérise le comportement hydrologique de la région méditerranéenne à partir des séries de données de précipitations et de ruissellement rassemblées pour 55 bassins versants appartenant à 15 pays différents. Il présente les régimes d'écoulement selon la classification de Haines (1988), l'application du modèle du bilan énergétique avancé par Budyko (1974), le modèle de partitionnement de L'vovich (1979), le modèle conceptuel de Ponce & Shetty (1995a, 1995b) et sa formulation non dimensionnelle de Sivapalan et al., (2011). Les modèles fonctionnels sont les mieux adaptés à notre approche puisqu'ils fournissent une méthode claire et simple pour caractériser chacune des composantes du bilan et leurs interactions tout en donnant la possibilité d'étudier la variabilité spatio-temporelle, interannuelle et intra-annuelle. Ces modèles adoptent principalement les analogies de substitution «Time for time» et «Space for time», où l'analyse du comportement hydrologique d'un ensemble de bassins versants explique le changement de comportement potentiel qui pourrait se produire dans le temps et l'espace.

Le modèle de Budyko (1974) a été utile pour positionner tous les bassins versants en fonction de leurs précipitations et évapotranspirations, indiquant ainsi le forçage climatique sur l'hydrologie. La courbe de Budyko peut indiquer la disponibilité globale en eau d'un bassin versant, mais reste insuffisante pour estimer les ressources en eau. Le modèle de L'Vovich (1979) a montré une décomposition du bilan hydrique annuel donnant ainsi plus d'informations sur l'écoulement surfacique S et de base U, ce qui aide à déterminer le forçage physiographique sur l'hydrologie du bassin. Ce modèle a permis également une comparaison interannuelle précise avec des informations précieuses sur les ressources en eau. Ponce et Shetty (1995a) ont défini les équations des courbes du modèle de L'vovich, ce qui aide à prévoir les ressources en eau disponibles. Ces équations dépendent des paramètres des seuils d'écoulement, spécifiques à chaque bassin versant, ce qui permet une comparaison inter bassins plus précise, mettant en évidence la variabilité méditerranéenne. Ces paramètres reflètent également le forçage physiographique sur l'hydrologie. Le modèle de Sivapalan (2011) a rendu les équations de Ponce et Shetty adimensionnelles ce qui permet une comparaison interannuelle et inter bassins, ainsi qu'une comparaison inter climatique et inter physiographique, utile pour analyser la variabilité et l'homogénéité des bassins versants méditerranéens à travers des coefficients d'écoulement adimensionnels K_H , K_B, K_R et K_V. Ces coefficients, ont montré une configuration particulière des bassins versants méditerranéens en correspondance avec l'indice d'aridité $\varphi = \tilde{V} / \tilde{P}$. Le modèle de Sivapalan a montré une symétrie spatio-temporelle où les courbes fonctionnelles conviennent à l'analyse interannuelle pour chaque bassin seul ou à l'analyse inter bassins avec les bilans hydrologiques annuels moyens.

De plus, le Chapitre 5 présente l'analyse des coefficients d'écoulement total K_r et d'écoulement de base K_u et leurs gains par rapport aux précipitations annuelles selon la notion avancée par Ponce et Shetty

(1995b) et élaborée ensuite comme sensibilité aux précipitations par Harman et al., (2011) et nommée élasticité.

L'analyse du bilan hydrologique a mis en évidence une tendance méditerranéenne alignée avec le contexte climatique général, de la région humide au Nord vers la région aride au Sud; L'analyse a également montré une homogénéité hydrologique pour des classes physiographiques spécifiques telles PC4 des bassins versants montagneux karstiques et influencés par la neige qui produisent les débits de base et coefficients de ruissellement les plus élevés, en particulier ceux situés dans les régions CC3, ces bassins sont les moins sensibles à l'indice d'humidité P/ET_p qui rend leur comportement hydrologique très intéressant à étudier sous les scénarios de changement climatique RCP 4.5 ou RCP 8.5.

La distribution spatiale des paramètres du bilan hydrologique de Ponce et Shetty W_p, V_p, $\lambda_s W_p$ et $\lambda_u V_p$ reflète une variabilité géographique étendue à travers la Méditerranée sans aucune indication claire d'une organisation spatiale. Pour cela, l'application de la formulation non dimensionnelle de Sivapalan permet le traçage de toutes les composantes du bilan hydrologique des 55 bassins versants sur le même graphique et la discussion de leurs variabilités par rapport aux classes climatiques et physiographiques.

L'illustration climatique des courbes de l'humectation W^*et de l'écoulement surfacique S^*en fonction de la précipitation rééchelonnée $(\tilde{P})$ a indiqué que la compétition entre W^* et S^* évolue progressivement avec le climat allant de CC2 au Sud, où les précipitations sont faibles et les débits surfaciques sont faibles aussi, vers CC5 au Nord, où les précipitations sont fortes et les débits surfaciques élevées dominent. La même tendance peut être aussi observée pour U^*et V^* en fonction de l'humectation rééchelonnée $(\widetilde{W})$ néanmoins avec des perturbations provenant des bassins versants libanais CC3.

L'illustration physiographique des mêmes graphiques n'a montré aucune tendance interclasse ou regroupement sauf pour les bassins forestiers PC2 produisant le débit surfacique le plus élevé S^* et l'humectation la plus faible W^*; ceci peut être due à leurs positions géographiques dans la région humide CC5 ce qui justifie également leur couverture forestière et sa densité. Un autre groupe, celui des bassins versants montagneux influencés par la neige et le karst PC4 et qui sont répartis à travers la Méditerranée mais produisent le débit de base le plus élevé U^* et la vaporisation la plus faible V^*, n'importe la classe climatique.

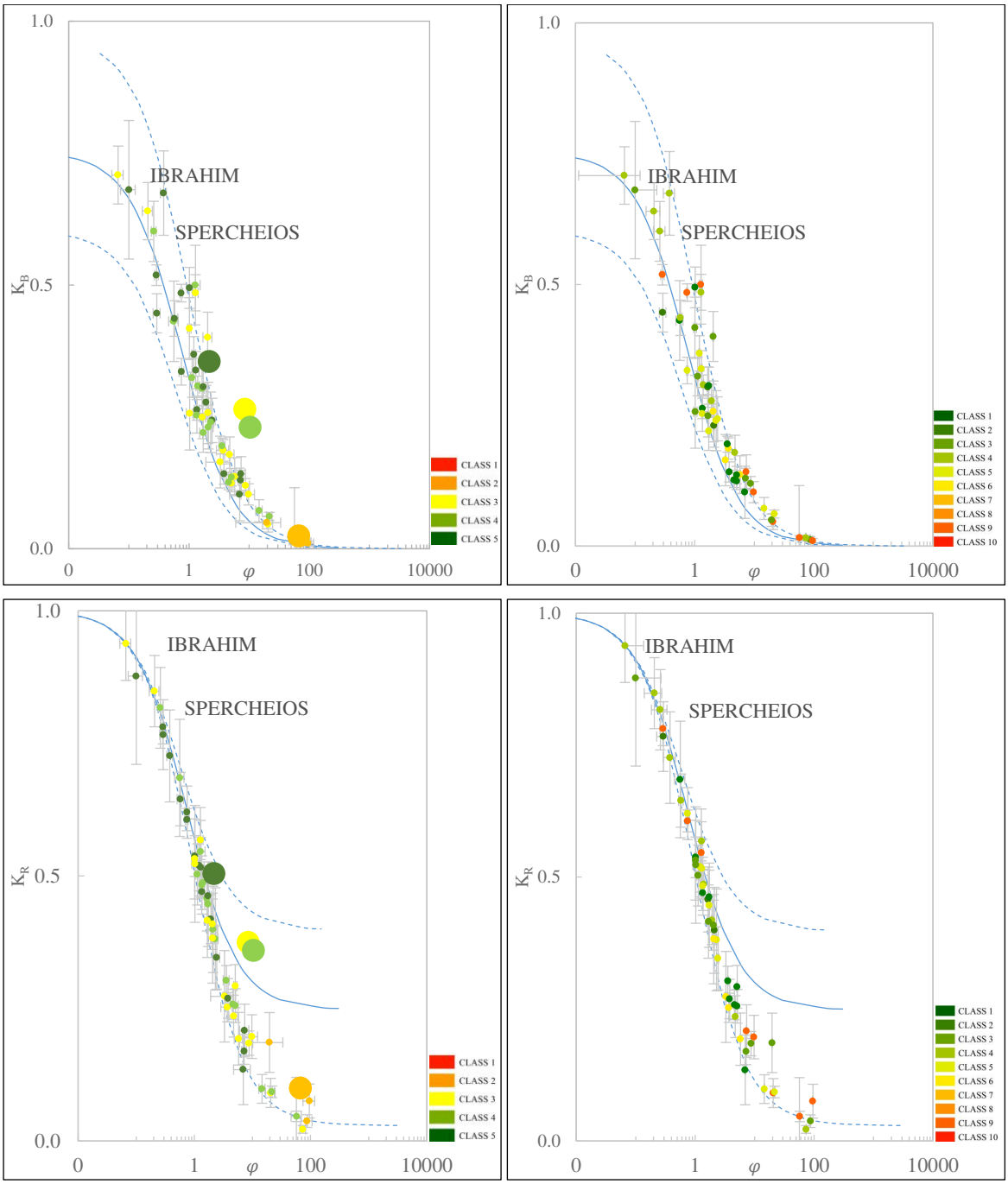

Figure d : Estimation des indices non dimensionnel K_B et K_R en fonction de l'indice d'aridité φ pour les 55 bassins et coloré selon la classification climatique (gauche) et physiographique (droite). Les petits points représentent les bassins, les gros points représentent les moyennes par classe.

Le calcul des variables adimensionnelles du bilan hydrologique K_H, K_B, K_V, K_R confirme les résultats précédents puisque l'indice d'aridité $\varphi = \tilde{V}/\tilde{P}$ s'est avéré un déterminant principal du bilan hydrologique. Les graphiques ont montré que K_H et K_V augmentaient avec l'aridité, suggérant qu'en général, la vaporisation V (et par conséquence l'énergie) prend le dessus sur l'humectation W et par conséquent le débit de base U. Inversement, K_B et K_R diminuaient avec l'aridité, à l'exception, encore une fois, des bassins versants PC4 qui se sont révélés indépendants de la variabilité climatique.

Les mêmes tendances climatiques et positionnement séparé des bassins PC4 ont été également observés pour les coefficients de ruissellement et d'écoulement de base dans la section 5.4.3; par conséquent, nous concluons qu' *en Méditerranée, les bassins versants montagneux, influencés par la neige et le karst, produisent le débit de base et le ruissellement les plus élevés, surtout s'ils sont situés dans une région à saisonnalité élevée (telle CC3 au Sud de la Méditerranée) où les précipitations sont concentrées en hiver et le ruissellement est concentré en hiver et au printemps (ayant pour régime le Groupe G13 de Haines ou G14 au Nord du Liban), lorsque la végétation couvre le minimum de terre et que la vaporisation (ou évapotranspiration) est la plus basse, ceci s'inscrit, mais à l'échelle intra-annuelle, dans l'auto-organisation de la végétation avec le climat comme proposé par Horton (1933).*

A la lumière de ce qu'on a déduit que les caractéristiques des bassins PC4 sont indépendants de la variabilité du climat, il est fort probable que l'impact de l'évolution climatique sur le comportement hydrologique, comme vu au Chapitre 3, aura une incidence moins grave sur les régimes hydrologiques des bassins versants PC4 étant donné que l'aridité devrait diminuer en raison de la diminution de la Vaporisation V lorsque la saison des précipitations se raccourcira et, par conséquent, le débit de base U et l'humectation W devraient augmenter tant qu'ils restent sous l'influence de la neige.

Chapitre 6 – Analyse de l'homogénéité et de la variabilité hydrologique

Les observations et conclusions du Chapitre 5 ont été vérifiées et complétées au Chapitre 6 en transférant les coefficients et les indices hydrologiques à 1270 bassins de 100 km^2 et 3000 km^2 à partir des équations de régression issues de l'analyse canonique de corrélations. L'analyse canonique de corrélation a déterminé quels indices climatiques et physiographiques spécifiques régissent le comportement hydrologique méditerranéen, principalement des coefficients K_r et K_u et les indices de crues de 90 jours (DH_5, FH_1) et d'étiage de 90 jours (DL_5, FL_1) choisis pour leur rôle dans la gestion des ressources en eau.

L'ACC a montré que les indices physioclimatiques A, MAP, $T_{25\%}$, I_{Arid} sont hautement corrélés avec (DH_5 ; DL_5) tandis que T_AWC est corrélé avec FH_1. L'ACC intra-classes des bassins versants PC1 et PC9 a montré une corrélation supplémentaire entre ZS_{Mean} et (DH_5; DL_5). Tandis que pour les bassins versants PC4, l'ACC n'a remarquablement pas indiqué de corrélation avec I_{Arid} ce qui fait que DH_5 et DL_5 sont en quelque sorte indépendant de l'indice d'aridité annuel. Néanmoins, l'ACC a montré que MAP, ZS_{Mean}, TC_BDC, $T_{25\%}$, I_{Arid} sont fortement corrélés à K_r et K_u et ont été validé par la méthode Jack-knife.

La représentation des diagrammes canoniques en fonction de leurs régions climatiques et physiographiques a permis d'identifier l'existence d'amas homogènes dans les espaces canoniques. La contribution des indices climatiques dans l'ACC a forcé un certain regroupement spatial malgré le fait que les indices physiographiques sont variables à travers la Méditerranée, mais ils sont également affectés par les caractéristiques climatiques comme mentionné ci-dessus.

La régionalisation des indices de débit (DH_5 ; DL_5) a montré que le climat méditerranéen force une homogénéité hydrologique malgré la variabilité physiographique**.** Cependant, la régionalisation des coefficients K_r et K_u a montré que les bassins versants PC4 produisent les coefficients de ruissellement les plus élevés sur différentes classes climatiques, d'où on déduit que certaines caractéristiques physiographiques, principalement le relief, la neige et le karst dominent les caractéristiques climatiques et ainsi on peut dire que *les bassins versants climatiquement homogènes sont plus susceptibles d'avoir un comportement hydrologique homogène malgré leur variabilité physiographique, sauf pour les bassins versants montagneux influencés par la neige et le karst qui produisent un comportement hydrologique homogène malgré un climat différent.*

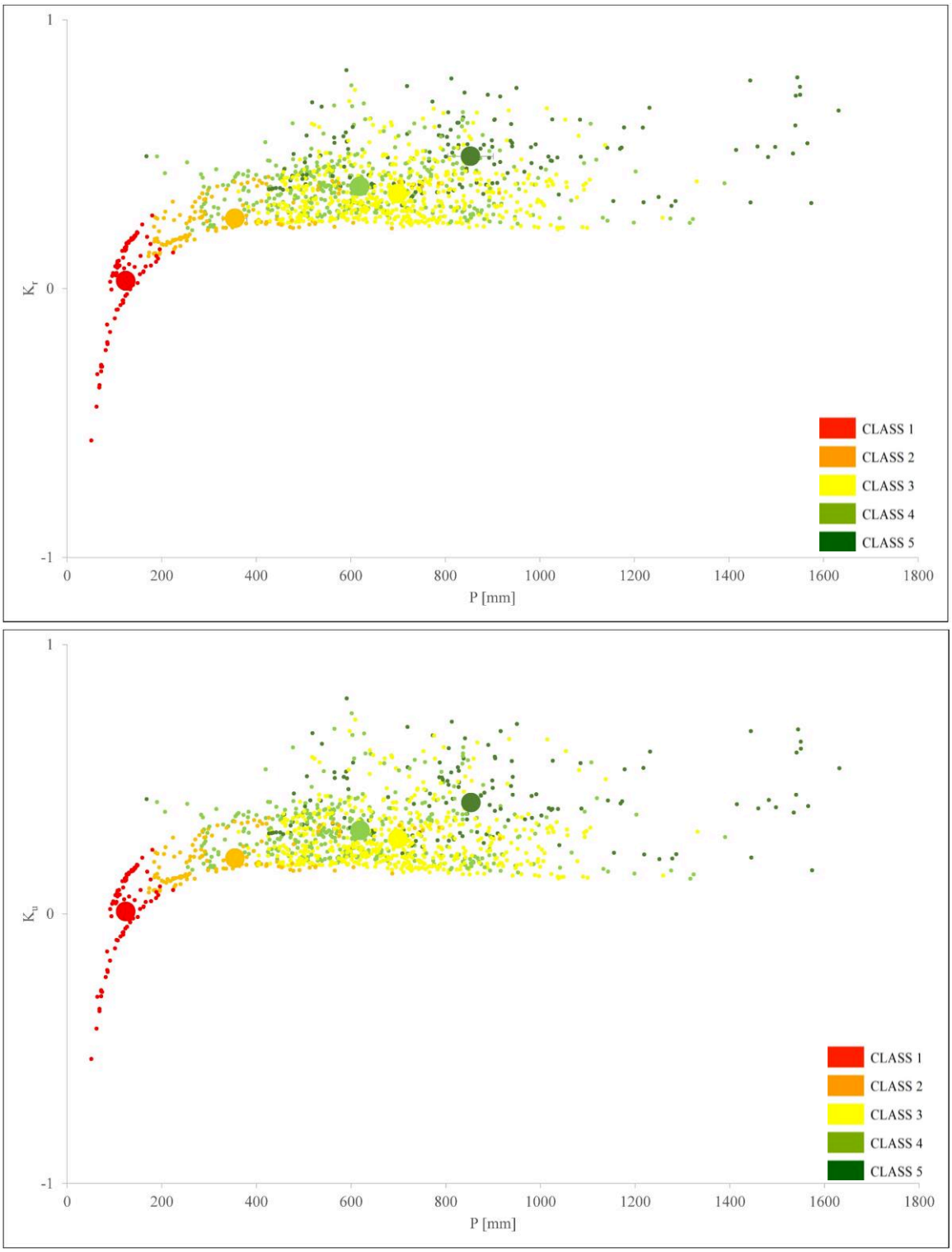

Figure e: Coefficients régionalisés d'écoulement total K_r et de base K_u selon les classes climatiques. Les petits points représentent les bassins, les gros points représentent les moyennes par classe.

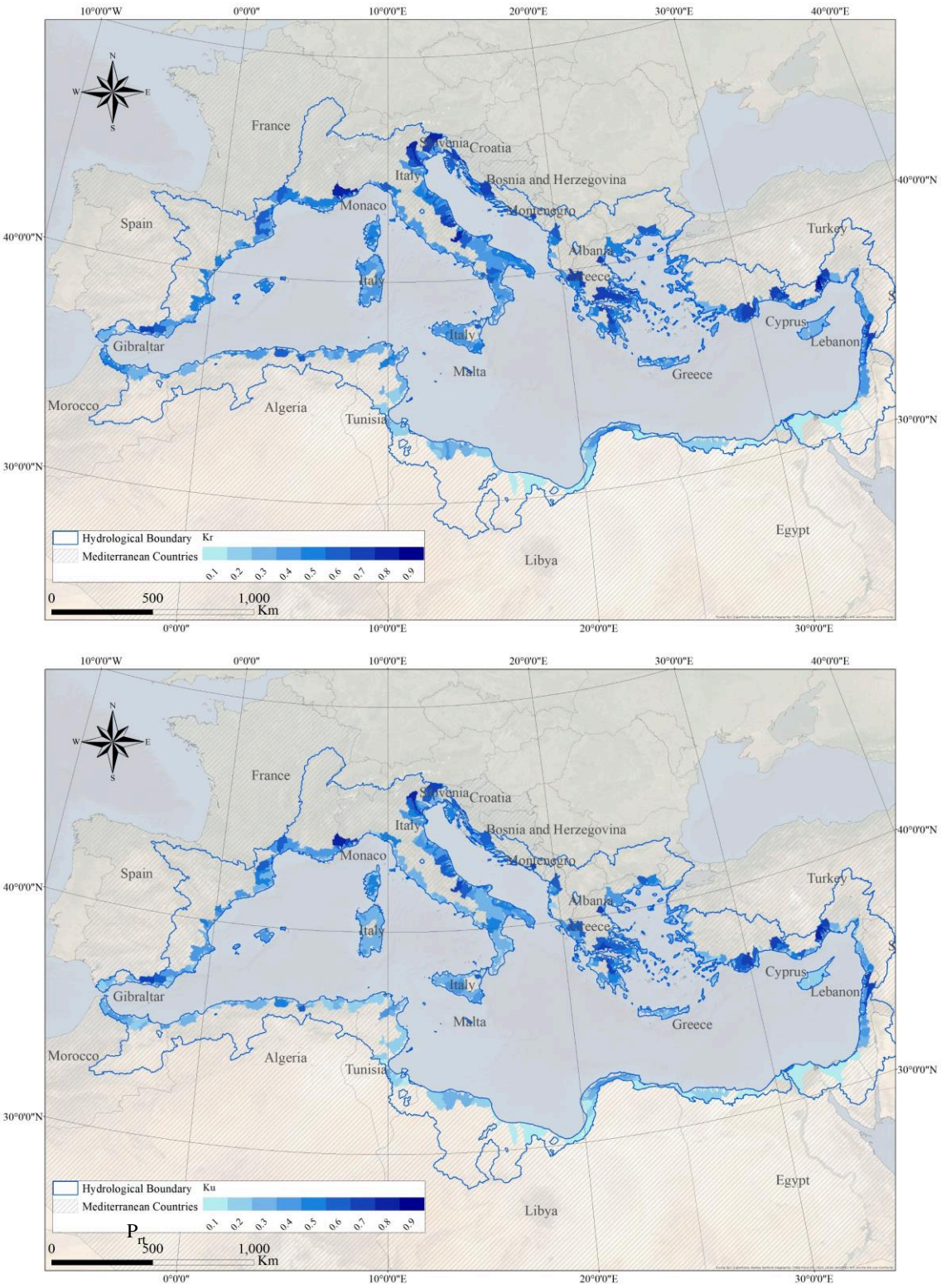

Figure f: Distribution spatiale des coefficients régionalisés d'écoulement total K_r et de base K_u allant de 0 (bleu clair) à 1 (bleu foncé)

La classification K-moyennes des indices physioclimatique obtenus par ACC I_S, I_{Arid}, ZS_{Mean}, P_{Karst}, T_AWC, TC_BDC et les coefficients K_r et K_u montrent que la dimension climatique méditerranéenne est à l'origine de la proximité spatiale de certains bassins versants appartenant à une même classe hydrologique HC1. Cependant, la plupart des bassins versants qui appartiennent à HC2, HC3 ; HC4 et HC5 ont montré une homogénéité hydrologique entre bassins versants non adjacents.

Ainsi, en associant tous les résultats de caractérisation, on déduit que l'hydrologie méditerranéenne est conditionnée par un forçage climatique de 1er degré, généré par le complexe des oscillations de Nord Atlantique, d'autres cyclones balayant la Méditerranée, exprimés dans cette thèse par les indices de saisonnalité et d'aridité I_S et I_{Arid} et d'un forçage physiographique de 1er degré tels les reliefs, qui eux-mêmes sont des générateurs de microclimats. Les microclimats sont le forçage climatique de 2nd degré exprimé par la quantité et le type de précipitations qui façonnent la physiographie du 2nd degré tels les types de couverture végétale, le T_AWC et d'autres caractéristiques physiographiques qui résultent d'une longue exposition climatique. Cette organisation paysagère-climat spécifique à la Méditerranée façonne indirectement le bilan annuel, les ruissellements, l'infiltration et l'évapotranspiration, ce qui les rend plus alignés avec le climat que le paysage.

Cependant, le karst exposé s'impose comme «intrus» à cette organisation paysage-climat. Le karst est une spécificité assez présente en Méditerranée datant depuis la période Messénienne de 5,96 à 5,33 Ma lorsque le niveau de la mer a chuté de façon spectaculaire, provoquant la Karstogenèse des Lapiaz, des grottes et d'autres formations souterraines. Les bassins montagneux karstiques ont défié le comportement hydrologique d'autres bassins, plutôt alignés avec le climat et qui ont montré un comportement homogène indépendant des forçages climatiques. Un autre «intrus» aussi spécifique à la Méditerranée serait la gestion des ressources en eau PC1 ou PC9 mais qui restent toujours alignés avec le climat au moins pour les bassins versants choisis dans cette étude.

Le climat est en effet le déterminant principal de l'hydrologie méditerranéenne, mais pas le seul, puisqu'une contribution majeure aux régimes d'écoulement provient d'indices physiographiques tels le ZS_{Mean}, TC_BDC et T_AWC. Par conséquent, la définition de bassins versants méditerranéens hydrologiquement homogènes consiste à trouver les caractéristiques climatiques et physiographiques du 1er et 2nd degré.

La régionalisation a permis aussi de prévoir l'impact du changement climatique sur les coefficients K_r et K_u des bassins versants de type II, selon les scénarios RCP du MED-CORDEX. Dans l'ensemble, l'évolution projetée a principalement affecté les extrêmes, minimisant ainsi la variabilité interclasse et augmentant l'homogénéité des bassins versants. Les bassins versants se sont rapprochés des classes CC3

et CC4 les plus méditerranéens sans changer leurs tendances ayant toujours les bassins PC4 les plus productifs. Le changement climatique entraînerait également un changement physiographique, affectant principalement la végétation et le couvert végétal, mais ceci n'a pas été pris en compte mais pourrait être envisagé dans des études ultérieures.

Conclusion

Nous avons répondu aux quatre objectifs annoncés au départ. Une base de données hydrologique a été rassemblée comprenant les bassins versants, les données climatologiques et hydrométriques et les caractéristiques physiographiques. Une nouvelle classification climatique pour l'hydrologie a été établie, basée sur des indices climatiques spécifiques à la Méditerranée tels que la saisonnalité des précipitations et l'aridité. Cette classification a servi pour la projection de scénarios climatiques futurs. Une classification physiographique de tous les bassins versants méditerranéens a été effectuée en fonction des indices physiographiques de relief, d'occupation du sol etc. mettant ainsi la variabilité méditerranéenne. Cette classification a permis de découvrir l'interaction physioclimatique et son rôle dans la formation de l'hydrologie et des régimes d'écoulement méditerranéens. Et finalement, une analyse hydrologique approfondie a été effectuée sur 55 bassins versants méditerranéens selon les différents modèles fonctionnels où la variabilité hydrologique et la similarité entre tous les bassins versants et entre les mêmes classes climatiques et / ou physiographiques a été vérifiée.

L'alerte climatique et les effets anthropiques appellent à des mesures d'adaptation et d'atténuation urgentes qui devraient être incluses dans les futures stratégies nationales et plans de gestion des ressources en eau et qui devraient être davantage basées sur la recherche régionale en approfondissant les connaissances sur la variabilité spatiale et temporelle des ressources hydrologiques partout dans la Méditerranée.

La cartographie des bassins versants méditerranéens hydrologiquement homogènes est l'une des études de base à utiliser par les chercheurs, les laboratoires, les ingénieurs, les gouvernements et les organisations internationales dont la région méditerranéenne forme leurs zones d'étude cibles. Ces résultats pourraient aider dans des études à l'échelle du bassin versant comme la prévision sur les bassins non jaugés ou en outre des études à l'échelle régionale comme la prévision de l'impact du changement global sur l'hydrologie méditerranéenne conduisant à des politiques et pratiques d'adaptation et d'atténuation.

Cette thèse a été valorisée par 3 publications :

Allam A., Moussa R., Najem W., Bocquillon C., 2020. “Chapter 1: Hydrological cycle, Mediterranean basins hydrology”. In Water Resources in the Mediterranean Region, Editors Mehrez Zribi, Luca Brocca, Yves Tramblay and Francois Molle, Elsevier, pp. 1-21. https://doi.org/10.1016/B978-0-12-818086-0.00001-7

Allam A., Moussa R., Najem W., & Bocquillon C., 2020. Specific climate classification for Mediterranean hydrology and future evolution under Med-CORDEX regional climate model scenarios. Hydrol. Earth Syst. Sci., 24(9), 4503-4521. https://hess.copernicus.org/articles/24/4503/2020/

Allam A., El Hassan J., Najem W., Bocquillon C., Moussa R., 2020. Classification climatique méditerranéenne pour l'hydrologie. La Houille Blanche Vol. 1, 60 – 69. https://doi.org/10.1051/lhb/2020008

Perspectives

Pour surmonter les défis posés par la culture et la gestion des ressources en eau douce en Méditerranée, nous souhaitons élaborer quelques propositions à prendre en compte dans les futures stratégies et plans de gestion sur la base des résultats de cette thèse.

1- Perspectives pour la recherche hydrologique en Méditerranée

Premièrement, nous souhaitons valider cette étude sur tous les sous-bassins versants méditerranéens disponibles pour étudier l'homogénéité et la variabilité à l'échelle régionale et locale, et pour augmenter la précision des caractéristiques physioclimatiques et des indices hydrologiques. Nous inclurions des indices supplémentaires tels que les débits de pointe quotidiens, intéressants pour les études des risques d'inondation des petits bassins versants et une analyse de l'incertitude des indices.

Deuxièmement, cette étude pourrait être reproduite au niveau mondial, pour localiser les bassins versants méditerranéens d'autres bassins versants sous différents forçages climatiques et physiographiques. Nous inclurions également d'autres bassins versants sous climat méditerranéen en Californie, en Amérique du Sud ou en Afrique du Sud.

Troisièmement, nous aimerions appliquer, en plus des scénarios de changement climatique (modèles RCM), certains changements climatiques en forçant le climat de CC5 sur les bassins versants CC3 et vice versa pour les bassins versants des mêmes classes physiographiques. Aussi, nous aimerions appliquer certains scénarios paysagers pour suivre l'évolution globale des régimes hydrologiques en cas d'augmentation des cultures, d'urbanisation, de déforestation et d'autres scénarios, tout en ciblant des classes physiographiques ou climatiques spécifiques. Cela serait également possible en utilisant la même approche fonctionnelle que l'outil de suivi simple.

2- Perspectives pour la gestion des ressources en eau

a. Optimisation des stratégies nationales et des stratégies de collaborations

Les avantages de l'analyse d'homogénéité ne se limitent pas au transfert de caractéristiques hydrologiques entre bassins versants similaires, mais les dépassent pour le transfert d'expériences et de meilleures pratiques de gestion de ressources entre deux services où établissements d'eau de pays différents gérant des bassins versants similaires peuvent partager leur savoir-faire et optimiser les plans de gestion. Par conséquent, nous appelons à un projet méditerranéen de «bassins versants jumeaux», similaire aux «villes jumelles» ou «ville sœur», afin de transférer des stratégies durables réussies et de les mettre en œuvre sur des projets de développement sous-développés. Ce projet remodèlera les stratégies nationales du secteur de l'eau dans les pays en développement, le rendant scientifiquement fondé avec des plans personnalisés pour chaque bassin versant ciblant la gestion des ressources en eau, l'agriculture, le traitement de l'eau, la réutilisation des eaux usées.

b. Atténuation des pénuries d'eau douce

Cette étude a détecté l'importance des bassins versants montagneux karstiques sous influence neigeuse qui produit les coefficients de ruissellement et d'écoulement de base les plus élevés. Ces bassins versants sont les principaux fournisseurs d'eau douce et pourraient changer le jeu contre les problèmes de pénurie. Par conséquent, tout plan de gestion ou stratégie nationale supplémentaire devrait d'abord cibler ces bassins versants et profiter de leurs ressources en eau douce pour les futurs citoyens et touristes méditerranéens. Cependant, ces bassins versants sont les plus sensibles à l'environnement à la contamination et à la pollution et il faut faire attention à leur gestion.

c. Mesures d'atténuation du changement climatique

L'impact du changement climatique a mis en évidence l'évolution des bassins versants en CC5 vers les CC4 et CC3 avec une saisonnalité et une aridité croissantes provoquant l'évolution des régimes de débit printanier vers des régimes de débit hivernal extrême, ce qui raccourcit les saisons de stockage et d'arrosage. Par conséquent, pour atténuer ce changement, qui affectera principalement les bassins versants gérés et cultivés PC1 et PC9, les pays du Sud incluront dans leurs stratégies nationales l'augmentation des capacités de stockage et les pays du Nord prévoient de passer à l'agriculture saisonnière.

[This page was left intentionally blank]

INTRODUCTION

GENERAL MEDITERRANEAN CONTEXT

Mediterranean water resources and hydrology has long triggered research topics as its coastal areas and marine environment are one of the most sensitive regions around the globe enhancing more challenges. Water resources usually available in this region are now, more than ever, exposed to continuous increasing demand for agriculture, industry, tourism, urban and demographic development to improve the standards of living; add to this a challenging climate evolution mostly affecting freshwater resources. These concerns lead the Mediterranean-rim countries in 1976 to adopt the Barcelona Convention for the protection of marine resources, launch the regional activity centre of the Mediterranean Plan Bleu in 1977, an observatory on environment and Sustainable Development, and initiate several research programs with the main focus on Mediterranean water resources like MEDFRIEND in 1991, MEDHYCOS in 1995, EMWIS in 1996, and lately HyMEX Hydrological cycle in the Mediterranean EXperiment launched in 2007.

Mediterranean water resources are unevenly distributed, hence constituting hard political and social challenge in face of the increasing demand. This uneven distribution might be caused by the highly fragmented morphology with 3681 catchments of different sizes where 35% of them have a middle range area between 100 km^2 and 3000 km^2. Water management challenges facing small to medium administrative divisions require mandatory measures to benefit from small catchments, as most of the wide catchments' resources are already reserved to cultivated and managed areas covering 30% of the Mediterranean.

Mediterranean climate has proved for the last 20 years to be the most convenient for tourism leading the touristic destinations by attracting 410 Million tourists in 2018 against 160 Million only in 1995 showing a 4.2% average annual growth (World Tourism Organization, 2019), and climate change has serious impacts over it. In a 2011 study based on physical-impact model, Ciscar, (Ciscar et al., 2011) details the expected climate change impacts on agricultural, flooding, coastal systems and touristic activities in 2080 whereas agricultural yield change is expected to decrease by -27% in southern Europe, touristic activity expected to decrease by -4% in southern Europe but to increase by 17% in Central Europe. In a 2013 study, Milano et al., (2013) point out the current water stress that Southern and Eastern Mediterranean rim countries are experiencing with an increasing trend over the whole Mediterranean basin, as 30 to 50% decline in freshwater resources is expected and it is estimated that about ten Eastern and Southern Mediterranean countries will be below the scarcity level, generally estimated at 1000 cubic meters available per year and per inhabitant, all requirements considered.

The alerting climatic and anthropogenic impacts call for urgent adaptation and mitigation measures and water management policies that should be more based on regional research by deepening the knowledge on the spatial and temporal variability of hydrological resources all over the Mediterranean, hence the

importance of this thesis qualifying it as pioneering work in this direction for collecting a physioclimatic database covering all the Mediterranean and a hydrometric dataset of 55 catchments from 15 Mediterranean-rim countries. We do not claim that we have built the first and most extensive, complete, and valid Mediterranean hydrological database, however, the collected data are representative of the studied area. In addition, the methodology adapted in this study deserved to be tested as it showed promising findings for hydrological characterisation and prediction on ungauged basins that can be expanded and replicated on another database when available.

Mediterranean climate is known for its seasonality and the alternation of humid winters and dry summers (Köppen, 1936; Emberger, 1955) which conditions rivers flow regimes, landcover, agriculture and consequently any water resources management plan. The most notable characteristic of the Mediterranean climate is the precipitation seasonality and alternation between short humid seasons, 3 to 6 months accompanied with cold weather and heavy rains and floods, and somehow longer dry seasons, 6 to 9 months accompanied with warm weather and harsh droughts.

Mediterranean region shares several physiographic traits that could be observed across the Mediterranean, like the elevated and exposed karstic features, dating since the Messinian period 5.96 - 5.33 Ma when sea level dropped dramatically (Krijgsman et al., 1999; Audra et al., 2004). Karst landscapes could be observed in Mount Lebanon, Syria, Turkish coast from Adana to Antalya, Balkans countries, centre of Italy, the French riviera and eastern Spain. (Chen et al., 2017). On the other hand, cultivated and managed areas cover 30% of the Mediterranean, and olive tree, seen all over the region, is considered one of its iconic bioindicators mainly for the convenience of its climate, as olive reproductive cycle and flowering intensity is influenced by seasonal temperature and water availability (Moreno, 2014; Fraga et al., 2019).

OBEJCTIVES AND METHODOLOGY

Hydrological similarity between catchments should be judged based on specific metrics taking into account the complexity of the environmental factors impacting the catchment response (Wagener et al., 2007). Global river regimes were classified by Haines et al., (1988) based on monthly average flows only, and Mediterranean regimes were identified under 3 of the 15 global classes, finding a clear relation to Köppen's Mediterranean climate. Mediterranean rivers were classified into 6 flow regimes by Oueslati et al., (2015) based on Richter et al., (1996) hydrological indices and broad-scale catchment characteristics and the classification of 300 Italian catchments was carried out by Di Prinzio et al., (2011) making use of Self Organization Maps. However, to our knowledge, no Mediterranean study has tackled a climatic and physiographic classification before assessing the hydrological similarity. In a meta-analysis of hydrological response characteristics of Mediterranean catchments, Merheb et al., (2016) has highlighted the lack of

multidisciplinary studies using multinational databases of the region and which still until now slightly addressed in the literature as a hydrological entity. This lack of studies is mainly due to the geopolitical diversity with 23 bordering countries and more than 15 different official languages.

In result, a climatic, physiographic, and hydrological homogeneity has been detected but not yet confirmed across the Mediterranean. A specific Mediterranean hydrology is long to be defined yet and requires additional research to determine the relation between catchments climatic and physiographic indices on one hand and the hydrological processes on the other and which remains weakly addressed with several questions to be answered yet, what is the climate and landscape contribution into Mediterranean hydrology? Which are the similar catchments and what is unique about it? Are water resources available across the Mediterranean? And how does climate change impacts hydrology?

This PhD presents a comprehensive study that aims to hydrologically characterise Mediterranean catchments, from a climatic, physiographic and water balance point of view, putting it in the domain of comparative hydrology as defined by (Falkenmark & Chapman, 1989). Since there is a great interest and benefit in sharing knowledge for sustainable water resources management between developed countries, mostly in the North, and underdeveloped countries in the South, a quest to understand the actual and future hydrological behaviour of Mediterranean catchments was launched through the analysis of Mediterranean catchments hydrological similarity and variability. Thus, a four steps approach was adopted.

The first considers the feasibility of a multinational hydrology research project beneficial for countries and communities where hydrological services and water resources management are underdeveloped. Thus, a considerable effort was put to develop an inclusive hydrological database including catchments delineation with all their physiographic characteristics and climatological and hydrometric data.

The second consists of understanding the climatic contribution to Mediterranean hydrology by establishing a new high-resolution climatic classification for hydrology purposes based on Mediterranean specific climate indices like precipitation seasonality and aridity that play an important role in the mechanisms of Mediterranean catchments and flow intermittence. This classification is useful for the projection of future scenarios and following up hydrological (water resources management, floods, droughts, etc.) and ecohydrological applications such as Mediterranean cultivation of olive and other environmental practices.

The third consists of understanding the Mediterranean landscape variability by carrying out a physiographic classification of all Mediterranean catchments based on landform, landcover and soil indices. This classification shall uncover the physioclimatic interaction, (microclimates, landcover distribution, etc.) as part of the self-organisation of the vegetation with the climate as proposed by Horton (1933), and its role in shaping Mediterranean hydrology and flow regimes.

The fourth, to carry out an extensive water balance analysis of 55 Mediterranean catchments based on different water balance functional models as advanced by L'vovich (1979) then elaborated by Ponce & Shetty (1995a, 1995b) and Sivapalan et al., (2011) to check the hydrological variability and similarity between all catchments and between same climatic and/or physiographic classes catchments. The functional models are best fitted for our approach as they provide a clear and simple way to characterise each water balance component and their interaction while giving the ability to discover their time-space, interannual and intra annual variability. These approaches mainly adopt the "Time for time" and "Space for time" substitution analogies, also adopted by Budyko (1974) and L'vovich (1979) where the analysis of the hydrological behaviour of a set of catchments explains the potential behavioural change that might occur in time and space. The water balance metrics and hydrological indices will then be exported to 1270 catchments ranging between 100 km^2 and 3000 km^2 using Canonical Correlation Analysis regression equations. The hydrological variability analysis will help in setting better management plans for Mediterranean catchments to adapt and mitigate the expected change impact, expressed by temperature increase, seasonal shifting, early snowmelt and anthropogenic pressures on Mediterranean runoff mainly through transformation of agriculture, landuse and tourism (Cudennec et al., 2007; Hreiche et al., 2007; García-Ruiz et al., 2011; Verdier & Viollet, 2015).

This thesis is structured into 6 main chapters; CHAPTER 1 presents the literature review which includes the definition of the Mediterranean boundaries and Mediterranean climate, the different water balance approaches and hydrological classification and regionalisation; CHAPTER 2 presents the Mediterranean database including an extensive description of climatic and physiographic characteristics of all catchments and the hydrological datasets of 55 selected catchments. This chapter constitutes the introductory chapter of the book « Hydrological cycle" from "Water Resources in the Mediterranean Region" (Allam et al., 2020b) (see APPENDIX A1); CHAPTER 3 presents the results of the Mediterranean specific climate classification and the results of future RCP 4.5 and RCP 8.5 scenarios; This chapter was validated through two different articles; the first article accepted at La Houille Blanche (Allam et al., 2020a) (see APPENDIX B1) and the second article in HESS (Allam et al., 2020c) (see APPENDIX B2); CHAPTER 4 presents the results of the physiographic classification of Mediterranean catchments; CHAPTER 5 presents the hydrological characterisation of the 55 selected Mediterranean catchments through water balance calculation based on the functional approach; CHAPTER 6 the hydrological variability analysis through the regionalisation of hydrological indices from the 55 donor catchments to the 1270 Mediterranean catchments with the results of RCP scenarios ; and a GENERAL DISCUSSION of all the thesis findings.

This PhD gave until now 3 publications:

Allam A., Moussa R., Najem W., & Bocquillon C., 2020. Specific climate classification for Mediterranean hydrology and future evolution under Med-CORDEX regional climate model scenarios. Hydrol. Earth Syst. Sci., 24(9), 4503-4521. https://hess.copernicus.org/articles/24/4503/2020/

Allam A., El Hassan J., Najem W., Bocquillon C, Moussa R., 2020. Classification climatique méditerranéenne pour l'hydrologie. La Houille Blanche Vol. 1, 60 – 69. https://doi.org/10.1051/lhb/2020008

Allam A., Moussa R., Najem W., Bocquillon C., 2020. "Chapter 1: Hydrological cycle, Mediterranean basins hydrology". In Water Resources in the Mediterranean Region, Editors Mehrez Zribi, Luca Brocca, Yves Tramblay and Francois Molle, Elsevier, pp. 1-21. https://doi.org/10.1016/B978-0-12-818086-0.00001-7

Chapter 1 Literature Review

- Mediterranean hydrology
- Functional modeling

Chapter 2 Mediterranean Database

- Climatic database (grids and stations)
- Physiographic database (maps)
- Hydrological data for 55 catchments on 15 countries

Chapter 3 Climatic Characterisation

- Hydrology driven climatic indices
- Climatic classification
- MEDCORDEX climate change RCP scenarios

Chapter 4 Physiographic Characterisation

- Physiographic indices
- Physiographic classification

Chapter 5 Hydrological Characterisation

- Mediterranean flow regimes
- Mediterranean catchments waterbalance analysis

Chapter 6 Hydrological Homogeneity and Variability Analysis

- Hydrological homogeneity
- Hydrological regionalisation
- MEDCORDEX climate change RCP scenarios

NOTE TO THE READER

To lead the reader through the thesis, we chose two catchments representing God Rivers in Greek mythology, Nahr Ibrahim in Lebanon, and Spercheios in Greece. We will progressively develop their characteristics in a fight card at the end of each chapter in what we liked to call:

"God Rivers Duel, a Mediterranean Epic".

In Greek mythology, Nahr Ibrahim (Nahr in Arabic means river) is also known as Adonis River after the God of beauty and desire. The region of Nahr Ibrahim is one of the most beautiful and green areas of Lebanon, hence its name. Adonis was killed by Ares at the foot of the falls of Afqa, where Nahr Ibrahim emerges and bled to death from a deep wound in the groin. Aphrodite, his lover, despaired at his death and out of pity for her, the gods allowed Adonis to ascend from Hades for a short period each year, and as she mourned Adonis's death, she caused anemones to grow wherever his blood fell. In reality, Adonis river colour turn to red each February due to the volume of soil washed off the mountains by heavy winter rains, making it appear as if the water is filled with blood (Lucian et al., 1913).

In Greek mythology, Spercheios is a God River, son of Okeanos and his sister wife Tethys, both were Titans. Okeanos was the source of all fresh water, as for Tethys, she was the mother of the river gods and Oceanids. Both were the offspring of Uranus (Sky) and Gaia (Earth). According to Homer Iliad, Achilles was supposed to cut his hair and offer it to Spercheios as his father Peleus vowed, instead, Achilles gave it to his companion Patroklos. In Modern history, Eduard Suess, an Austrian geologist, and an expert on the geography of the Alps hypothesised the existence of the supercontinent Gondwana (proposed in 1861) and the Tethys Ocean (as he named it). During Mesozoic Era, Tethys ocean separated between Gondwana and Laurasia, and the latest successor of the Tethyan Sea is the present Mediterranean (Suess, 1893).

[This page was left intentionally blank]

CHAPTER 1. LITTERATURE REVIEW

Chapter summary

This chapter presents an overview of the theoretical background of the thesis. It starts by defining the climatic, hydrological, agro-bioclimatic, and administrative study area boundaries with a general and historical definition of the Mediterranean climate. It then extensively details the functional modelling theories since the heat balance model of Budyko (1974), the water balance two stage partitioning model of L'vovich (1979), the conceptual model of Ponce and Shetty (1995a, 1995b), its nondimensional formulation by Sivapalan et al., (2011) and the flow elasticity by Harman et al. (2011). The chapter also tackles the hydrological classification and similarity analysis.

1.1 INTRODUCTION

This chapter presents a theoretical background overview of the thesis. It starts by defining the climatic, agro-bioclimatic, administrative and hydrological Mediterranean boundary which will be adopted as study area for the data collection in CHAPTER 2. It states a general and historical definition of the Mediterranean climate which will be more detailed in CHAPTER 3. The chapter then extensively details the hydrological characterization methodology based on functional modelling theories since the heat balance model of Budyko (1974) considered as reference model in this thesis, to the flow elasticity by Harman et al. (2011) which will be applied later in CHAPTER 5. The chapter also tackles the hydrological classification and similarity analysis that will be used in CHAPTER 6 to identify Mediterranean patterns.

The Mediterranean hydrological studies vary between catchment scale studies that deal with special events such as flash floods well spread in the Mediterranean (Llasat et al., 2013), erosion problems, annual water balance (García-Ruiz et al., 2011), regional climate change impact studies on Mediterranean resources (García-Ruiz et al., 2011; Thiébault & Moatti, 2016) and global scale studies that dealt with Mediterranean specificities such as climate classification studies (Köppen, 1936), and river flow regimes classification (L'vovich, 1979; Haines et al., 1988; Oueslati et al., 2015).

1.2 MEDITERRANEAN HYDROLOGY

1.2.1 Defining Mediterranean boundaries

From the Latin word Mediterranĕus meaning 'middle land' the Mediterranean refers to the sea and bordering region located in the middle of the Ecumene between the European, African, and Asiatic continents. With Köppen's classification (Köppen, 1936) the definition designated henceforth a moderate climate and extended geographically beyond the limits of the Mediterranean Sea. The question that arises is how would the Mediterranean boundary be defined? Several alternatives are considered in this case based on the field of practice; hydrological boundary was adopted for this study as shown in Figure 1-1.

- The climatic boundary could be defined according to Köppen's classification where a set of regions share similar temperature and precipitation characteristics and known for their warm and dry summers and cold and humid winters. It is limited by the African desert to the South and the temperate European countries to the North. This boundary might change according to the definition of this similarity. Some regions share a similar Mediterranean climate although located far outside the Ecumene such as Chile, California, or South Africa.

- The hydrological boundary is defined by the set of catchments draining towards the Mediterranean Sea (Milano et al., 2013). This definition neglects some of Mediterranean climate regions like Portugal, part of Spain and favours geographically adjacent regions like Egypt and Libya.
- The agricultural-bioclimatic boundary consists of the set of regions sharing the same types of vegetation considered as indicators of the Mediterranean region such as olives, (Moreno, 2014). This definition is linked to human activity with the same nuances as the climatic limit.
- The administrative boundary of countries adjacent to Mediterranean Sea has a problematic definition independent of any natural base (Wainwright & Thornes, 2004). These boundaries include several climatic classes and cover larger areas than the topographical limits.

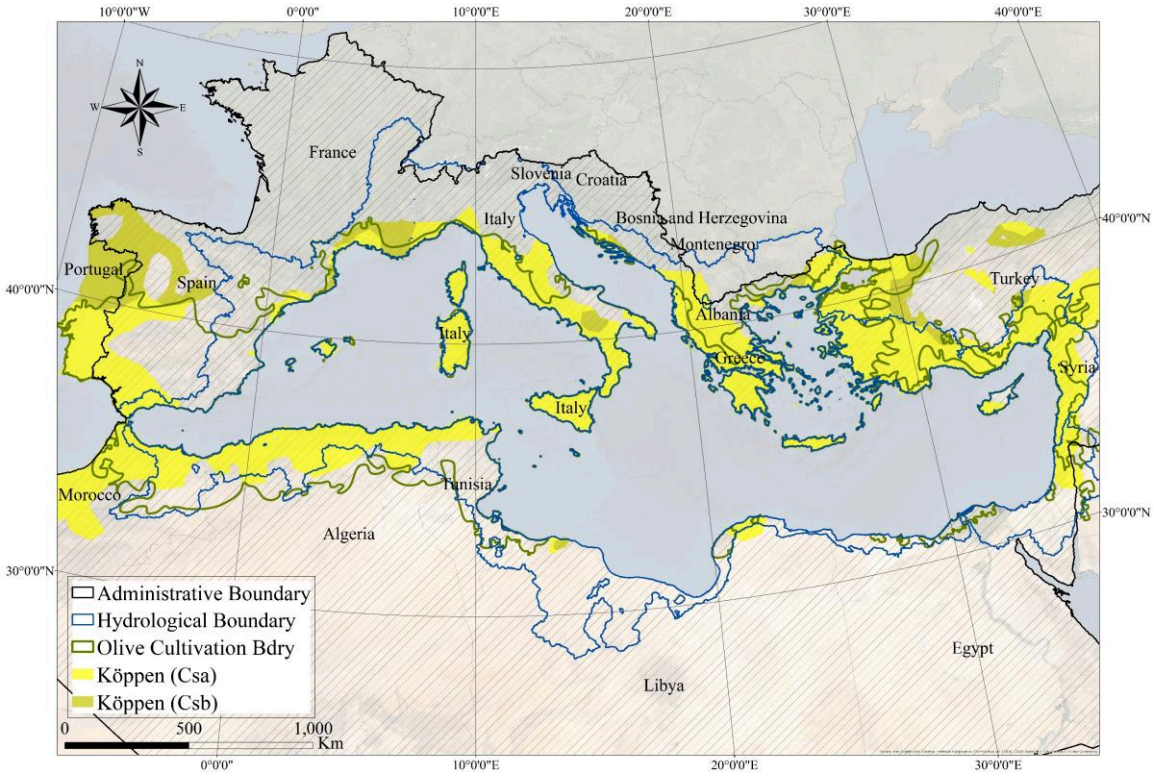

Figure 1-1: Four Mediterranean region boundaries (Merheb et al., 2016); first administrative, second topographic (Milano et al., 2013), third olive cultivation (Moreno, 2014); and fourth climatic (Peel et al., 2007).

1.2.2 Mediterranean climate

Mediterranean climate is the result of a complicated cyclonic system swiping a large evaporative basin. The distribution of marine and continental air masses creates an alternation of low-pressure zones coming over from Iceland and the Persian Gulf or high-pressure zones from Siberia and Azores. The seasonal shifts of these zones are magnified by the North Atlantic Oscillation (NAO) that plays an important role in shaping Mediterranean climate and influencing the evolution of farming and social activities on the long-term

(Rodwell & Hoskins, 1996). During the positive phases of the NAO, oceanic disturbances bring the most humid to northern Europe and less humid to North Africa and the Middle East (Douguédroit & Lionello, 2015). Winter hydroclimatic variables are negatively correlated with NAO in southern and western Italy and positively correlated with eastern and northern Africa. This modulation of winter precipitation by the NAO improves our current understanding and our ability to predict interannual rainfall variability in the greater part of the Mediterranean (Brandimarte et al., 2011). The influence of the NAO has also been demonstrated on river flows in the Iberian Peninsula (Trigo et al., 2004). In addition, mesoscale cyclones over the Mediterranean generate regional weather regimes, generally characterized by shorter life-cycles and smaller spatial scales than extra-tropical cyclones developed in the Atlantic (Lionello et al., 2006).

According to the Köppen-Geiger classification, the major part of the Mediterranean rim belongs to the temperate climate with a dry summer (Csa and Csb) limited to the south by the arid desert climate (Bwh), to the north by the temperate climate without a dry season (Cfb) and to the West by the cold climate without a dry season (Dfb). A similar Mediterranean climate could also be found in some regions of the world like California and Central Chile, South Africa, and South Australia. Nevertheless, there are some exceptions within the Mediterranean rim like Egypt and Tripolitania at the edge of the desert, Thessaloniki, and Veneto, where the seasonality disappears with classification (Cf).

This continuous alternation of high and low pressure, cold and humid winters followed by a hot and dry summers, marks the Mediterranean seasonality which makes the region attractive to social activities, thus its sensitivity to climate change and anthropogenic pressures (Milano, 2012). Climate change and anthropogenic pressures are expected to have severe consequences on Mediterranean runoff with a serious risk of water shortages (Cudennec et al., 2007; Hreiche et al., 2007; García-Ruiz et al., 2011; Verdier & Viollet, 2015).

Hydrologically, this seasonality plays a role in shaping rivers runoff as Haines classified the Mediterranean hydrological regimes under Group 12 Winter Moderate, Group 13 Extreme Winter and Group 14 Early Spring, and found a clear relation to the Köppen Csa and Csb climates and a close equivalent of the ‘Mediterranean Seasonal’ categories of Gentilli (Haines et al., 1988). Seasonality is a main factor in the Mediterranean but to our knowledge its use is still limited as a characterising index for climatic and hydrological classification.

Each climatic year is an independent realisation of a random phenomenon defined by a stochastic process and characterised by stationary parameters such as monthly averages, variance etc. The spatial distribution of this process characteristics leads to the classification of different climates. The complexity of climatic mechanisms, combined with regional landform diversity, creates extremely variable microclimates at the spatio-temporal scale. Climatic conditions have a decisive influence on hydrological mechanisms as they

constitute the main component of their functioning. Stream flows, groundwater recharge and the evapotranspiration of soils and plants are constrained by climatic variables: rain, temperature, wind, sunshine. In the same way as for climate, river flows constitute a stochastic process depending on the climatic and physiographic characteristics of the corresponding catchment.

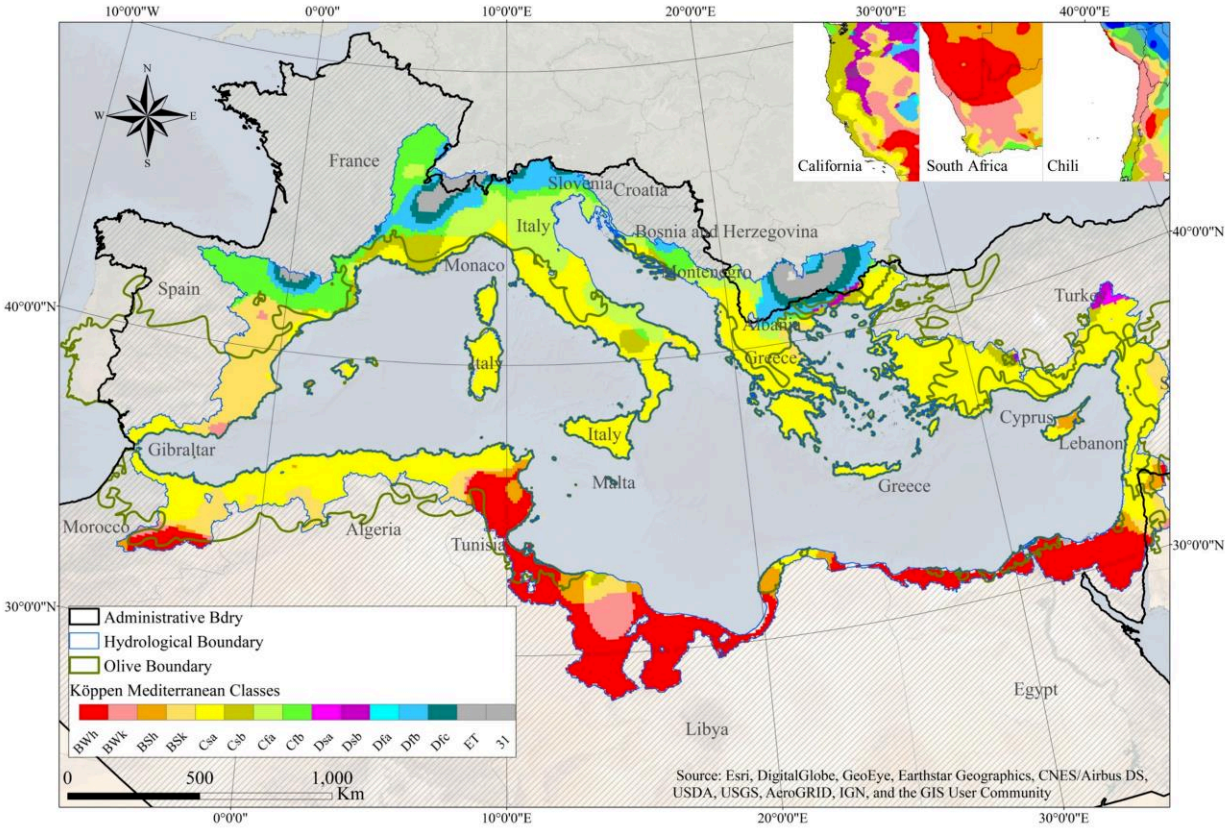

Figure 1-2: Köppen-Geiger climatic classification for the Mediterranean region and other Cs regions from (Peel et al., 2007).

1.2.2.1 Mediterranean seasonality

Precipitation seasonality, main characteristic of Mediterranean region, could be expressed by a seasonality index I_S. It corresponds to the precipitation difference between humid and dry seasons, which is also an index to identify the Mediterranean climate according to Köppen-Geiger classification. Knowing the monthly rain at each station, the calculation of this index is as the following:

$$I_s = 1 - \frac{min\, C_i}{max\, C_i} \qquad 1$$

With

$$C_i = \sum_{i=1}^{i+2} P_i \qquad 2$$

Where P_i is the monthly precipitation of the month i in mm, with i as the rank of the month starting from the first month of the hydrological year, September for the Mediterranean region.

The charts below in Figure 1-3, indicate the monthly distribution over the hydrological year of the non-dimensional precipitation ratio (P_i / P_m) (P_i being the monthly precipitation divided by the P_m the monthly annual precipitation) corresponding to Polis station in Cyprus with a strong I_S = 0.992 and centred distribution indicating the seasonal precipitation in contrary to Perpignan in France with a low I_S = 0.553 and flattened distribution indicating a regular distribution of rain all over the year (Hreiche, 2003). The Mediterranean would be qualified by high seasonality (see Figure 1-4), an interesting criterion for the study of interannual variability.

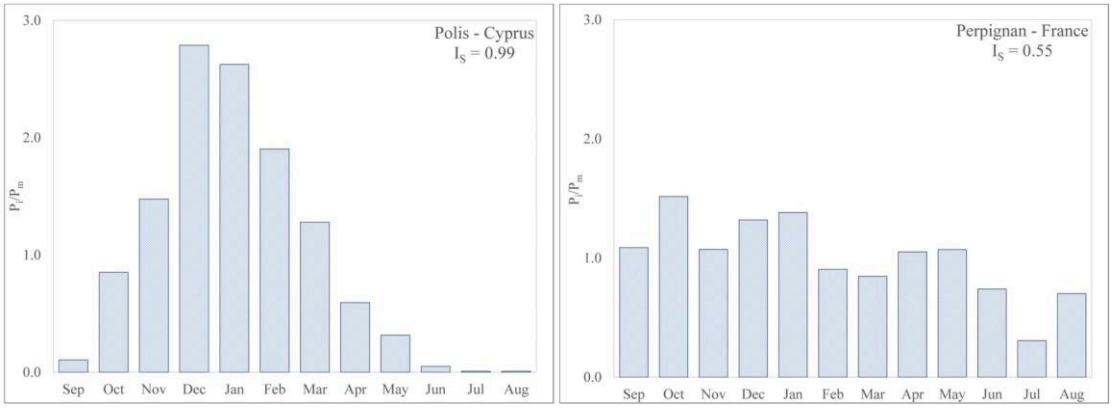

Figure 1-3: Monthly distribution of the precipitation at Polis-Cyprus and Perpignan-France from (Hreiche, 2003).

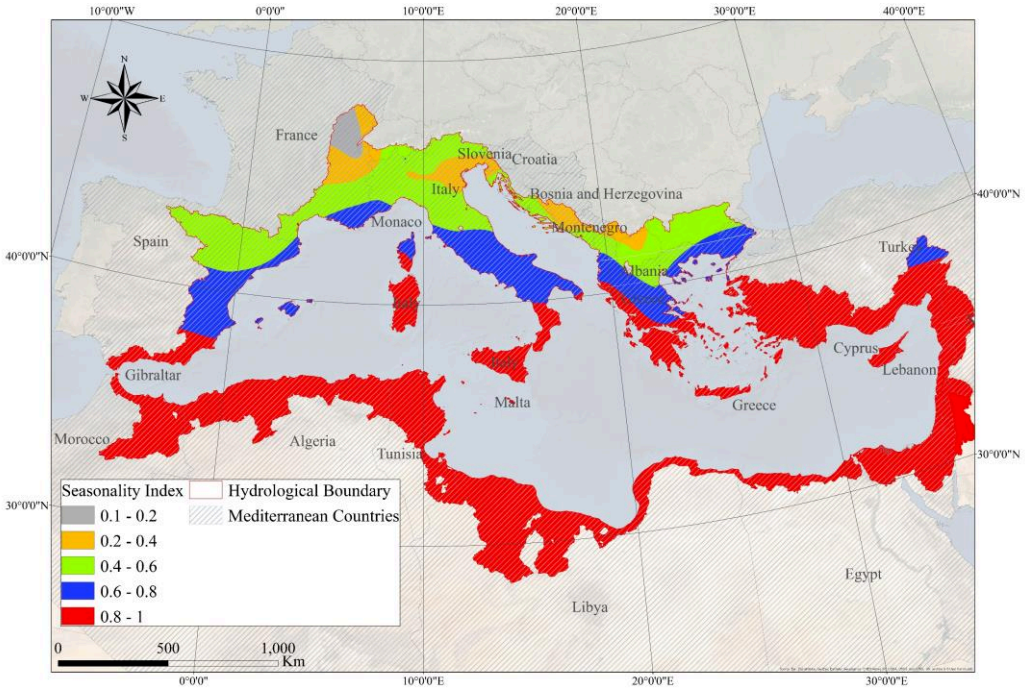

Figure 1-4: Seasonality index distribution over the Mediterranean from (Hreiche, 2003).

1.2.2.2 Stochastic model of Mediterranean precipitation

A stochastic process is a temporal phenomenon involving hazard represented by a random variable evolving over time. Thus, a stochastic process $\{Xt: \in T\}$ is a series of random variables indexed by t with values in a set X. T is the set of indices and X is the set of the process states. In summary, the basic characteristic of a stochastic process is the fact that the variable Xt is a function of t.

Several authors pointed out the stochastic behaviour of wet and dry periods alternation in the Mediterranean to synthetically describe the climatic variability. The single-site stochastic precipitation models that include precipitation occurrence and intensity were useful to generate long daily rainfall series and model hydrological responses to predict flood and erosion impacts. Efremides & Tsakiris, (1994) proposed a one-part stochastic rainfall model to simulate the rainfall process in the Greek islands of Rhodes and Chios. The Markovian process was found suitable for modelling daily precipitation data in Andalusia, Spain (Ramírez-Cobo et al., 2014) and middle east (Mhanna & Bauwens, 2009), Najem have demonstrated that precipitation in Lebanon, which is a unidimensional time-series observed and recorded over time at a certain location, follows a stochastic model (Catafago & Najem, 1976; Najem, 1988). The model is composed of 2 mechanisms with 4 parameters

- The first mechanism is the alternation of rain and non-rain events, which is a first-rate Markovian process with T1 the average duration of non-rain episodes, T2 the average duration of rainy episodes.
- The second mechanism is the rain impulses within same rain episode which have a structure of non-zero random variables and follow a Markovian order 0 process. With N the mean duration between two successive showers within the same rain episode and G the rain intensity. In other words, the intensity of today's rain is independent of the intensity of the previous day.

As part of the research conducted at CREEN, this stochastic model was verified (Hreiche, 2003), and its parameters were identified on a set of stations around the Mediterranean which helped in finding climate variability indicators. This verification helped in the search for climate variability indicators in the Mediterranean (see Figure 1-5).

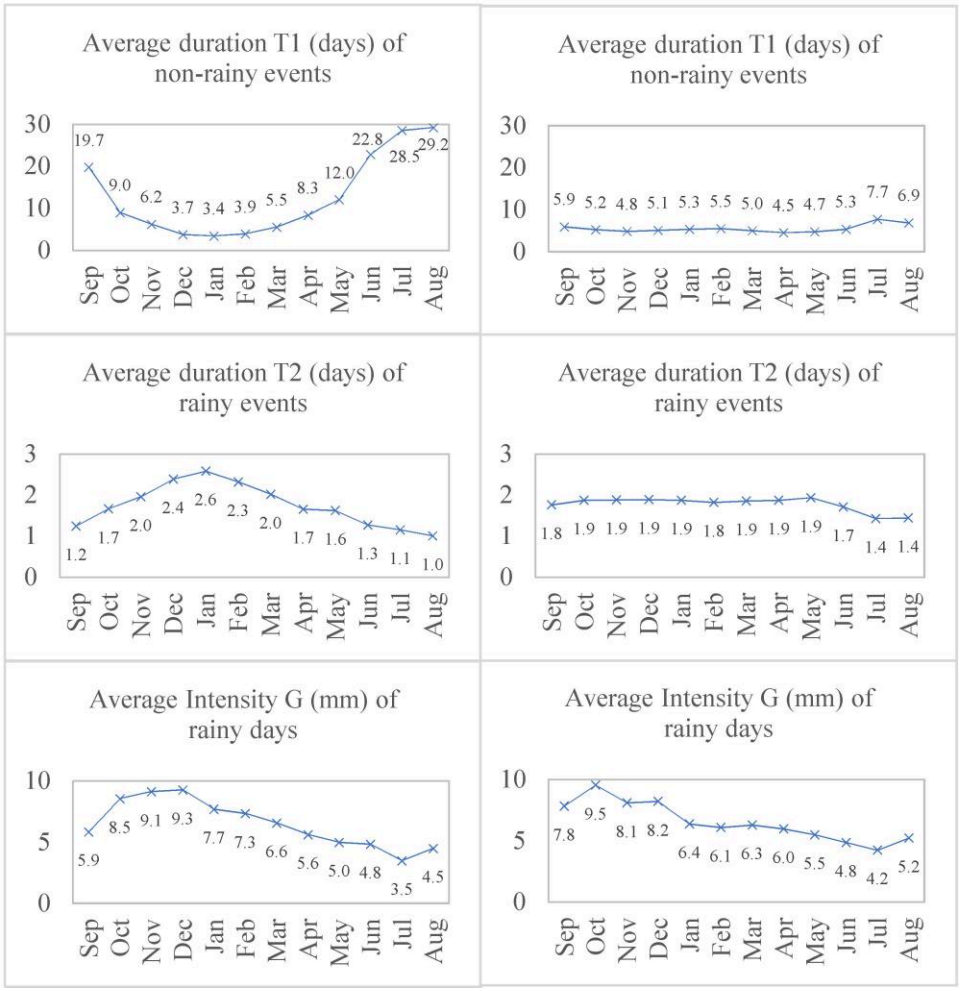

Figure 1-5: Stochastic parameters for precipitation time series in Polis-Cyprus (left); Perpignan-France (right) (Hreiche, 2003).

The global climatic classification, the seasonality index I_S and stochastic model parameters, have proven that precipitation seasonality is the main feature of the Mediterranean climate. This feature and its impact on Mediterranean landscape and hydrology will be analysed furthermore throughout the thesis.

1.2.3 Annual water balance of Mediterranean catchments

In his work, "World Water Resources and their Future", L'vovich (1979) assessed Earth's rivers water balance components, runoff and their underground component, and their patterns over the globe. In the subtropical belt, he defined 3 types of river regimes, the Mediterranean type, the one of the enormous deserts (Sahara, Arabian) and the one typical of terrains in which wet forests predominate (south-eastern China, Gulf of Mexico).

The Mediterranean type of river regime is widespread in southern Europe, on the west and south of the Iberian Peninsula, on the Italian Peninsula, and in the Balkans; in Asia: in the south of Asia Minor, the Near East, in the south and east of Iran and the Arabian Peninsula; in Australia: in the south and west of the

continent; in Africa: in Algeria, Tunisia, Morocco and the extreme south of the continent; in North America: California and Baja California; in South America: in the coastal strip of Chile, excluding its Patagonian part. In these areas, runoff has an uneven distribution, but generally rivers with comparatively small volume, with a flow of less than 100 to 200 mm are dominant. A higher runoff is associated with the relief, when confined to mountains or hills, like in southern Europe. An even higher runoff is associated with extensive Karstic landscape such as Balkans and Apennines. If the karstic rocks crop out on the surface, the water seeps down quickly and is preserved from evaporation.

L'vovich distinguished 2 types of Mediterranenan water balance, one group in Southern Europe: Balkans and the Near East, typified by high groundwater runoff, ranging approximately between 25% to 50% of total runoff, or even higher in rare cases where groundwater coefficient K_U (U/W) is usually higher than 0.20 mostly because of the open karst landscape and the large amount of rain, more than 1000 mm, with total runoff exceeding 500 mm.

"Mediterranean climatic influences extend to the south of the country; this being manifested in the predominance of winter runoff in rivers whose catchment areas have an average altitude of less than 1000 m. At higher altitudes, a substantial amount of the wintertime precipitation typical of the Mediterranean falls as snow, and spring runoff is therefore predominant. Steady predominance of spring runoff is typical of the zone of continental influences in the range of altitudes up to 2200 m. At higher altitudes, the snow melts in the summer, and summertime runoff therefore predominates. Summer runoff is small not so much because much less precipitation occurs in this season, but mainly because this is the time of the year when evapotranspiration increases. But at altitudes exceeding 1 200 m the predominance of spring runoff is also related to the melting of the snow cover."

The other group, in North Africa typified by low groundwater runoff ranging between 20% and 25% of total runoff with K_U usually less than 0.10 with sharp seasonal wetting fluctuations due to dry summer and wet winter with frequent heavy rains which prevents the water from being absorbed into the soil, with total runoff rarely exceeding 100 mm. The water balance components averages are presented in Figure 1-6.

"The second type of proportional pattern in Africa's water balance pertains to the sclerophyll evergreen forests and scrub in the mountainous areas of the African Mediterranean and the extreme south of the continent. Here the rainfall is 500 to 800 mm, of which 100 to 200 mm become runoff, 15 to 20 percent of that coming from groundwater. The comparatively low groundwater runoff and the high surface runoff results, first, from the high PE, so that soil moisture is spent primarily for evapotranspiration, and second, from the properties of red soils (terra rosa) which are developed on limestone eluvium, These soils have a high field capacity, but at the same time they have a high water retention capacity as well, and this prevents the water from percolating downward. At the same time, after soils of this kind are saturated with water, they become aquicludes (Shokal' skaya, 1948). For this reason, the first rains in the rainy season, which is in the winter, yield little runoff, since the water goes for infiltration, but subsequent rains, which fall on wet soil, form abundant surface runoff and high floods."

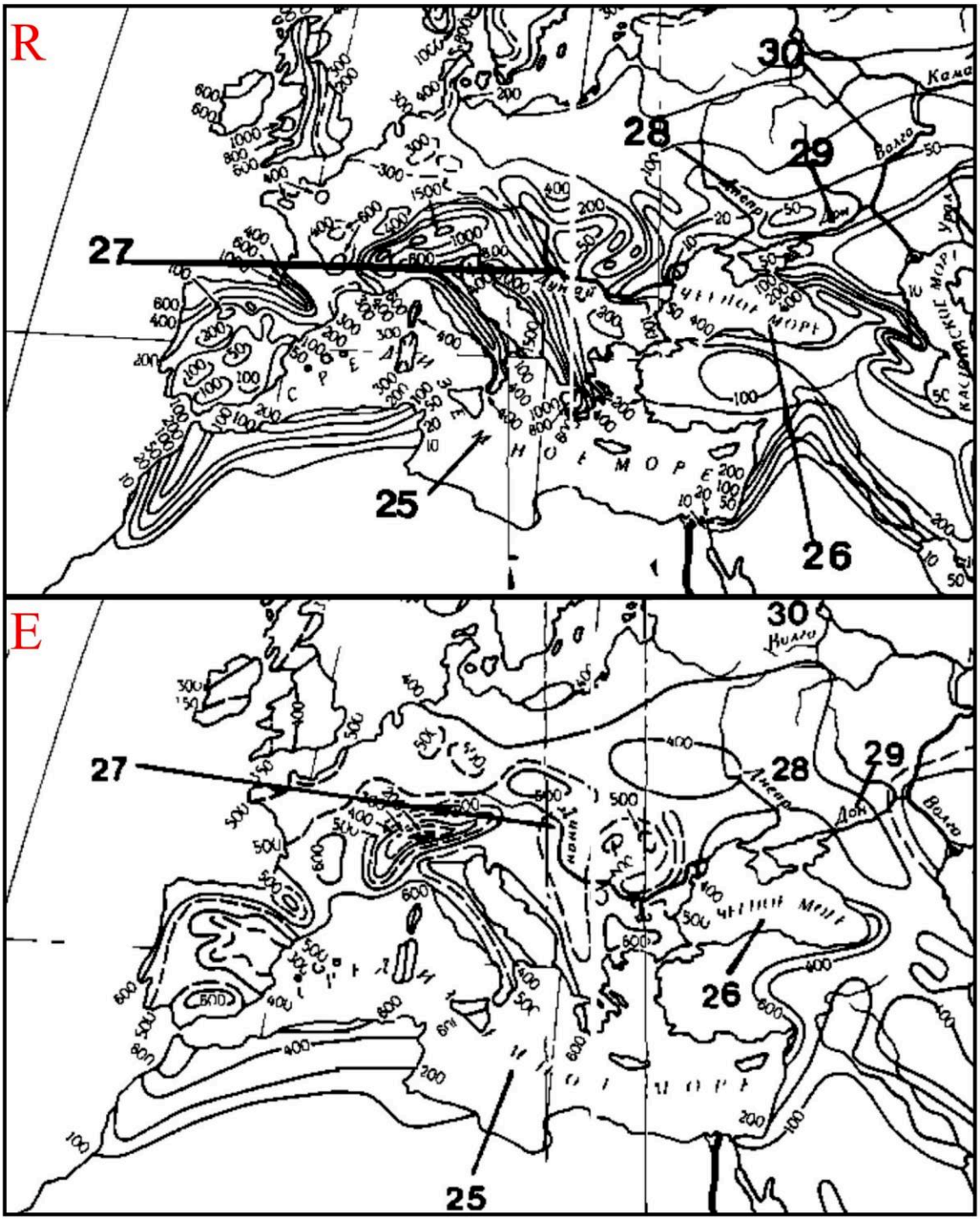

Figure 1-6: Water balance components maps for the Mediterranean region runoff (R) and evaporation (E) from (L'vovich, 1979).

In a meta-analysis, Merheb et al., (2016) collected a set of 140 published studies on the Mediterranean, including 58 studies annual water balance mostly of a single basin, 49 published studies on floods and 33 studies on low flows and drought. To study Mediterranean trends, Merheb divided geographically the Mediterranean into 3 subregions:

- The North Western Mediterranean (NWM) including Albania, Croatia, France, Italy, Montenegro, Portugal, Slovenia, and Spain.
- The Eastern Mediterranean (EM) including Cyprus, Egypt, Israel, Lebanon, Palestinian territories, Syria, and Turkey
- The Southern Mediterranean (SM) including Algeria, Libya, Morocco, and Tunisia.

It should be noted that the annual water balance studies were intended either for simulation, the presentation of hydrological processes, the improvement of the models' performance, or for future scenarios studies such as climate change and landscape change impacts.

The water balance across the Mediterranean showed a wide variability of Mean Annual Precipitation (MAP), Evapotranspiration (ET) and Mean Annual Runoff (MAQ). This variability could be easily observed between catchments where for the same MAP (900 mm), two different MAQ could be obtained, 30 mm for the first and MAQ exceeding MAP for a second. This variability also extended to the hydrological responses of these catchments hence the encountered modelling difficulties. However, Merheb has identified a high correlation r^2=0.69 between MAP and MAQ of all the studies. This correlation could be justified by the similarity between Mediterranean catchments where NWM catchments gave high MAQ and low aridity coefficients while SM were the driest.

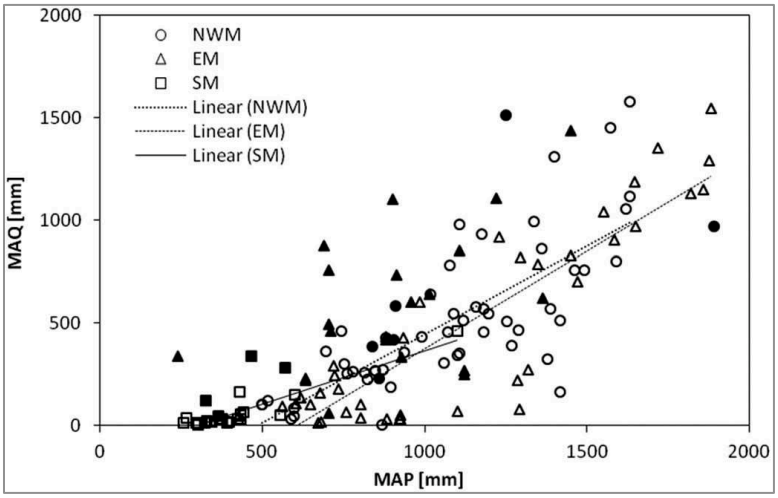

Figure 1-7: Relationship between mean annual runoff (MAQ) and mean annual precipitation (MAP) for the three studied sub-regions (NWM, EM and SM). Filled symbols indicate karstic catchments in each sub-region from (Merheb et al., 2016).

1.3 FUNCTIONAL MODELLING

Several rainfall runoff modelling approaches can be found in literature, we focus here on the functional approach for annual water balance estimation; The functional approach took birth from the empirical model of L'vovich and the process-based approach of Horton; L'vovich advanced an empirical approach for the two-stage distribution of the water balance (L'vovich, 1979) while Horton introduced the ratio of the vaporisation V to the wetting W and named as Horton index, H = V / W in a trial to search for catchments capacity to store the infiltrated water, depending on the soil type and the evaporation controlled by the vegetation type (Horton, 1933). The work of Horton and L'vovich could be considered as characterising of catchments functioning on an annual scale described as a functional approach.

In the empirical approach, the annual water balance is estimated based on a systematic analysis of long-term rainfall and runoff series observed in different climatic regions and an empirical analysis of the effect of physiographic and climatic descriptors on the water balance. The value of the empirical approaches lies in the simplicity of the relations which govern the annual assessment on the long term, and which appeared from the coevolution and the self-organization of climates, soils, topography and vegetations of the different regions. One of the empirical approaches would be the Budyko E/P aridity index (Budyko, 1974).

In the process-based approach, the annual water balance would be estimated based on the illustration of the various processes of the balance such as infiltration, storage, drainage, and evaporation. These processes constitute the water balance equation and the interactive roles of climate, soil, topography, and vegetation. (Eagleson, 1978; Eagleson & Tellers, 1982; Milly, 1994a, 1994b; Reggiani et al., 2000; Potter et al., 2005; Yokoo et al., 2008).

Horton's hypothesis that his index H is constant for each catchment from one year to the next, was verified by (Troch et al., 2009) when he estimated the Horton index of 89 catchments in the United States. Troch also found that if the aridity index Ep/P increased, the Horton index also increased while its variability decreased significantly. In addition, the symmetry induced by Horton index' variability, spatially and intra-annually, assumed that the vegetation of each region adapted to the spatial and temporal variability of the water availability and energy.

Furthermore, the interannual variability is affected by seasonality, intra-annual variability and hydrological processes (Sivapalan et al., 2011). Therefore, the empirical and process-based approaches should be generalised to account for these intra-annual variations. Horton and L'Vovich are considered pioneers in their work in this direction.

We present in chronological order the different water balance functional models, (see Table 1-1) and detail at the end the baseflow separation methods which shall be used to apply these models in CHAPTER 5.

Table 1-1: List of different water balance functional models detailed in sections below and applied in CHAPTER 5.

Water balance model	Author, Year	Equation
The heat and water balance reference model	Budyko, 1974	$E = f(P, E_p)$
The empirical water balance partitioning model	L'vovich, 1979	$P = S + W$; $W = U + V$
The conceptual water balance model	Ponce et Shetty, 1995a	$S = \frac{(P-\lambda_s W_p)^2}{P+(1-2\lambda_s)W_p}$; $U = \frac{(W-\lambda_u V_p)^2}{W+(1-2\lambda_u)V_p}$;
The nondimensional water balance model	Sivapalan, 2011	$S^* = \frac{S}{P-\lambda_s W_p}$; $W^* = \frac{W-\lambda_s W_p}{P-\lambda_s W_p}$;

1.3.1 The heat and water balance model of Budyko (1974)

The water balance equation of Budyko (1974) illustrates the relationship between annual evapotranspiration and long-term water and energy balance at the catchment scale. Although its simplicity, this formula has been generally applied especially recently with the climatic and urban evolution mainly affecting water resources management schemes. Since Budyko's formula contains in it the transformation of liquid water into vapor, the evapotranspiration then reflects not only a distribution of water but also the radiative energy of the atmosphere-soil interface (Sposito, 2017).

According to Budyko, the long-term annual transfer flow of the atmosphere-soil interface is subject to the same separation hypothesis of the water and energy balance applied to the total available water for exchange in the unsaturated zone. Hence the following expression of the long-term average flow of water and energy balance at the catchment scale:

$$P = E + Q \qquad 3$$

Where P = Precipitation

E = Evapotranspiration

Q = Runoff

Equation (4) states that solar radiation falling over a catchment is also not stored in the vadose zone, leaving it either as heat carried off by the evapotranspiration (L.E) or as thermal radiation from the upper boundary of the vadose zone back into the atmosphere (H). Furthermore, because evapotranspiration and latent heat flux are equivalent processes, the division of Equation (4) by L leads to an energy-balance constraint on E analogous to the water-balance constraint expressed by equation (4):

$$\frac{R_n}{L} = E + \frac{H}{L} \qquad 4$$

Equation (4) suggests that the maximal Evapotranspiration E is attained when the total radiation energy is consumed by water evaporation from the land surface, this quantity being unlimited and the sensible heat flux H being negligible (Budyko, 1974). Maximal E is then equal to R_n/L, and called potential

evapotranspiration symbolised by E_p. Hence, Budyko's hypothesis on the existence of a functional relationship between the evapotranspiration E, the Precipitation P, and potential Evapotranspiration E_p:

$$E = f(P, E_p) \quad 5$$

And subject to limiting the conditions:

$$E \to E_p \; as \; P \uparrow \infty \quad 6$$

$$E \to P \; as \; E_p \uparrow \infty \quad 7$$

With Equation (6) describing the wet condition (energy limited) and Equation (7) the dry condition (water limited).

We then define the aridity index E_p/P symbolised by $\emptyset$ with $\emptyset$ <1 indicating wet climate and $\emptyset$ >1 indicating dry climate. Equation (8) becomes then:

$$\frac{E}{P} = F(\emptyset) \quad 8$$

And equations (9) and (10) become

$$\frac{E}{P} \downarrow \emptyset \; as \; \emptyset \downarrow 0 \quad 9$$

$$\frac{E}{P} \uparrow 1 \; as \; \emptyset \uparrow \infty \quad 10$$

Hence the shape of a Budyko curve which starts tangent to the first bisector and then turns concave towards the axis of the coordinates $\emptyset$ to approach asymptotically to the horizontal line representing E/P. These equations were verified by Budyko by applying them on a set of 1000 catchments.

To consider in Budyko's functional approach, the important role of evapotranspiration, which is directly related to solar irradiance and water availability. While the Mediterranean climate is characterised by a seasonal alternation of rain and temperature with 6 months delay of these variables; the maximum rainfall coincides with the minimum temperature.

These specific climatic characteristics play an important role in hydrological mechanisms with low evapotranspiration when water is available and high evapotranspiration when this availability is depleted. This makes the hydrological balance weakly influenced by evapotranspiration in the Mediterranean.

1.3.2 The water balance partitioning model of L'vovich (1979)

L'vovich empirical approach is based on a two-stage partitioning of annual precipitation into three components: quick flow here and after symbolised as (S), slow flow as (U), and vaporisation as (V), illustrated in Figure 1-8 below (L'vovich, 1979).

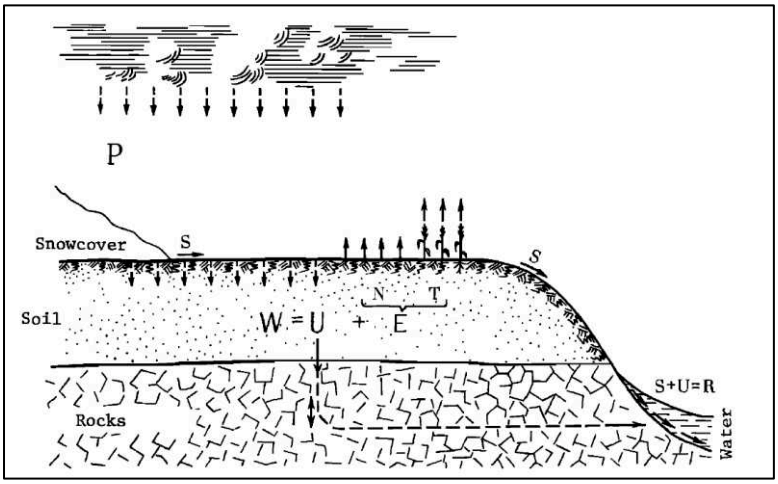

Figure 1-8: Diagram of the water balance of land area with P-Precipitation; R-total runoff; U-groundwater runoff; S-surface runoff; W-total wetting of the area (annual infiltration) including surface retention; N-unproductive evaporation (proper evaporation); T-transpiration of plants; E-Evapotranspiration; from (L'vovich, 1979).

At the first stage, precipitation P is partitioned into a quick flow component S and an infiltrated component called catchment wetting W. At the second stage, the resulting catchment wetting W is then further partitioned into a slow flow component U and an energy-dependent component E evapotranspiration.

This two-stage hydrological partitioning can be mathematically represented as follows:

$$P = S + U + E = S + W \quad (11)$$

$$W = U + E \quad (12)$$

The combined annual water balance, neglecting carryover of storage between consecutive years, can then be written as:

$$P = E + R \quad (13)$$

$$R = S + U \quad (14)$$

Where P = Precipitation.

S = Surface Runoff.

U = Underground Runoff, baseflow.

E = Evapotranspiration or Vaporisation, also symbolised as V.

R = Total Runoff, also symbolised as Q.

W = Wetting of the surface.

Equation 12 is henceforth the basis of the "proportional curve" of L'vovich, shown in Figure 1-9, where E=f(W) is located near the first bisector and then approaches the asymptote E_{max} each time the heat balance changes with E_{max} corresponding to potential evapotranspiration. Likewise, the wetting W tends towards a value W_p when the precipitation P and runoff S tend towards infinity. At the limit, the Evapotranspiration E would be equal to the wetting W, which means that the total amount of water reaching the ground has evaporated and nothing remains for groundwater runoff U. The curve U=f(W) would then be complementary to the evapotranspiration curve E=f(W) graphically and correspond to the difference between the curve E=f(W) and the first bisector.

L'vovich calculated the water balance elements for several catchments across four continents (Europe, Asia, Africa, Americas) and drew the proportional curves for each catchment; he then observed the correlation between E and U of the water balance and deduced that for each climatic and/or geographical region corresponded a pair of specific proportional curves, since they are governed by prevailing regional climatic and landscapes patterns; a simple global scale classification and regionalisation system based on a functional approach. Thus, he also defined the coefficient for each element, the baseflow or groundwater K_U = U/W, evaporation K_E = E/W, runoff coefficients K_R = R/P and wetting coefficient K_W = W/P useful for the characterisation and analysis of water balances.

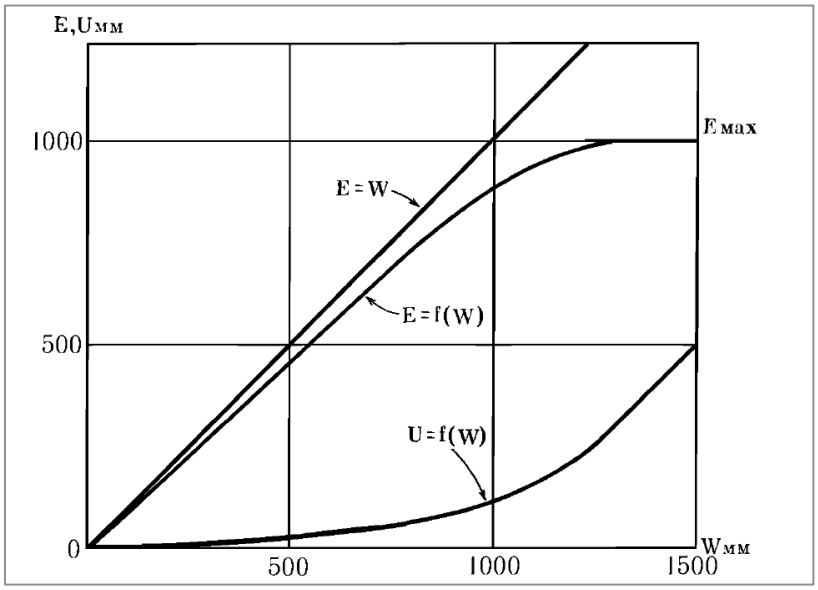

Figure 1-9: Diagram of proportional water balance curves from (L'vovich, 1979); with W = total wetting, E = Evapotranspiration, U=Underground runoff, E_{max} = Potential Evapotranspiration).

1.3.3 The conceptual water balance model of Ponce et Shetty (1995a)

Ponce and Shetty have developed a simple conceptual model from the water balance equations to separate precipitation into different flows (Ponce & Shetty, 1995a, 1995b). This model has been proposed as an alternative to empirical models, which have a limited applicability and to simulation models that require extensive simulations, for the calculation of river flows.

All the water balance equation has the same structure where, X is equal to the sum of two terms Y and Z. Ponce & Shetty, indicated a similarity to the SCS Curve number model and a similarity to its solution. Thus, the initial abstraction $I_a = \lambda Z_p$ with λ the initial abstraction coefficient, ranging between 0 and 1, and Zp the potential value or upper limit. Hence, the following solutions to L'vovich model suggested by Ponce & Shetty:

First stage partitioning, $P = S + W$

$$P < \lambda_s W_p,\ S = 0, W = P \qquad 15a$$

$$P > \lambda_s W_p,\ S = \frac{(P-\lambda_s W_p)^2}{P+(1-2\lambda_s)W_p} \qquad 15b$$

$$W = P - \frac{(P-\lambda_s W_p)^2}{P+(1-2\lambda_s)W_p}$$

$$P \to \infty, S \to P - W_p,\ W \to W_p \qquad 15c$$

Second stage partitioning, $W = U + V$

$$W < \lambda_u V_p, U = 0, V = W \qquad 16a$$

$$W > \lambda_u V_p, U = \frac{(W-\lambda_u V_p)^2}{W+(1-2\lambda_u)V_p} \qquad 16b$$

$$V = W - \frac{(W-\lambda_u V_p)^2}{W+(1-2\lambda_u)V_p}$$

$$W \to \infty, U \to W - V_p, V \to V_p \qquad 16c$$

Ponce et Shetty has calibrated the initial abstraction coefficients surface runoff λ_s, baseflow λ_u, wetting potential W_p, and vaporisation potential V_p through the application of their equations on L'vovich database and tented to classify the climatic regions according to the range of values they obtained; The results of the calibration are shown in Table 1-2.

Table 1-2: Calibration des coefficients λ_s, λ_u, W_p et V_p (Ponce & Shetty, 1995a, 1995b).

Region	Description	λ_s	W_p	λ_u	V_p
Africa	Mountain conifer forests	0.02	2164	0.35	903
	Evergreen sclerophyll forests and scrub	0.23	1517	0.37	1405
Canada	Arctic-subarctic (wooden tundra)	0.00	889	0.19	2047
	Subarctic forests (taiga)	0.00	1578	0.10	796
South America	Mountain meadows, steppes, and savannas	0.06	1789	0.25	977
	Wet evergreen forests in the mountains	0.31	1326	0.10	1856
	Steppes and savannas in the plains	0.22	2627	0.48	1721

Runoff gain K'_r is defined as the derivative of the runoff coefficient K_r and the baseflow gain K'_u as the derivative of the baseflow coefficients K_u (Ponce & Shetty, 1995a, 1995b). The analysis of the runoff and baseflow gain charts for each of the considered cases led to the following conclusions:

- Runoff gains are always positive, reaching a peak K'_{rp} at a runoff threshold precipitation P_{rt}.
- Baseflow gains are always positive, reaching a peak K'_{up} at a baseflow threshold precipitation P_{ut}.
- An increase/decrease in runoff or baseflow gain corresponds to a decrease/ increase in vaporisation gain, i.e. an increase/decrease in vaporisation loss.

Ponce & Shetty were able to characterise the climatic region from baseflow and runoff threshold precipitation, P_{ut} and P_{rt} and their ratio to the average precipitation P_a see Table 1-3. The analysis of these findings led to the discussion of the competition between runoff and vaporisation on one side and baseflow and vaporisation on the other side. This competition between different water balance elements is reigned by the magnitude of the average annual precipitation to the runoff threshold precipitation P_{rt}:

- If $P< P_{rt}$: increases in annual precipitation lead to increases in runoff gain and proportionally larger increases in runoff.
- If $P> P_{rt}$: increases in annual precipitation lead to decreases in runoff gain and proportionally smaller increases in runoff.
- For semiarid regions $P_{rt}/P_a \approx 1$.

They concluded that runoff is a strong competitor over vaporisation in semi-arid regions when annual precipitation is below average. This means that in a semi-arid region, a raindrop is more likely to flow if it is on the dry side of the annual precipitation spectrum ($P <P_a$). Conversely, a raindrop is more likely to vaporize if it is on the wet side of the annual precipitation spectrum ($P>P_a$). Similarly, the competition between baseflow and vaporisation is like the one between runoff and vaporisation.

Table 1-3: Summary of threshold precipitation and ratio to annual precipitation P_a according to climatic regions from (Ponce & Shetty, 1995a, 1995b).

Case	Description	P_a	P_{rt}	P_{rt}/P_a	K'_{rp}	P_{ut}	P_{ut}/P_a	K'_{up}
1	Semiarid Africa: Evergreen sclerophyll forests and scrub	750	725	0.97	0.000560	825	1.1	0.000186
2	Subhumid Africa: Mountain conifer forests	750	525	0.7	0.000634	575	0.77	0.000412
3	Subarctic North America (Canada): Subarctic forests (taiga)	800	175	0.22	0.001123	175	0.22	0.000705
4	Humid South America: Wet evergreen forests in the mountains	2000	575	0.29	0.000623	375	0.19	0.000409
5	Seasonally humid Asia (India): Semideciduous forests in the mountains (Western Ghats)	3000	900	0.3	0.000390	850	0.28	0.000239

1.3.4 The nondimensional water balance functional model of Sivapalan et al. (2011)

Sivapalan presented a detailed analysis of the regional and interannual variability from the annual water balance of 431 catchments of the MOPEX database in the United States by studying the of the two-stage water balance partitioning according to the model of L'vovich (1974) and the equations of Ponce and Shetty (1995a) fitting and the analysis of the spatial and temporal similarity from the obtained parameters (Sivapalan et al., 2011). Figure 1-10 illustrates the distribution of the different parameters of the 431 catchments in the United States, indicating a clear inter-catchment variability. He then searched for a non-dimensional form of Ponce and Shetty equations aiming to simplifying it.

In the case of precipitation P exceeding the threshold $\lambda_s W_p$, the precipitation excess could be partitioned between runoff and wetting excess, hence:

$$(P - \lambda_s W_p) = S + (W - \lambda_s W_p) \qquad 17$$

In the same way, if the wetting exceeds the threshold $\lambda_u V_p$, the wetting excess could be partitioned between baseflow and vaporisation excess, hence:

$$(W - \lambda_u V_p) = S + (W - \lambda_u V_p) \qquad 18$$

When replacing these relations in the equations of Ponce and Shetty 15b and 16b, Sivapalan reformulated Ponce and Shetty equation in the following non dimensional form:

$$S^* = \frac{S}{P - \lambda_s W_p}; W^* = \frac{W - \lambda_s W_p}{P - \lambda_s W_p} \qquad 19$$

$$U^* = \frac{U}{W - \lambda_u V_p}; V^* = \frac{V - \lambda_u V_p}{W - \lambda_u V_p} \qquad 20$$

And defined the following driving variables:

$$\tilde{P} = \frac{P-\lambda_s W_p}{(1-\lambda_s)W_p}; \tilde{V} = \frac{V_p-\lambda_u V_p}{(1-\lambda_s)W_p}; \widetilde{W} = \frac{W-\lambda_u V_p}{(1-\lambda_u)V_p} \quad 21$$

$\widetilde{P}$ is a rescaled annual precipitation, $\widetilde{W}$ a rescaled annual soil wetting and $\widetilde{V}$ a rescaled vaporisation limit equivalent to the potential evapotranspiration E_p. hence the new non dimensional and non-parametric equations

$$S^* = \frac{\tilde{P}}{1+\tilde{P}}; W^* = \frac{1}{1+\tilde{P}} \quad 22$$

$$U^* = \frac{\widetilde{W}}{1+\widetilde{W}}; V^* = \frac{1}{1+\widetilde{W}} \quad 23$$

Taken together these equations verify that:

$$S^* + W^* = 1; U^* + V^* = 1 \quad 24$$

Sivapalan reformulated the non-dimensional water balance metrics equations (25) Horton index K_H, runoff fraction K_R, baseflow fraction K_B and vaporisation fraction K_V; using the driving variables $\widetilde{P}$ et $\widetilde{V}$ to obtain new simplified equations (26). Therefore, the water balance would then be governed by the aridity index $\varphi = \frac{\widetilde{V}}{\tilde{P}}$ and the rescaled precipitation $\tilde{P}$ (Figure 1-11).

The non-dimensional equations of the water balance metrics:

$$K_H = \frac{V-\lambda_u V_p}{W-\lambda_u V_p}; K_B = \frac{U}{P-\lambda_u V_p}; \quad 25$$

$$K_V = \frac{V-\lambda_u V_p}{W-\lambda_u V_p}; K_R = \frac{S+U}{P-\lambda_u V_p};$$

The water balance metrics equations reformulated using the driving variables $\widetilde{P}$ et $\widetilde{V}$:

$$K_H = \frac{(1+\tilde{P})\varphi}{1+\varphi+\tilde{P}\varphi}; K_B = \frac{1}{(1+\tilde{P})(1+\varphi+\tilde{P}\varphi)}; \quad 26$$

$$K_V = \frac{\varphi}{1+\varphi+\tilde{P}\varphi}; K_R = \frac{1+\tilde{P}\varphi}{1+\varphi+\tilde{P}\varphi};$$

Furthermore, in their work on the US MOPEX dataset, Harman et al. (2011) used the same framework as Ponce and Shetty (1995b) to quantify the sensitivity of the fast flow or quick flow (S) and slow flow (U) to interannual variations in precipitation (expressed as elasticity), and determine which of the functional parameters (λ_s, λ_u, W_p, V_p) plays the most important role in determining this sensitivity.

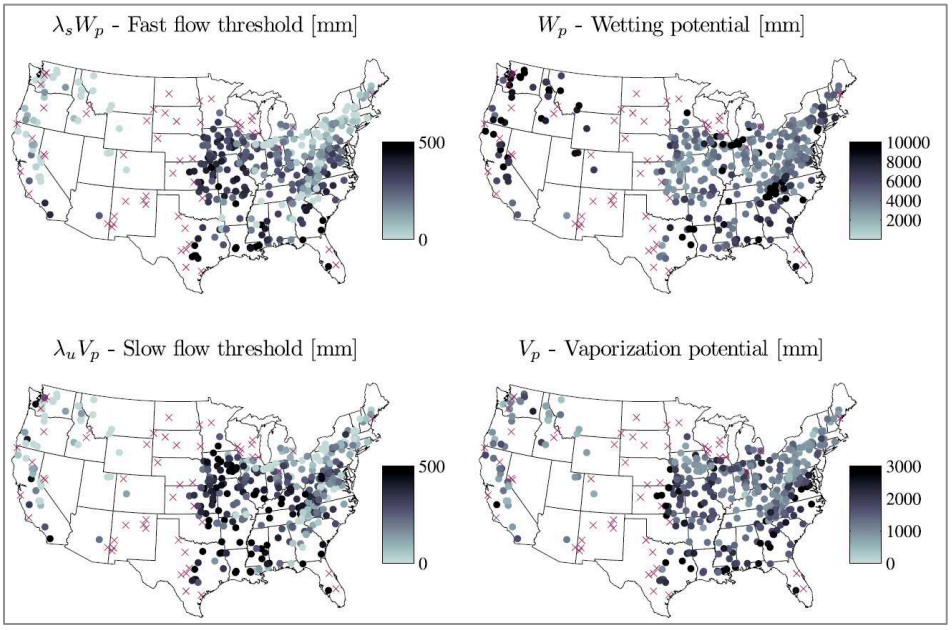

Figure 1-10: Threshold values $\lambda_s W_p$, and $\lambda_u V_p$ and potentials W_p and V_p of soil wetting W and vaporisation V from (Sivapalan et al., 2011).

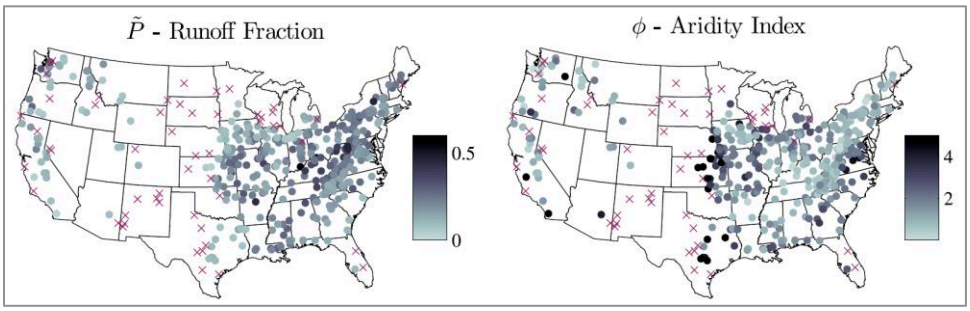

Figure 1-11: Spatial variations of mean annual values of the aridity index φ and mean annual rescaled precipitation $\tilde{P}$ from (Sivapalan et al., 2011).

They aimed to observe how patterns in the spatial and (long-term) climatic controls on catchment function determine the sensitivity of the streamflow components to (short-term) precipitation variations.

To bypass the wide variety of climatic and landscape factors that control water balance, which complicate the task of assessing regional patterns of sensitivity, two alternatives could be adopted. The first is a "time-for-time" by using data on the historical sensitivity to interannual variations in precipitation as a surrogate for the long-term effects as proposed by (Risbey & Entekhabi, 1996) and the second "space-for-time" approach by using data from different catchments to look for patterns in the relationship between long term average metrics of the climate and partitioning of rainfall into runoff as applied by (Budyko, 1974).

The "time-for-time" approach assumes that the changes in catchment response due to small climate shifts toward a wetter (or drier) climate are reasonably predicted by considering the behaviour of catchments in

the wetter (or drier) years it currently experiences. The “space-for-time” approach assumes that the trajectory of short-term (decades to century) responses of catchments to environmental change can be derived from the (dis)similarity between catchments that have been exposed to the projected climate and land cover conditions over long time periods (Risbey & Entekhabi, 1996).

Harman et al. (2011) suggested that patterns in the functional parameters would allow the application of both approaches where short term variations in climate are characterised by the interannual variability while the long term variations are described by the between-site patterns of the parameters. Hence, Harman derived an elasticity metric of sensitivity (ρ) within the framework of Ponce and Shetty model, based on the economic metric of “elasticity” and generically defined as the percent change in one variable given a unit percent change in another. They applied it to US MOPEX data set and tested its robustness using a Markov chain Monte Carlo algorithm to determine the uncertainty bounds on the sensitivity metrics, determine which of the functional parameters most strongly determine the sensitivity and examine the spatial and climatic variations in relation to the humidity index (P/Ep) and Horton index H =V/W. The analysis of the runoff gains and elasticity across the Mediterranean and through the climatic and physiographic classes will characterise the hydrological behaviour similarity and variability, and the competition between the water balance components of the Mediterranean catchments.

Considering the change in streamflow per change in precipitation, Harman et al., (2011) approximated the derivative of the total flow Q to P the annual precipitation:

$$\Delta Q = \Delta P \frac{\partial Q}{\partial P} \qquad 27$$

They expressed the similar expressions with *U* and *S* substituted for *Q* and wrote:

$$\frac{\Delta S}{S} = \rho_S \frac{\Delta P}{P} \qquad 28$$

$$\frac{\Delta U}{U} = \rho_U \frac{\Delta P}{P} \qquad 29$$

$$\frac{\Delta Q}{Q} = \rho_Q \frac{\Delta P}{P} \qquad 30$$

Hence defined the elasticity metrics that give the percent of change in the water balance component per percent of change in precipitation

$$\rho_S = \frac{\partial S}{\partial P} \Big/ \frac{S}{P} \qquad 31$$

$$\rho_U = \frac{\partial U}{\partial P} \Big/ \frac{U}{P} \qquad 32$$

$$\rho_Q = \frac{\partial Q}{\partial P} \Big/ \frac{Q}{P} \qquad 33$$

And since $Q = S + U$ and $\partial Q = \partial S + \partial U$:

$$\frac{\partial Q}{\partial P} = \frac{\partial S}{\partial P} + \frac{\partial U}{\partial P} \quad 34$$

Thus, they expressed the elasticity of the total discharge from its components S and U and their elasticities

$$\rho_Q = \frac{S}{S+U}\rho_S + \frac{U}{S+U}\rho_U \quad 35$$

They then substituted the Ponce and Shetty model in the definition and took the partial derivatives to express the elasticity with the water balance parameters around the mean precipitation $\overline{P}$

$$\bar{S} = \frac{(\bar{P}-\lambda_s W_p)^2}{W_p - 2\lambda_s W_p + \bar{P}} \quad 36$$

$$\bar{W} = \frac{\left(W_P \bar{P} - (\lambda_s W_p)^2\right)}{W_p - 2\lambda_s W_p + \bar{P}} \quad 37$$

$$\bar{U} = \frac{(\bar{W}-\lambda_u V_p)^2}{V_p - 2\lambda_u V_p + \bar{W}} \quad 38$$

Values of the required partial derivatives with respect to $\overline{P}$ are then given by the following equations which calculates the sensitivity parameter evaluated around the mean precipitation (Harman et al., 2011).

$$\left.\frac{\partial S}{\partial P}\right|_{\bar{P}} = \frac{2(\bar{P}-\lambda_s W_p)}{W_p - 2\lambda_s W_p + \bar{P}} - \frac{(\bar{P}-\lambda_s W_p)^2}{(W_p - 2\lambda_s W_p + \bar{P})^2} \quad 39$$

$$\left.\frac{\partial W}{\partial P}\right|_{\bar{P}} = \frac{W_p}{W_p - 2\lambda_s W_p + \bar{P}} - \frac{W_P \bar{P} - (\lambda_s W_p)^2}{(W_p - 2\lambda_s W_p + \bar{P})^2} \quad 40$$

$$\left.\frac{\partial U}{\partial P}\right|_{\bar{P}} = \frac{2\frac{\partial W}{\partial P}(\bar{W}-\lambda_u V_p)}{V_p - 2\lambda_u V_p + \bar{W}} - \frac{\frac{\partial W}{\partial P}(\bar{W}-\lambda_u V_p)^2}{(V_p - 2\lambda_u V_p + \bar{W})^2} \quad 41$$

1.3.5 Baseflow separation methods

Runoff is an essential component of the hydrological cycle. The precipitated water on a catchment will be divided into intercepted, evaporated, infiltrated, and drained water. The amount of water collected and drained by the river result from direct runoff on the watercourse and catchment surface, and from underground flows participation to its outlet. The proportion between these two types of flow is defined by the amount of water infiltrated into the soil. The various infiltration and flow processes involved in flood generation are shown schematically in Figure 1-12. The separation of the baseflow from the total runoff will serve the application of the different water balance models explained above.

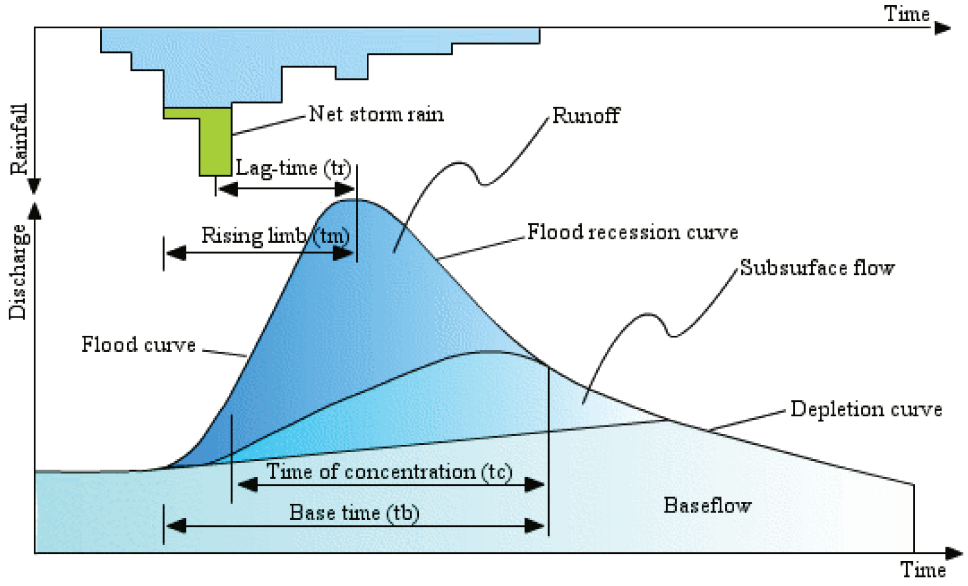

Figure 1-12: Hyetograph and hydrograph resulting from a storm event (rain - flow) (Musy, 2001).

1.3.5.1 Surface runoff

After interception by the vegetation, the available water is divided at the ground level, between the portion which infiltrates slowly through the soil layers and contributes to the groundwater recharge and baseflow, and the portion that contributes to the surface runoff as soon as the intensity of the rain exceeds the infiltration capacity of the soil; the soil infiltration capacity is also variable, depending on the initial soil moisture among other things. This surface flow forms the bulk of the quick flood flow and is called the Hortonian overland flow or infiltration capacity excess flow; and is considered relevant to explain the hydrological response of semi-arid catchments as well as under high rainfall intensity conditions. It is generally assumed that even natural soils with high hydraulic conductivity in temperate and humid climates may have an infiltration capacity lower than the maximum recorded rainfall intensities.

However, floods are frequently observed for intensities below the infiltration capacity of the soil, in this case, other processes such as saturated surface runoff could explain the generation of flows. Saturated surfaces might exist either by the contribution of the groundwater returned by exfiltration (from a shallow water table, for example), or through direct precipitation falling on these surfaces.

1.3.5.2 Baseflow separation

According to the International Glossary of Hydrology, (WMO, 2012), the baseflow is the discharge which enters a stream channel mainly from groundwater, but also from lakes and glaciers, during long periods when no precipitation or snowmelt occurs, therefore, most summer flows, in temperate regions, are comparable to baseflow. However, the baseflow still exists during rainy periods, for this there are several methods for the baseflow separation. Baseflow separation methods could be divided into two categories

manual and automated separation. The manual method consists in separating the components of the flow hydrograph manually according to the procedure proposed by (Barnes, 1939) and quoted by Gray in his Manual of Principles of Hydrology (Gray, 1970)

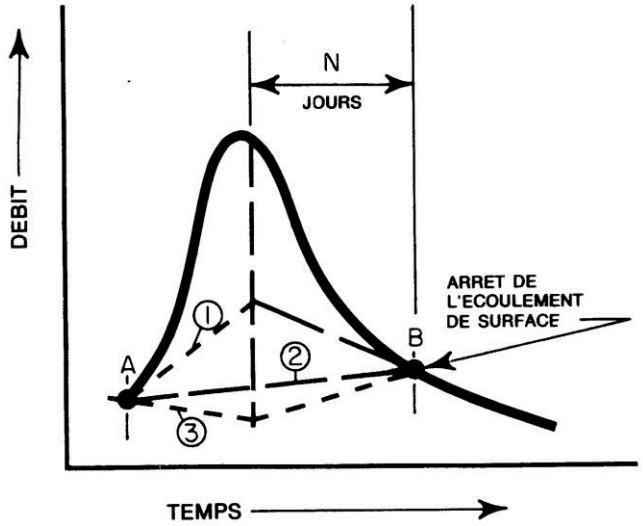

Figure 1-13 : Manual baseflow separation method as proposed by (Barnes, 1939) from (Gray, 1970).

1. Plot the hydrograph on semi logarithmic paper
2. Estimate the natural fall in groundwater levels by a line extended to the left under the hydrograph
3. Trace Residual Flow Values (Runoff and Hypodermic Flow)
4. Adjust a straight line to the dry curve (item 3) and extend it under the hydrograph
5. Trace residual runoff values for runoff

The first automated single-parameter separation method is Lyne & Hollick, (1979) and the second two-parameter method is BFImax (Eckhardt, 2005) which takes into consideration the river type and the soil type of its correspondent catchment. Since we are trying to classify the catchments from climatic and physical characteristics, it was preferable to use the method of Lyne and Hollick so that there is no pre-classification due to the separation of the baseflow if the BFImax was used.

1st Method: Lyne and Hollick, 1979

$$Q_{d_{(i)}} = \alpha Q_{d_{(i-1)}} + \beta(1+\alpha)(Q_{T_{(i)}} - Q_{T_{(i-1)}}) \qquad 42$$

With: Q_d = Direct runoff

Q_T = Total runoff (baseflow + direct runoff)

α = coefficient = 0.925

β = coefficient = 0.5

2nd Method: BFI max Eckhardt, 2005

$$B_{k+1} = \frac{(1-BFI_{max}).\alpha.B_k+(1-\alpha).BFI_{max}.Q_{k+1}}{1-\alpha.BFI_{max}} \quad 43$$

Where: α Baseflow coefficient = 0.98

BFImax River type coefficient (the long-term ratio of baseflow to total streamflow)

0,80 for perennial streams and porous aquifers.

0,50 for ephemeral streams, porous aquifers.

0,25 for Perennial streams, hard rock aquifers.

If $B_{k+1} > Q_{k+1}$ then $B_{k+1} = Q_{k+1}$ and $R_{k+1} = Q_{k+1} - B_{k+1}$

Below, an example of baseflow separation according to one filter Lyne & Hollick method, the hydrographs of observed and baseflows at Pescara, Italy for the hydrological years 2010 - 2011.

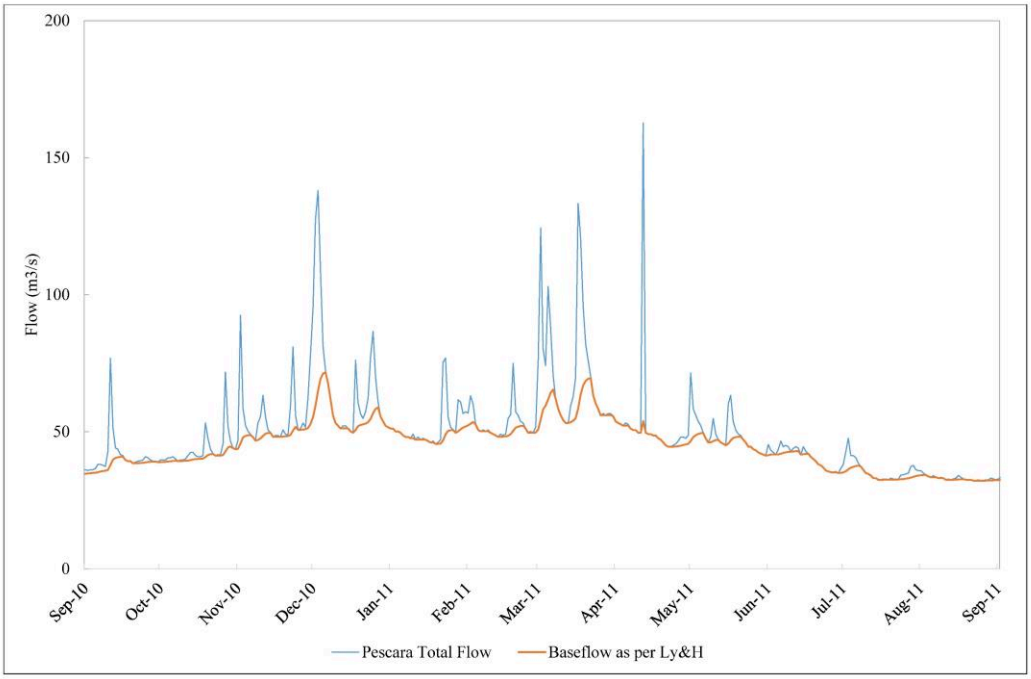

Figure 1-14 : Baseflow separation according to (Lyne & Hollick, 1979) method for Pescara, Italy 2010-2011.

1.3.6 Conclusion

This section has presented the development of the water balance functional models. All the models have shown a decisive relation to the evapotranspiration which varies with each catchment climate and landscape characteristics since the simple formulation of Budyko to the nondimensional formulation of Sivapalan applicable to multiple catchments capable of identifying hydrological patterns throughout a set of catchments.

1.4 HYDROLOGICAL CLASSIFICATION

1.4.1 Classification systems philosophy

Taxonomy aims to sort a population into several groups of similar characters. It was mainly developed by naturalists (Linnaeus, 1748). Thornthwaite pointed out that climate classification does not follow the same approach since one goes from one climate to another continuously, whereas the various species of fish, for example, are all different, in fact individualised (Thornthwaite, 1948). This continuity can be demonstrated using a fine intra-climate classification. To achieve any classification, it is essential to introduce measurable indices ensuring continuous variable scale. An index is a value that characterizes a set of data. In the case of timeseries, there are two types of indices, the time-independent (mean, variation coefficient) and the time dependent (autocorrelation coefficient). The purpose of automatic classification methods is to divide a set of objects into classes in a way that objects in the same class will be as homogeneous as possible while classes by themselves are as much heterogeneous as possible. Two of the main objectives of identifying the homogeneous regions is regionalisation and prediction on ungauged basins. The different approaches used are variously based on a combination of cluster analysis, multiple regression, principal component analysis, and the graphical representation of multi-dimensional data (Nathan & McMahon, 1990).

Cluster analysis consists of data points partitioning into isolated groups while minimizing the distance between same cluster data points and maximizing it between different clusters. There are 2 types of classification systems, partitioning methods (K-means) and hierarchical classification (multiple regression) K-means is one of the most popular clustering methods is the method introduced by Edward Forgy (Forgy, 1965) and MacQueen (MacQueen, 1967). It aims to minimize the square error objective function for distance optimization. The quality of the solution thus found strongly depends on the initial kernels. In its turn, kernel initialization is sensitive to the data dimensionality. The application of K-means requires setting a certain number of classes, otherwise the optimization leads to as many classes as individuals.

The optimization steps begin with:

1) Kernels initialization, the kernel being a virtual point representing the statistical centre of a class
2) Updating classes
3) Re-evaluation of kernels
4) Repetition of steps (2) and (3) until stabilization

This discrimination techniques are limited when addressing prediction on ungauged basins problem, where a new catchment will be allocated to one or other of the available groups, regardless of the range of similarity (Nathan & McMahon, 1990).

A classification system should provide an important organizing principle in itself, help with both modelling and experimental approaches to hydrology by providing guidance on the similarities and differences between catchments and provide, to first order, insights into the potential impacts of land use and climate changes on the catchment scale hydrological response in different parts of the world (Wagener et al., 2007). The hydrological similarity assessment should be based on clear metrics to judge the similarity or dissimilarity between catchments, as well as advantages and disadvantages of metrics and schemes for discrete classification (as in biology) or for continuous similarity variables (as in fluid mechanics). Thus, catchments classification shall take into consideration:

i. First order dominant physiographic characteristics avoiding the complexity of environmental factors impacting the catchment response.
ii. The uncertainty in the variables underlying the classification metrics.
iii. A uniformly available data distribution.

In addition, and always according to Wagener et al., (2007) a classification framework must respect four conditions:

1- Illustrate catchment form/hydro-climatic conditions on catchment function across spatial and temporal scales.
2- Catchment functions should include partition, storage, and release of water. With transmission within the catchment as a connecting process.
3- It needs to explicitly consider uncertainty in the metrics/variables used and mappings established.
4- It should initially be based on functions characterised by streamflow to be widely applicable, and graduate to other more complex functions subsequently.

Thus, our Mediterranean characterisation approach will be based on:

1- Representation of catchments climatic and physiographic characteristics by coverage ratio indices and normalised values and their classification.
2- A water balance partitioning functional model which represent the change with spatial and temporal scale

1.4.2 Climatic classification

1.4.2.1 Global climatic classification

Since antiquity, Greeks (Strabo, 63 B.C), have noted the climate evolution with latitude. Starting 19th century, under the impetus of biologists, several classifications have emerged. Automatic classification methods partition a set of objects knowing their distances by pairs in a way to keep the classes as much

homogeneous as possible while remaining distinct from each other. Like any classification, the adopted method depends on the objective and its specificity. There are several modes of climatic classification:

(a) Genetic classifications related to meteorological causes and the origin of air masses (Bergeron, 1928; Barry & Chorley, 2009).

(b) Bioclimatic classifications based on the interrelation between vegetation type and climate (Holdridge, 1947; Mather & Yoshioka, 1968; Harrison et al., 2010)

(c) Agro-climatic method based on the assessment of the Rainfall - Evapotranspiration balance for the estimation of agricultural productivity (Thornthwaite, 1948).

(d) Climatic methods based on precipitation and temperature indices similarly to the classification of Köppen in 1936 (Köppen, 1936) updated by Peel in 2007 (Peel et al., 2007) and which remains the most used.

Köppen's classification divided the globe into thirty climate zones and was based on a hierarchical approach. The Mediterranean climate corresponds to dry hot or dry warm summer where either the precipitation in the driest month in summer is below 40 mm or below the third of the precipitation in the wettest month in winter (Cs) and the air temperature of the warmest month is above 22 (Csa) or the number of months with air temperature above 10°C exceeds 4 (Csb) (see Figure 1-15).

The (Cs) climate does not reign all over the Mediterranean region, some exceptions could be observed. A Desertic climate (BWh) dominates Egypt and Libya, (Bsk) Southeast Spain and (Cf) the regions of Thessaloniki and Veneto. On the other hand, and at a global scale, (Cs) climate is present in California, Chile and South Africa, Figure 1-16.

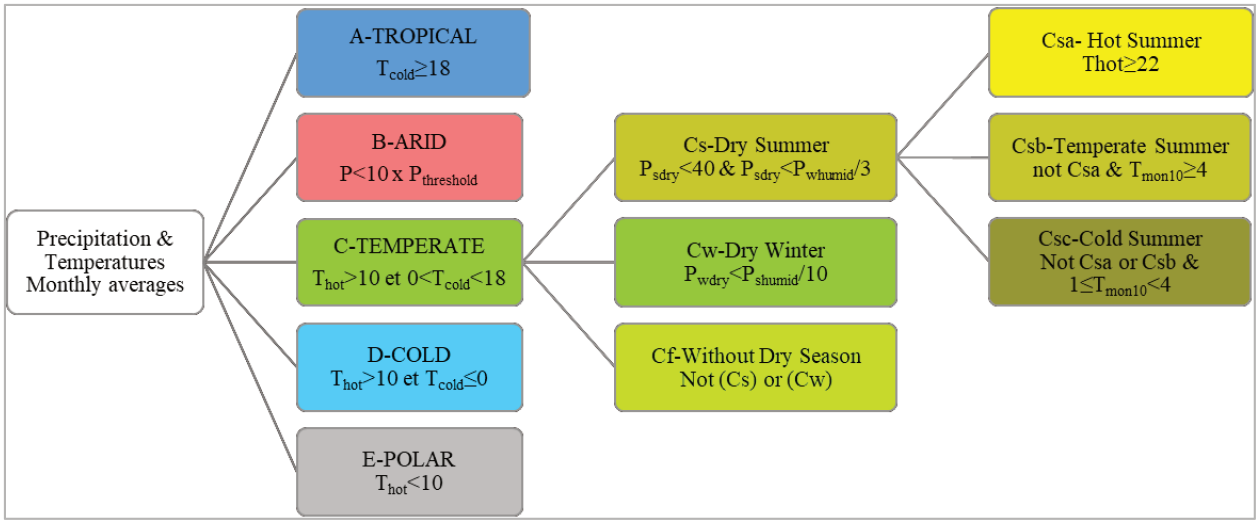

Figure 1-15: Organisation chart of the Köppen Classification System simplified for the Mediterranean Climate.

In climate classification, climatic indices based on monthly rainfall and temperature averages are interesting to observe. The seasonal nature of climatic variables means that these indices consist of a set of twelve ordered but cyclic values (following the 12th month, the 1st starts again) which follow the hydrological year. The hydrological year in the Mediterranean starts on September 1st.

Climatic indices highlight regional similarities and consequently highlight certain climatic classification. These indices describe different elements like precipitation, temperature, humidity, wind, etc.

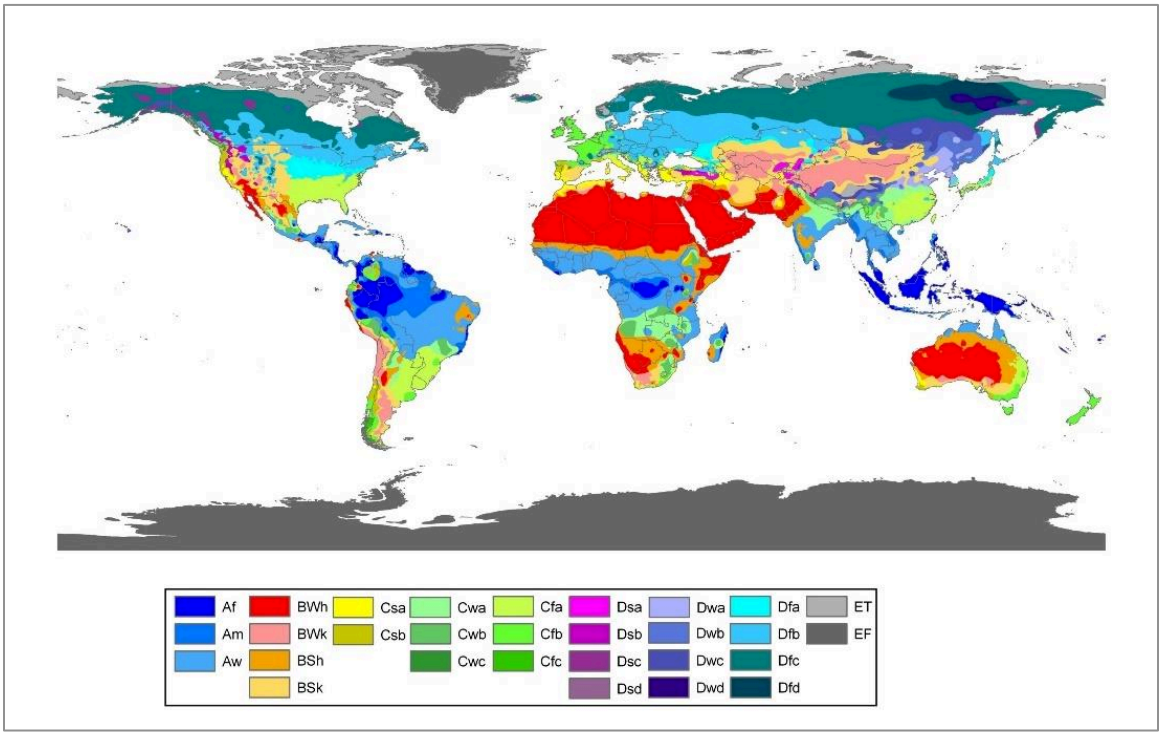

Figure 1-16: Global Köppen-Geiger climatic classification from (Peel et al., 2007).

1.4.3 Hydrological classification

The International Glossary of Hydrology defines the hydrological regime as the "Variations in the state and characteristics of a water body which are regularly repeated in time and space and which pass through seasonal or other phases" (WMO, 2012).

Despite the considerable effort the last two decades to classify the hydrological regimes of rivers at the global, regional, and national scales (Gentilli, 1952; Beckinsale, 1969; Haines et al., 1988; Oueslati et al., 2015), "Hydrology does not yet possess a generally agreed upon catchment classification system" (Wagener et al., 2007) and a "generic catchment classification framework has not been emphasised" (Sivakumar et al., 2015). The mentioned trials were limited to one of the characteristics or avoided covering the necessary

parameters for a relevant classification. However, several frameworks for hydrological classification have been introduced by Wagener (2007), Olden (2012) and Sivakumar (2015).

In the following section, some hydrological regimes classification systems at the global and regional scales are presented.

1.4.3.1 Global scale river regime classification examples

L'vovich developed a typology of the world streamflow regimes based on two criteria. The first corresponds to the types of water resources feeding the stream (rain, snow, glacier, or groundwater) according to their ratio of contribution (>80% almost exclusively; 50% to 80% predominantly; <50% leading source). The second corresponds to the seasonal distribution of the runoff with the same gradations as the first criteria, to describe the seasons that have prevalence as to the relative amount of runoff as compared to annual runoff. This typology is presented in Table 1-4 below and mapped for the Mediterranean in Figure 1-17.

L'vovich identified 6 types of stream flow regimes in the Mediterranean:

- Rx-Hy (23): Eastern Mediterranean coast from Turkey to Sinai, southern Greece, Italy, and Andalusian coast. Rain is exclusively the type of resource and it is predominant in winter.
- Rx-hy (24): Western Mediterranean, Morocco, and south western Spain. rain is the predominant type and mainly occurring in winter.
- rx-py (25): Southern European countries from Spain to Northern Turkey with rain and main resource and mainly occurring in spring.
- rx-hy (30): Central Italy, with rain as main resource, mainly occurring in winter
- sx-py (7): Typical of Alps, snow is the main source with flow peaks mainly occurring during spring due to snowmelt.
- sx-ey (9): Typical of Pyrenees mountains, snow is the main source with flow peaks mainly occurring during summer due to late snowmelt.

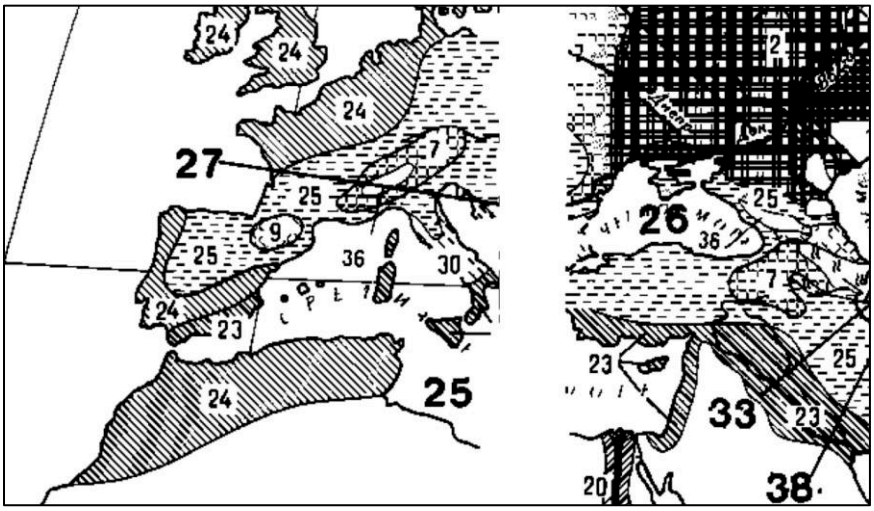

Figure 1-17: River regimes in the Mediterranean region, from (L'vovich, 1979).

Table 1-4: Typological chart of streamflow regime of the world's rivers,("+" streamflow found in ex USSR, "x" streamflow found elsewhere), with cases in red for the regimes found across the Mediterranean, from (L'vovich, 1979) figure 38.

Seasonal runoff distribution / Type of resources			Spring P			Summer E			Autumn A			Winter H		
			>80%	50-80%	<50%	>80%	50-80%	<50%	>80%	50-80%	<50%	>80%	50-80%	<50%
			P	Py	py	E	Ey	ey	A	Ay	ay	H	Hy	hy
Snow	>80%	S	+						NO DATA					
	50%-80%	Sx		+	+	+	+	+						
	<50%	sx			+(7)		+	+(9)						
Rain	>80%	R				x	x	x		x	x		x	x
	50%-80%	Rx			+		+	+		x	x	x	x(23)	x(24)
	<50%	rx			+(25)	+	x	x					x	x(30)
Glacier	>80%	G				+	x							
	50%-80%	Gx				x	+							
	<50%	gx				+	+	+						
Groundwater	>80%	U	NO DATA											
	50%-80%	Ux						x						
	<50%	ux			+			+						

In his turn, Haines (1988) developed a new global river regime classification, based only on monthly average flows and Köppen climatic classes without including physical characteristics; This classification showed several similarity to Gentilli's and Beckinsale's (Gentilli, 1952; Beckinsale, 1969). Haines gathered a global set of rivers runoff and produced a flow regime classification based on monthly average flows expressed as the ratio of the mean annual runoff. The clustering was carried out using the within-group average method with cosine similarity measure after removing streams with no significant seasonal fluctuations. A hierarchical decision tree with classification algorithms is shown in Figure 1-18; These

algorithms could be used to classify any river and the classification process could be stopped at any level of subdivision up to 15-group level for global mapping.

Group 13 – Extreme winter of Haines' classification, Figure 1-20 showed a clear relation to Köppen's Csa and Csb Mediterranean climatic classes and also referred to Gentilly's and Beckinsale's Mediterranean river *regimes; A preliminary global mapping of river regime types according to Haines (1988) is shown in Figure 1-19 is the first to be only based on flow characteristics. Nevertheless, Haines indicated that, in general, the relation of river* regimes to Köppen climatic classes was not too good and that the extrapolation of river regimes using climatic classification systems of the same type is unreliable.

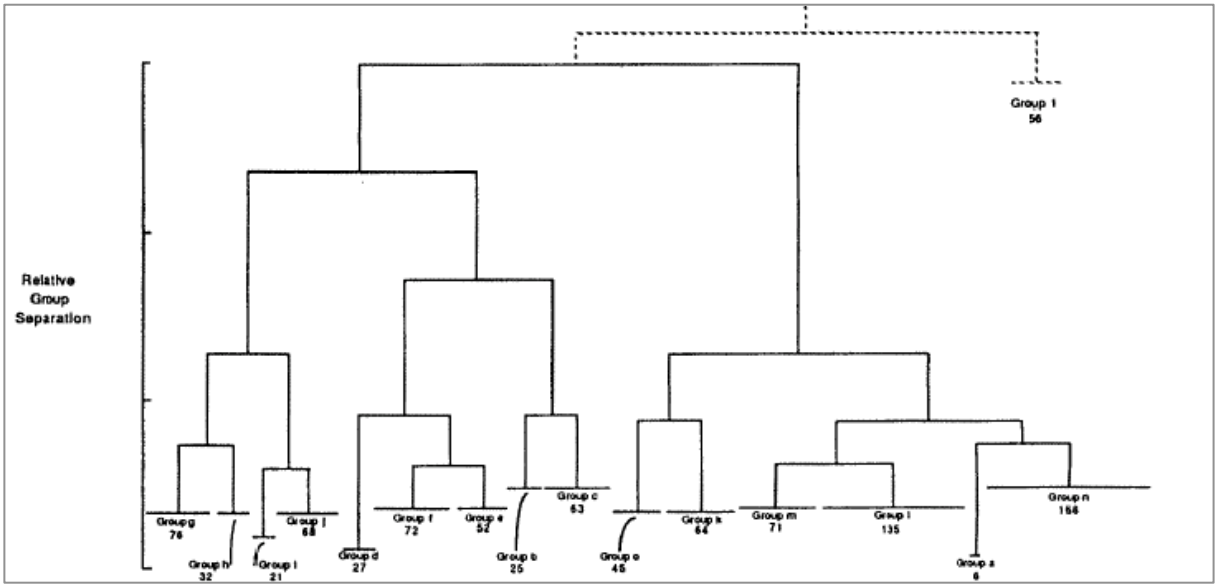

Figure 1-18: Hierarchical relations between the 15 groups defined by cluster analysis from (Haines et al., 1988)

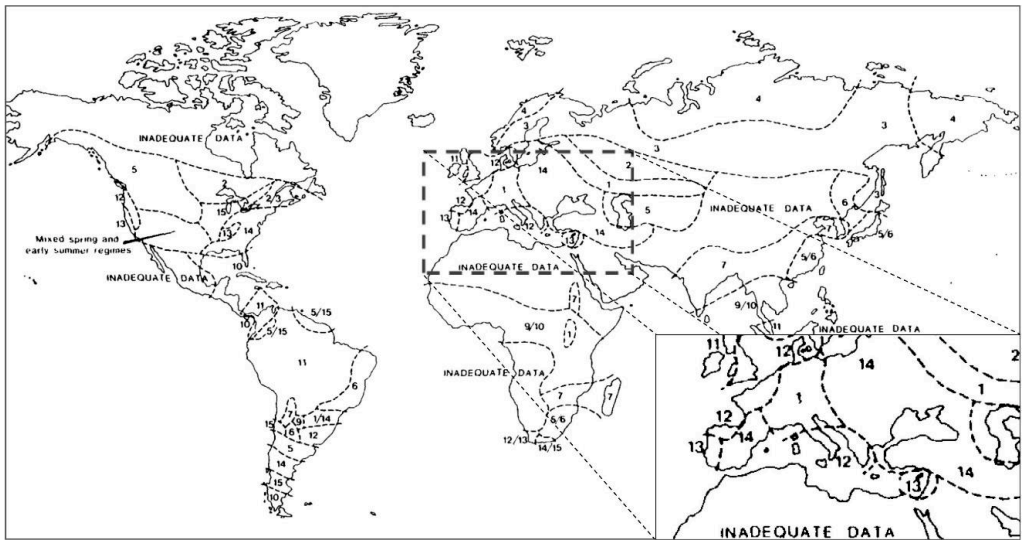

Figure 1-19: World map of the global regime classification based on runoff data from (Haines et al., 1988)

We will apply the classification of Haines in CHAPTER 5 to characterise and classify the regimes of 55 Mediterranean catchments.

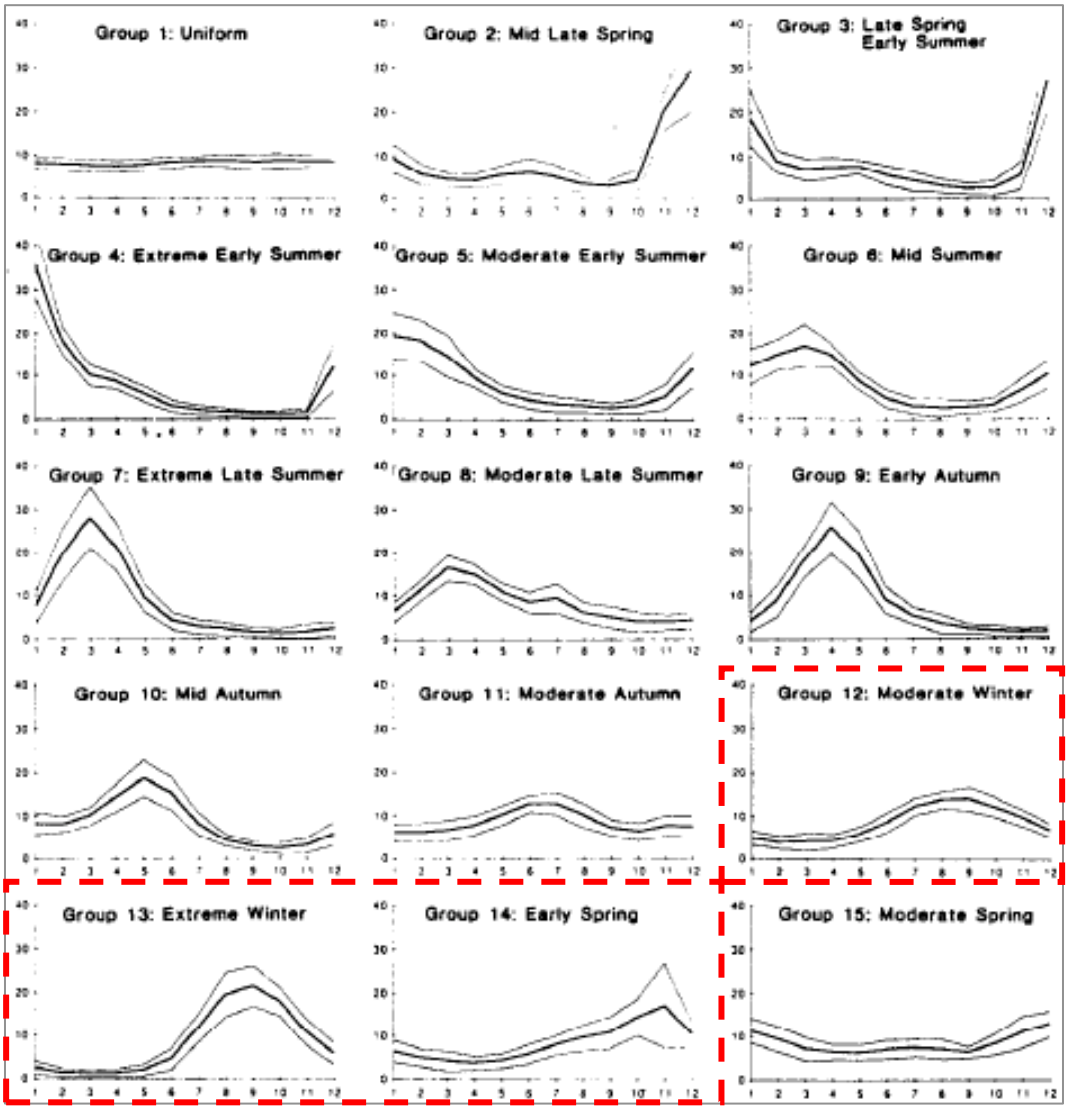

Figure 1-20: Average flow regime with bands of standard deviation with Mediterranean regimes highlighted in red from (Haines et al., 1988)

1.4.3.2 Mediterranean river regime classification example

River flow regime classification studies at the Mediterranean scale are rare due to the geopolitical diversity in the region with 23 countries spread over 3 continents in addition to language variety making the communication harder. However, a new elaborate work was recently carried out in a collaboration between an Italian, Moroccan and British research centres (Oueslati et al., 2015) funded by the Seventh Framework Program of the European Community FP7/2011.

This work tried to classify the flow regimes of Mediterranean rivers based on Richter's hydrological indices of a set of river from 8 different countries: 26 France, 13 Cyprus, 5 Italy, 4 Morocco, 5 Algeria, 4 Portugal, 2 Israel and 1 Tunisia; (Richter et al., 1996)

In a similar way to Haines work, classical statistical methods were applied like Principle Component Analysis (PCA) and agglomerative hierarchical clustering. PCA application reduced the hydrological indices to 3 main indices:

- Number of zero flow days.
- Flow predictability index.
- Flashiness index indicating frequency and speed of short-term changes in stream flow.

The agglomerative clustering based on the 3 hydrological indices resulted with a classification of 6 different flow regimes:

(1) Harsh intermittent flashy
(2) Harsh intermittent
(3) Intermittent flashy
(4) Intermittent
(5) Perennial
(6) Perennial flashy

A second clustering was carried out using stepwise multiple regression analysis and statistically significant relationships were derived by introducing topography, soil type, land cover and mean precipitation was carried out, for a small set of basins whose long term data existed, in the attempt to find a relationship with physical characteristics and transpose the classification to ungauged basins. The relationship found between hydrological indices and physical indices has been validated on five Italian catchments. Figure 1-21 illustrates the distribution of basins and classes of river regimes.

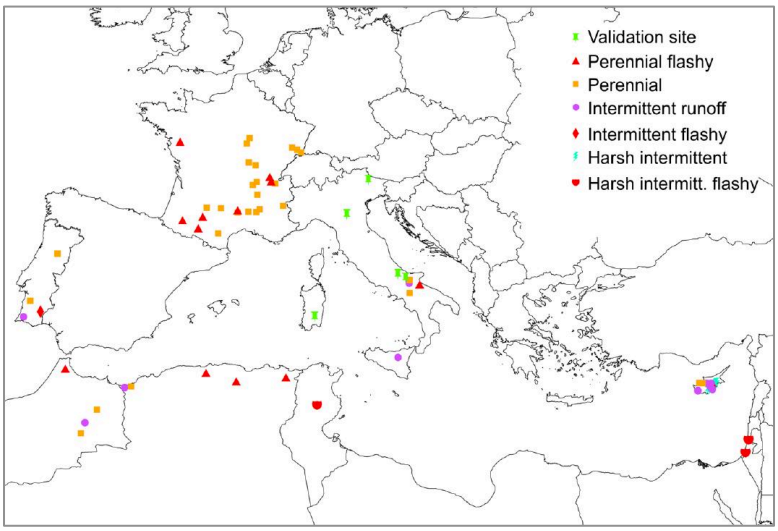

Figure 1-21: Location of the Mediterranean rivers with corresponding flow regimes from (Oueslati et al., 2015)

1.4.3.3 Catchments classification systems

Motivated by the lack of a generally accepted classification systems, (Wagener et al., 2007)) proposed a rule of thumb for catchment classification based on existing hydrological similarity approaches The perceptual model catchment function adopted in his study consists of the partitioning, the storage and the drainage of the water received by precipitation. These processes take place in a variable spatial and temporal frame governed by various climatic and physical conditions (Woods, 2005). A similar description to that given by L'Vovich for the catchment function.

Wagener et al. (2007) assumed that similarity assessments should then include the static and dynamic characteristics of the basin. Static characteristics (or physical or shape characteristics) are defined as landscape, morphology, pedology, land use, and dynamic characteristics such as surface runoff, groundwater runoff or soil moisture (Chapman, 1989).

They also assume, as a first approximation, that the hydro-climatic conditions could be considered as static characteristics if the region climate remains sufficiently invariable on the long term. He also considers that an understanding of the relation between structure, hydro climate, and response behaviour would advance hydrological understanding and predictive ability (McDonnell & Woods, 2004).

1.4.3.4 Catchments classification based on physiographic characteristics

Physiography used to be defined in 19th century as the study of regional-scale geomorphology which resulted in a confusion with the current definition. The definition evolved to become a contraction of "physical" and "geography", and therefore synonymous with physical geography. The U.S. Geological Survey defines physiography as a study of "Features and attributes of earth's land surface" which was adopted for this thesis, while geomorphology is defined separately as "Branch of geology dealing with surface land features and the processes that create and change them".

Flow indices and their relationship to catchments physiographic characteristics have been extensively addressed in various research studies and have even resulted in an overall classification of 15 regions of seasonal hydrology with Haines (Haines et al., 1988) by examining long-term monthly flows (Richter et al., 1996; Richter et al., 1997; Richter et al., 1998; Clausen & Biggs, 2000; Hannah et al., 2000; Yu & Yang, 2000; Morin et al., 2002; Atkinson et al., 2003; Olden & Poff, 2003; Shamir et al., 2005a; Shamir et al., 2005b; Yadav et al., 2006); assuming that if rivers can be subdivided a priori into groups that are hydrologically distinctive at landscape scales, the patterns that are defined can be expected to discriminate differences in ecological character (Resh et al., 1988; Poff et al., 1997).

Most physiographic classification were carried on separately for each physiographic feature, like topography, soil, landcover, but only few trials were carried on for an inclusive classification which

considers all three landform, landcover and edaphic factors such for Host ecosystems classifications who integrated climatic, physiographic, and edaphic databases and produced a classification of regional landscape ecosystems for north western Wisconsin. (Host et al., 1996),

River classification was first introduced by Davis who classified the streams into three groups based on relative age of adjustment, youthful, mature and old (Davis, 1899). Physiographic classification has been conducted to identify homogeneous regions sharing a specific hydrological aspect like floods, droughts and to yield an estimate of a regional dimensionless flood frequency relationship (Acreman & Sinclair, 1986). The classification was also used to resolve social issues and produce integrated assessments of the condition, health and sustainability of aquatic ecosystems based on ecological and socioeconomic information compiled at the scale of estuarine segments and small catchments (Wardrop et al., 2005).

The classifications based on physical characteristics as proposed by different hydrologists are the following:

- Dimensionless numbers:
    - Drainage density
    - Hydrographic network classification, stream order
    - Area, Slope, Perimeter
    - Bifurcation ratio
    - Hillslope Peclet number Pe
    - Concentration time
- Curves and distribution
    - Hypsometric curves (Langbein, 1947)
    - Topographic indices (Kirkby, 1975)
    - Digital Elevation Models (DEM)
- Conceptual models (Not to be confused with hydrological conceptual models)
    - Hydrological Landscape (Winter, 2001; Wolock et al., 2004)
    - Type of soil models in United Kingdom, HOST (Boorman et al., 1995) from which resulted the baseflow index BFI HOST
- Mathematical models
    - Bottom up, mechanistic, reductionist.
    - Top-down (Klemeš, 1986)

1.4.3.5 Catchments classification based on hydroclimatic regions

Wagener et al. (2007) highlighted the climatic impact on catchments hydrological behaviour citing the works of Köppen (1936), Budyko (1974) and L'vovich (1979) on the climatic classification based on long term climatic data. These works were detailed in the previous section. Other works also identified the role of climatic variables in the hydrological response, where a catchment location within a hydroclimatic region was found playing an important role in any classification system despite their limitation in identifying seasonal and inter-annual variations (Chapman, 1989).

We found out that indices combining soil characteristics and climate (including seasonality and intermittence) could explain the observed variability in the hydrological response by using a small number of dimensionless similarity parameters characterising climatic seasonality (Milly, 1994a). Consequently, Woods proposed three families of similarity indices to characterize average annual and average seasonal response of hydrological systems according to the based on the predominant water stock (i) snow or frozen water, (ii) pore water, or (iii) open water (Woods, 2006). Hence, the dimensionless number for pore water, used to estimate the annual or seasonal characteristics of throughfall and canopy evaporation, infiltration excess runoff and saturation excess runoff, root-zone water balance, and shallow water table position (Woods, 2003).

1.4.3.6 Catchments classification based on functional response

It is widely accepted that the main differentiating metric between catchments, from a hydrological point of view, must be the catchment's response behaviour and storage characteristics. Such behavioural characteristics or signatures should include streamflow, but could also extend to evaporation, groundwater dynamics, soil moisture dynamics, snow cover, distributions of residence time and water age, isotopic composition, concentrations of chemicals such as chloride and nitrate (Sivapalan, 2005).

But what would the relevant characteristics be at a specific time scale and what would be the physical and climatic characteristics that best reflect them? These different factors could vary, hence the interest of defining a classification according to their spatial and temporal extent.

McDonnell and Woods (2004) suggest two functional characteristics:

- The state in which water is predominantly stored: either frozen (snow and glaciers), or pore water (in soils and rocks), or open water (lakes, wetlands, river channels), and especially their magnitudes.
- The response time in the dominant catchment storage (volume of storage which has the largest flux, divided by the flux).

1.4.4 Hydrological similarities mapping

The aim of a classification is to understand the main climatic and physiographic factors controlling its hydrological function. Wagener assumes that a simple and meaningful classification system based on the physiographic and climatic characteristics and which explains the functioning of the catchment, will have a powerful tool of regionalisation. A necessary step to improve our understanding of hydrology knowing that at this point, a prediction of the hydrological response from the physical characteristics alone remains not feasible.

The classification systems mapping should carry out in a frame of uncertainty recommended by Beven (Beven, 2000). Uncertainty would be useful to identify which physiographic or climatic characteristics would be responsible for some hydrological behaviour (Yadav et al., 2007). Nevertheless, Wagener warns to limit the number of classes so not to induce an over classification with a large number of correlated and sensitive geographical regions.

Uncertainty should encourage the development of comprehension and measurement abilities. A refinement of perceptual models, an understanding of the catchment function in all its complexity and evolution and a representation of the function in terms of competition between different processes (distribution, storage and drainage according to L'vovich (1979) will have to progressively lead to a better understanding and possibly more targeted measures, which together will advance the cause of the classification.

1.5 CONCLUSION

The characterisation of a specific Mediterranean hydrology is still inconspicuous despite the last decades progress and efforts to carry on common research programs across the Mediterranean that focus on droughts, erosion, extreme events, flash floods and climate change. Thus, different aspects are still to be treated yet to characterise the Mediterranean climate, landscape, catchments water balance and their relation to hydrological specifications, with the progress of data collection and open access, remote sensing, and observational resolution.

To complete the characterisation of the Mediterranean climate, the role of seasonality and aridity in shaping hydrological regimes leading to an unequal distribution of water resources should be analysed closely and in detail over the whole region through a fine scale climatic classification in CHAPTER 3. A comprehensive description of the landscape for hydrological purposes shall also be carried out overall Mediterranean basin and at the catchment scale including landform, geology, karst, soil, landcover and other characteristics. This physiographic description, expressed by coverage ratios and indices values, shall be valorised through a classification that emphasize catchments variability and similarity in CHAPTER 4.

The hydrological characterisation of Mediterranean catchments shall be carried out on two phases, the first in CHAPTER 5 details the water balance components through the functional approach described previously and the second in CHAPTER 6 through multivariate analysis with physioclimatic indices. The water balance calculation and its component analysis should reflect the hydrological variability; but an analysis of a representative sample will lead to the detection of a general Mediterranean hydrological behaviour when cross analysed with climatic and physiographic classification. As for the multivariate analysis, it should detect the most contributing climatic and physiographic factors of the Mediterranean hydrology.

CHAPTER 2. MEDITERRANEAN DATABASE

Chapter summary

This chapter includes the hydrometric, climatic, and physiographic database collected for this study. It first describes the delimitation of the Mediterranean catchments and the criteria for the selection of the 55 catchments along with the compilation of their hydrometric data from different national and regional services and projects. Second, it describes climatic timeseries, historical grids and RCM projected gridded climatic data. Third, it describes the physiographic characteristics of the Mediterranean region derived from global data sets of topography, geology, landcover, lithology, soil, and karst.

Complementary material to Chapter 2 was added in Appendix A

APPENDIX A1 (Allam et al., 2020b)

Allam A., Moussa R., Najem W., Bocquillon C., 2020. "Chapter 1: Hydrological cycle, Mediterranean basins hydrology". In Water Resources in the Mediterranean Region, Editors Mehrez Zribi, Luca Brocca, Yves Tramblay and Francois Molle, Elsevier, pp. 1-21. https://doi.org/10.1016/B978-0-12-818086-0.00001-7

APPENDIX A2 Additional information on the Mediterranean research programs

APPENDIX A3 Hydrometric data quality check

2.1 INTRODUCTION

Several international research programs and networks tried to improve the knowledge on Mediterranean hydrology by establishing or enhancing hydrological information systems across the Mediterranean, mutual exchange of data, knowledge and techniques at a regional level hence covering topics like extreme events, erosion and solid transport, flow regimes and water resources, assessment of global changes, karstic hydrogeology and coastal ecohydrology, discussing water resources assessment and management challenges and organizing international conferences. A chronological description of Mediterranean programs was added in APPENDIX A2 and includes details about PLAN BLEU, MEDFRIEND, POEM, PRIMO, WMGE, EU/MAST/MTP I & II, MEDHYCOS, EMWIS and HyMEX. In addition, several international scientific conferences and related works have focused on Mediterranean hydrology to increase the scientific knowledge in face of water resources management challenges, like the International seminar between FRIEND-AMHY and HYDROMED on Hydrology of Mediterranean Regions (Montpellier, 11-13 October 2000), the IAHS conference on Hydrology of Mediterranean and Semi-Arid Region (Montpellier, 1 - 4 April 2003) and side session within EGU conferences.

Despite that all the programs tried to involve in a way or another every national hydrological service with one shared objective of collecting data, they failed until now to create a comprehensive hydrometric database, except for MEDHYCOS to certain extent. Thus, a huge work is yet to be done before obtaining a common Mediterranean hydrological database similar to the US MOPEX dataset (Schaake et al., 2006), that all researchers working in the water sector could easily use. However, a huge progress was noticed at the European scale in relation to landcover, geology, soil cartographic data which facilitated the extraction of common physiographic characteristics for all the study area. Main climatic parameters, Precipitation and Temperature, were also extracted from global networks of thousands of stations to create long term average values gridded data.

We do not claim that we have built the first and most extensive and complete Mediterranean hydrological database, however, the collected hydrometric data cover 15 different countries and are representative of the studied area. In addition, the methodology adapted in this study for hydrological characterisation deserve to be tested.

This chapter includes a detailed description of the study area starting with an overview of Mediterranean catchments, second the different climatic dataset used for climatic classification and climate change scenario in CHAPTER 3, third, the physiographic data used for physiographic classification in CHAPTER 4, fourth and finally the hydrometric data of the selected catchments for the hydrological characterisation in CHAPTER 5.

2.2 DATABASE DESCRIPTION

2.2.1 Mediterranean catchments

Since the geographic extent of the study is very wide, the delimitation of Mediterranean catchments was imported from international references. The European Commission and Joint Research Centre (JRC) has done extensive and elaborate work on the delimitation of catchments in Europe and some adjacent countries as part of the "Catchment Characterization and Modelling" (CMM) project (De Jager & Vogt, 2010). For catchments in the Middle East and Northern Africa, catchments from HydroSHEDS, the World Wildlife Fund's project, were used (Lehner & Grill, 2013). Catchments were extracted at their main stem outlet to Mediterranean coastline. According to these databases, the total number of catchments exceeding 1 km^2 and having a Mediterranean Sea mouth outlet is 3681 covering a total area of 1,781,645 km^2. It should be noted that the Nile was omitted for its extent 3500 km to the south of the Mediterranean. These catchments were divided into three types based on their areas.

- Type I, very small catchments below 100 km^2, usually showing little to no water resources hence the low management interest.
- Type II, between 100 km^2 and 3000 km^2, showing serious water resources potential but still undermanaged, focus of this study.
- Type III, above 3000 km^2, usually anthropized and managed wide catchments.

Catchments area distribution is shown in Table 2-1 where 1270 type II catchments constitute 35% of the total and cover 28% of the total area.

Table 2-1: Catchments distribution per area and ratio to total area

TYPE	Area range	Catchments	Ratio	Total Area	Ratio Area
I	A < 100km^2	2333	63%	80,157	4%
II	100 km^2 < A < 3000 km^2	1270	35%	498,614	28%
III	A > 3000 km^2	78	2%	1,202,874	68%

Catchments selection for the hydrological analysis was carried out geographically using Geographical Information System GIS. A huge number of hydrometric records was found across the Mediterranean; however, those records were mostly of short term and corresponded to sub catchments on highly managed wide catchments like Rhône, Po, Ebro etc.

A study of all Mediterranean catchments or sub catchments would be very interesting, however, the available hydroclimatic data forced us to reduce the number to 55 Type II catchments in order to deepen the analysis (see Table 2-14) Therefore, the following criteria were set for this study nevertheless respected with some exception:

- Mediterranean coastal catchments of an area ranging between 100 and 3000 km^2
- Hydrometric data at sea mouth
- Continuous long term daily timeseries of at least 10 concomitant years with climatic data
- Climatic stations within catchment boundaries or at vicinity
- Minimum influence of hydraulic structures on the flow regimes
- At least 1 catchment per country

Table 2-2: Catchments distribution per country ranked according to Area.

ID	Country	Number of Catchments	% Number	Total Area (km^2)	% Area
1	ITALY	798	20.9%	301015.7	16.9%
2	TURKEY	229	6.0%	223798.6	12.6%
3	GREECE	760	19.9%	211746.9	11.9%
4	LIBYA	416	10.9%	205333.5	11.5%
5	SPAIN	246	6.5%	187590.0	10.5%
6	FRANCE	174	4.6%	136389.2	7.7%
7	ALEGERIA	236	6.2%	122148.6	6.9%
8	EGYPT	193	5.1%	85575.9	4.8%
9	TUNIS	254	6.7%	83359.1	4.7%
10	MOROCCO	97	2.5%	66456.8	3.7%
11	JORDAN	1	0.0%	43237.2	2.4%
12	ALBANIA	37	1.0%	35967.1	2.0%
13	CROATIA	193	5.1%	18581.3	1.0%
14	BOSNIA AND HERZEGOVINA	2	0.1%	13249.0	0.7%
15	ISRAEL	25	0.7%	12616.4	0.7%
16	CYPRUS	52	1.4%	9059.2	0.5%
17	MONTENEGRO	26	0.7%	7421.6	0.4%
18	LEBANON	35	0.9%	7018.1	0.4%
19	SYRIA	24	0.6%	5472.2	0.3%
20	SLOVENIA	8	0.2%	5327.7	0.3%
21	MALTA	5	0.1%	310.6	0.0%

Table 2-3: Statistical summaries of the selected catchments.

	A (km^2)	P (km)	Z_{Max} (m)	Z_{Mean} (m)	S_A (%)	MAP (mm)	MET_p (mm)	Data Length (years)
Minimum	77.0	35.4	484	93	0.2%	230.3	556.0	11
Mean	891.7	306.3	1782	586	1.9%	845.4	833.2	36
Maximum	3125.0	1528.6	2980	1572	6.8%	3383.4	1000.0	84
50th	634.0	219.4	1632	506	1.4%	675.0	834.9	35

2.2.2 Climatic data

Four types of climatic data were used in this study, (1) WorldClim-2 new 1-km spatial resolution climate surface data (Fick & Hijmans, 2017), (2) Monthly average times series of 144 stations from NOAA database of 20 different Mediterranean countries covering a period of 30 to 120 years used for validation purpose (3) 232 In-situ stations falling inside or at the vicinity of the 55 selected catchments served for water balance calculations and (4) MED-CORDEX historical and projected data simulated under RCP 4.5 and 8.5 scenarios for future projections (Tramblay et al., 2013). It should be noted that we respected the conditions for the acquisition and use of these data, according to the recommendations for each database. In details,

(1) WorldClim-2 new 1-km spatial resolution climate surface data, which consists of long-term average monthly temperature and precipitation, solar radiation, vapor pressure and wind speed data, aggregated across a target temporal range of 1970–2000, using data from 9000 to 60000 weather stations (Fick & Hijmans, 2017). Worldclim-2 database is a refined and expanded version of the 2005 "WorldClim-1 database" (Hijmans et al., 2005). This database covers the whole study area, thus climatic classification of Mediterranean catchments was possible. The WorldClim-2 database was built over 23 regions with different coverage for each parameter. For the precipitation, an overlap of 3 regions covered the Mediterranean area with a total of 10410 stations for the 3 regions (Western Europe euw n= 3730; Eastern Europe eue n = 3632; North Africa n = 3048). For average temperature, the Mediterranean was covered by one region (eu1) with number of stations n = 1760; n = 1627 for Maximum temperature and n = 1626 for Minimum temperature; Refer to figures S1 and S2 in the supporting information of Fick and Hijmans (2017) article. Monthly precipitation and temperature were averaged for each catchment and then climatic indices were calculated at both catchment and grid scale. Both classifications were compared for validation. Climatic characteristics of Mediterranean catchment are summarised in Table 2-3 and illustrated in Figure 2-1, reflecting the wide variability of mean annual precipitation ranging between 5 ("Jabal el Aswad desert in Libya") and 3000 mm (Kobarid in Slovenia) and mean annual temperature ranging between -14°C (Mont Blanc, Alps, France) and +26°C (Karak, Jordan) where some catchments receive 50 times more than others the amount of precipitation while being 4 times colder.
(2) 144 ground weather station data covering the whole study area served to validate the Mediterranean climate classification with 105 stations located within catchments boundary and 39 outside. Also, 102 of these stations located within Köppen's (Csa) and (Csb) Mediterranean climate and 42 outside. These stations belong to Global Historical Climatology Network GHCN (Menne et al., 2012) and recognised by the World Meteorological Organization (WMO), they are available for free access on the portal of the National Administration of Oceans and Atmosphere of the United States (NOAA). The average

length of data series is 60 years and range between 30 and 120 years at monthly time step. The 1960 - 1990 period is common to all stations. The data quality was verified (i.e. ellipse of Bois (Bois, 1986)) and only complete hydrological years were retained for indices calculation.

(3) 232 In-situ stations falling inside or at the vicinity of the 55 selected catchments served for water balance calculations. These timeseries were collected from several references and meteorological agencies. The Italian ISPRA archive and Yugoslavian archive were consulted and precipitation daily and monthly data were digitised. Other national and regional agencies were consulted also like, the Hellenic Meteorological Service (HNMS) for Greece and the SIEREM for Tunisia, Algeria, and Morocco. The data was then completed using the World Meteorological Organization (WMO) network available on the US National Oceanic and Atmospheric Administration (NOAA) portal and the European Climate Assessment & Dataset (ECAD) database. Table 2-4 summarised the number of stations per agency.

Table 2-4: List of Meteorological agencies and services source of the selected catchments climatic data.

Agency	Country	Number of Stations
Catalan Agency for Water - ACA, Hydrological Automatic Information System - SAIH	Spain	30
Superior Institute for the Protection of Environmental Resources - ISPRA	Italy	86
Meteorological Service of the Democratic Federal Yugoslavia	Montenegro, Croatia	11
European Climate Assessment & Dataset - ECAD	Europe	10
Lebanese Meteorological Service - LMS	Lebanon	20
Hellenic National Meteorological Service - HNMS	Greece	5
National Oceanic and Atmospheric Administration – NOAA WMO Stations	International	61
Système d'Informations Environnementales sur les Ressources en Eau et leur Modélisation - SIEREM	Algeria, Morocco, Tunis	9
TOTAL		232

(4) MED-CORDEX simulations of the Regional Climate Models (RCM) ALADIN-Climate v5.2 at 12 km and CCLM at 50 km spatial resolution grid were used to analyse the climate change impacts on the climatic classification for the end of the century projection period 2070-2100, and for two different RCP 4.5 and 8.5 scenarios in comparison to the historical 1970-2000 baseline period (Rockel et al., 2008; Tramblay et al., 2013). The climate change study was limited to ALADIN and CCLM models since those were the only MED-CORDEX models to present the simulation results for RCP 4.5 and 8.5 for 2070-2100 period with the three required variables available (average temperature (tas), average precipitation (pr) and average radiation (rlds)).

Radiative Concentration Pathway (RCP) is a greenhouse gas (GHG) concentration trajectory adopted by the International Panel for Climate Change (IPCC) for its fifth Assessment Report (AR5) in 2014. RCP 4.5 and 8.5 were chosen between 4 available scenarios being the most focused on in literature. RCP 4.5 assumes

that global annual emissions measured in CO_2-equivalents peak around 2040, with emissions declining substantially thereafter while under RCP 8.5 emissions continue to rise throughout the 21st century. The RCP 4.5 (resp. RCP 8.5) means that the GHG and aerosols concentrations evolve in a way that leads to an additional radiative forcing equal to +4.5 W/m^2 (resp. + 8.5 W/m^2) at the end of the 21st century with respect to the pre-industrial climate. Consequently, the RCP 4.5 can be considered as an optimist scenario whereas RCP 8.5 is a more pessimist option (Giorgi et al., 2009; IPCC, 2013; Ruti et al., 2016).

While temperature increase and precipitation decrease have been already observed (IPCC, 2013), MED-CORDEX RCP 4.5 scenario projections, as simulated by ALADIN v5.2 for the 2071–2100 period (Tramblay et al., 2013; Dell'Aquila et al., 2018; Drobinski et al., 2018; Tramblay & Somot, 2018), estimates a spatially distributed temperature increase of 1.4 to 3.5°C and a precipitation evolution of ± 10% while RCP 4.5 projects an increase of 2.2 to 6.4°C and a precipitation evolution of ± 20% compared with the baseline period 1970-2000 with expected shifts of Mediterranean climate and expansion of arid regions (Beck et al., 2018; Barredo et al., 2019), related water restrictions and legal processes (Sauquet et al., 2018).

The use of ground-based stations time series or gridded observational data is limited by several uncertainties mainly density and interpolation processing methods, especially in Mediterranean region where North African and Levantine countries are poorly covered (Raymond et al., 2016; Zittis, 2018). Nevertheless, the use of specific indices like seasonality and aridity, which are averaged on 30 years periods and based on monthly and annual values, while avoiding extreme event indices, reduces data quality uncertainties. On the other hand, several studies have revealed the uncertainties connected to the resolution of RCM simulated gridded data in the Mediterranean complex domain (Romera et al., 2015) hence the use high-resolution data like MED-CORDEX 12 and 50 km grids and WorldClim-2 1-km and overall, the regional aspect of this study makes it less sensitive to local errors.

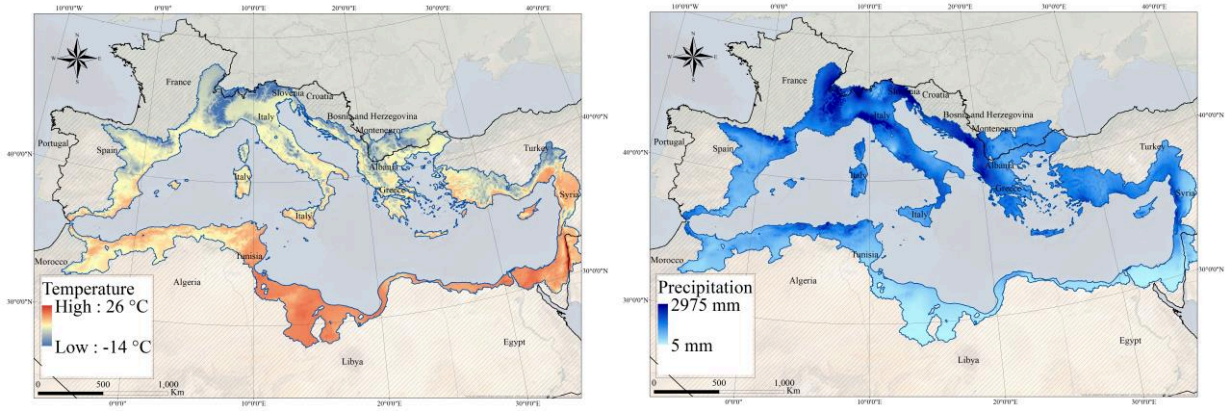

Figure 2-1: WorldClim-2 Temperature and Precipitation.

2.2.3 Physiographic data

The physiographic characteristics of the Mediterranean region were derived from global data sets for each catchment using Zonal Statistics and Tabulate Intersection from ESRI's ArcGIS software. These characteristics served first for catchments classification and then for the similarity analysis and the hydrological characterisation of Mediterranean catchments. These characteristics expressed by indices, describe catchment sizes, landforms, snow cover, geology, lithology, landcover, soil, and Karst. Some are described in the section below and a complete list is in Table 2-12. The location of catchments was omitted from PIs as climatic classification proved to have uniform spatial distribution and therefore catchment location might provoke a climatic overlapping effect over the physiographic classification.

2.2.3.1 Topography

Landform indices, Z_{Mean}, Z_{Min}, Z_{Max} and Z_{Med} indicating the mean, min, max and median catchments altitudes with a hypsometric index I_{Hypso} as a ratio of median and mean altitude indices were derived from the Digital Elevation Map of the Shuttle Radar Topography Mission (SRTM) (Jarvis et al., 2008) see Figure 2-2. Few catchments had below sea level mean altitudes mainly in Venice and some coastal areas in France usually submerged by sea water. About 50% of the Mediterranean catchments have a mean altitude below 200 m and cover 28% of the area, marking the wide plains in the region, while only 2% of the catchments have a mean altitude above 1000 m but cover 19 % of the area. The topographical map clearly showed that the Mediterranean Sea is surrounded by high mountains except for Egypt and Libya. These mountains were shaped mostly during the Oligocene and Miocene epochs when the African-Arabian continent collided with the Eurasian continent (Hsü et al., 1977). The collision pushed up a vast system of mountains, extending from the Pyrenees in Spain, Alps between France, Italy, and Switzerland to the Zagros Mountains in Iran.

Table 2-5: Mediterranean catchments Mean Altitude, see Figure 2-2.

Mean Altitude (m)	Number of Catchments	Percentage of Number of Catchments	Cumulated Percentage of Number of Catchments
<0	25	1%	100%
0-100	1139	31%	99%
100-200	733	20%	68%
200-300	548	15%	48%
300-400	387	11%	34%
400-500	286	8%	23%
500-600	199	5%	15%
600-700	120	3%	10%
700-800	81	2%	7%
800-900	68	2%	4%
900-1000	34	1%	3%
>1000	62	2%	2%

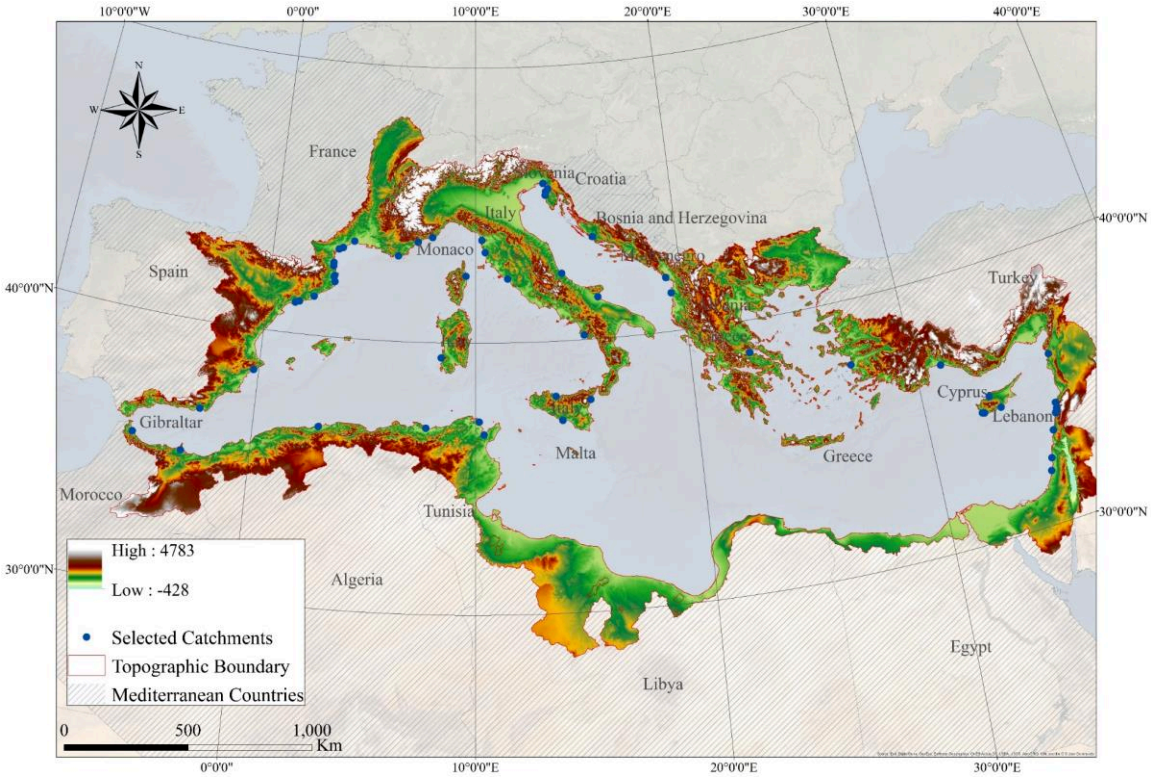

Figure 2-2: Mediterranean topography map using SRTM Data (Jarvis et al., 2008). See Table 2-5.

2.2.3.2 *Snow cover*

The snow index ZS_{Mean}, expresses the mean altitude of a catchment's snow cover which lasts at least 1 month per year. This index was estimated from the MODIS/Terra Snow Cover Daily L3 Global 0.05Deg CMG, Version 6 (Hall & Riggs, 2016). This data set was generated from Normalized Difference Snow Index (NDSI) snow cover in the MOD10A1 data set from 2000 to 2013. The MOD10A1 data set contains daily gridded snow cover and albedo observations at 500 m, mapped into 0.05° (approx. 5 km) CMG cells, derived from radiance data acquired by the Moderate Resolution Imaging Spectroradiometer (MODIS) on board the Terra satellite. Although ZS_{Mean} is a climatic index if considered at a timely step for its relation to temperature and precipitation, it could be considered as a physiographic index if the average value were calculated for a long period. The map in Figure 2-3 and corresponding Table 2-6 show that snow covers for at least 1 month per year 6% of the Mediterranean catchments and 12.2% of its area, mainly in Northern countries in addition to Mount Lebanon and Turkish mountains in the East and Moroccan Atlas Mountains in the South West.

Table 2-6: Mediterranean Snow Cover average altitude and area for catchments covered for at least 1 month per year. See Figure 2-3.

ZS_{Mean}	Number of Catchments	Snow Covered Area (km^2)	Covered Area ratio
-	3444	0	0.0%
300-600	2	50	0.0%
600-900	21	1675	0.1%
900-1200	61	33675	1.9%
1200-1500	88	83250	4.7%
1500-1800	44	93775	5.3%
1800-2100	17	3775	0.2%
2100-2400	3	450	0.0%
>2400	1	575	0.0%

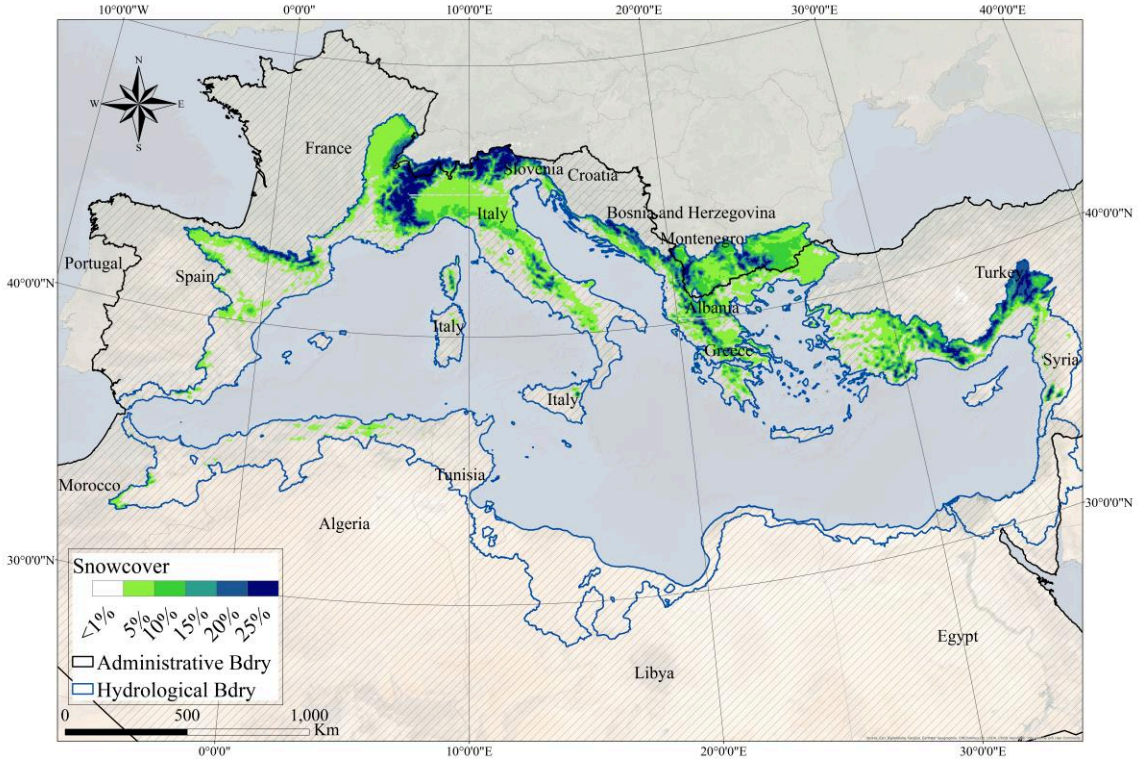

Figure 2-3: Mediterranean snow cover duration map (ratio of the year) from the MODIS/Terra Snow Cover Daily L3 (Hall & Riggs, 2016) see Table 2-6.

2.2.3.3 Geology

The Mediterranean geologic age layers were imported from the 1:5 Million International Geological Map of Europe and Adjacent Areas (IGME 5000) which shows the pre-quaternarian geology of Europe and adjacent countries onshore and offshore. Aside from the geology attributed by age, petrography and genesis, also magnetic anomalies, tectonic structures, continental edges, metamorphism, and crusts are shown. The map was developed under the leadership of BGR and the auspices of the World Map Commission (CGMW) in cooperation with Geological Surveys of 48 countries and more than 20 scientific institutes, (Asch & Bellenberg, 2005). Geologic age indices showed limited contribution to the classification therefore were omitted from the PCA and clustering to keep rigorous results given by landcover, karst and soil types. The layers covering more than 1% of the total Mediterranean area are shown in Table 2-7 and represented on the map in Figure 2-4

Table 2-7: Mediterranean geologic ages for layers covering more than 1% of the total area; with colour ID; see Figure 2-4.

Colour ID	Geologic Age Name	Age (MYears)	Area (km^2)	Percentage
	Miocene	23.8 - 5.32	198957	11.6%
	Late Cretaceous	98.9 - 65.5	197167	11.4%
	Pliocene	5.32 - 1.81	152630	8.9%
	Neogene	23.8 - 1.81	117227	6.8%
	Quaternary	1.81 - 0	101116	5.9%
	Early Cretaceous	142 - 98.9	70081	4.1%
	Eocene	55 - 33.7	67089	3.9%
	Pliocene - Quaternary	5.32 - 0	52118	3.0%
	Palaeocene	65.5 - 55	41537	2.4%
	Palaeozoic	545 - 250	41051	2.4%
	Jurassic	205.1 - 142	40593	2.4%
	Oligocene	33.7 - 23.8	38675	2.2%
	Eocene - Oligocene	55 - 23.8	36556	2.1%
	Late Jurassic	159.4 - 142	34740	2.0%
	Palaeocene - Eocene	65.5 - 33.7	29629	1.7%
	Cretaceous	142 - 65.5	26651	1.6%
	Triassic	250 - 205.1	26348	1.5%
	Jurassic - Cretaceous	205.1 - 65.5	24322	1.4%
	Oligocene - Miocene	33.7 - 5.32	23102	1.3%
	Middle Jurassic	180.1 - 159.4	20799	1.2%
	Permian	292 - 250	19974	1.2%
	Mesozoic	250 - 65.5	19096	1.1%
	Pliocene - Pleistocene	5.32 - 0.01	18431	1.1%

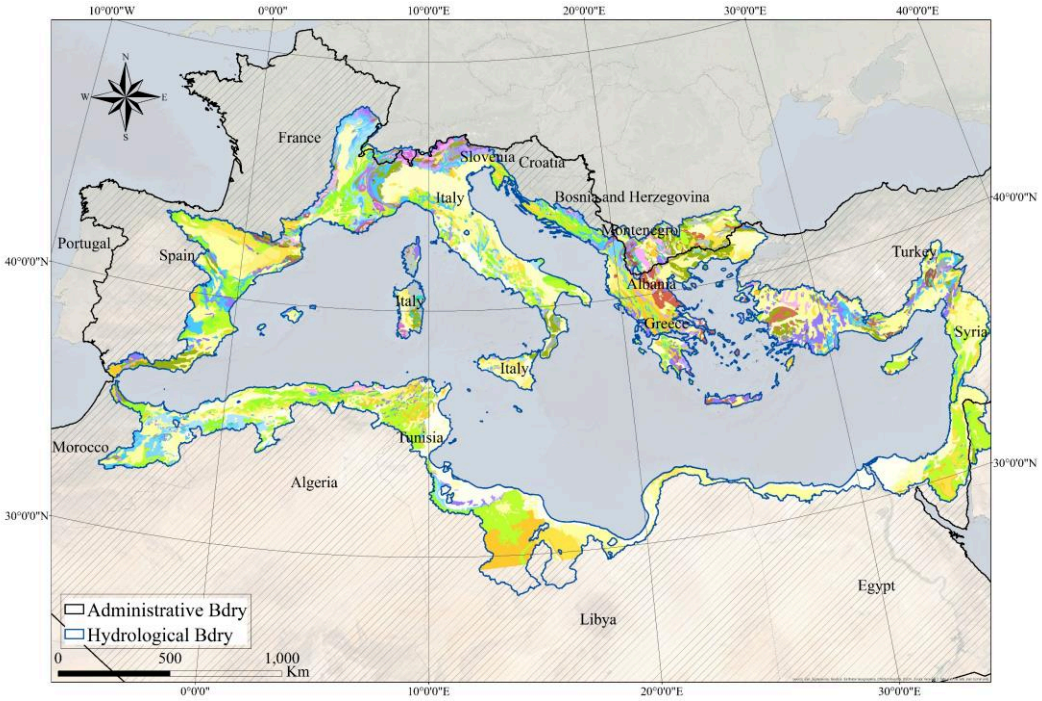

Figure 2-4: Mediterranean Geology Map from (Asch & Bellenberg, 2005); the map colour coding is the same as original and shown in the first column of Table 2-7.

2.2.3.4 Lithology

Lithology describes the physical properties of rocks which plays a key role in hydrological processes. Understanding these processes at the regional scale requires a high-resolution description of lithology. The lithologic structure of Mediterranean catchments was deduced from the new Global Lithological Map database GLiM (Hartmann & Moosdorf, 2012). GLiM was assembled from existing regional geological maps translated into lithological information with the help of regional literature. According to the GLiM, the Mediterranean is covered by 85% of sedimentary rocks mainly carbonate sedimentary rocks (33%) see Table 2-8 and Figure 2-5. The main lithologic composition, carbonated sedimentary rocks, showed high correlation with the percentage of karstifiable rocks per catchment, therefore lithologic indices where disregarded from the classification.

Table 2-8: Mediterranean lithology types with ratio to total area, colour coded as original; see Figure 2-5.

Colour ID	Lithology type	Code	Area (km^2)	Percentage area
	Carbonate sedimentary rocks	sc	576222	33%
	Mixed sedimentary rocks	sm	308533	18%
	Unconsolidated sediments	su	301987	17%
	Siliciclastic sedimentary rocks	ss	288115	17%
	Metamorphic rocks	mt	120331	7%
	Plutonic rocks	pa/pb/pi	64290	4%
	Volcanic rocks	va/vb/vi	53636	3%

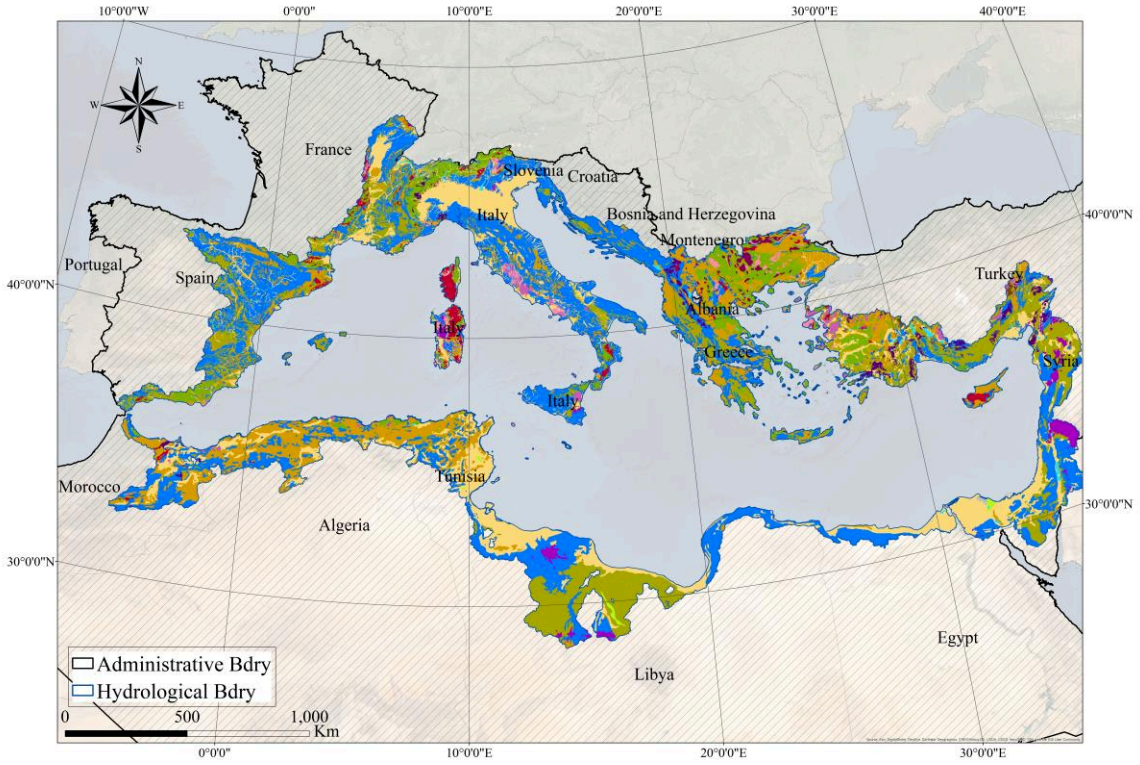

Figure 2-5: Mediterranean Lithology Map from (Hartmann & Moosdorf, 2012); colour coding as original see *Table 2-8.*

2.2.3.5 Landcover

Landcover was expressed according to Global Land Cover GLC 2000 major types (Bartholome et al., 2002). A newer and a higher resolution landcover map is available for the European countries from the Copernicus Landcover database Corine Land Cover (Buchhorn et al., 2017) however the GLC 2000 was adopted for having a coverage of south Mediterranean countries and a temporal coverage of the same era as the hydroclimatic data. The Mediterranean landcover map in Figure 2-6 and corresponding summary Table 2-9, show that in the top rank comes the Cultivated and Managed Areas that dominate the Mediterranean catchments with 31% of the total area, all type of shrub cover come in second rank with a total of 23%, all tree cover types in the third with 20% and Bare Areas 13% mainly in the southern countries. The landcover indices were calculated at the catchment scale according to each type coverage area ratio.

Table 2-9: Mediterranean Landcover major types according to GLC 2000; See Figure 2-6.

Colour ID	Global Landcover Type	Code	Area (km^2)	Percentage area
	Cultivated and managed areas	CMA	553874	31%
	Shrub Cover, closed-open, deciduous	SC_CO_D	278599	16%
	Bare areas	BA	235192	13%
	Sparse herbaceous or sparse shrub cover	SH OR SHC	216329	12%
	Tree Cover, broadleaved, deciduous, closed	TC_BD_C	166171	9%
	Tree Cover, needle-leaved, evergreen	TC_NL_E	127713	7%
	Tree Cover, mixed leaf type	TC_MLT	70192	4%
	Herbaceous Cover, closed-open	HC_CO	37566	2%
	Shrub Cover, closed-open, evergreen	SC_CO_E	27045	2%
	Mosaic: Cropland / Shrub and/or grass cover	MOSAIC	24229	1%
	Water Bodies	WA	17204	1%
	Artificial surfaces and associated areas	AS	13056	1%

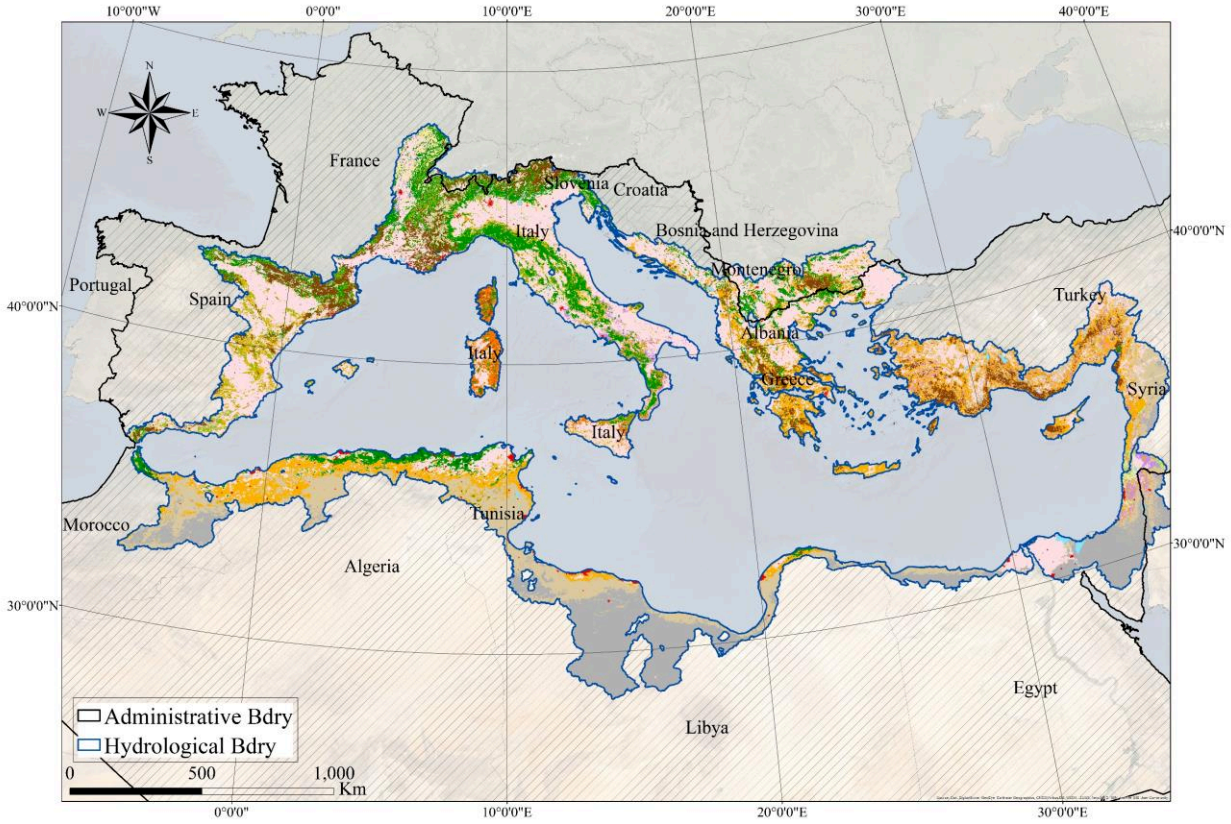

Figure 2-6: Mediterranean landcover Map from (Bartholome et al., 2002) colour coded as original see Table 2-9.

2.2.3.6 Soil

Hydropedology consists of combining the best of the field expertise of soil scientists with process knowledge of soil physicists and hydrologists. Widely used pedotransfer functions have been proposed to "translate" static soil properties needed for classification into dynamic properties to be used for simulating soil water regimes in soils and catchment areas (Bouma et al., 2011). Soil characteristics were obtained from two different database according to the adopted indices. First, Leptosols and Luvisols ratios per catchment were considered as soil indices for their widespread presence across the Mediterranean catchments and major contribution to the cultivation and landcover types. Leptosols represent mineral soils whose formation was conditioned by the topography/ physiography of the terrain and Luvisols was conditioned by sub-humid temperate regions climate hence their Mediterranean specificity. Leptosols and Luvisols were derived at catchment scale from the Harmonized World Soil Database (HWSD) (FAO & ISRIC, 2012) see Figure 2-7. Second, the Available Water Capacity (AWC), one of the main soil characteristics describing the hydrological dimension of all soil types, is the amount of water that can be stored in the soil and be available for vegetation. It has a considerable influence on hydrological processes in a river catchment affecting both the infiltration rate and the amount of surface run-off (Oueslati et al., 2015). Topsoil and subsoil available water capacity (T_AWC and S_AWC) were considered as indices and derived from the European Soil Data Centre (ESDAC) JRC project (Panagos et al., 2012; Hiederer, 2013).

Table 2-10: Mediterranean soil types table as per the Harmonized World Soil Database; See Figure 2-7.

ID	Soil Type	Code	Area (km^2)	Percentage area
	CaMbisols	CM	470896	26.4%
	CaLcisols	CL	396947	22.3%
	LePtosols	LP	353463	19.8%
	LuVisols	LV	182671	10.3%
	FLuvisols	FL	114409	6.4%
	ReGosols	RG	63978	3.6%
	VeRtisols	VR	48205	2.7%
	GYpsisols	GY	31462	1.8%
	Not Identified	NI	37615	2.1%
	Other	Other	82026	4.6%

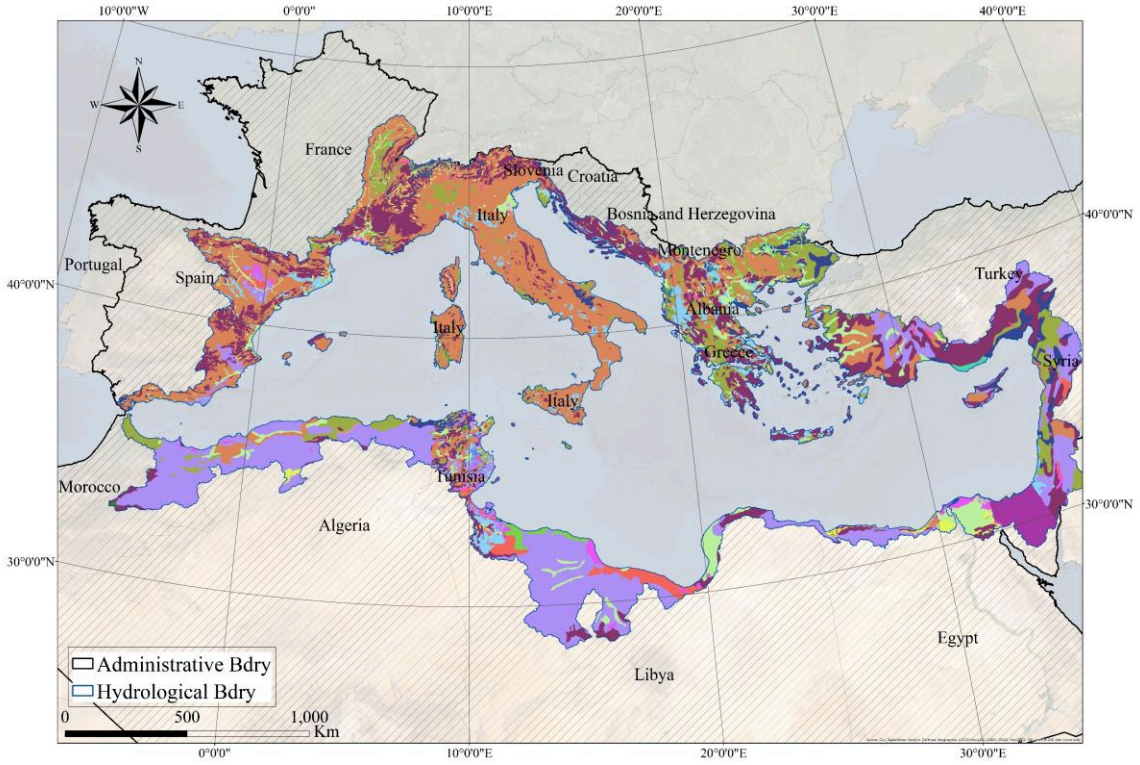

Figure 2-7: Mediterranean Soil Map from the HWSD (FAO & ISRIC, 2012), colour coded as original see Table 2-10.

2.2.3.7 Karst

Karst ratio index P_{Karst} was estimated as percentage of the catchment area covered by karstifiable rocks from the World Kart Aquifers Mapping project WOKAM. For further detailed mapping procedure, one can refer to the corresponding paper that presents "the basic concepts and illustrate the step-by-step workflow, which includes generalization, differentiation of continuous and discontinuous carbonate and evaporite rock areas, and the identification of non-exposed karst aquifers" (Chen et al., 2017). The Mediterranean karst map in Figure 2-8 and corresponding Table 2-11 below show that overall 41% of the Mediterranean contains what is qualified as karstifiable rocks and Continuous Carbonate Rocks.

Table 2-11: Mediterranean karstifiable rocks See Figure 2-8

Colour ID	Karstifiable Rocks	Area (km^2)	Percentage area
	Continuous Carbonate Rocks	582179	32.68%
	Discontinuous Carbonate Rocks	122793	6.89%
	Continuous Evaporite Rocks	13038	0.73%
	Discontinuous Evaporite Rocks	2661	0.15%
	Mixed Carbonate and Evaporite Rocks	1677	0.09%

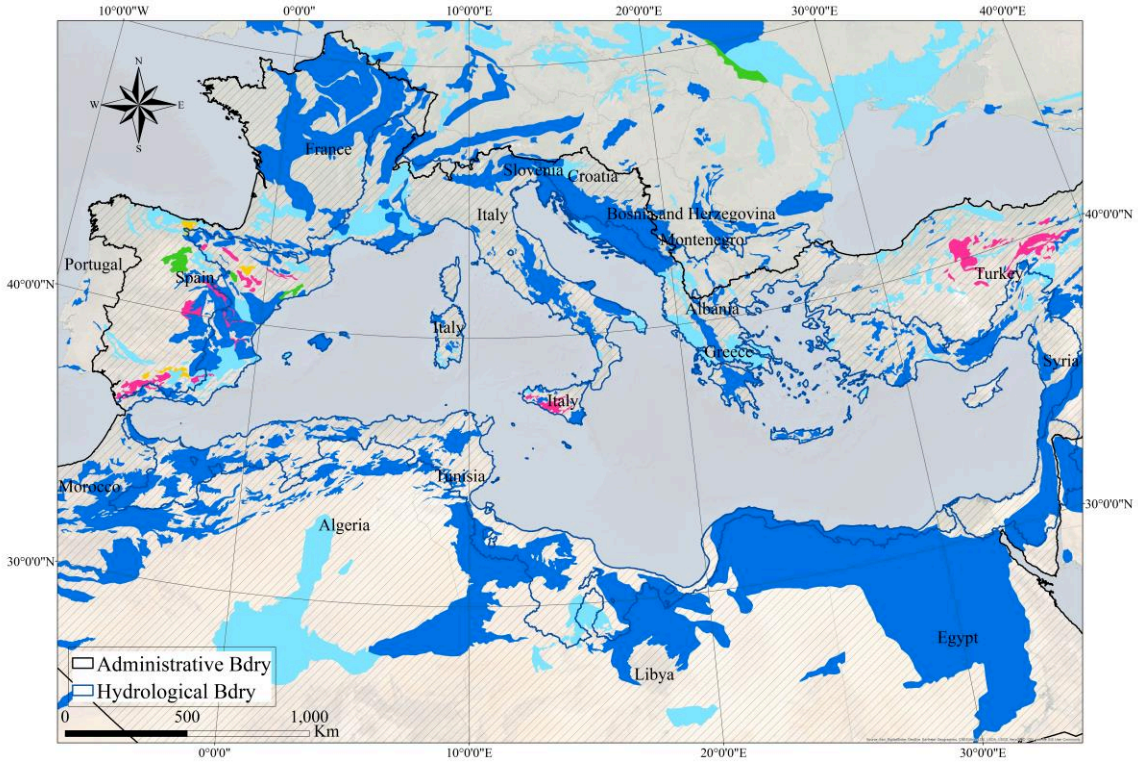

Figure 2-8: Mediterranean Karst Map from WOKAM (Chen et al., 2017) original colour coding see Table 2-11.

Table 2-12: Physiographic Indices description summary (check list of acronyms for additional description).

GROUP	TYPE	INDICES	DESCRIPTION
I	LANDFORM	A (km^2)	Area of Catchment
		I_{Hypso}	Hypsometric index, ratio of Z_{Mean} and Z_{Med}
		LargEq (km)	Equivalent rectangle width
		LongEq (km)	Equivalent rectangle length
		P (km)	Catchment Perimeter
		S_A	Catchment Average Slope
		Tc (min)	Concentration time
		Z_{Max} (m)	Catchment Maximum Altitude
		Z_{Mean} (m)	Catchment Mean Altitude
		Z_{Med} (m)	Catchment Median Altitude
		Z_{Range} (m)	Catchment Altitude Range (Maximum - Minimum)
		ZS_{Mean} (m)	Mean Snow Cover altitude when it exceeds 1 month per year
II	LANDCOVER	BA	Bare Areas
		CMA	Cultivated and managed areas
		P_{Karst}	Percentage of Karst Cover
		SC_COD	Shrub Cover, closed-open, deciduous
		SHC	Sparse herbaceous or sparse shrub cover
		TC_BDC	Tree Cover, broadleaved, deciduous, closed
		TC_MLT	Tree Cover, mixed leaf type
		TC_NLE	Tree Cover, needle-leaved, evergreen
III	SOIL	Leptosols	Type of very shallow soil over hard rock or highly calcareous material
		Luvisols	Type of soil in temperate climates, generally fertile used for agriculture
		S_AWC (mm)	Sub soil Available Water Capacity
		T_AWC (mm)	Topsoil Available Water Capacity

2.2.4 Hydrometric data

The data collection of the set of catchments with their hydroclimatic data was very challenging as no common database gathers all the available stations in the region and one had to consult national database for every country, hence the limited number of 55 catchments. Although an extensive job was performed some minor exceptions were still to be found. Some timeseries presented discontinuities and therefore only complete hydrological years were considered. All hydrometric data timeseries quality was tested for dependence using Spearman's rank correlation (Spearman, 1904) and for change detection using ellipse of Bois (Bois, 1986), the non-parametric approach to the change-point test Pettitt (Pettitt, 1979), shift detection test of Buishand (Buishand, 1984), and segmentation of Hubert (Hubert et al., 1989). 50 out of the 55 timeseries were found accepted for Pettitt at 99% and 48 for Spearman's rank test at 99%. Complete test results are presented in APPENDIX A3.

For a better organization, runoff timeseries were collected first and corresponding climatic data later. Streamflow timeseries were collected from several national and Regional hydrological agencies and services summarised in Table 2-13. It is worth noting that only 10 sub catchments were considered so the whole study area could be covered. Statistical summaries are presented in Table 2-14 below showing the wide inter-catchment variability of physioclimatic characteristics. The selected rivers cover a wide geographic domain spread across 15 countries (See Figure 2-9) in different geologic, soil and landcover settings.

Table 2-13: List of hydrological agencies and services source of the selected catchments hydrometric data.

Agency	Country	Number of Catchments
Catalan Agency for Water - ACA, Hydrological Automatic Information System - SAIH	Spain	8
Banque HYDRO	France	8
Superior Institute for the Protection of Environmental Resources - ISPRA	Italy	11
Slovenian Republic Environment Agency - ARSO	Slovenia	3
Croatian Meteorological and Hydrological Service - DHMZ	Croatia	2
Litani River Authority - LRA	Lebanon	6
Greek ministry of Environment and Energy - YPEKA	Greece	1
Système d'Informations Environnementales sur les Ressources en Eau et leur Modélisation - SIEREM	Algeria, Morocco, Tunis	6
Global Runoff Discharge Centre - GRDC	Cyprus, Turkey, Israel	7
Mediterranean Hydrological Cycle Observing System - MedHyCOS	Albania, Cyprus, Montenegro	3
TOTAL	15	55

Table 2-14: The 55 selected catchments with Area at flow station, Mean Annual Precipitation (MAP), Mean Annual Flow (MAQ) and runoff coefficient (CE) calculated based on available data.

ID	Code	Name	Coverage period	No. of Years	Water Balance Years	Area (km^2)	MAP (mm)	MAQ (mm)	CE
4	ME	MELAH*	1976-2003	28	15	552	587	174	0.30
5	MA	MAZAFRAN	1976-1995	20	14	1912	574	57	0.10
15	ER	ERZENIT	1954-1992	38	37	760	1202	553	0.46
47	SR	SERRAKHIS*	1965-1998	32	30	77	1006	188	0.19
51	VA	VASILIKOS	1965-2014	21	21	150	629	32	0.05
56	EZ	EZOUSAS	1965-2002	37	25	210	669	58	0.09
63	DH	DHIARIZOS	1965-1996	30	27	125	675	173	0.26
88	CE	CENIA	1957-2014	51	51	97	529	281	0.53
103	AM	AMADORIO	1959-1985	26	26	185	359	38	0.11
162	FL	FLUVIA	1991-2017	26	26	842	802	221	0.28
165	MU	LA MUGA	1974-2017	39	39	854	714	77	0.11
169	EL	ELTER	1990-2017	25	25	2350	701	129	0.18
174	EB	EL BESÒS	1975-2016	28	28	1036	644	126	0.20
175	GA	GAIA	2001-2015	15	15	424	462	17	0.04
194	AN	ANDARAX	1998-2017	20	20	490	242	2	0.01
206	FA	FIUM-ALTO	1960-2012	52	43	114	749	390	0.52
297	LE	LEZ	1998-2017	20	19	150	629	382	0.61
319	LO	LOUP	1980-2017	36	26	264	755	541	0.72
531	HE	HERAULT	1953-2017	64	60	2625	629	502	0.80
541	AU	AUDE*	1969-2017	48	47	1754	557	342	0.61
550	GP	GAPEAU	1961-2017	56	19	517	536	252	0.47
559	TC	TECH	1985-2017	32	28	729	554	351	0.63
561	TE	TET	1970-2017	46	46	1371	557	244	0.44
634	SP	SPERCHEIOS	1952-2011	50	50	1282	701	572	0.82
677	MI	MIRNA	1955-2016	62	36	579	1164	384	0.33
681	KR	KRKA	1947-2017	71	66	2103	1074	771	0.72
692	AX	ALEXANDER	1967-1993	27	18	953	603	11	0.02
693	SO	SOREQ	1960-1992	32	27	492	543	18	0.03
710	FI	FIORA	1950-1993	44	21	818	959	287	0.30
722	AC	ALCANTARA	1981-1999	14	14	475	658	14	0.02
725	FM	FLUMINIMAGGIORE	1952-2004	52	37	83	747	320	0.43
800	SE	SERCHIO	2000-2014	15	15	1525	1831	997	0.54
803	AR	ARGENTINA	1925-1996	58	34	209	982	703	0.72
822	CI	CECINA	1957-1997	22	22	634	857	262	0.31
845	PE	PESCARA	1990-2012	23	23	3125	783	487	0.62
887	AL	ALENTO	1961-1993	26	26	285	1253	462	0.37
903	SL	SAN LEONARDO	1951-1981	30	29	522	660	195	0.30
908	IM	F. IMERA MERIDIONALE	1963-2003	40	27	1725	633	102	0.16
913	CR	CERVARO	1966-1996	30	26	657	713	103	0.14
928	JA	NAHR EL JAOUZ	1964-2004	40	13	189	1413	304	0.21
929	BE	NAHR BEYROUTH	1958-2015	57	31	217	1032	454	0.44
930	KA	NAHR EL KALB	1949-2015	66	31	249	1440	904	0.63
934	IB	NAHR IBRAHIM	1965-2015	50	16	326	1450	1052	0.73
936	AS	NAHR ASSI	1931-1973	42	17	1507	661	266	0.40
937	LI	NAHR LITANI	1931-2015	60	26	1808	637	289	0.45
938	MO	MORACA*	1948-1990	42	26	2628	3383	1778	0.53
949	KE	KERT*	1969-1987	18	18	1353	230	16	0.07
951	EM	EMSA	1971-1988	18	15	110	572	203	0.35
959	RI	RIŽANA	1988-2015	27	27	205	941	606	0.64
960	DR	DRAGONJA	1955-2015	35	26	147	956	216	0.23
962	IS	ISONZO*	1980-2015	35	31	1800	2254	1569	0.70
1035	KO	KOEPRUE*	1977-1987	11	8	1942	632	336	0.53
1042	CC	CINE CAYI*	1977-1987	11	8	948	632	217	0.34
1048	MJ	MEJERDA*	1950-1996	45	44	1490	450	99	0.22
1074	ML	MILIANE*	1970-2008	37	36	1070	413	64	0.15

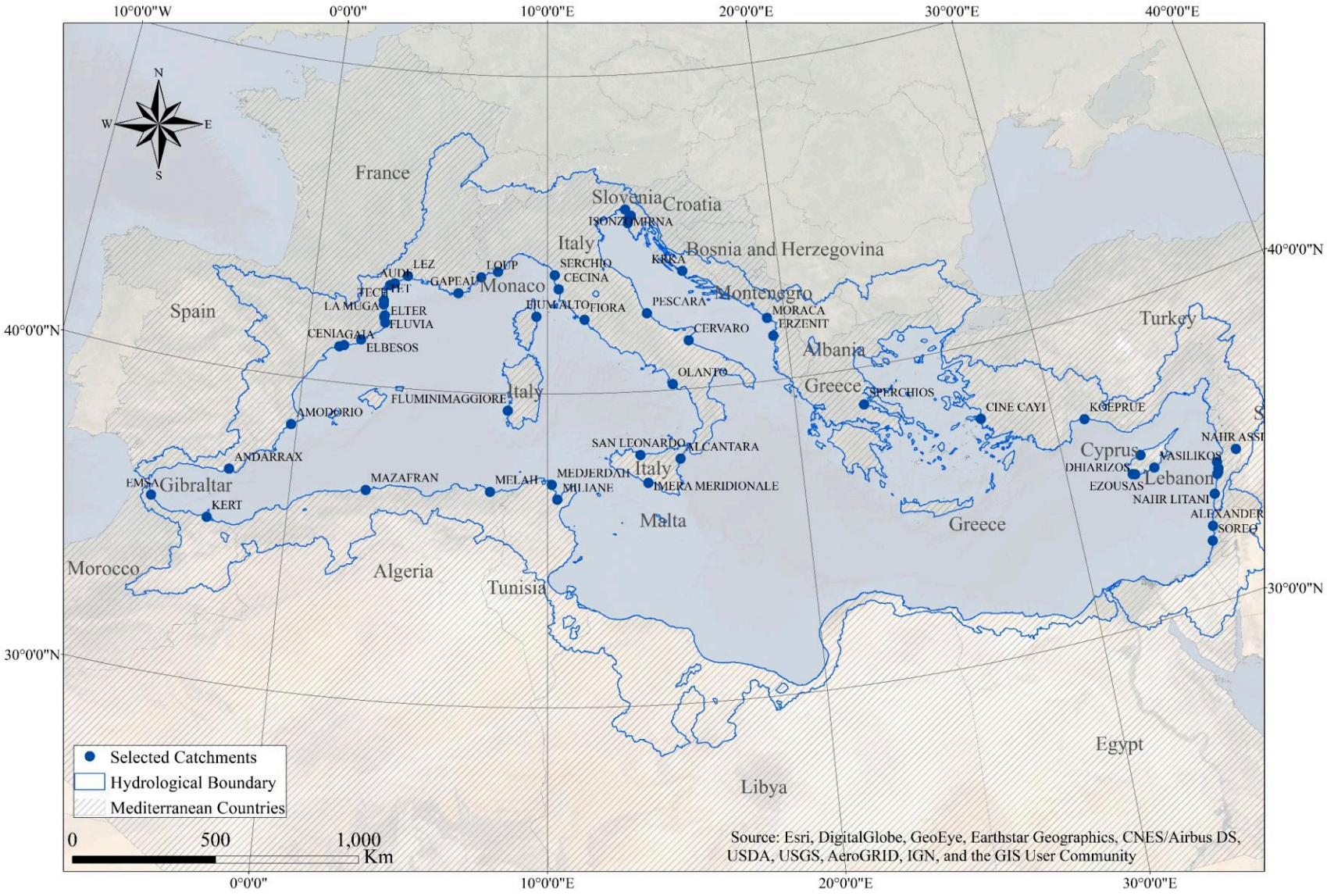

Figure 2-9: The 55 selected Mediterranean catchments for hydrological characterisation (see Table 2-14).

2.3 CONCLUSION

This chapter presented an elaborate description of the Mediterranean region with the collected climatic, physiographic, and hydrometric database. First, various definitions of the boundaries of the Mediterranean region according to climatic, hydrological, agro-bioclimatic and administrative consideration were discussed; then hydrometric data was collected for the 55 selected catchments, climatic data were derived from precipitation and temperature global data sets and weather stations networks; and physiographic data were derived from cartographic data of topography, geology, landcover, lithology, soil, and karst;

The collected database will be used to extract and calculate climatic, physiographic, and hydrological characteristics at the catchment scale. However, at this level we cannot yet assume if these characteristics are enough to reflect the hydrological behaviour of the catchment, or enough to define the hydrological similarity in the Mediterranean. Therefore, progressively in the following chapters we will hydrologically characterise the Mediterranean catchments using multivariate analysis starting with a specific climatic classification in CHAPTER 3 and physiographic classification in CHAPTER 4.

"God Rivers Duel, A Mediterranean Epic"

First encounter: Greek and Canaanites get ready for the battle

ΠΟΤΑΜΙ ΕΝΑ	
Name	Ibrahim, Adonis
Country	Lebanon
Area	329 km^2
MAP	1450 mm
MAQ	1052 mm

ΠΟΤΑΜΙ ΔΥΟ	
Name	Spercheios
Country	Greece
Area	1592 km^2
MAP	701 mm
MAQ	575 mm

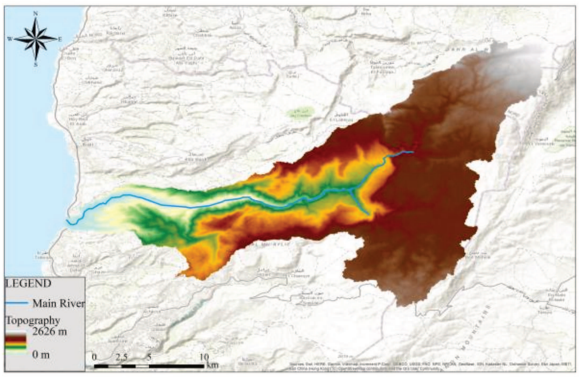

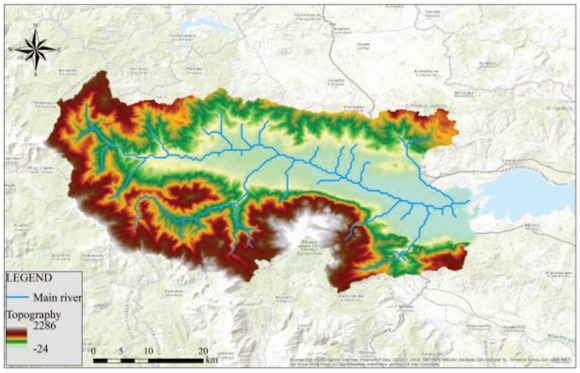

CHAPTER 3. CLIMATIC CHARACTERISATION

Chapter summary

This chapter aims to establish a new high resolution classification for hydrology purposes based on Mediterranean specific climate indices. This classification is useful in following up hydrological (water resources management, floods, droughts, etc.), and ecohydrological applications such as Mediterranean agriculture like olive cultivation and other environmental practices. The proposed approach includes the use of classic climatic indices and the definition of new climatic indices mainly precipitation seasonality index I_S, a Principal Component Analysis to reduce the number of indices, K-means classification to distribute them into classes. The classification was set and validated by WorldClim-2 at 1-km high resolution gridded data for the 1970-2000 baseline period and 144 stations data over 30 to 120 years, both at monthly time steps. Climatic classes coincided with a geographical distribution in the Mediterranean ranging from the most seasonal and dry CC1 in the south to the least seasonal and most humid CC5 in the North, showing up the climatic continuity from one place to another and enhancing the visibility of change trends. The MED-CORDEX ALADIN and CCLM historical and projected data at 12-km and 50-km resolution simulated under RCP 4.5 and 8.5 scenarios for the 2070-2100 period served to assess the climate change impact on this classification by superimposing the projected changes on the baseline grid based classification. ALADIN and CCLM RCM models have demonstrated an evolution of the Mediterranean region towards arid climate. The classes located to the north are slowly evolving towards moderate coastal classes which might affect hydrological regimes due to shorter humid seasons and earlier snowmelts.

Complementary material to Chapter 3 was added in Appendix B

Two papers were published from this chapter:

APPENDIX B1

Allam A., El Hassan J., Najem W., Bocquillon C, Moussa R., 2020. Classification climatique méditerranéenne pour l'hydrologie. La Houille Blanche Vol. 1, 60 – 69. https://doi.org/10.1051/lhb/2020008

APPENDIX B2

Allam A., Moussa R., Najem W., & Bocquillon C., 2020. Specific climate classification for Mediterranean hydrology and future evolution under Med-CORDEX regional climate model scenarios. Hydrol. Earth Syst. Sci., 24(9), 4503-4521. https://hess.copernicus.org/articles/24/4503/2020/

APPENDIX B3 Climatic Indices for selected catchments

3.1 INTRODUCTION

Mediterranean climate is a result of a complicated global cyclonic system swiping a large evaporative basin. The distribution of marine and continental air masses creates an alternation of low-pressure zones coming over from Iceland and the Persian Gulf or high-pressure zones from Siberia and Azores (Clerget, 1937). The seasonal shifts of these zones are magnified by the North Atlantic Oscillation (NAO) that plays an important role in shaping Mediterranean climate and influencing the evolution of farming and social activities in the long-term (Rodwell & Hoskins, 1996). During the positive phases of the NAO, oceanic disturbances bring the most humid to northern Europe and less humid to northern Africa and the Middle East (Douguédroit & Lionello, 2015). This continuous alternation of high- and low-pressure, cold and humid winters followed by a hot and dry summers, marks the Mediterranean seasonality which makes the region attractive to social activities, thus its sensitivity to climate change and anthropogenic pressures (Milano, 2012). A north–south general precipitation and evapotranspiration gradient has been identified in Tunisia through the analysis of directional variograms that results from partial gradients evolving through seasons (Slimani et al., 2007; Baccour et al., 2012; Feki et al., 2012). These spatial gradients mainly depend on topographic structures through the interception of rainfall-generating air masses. The climatic classification will try to identify the general spatial gradients across the Mediterranean. Hydrologically, the precipitation seasonality characterizing the Mediterranean climate is reflected in the flow regimes of Mediterranean rivers, as pointed out by Haines (1988), who classified the Mediterranean rivers under Group 12 Winter Moderate hydrological regimes, Group 13 Extreme Winter and Group 14 Early Spring, and found a clear relation to the Köppen Csa and Csb climates and a close equivalent of the ‘Mediterranean Seasonal’ categories of Gentilli (Haines et al., 1988). Seasonality is a main factor in the Mediterranean but to our knowledge its use is still limited as a characterising index for climatic and hydrological classification.

Climate change is expected to have severe consequences on Mediterranean runoff with a serious risk of fresh water availability decrease of 2% to 15% for 2°C of warming (Cramer et al., 2018) and significant increase of droughts period particularly in the South and East (Cudennec et al., 2007; Hreiche et al., 2007; García-Ruiz et al., 2011; Verdier & Viollet, 2015). The CMIP5 simulations (Coupled Model Intercomparison Project, Phase 5) expected a mean precipitation decrease of -4%/°C and a temperature increase of 20%, more than the global average, with a maximum precipitation reduction reaching -7%/°C in winter in the southern Mediterranean region and -9%/°C in the summer in the Northern region (Lionello & Scarascia, 2018). At 1.5 °C global warming, some Mediterranean areas are under aridification while moving to drier state due to the decrease in precipitation combined with a potential evapotranspiration PET increase leading to an expansion of drylands, thus affecting more people (Koutroulis, 2019).

Automatic classification methods partition a set of objects, knowing their distances by pairs in a way to keep the classes as much homogeneous as possible while remaining distinct from each other. Like any classification, the adopted method depends on the objective and its specificity. There are several modes of climatic classification: (a) genetic classifications related to meteorological causes and the origin of air masses (Bergeron, 1928; Barry & Chorley, 2009); (b) bioclimatic classifications based on the interrelation between vegetation type and climate (Holdridge, 1947; Mather & Yoshioka, 1968; Harrison et al., 2010); (c) agro-climatic method based on the assessment of the rainfall - evapotranspiration balance for the estimation of agricultural productivity (Thornthwaite, 1948); and (d) climatic methods based on precipitation and temperature indices similarly to the classification of Köppen (1936) updated by Peel in 2007 (Peel et al., 2007) and which remains the most used.

There are several climate classification studies of the Mediterranean region; among these we cite Köppen-Geiger classification at the global scale in which the Mediterranean climate is well distinctive (Köppen, 1936; Peel et al., 2007; Eveno et al., 2016). Köppen's classification divides the globe into 30 climate zones and relies on a partition hierarchy. It is based on precipitation and temperature indices where Mediterranean climate corresponds to dry hot or dry warm summer where the precipitation in the driest month in summer is either below 40 mm or below the third of the precipitation in the wettest month in winter (Cs) and the air temperature of the warmest month is above 22 °C (Csa) or the number of months with air temperature above 10 °C exceeds 4 (Csb). The (Cs) climate does not reign all over the Mediterranean region, as Köppen (B) classes are also observable. (B) classes correspond to arid climate in general, with (BWh) the desertic and hot climate that dominates Egypt and Libya, characterized by very low precipitation (MAP < 5 x $P_{threshold}$ with $P_{threshold}$ = 2 x MAT) and high temperature (MAT ≥ 18 °C), (BSk) the arid steppe cold climate that dominates south-eastern Spain characterized by low precipitation (5 x $P_{threshold}$ > MAP > 10 x $P_{threshold}$) and low temperature (MAT < 18 °C), (Cf) the temperate climate without any dry season in the regions of Thessaloniki and Veneto, and finally (D) cold climate present further north. On the other hand, and at a global scale, some regions share a similar Mediterranean (Cs) climate, such as California, Chile, South Africa, and Australia (Fig. 1). Rivoire et al. (2019) classified 160 Mediterranean rain gauges according to monthly net precipitation (P - ET). The classification showed a marked distinction between two clusters with northern stations having a precipitation deficit from April to September and southern stations having a precipitation deficit from March to October. Other climatic classification were also carried out in the Mediterranean but at the national scale like in France, using ascending hierarchical automatic classification based on a 1976 rain gauges network for the 1971-1990 period (Champeaux & Tamburini, 1996). In Turkey seven different climate zones were identified by using Ward's hierarchical cluster analysis based on data from 113 climate stations for the 1951-1998 period (Unal et al., 2003). Another reclassification of rainfall regions of Turkey was also carried out in 2011 by K-means based on 148 stations covering the 1977-2006

period (Sönmez & Kömüşcü, 2011). We also mention the classification of cyclonic trajectory information using K-means clustering for an 18 years period over the Mediterranean (Trigo et al., 1999). Synoptic meteorology using discriminant analysis over the eastern Mediterranean for 1948–2000 (Alpert et al., 2004); Cloud physical properties classification at the pixel level using K-means applied over European Mediterranean region (Chéruy & Aires, 2009); The hydrological classification of 40 Mediterranean streams natural flow regimes using PCA to identify the most representing Richter's hydrological indices and agglomerative cluster analysis (Oueslati et al., 2015); However, no specific classification based on precipitation and temperature series has yet treated the Mediterranean region as a climatic or hydrological unit, hence the aim of our study.

The objective of this study is first to establish a Mediterranean-specific climatic classification for hydrology purposes based on a set of indices, mainly seasonality and aridity, and second to estimate future evolution of this classification based on Radiative Concentration Pathway (RCP) scenarios with an easy follow up tool using olive cultivation boundary as an evolution indicator for the Mediterranean.

Through the classification of the Mediterranean catchments climatically and, in a second step physiographically in CHAPTER 4, we will be able to characterize their hydrological patterns and identify homogeneous regions which will be useful for the prediction on ungauged basins (Wagener et al., 2007; Hrachowitz et al., 2013). This study is a contribution to the HyMeX program and to the Med-CORDEX initiative. The HyMeX program (HYdrological cycle in the Mediterranean Experiment) aims at a better understanding of the Mediterranean hydrology, with emphasis on the predictability and evolution of decadal variability in the context of global change. Med-CORDEX, a HyMeX initiative, (Ruti et al., 2016), is part of the COordinated Regional Downscaling EXperiment specific for the Mediterranean that aims at improving our understanding of climate change through high resolution atmosphere Regional Climate Models (RCM). RCMs were introduced in late 1980s as a nested technique into Global Climate Models (GCMs) to consider regional scale climatic forcings caused by the complex physiographic features and small-scale circulation features (Giorgi, 2006). The primary application of RCMs has been in the development of climate change scenarios of which we mention ALADIN RCM (Aire Limitée Adaptation dynamique Développement InterNational) developed by Météo France and CCLM (Cosmo Climate Limited-area Model) developed by the German Weather Service (DWD) both applied for EURO-CORDEX and MED-CORDEX projects (Rockel et al., 2008; Tramblay et al., 2013). We aim in this study to discuss the results of the individual models and not to compare their performances, such study was carried out for EURO-CORDEX with 17 RCM models for the representation of the basic spatiotemporal patterns of the European climate for the period 1989–2008 (Kotlarski et al., 2014).

This chapter is structured into seven sections; Section 3.1 Introduction, Section 3.2 the classification approach based on PCA, K-means and the decision tree with the presentation of MED-CORDEX atmosphere-RCM climate change scenarios; Section 3.3 the results of WorldClim-2 classification of catchment indices and on gridded indices and stations, in Section 3.4 classification projection and impacts under MED-CORDEX scenarios followed by a discussion in Section 3.5 before concluding the chapter with Section 3.6.

3.2 METHODOLOGY

The suggested methodology includes first the definition of the climatic indices, of which some are classic, like the frequency indices, and other are specific of the Mediterranean climate, like precipitation seasonality. Second, there is a Principal Component Analysis (PCA) to reduce the number of climate indices and consider only the most contributing. Third, there are K-means classification according to the most contributing indices and finally the construction of a decision tree based on distances to class kernels to determine whether or not a place has a Mediterranean climate, and to which type it belongs. This approach was applied at grid scale, verified on a set of ground stations, and then compared to a catchment-scale classification where indices are calculated from averaged climatic variables of each catchment. Each class was described and characterised by its corresponding climatic indices. The Mediterranean climatic class evolution was assessed according to indices variation based on simulated RCP scenarios and by following up the olive tree cultivation boundary as an example of a historical Mediterranean specific bioindicator. The olive reproductive cycle displays considerable variations due to climate evolution among others, influencing flowering intensity mainly affected by seasonal temperature and water availability (Moreno, 2014).

3.2.1 Hydrology-driven climatic indices

The hydrology-driven independent climatic indices were chosen subjectively and developed at the grid and catchment scales from WorldClim-2 monthly average data and divided onto four groups to highlight the Mediterranean seasonality and precipitation intermittence hypothesis of the climate and its corresponding hydrological response. The climatic indices were inspired by Köppen's definition of Mediterranean climates to emphasize the precipitation and temperature variability between seasons and from the components of the water balance in its general form to highlight the link between climate and hydrology. Hence Group I and III indices I_S, $P_{25\%}$, $P_{75\%}$, and I_{Decal} characterize Mediterranean precipitation P in its seasonality and monthly distribution. Group II and IV indices S_{PET}, I_{Arid}, $T_{25\%}$, and $T_{75\%}$ characterize the hydrological loss to evapotranspiration in the Mediterranean. While the flow seasonality is clearly affected

by the precipitation seasonality, the other indices help in fine-tuning this theory, like monthly temperature and potential evapotranspiration variation. A complete list of indices with description is in Table 3-1.

Table 3-1: Climatic Indices definition.

GROUP	TYPE	CLIMATIC INDICES	DESCRIPTION
I	Climatic Indices based on average monthly rainfall	Seasonality Index I_S	One minus the precipitation ratio between the driest three months over the three humid months
		Precipitation Index $P_{25\%}$ and $P_{75\%}$	Rain value exceeded 25% or 75% of the time
		Peak index $S_{P1.5}$ $S_{P1.7}$ S_{P2}	Number of months exceeding the average monthly precipitation by 1.5, 1.7 and 2 times
		Horizontal Inertia Index I_{Hor}	Dispersion of monthly rainfall compared to the annual average
II	Climatic Indices based on average monthly temperature	ΔT_1	Temperature lag between the coldest and warmest months
		ΔT_2	Temperature lag between the coldest and warmest three consecutive months
		Temperature Index $T_{25\%}$ and $T_{75\%}$	Temperature value exceeded 25% and 75% of the time
		Peak Index $S_{T1.2}$	Number of months exceeding the average temperature by 1.2 times
		Degree Day D_j	Decomposition according to the need for habitat heating
		Mean temperature Index S_{Tm}	Number of months exceeding the Mediterranean monthly average temperature Tm 16.4 °C
III	Climatic Indices based on precipitation and temperature	Time Lag Index I_{Decal}	Time lag between the coldest and most humid month
IV	Climatic indices of Evapotranspiration	Aridity Index I_{Arid}	Annual evapotranspiration over annual precipitation I_{Arid} = PET/P
		Threshold Index S_{PET}	Number of month where precipitation P exceeds evapotranspiration PET, (PET calculated using Turc (1961) formula)

Group I: indices based on monthly precipitation from which we mention seasonality index I_S, peak indices $P_{1.5}$, P_2 and frequency indices $P_{25\%}$, $P_{75\%}$. I_S is directly linked to Mediterranean flow regimes for expressing the precipitation ratio between the 3 most humid months and the 3 most dry months with values ranging from 0 to 1 (Hreiche, 2003). I_S values tending towards 0 express uniform distribution of precipitation along the year with a hydrological response lacking flood and drought seasons while I_S values tending towards 1 correspond to a normal distribution of precipitation with a hydrological response more likely to show flood and drought seasons.

Group II: indices based on monthly temperature expressed by the temperature lag between the coldest and warmest months ΔT_1, frequency indices $T_{25\%}$, the number of months exceeding the average Mediterranean temperature S_{Tm}.

Group III: indices based on both temperature and precipitation expressed by I_{Decal} the time lag between the coldest and most humid month.

Group IV: indices based on precipitation and evapotranspiration expressed by aridity index I_{Arid}. The evapotranspiration was estimated according to Turc's formula (Turc, 1961), chosen for its application simplicity and adequacy to Mediterranean areas as it was originally developed for southern France and North African countries (Trajković & Stojnić, 2007; Trajković & Kolaković, 2009; Jensen & Allen, 2016). Turc's formula is mainly based on temperature and radiation, two stable parameters on the regional scale which reduces the uncertainties when using regionalised dataset such as WorldClim-2. Group II and IV indices describe the seasonality and variability of evapotranspiration and intermittence of wet and dry seasons.

3.2.2 Principle Component Analysis

Principal Component Analysis (PCA) is widely applied to reduce the dimensionality of datasets and keep the most representing and uncorrelated variables. This section presents a brief description of the method along with some of their applications in hydrology. For an extensive mathematical description and demonstration of these methods we advise the reader to consult (Krzanowski, 1988) and (Jolliffe, 2002).

PCA was first introduced by Karl Pearson (Pearson, 1901) and then developed by Harold Hotelling (Hotelling, 1933). Hotelling's motivation is that there may be a smaller *fundamental set of independent variables which determine the values* and conserve the maximum amount of information of the original variables (Jolliffe, 2002). This is achieved by transforming a vector of p random variables to a new set of variables, named Principal Components (PCs), by looking for a linear function of the elements having maximum variance. And next looking for another linear function uncorrelated with the first and having maximum variance and so on up to p PCs. It is hoped in general, that most of the variation will be accounted for by m PCs, where $m \prec p$.

The number of indices is reduced at two steps. The first step is based on the correlation matrix, where strongly correlated indices higher were eliminated (a threshold of 0.85 was chosen for this study). The second is based on PCA results where indices that do not contribute into the principal components that represent the greatest variabilities are eliminated.

3.2.3 K-means clustering technique

Cluster analysis consists of data points partitioning into isolated groups while minimizing the distance between same cluster data points and maximizing it between different clusters. One of the most popular clustering methods is the K-means method introduced by Edward Forgy (Forgy, 1965) and MacQueen (MacQueen, 1967). It aims to minimize the square error objective function for distance optimization. The optimization steps begin with (1) kernel initialization, the kernel being a virtual point representing the statistical centre of a class, (2) updating classes, (3) re-evaluation of kernels and (4) repetition of steps (2) and (3) until stabilization. The quality of the solution thus found strongly depends on the initial kernels. In its turn, kernel initialization is sensitive to the data dimensionality. Classification gives a deterministic result where each point should belong to one of the classes, a result of a set of decision rules based on its distances to class kernels.

The application of K-means requires setting a certain number of classes; otherwise the optimization leads to as many classes as individuals. The optimum number of classes 'K' could be defined according to the elbow method (Bholowalia & Kumar, 2014).

K-means has gained in reputation the last decades and was widely applied in hydrology field for clouds classification from satellite imagery (Desbois et al., 1982), for climatic classification using measured and simulated timeseries (Moron et al., 2008; Carvalho et al., 2016) for catchment classification based on streamflow characterisation and precipitation (Toth, 2013). K-means classification was applied, and catchments were distributed into 5 classes kernels to determine whether they belong, or not, to a Mediterranean climate and to which type they belong to, if so. We hoped for a classification that delimits the Mediterranean climate from South and North and divides the intermediate coastal zone. Therefore, a distribution into 5 classes was chosen despite that 3 classes would be optimal as per the elbow method. In detail, one class that covers the southern desertic region, another class that covers the northern continental region of non-Mediterranean climate and 3 classes that cover the intermediate coastal region. A larger number of classes would produce an uninterpretable fragmented classification.

3.2.4 Decision Tree

A decision tree is a set of distance criteria or questions in the form of hierarchy that leads to an intended classification (Breiman et al., 1984). To classify new points, or stations or to reproduce the classification on another dataset, it suffices to define the distance criterion to the various kernels of the climatic classes by predicting values of a dependent variable based on values of predictor variables from a reference classification. This procedure provides validation tools for exploratory and confirmatory classification analysis.

We generated a decision tree based on the distances to the clusters' kernels obtained from the gridded indices classification. The aim of this decision tree is to easily reproduce the classification with the same kernels rather than repeat the whole classification process which will modify the clusters and their kernels. By conserving the same kernels, the decision tree will permit to follow up the climate evolution and its impact on the classification under other scenarios.

In our case, the dependent variables are the climatic classes obtained from K-means clustering, while the predictor variables are the distances to each cluster's kernels. This procedure was done for both gridded and catchment classification. The decision tree generates a set of classification rules usually used to classify new stations based on their distances to classes kernels. In this study, these rules were used in Section 3.4 to classify the projected indices. This has fixed the classes kernels indices of the 1970-2000 baseline period and calculated the distances of the 2070-2100 projected grid to the baseline to compare both the classification indices and spatial evolution.

3.2.5 RCP scenarios

For climate change impact assessment, temperature and precipitation delta change were calculated between both baseline period 1970-2000 and projected period 2070-2100 for the MED-CORDEX RCM ALADIN and RCM CCLM grids and for two different RCP scenarios (RCP 4.5 and RCP 8.5). Those delta changes were then superimposed on the WorldClim-2 grid, based on the nearest Euclidean distance between MED-CORDEX grid cells and WorldClim-2 grid cells using the GIS spatial join toolbox. The indices were then recalculated using the projected values of monthly temperatures and precipitation. The decision tree rules from Table 3-4 were then applied for the projected period and the climate change under RCP was illustrated in Figure 3-6 and Figure 3-7 and expressed by indices evolution between classes in Table 3-5.

3.2.6 Adopted Methodology

The proposed methodology consisted first in calculating the grid-based climatic indices using WorldClim2 monthly data, second in reducing the number of indices with the PCA, and third in classifying it using K-means clustering. The gridded indices classification was later verified on the ground station indices and then compared to the catchment-scale-averaged data for future hydrological applications. In addition, a hierarchical decision tree was constructed to avoid repeating the whole process. All PCAs, K-means and decision trees where calculated using SPSS software. Projected indices under RCP scenarios were calculated and classification evolution were then deduced.

3.3 CLASSIFICATION RESULTS AND VERIFICATION

This section details the climatic indices derived from the collected database, the results of PCA/K-means classification of each set of indices and their validation on gridded and station indices with a decision tree for replicating the classification on new stations or grids.

3.3.1 PCA results for WorldClim-2 grid-based indices

The number of indices was reduced the first time based on the correlation matrix and the second based on PCA results. We eliminated the strongly correlated indices (correlation higher than 0.85), and 10 indices were kept upon the first step.

- I_S and $P_{75\%}$ are strongly inversely correlated (-0.947). I_S was kept.
- ΔT_1 and ΔT_2 are strongly correlated (0.992). ΔT_1 was kept.
- $T_{25\%}$ and $T_{75\%}$ are strongly inversely correlated (-0.999). $T_{25\%}$ was kept.
- $P_{25\%}$, $SP_{1.7}$, and SP_2 are strongly correlated (0.885, 0.852). $P_{25\%}$ was kept.
- I_{Hor} and I_{Arid} are strongly correlated (0.856). I_{Arid} was kept.
- S_{Tm} and D_j are strongly inversely correlated (-0.949). S_{Tm} was kept.

Once the correlation matrix transformed into a diagonal one, it was possible to find the eigenvalues representing the projection from p to k dimensions. The eigenvector matrix is the linear expression of the indices with respect to the principal components. The first eigenvalue 4.8 represents 48% of the variability, the second 1.09 represents 11%, and the third 1.02 represents 10%. The first three factors represent the three greatest variabilities with respect to the following factors and 68% of the total variability is thus preserved with this choice. Upon PCA, the number of indices was reduced to 7 showing that I_s, $SP_{1.5}$, $P_{25\%}$, S_{Tm}, I_{Arid}, $T_{25\%}$ and S_{PET} were the most contributing climatic indices, with 68% of total variance explained. Statistical summaries are shown in Table 3-2 with I_S values ranging between 0.06 and 1 with an average of 0.7 highlighting Mediterranean seasonality.

Table 3-2: Statistical summaries of the PCA selected grid based climatic indices using WorldClim-2 monthly data.

	I_S	$S_{P1.5}$	$P_{25\%}$	S_{Tm}	I_{Arid}	$T_{25\%}$	S_{PET}
Minimum	0.1	0.0	0.0	0.0	0.3	1.2	0.0
Mean	0.7	1.9	0.3	5.9	3.2	1.4	4.0
Maximum	1.0	6.0	0.9	10.0	38.3	2.3	12.0
Median	0.8	2.0	0.3	6.0	1.8	1.3	5.0

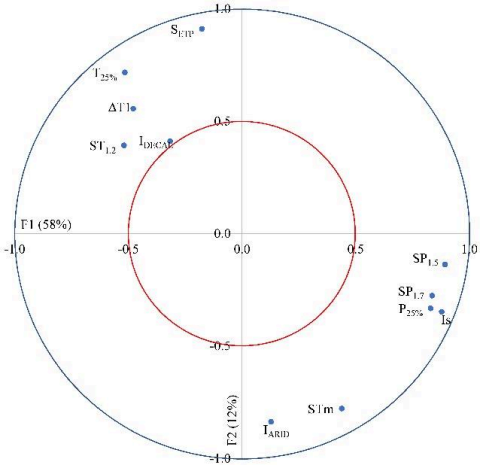

Figure 3-1: Correlations Circle.

3.3.2 Grid-based classification

The K-means classification shown in Figure 3-2 and Figure 3-3 is distributed into 5 classes.

- Class 1: present between Egypt and Libya, highlighting a desertic influence with few rain episodes registered per year, if any, expressed by I_S = 0.99 and I_{Arid} = 39.8 on average. Precipitation never exceeds evapotranspiration in this region, hence S_{PET} = 0.
- Class 2: mainly present in the south and east of the Mediterranean, characterised by a high seasonality I_S =0.98 and high aridity I_{Arid} = 9.27.
- Class 3: dominates the central region from the southern tip of Spain to Syria with an average seasonality I_S = 0.87.
- Class 4: covers mainly coastal catchments in north-west countries, south-east Italy, western Greece and present discontinuously in the south-west. I_S = 0.62 in this class.
- Class 5: present in northern non-coastal catchments and characterised by a low seasonality I_S = 0.42.

In comparison to Köppen's, classes 2-4 match with (Csa) while classes 1 and 5 are mainly outside (Csa) and (Csb), henceforth defined as non-Mediterranean climate. The main difference with Köppen's Mediterranean classes resides in southern Spain, defined as arid climate (Bsk), while in the present classification it varies between classes 2 and 4. This new distribution indicates climate variability within (Csa) or (Csb), hence the importance of a fine gridded classification. This variability is highlighted in the class kernels indices (see Figure 3-2) and is mainly due to the complex seasonality across the Mediterranean. This complexity is shown here more delicately than the one defined by Köppen which is climate oriented only and limited to the simple criteria of a wet winter and dry or temperate summer. Therefore, we think that a hydrology oriented climatic classification should account for an intra climate

characteristic expressed by specific indices like the one shown here, specific to the Mediterranean and expressed by I_S.

Olive is one of the best Mediterranean-specific physiographic indices and we noticed that its cultivation boundary is limited by those of classes 1 and 5 where 13% is in Class 2, 49% in class 3 and 34% in class 4. This observation gives an accurate idea of suitable climate conditions for olive cultivation, deducing that extreme seasonality combined with very high aridity (South) or very low seasonality combined with high humidity (North) are avoided by olive trees. In a similar way, other tree types like pine trees also characterise Mediterranean landscape putting forward the need for a physiographic classification to interpret in parallel to this climatic classification under the umbrella of hydrological characterisation. The future of Mediterranean cultivation in case of climate change is to be checked under RCP 4.5 and 8.5 scenarios in next section.

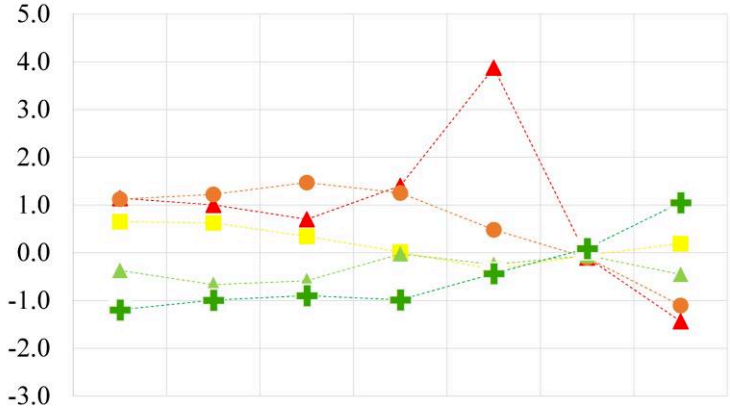

	I_s	$S_{P1.5}$	$P_{25\%}$	S_{Tm}	I_{Arid}	$T_{25\%}$	S_{PET}
▲ CLASS 1	1.14	1.00	0.70	1.40	3.88	-0.10	-1.44
● CLASS 2	1.12	1.22	1.47	1.25	0.48	-0.10	-1.10
■ CLASS 3	0.65	0.63	0.34	0.02	-0.34	-0.05	0.19
▲ CLASS 4	-0.37	-0.66	-0.58	-0.02	-0.24	-0.06	-0.45
✚ CLASS 5	-1.19	-0.99	-0.89	-0.98	-0.43	0.09	1.05

Figure 3-2: Normalised indices values of the five climatic classes kernels from the Mediterranean grid based classification using WorldClim-2 data.

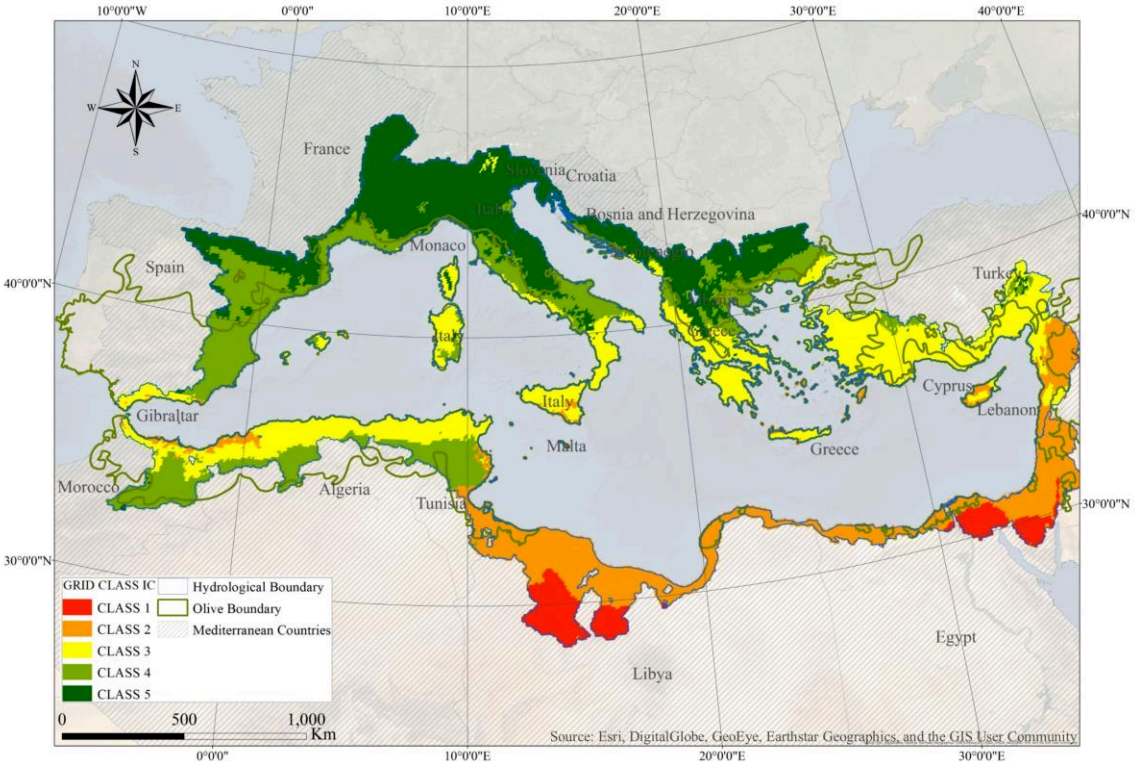

Figure 3-3: Geographical distribution of the Mediterranean climatic classes based on gridded indices using WorldClim-2 monthly data.

3.3.3 Verification on stations indices

The 144 stations were also K-Means clustered based on the selected indices from the PCA. The resulting geographical distribution differed only by some shifting due to averaging and normalization as the sample is much less than the gridded cells. There is no coverage of class 1 as no weather station was found in that region (see Figure 3-4). Despite the shifting, there is an 82% accuracy rate or 86 out of 105 stations that matched the gridded distribution, the rest is located within the adjacent classes boundaries. As for olive boundary, there was only one class 5 station corresponding to Firenze that was located within the boundary.

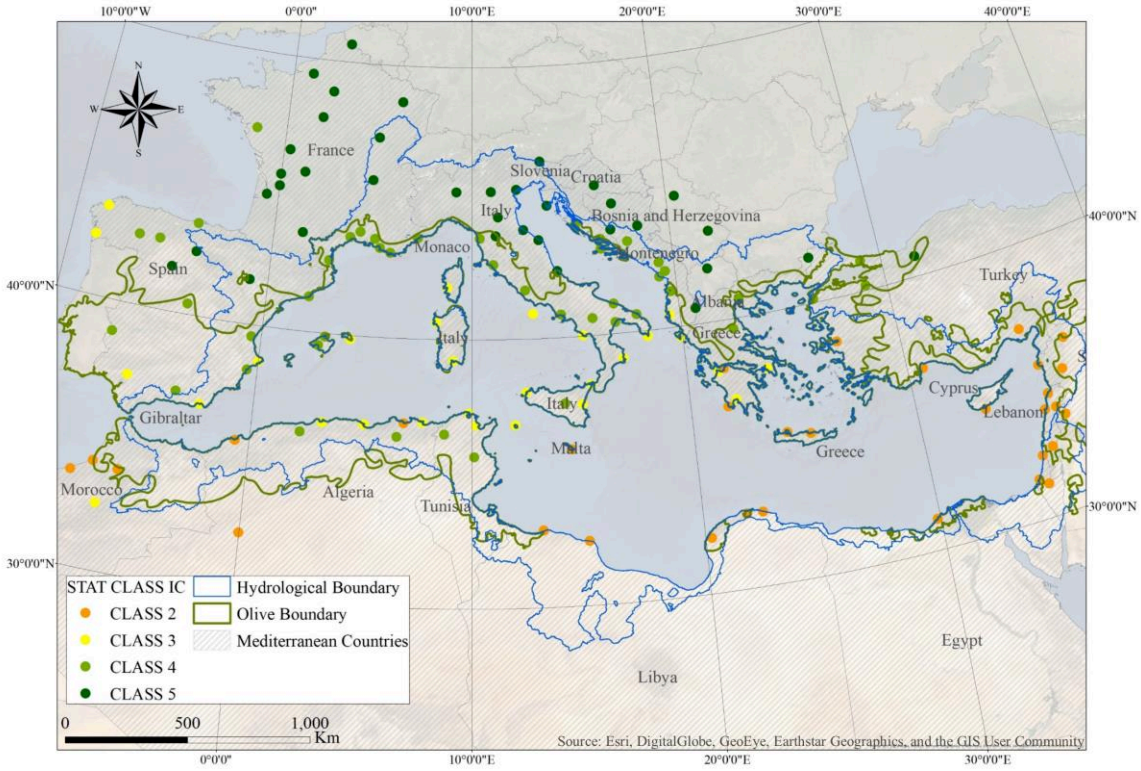

Figure 3-4: Geographical distribution of the Mediterranean climatic classes based on 144 stations climatic indices.

3.3.4 Comparison to catchment-based classification

The K-means clustering of the catchment indices classification resulted with a spatial distribution similar to WoldClim-2 grid based classification where class 1 catchments dominate the south, class 5 the north and classes 2, 3 and 4 the central region (Figure 3-5). This classification has shown lower resolution and revealed the shifts of some regions to adjacent classes. Class 1 dominated Egypt and Libya, class 5 climate disappeared from northern Spanish coasts, class 3 climate from Sardinia and Greece, Class 2 from Syria, and the limited spread of class 4 and 5 also disappeared from Eastern Turkey. However, climate continuity is conserved in this classification for indices are gradually increasing or decreasing from North to South. We believe that this classification is useful both for hydrological and ecohydrological applications like cultivation and other related environmental practices affected by water resources and river flows.

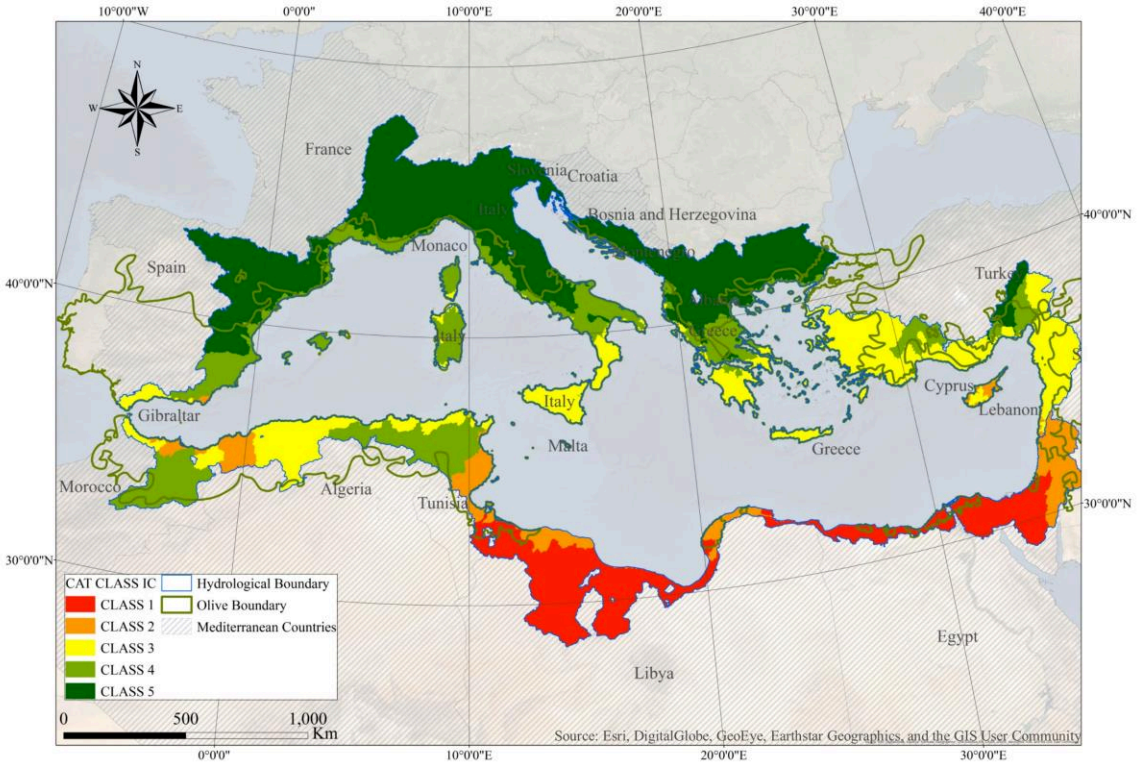

Figure 3-5: Geographical distribution of the Mediterranean climatic classes based on average catchments indices using WorldClim-2 monthly data.

3.3.5 Decision tree analysis

A decision tree was generated based on the gridded indices and their distances to cluster's kernels. The total population of gridded indices was divided randomly into two equal subsets, one for training and the second for testing. The predicted classes values of both sets were then compared to the original classification of the gridded indices obtained in Section 3.3.2 and both yielded an overall 93% accuracy (Table 3-3). We notice that some grids have joined one of the adjacent classes due to interclass connectivity; this confirms once more the continuity of climate. The generated decision tree of 3 levels includes 75 nodes in total due to high population number with 75 classification rules sampled in (Table 3-4). As an example, for class 1, if the distance to kernel 1 (D1) is below 3.5 and the distance to kernel 2 (D2) is above 2.2, then the grid cell belongs to class 1. This decision tree permits to follow up the climate evolution and its impact on the classification applied in section 3.4.

Table 3-3: Gridded classification decision tree accuracy table. The accuracy rate is calculated in comparison to the K-means classification of the gridded indices in Section 3.3.2

Sample		1	2	3	4	5	Accuracy
Training	1	636	26	1	1	2	95.5%
	2	86	1915	131	0	0	89.8%
	3	0	118	3537	186	17	91.7%
	4	1	0	135	2860	68	93.3%
	5	0	0	1	72	3511	98.0%
	Overall Percentage	5.4%	15.5%	28.6%	23.4%	27.0%	93.6%
Test	1	637	33	2	2	0	94.5%
	2	71	1889	166	0	0	88.9%
	3	1	124	3635	197	11	91.6%
	4	0	0	167	2912	69	92.5%
	5	0	0	0	83	3389	97.6%
	Overall Percentage	5.3%	15.3%	29.7%	23.9%	25.9%	93.1%

Table 3-4: Sample of the decision tree set of rules for the gridded classification (D1, D2, D3, D4 and D5 correspond to distance to kernel of class 1, 2, 3, 4 and 5). As an example, for class 1, if the distance to kernel 1 (D1) is below 3.5 and the distance to kernel 2 (D2) is above 2.2, then the grid cell belongs to class 1.

CLASS 1 (4 rules)	(D1) < 3.5 and (D2) > 2.2
CLASS 2 (13 rules)	(D1) < 3.5 and 1.9 < (D2) < 2.2 3.5 < (D1) < 4.2 and 2.4 < (D4) < 2.8 and (D2) < 2.2 3.5 < (D1) < 4.2 and 2.8 < (D4) < 3.4 4.7 < (D1) < 4.8 and (D4) > 3.4 4.8 < (D1) < 5.1 and (D4) > 3.4
CLASS 3 (23 rules)	3.5 < (D1) < 4.2 and 1.8 < (D4) < 2.1 and (D2) < 2.2 3.5 < (D1) < 4.2 and 2.1 < (D4) < 2.4 5.1 < (D1) < 5.5 and 1.5 < (D4) < 1.8 and (D5) > 1.7 5.1 < (D1) < 5.5 and 1.5 < (D4) > 1.8
CLASS 4 (23 rules)	3.5 < (D1) < 4.2 and (D4) < 1.8 3.5 < (D1) < 4.2 and 1.8 < (D4) < 2.1 and (D2) > 2.2 5.5 < (D1) < 5.9 and 1.3 < (D5) < 1.7 and 1.2 < (D4) < 1.5 5.5 < (D1) < 5.9 and (D5) > 1.7
CLASS 5 (12 rules)	5.1 < (D1) < 5.5 and 1 < (D4) < 1.2 and (D5) < 1.3 5.1 < (D1) < 5.5 and 1.5 < (D4) < 1.5 and (D5) < 1.7 5.9 < (D1) < 6.5 and 1.5 < (D4) < 2.4 and (D5) > 1.7 5.9 < (D1) < 6.5 and (D4) > 2.4 (D1) > 6.5

3.4 CLASSIFICATION EVOLUTION UNDER CLIMATE CHANGE SCENARIO

3.4.1 MED-CORDEX ALADIN RCP Scenarios Climate Evolution

The climate change impact on the classification under RCP scenarios was illustrated in Figure 3-6 and Figure 3-7 and expressed by indices evolution between classes in Table 3-5. Under RCP 4.5 scenario, temperature is increasing by 1.4 to 3.5°C (average 2.2°C), with the lowest rates during winter and the highest during summer. In the South, on average, precipitation is increasing by 25% during winter and 70% during summer and decreasing by 15% during spring and 5% during fall. In the North it is increasing by 10% during winter, spring and fall while staying stable along the year in the central region. No major area changes are occurring between classes. In detail, class 5 is reducing its extent in Greece and Albania in favour of classes 3 and 4 but compensating in central Spain; class 3 extent is decreasing in Turkey and Corsica in favour of class 4 in Lebanon and class 2 in Cyprus. Classes 1, 2 and 3 seasonality indices I_S are stable while classes 4 and 5 are increasing by 7% and 9%. Also for classes 4 and 5, $S_{P1.5}$ is highly increasing (70%) with $P_{25\%}$ staying almost the same (3%) which means that precipitation change is temporally distributed in a way that more months are exceeding the average monthly precipitation by 1.5 times and that the humid season has shortened, enhancing seasonality variation. Another remarkable change is class 5 I_{Arid} 20% increase pushing it towards class 4.

Under RCP 8.5 scenario, the case is accentuated for temperature which is increasing evenly across the Mediterranean by 2.5 to 5.6°C (average 3.8°C) with the lowest rates during winter and the highest during summer. In the South, on average, precipitation is increasing by 60% during summer and decreasing by 10% during winter. In the North it is increasing by 5% during spring and summer while staying almost stable along the year in the central region. The area also did not change much under RCP 8.5; in detail class 3 is taking over the south eastern coast of Spain but retreating in favour of class 4 from North West Africa and Turkey. The difference with RCP 4.5 scenario resides first in the indices' evolution where I_S is increasing by 9% in class 5 and $S_{P1.5}$ highly increasing by 96%. This has caused an area change of 2% towards class 4 mainly in Spain, Greece, and Albania. Another change is class 3 I_{Arid} increasing by 19% and S_{PET} decreasing by 10% which means that this moderate region is pushing towards more arid climate

3.4.2 MED-CORDEX CCLM RCP Scenarios Climate Evolution

Under RCP 4.5 scenario, temperature is increasing by 1.9 to 3.5°C (average 2.9°C), with the lowest rates in the South during winter and the highest in the North during summer. In the South, on average, precipitation is increasing by 20% during winter and 10% during fall and decreasing by 10% during summer but stable during spring. In the North it is increasing up to 10% during fall and winter and decreasing down

to 30% during spring and summer. The spatial extent of class 5 is increasing by 4% mostly in northern Spain, Albania, Morocco and Algeria in favour of class 4 which is decreasing by 5%; class 3 appeared between Italy and France on the Ligurian Sea, at San Marino and on the Spanish coast; class 2 expanding over the Turkish coast and in Morocco; class 1 remained almost unchanged. Classes 1 and 2 seasonality indices I_S are constant while of classes 3, 4 and 5 are increasing by 4%, 27% and 42%. Also, $S_{P1.5}$ is increasing by 14%, 120% and 320% for classes 3, 4 and 5 with a little change of $P_{25\%}$ (less than 10%); same observation as ALADIN RCP4.5 scenario but more accented. I_{Arid} is increasing by 56% in class 5 while S_{PET} is increasing by 25%.

Under RCP 8.5 scenario, temperature is increasing by 3.6 to 6.4°C (average 5.1°C), with the lowest rates in the South during winter and the highest in the North during summer. In the South, on average, precipitation is increasing by 30% during winter and 10% during fall and decreasing down to 25% during summer but stable during spring. In the North it is increasing up to 10% during fall and winter and decreasing down to 60% during spring and summer. Spatially, class 3 is increasing by 9% mostly in Italy, France, Spain, northern Greece, and Algeria in favour of class 4 which is decreasing by 7%; classes 1, 2 and 5 remained almost unchanged. Classes 3, 4 and 5 seasonality indices I_S are increasing by 8%, 39% and 80%. $S_{P1.5}$ is increasing by17%, 215% and 516% for classes 3, 4 and 5 with a change of $P_{25\%}$ of maximum 17%. Aridity indices are increasing of 24% to 50% for classes 3, 4 and 5 while S_{PET} is decreasing between 13 and 26 % for the same classes. In summary, the Mediterranean is evolving towards an arid region under both CCLM RCP 4.5 and 8.5 scenarios.

Table 3-5: Climatic indices values under ALADIN and CCLM RCP scenarios with evolution ratio in italic.

		AREA		ΔT	ΔP	I_s		$S_{P1.5}$		$P_{25\%}$		S_{Tm}		I_{Arid}		$T_{25\%}$		S_{PET}	
BASELINE 1970-2000	CLASS 1	5%				0.99		3.53		1.70		9.10		39.80		1.33		0.00	
	CLASS 2	18%				0.98		3.88		1.94		8.76		9.18		1.32		1.00	
	CLASS 3	27%				0.87		2.90		1.58		5.98		1.75		1.48		4.85	
	CLASS 4	22%				0.61		0.77		1.29		5.81		2.58		1.47		3.05	
	CLASS 5	28%				0.41		0.29		1.20		3.66		0.89		1.94		7.56	
ALADIN RCP 4.5 2070-2100	CLASS 1	4%	*0%*	2.13	19%	0.99	*0%*	3.45	*-2%*	1.79	*6%*	9.00	*-1%*	39.46	*-1%*	1.32	*-1%*	0.00	*0%*
	CLASS 2	19%	*1%*	2.14	12%	0.98	*0%*	3.65	*-6%*	1.99	*3%*	8.43	*-4%*	9.94	*8%*	1.31	*-1%*	0.99	*-1%*
	CLASS 3	26%	*-1%*	2.26	1%	0.87	*0%*	2.90	*0%*	1.60	*1%*	5.91	*-1%*	2.01	*15%*	1.44	*-3%*	4.51	*-7%*
	CLASS 4	23%	*0%*	2.14	2%	0.66	*9%*	1.31	*70%*	1.32	*3%*	5.64	*-3%*	2.73	*6%*	1.44	*-2%*	2.80	*-8%*
	CLASS 5	28%	*0%*	2.21	7%	0.45	*7%*	0.50	*71%*	1.22	*2%*	3.67	*0%*	1.06	*20%*	1.87	*-4%*	7.11	*-6%*
ALADIN RCP 8.5 2070-2100	CLASS 1	4%	*0%*	3.80	11%	0.99	*0%*	3.44	*-3%*	1.83	*8%*	8.90	*-2%*	38.43	*-3%*	1.32	*-1%*	0.00	*0%*
	CLASS 2	19%	*1%*	3.79	8%	0.98	*0%*	3.60	*-7%*	1.98	*2%*	8.45	*-4%*	10.11	*10%*	1.31	*-1%*	1.02	*2%*
	CLASS 3	26%	*-1%*	3.84	-3%	0.86	*0%*	2.79	*-4%*	1.58	*0%*	5.92	*-1%*	2.08	*19%*	1.44	*-3%*	4.38	*-10%*
	CLASS 4	24%	*2%*	3.76	-2%	0.65	*7%*	1.33	*74%*	1.34	*4%*	5.57	*-4%*	2.66	*3%*	1.44	*-2%*	2.95	*-3%*
	CLASS 5	26%	*-2%*	3.67	3%	0.45	*9%*	0.57	*96%*	1.23	*3%*	3.62	*-1%*	0.93	*4%*	1.89	*-3%*	7.32	*-3%*
CCLM RCP 4.5 2070-2100	CLASS 1	5%	*0%*	2.67	6%	0.99	*0%*	3.51	*-1%*	1.72	*2%*	9.06	*0%*	38.26	*-4%*	1.30	*-2%*	0.00	*0%*
	CLASS 2	19%	*1%*	2.58	6%	0.99	*0%*	3.87	*0%*	2.02	*4%*	8.43	*-4%*	9.01	*-2%*	1.28	*-3%*	1.05	*5%*
	CLASS 3	27%	*-1%*	2.89	-3%	0.90	*4%*	3.31	*14%*	1.68	*6%*	5.97	*0%*	1.96	*12%*	1.39	*-6%*	4.59	*-5%*
	CLASS 4	17%	*0%*	3.00	-7%	0.77	*27%*	1.69	*120%*	1.37	*7%*	5.86	*1%*	2.89	*12%*	1.40	*-5%*	2.97	*-3%*
	CLASS 5	32%	*0%*	3.07	-7%	0.59	*42%*	1.22	*316%*	1.31	*9%*	3.93	*8%*	1.39	*56%*	1.69	*-13%*	5.70	*-25%*
CCLM RCP 8.5 2070-2100	CLASS 1	5%	*0%*	4.66	6%	0.99	*0%*	3.57	*1%*	1.85	*9%*	8.48	*-7%*	36.64	*-8%*	1.27	*-4%*	0.00	*0%*
	CLASS 2	17%	*1%*	4.61	1%	0.99	*1%*	3.89	*0%*	2.09	*8%*	8.10	*-8%*	9.49	*3%*	1.26	*-4%*	1.00	*0%*
	CLASS 3	36%	*-1%*	5.22	-11%	0.93	*8%*	3.40	*17%*	1.76	*11%*	5.82	*-3%*	2.19	*25%*	1.36	*-8%*	4.02	*-17%*
	CLASS 4	15%	*2%*	5.31	-18%	0.84	*39%*	2.41	*215%*	1.50	*17%*	5.60	*-4%*	3.20	*24%*	1.38	*-6%*	2.64	*-13%*
	CLASS 5	28%	*-2%*	5.36	-23%	0.75	*80%*	1.79	*514%*	1.39	*16%*	3.69	*1%*	1.40	*58%*	1.48	*-24%*	5.61	*-26%*

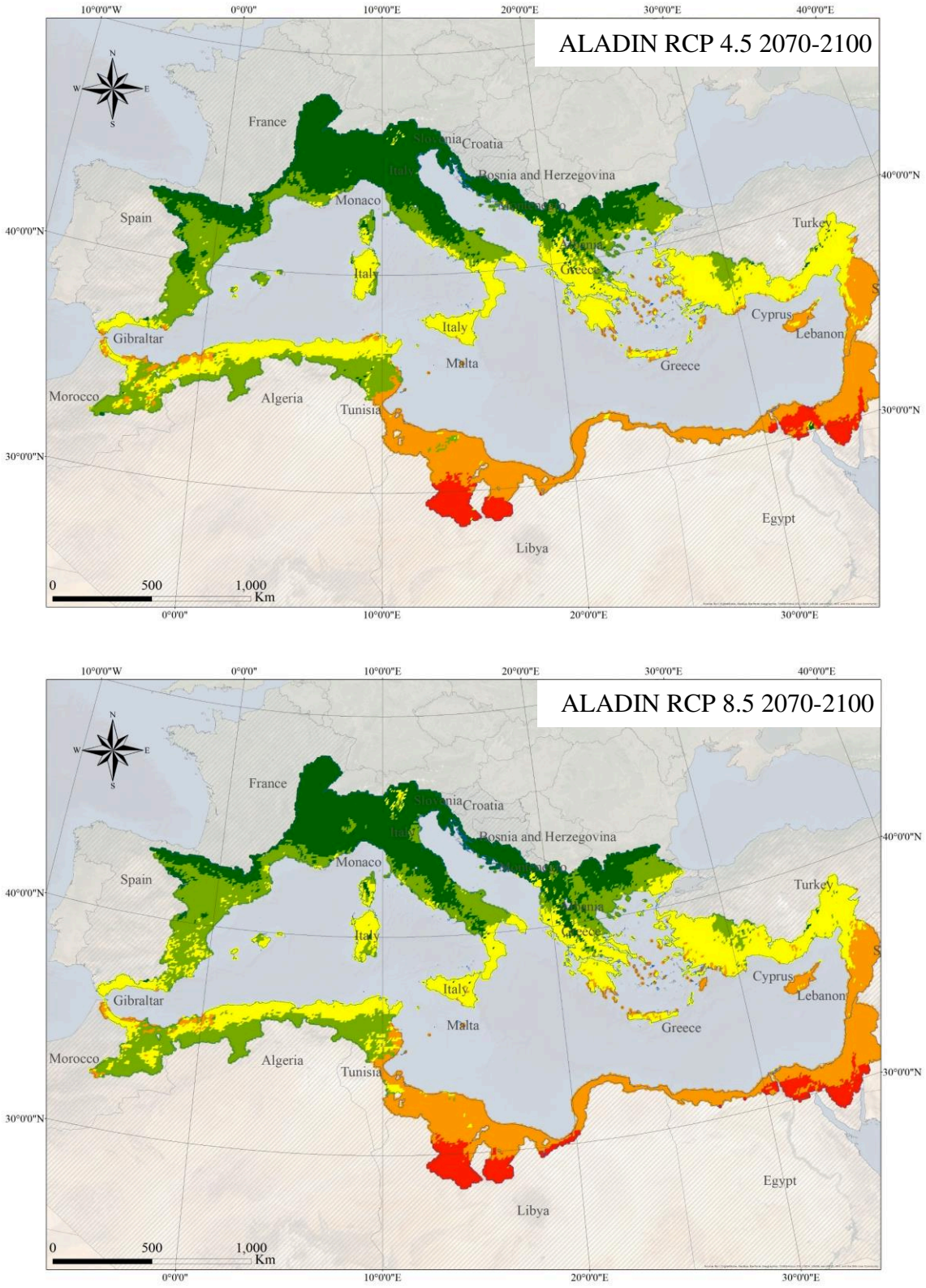

Figure 3-6: Projected geographical distribution of the Mediterranean climatic classes based on WorldClim-2 gridded climatic indices using projected data under ALADIN RCP 4.5 and 8.5 scenarios for the 2070-2100 period..

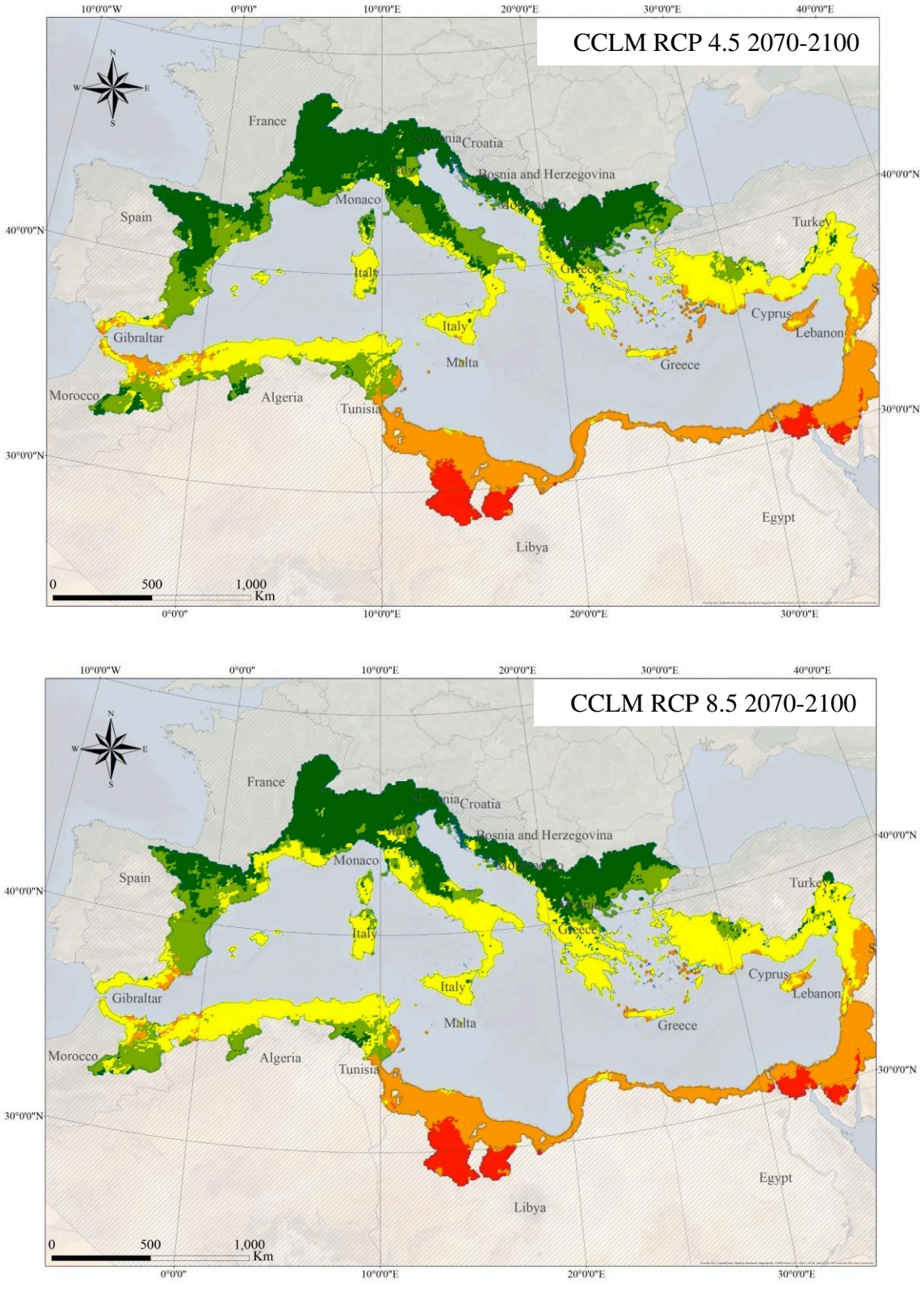

Figure 3-7: Projected geographical distribution of the Mediterranean climatic classes based on WorldClim-2 gridded climatic indices using projected data under CCLM RCP 4.5 and 8.5 scenarios for the 2070-2100 period.

3.5 DISCUSSION

The objective of this study is first to establish a Mediterranean specific climatic classification for hydrology purposes based on a set of indices mainly seasonality and aridity, second, to estimate future evolution of this classification based on RCP scenarios.

In this chapter, the climatic classification was applied and verified on three datasets of different resolutions; the grid based, the station based, and catchment based classification using the same climatic indices. We can clearly notice that the grid based classification yielded the best resolution, however, despite the variability of the class boundaries between classifications, where some region shift from class to another, the continuous evolution of climate across the Mediterranean was demonstrated by the indices values uniformly increasing or decreasing from North to South in all classifications. In general, precipitation seasonality is highest in the South and lowest in North, same for other precipitation indices and aridity, hence, the overall classification gradient was maintained from class 1 in the South to class 5 in the North which confirms that I_S and I_{Arid} are the main contributors to the classification taking over precipitation and temperature frequency indices. (Figure 3-3, Figure 3-4 and Figure 3-5)

The catchment based classification put the whole catchment within the same class despite the intra climatic diversity which mostly affected wide catchments (above 10000 km^2) like Rhône, Ebro and Po and to less extent, smaller catchments (less than 3000 km^2) as climatic diversity decreases with area and spatial spread.. The grid based classification refined the catchment based classification showing different climatic classes within the same catchment mainly between coastal low land areas, valleys, and mountainous high land areas. However, we could still notice in Figure 3-4 that Alps mountains and Po valley are still in the same class according to our classification approach as they both share close seasonality index ($I_S \approx 0.47$) and aridity index ($I_{Arid} \approx 1.06$). Nevertheless, class 3 spots were seen in Northern Italy mountains at the boundary with Austria which upon checking appeared to have a higher seasonality and aridity ($I_S \approx 0.70$; $I_{Arid} \approx 0.98$) than the surrounding region ($I_S \approx 0.61$; $I_{Arid} \approx 0.78$), an anomaly that might be caused by variables interpolations in the area. It is interesting to cross analyse this classification with a catchment based physiographic classification (article in preparation) which both classifications will be used for a hydrological characterization of Mediterranean catchments.

In the North, where seasonality is low and precipitation is regular along the year, RCP 4.5 and 8.5 scenarios impacts on hydrology are more accentuated for CCLM than ALADIN as the first is projecting a high precipitation decrease, down to -30% and -60% and a warming of 3.8°C and 6.8°C for RCP 4.5 and 8.5 consequently during dry spring and summer seasons, hence increasing I_S by +80% and I_{Arid} by +60% causing the wet seasons shortening and river regimes modification with the migration North of Group 13

Extreme Winter regimes instead of Group 12 Moderate winter and Group 14 Early Spring regimes. ALADIN is projecting a moderate precipitation variation of ± 10% with a warming of 2.7 °C and 4.5°C and increasing I_S by only +9% and I_{Arid} by +20% (see Table 3-5).

In the South, where seasonality is very high already, and precipitation is limited to fall and winter, models have projected little to no modification. RCP 4.5 and 8.5 scenarios impacts on hydrology is more accentuated for ALADIN than CCLM as the first is projecting a precipitation change between -5% and +25% for RCP 4.5 and between -12% and -2% for RCP 8.5 during fall and winter consequently with I_{Arid} change reaching 10%; CCLM is projecting a precipitation increase between +8% and +22% for RCP 4.5 and between +5% and +32% for RCP 8.5 with only +3% I_{Arid} change while I_S didn't change for both. A modification of hydrologic regime from Group 14 Early Spring to Group 13 Extreme Winter is expected.

Looking to the maps in Figure 3-6 and Figure 3-7 we can easily notice that class 2 and 3 are expanding to the North for RCM CCLM while this change is limited for RCM ALADIN; looking South, we don't see much change on the maps, hence confirming our previous observations.

The use of ALADIN and CCLM models is not enough to fully assess the uncertainties which is beyond the scope of this thesis. Nevertheless, the seasonal variability between models and scenarios, despite the general trend towards warming, aridity and accentuated seasonality, incited us to address the main reasons behind. This uncertainty usually depends on adopted climate variables, the region, seasons (Lionello & Scarascia, 2018). In addition, the adopted models in this study are atmosphere-RCM and not fully coupled models, as they are not yet achieved by the MED-CORDEX, which could have returned different results.

ALADIN and CCLM RCM models have demonstrated an evolution of the Mediterranean region towards arid climate, more emphasised with CCLM especially for RCP 8.5. These scenarios might look Mediterranean friendly as classes 4 and 5 seasonality indices are evolving towards class 3 in addition to some spatial expansion which might look favourable for Mediterranean cultivation however, the expected impact on water resources and flow regimes will sure expand and directly hit ecosystems, food, health and tourism as risk is interconnected between domains (Cramer et al., 2018).

3.6 CONCLUSION

The Mediterranean climate characteristics and specifically precipitation seasonality, main contributor according to PCA, plays an important role in the hydrological mechanisms of Mediterranean catchments and flow intermittence. A decision tree makes it possible to define, from distances to class kernels, if any place has a Mediterranean climate or not, and to which type of Mediterranean climate does it belong to, for present and future scenarios. On the other hand, the superposition of olive cultivation boundary as Mediterranean-specific physiographic index highlighted the utility and importance of physiographic-climatic coupled scenario models that could be extended to other Mediterranean physiographic or bio-climatic indices. The climatic classification and corresponding indices evolution under RCP scenarios helped in identifying the general climate change impact on Mediterranean seasonality that might uncover valuable findings about water balance, floods, and droughts for water sector stakeholders. Both ALADIN and CCLM scenarios showed an increase of the average seasonality and aridity indices affecting hydrologic regimes due to shorter humid seasons and earlier snowmelts. The results of this study are useful for future water resources and cultivation management policies to identify the most impacted zones and propose preventive and adaptative measures for a more resilient and sustainable region. This kind of classification might be reproduced at the global scale, using same or other region-specific climatic indices highlighting their physiographic characteristics and hydrological response.

"God Rivers Duel, A Mediterranean Epic"

Second encounter: Zeus helps Spercheios, Adonis attacked by a wild boar

ΠΟΤΑΜΙ ΕΝΑ	
Name	Ibrahim, Adonis
Country	Lebanon
Area	329 km^2
MAP	1450 mm
MAQ	1052 mm

ΠΟΤΑΜΙ ΔΥΟ	
Name	Spercheios
Country	Greece
Area	1592 km^2
MAP	701 mm
MAQ	575 mm

Climatic characteristics	
Climatic Class	CC3
I_S	0.99
$SP_{1.5}$	4
$P_{25\%}$	2.12
S_{Tm}	6
I_{Arid}	0.99
$T_{25\%}$	1.52
S_{PET}	5

Climatic characteristics	
Climatic Class	CC4
I_S	0.75
$SP_{1.5}$	2
$P_{25\%}$	1.36
S_{Tm}	6
I_{Arid}	1.26
$T_{25\%}$	1.56
S_{PET}	6

[This page was left intentionally blank]

CHAPTER 4. PHYSIOGRAPHIC CHARACTERISATION

Chapter summary

This chapter aims to highlight Mediterranean variability through the physiographic classification of all Mediterranean catchments based on physiographic indices of landform, landcover and soil indices. This classification should help in exposing the physioclimatic interaction expressed by microclimates, landcover distribution and variability. The proposed approach includes the use of Principal Component Analysis to reduce the number of indices to the most contributing and K-means classification to distribute them into classes. The number of classes was set to 10 according to the elbow method. This classification provided a unique overview on the physiography of Mediterranean catchments. When the physiographic features, and mainly landform were analysed with the local climatic features, a micro-climatic variability was found but shadowed by the macro climate homogeneity. This micro-climatic variability is the main reason behind natural landcover variability like different tree cover.

Complementary material to Chapter 4 was added in Appendix C

APPENDIX C1 Physiographic indices of the selected catchments

4.1 INTRODUCTION

In the previous chapter, we identified the main Mediterranean climatic characteristics, their spatial distribution and temporal evolution in case of climate change. In this chapter we will try to identify the main Mediterranean catchments physiographic characteristics and understand their diversity following the same approach used for climatic classification, PCA to reduce the number of physiographic characteristics and K-means clustering to classify the catchments based on the results of the PCA, then discuss their interaction with climatic features and role in the hydrological behaviour of Mediterranean catchments.

This chapter aims to understand the landscape contribution into the Mediterranean hydrology and highlight the physiographic variability through the classification of all Mediterranean catchments based on landform, landcover and soil indices. This classification should help in exposing the physioclimatic interaction expressed by microclimates, landcover distribution and variability. It shall help identifying the physiographic role in shaping Mediterranean hydrology and flow regimes which stand as one of the main research inquiries of the PUB, and help in the comprehension of the physiographic forcings on the variability of the Mediterranean hydrological processes (Schröder, 2006). Hence validating Eagleson's suggested idea that the biosphere, the climate, the hydrology, and the soil were in a synergistic waltz trying to reach a point of "ecological optimality" (Eagleson, 1978; Eagleson & Tellers, 1982).

Catchments physiographic characteristics and classification for hydrological purposes have been extensively discussed in literature where several have searched to understand hydrological fluxes and regimes by studying one or a combination of multiple physiographical features starting with Horton (1933) ideas on catchments capacity to store the infiltrated water depending on the soil and vegetation types. The slope-discharge relationships were quantitatively developed by Lane for the three types of streams braided, intermediate, and meandering streams (Lane, 1957). In their physically based model Beven and Kirkby (Beven & Kirkby, 1979) highlighted the major role that topography plays in the redistribution of moisture which hence influences the nature of runoff production, (Bras, 1999). Geomorphological properties and river network were also used for hydrological analysis, modelling and classification (Gaucherel et al., 2017). Remote sensing was introduced to hydrological modelling and classification in late 1970's by the Hydrologic Engineer Centre of the US Army Corps of Engineering (Cermak et al., 1979), more recently, the remote sensing indices like Soil-Adjusted Vegetation Index (SAVI), Leaf Area Index (LAI), Normalized Difference Moisture Index (NDMI), Normalized Difference Vegetation Index (NDVI), Forest Canopy Density model (FCD), snow cover, landuse and landcover, crop type derived information and other indices became popular to catchments classification to determine the similar hydrological properties (Jang et al., 2009; Choubin et al., 2017). Modern informatic tools, and big data have also contributed in the

advance of the classification such as Data driven tools, machine learning, artificial neural networks and fuzzy sets (Hall & Minns, 1999), (Praskievicz, 2018), Self-Organization Maps (SOM) (Di Prinzio et al., 2011; Boscarello et al., 2015).

Across the Mediterranean, similar physiographic traits could be easily observed like karstic features, dating since the Messinian period 5.96 - 5.33 Ma when sea level dropped dramatically (Krijgsman et al., 1999; Audra et al., 2004). Karst landscapes could be observed in Mount Lebanon, Syria, Turkish coast from Adana to Antalya, Balkans countries, centre of Italy, the French riviera and eastern Spain. (Chen et al., 2017). On the other hand, cultivated and managed areas cover 30% of the Mediterranean, and olive tree is considered one of its specific bioindicator that could be seen all over the region mainly because of the climate that is convenient for its cultivation, as olive reproductive cycle and flowering intensity is influenced by seasonal temperature and water availability (Moreno, 2014; Fraga et al., 2019).

Most of the physiographic characteristics remain unchanged for the time scale of the study like landform, geology and karst, but landcover is dynamic and affected by anthropogenic activities like cultivation, urbanisation and deforestation and its mapping is usually performed during one time-limited campaign causing a distortion with hydrometric data continuously measured. Another dynamic index is snow cover which is marked by climate change and climate variability and could have differed if it were possible to calculate for the whole period. These physiographic limitations are one main source of uncertainty; however, we assume they have a limited impact on the physiographic classification.

This chapter is structured into four sections; Section 4.1 introduction; Section 4.2 presents the physiographic classification approach based on PCA and K-means; Section 4.3 presents the results of physiographic classification for Type II catchments, between 100 km^2 and 3000 km^2 and then project it to Type I less than 100 km^2 and Type III above 3000 km^2; and Section 4.4 presents the discussion and conclusion.

4.2 METHODOLOGY

The proposed methodology consists of optimizing the number of physiographic indices using Principal Components Analysis (PCA) and classifying the set of catchments into 10 classes using K-means clustering technique. The PCA/K-means approach is widely applied to first reduce the dimensionality of datasets and keeping the most representing and uncorrelated variables and then classify the dataset according to the predetermined number of clusters k. An extensive mathematical description and demonstration of this method was detailed in Section 3.2.1.

The main physiographic characteristics were collected for all the Mediterranean catchments. The physiographic indices were then calculated, normalised, and standardised for the PCA/K-means application. 24 physiographic indices were considered for PCA optimization and divided into three groups summarised in CHAPTER 2 and repeated here in Table 4-1.

Group I: indices based on landform and topography mainly area A, Z_{Mean} and ZS_{Mean} describing snow cover mean altitude.

Group II: indices based on landcover like Cultivated and Managed Areas (CMA), TC_BDC and Karst P_{Karst}.

Group III: indices based on soil characteristics mainly the Topsoil Available Water Capacity T_AWC.

Table 4-1: Physiographic Indices description

GROUP	TYPE	INDICES	DESCRIPTION
I	LANDFORM	A (km^2)	Area of Catchment
		I_{Hypso}	Hypsometric index, ratio of Z_{Mean} and Z_{Med}
		LargEq (km)	Equivalent rectangle width
		LongEq (km)	Equivalent rectangle length
		P (km)	Catchment Perimeter
		S_A	Catchment Average Slope
		Tc (min)	Concentration time
		Z_{Max} (m)	Catchment Maximum Altitude
		Z_{Mean} (m)	Catchment Mean Altitude
		Z_{Med} (m)	Catchment Median Altitude
		Z_{Range} (m)	Catchment Altitude Range (Maximum - Minimum)
		ZS_{Mean} (m)	Mean Snow Cover altitude when it exceeds 1 month per year
II	LANDCOVER	BA	Bare Areas
		CMA	Cultivated and managed areas
		P_{Karst}	Percentage of Karst Cover
		SC_COD	Shrub Cover, closed-open, deciduous
		SHC	Sparse herbaceous or sparse shrub cover
		TC_BDC	Tree Cover, broadleaved, deciduous, closed
		TC_MLT	Tree Cover, mixed leaf type
		TC_NLE	Tree Cover, needle-leaved, evergreen
III	SOIL	Leptosols	Type of very shallow soil over hard rock or highly calcareous material
		Luvisols	Type of soil in temperate climates, generally fertile used for agriculture
		S_AWC (mm)	Sub soil Available Water Capacity
		T_AWC (mm)	Topsoil Available Water Capacity

The determination of the number of clusters in K-means beforehand is required, however the choice of k still poses a dilemma for any classification approach. Several methods have been tested in literature to determine the number of clusters; Milligan, (Milligan & Cooper, 1985) assessed 30 different procedures for determining the number of clusters for hierarchical clustering working as stopping rules. Kodinariya in his turn reviewed 6 methods for K-means clustering; rule of thumb, elbow method, cross validation, information criterion approach, information theoretic approach and cross validation. (Kodinariya & Makwana, 2013).

The elbow method is considered as one of the most applied methods for the determination of k, therefore it was adopted for the physiographic classification. This method exists upon the idea that one should choose a number of clusters so that adding another cluster doesn't give much better modelling of the data. (Bholowalia & Kumar, 2014). It consists of calculating the "cost" for each number of clusters k, where k increases by 1 at each step. The optimal number of clusters corresponds to when the cost drops dramatically creating an elbow on the chart cost = f(k). The sum of squared distances (SSD) could be employed as the cost function. The main problem with elbow method is when the elbow cannot be clearly identified, in other words, the cost does not drop dramatically. In the present physiographic classification, the cost drops rapidly until k =10 and then goes very slowly after that as seen in Figure 4-1, hence the number of clusters needed for the physiographic classification of Mediterranean catchments is 10.

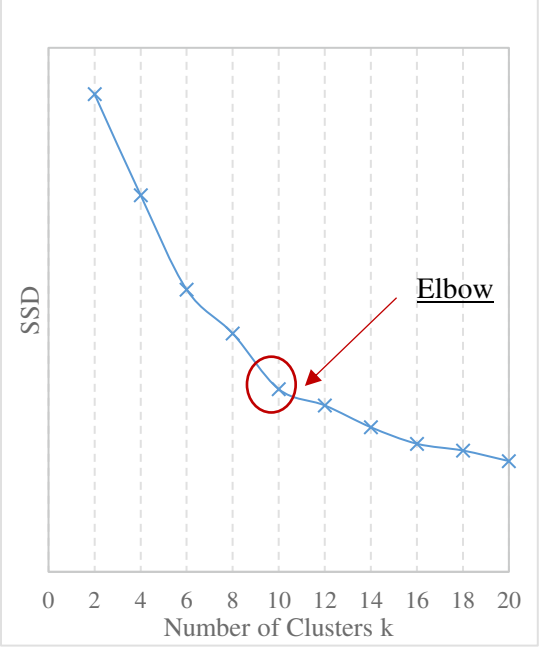

Figure 4-1: Elbow method chart for the determination of the number of clusters k for the physiographic classification

4.3 RESULTS

4.3.1 Physiographic indices selection using PCA

The PCA/K-means resulted with 10 different types of catchments which will be tested for inter-class and intra-class hydrological similarity in CHAPTER 6.

The number of indices was first reduced based on the correlation matrix by eliminating those strongly correlated in order not to overemphasize their contribution. In total 17 indices were kept for PCA.

- P, LargEq and LongEq are strongly correlated with A, (0.92; 0.91; 0.87), A was kept.
- Z_{Med}, Z_{Max}, Z_{Range} are strongly correlated with Z_{Mean}, (0.98; 0.88; 0.88), Z_{Mean} was kept.
- S_AWC is correlated with T_AWC (0.76); Leptosols is inversely correlated with S_AWC (-0.74) and T_AWC (-0.63); T_AWC and Leptosols were kept for their significance in runoff and role in landcover determination.

The PCA reduced the number of physiographic indices to 13 showing A, Z_{Mean}, ZS_{Mean}, I_{Hypso}, P_{Karst}, T_AWC, Leptosols, and Landcover types, Tree Cover Mixed Leaf Type (TC_MLT), Tree Cover Broadleaved Closed Deciduous (TC_BCD), Shrub Cover Closed-Open Deciduous (SC_COD), Bare Areas (BA), Sparse Herbaceous Cover (SHC) and Cultivated and Managed Areas (CMA) as the most contributing indices in the first 6 components with 70% of total variance explained (see Figure 4-2). The other 4 indices were eliminated as they have shown little interest in the classification or low contribution to the extracted principle components concentration time (Tc), catchment slope (S_A), Tree cover needle leaved (TC_NLE) and Luvisols. Table 4-2 below summarizes the 55 selected catchments physiographic indices.

Table 4-2: Statistical summaries of the 55 selected catchments physiographic indices

	A (km^2)	Z_{Mean} (m)	ZS_{Mean} (m)	I_{Hypso}	P_{Karst} (%)	T_AWC (mm)	Leptosols (%)	TC_MLT (%)	SC_COD (%)	BA (%)	CMA (%)	SHC (%)	TC_BCD (%)
Minimum	77.0	93	-	-0.5	0.0	22.2	10.0	0.3	0.1	0.1	0.4	0.2	0.3
Mean	891.7	586	611.5	-0.1	46.9	48.3	39.8	10.0	21.4	1.3	30.1	13.7	20.0
Maximum	3125.0	1572	2092.0	0.2	100.0	56.1	90.0	36.5	94.6	3.6	86.9	73.0	96.8
Median	634.0	506	0.0	-0.1	42.9	49.3	37.5	6.4	7.7	1.4	22.2	4.4	12.3

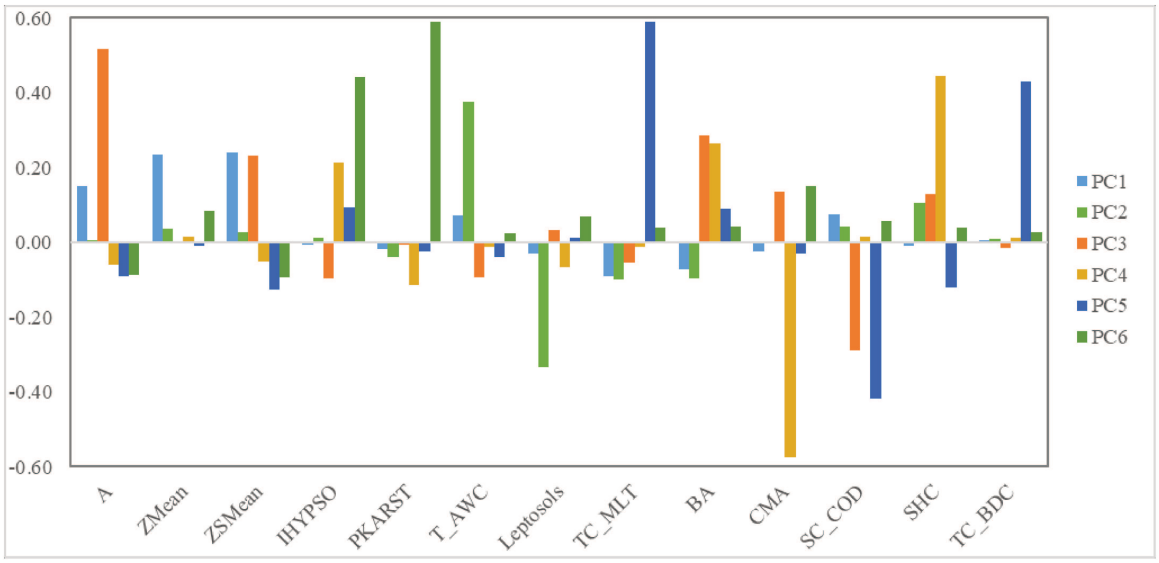

Figure 4-2: Standardised coefficients for the first 6 Principal Components (PC1 to PC6) of the Physiographic Indices

4.3.2 K-means classification

The K-means classification highlighted the inter-class variability of physiographic characteristics with kernels' indices showing mixed distribution in Table 4-3 and Figure 4-3 along with random geographical distribution across the study area in Figure 4-4.

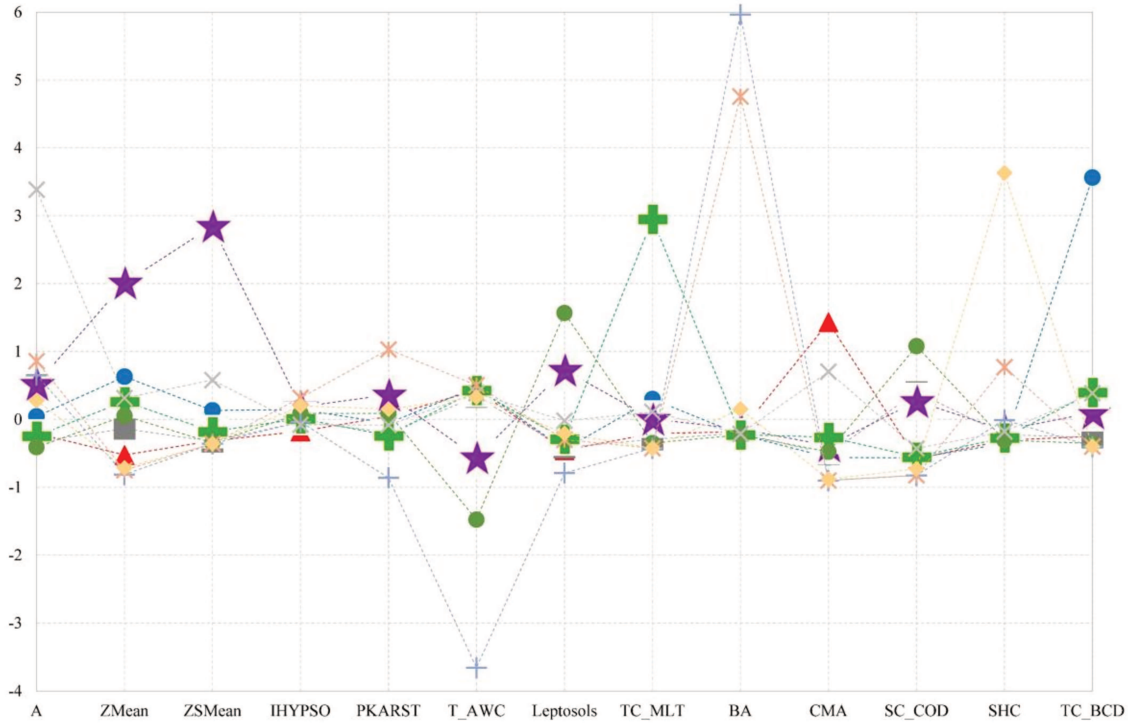

Figure 4-3: Physiographic classes kernels

Average area A ranges between 180 and 838 km^2 except for PC9 representing wide cultivated catchments of 2146 km^2 average area. Landform indices Z_{Mean}, ZS_{Mean} and I_{Hypso} indicate morphological contribution to the classification, where Z_{Mean} varying between 107 and 871m. All classes except class 7 include catchments with karstic features but with different rates ranging between 29% and 80%. Leptosols presence is associated to low T_AWC and SC_COD, in this classification either Leptosols are absent, lower than 20% and T_AWC around 50 mm or Leptosols are present and T_AWC is low, case of PC4 and PC8. Landcover vary with little overlap from class to class, in ex. cultivated catchment show little tree or shrub cover, bare areas do not show any tree cover.

Table 4-3: Mediterranean type II catchments physiographic classification kernel indices original values, see Figure 4-4 for classified catchments geographical distribution. The number of selected catchments from each class is mentioned between ().

CLASS	No	REGION	DESCRIPTION	A (km^2)	Z_{Mean} (m)	ZS_{Mean} (m)	P_{KARST} (%)	T_AWC (mm)	LpSols (%)	TC_MLT(%)	BA (%)	CMA (%)	SC_COD (%)	SHC (%)	TC_BCD (%)
PC1	306 (10)	North West	Small, Highly Cultivated and Managed at 70%	286	184	-	40%	50.8	11%	2%	1%	71%	7%	1%	2%
PC2	62 (3)	South West and Italy	Broadleaved Tree Covered at 60%	415	497	224	36%	51.3	12%	6%	0%	10%	7%	0%	60%
PC3	351 (10)	Mediterranean	No specific overwhelming influence	221	289	-	30%	49.6	13%	1%	1%	12%	34%	3%	2%
PC4	105 (11)	North and East	High altitude with Snow and Karst influence	662	871	1462	53%	38.6	51%	3%	1%	16%	30%	4%	8%
PC5	88 (9)	North West	Mixed leaf Tree Covered 26 %	266	398	-	29%	50.8	17%	26%	0%	19%	8%	2%	12%
PC6	190 (4)	East and Libya	Shrub Covered at 52 %, low T_AWC and Leptosols at 79%	181	341	-	42%	27.4	79%	1%	0%	13%	52%	1%	1%
PC7	14 (0)	Sinai	Desertic	730	107	-	3%	0.8	0%	0%	87%	0%	0%	8%	0%
PC8	29 (0)	Egypt, Libya	Desertic	838	124	-	80%	51.6	16%	0%	70%	0%	0%	25%	0%
PC9	49 (8)	Mediterranean	Wide and Highly Cultivated and Managed at 50% with Snow Influence	2146	411	428	35%	50.3	26%	4%	0%	49%	11%	4%	12%
PC10	76 (0)	Egypt Libya Tunisia	Semi Desertic, Sparse Herbaceous or Shrub Covered at 87%	537	133	-	44%	49.5	19%	0%	5%	1%	3%	87%	0%

PC1 and PC9 (see Figure 4-5 and Figure 4-13) include highly cultivated and managed catchments and are dominant in North Mediterranean countries and Italy where lowlands and wide fields are suitable for agricultural activities. It is worth noting that Italian plains have undergone an important land improvement activities for wheat and corn cultivation, mainly in the 16th century marking an important anthropogenic interference, with the available means they disposed back then (Braudel, 1949).

PC2 (see Figure 4-6) are characterised with broadleaved trees forests and preferred South Western Mediterranean and Italy where high T_AWC and low seasonality reigns.

PC3 (see Figure 4-7) has not shown any dominating characteristic, however, they might hold a potential for agriculture as they share same soil characteristics as PC1.

PC4 (see Figure 4-8) are characterised by high landforms that provoke orographic precipitations and snow fall if exposed to cold fronts and elevated enough. It is highly probable that many karstic springs emerge in these catchments which contribute into summer flows showing a specific hydrological regime.

PC5 (see Figure 4-9) mixed leaved tree forests catchments are mostly present in North Western Mediterranean countries, without any bare areas and still unmanaged. These catchments are very interesting to follow up in the context of global change as they represent the old Mediterranean physiographical status.

PC6 (see Figure 4-10) are widely present in the Eastern Mediterranean region and is characterised by low T_AWC which normally conditions natural landcover. It was deduced that in leptosols, where T_AWC is low, only shrubs and needle leaved trees grow if exposed to high seasonality.

PC7, PC8 and PC10 are characterised by low landforms that have little contribution to precipitation genesis which permit North African desertic influence on coastal areas through low corridors preventing any vegetation except for sparse shrubs or herbaceous covers. PC7 (see Figure 4-11) is limited to Sinaii desert with very low T_AWC, PC8 (see Figure 4-12) desertic catchments with 70% of Bare Areas and PC10 (see Figure 4-14) semi desertic catchments covered by shrubs and herbs at 87%. Both PC8 and PC10 are located between Egypt, Libya, and Tunisia.

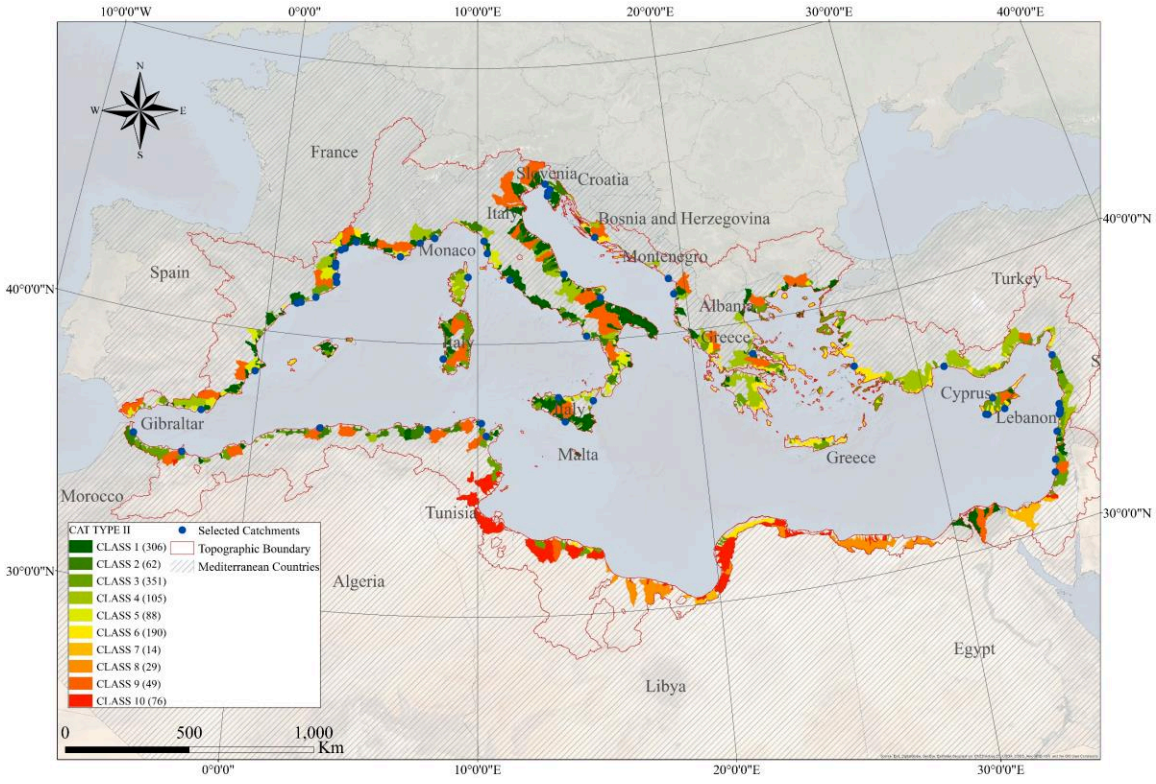

Figure 4-4: Geographical distribution of Mediterranean type II catchments (between 100 and 3000 km2) physiographic classes.

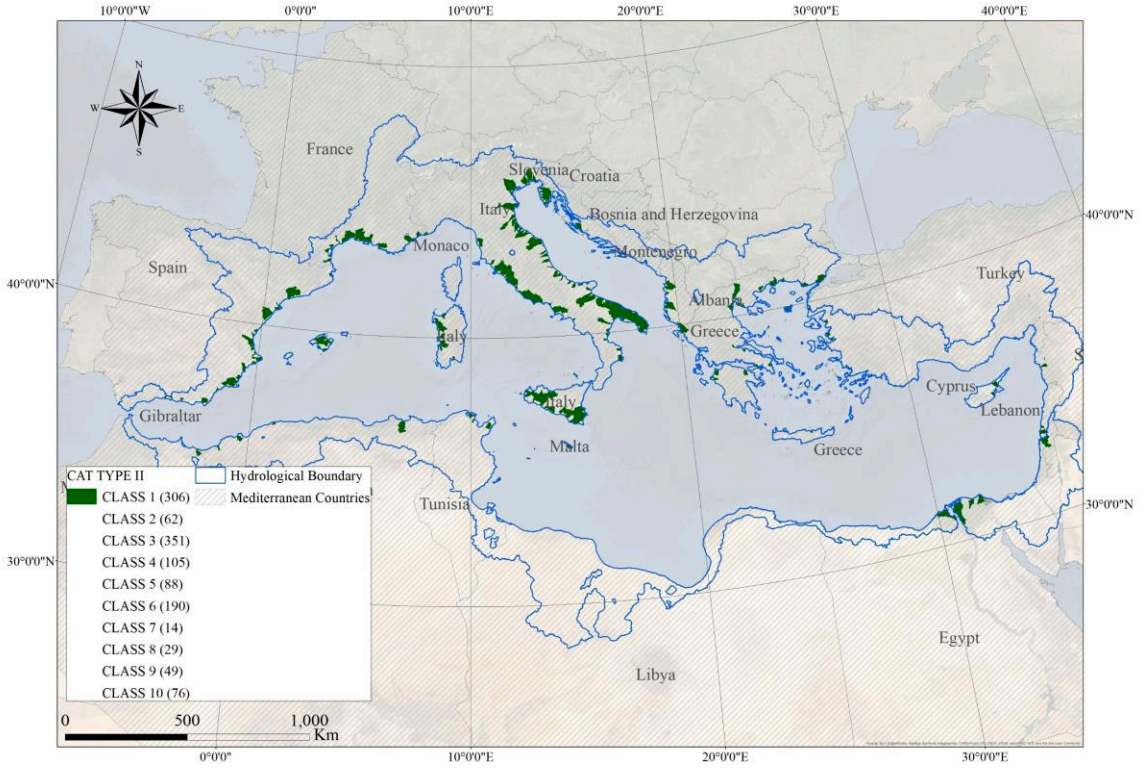

Figure 4-5: Geographical distribution of PC1 small, highly cultivated and managed at 70% Mediterranean type II catchments mostly in North Western region .

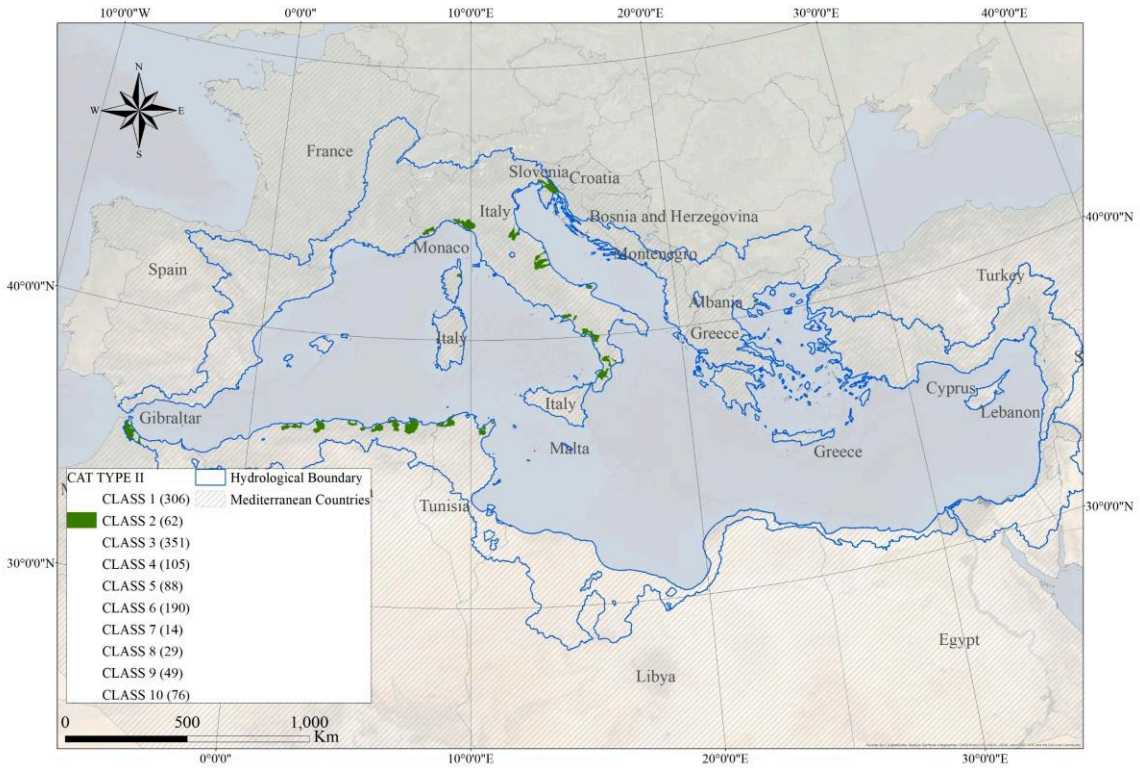

Figure 4-6: Geographical distribution of PC2 broadleaved tree covered at 60% Mediterranean type II catchments mostly present in South West and Italy.

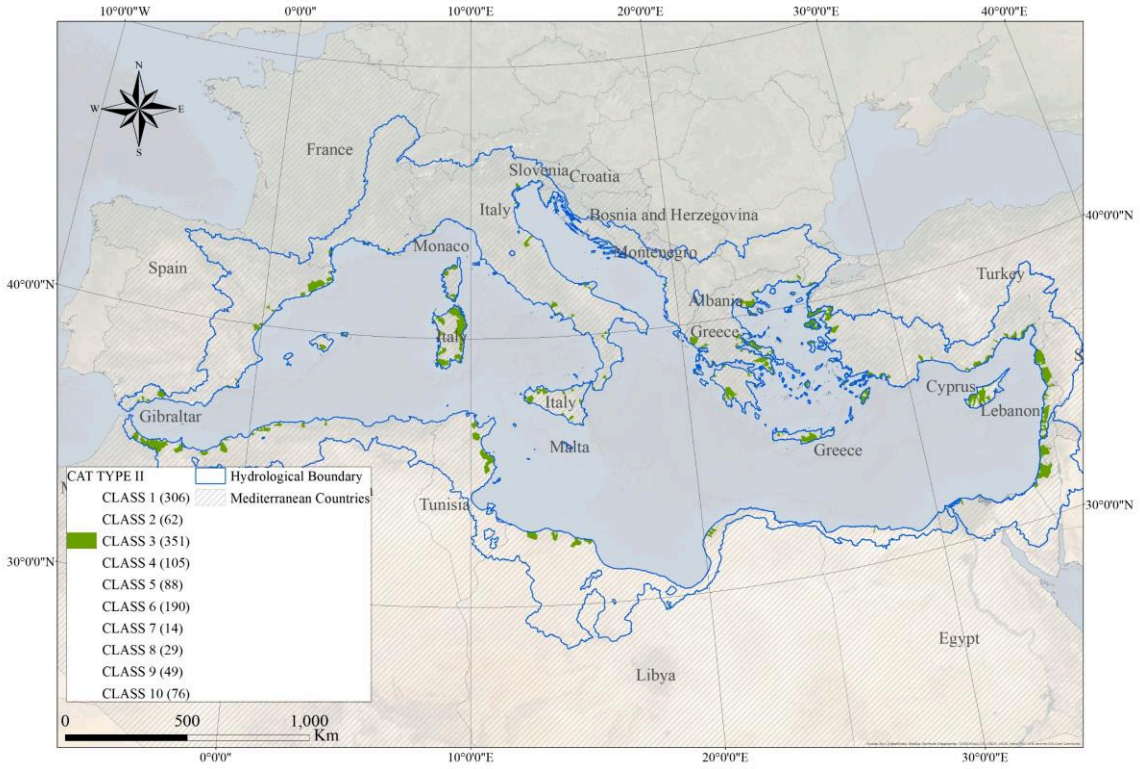

Figure 4-7: Geographical distribution of PC3 without a specific overwhelming influence Mediterranean type II catchments.

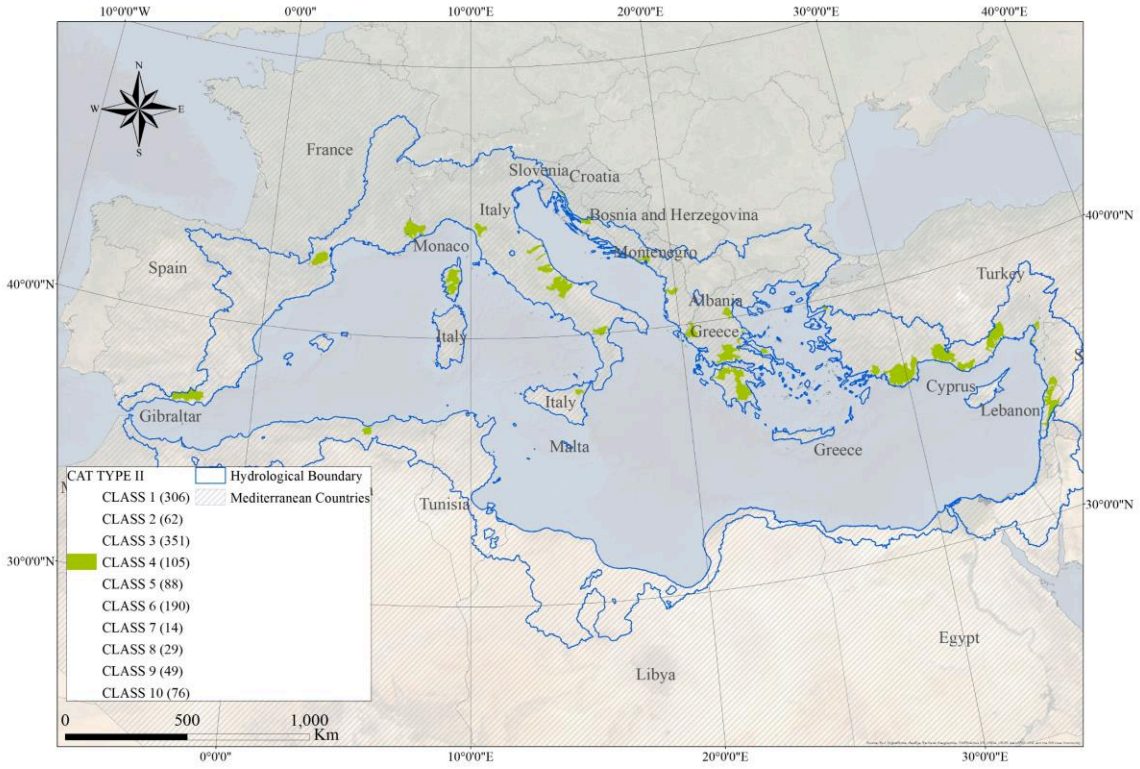

Figure 4-8: Geographical distribution of PC4 high altitude with Snow and Karst influence Mediterranean type II catchments mostly in North and Eastern region.

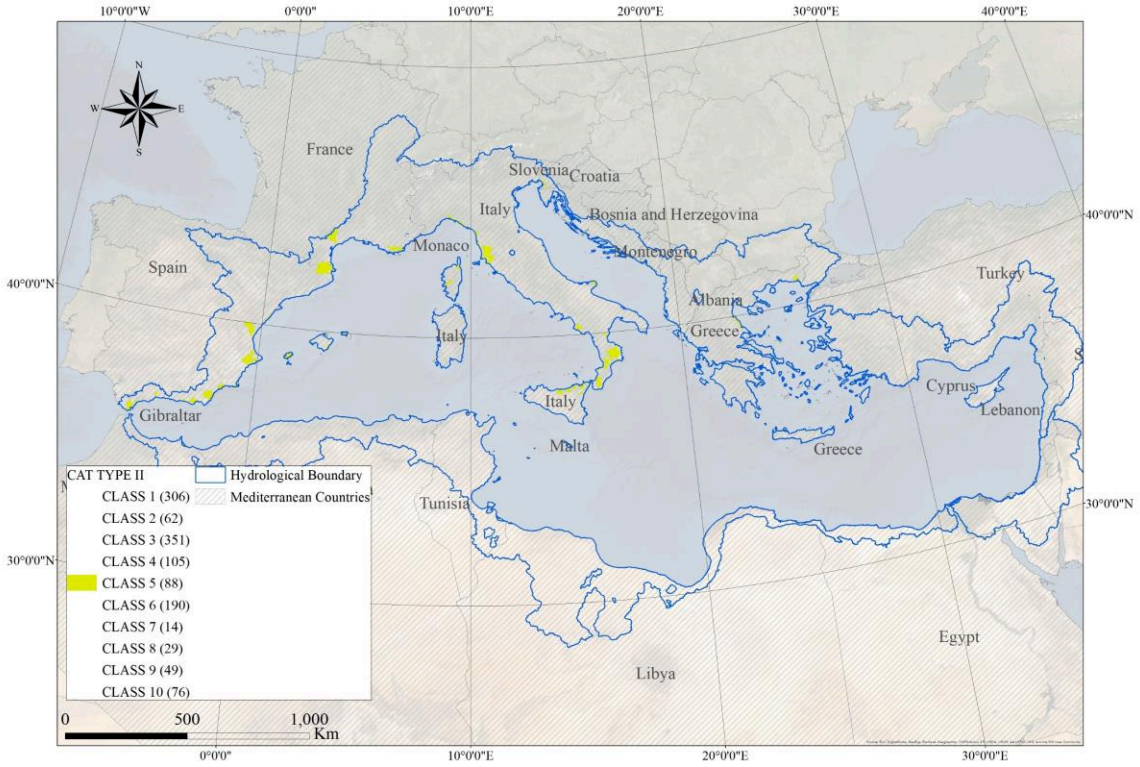

Figure 4-9: Geographical distribution of PC5 mixed leaf tree covered 26 % Mediterranean type II catchments mostly in North West.

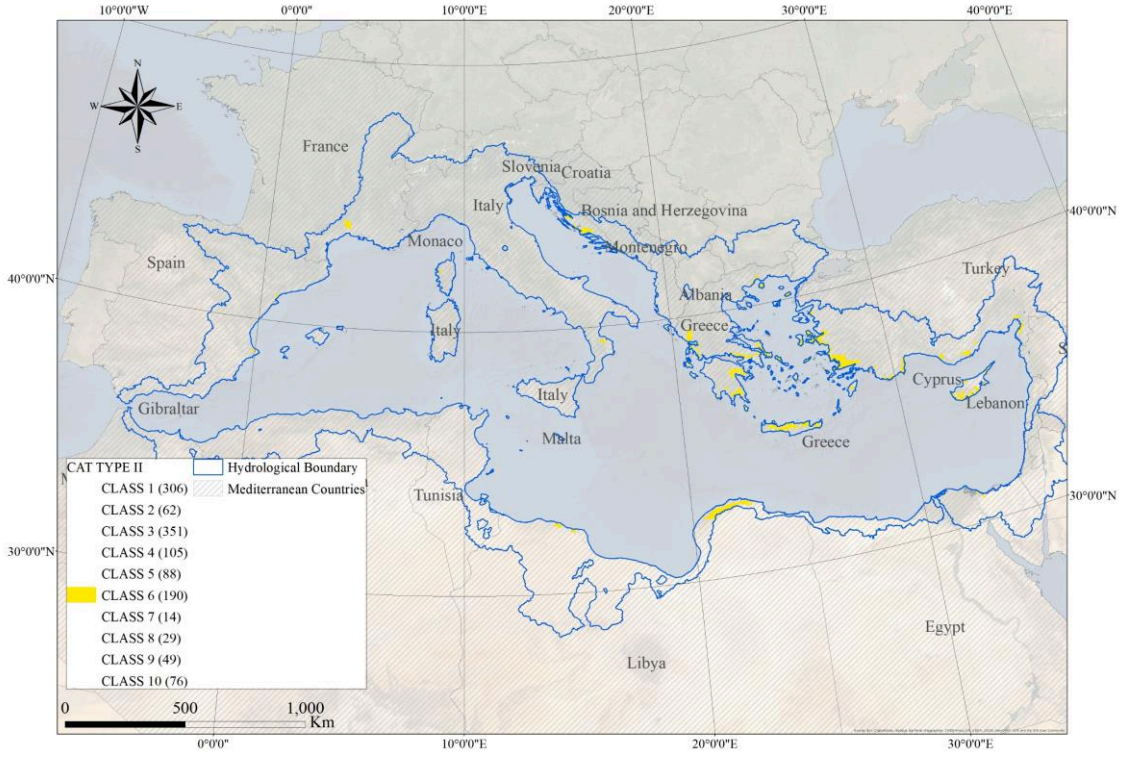

Figure 4-10: Geographical distribution of PC6 Shrub Covered at 52 % low T_AWC and Leptosols at 79% Mediterranean type II catchments mostly in East and Libya.

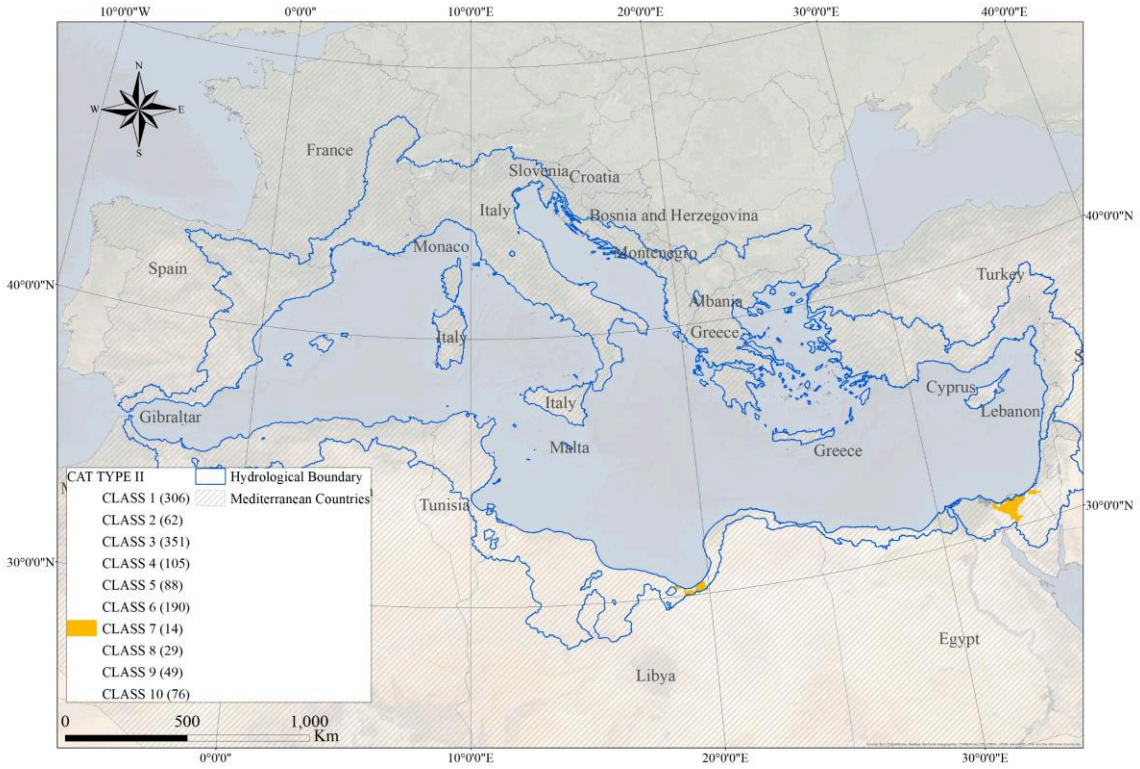

Figure 4-11: Geographical distribution of PC7 desertic Mediterranean type II catchments in Sinai.

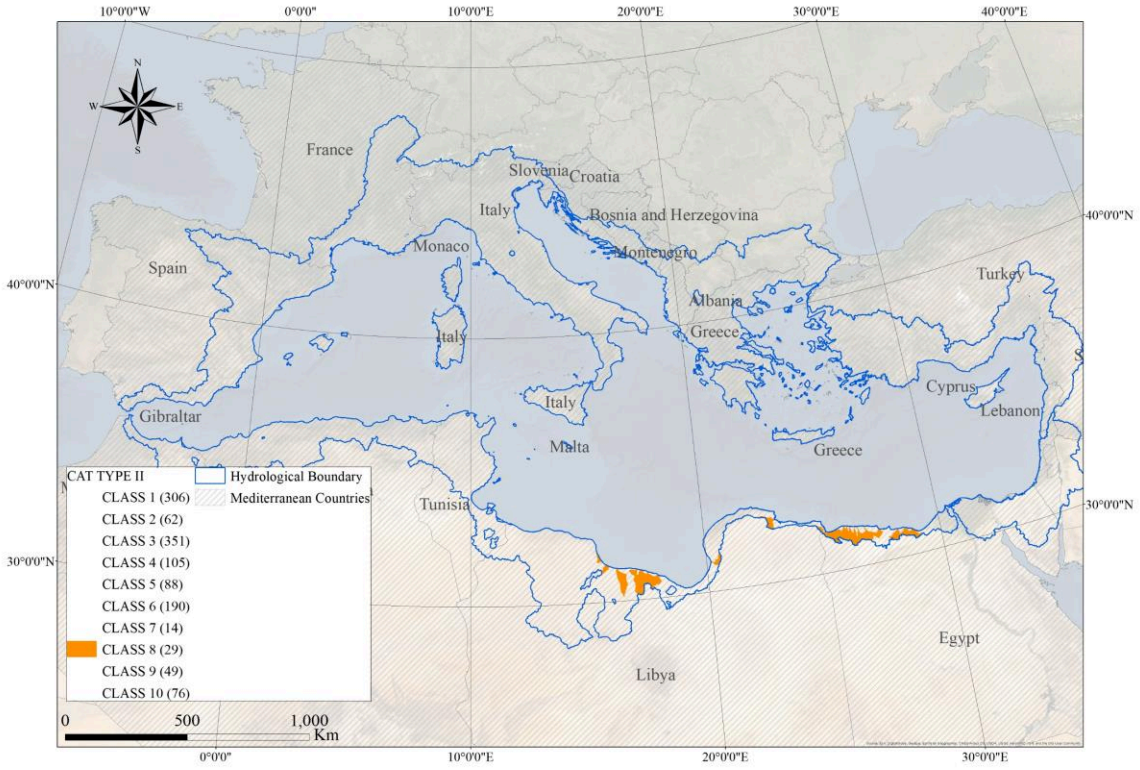

Figure 4-12: Geographical distribution of PC8 Desertic Mediterranean type II catchments in Egypt, Libya.

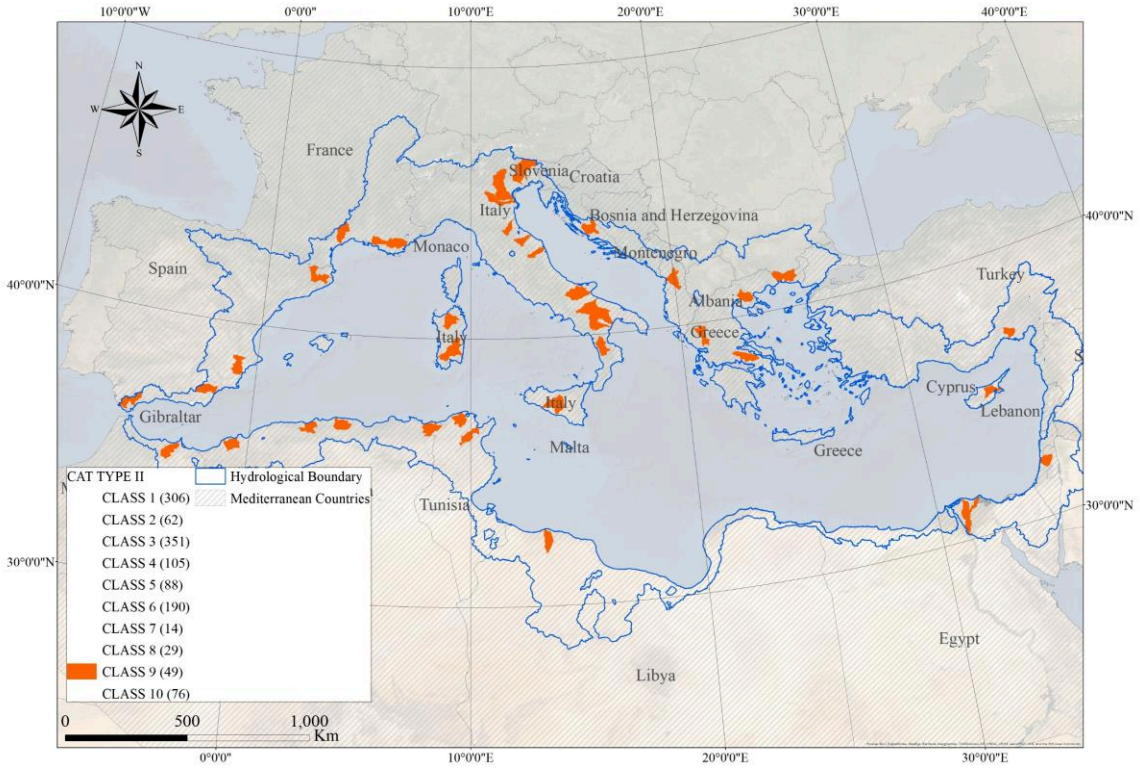

Figure 4-13: Geographical distribution of PC9 of wide and highly cultivated and managed at 50% with Snow Influence Mediterranean type II catchments.

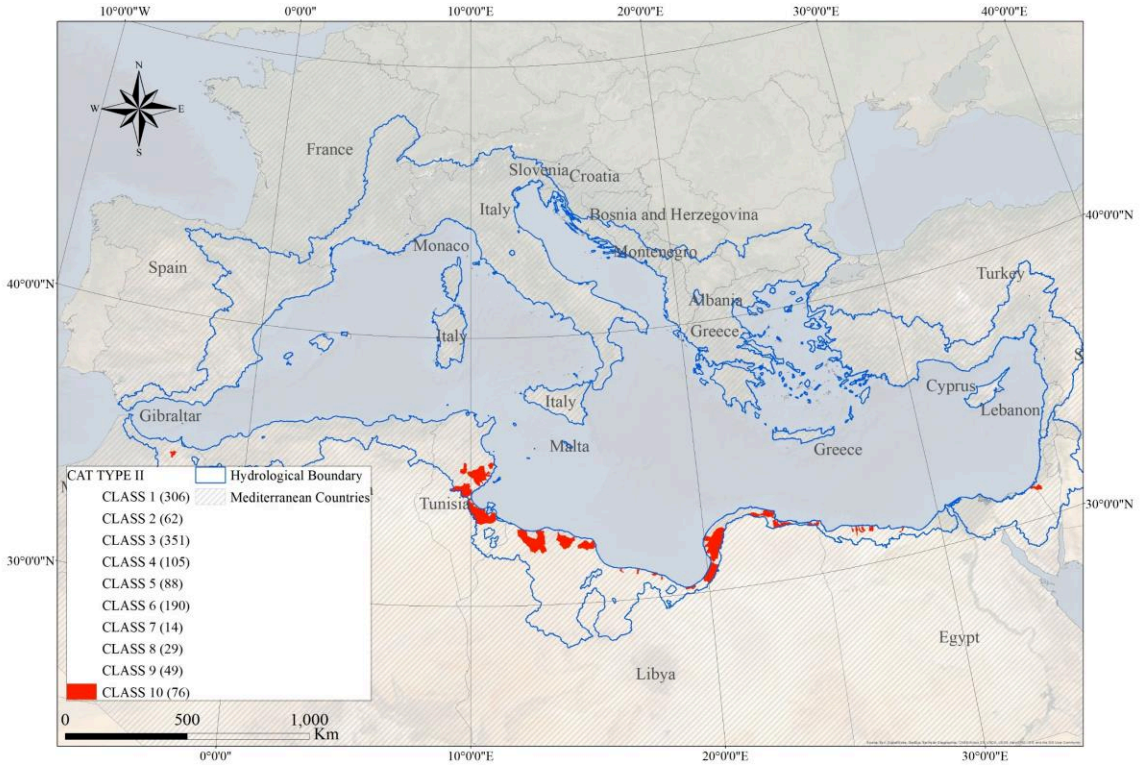

Figure 4-14: Geographical distribution of physiographic class 10 Semi Desertic, Sparse Herbaceous or Shrub Covered at 87% Mediterranean type II catchments Egypt Libya Tunisia.

4.3.3 Classification of type I & III catchments

To complete the physiographic map of Mediterranean catchments, the Euclidian distance was calculated for type I & III catchments to classes kernels of type II catchments. Type I and III catchments were then classified according to their nearest kernel. It is assumed that this method will yield a better homogeneity with type II classification as a separate K-means classification for type I and type III will generate new classes which kernels differ from the ones obtained from the type II classification. However, to validate this method, the K-means classification was carried out on the 2333 type I catchments and yielded 86% accuracy in comparison to their classes according to distances to Type II Kernels.

This regionalisation appeared spatially compatible with the original classification (see Figure 4-15) where no major modification was observed, in ex. Turkish, Greek and Balkans catchments joined PC4, Sinai catchments joined PC7, Libyan and Egyptian wide desertic catchments joined PC8, highly cultivated & managed catchments with Snow Influence joined PC9.

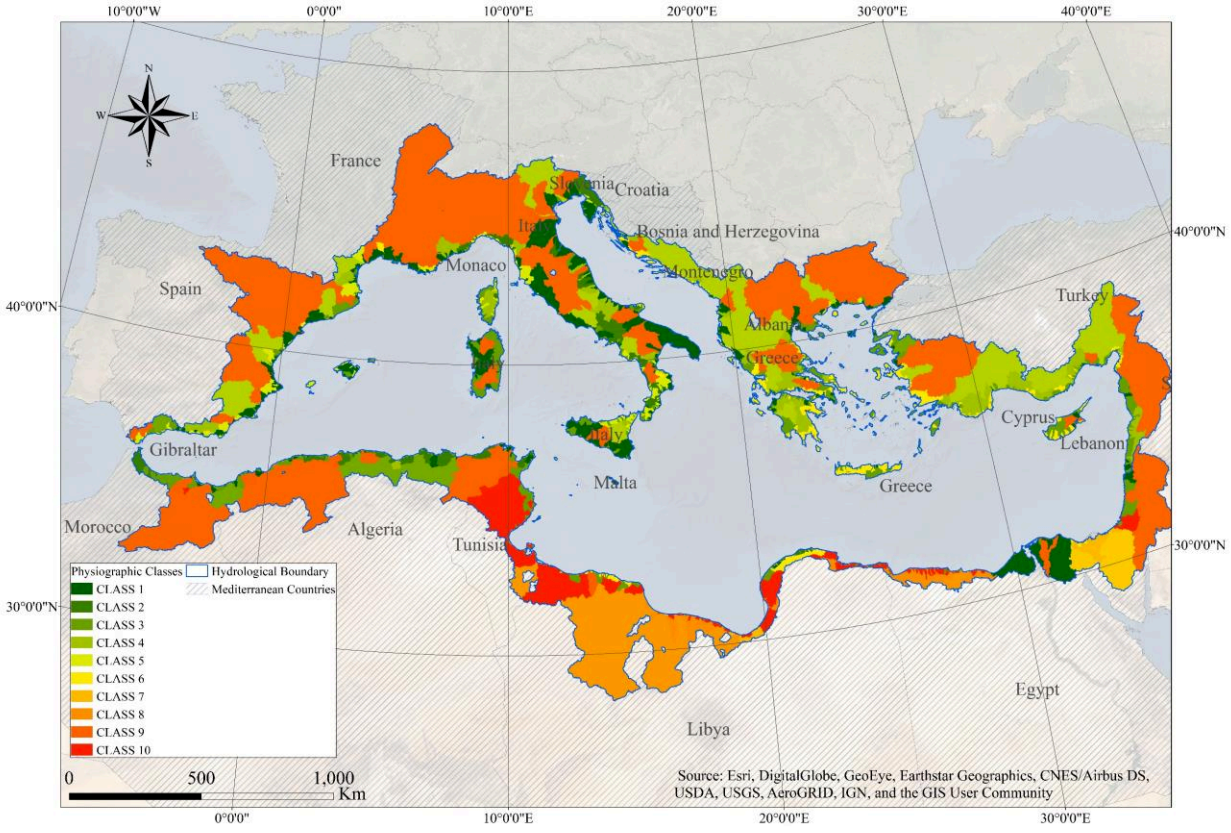

Figure 4-15: Physiographic classification of all Mediterranean type I, II and III catchments.

4.4 CONCLUSION

A physiographic database was developed for the Mediterranean region and included different maps to extract all landform indices, snow cover, geology, lithology, landcover, soil and karst. The main constraint consisted of the spatial spread and the work on a very wide and diversified area. It is possible to add maps and indicators relevant to society such as population density maps, touristic flows but they are very dynamic which increases the uncertainty. Therefore, the societal indicator was limited to the Cultivated and Managed Areas within landcover maps, being less dynamic and more accurate. Relying on PCA and K-means, it was possible to identify 10 Mediterranean classes according to their physiographic indices highlighting the existence of some homogeneous regions with similar descriptions despite the general variability.

The landform impact is widely observable across the Mediterranean, like Andarax catchment located in southern Spain in the shade of Sierra Nevada mountains to the Mediterranean side making it one of the most arid regions in Spain with MAP = 240 mm. Another example is “Jabal el Akhdar” or “green mountain” the only green and elevated spot between Alexandria and Tunis reaching a maximum altitude of 875m. The “green mountain” creates a natural boundary between Mediterranean Sea and Libyan desert, receiving more precipitation than adjacent catchments, making it more homogeneous with PC6, while adjacent lower PC8 catchments have dominant bare lands, lacking tree, and shrub cover. Anthropogenic activity has played an important role in shaping Mediterranean catchments and related hydrological regimes as 31% of its area is highly cultivated and managed, (PC1 and PC9). This human interference has disrupted the Mediterranean continuous landscape and contributed to its diversity. However, some continuity could still be observable where human activity was limited due to weather condition (Egypt, Libya) PC7, PC8 and PC10; or landform and geological condition, difficult and inconvenient for cultivation, case of PC6.

This classification provided a unique overview on the physiography of Mediterranean catchments, and when physiographic features, mainly landform, were analysed with the local climatic features, a micro-climatic variability was deduced but shadowed by the macro climate homogeneity. This micro-climatic variability is the main reason behind natural landcover variability between tree cover (needle leaved, broadleaved, and mixed leaved), shrubs and herbaceous cover. As for the anthropogenic impact, with Cultivated and Managed Areas already covering 30%, the Mediterranean still hold a potential for agriculture or management expansion if water resources allowed. This potential shall ease the stress on focused areas and redistribute the resources, hence the importance of pursuing a hydrological homogeneity and regionalisation analysis and assess the hydrological potential of the main classes. The identified climatic and physiographic homogeneity and variability across the Mediterranean shall be tested to identify any hydrological homogeneity or variability in CHAPTER 5 and CHAPTER 6.

"God Rivers Duel, A Mediterranean Epic"

Third encounter: Gaia rescue Adonis, Achilles did not keep his promise to Spercheios

ΠΟΤΑΜΙ ΕΝΑ	
Name	Ibrahim, Adonis
Country	Lebanon
Area	329 km^2
MAP	1450 mm
MAQ	1052 mm

ΠΟΤΑΜΙ ΔΥΟ	
Name	Spercheios
Country	Greece
Area	1592 km^2
MAP	701 mm
MAQ	575 mm

Physiographic characteristics	
Physiographic Class	PC4
Z_{Mean}	1572 m
ZS_{Mean}	1928 m
I_{Hypso}	0.13
P_{Karst}	100%
T_AWC	34.2 mm
Leptosols	0.35
TC_MLT	0%
SC_COD	47%
BA	1.5%
CMA	0%
SHC	48.4%
TC_BDC	0%

Physiographic characteristics	
Physiographic Class	PC4
Z_{Mean}	714 m
ZS_{Mean}	1344 m
I_{Hypso}	-0.1
P_{Karst}	58%
T_AWC	42.1 mm
Leptosols	0.35
TC_MLT	9%
SC_COD	4%
BA	0%
CMA	17%
SHC	0%
TC_BDC	10%

[This page was left intentionally blank]

CHAPTER 5. HYDROLOGICAL CHARACTERISATION

Chapter summary

This chapter characterises the Mediterranean hydrological response through the annual water balance analysis of the 55 selected catchments. We studied the flow regimes of selected catchments according to Haines (1988) and the different water balance functional models as advanced by Budyko (1974), the water balance two stage partitioning model of L'vovich (1979), the conceptual model of Ponce and Shetty (1995a, 1995b) and its nondimensional formulation by Sivapalan et al., (2011). In addition, we analysed the total runoff and groundwater runoff coefficients and gains to annual precipitation, a notion advanced by Ponce and Shetty (1995b) and then elaborated as a sensitivity to precipitation called elasticity by Harman (2011). The water balance analysis highlighted the Mediterranean trend following the general climatic setting from the wet Northern region to the arid Southern region; it also showed hydrological homogeneity for specific physiographic classes like PC4 mountainous karstic and snow influenced catchments which yield the highest baseflows and runoff coefficients, especially those located in CC3 regions however they are the least sensitive to the humidity index P/Ep which make their hydrological behaviour very interesting to study under RCP 4.5 or RCP 8.5 climate change scenarios.

Complementary material to Chapter 5 was added in Appendix D

APPENDIX D1 Flow regime types for all catchments according to the classification of Haines (1988)

APPENDIX D2 Summary table of all water balance parameters

APPENDIX D3 The water balance partitioning model of L'vovich and fitting curves of Ponce & Shetty

APPENDIX D4 The nondimensional water balance curves of Sivapalan

5.1 INTRODUCTION

In the previous CHAPTER 3 and CHAPTER 4, we carried out a climatic and physiographic characterisation of Mediterranean catchments in the aim of discovering the forcing factors of the hydrological behaviour as rivers regimes are the direct response of the regional and local climate and corresponding landscape. We mainly found that climate presents a continuous and gradual evolution from the most arid and seasonal region in the South to the most humid and least seasonal region in the North and was classified into 5 climatic classes (see Figure 3-5). We also found that Mediterranean landscape presents a rich and wide variability at the catchment scale showing different natural landcover, enhanced by micro-climatic characteristics and by anthropogenic activity like cultivated and managed areas, urban areas. The landscape was classified into 10 physiographic classes (see Figure 4-4).

The general approach to characterise the hydrological behaviour of any catchment is to study its long term flow regime and water balance. Hence, to characterise the Mediterranean region, this approach was expanded to cover the Mediterranean where we collected long enough rainfall and runoff series for 55 catchments across 15 countries. Hydroclimatic data were obtained from several hydrological services of different countries, measured by different instruments and data was processed using different methodologies. These uncertainties have a serious impact on runoff data, hydroclimatic indices and consequently the similarity analysis but somehow limited effect on the physiographic classification. An uncertainty analysis was not considered in the scope of this thesis as here we present a methodology to define catchments variability and homogeneity at regional scale, nevertheless they deserve to be treated separately and extensively in light of the previous studies that tackled the indices uncertainty (Westerberg & McMillan, 2015; Westerberg et al., 2016; McMillan et al., 2018)

We first studied the flow regimes of selected catchments according to Haines (1988) as detailed in Section 1.4.3.1. to verify if Mediterranean rivers fall into same regime class. Second, we characterised the Mediterranean hydrological response through different water balance functional models as advanced by Budyko (1974), L'vovich (1979) and elaborated by Ponce & Shetty (1995a, 1995b) and Sivapalan et al., (2011) as detailed in Section 1.3 and briefed in Section 5.2 of this chapter. The functional models are best fitted for our approach as they provide a clear and simple way to characterise each water balance component and their interaction while giving the ability to discover their time-space, interannual and intra annual variability.

We also defined from the functional model results the total runoff and groundwater runoff gains as the ratio of the runoff coefficients to annual precipitation, a notion advanced by Ponce and Shetty (1995b) and elaborated as a sensitivity to precipitation and called it elasticity by Harman (2011) detailed in Section 1.3.4

and Section 5.2. The analysis of the runoff gains and elasticity across the Mediterranean and through the climatic and physiographic classes characterised furthermore the hydrological behaviour similarity and variability, and the competition between the water balance components of the Mediterranean catchments.

These approaches mainly adopt the “Time for time” and “Space for time” substitution analogies (also adopted by Budyko (1974) and L’vovich (1979) where the analysis of the hydrological behaviour of a set of catchments explains the potential behavioural change that might occur in time, case of CC5 translation to CC4 and CC3 as discussed in CHAPTER 3, and in space, case of physiographic change from forests to cultivated catchments PC3 to PC1 or PC9, discussed in CHAPTER 4.

This chapter is structured into four sections; Section 5.1 introduction; Section 5.2 the characterisation methodology; Section 5.3 the classification of the flow regimes according to Haines (1988); Section 5.4 the extensive water balance analysis for each catchment based on the functional approaches and Section 5.5 conclusion.

5.2 METHODOLOGY

5.2.1 Flow regimes classification

The flow regimes of the 55 selected catchments were classified according to the approach presented by Haines et al. (1988). For each river, the average monthly runoff was calculated and converted into the ratio from annual runoff, then ranked from June to May as recommended for the North Hemisphere, classification algorithms were then applied. These algorithms consider the monthly rank (J), the highest monthly ratio (Lj), and the 3 highest months ratio (Tj) in addition to the lowest monthly average flow (S). The different regime charts are presented in Section 5.3.

5.2.2 Functional modelling

The slow flow U (also called baseflow or groundwater runoff) and quick flow S (also called fast flow or surface runoff) were extracted for the 55 selected catchments based on the single-parameter separation method of Lyne and Hollick (1979) (See Section 1.3.5). Following the baseflow separation, annual water balance was calculated for each catchment based on the two stage proportional model presented previously in CHAPTER 1 (L'vovich, 1979). In the first stage, the precipitation P is divided into two components, quick flow S and wetting of the catchment W. In the second stage, the wetting W was divided into the slow flow U and energy-dependent vaporisation component V (also called Evapotranspiration). As this formulation neglects the storage carryover from year to year, the vaporisation component V, includes this

storage which for some catchments, like Assi in Lebanon, is not negligible, hence affecting the parameters values.

We were interested next in fitting the analytical expression from Ponce and Shetty (1995a) on L'vovich charts and the estimation of the different water balance parameters; potential wetting W_p, potential vaporisation V_p, quick flow coefficient λ_s and slow flow coefficient λ_u. For the first partitioning stage S = f (P) and W = f (P), the curve fitting adjustment was made by varying both W_p and λ_s to minimize the Root Mean Squared Error (RMSE) of the differences between the quick flow S, extracted from the flow separation process as per L'vovich and the one calculated by the model of Ponce and Shetty (1995a). This fitting was repeated for the second partitioning stage U = f (W) and V = f (W) to estimate the optimal values of V_p and λ_u. The values of W_p and V_p for the selected catchments showed a wide variability ranging from 100 to 80000 mm. The different models with their main equations are summarised in Table 5-1.

Table 5-1: List of the different water balance functional models applied in this study.

Water balance model	Author, Year	Equation
The heat and water balance reference model	Budyko, 1974	$E = f(P, E_p)$
The empirical water balance partitioning model	L'vovich, 1979	$P = S + W$; $W = U + V$
The conceptual water balance model	Ponce et Shetty, 1995a	$S = \frac{(P-\lambda_s W_p)^2}{P+(1-2\lambda_s)W_p}$; $U = \frac{(W-\lambda_u V_p)^2}{W+(1-2\lambda_u)V_p}$;
The nondimensional water balance model	Sivapalan, 2011	$S^* = \frac{S}{P-\lambda_s W_p}$; $W^* = \frac{W-\lambda_s W_p}{P-\lambda_s W_p}$;

5.2.3 Runoff gains and elasticity

To compare and discuss the results with previous works, the runoff and baseflow gains K'_r and K'_u were defined for each catchment as the ratio of the runoff and baseflow coefficients K_r and K_u to the precipitation. The runoff gain $K'_r = \frac{K_r}{P}$ and the baseflow gain $K'_u = \frac{K_u}{P}$. Not to mistaken K_r the runoff coefficient with the water balance metric runoff fraction K_R defined by Sivapalan (2011).

In reference to the hypothesis advanced by Ponce and Shetty (1995b) that peak gain corresponds to the runoff threshold, the total runoff threshold precipitation (P_{rti} and P_{rt}) and baseflow threshold precipitation (P_{uti} and P_{ut}) was estimated for the selected catchments and for each climatic or physiographic class (i) corresponding to the catchment that obtained the highest runoff gain (K'_{rp} and K'_{rp1}) and baseflow gain (K'_{upi} and K'_{up}). Their ratio to the average precipitation P_i and P was also calculated. The ratio P_{rti}/P_i characterises the class itself and the general ratio P_{rt}/P_i characterises it within the Mediterranean climate.

5.3 MEDITERRANEAN FLOW REGIMES

Upon the classification of flow regimes according to Haines (1988), 4 main classes were obtained in addition to Isonzo in group 11, described here below and illustrated in the charts of Figure 5-1. Their distribution in Figure 5-2 showed that group 12 dominated Northern Mediterranean catchments while group G13 dominated the Southern catchments. The charts for each river are presented in APPENDIX D1.

Group 1 : Uniform distribution along the year where monthly flows range evenly between 5% to 12% of the mean annual flows. Only 4 rivers out of 55 have shown a regular flow, Cenia and Muga in Spain, Pescara in Italy and Litani in Lebanon (see Figure 2-9). We can deduce that either these catchments are managed or their baseflow runoff contribution to total runoff is very high.

Group 11 : Moderate Autumn, this flow regime type shows 2 distinct peaks, the first in autumn and a secondary in winter-late spring. Only Isonzo river was classified as Group 11.

Group 12 : Moderate Winter, a very broad winter and early spring peak and a distinct yet low summer flow. 21 river out of 55 belong to this group, located to the North in Italy, France and Spain between CC4 and CC5, where low precipitation seasonality reigns.

Group 13 : Extreme Winter, a typical mediterranean flow regime with winter flow increase. Similar to Gentilli's Medierranean perennial & seasonal and coinciding with Köppen Csa and Csb climates (Haines et al. 1988); 20 out of 55 rivers belong to this group, mostly located in the Centre and South, between CC2 and CC3.

Group 14 : Early spring, This group shows an extended high flow exceeding 10% of the annual flow over 6 months building up to peak in spring due to snowmelt, before decreasing in summer with monthly flows below 5%; This group includes 8 catchments mainly PC4 mountainous karsitc catchments under snow influence, located between Spain and France and North Lebanon, hence defying CC2 and CC4 characteristics.

The flow regimes geographical distribution shows that groups 12 and 13 are always dominating the region, hence verifying the findings of Haines in 1988. In addition, the coincidence of the flow regimes distribution with the climatic classification could be clearly seen, but not totally as some physiographic features like cultivation (PC1, PC9) or mountainous catchments (PC4) could possibly overtake the climate and influence the flow regimes.

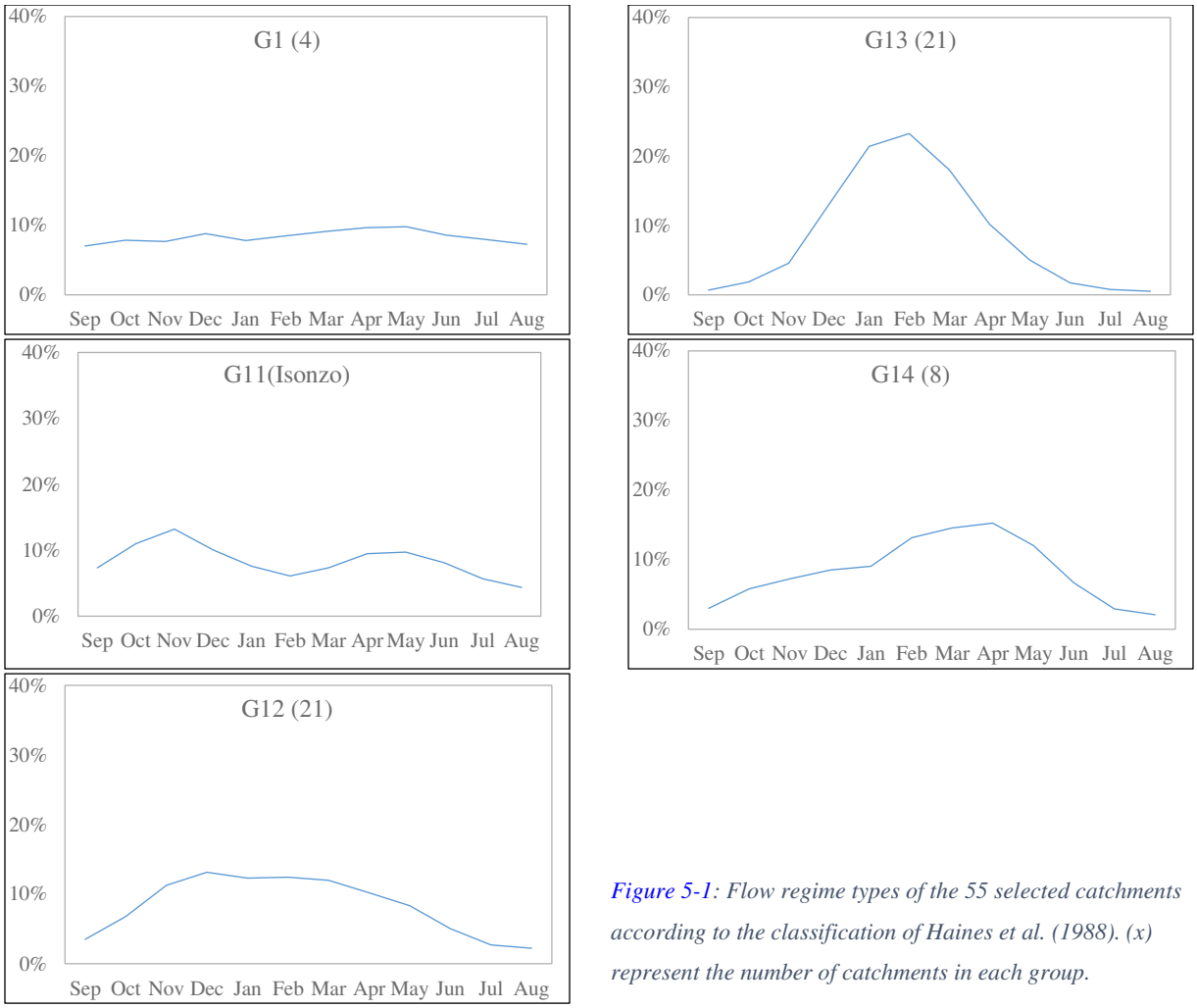

Figure 5-1: Flow regime types of the 55 selected catchments according to the classification of Haines et al. (1988). (x) represent the number of catchments in each group.

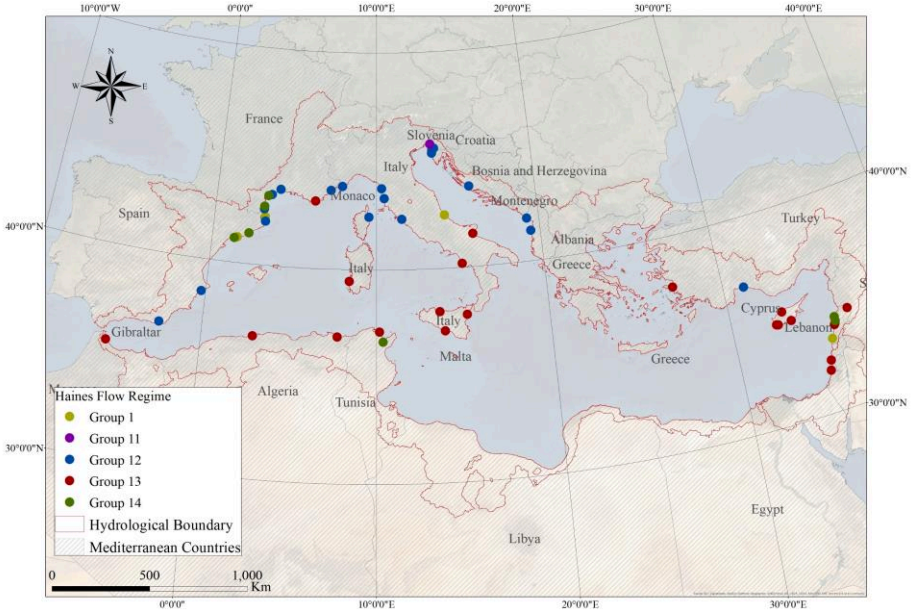

Figure 5-2: Flow regime types of the selected catchments according to the classification of Haines et al. (1988).

5.4 MEDITERRANEAN CATCHMENTS WATER BALANCE

5.4.1 Selected catchments climate and physiography

The selected catchments belong to different climatic and physiographic classes. Figure 5-3 shows that precipitation seasonality I_S ranges between 0.3 and 0.7 in North West Europe and gradually increase in the South reaching 1 in Lebanon. In Figure 5-4 the aridity index I_{Arid} shows an evolution from the most arid and seasonal region in the South to the most humid and least seasonal region in the North but with some exceptions where mountainous karstic catchments in North Lebanon have I_{Arid} less or equal to 1 or the Gulf of Lion catchments (Mediterranean region between Spain and France), showing somehow a marking variability of I_{Arid} ranging between 0.82 and 1.83. The selected sample is representative of the Mediterranean landscape as seen in Figure 5-5. Physiographic classes of the selected catchments are diverse without any geographical domination but a widespread distribution of PC1 and PC9 cultivated catchments, PC3 forest catchments and PC4 catchments, mainly observable in Golf du Lion where neighbouring catchments belong to different classes.

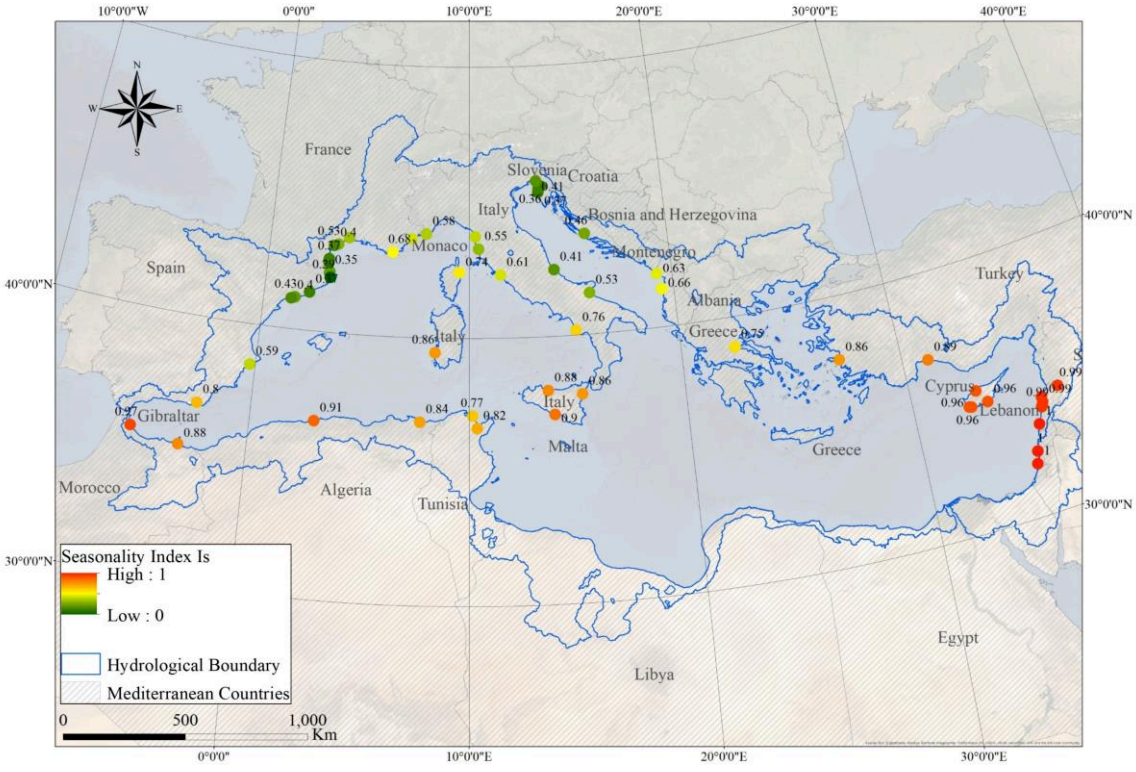

Figure 5-3: Spatial distribution of Seasonality Index I_S ranging from 0.3 for El Ter, Spain to 1.0 for Litani, Lebanon.

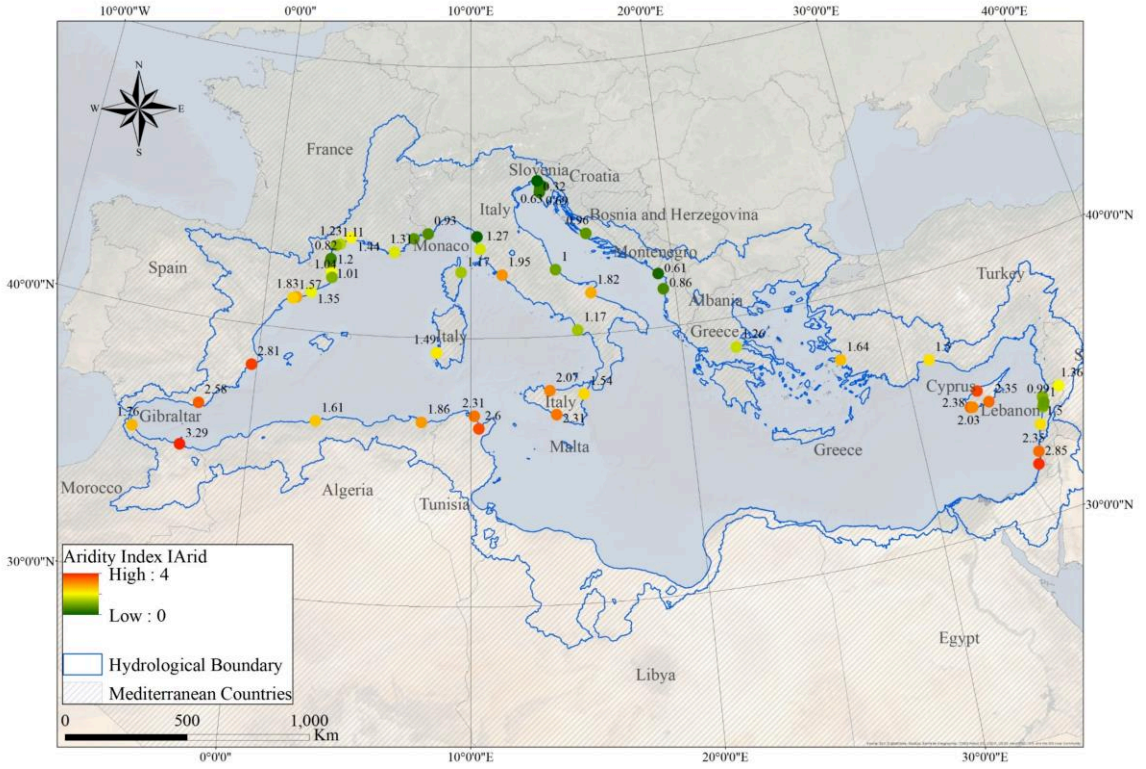

Figure 5-4: Spatial distribution of the aridity index I_{Arid} ranging from 0.24 Moraca, Montenegro to 4.07 for Andarax, Spain.

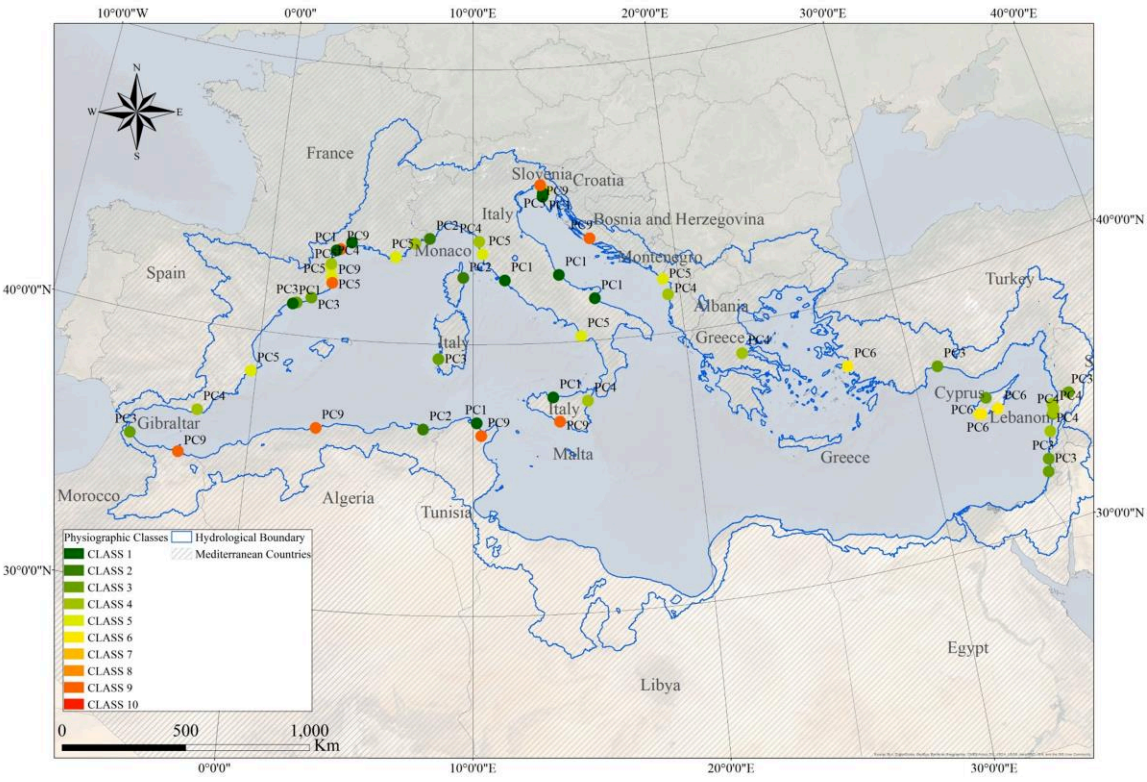

Figure 5-5: Physiographic classes of the 55 selected catchments.

5.4.2 Characterisation of Mediterranean catchments water balance

5.4.2.1 The heat and water balance model of Budyko (1974)

The functional model of Budyko (1974) characterises the relationship between the annual evapotranspiration and long-term water and energy balance at the catchment scale. Hence, the aridity index $\emptyset = ET_p/P$ was calculated by estimating the annual average evapotranspiration according to Turc (1961); and the annual flow deficit (P-Q) to the annual precipitation. Figure 5-6 and Figure 5-7 shows Equation (8) $\frac{E}{P} = F(\emptyset)$ from Section 1.3.1 with average values for each catchment and climatic classes, summarised in Table 5-2. The Budyko curve of all catchments annual values is added in Figure 5-8.

Table 5-2: Summary of the Budyko formulation components averaged by climatic classes.

Climatic Class (55 Catchments)	*P (mm)*	*E_p (mm)*	*E (mm)*	*E_p/P*	*E/P*
CC2 (3)	473	903	457	2.3	1.0
CC3 (17)	839	856	541	1.2	0.7
CC4 (17)	758	843	496	1.4	0.7
CC5 (18)	1047	796	525	1.0	0.5

The distribution of Mediterranean catchments follows the general shape of a Budyko curve with the humid CC5 catchments almost tangent to the first bisector and the most arid CC2 catchments approach asymptotically to the horizontal line representing E/P = 1. Looking to each catchment aside, we notice the interclass variability especially for CC3 and CC4. It was surprising to see two CC3 Lebanese catchments, Nahr el Kalb (KA) and Nahr Ibrahim (IB), between the most humid and flowing catchments and the spanish CC4 Andarax (AN) as the most arid and least flowing catchment. The aridity index I_{Arid} of Andarax was low enough to classify it in CC4 and the humidity of the Lebanese catchments was not high enough to classify it in CC4 as the PCA results in CHAPTER 3 showed that seasonality index I_S is the most contributing in the classification. According to the physiographic calssificaiton we notice that these catchments are PC4 mountainous, karstic and snow influenced catchments. However, (AN) is the most arid catchment between the selected mainly because of its positioning in the shadow of Sierra Nevada mountains and not receiving enough precipitation, in addition of being only 27% karstic.

The general distribution is aligned with the climatic classification and specifically the aridity, despite the average positioning making CC3 less arid than CC4 due to the huge distortion between the 3 catchments described previously. Budyko curve also shows that water resources are much more available in Northern catchments than Southern catchments. This variability shows the important role of evapotranspiration and water availability in hydrological processes and shall be discussed furthermore with the physiogrpaphic variability in next sections.

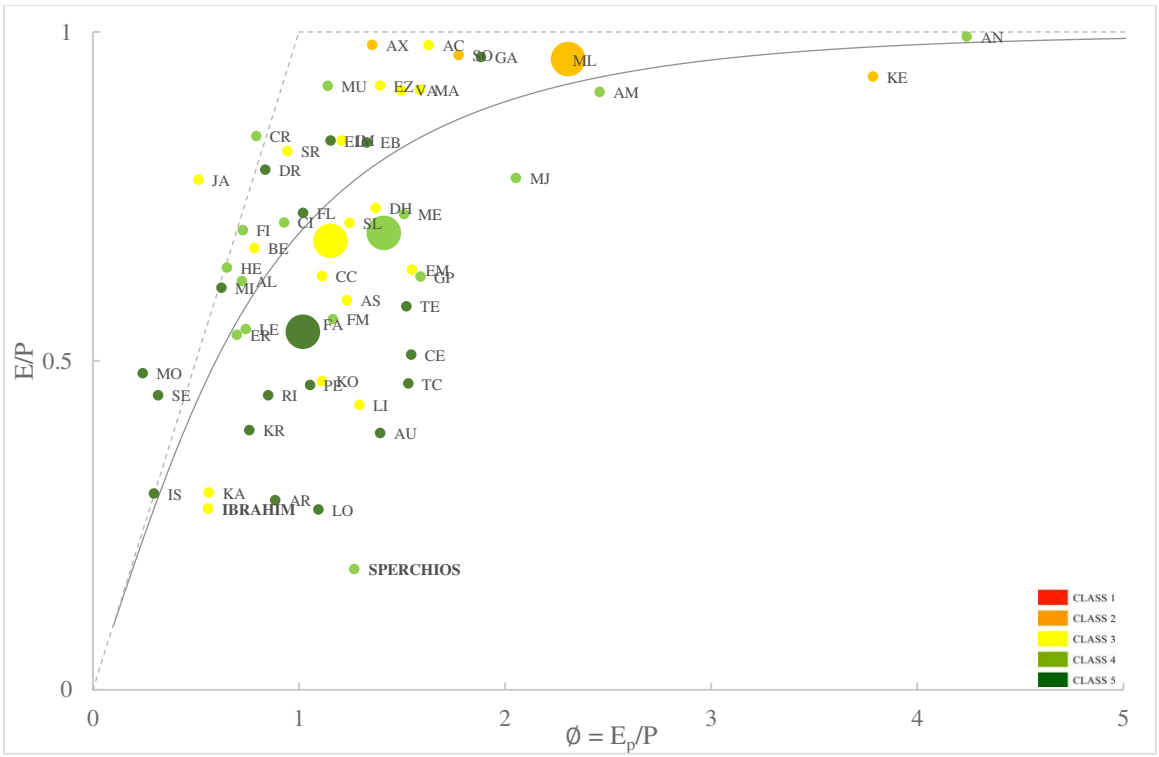

Figure 5-6: Budyko curve of the 55 Mediterranean catchments according climatic classes. Small points represent each catchment, large points represent class averages and dashed lines are theoretical (equations 9 and 10).

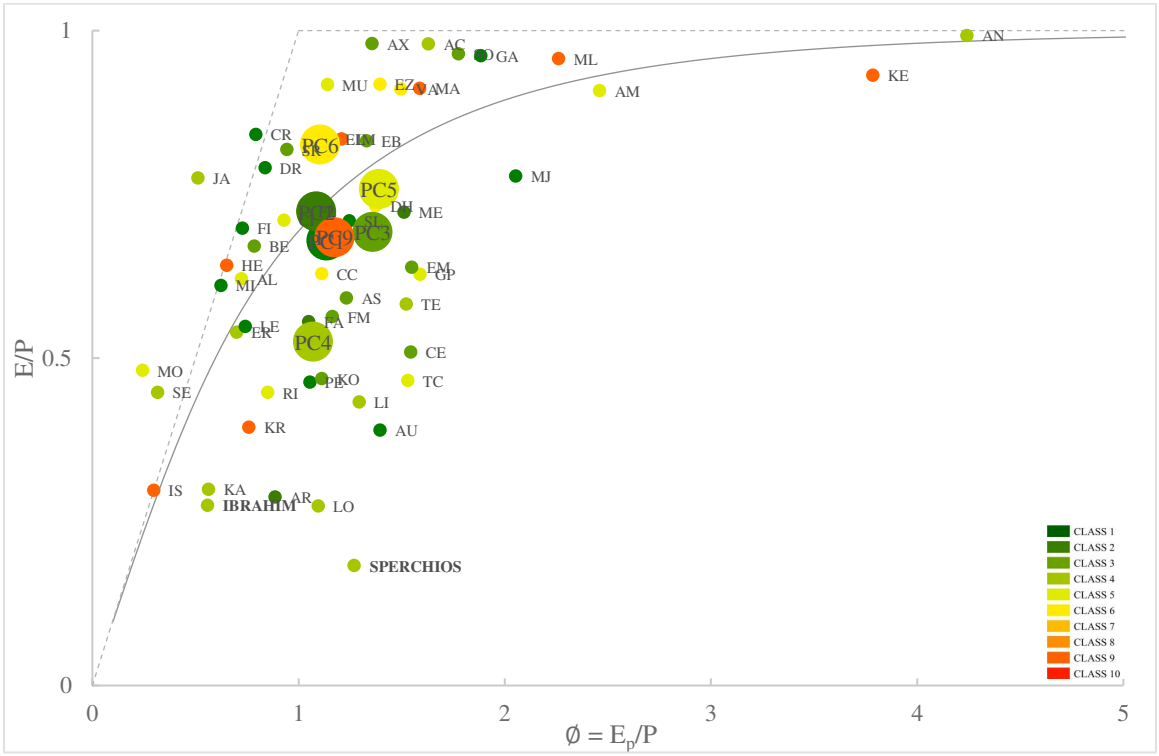

Figure 5-7: Budyko curve of the 55 Mediterranean catchments according to physiographic classes. Small points represent each catchment, large points represent class averages and dashed lines are theoretical (equations 9 and 10).

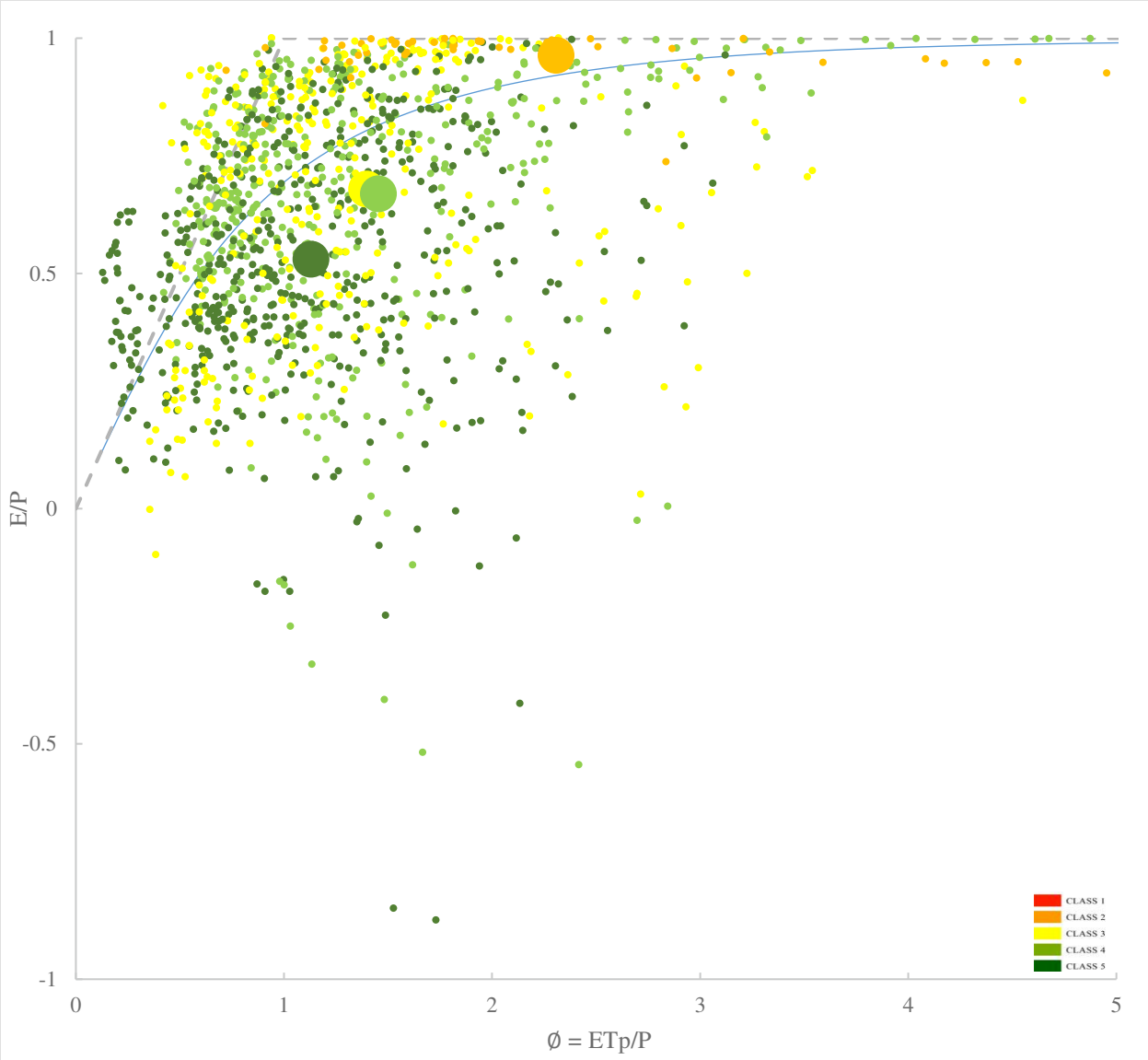

Figure 5-8: Budyko curve of all annual values of the 55 Mediterranean catchments according climatic classes. Small points represent each catchment, large points represent class averages and dashed lines are theoretical (equations 9 and 10).

5.4.2.2 *The water balance partitioning model of L'vovich (1979)*

The water balance components according to L'vovich (1979) are summarised in Table 5-3 and complete values are reported in APPENDIX D2. The partitioning for the catchments of Spercheios in Greece and Nahr Ibrahim in Lebanon are presented in Figure 5-9 and Figure 5-10 below, and for the rest of the catchments in APPENDIX D3. All the charts reproduced accurately the empirical relations for most of the Mediterranean catchments. The interannual variability is well marked for all water balance components, same for the inter-catchment variability with different ranges between catchments. Spercheios is a moderately watered catchment with MAP = 701 mm yielding a MAQ = 575 mm while Nahr Ibrahim is highly watered with MAP = 1450 mm yielding a MAQ = 1052 mm; Spercheios shows little precipitation variability in comparison to Nahr Ibrahim, however their surface flow S is almost similar ranging between 50 mm and 350 mm for the first and between 100mm and 550 mm for the second. The baseflow U shows remarkable high values ranging between 100 mm and 800 mm for the first and between 200 mm and 1350 mm for the second. Ibrahim's vaporisation curve seems interesting showing an upper limit of V, reached every year due to water availability in contrast with other catchments.

Table 5-3: Summary of the water balance components of the selected catchments according to the partitioning of L'vovich (1979)

Summary	*P* (mm)	*Q* (mm)	*U* (mm)	*S* (mm)	*W* (mm)	*V* (mm)
Average	862	239	106	345	755	516
Minimum	230	2	1	1	217	128
Maximum	3383	1756	1245	532	2872	1627
Standard Dev	510	358	257	113	417	251

5.4.2.3 *The conceptual water balance model of Ponce and Shetty (1995a)*

Table 5-4 summarises the runoff and baseflow threshold of all the catchments according to Ponce and Shetty (1995a). A sensitivity analysis conducted on 431 catchments of US MOPEX, showed that Ponce and Shetty curves fitting was insensitive to extremes and that the distribution returned a linear fit (Sivapalan et al., 2011). Those extremes were observed wherever the flow regime was dominated by the groundwater runoff, case of Nahr el Assi in Lebanon; or wherever the precipitation was very low, case of Andarax in Spain, or Alcantara in Italy. Some catchments did not yield very good results, this inaccuracy returns to either interrupted flows by dams and lakes, catchments interconnection or simply poor data quality.

Table 5-4: Summary of the fitting curves parameters according to Ponce and Shetty (1995a).

Summary	λ_s	λ_u	W_p	V_p	$\lambda_s W_p$	$\lambda_u V_p$
Average	0.02	0.10	10853	4213	88	118
Minimum	0.00	0.00	1897	182	3	0
Maximum	0.09	0.88	78982	39167	347	469
Standard Dev	0.02	0.18	14854	7353	101	131
Abs. Confidence interval	0.01	0.05	3926	1943	27	35
Rel. Confidence interval	39%	46%	36%	46%	30%	29%

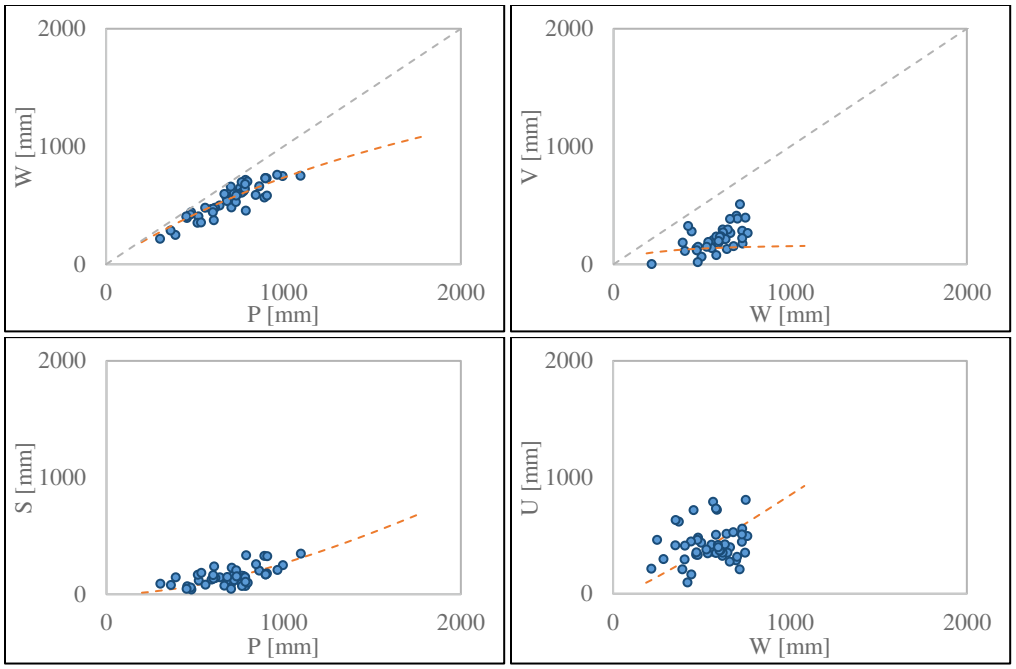

$\lambda_s W_p$	3
$\lambda_u V_p$	0
S-RMSE	60
W-RMSE	60
U-RMSE	133
V-RMSE	184

Figure 5-9: L'vovich water balance components proportional curves extracted for Spercheios, Greece.

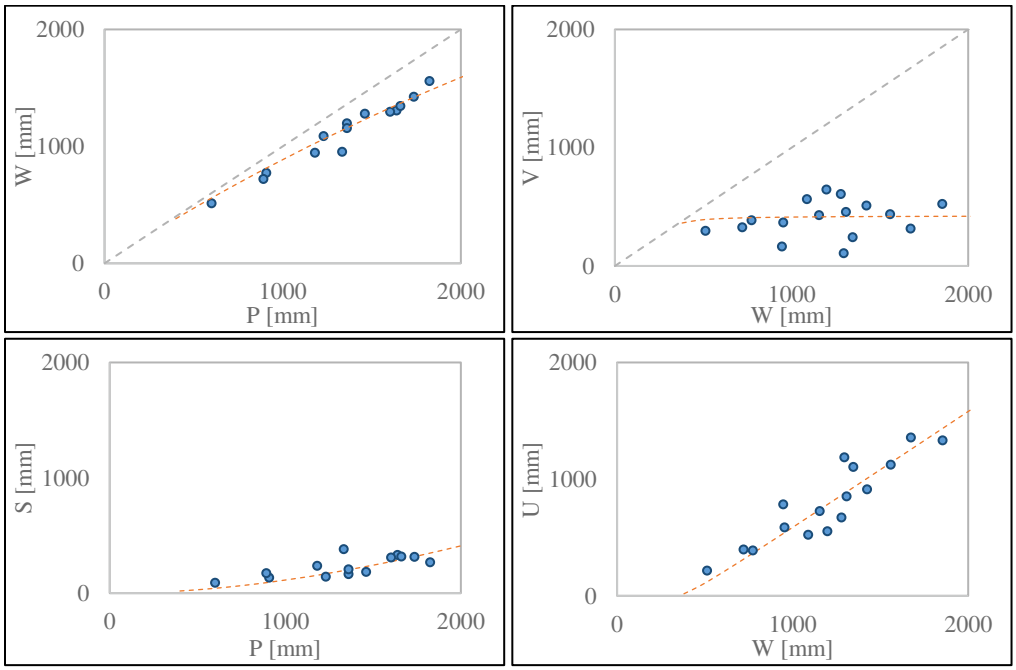

$\lambda_s W_p$	8
$\lambda_u V_p$	330
S-RMSE	75
W-RMSE	75
U-RMSE	124
V-RMSE	149

Figure 5-10: L'vovich water balance components proportional curves extracted for Ibrahim (Adonis), Lebanon.

The spatial distribution of Ponce and Shetty water balance parameters W_p, V_p, quick flow threshold $\lambda_s W_p$ and slow flow threshold $\lambda_u V_p$ estimated for the 55 selected catchments are presented in Figure 5-11 to Figure 5-14. The distribution reflected a wide geographical variability across the Mediterranean without any clear pattern or regional clustering despite some adjacent catchments yielding neighbouring values. The French catchments yielded the lowest values for all parameters with both $\lambda_s W_p$ and $\lambda_u V_p$ below 100 mm except for Hérault river which ($\lambda_s W_p$ = 122 mm; $\lambda_u V_p$ = 1 mm). In Cyprus, $\lambda_s W_p$ show close values ranging between 175 mm and 350 mm. These values are among the highest in the Mediterranean due to the high soil permeability on the island; this is confirmed with the high wetting potential W_p values ranging between 5000 mm and 9000 mm. The Lebanese coast have a wide variability of $\lambda_s W_p$ ranging from 7 mm to 270 mm between adjacent catchments as well as for W_p ranging from 5000 mm to 27000 mm (except for Nahr el Assi Lebanese sub catchment); same observations could be described for $\lambda_u V_p$ and V_p variability.

We noticed some matching catchments which share remarkable water balance similarities despite their geographical, climatic, or physiographic difference. These catchments could be considered twin catchments like Lez in Franc (PC1, CC4) and Erzenit in Albania (PC4, CC4); Fium-alto in France (PC2, CC4) and Fluminimaggiore in Italy (PC3, CC4); Mirna in Croatia (PC1, CC5) and Alento in Italy (PC5, CC5); Elter in Spain (PC9, CC5) and Imera Meridionale Italy (PC9, CC3). The water balance similarity between these catchments could be caused by an underlying physiographic similarity like snow or karst components which make these catchments interesting to examine closely.

The diversity of both microclimates and physiography between catchments as seen in CHAPTER 4 and Section 5-3 stands behind the water balance variability as hydrological response on the same climatic forcing differs according to catchments' landform, landcover soil types and other physiographic features, and despite some close catchments between Spain, France and Italy, no geographical pattern was detected. Similar water balance parameters could be found for subcatchments that belong to the same physioclimatic regions as mountainous Alpine catchments, or Italian cultivated catchments, but this is left for further research as this study only treats coastal catchments of an area ranging between 100 km^2 and 3000 km^2 at their outlet. Nevertheless, in the next section we will try to find water balance components patterns based on the formulations of Ponce & Shetty (1995a, 1995b) and Sivapalan et al. (2011) and on the climatic and physiographic classifications we developed in the previous chapters.

In comparison to the classification advanced by Ponce & Shetty (1995a), the initial obstruction coefficients (λ_s and λ_u) are low ($0<\lambda<0.15$). The wetting potential are high to very high ($W_p > 3000$) ranging between a minimum of 1897 mm for Lez in France and 80000 mm for Alcantara in Italy. The vaporisation potential is highly variable ranging between 200 mm for Spercheios in Greece and up to 40000 for Alcantara (19 catchments with $0<V_p<1000$ mm; 18 with $1000<V_p<3000$ mm; and 18 with $V_p>3000$ mm).

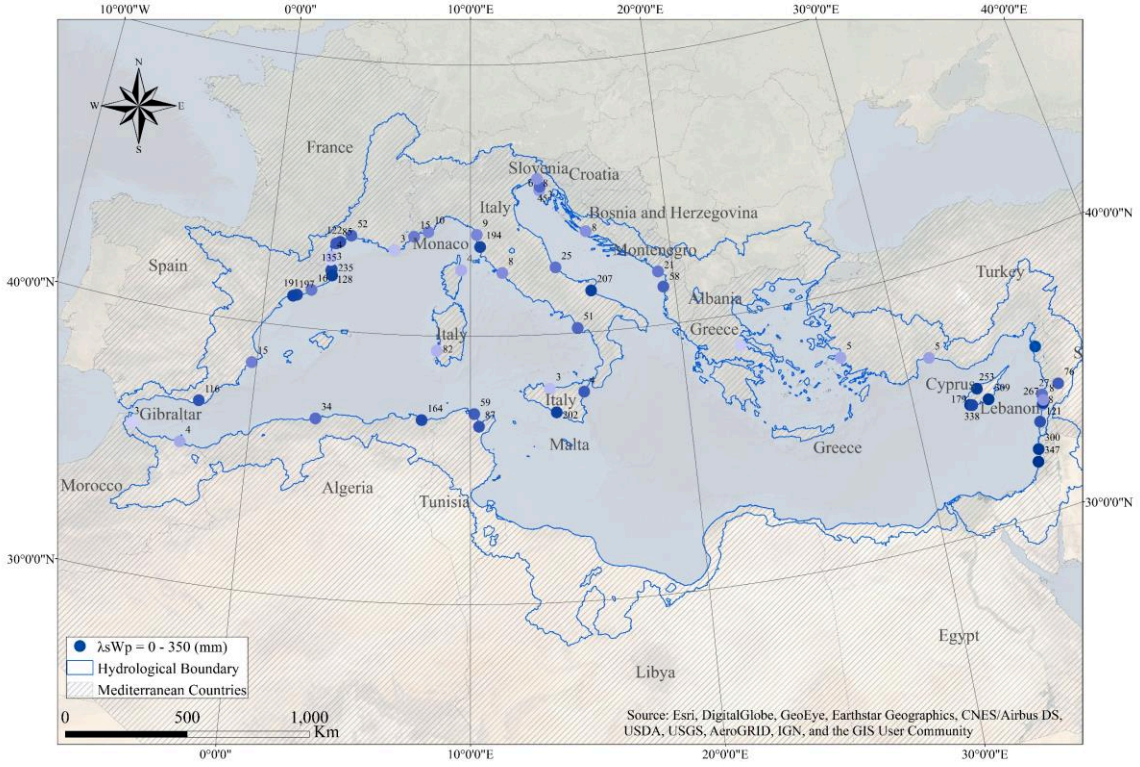

Figure 5-11: Spatial distribution of the water balance quick flow threshold parameter $\lambda_s W_p$, values reported in Appendix D2.

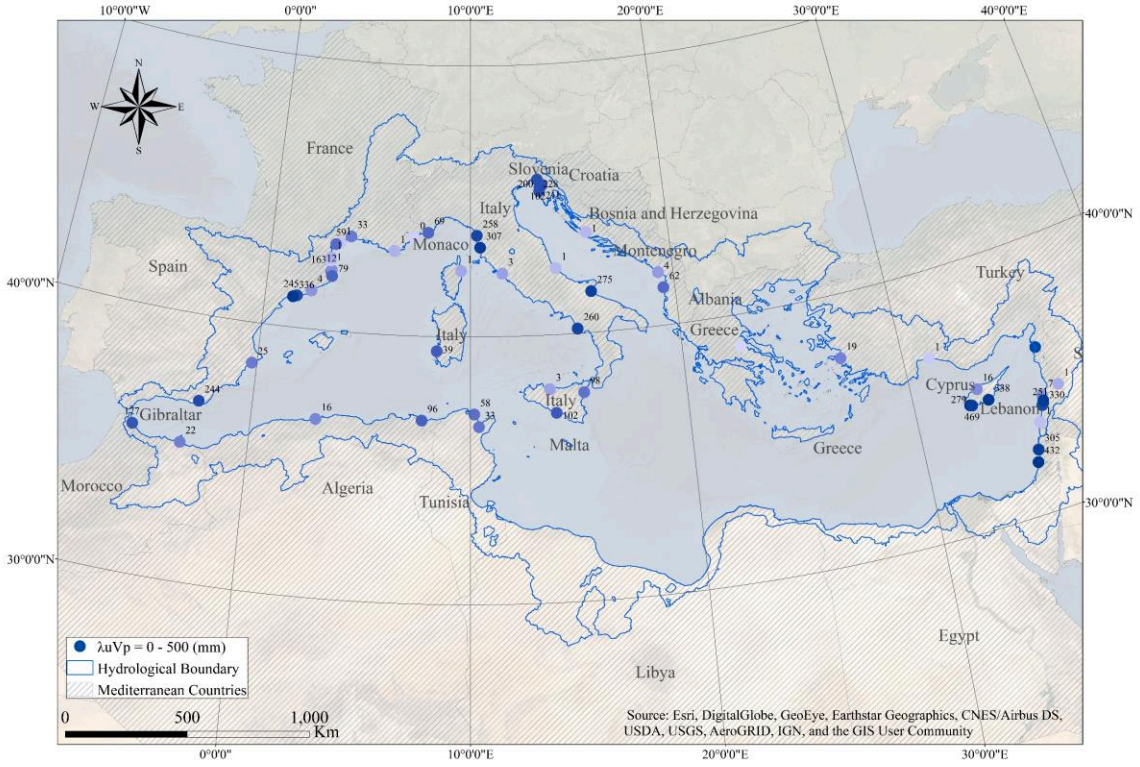

Figure 5-12: Spatial distribution of the water balance slow flow threshold parameter $\lambda_u V_p$, values reported in Appendix D2.

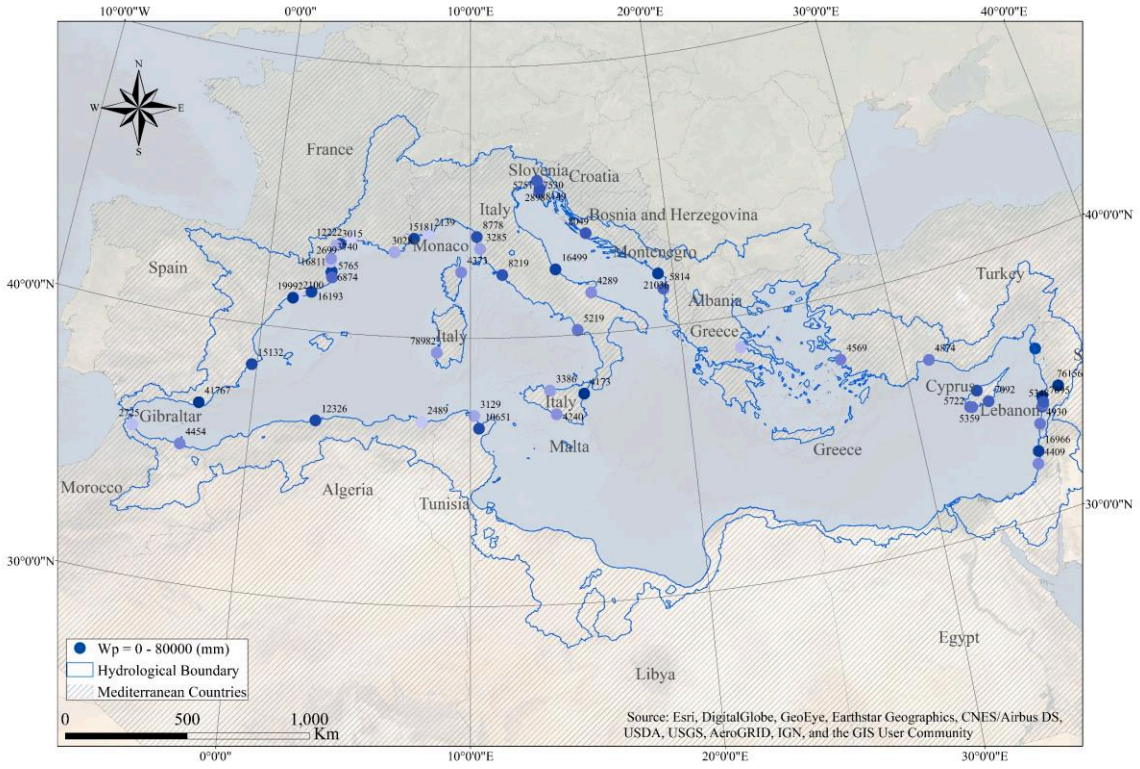

Figure 5-13: Spatial distribution of the water balance potential wetting parameter W_p, values reported in Appendix D2.

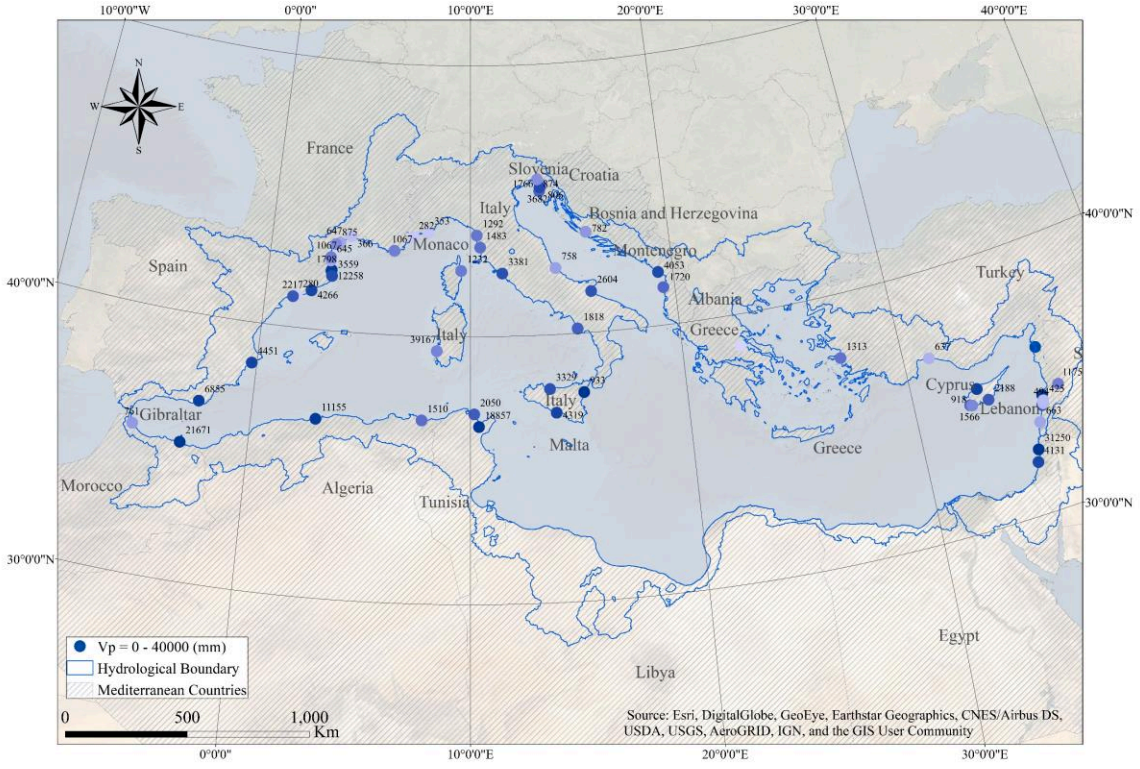

Figure 5-14: Spatial distribution of the water balance potential vaporisation parameter V_p, values reported in Appendix D2.

5.4.2.4 *The nondimensional water balance functional model of Sivapalan et al. (2011)*

In the previous sections, the formulations of L'vovich (1979) and Ponce and Shetty (1995) were verified on the selected catchments showing an interesting interannual and inter-catchment variability despite the general climatic homogeneity. In this section we will verify the nondimensional formulation of Ponce and Shetty theory as suggested by Sivapalan et al. (2011) to characterise Mediterranean hydrology according to the climatic and physiographic classifications and check if any water balance pattern could be extracted from Mediterranean site-specific water balance results that express their common hydrological behaviour.

The different non dimensional water balance components W*, S*, U* and V* were estimated from the values of W, S, U and V based on equations 19 and 20 and theoretical curves were fitted based on equations 22 and 23 detailed in Section 1.3. The charts in Figure 5-15 illustrate the annual values of 7 catchments each from different physiographic class showing the inter catchment and interannual variability; Table 5-5 summarises the properties of the seven catchments. Supplementary charts illustrating the annual values of catchments from same climatic or/and same physiographic class are added in APPENDIX D4. A summary is shown here representing the annual average of all the catchments and coloured according to their climatic classes in Figure 5-16 and physiographic classes in Figure 5-17 in a trial to discover any pattern behind, the averages values of each climatic and physiographic class were also added. The charts in Figure 5-15 to Figure 5-17 show the nature of competition between different water balance components of Mediterranean catchments as suggested by Sivapalan, where, at a first stage, quick flow S* is competing with the storage W* and at a second stage slow flow U* is competing with vaporisation V*.

Table 5-5: Summary of the seven catchments properties see Figure 5-15.

OID	*Name*	*Code*	*Country*	*CC*	*PC*	*No. of Years*	*S**	*W**	*U**	*V**
15	*ERZENIT*	*ER*	*AL*	*4*	*4*	*37*	*0.2*	*0.8*	*0.4*	*0.6*
47	*SERRAKHIS*	*SR*	*CY*	*3*	*3*	*30*	*0.1*	*0.9*	*0.1*	*0.9*
63	*DHIARIZOS*	*DH*	*CY*	*3*	*6*	*27*	*0.1*	*0.9*	*0.6*	*0.4*
165	*LA MUGA*	*MU*	*ES*	*4*	*5*	*39*	*0.0*	*1.0*	*0.1*	*0.9*
206	*FIUM-ALTO*	*FA*	*FR*	*4*	*2*	*43*	*0.2*	*0.8*	*0.4*	*0.6*
531	*HERAULT*	*HE*	*FR*	*4*	*9*	*60*	*0.1*	*0.9*	*0.5*	*0.5*
845	*PESCARA*	*PE*	*IT*	*5*	*1*	*23*	*0.0*	*1.0*	*0.5*	*0.5*

The charts of Figure 5-15 show that even if two catchments yield the same W* and S*, they do not necessarily yield the same U* and V*, in ex. Pescara (PE), La Muga (MU) and Hérault (HE) which all yield high W*and low S* but different U* and V* where PC5 forest catchment (MU) yield the lowest U* and high V* due to the high intake of trees while PC1 and PC9 managed catchment (PE) and (HE) yield average to high U* and average to low V*. Another observation is the similarity and high interannual variability of PC4 catchment Erzenit (ER) and PC2 forest catchment Fium Alto (FA) despite that both are from different countries but under the same climate CC4.

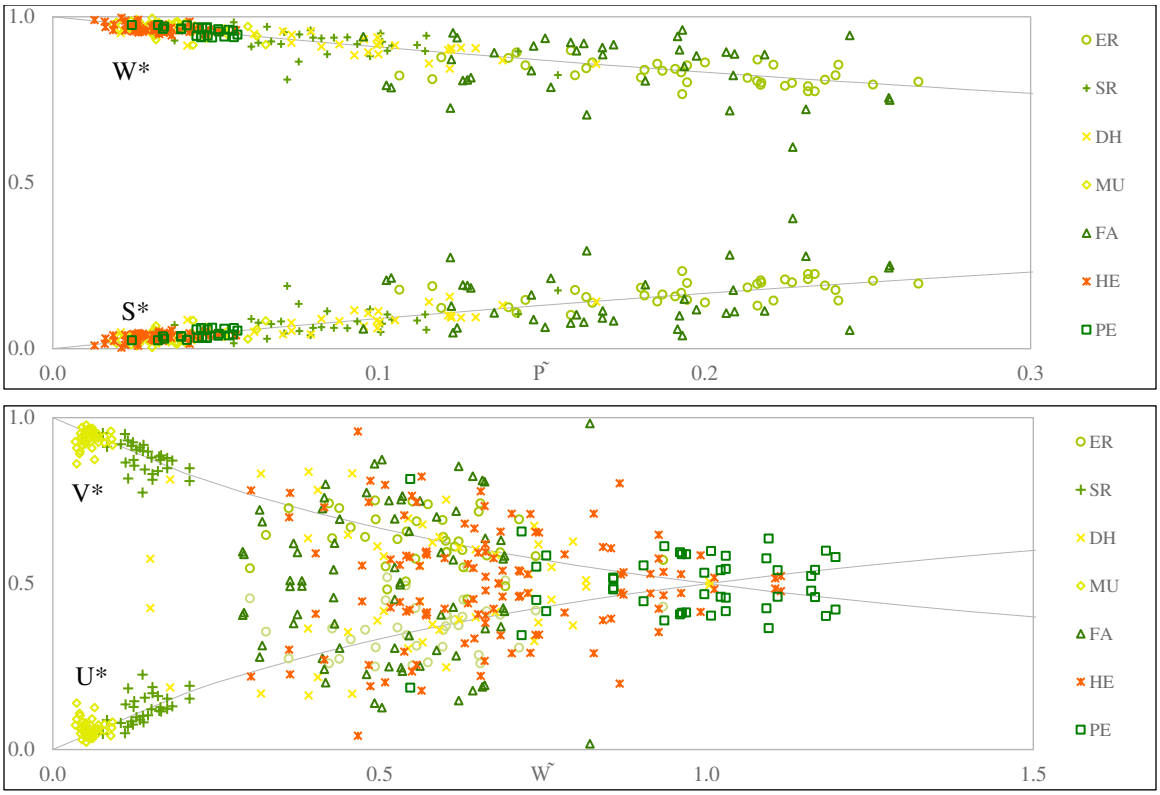

Figure 5-15: Inter-annual variability of water balance nondimensional estimates of W and S* versus annual climatic driver $\tilde{P}$ (up) and U* and V* versus annual climatic driver $\tilde{W}$ (down) for 7 representative catchments one from each physiographic classes. Points represent data (equations 19 and 20), and dashed lines are theoretical (equations 22 and 23).*

The climatic illustration of W* and S* vs $\tilde{P}$ in Figure 5-16 shows that this competition is gradually evolving from climatic CC2 in the South, where low precipitation and low quick flows dominate, to CC5 in the North where high precipitation and high quick flows dominate. This could also be observed for the climatic illustration of V* and U* vs $\tilde{W}$, however with a disturbance of climatic CC3. A closer examination revealed that two Lebanese catchments were behind this disturbance, which despite that they belong to CC3, they are well watered yielding high baseflow U* as they are elevated, snow covered and karstic PC4 catchments.

The physiographic illustration in Figure 5-17 shows a complex distribution reflecting once again the physiographic variability across the Mediterranean which is not directly correlated with the Mediterranean climatic distribution. Still, we could identify PC6 catchments mainly Cypriote and Turkish catchments yielding the lowest quick flows S* and highest wetting W*, PC2 catchments yielding the highest S* and W* while PC4 catchments, through snow contribution and emerging karstic springs, explain their position on the charts with the highest rescaled wetting $\widetilde{W}$, and highest U* but the lowest V*.

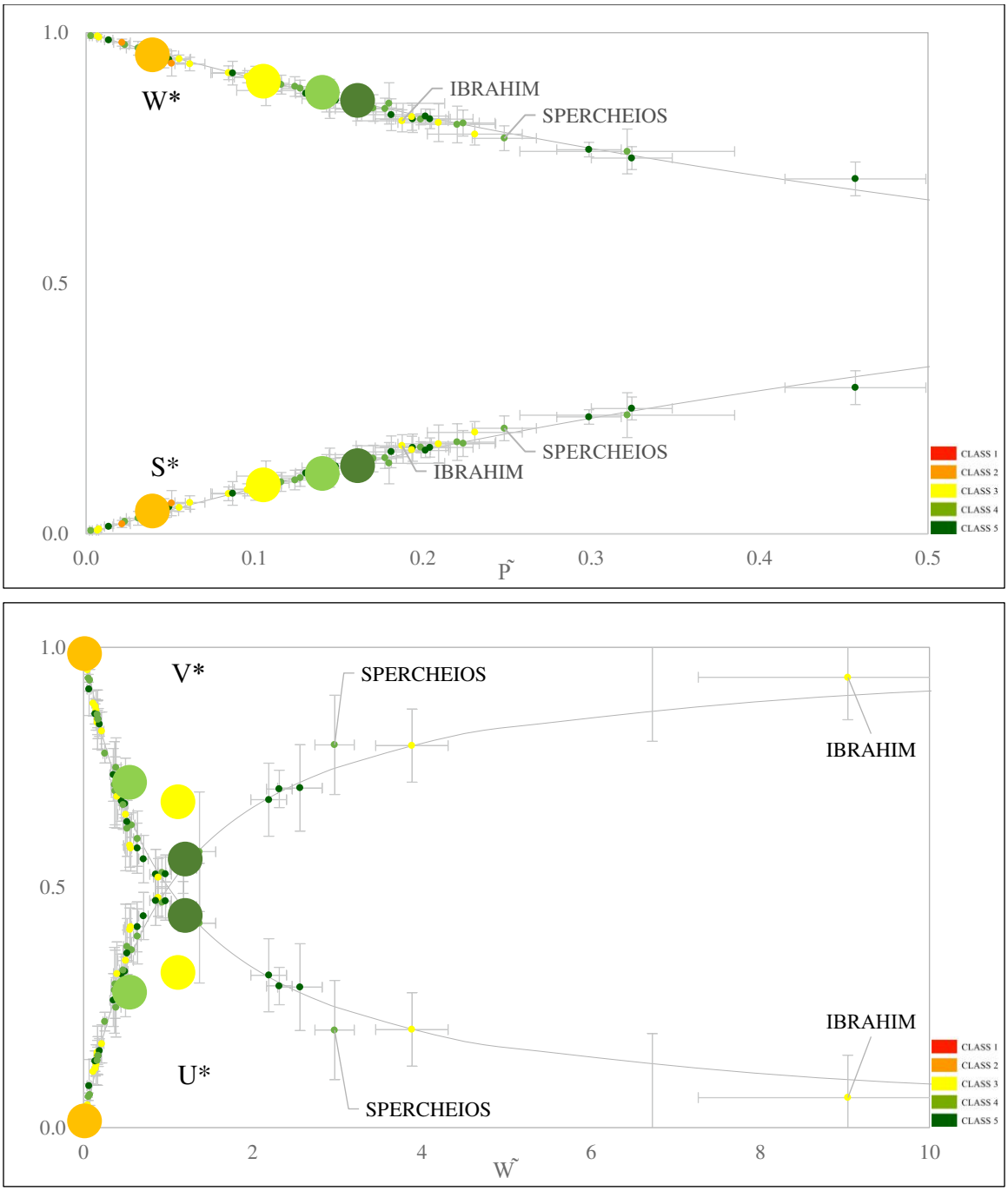

Figure 5-16: Inter-catchment variability of mean annual water balance nondimensional estimates of (left) W and S* versus annual climatic driver $\tilde{P}$ and (right) U* and V* versus annual climatic driver $\tilde{W}$ for all 55 catchments coloured according to climatic classification. Small points represent each catchment data (equations 19 and 20), large points represent class averages and dashed lines are theoretical (equations 22 and 23).*

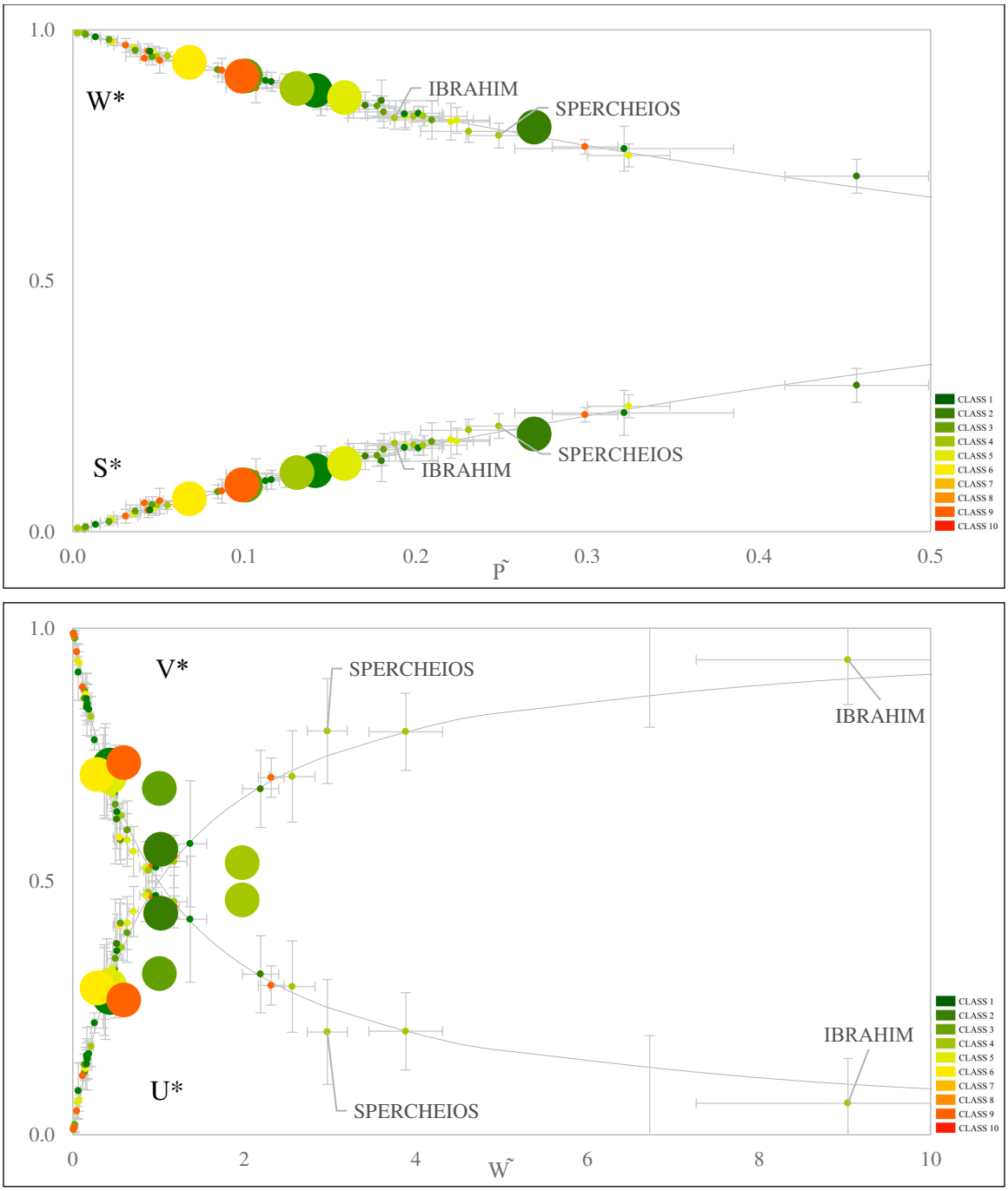

Figure 5-17: Inter-catchment variability of mean annual water balance nondimensional estimates of (left) W and S* versus annual climatic driver $\tilde{P}$ and (right) U* and V* versus annual climatic driver $\tilde{W}$ for all 55 catchments coloured according to physiographic classification. Small points represent data (equations 19 and 20), Large points represent class averages and dashed lines are theoretical (equations 22 and 23).*

We then calculated the different dimensionless water balance metrics K_H, K_B, K_V, K_R defined by Sivapalan et al. (2011) which suggest that the water balance are governed by two dimensionless variables, the aridity index $\varphi = \tilde{V}/\tilde{P}$ and the scaled precipitation $\tilde{P}$. The metrics were calculated for each catchment to assess the interannual variability. The mean annual water balances were also calculated to assess the inter catchments variability at the Mediterranean scale (see Table 5-6 to Table 5-8).

The mean annual water balance metrics fitting to the theoretical forms, as a function of the aridity index $\varphi = \tilde{V}/\tilde{P}$ in the charts of Figure 5-18 and Figure 5-19 illustrated according to their climatic and physiographic classes suggest that the aridity index φ is a primary determinant of the mean annual water balance, hence supporting the findings of Sivapalan (2011) on US MOPEX data. Figure 5-18 shows that K_H and K_V increase with increasing aridity, suggesting that the vaporisation V (energy), takes over the wetting W and consequently the slow flow component U, in arid catchments. We can see that for Mediterranean catchments, K_V fits properly to the lower bound of $\tilde{P} = 0.03$. In its turn, Figure 5-19 shows that K_B and K_R decrease with increasing aridity with on average, CC5 catchments yielding the highest baseflow and total runoffs but with some exceptions from PC4 catchments which also yielded the highest baseflow will be discussed furthermore later in this section. Same as for K_V, we can see that for Mediterranean catchments K_R and K_B fit properly to the lower bound of $\tilde{P} = 0.03$.

Table 5-6: Summary of the nondimensional Horton index K_H, Vaporisation index K_V, Baseflow index K_B and Runoff index K_R.

Summary	K_H	K_V	K_B	K_R
Average	0.68	0.60	0.27	0.40
Minimum	0.08	0.06	-0.11	-0.16
Maximum	1.10	1.16	0.71	0.94
Standard Dev	0.24	0.24	0.19	0.24

Table 5-7: Summary of the water balance components and nondimensional metrics averaged by climatic classes.

Climatic Class (55 Catchments)	*P (mm)*	*Q (mm)*	*U (mm)*	*S (mm)*	*W (mm)*	*V (mm)*	K_H	K_V	K_B	K_R
CC2 (3)	473	16	4	12	461	457	0.97	0.90	0.02	0.10
CC3 (17)	839	297	215	82	756	541	0.69	0.63	0.26	0.37
CC4 (17)	758	263	171	92	667	496	0.72	0.64	0.23	0.36
CC5 (18)	1047	522	365	158	885	521	0.57	0.50	0.35	0.50

Table 5-8: Summary of the water balance components and nondimensional metrics averaged by physiographic classes.

Physiographic Class (55 Catchments)	*P (mm)*	*Q (mm)*	*U (mm)*	*S (mm)*	*W (mm)*	*V (mm)*	K_H	K_V	K_B	K_R
PC1 (10)	782	263	170	92	690	519	0.73	0.63	0.23	0.37
PC2 (3)	791	407	247	160	631	384	0.57	0.46	0.33	0.54
PC3 (10)	714	211	148	63	651	503	0.69	0.62	0.26	0.38
PC4 (11)	998	518	387	131	867	480	0.54	0.50	0.38	0.50
PC5 (9)	1040	422	270	152	888	618	0.71	0.61	0.24	0.39
PC6 (4)	651	132	91	41	611	520	0.79	0.72	0.19	0.28
PC9 (8)	893	373	270	105	780	511	0.73	0.68	0.23	0.32

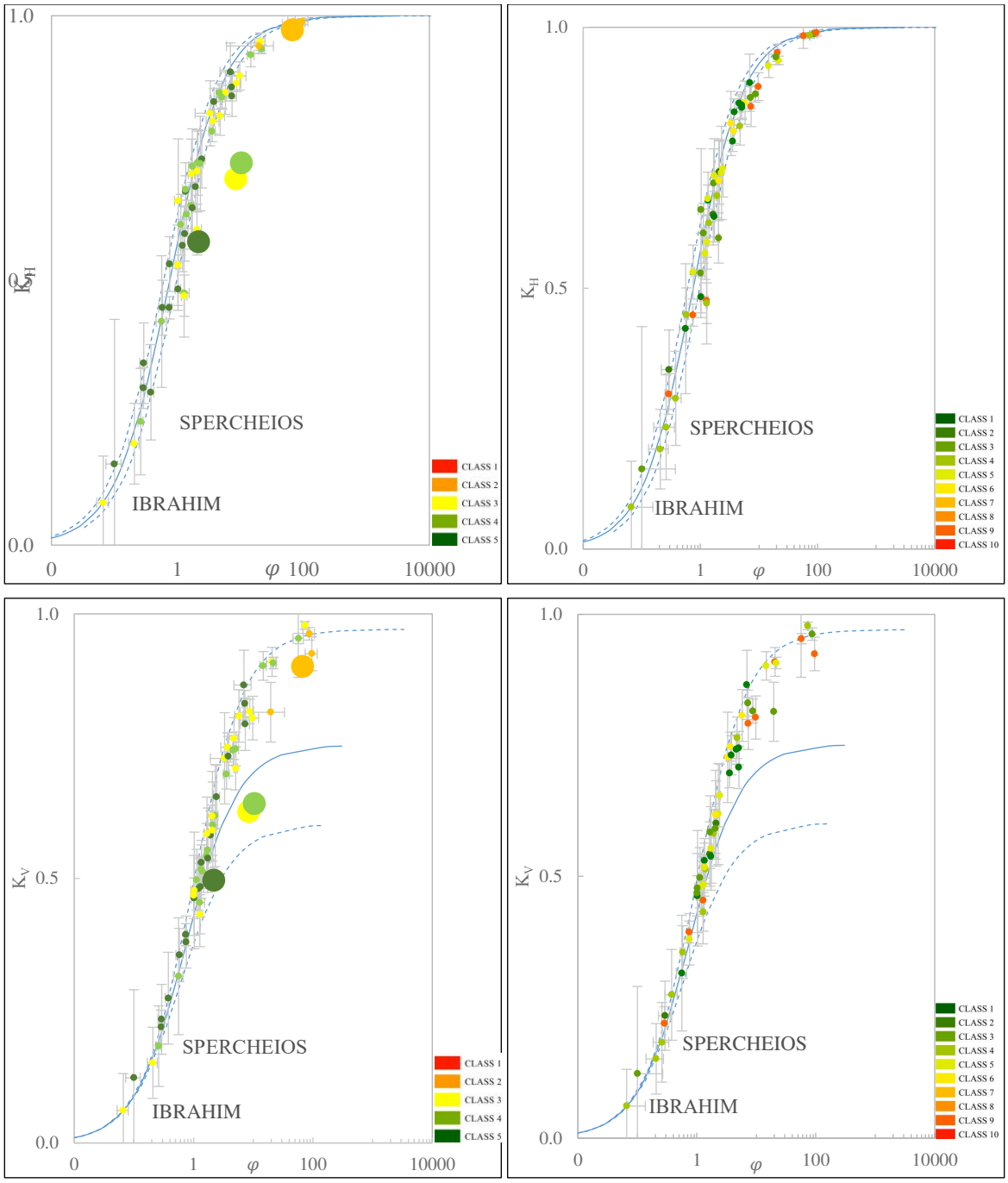

Figure 5-18: Estimation of the nondimensional Horton index K_H, Vaporisation index K_V versus aridity index *φ for all 55 catchments based on equations 25 (data points) and 26 (theoretic lines), coloured according to climatic classification (left) and physiographic classification (right) with large dots representing class averages.*

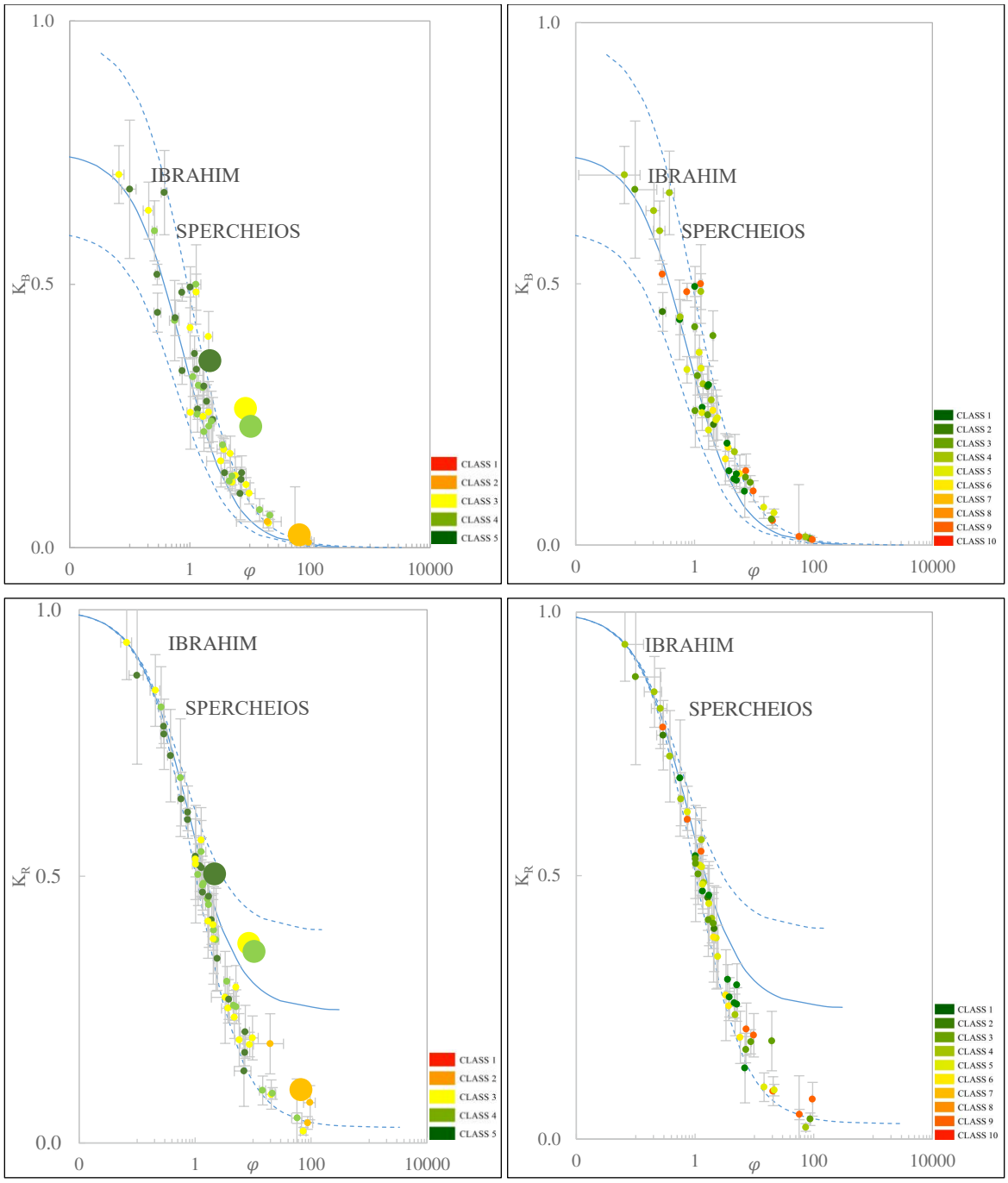

Figure 5-19: Estimation of the nondimensional Baseflow index K_B and Runoff index K_R versus aridity index *φ for all 55 catchments based on equations 25 (data points) and 26 (theoretic lines), coloured according to climatic classification (left) and physiographic classification (right) with large dots representing class averages.*

The maps in Figure 5-20 to Figure 5-23 show an interesting spatial distribution where K_H and K_V gradually decrease from South to North while K_B and K_R gradually decrease from North to South, nonetheless some exceptions were noticed where some Lebanese catchments showed an inverted distribution. Figure 5-24 shows the rescaled precipitation $\tilde{P}$ and Figure 5-25 the aridity index φ to cross validate the water balance indices distribution.

The geographical distribution coincides with the Mediterranean climatic classification, therefore we searched for which climatic index is mostly affecting this distribution and found that the water balance metrics of all catchments are slightly correlated with the mean annual aridity index Ep/P (R = 0.55) which is also correlated to the non-dimensional aridity index φ with R = 0.63 (r^2 = 0.4), hence supporting Sivapalan finding on US MOPEX data where r^2 = 0.46. It is therefore possible to say, to certain extent, that annual water balance metrics K_H and K_V increase while K_B and K_R decrease when seasonality increases, which suggests that intra-annual variability is responsible for the inter-catchment variability.

However, looking to Figure 5-17 to Figure 5-23 we noticed that some CC3 and CC4 catchments yielded lower aridity φ than CC5 which is unusual. And looking to their physiography, we noticed that those were PC4 catchments, case of Nahr Ibrahim in North Lebanon which yielded the highest slow flow peaking at 0.71 and total runoff at 0.94, due to high snowmelt contribution and high karstification with a similar observation for Spercheios, Nahr el Kalb and other.

This finding completes the one advanced by Sivapalan (2011) on baseflow metric variability when applied on the US MOPEX data stating that the wettest catchments have yielded the highest baseflow contribution and that soil types and topographic features govern the subsurface flow as part of the self-organisation of the vegetation with the climate as proposed by Horton (1933).

In our turn, we state that:

In the Mediterranean, the elevated, karstic and snow influenced (PC4) catchments yield the highest slow flow and runoff especially if located in high enough seasonal region (Southern Mediterranean CC3 regions) where precipitation are concentrated in winter and runoff (Haines Group 13 or 14 for North Lebanon) are concentrated in winter and spring seasons, when minimum vegetation cover the land and vaporisation (or evapotranspiration) is at lowest, part of the self-organisation of the vegetation with the climate as proposed by Horton (1933) but at the intra-annual scale.

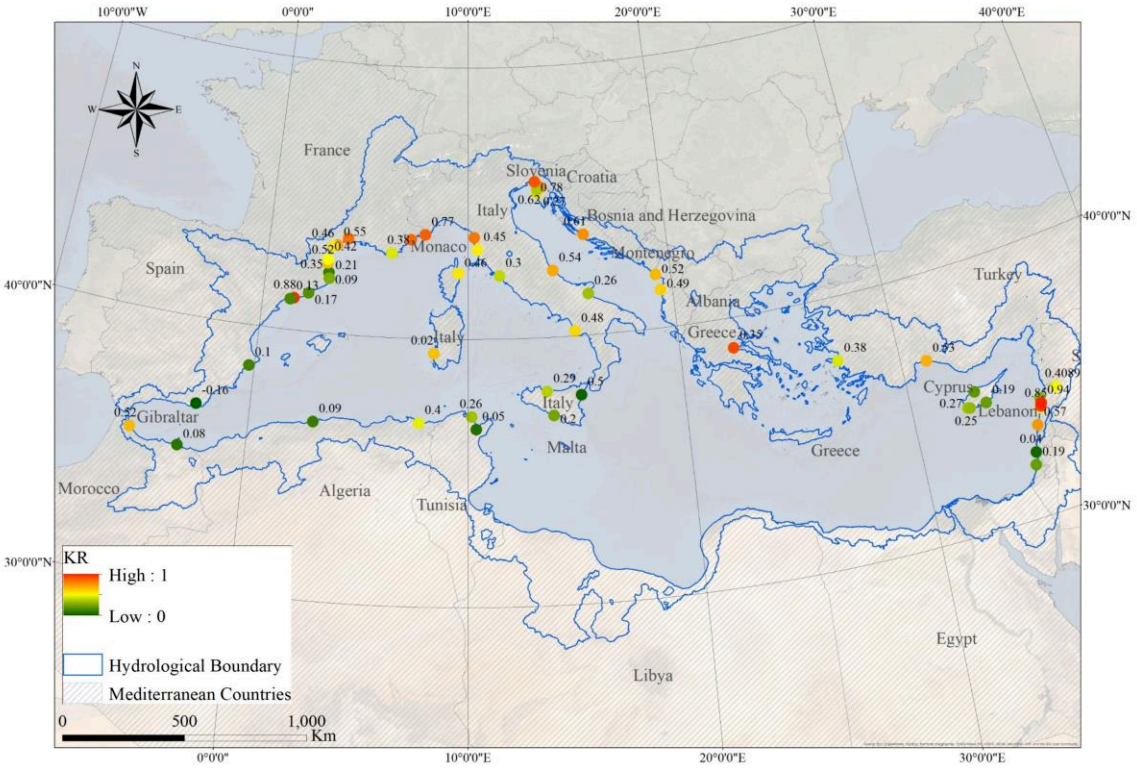

Figure 5-20: Spatial distribution of the water balance Runoff index K_R, values reported in Appendix D2.

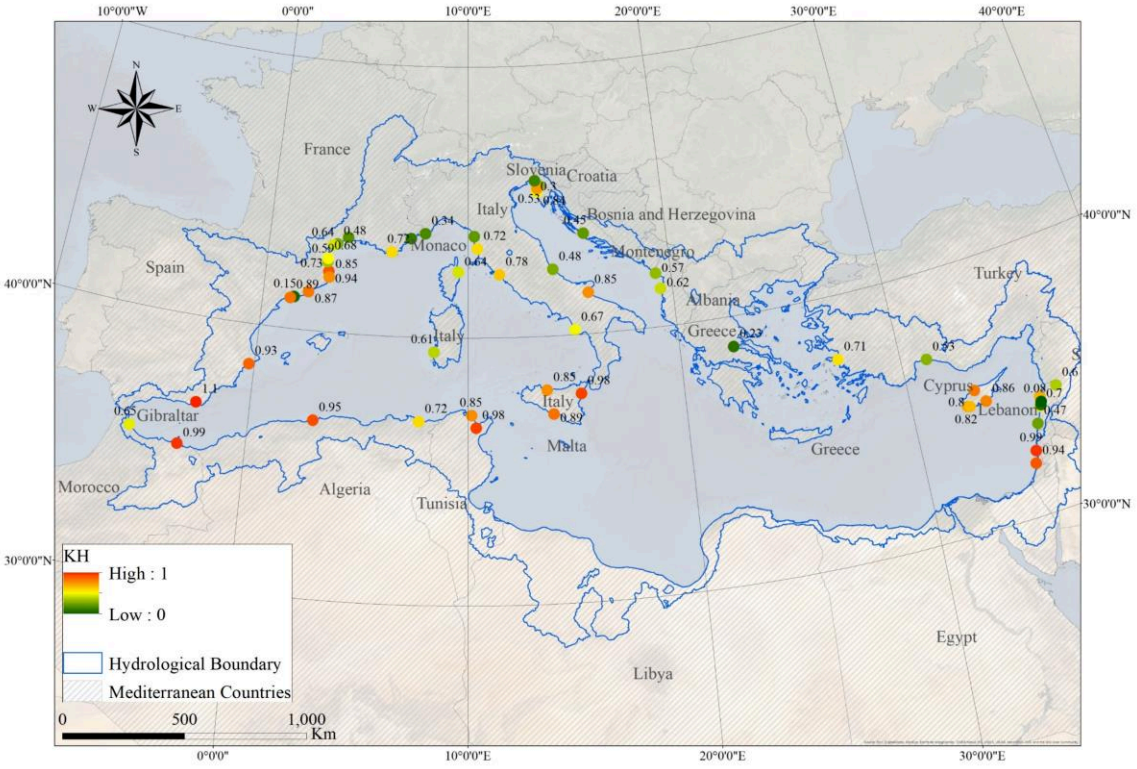

Figure 5-21: Spatial distribution of the water balance Horton index K_H, values reported in Appendix D2.

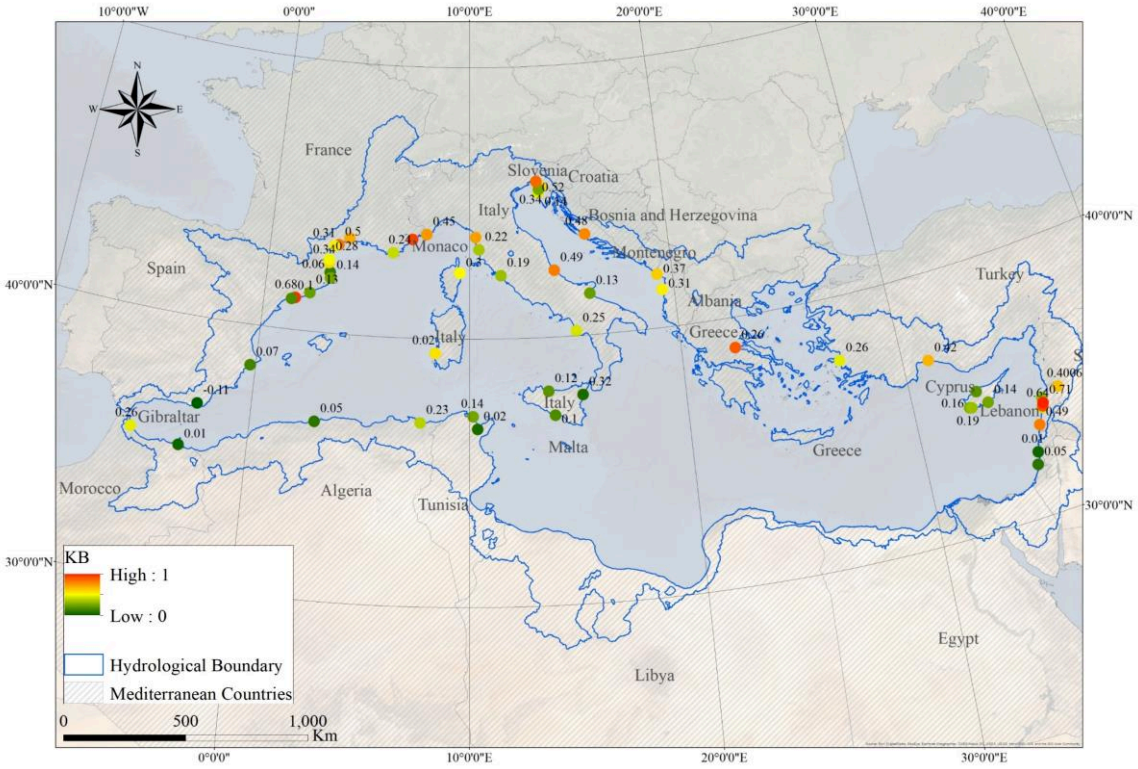

Figure 5-22: Spatial distribution of water balance Baseflow index K_B, values reported in Appendix D2.

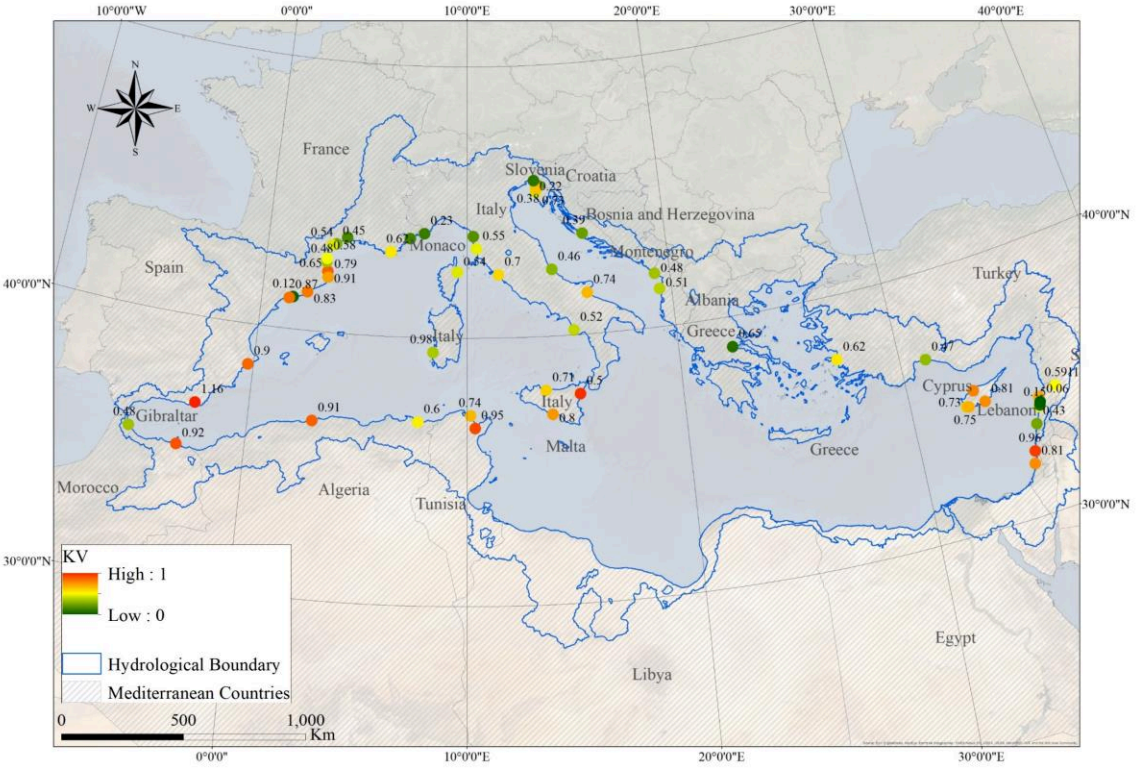

Figure 5-23: Spatial distribution of the water balance Vaporisation index K_V, values reported in Appendix D2

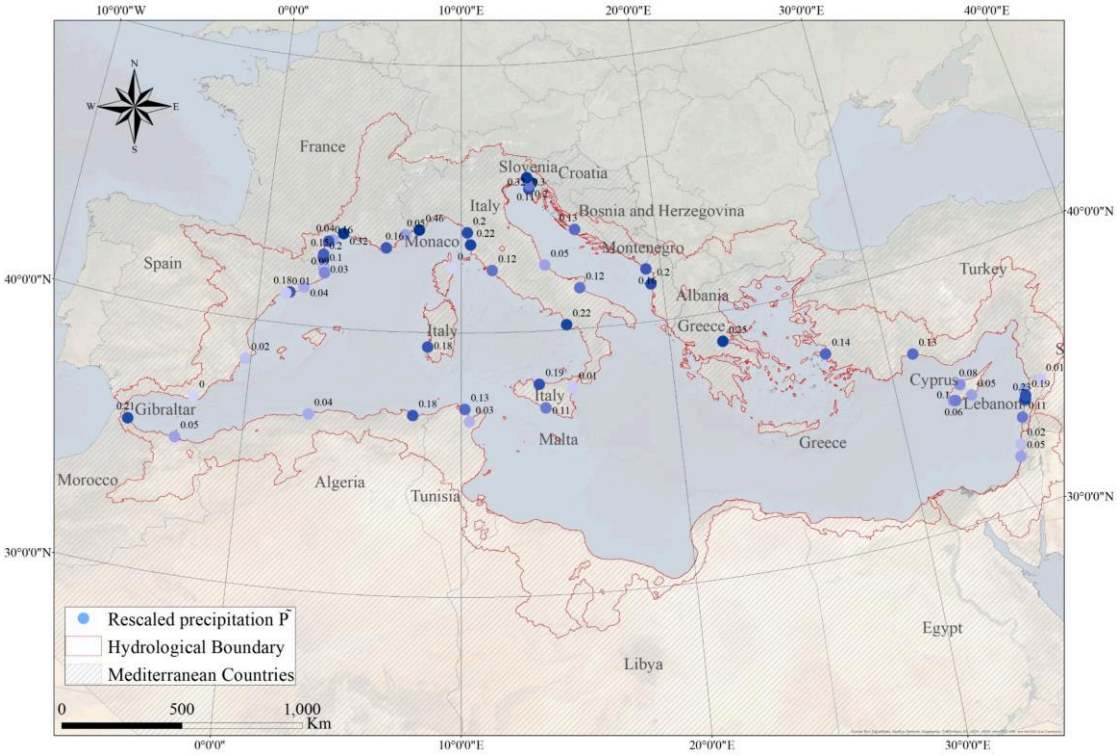

Figure 5-24: Spatial distribution of the rescaled precipitation $\tilde{P}$, values reported in Appendix D2.

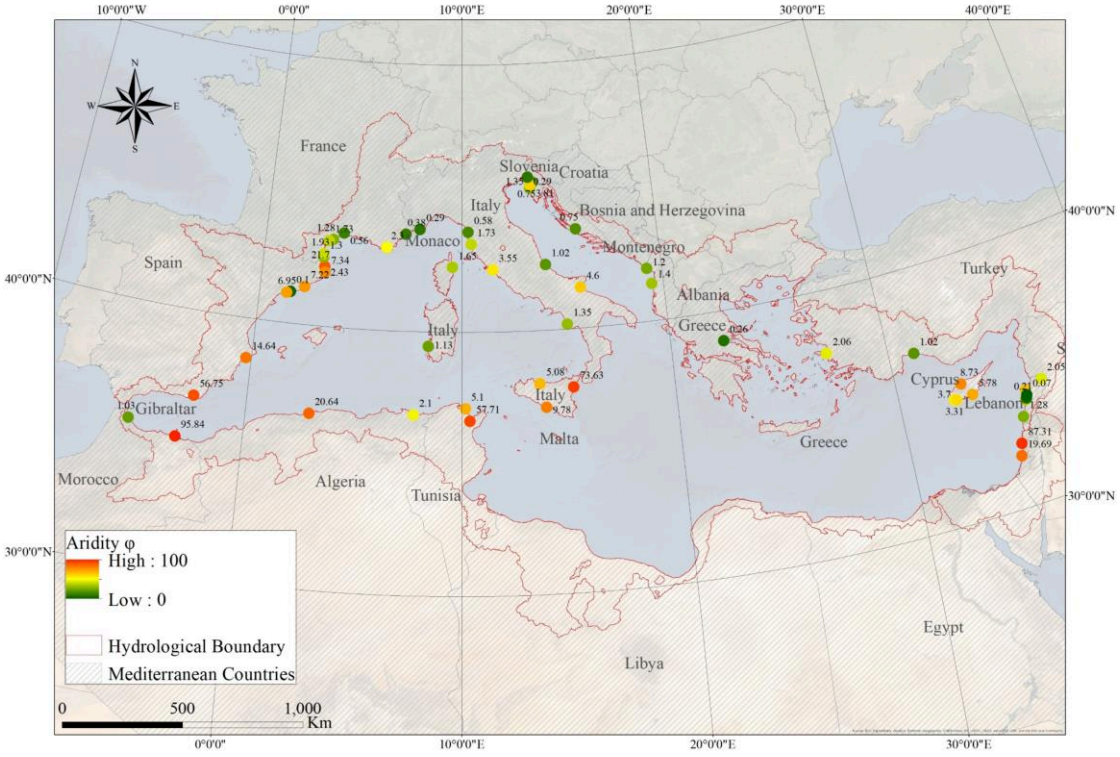

Figure 5-25: Spatial distribution of the aridity index φ, values reported in Appendix D2.

5.4.3 Characterisation of Mediterranean catchments runoff and baseflow

In this section, we studied the runoff gain to changes in mean precipitation as per Ponce & Shetty (1995b) and elasticity as per Harman et al. (2011). The runoff gains or elasticity characterise the catchments and allow the understanding of how water balance could change under a changing environment. Figure 5-26 and Figure 5-27 show the runoff and baseflow coefficients for the Mediterranean catchments illustrated according to the climatic classes and in Figure 5-28 and Figure 5-29 the runoff and baseflow gains illustrated according to the physiographic classes.

5.4.3.1 Water balance runoff and baseflow coefficients and gains

The climatic classification gradient from South to North was clearly observable on the water balance components despite the overlapping of some components between CC3 and CC4, due to higher precipitation over North Lebanon catchments. Precipitation P, runoff R, surface flow S and baseflow U increase with the classification. Wetting W and vaporisation V did not show any trend as they are not just energy dependent but also include runoff deficit and interconnection between catchments. The analysis of the catchments water balance components averages according to their climatic classes in Table 5-9 to Table 5-11 and corresponding Figure 5-26 and Figure 5-27 highlight once again the climatic forcing over the hydrological behaviour of Mediterranean catchments, thus we deduce:

1- The vaporisation potential (V_p) gradient is in line with the classification gradient where the highest potential corresponds to the most arid class CC2 and the lowest potential corresponds to the most humid class CC5. The wetting potential (W_p) do not follow the same trend.
2- The runoff and baseflow coefficients K_r and K_u are in line with the climatic classification. The lowest values correspond to CC2; they then quickly increase when average precipitation is close to 700 mm with high variability for CC3 and CC4 coefficients then stay within an upper bound of $K_r = 0.7$ and $K_u = 0.6$ for CC5 when precipitation >1500 mm.
3- The runoff and baseflow gains are always positive, they increase when the precipitation is below the thresholds $P_{rt} = P_{ut} = 700$ mm and then decrease when above it, with peak values $K'_{rp} = 0.00117$ mm^{-1} and $K'_{up} = 0.00109$ mm^{-1}. Thus, they characterise the climatic classes where arid catchments of CC2 are apt to increase their runoff coefficient with more precipitation while the wet catchments of CC5 are apt to decrease it with more precipitation.
4- The runoff and baseflow thresholds precipitation ratio to the average Mediterranean precipitation are high, they characterise the climatic setting of each class. For CC2, $P_{rt}/P_2 = 1.48$ thus runoff and baseflow coefficients tend to stay low (K_{r1} & $K_{u1} < 0.1$) characterising it as arid region. The ratio decreases with the seasonality where for CC5 it is as low as 0.67. The average precipitation of CC5 catchments is double the P_{rt} and the runoff and baseflow coefficient tend to reach their limit

(K_{r5} = 0.46 & K_{u5} = 0.38). For catchments in CC3 and CC4, their average precipitation is closer to the threshold precipitation, thus $P_{rt}/P \approx 1$.

Table 5-9: Summary of runoff and baseflow coefficients and gains according to Ponce and Shetty (1995b)

Summary	K_r	K_u	K'_r (mm^{-1})	K'_u (mm^{-1})
Average	0.34	0.28	0.000425	0.000335
Minimum	0.01	0.01	0.000031	0.000010
Maximum	0.82	0.77	0.001166	0.001094
Standard Dev	0.22	0.21	0.000285	0.000268
Abs. Confidence interval	0.06	0.05	0.000075	0.000071
Rel. Confidence interval	17%	20%	18%	21%

Table 5-10: Summary of the water balance components of the selected catchments averaged by climatic classes.

Climatic Class (55 Catchments)	K_r	K_u	λ_s	λ_u	W_p (mm)	V_p (mm)	$\lambda_s W_p$ (mm)	$\lambda_u V_p$ (mm)
2 (3)	0.04	0.01	0.03	0.04	8610	19017	217	253
3 (17)	0.32	0.26	0.02	0.14	15849	4934	113	135
4 (17)	0.31	0.23	0.02	0.05	8544	3613	76	89
5 (18)	0.46	0.38	0.01	0.12	8688	1631	56	109

Table 5-11: Runoff and Baseflow threshold, gains averaged by climatic classes.

Climatic Class (55 Catchments)	P_{rti} ; P_{uti}	P_{rti}/P_i; P_{uti}/P_i	P_{rt}/P_i; P_{ut}/P_i	K'_r (mm^{-1})	K'_u (mm^{-1})	K'_{rp} (mm^{-1})	K'_{up} (mm^{-1})
2 (3)	230	0.49	1.48	0.000131	0.000024	0.000297	0.000042
3 (17)	637	0.76	0.84	0.000394	0.000313	0.000890	0.000829
4 (17)	701	0.92	0.92	0.000395	0.000294	0.001166	0.001094
5 (18)	556	0.53	0.67	0.000529	0.000447	0.001098	0.000982

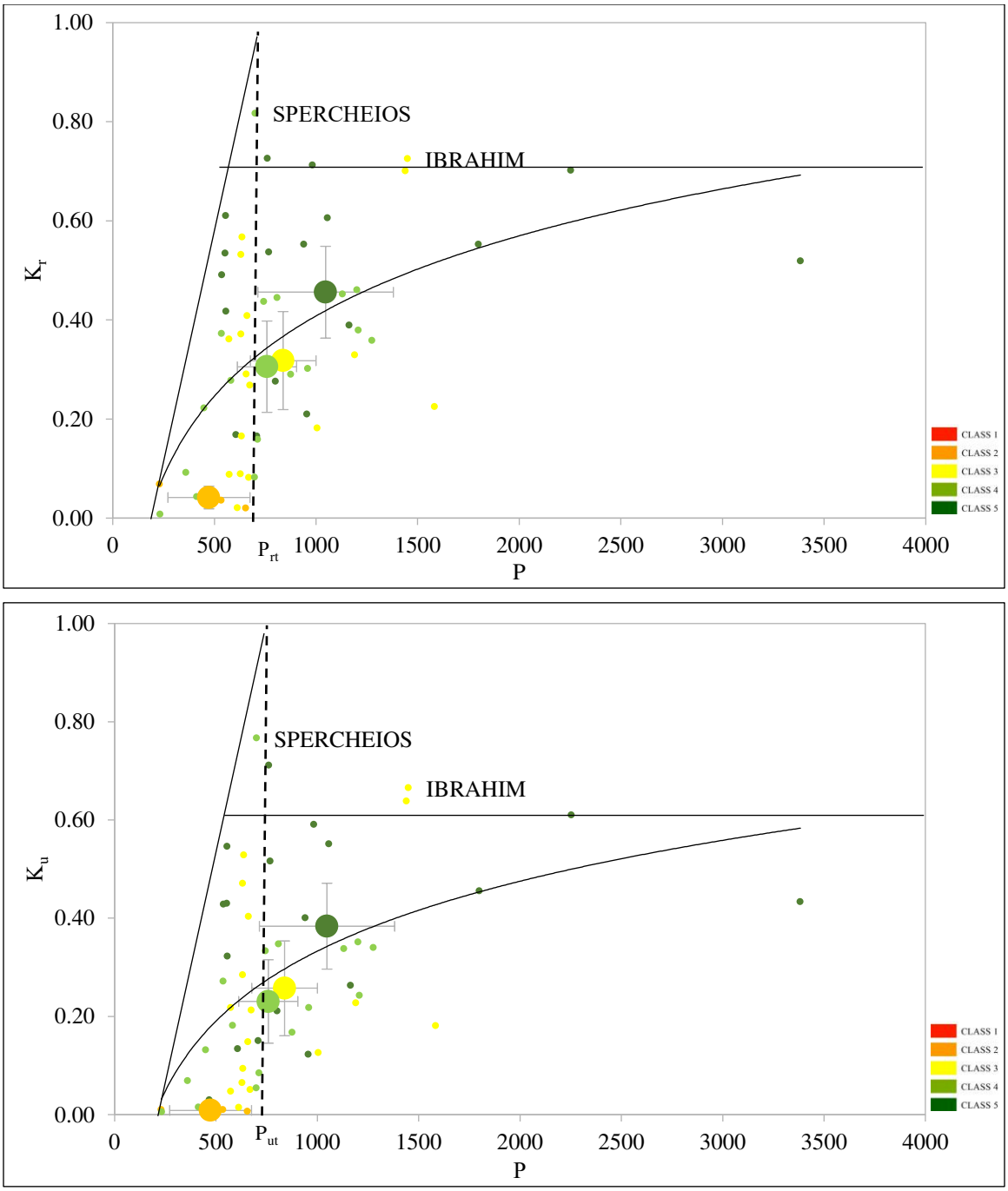

Figure 5-26: Runoff coefficient K_r and baseflow coefficient K_u with average values coloured according to climatic classes. Small points represent catchment and large points represent class averages with 95% confidence interval bars. Dashed line represents the runoff threshold precipitation and continuous lines are theoretical envelopes.

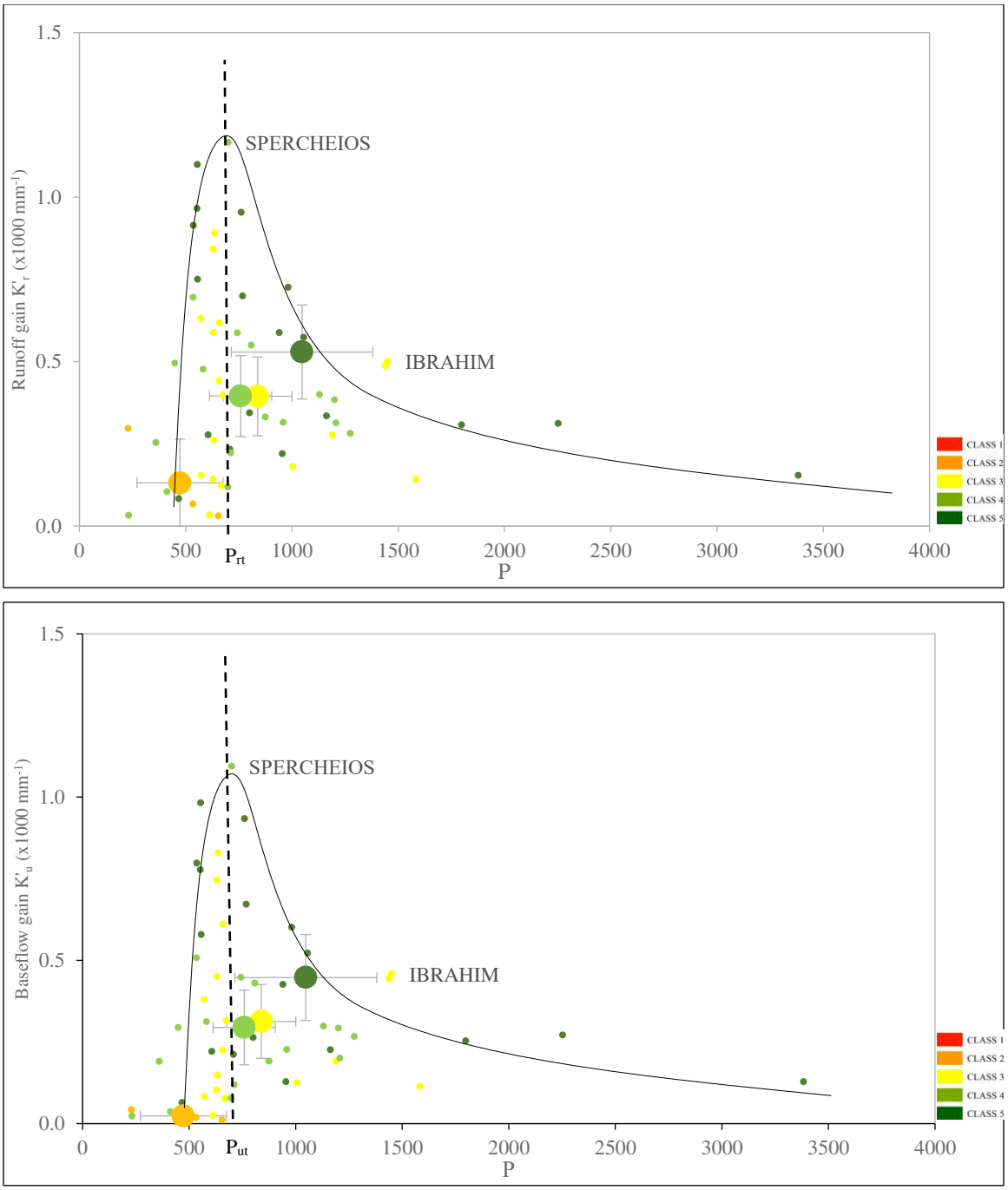

Figure 5-27: Runoff and baseflow gains K'$_r$ and K'$_u$ with average values coloured according to climatic classes. Small points represent catchment and large points represent class averages with 95% confidence interval bars. Dashed line represents the runoff and baseflow threshold precipitation and continuous lines are theoretical trendline.

We completed the observations with the analysis of Table 5-12 and Table 5-13 and Figure 5-28 and Figure 5-29 illustrated according to the physiographic classes which shed the light on some physiographic features forcing over the Mediterranean water balance mainly landform, dense forests and karst. In details:

1- The lowest wetting and vaporisation potential (W_p; V_p) correspond to PC2 catchments broadleaved tree covered at 60% (3000 mm; 1032 mm) and the highest corresponded to PC4, characterised with karstic features, mountains, and snow influence (18470 mm; 5372 mm)

2- The runoff and baseflow coefficients K_r and K_u characterise the physiographic types of the catchments. The highest values are (0.47; 0.42) and correspond to PC4 while the lowest values are (0.20; 0.15) and correspond to PC6 where Leptosols dominate and T_AWC is the lowest.

3- The highest runoff and baseflow gain peaks K'_{rp} and K'_{up} correspond to PC4 catchments (0.001166 mm^{-1};0.001094 mm^{-1}) and the lowest gain peaks to PC6 (0.000588 mm^{-1}; 0.000450 mm^{-1}).

4- We were intrigued by the positioning of the catchments according to their climatic and physiographic illustration. CC3 catchments belong to several physiographic classes, however PC4 has yielded the highest precipitation and runoff and baseflow gains and we can notice that these catchments are positioned further to the right than other catchments despite that their climatic class CC3 is more arid than CC4 and CC5. We can deduce that the mountains have taken over the climatic feature especially for Lebanese catchments.

Table 5-12: Summary of the water balance components of the selected catchments averaged by physiographic classes.

Physiographic Class (55 Catchments)	K_r	K_u	λ_s	λ_u	W_p (mm)	V_p (mm)	$\lambda_s W_p$ (mm)	$\lambda_u V_p$ (mm)
1 (10)	0.32	0.24	0.02	0.06	7433	2103	69	118
2 (3)	0.48	0.37	0.02	0.09	3000	1032	60	56
3 (10)	0.30	0.24	0.02	0.14	14544	5225	120	153
4 (11)	0.47	0.42	0.01	0.14	18470	5372	65	108
5 (9)	0.34	0.25	0.01	0.06	8553	3153	61	97
6 (4)	0.20	0.15	0.03	0.19	5685	1496	208	276
9 (8)	0.27	0.23	0.01	0.04	8155	7733	88	60

Table 5-13: Runoff and Baseflow threshold, gains averaged by physiographic classes.

Physiographic Class (55 Catchments)	P_{rti} ;P_{uti}	P_{rti}/P_i; P_{uti}/P_i	P_{rt}/P_i; P_{ut}/P_i	K'_r (mm^{-1})	K'_u (mm^{-1})	K'_{rp} (mm^{-1})	K'_{up} (mm^{-1})
1 (10)	556	0.71	0.90	0.00043	0.00032	0.00110	0.00098
2 (3)	983	1.24	0.89	0.00058	0.00045	0.00073	0.00060
3 (10)	537	0.75	0.98	0.00044	0.00036	0.00091	0.00080
4 (11)	701	0.70	0.70	0.00051	0.00046	0.00117	0.00110
5 (9)	554	0.53	0.67	0.00042	0.00031	0.00096	0.00078
6 (4)	632	0.97	1.08	0.00031	0.00024	0.00059	0.00045
9 (8)	1057	1.18	0.78	0.00028	0.00020	0.00057	0.00052

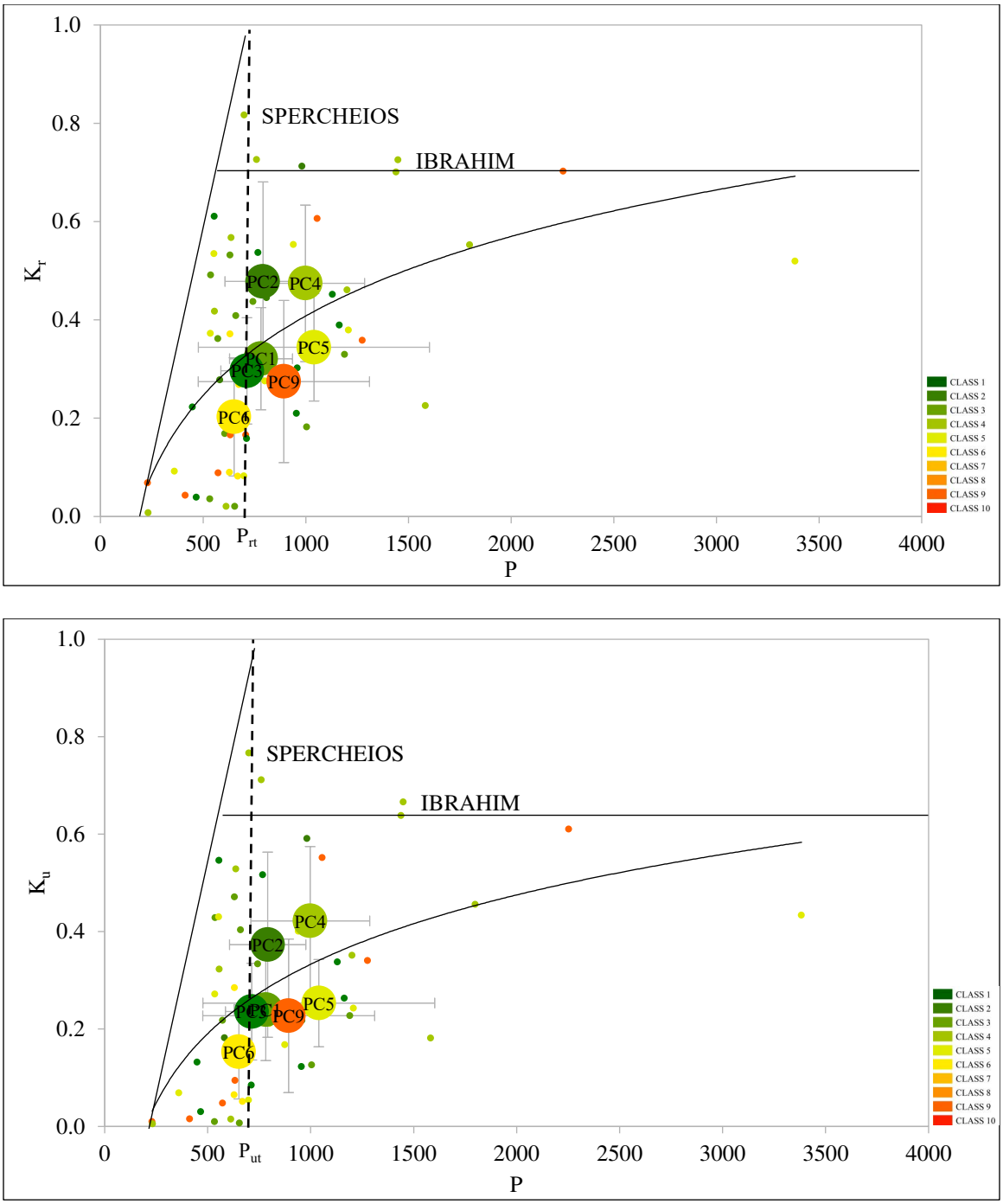

Figure 5-28: Runoff coefficient K_r and baseflow coefficient K_u with average values coloured according to physiographic classes. Small points represent catchment and large points represent class averages with 95% confidence interval bars. Dashed line represents the runoff and baseflow threshold precipitation and continuous lines are theoretical trendline.

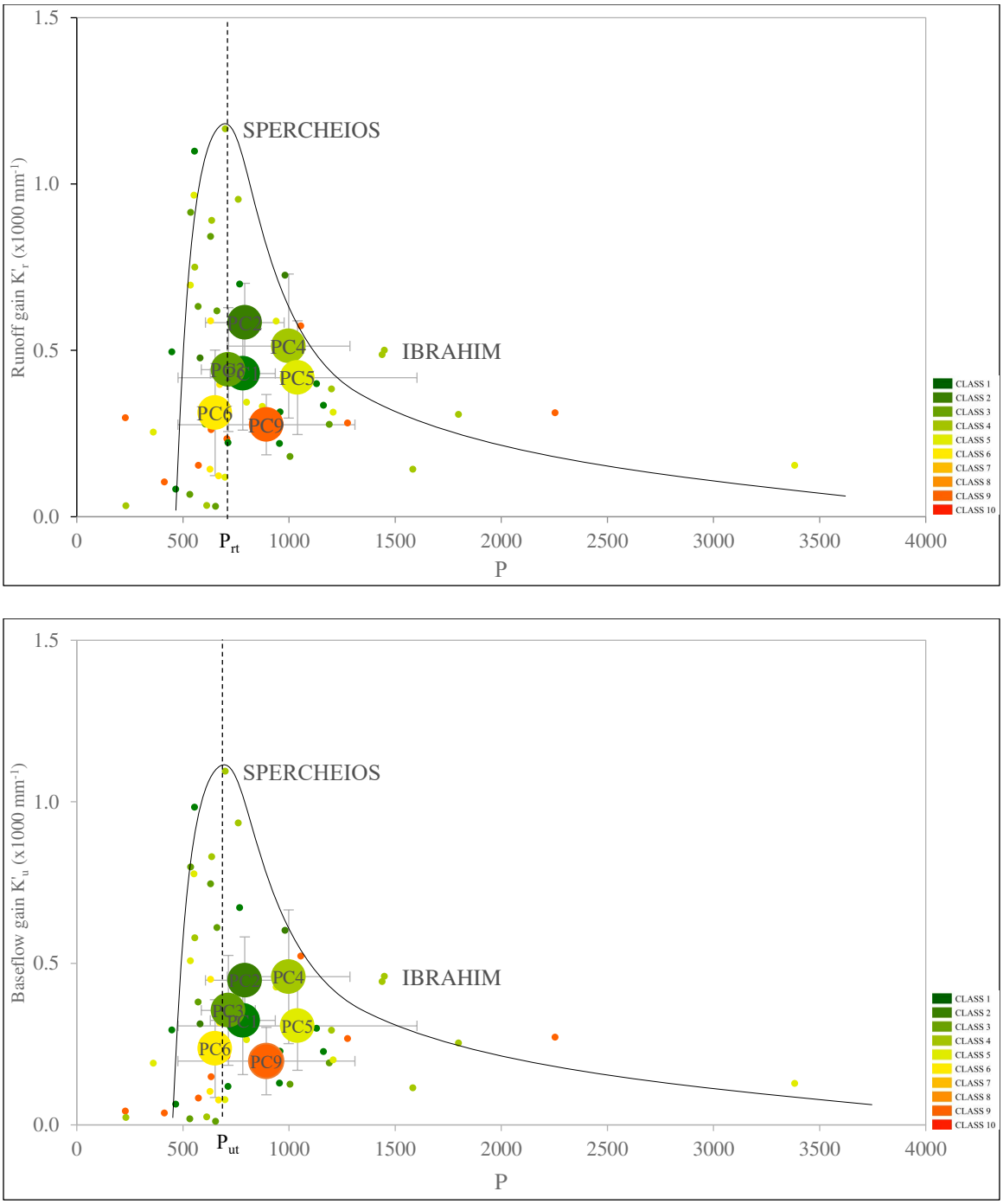

Figure 5-29: Runoff and baseflow gains K'$_r$ and K'$_u$ with average values coloured according to physiographic classes. Small points represent catchment and large points represent class averages with 95% confidence interval bars. Dashed line represents the runoff and baseflow threshold precipitation and continuous lines are theoretical trendline.

5.4.3.2 *Elasticity of water balance flow components to precipitation*

In addition to the runoff and baseflow gain assessment in the previous section, we characterise in this section the water balance of Mediterranean catchments through the elasticity to the precipitation of the total flow components Q expressed by ρ_Q, quick flow S expressed by ρ_S and slow flow U and expressed by ρ_U as defined by Harman et al., (2011) and detailed in Section 1.3.4. The elasticity is the percent of change in flow per percent of change in annual precipitation.

The results of the elasticity calculation are summarised in Table 5-14, Table 5-15 and Table 5-16 according to the climatic and physiographic classes. The elasticities ranged between $0.28 < \rho_Q < 4.33$; $1.59 < \rho_S < 5.95$; $1.06 < \rho_U < 4.91$ with a lonely surprising and exceptional negative value $\rho_U = -0.66$ which correspond to Andarax river in southern Spain. Average values of the elasticities across all sites was highest for ρ_S at 2.18, while ρ_U yielded 2.02, and ρ_Q yielded 2.01. The variability between sites (measured by the standard deviation across sites) was smallest for ρ_Q at 0.67, ρ_S at 0.71 and highest for ρ_U at 0.86.

Table 5-14: Summary of flow components elasticity according to Harman et al. (2011).

Summary	λ_s	λ_u	W_p (mm)	V_p (mm)	$\lambda_s W_p$ (mm)	$\lambda_u V_p$ (mm)	ρ_Q	ρ_S	ρ_U
Average	0.02	0.10	10853	4213	88	118	2.01	2.18	2.02
Minimum	0.00	0.00	1897	182	3	0	0.28	1.59	-0.66
Maximum	0.09	0.88	78982	39167	347	469	4.33	5.95	4.91
Standard Dev	0.02	0.18	14854	7353	101	131	0.67	0.71	0.86
Abs. Confidence interval	0.01	0.05	3926	1943	27	35	0.18	0.19	0.23
Rel. Confidence interval	39%	46%	36%	46%	30%	29%	11%	9%	9%

The relationship between the flow elasticities and the humidity index (P/E_P) are represented in Figure 5-30 and Figure 5-31 according to their climatic and physiographic classes with average values and corresponding distribution maps. The scatter seems to be enclosed by two envelopes, same as Harman (2011), an upper bound with a roughly hyperbolic shape that declines with humidity, and a lower bound that is invariant with climate. These bounds appear to converge for $P/E_P > 2$, although there are only 3 sites in the dataset that are that humid mainly located in the north eastern Mediterranean region.

According to the climatic classification, the elasticities are generally larger for CC2 arid catchments and decrease with the gradient to CC5 humid catchments, however with a wide variability among regions. This variability is clearly notifiable in Eastern Mediterranean (Lebanon, Cyprus, Israel) where CC2 and CC3 dominate with wide range of ρ_Q and ρ_U values but ρ_S values seem close enough. Same observation as for north western region. Other regions yielded consisting values of elasticities for the three different flows; this is observable between southern Italy, North Tunisia and eastern Algeria (CC3 and CC4) where elasticity values range between $1.79<\rho_Q<2.24$; $1.78<\rho_S<2.40$; $1.80<\rho_U<2.55$ and on the coastal North

Eastern Mediterranean region between Turkey, Greece, Albania, Croatia and Slovenia where elasticity values range between $1.38<\rho_Q<2.17$; $1.59<\rho_S<1.95$; $1.27<\rho_U<2.65$.

Table 5-15: Flow components elasticity averaged by climatic classes.

Climatic Class (55 Catchments)	ρ_Q	ρ_S	ρ_U	ρ_Q *Stdev*	ρ_S *Stdev*	ρ_U *Stdev*	ρ_Q *Conf Inter*	ρ_S *Conf Inter*	ρ_U *Conf Inter*
2 (3)	2.82	2.65	3.31	0.88	0.76	1.21	0.99	0.86	1.37
3 (17)	2.11	2.15	2.14	0.74	0.51	0.88	0.35	0.24	0.42
4 (17)	1.94	2.35	1.85	0.53	0.99	0.74	0.25	0.47	0.35
5 (18)	1.86	1.95	1.85	0.56	0.36	0.64	0.26	0.17	0.29

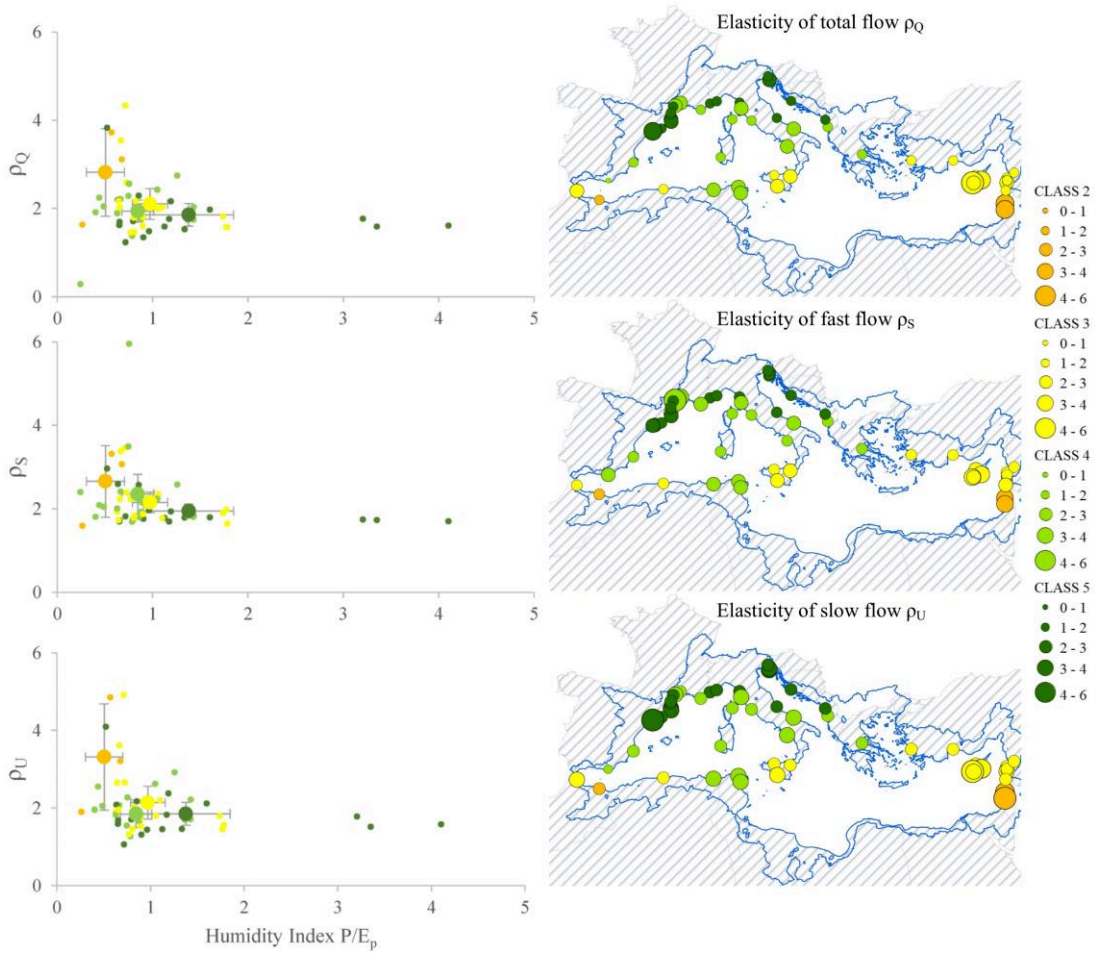

Figure 5-30: Left: Relationships between total flow Q, quick flow S and slow flow U elasticities ρ_Q, ρ_S, ρ_U and the humidity index P/E_P with average values coloured according to climatic classes. Small points represent catchments and large points represent class averages with 95% confidence interval bars. Right: Spatial distribution of the elasticities ρ_Q, ρ_S, ρ_U on the Mediterranean coloured according to climatic classes with a variation of size according to elasticity values.

According to the physiographic classification, the PC4 mountainous catchments under snow and karst influence yielded the lowest elasticities for the highest humidity indices $0.28<\rho_Q<2.03$; $1.64<\rho_S<2.39$; $-0.66<\rho_U<1.95$ with low ρ_S variability; while PC6 catchments (shrub covered at 52%, low T_AWC and

Leptosols at 79%) yielded the highest elasticities for the lowest humidity indices, 1.80 <ρ_Q<4.33; 1.87<ρ_S<3.46; 1.76<ρ_U<4.91 with the highest ρ_Q and ρ_U variability; The north western PC5 catchments (mixed leaved tree cover) yielded the lowest ρ_S = 1.91 and ρ_S variability of 10%.

Table 5-16: Flow components elasticity averaged by physiographic classes.

Physiographic Class (55 Catchments)	ρ_Q	ρ_S	ρ_U	ρ_Q *Stdev*	ρ_S *Stdev*	ρ_U *Stdev*	ρ_Q *Conf Inter*	ρ_S *Conf Inter*	ρ_U *Conf Inter*
1 (10)	2.13	2.22	2.10	0.69	0.56	0.82	0.43	0.35	0.51
2 (3)	1.85	2.04	1.73	0.26	0.27	0.25	0.30	0.30	0.29
3 (10)	2.19	2.20	2.34	0.67	0.56	0.98	0.41	0.35	0.61
4 (11)	1.51	1.92	1.38	0.44	0.25	0.68	0.26	0.15	0.40
5 (9)	1.92	1.91	1.95	0.24	0.20	0.31	0.16	0.13	0.20
6 (4)	3.06	2.77	3.23	0.96	0.67	1.17	0.94	0.66	1.14
9 (8)	1.99	2.49	1.97	0.36	1.34	0.34	0.25	0.93	0.24

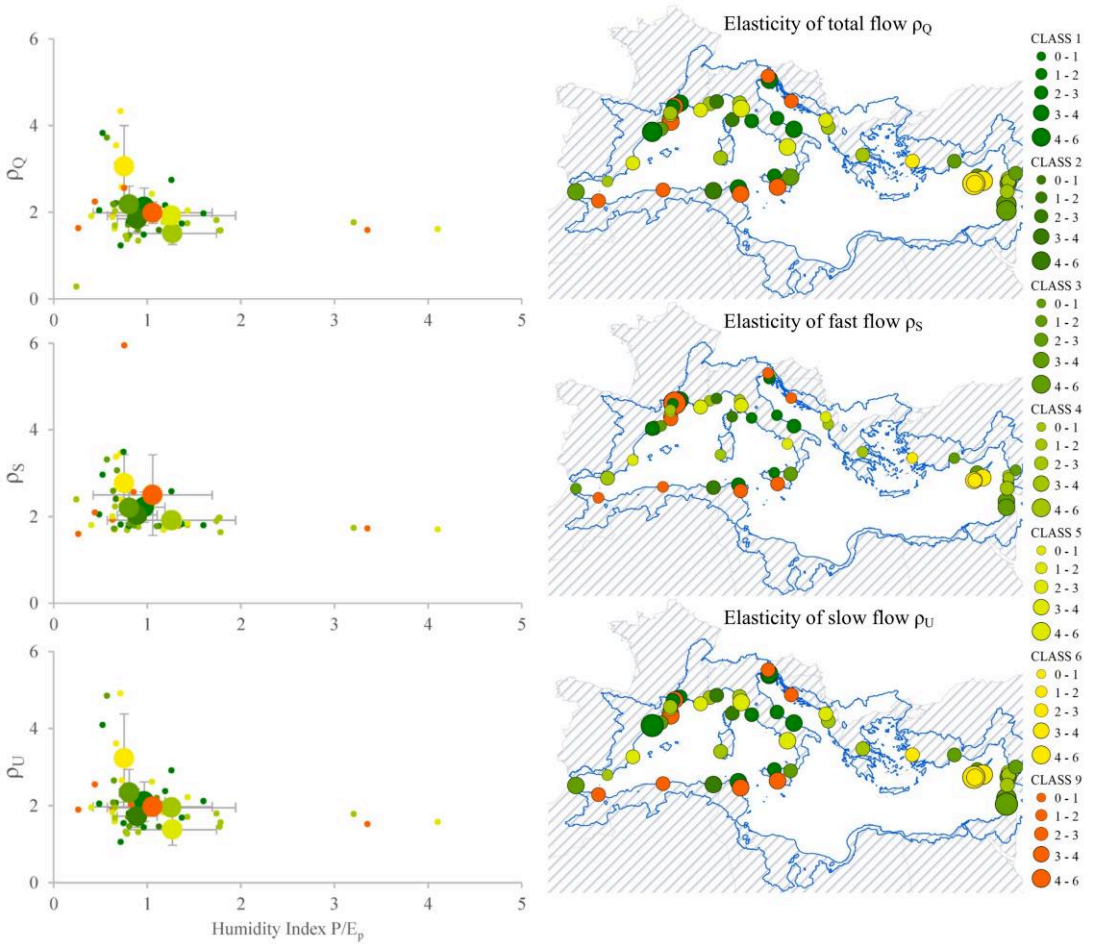

Figure 5-31: Left: Relationships between total flow Q, quick flow S and slow flow U elasticities ρ_Q, ρ_S, ρ_U and the humidity index P/EP with average values coloured according to physiographic classes. Small points represent catchments and large points represent class averages with 95% confidence interval bars. Right: Spatial distribution of the elasticities ρ_Q, ρ_S, ρ_U on the Mediterranean coloured according to physiographic classes with a variation of size according to elasticity values.

The somehow distinct climatic patterns seen on the charts of Figure 5-30 did not necessarily create distinct spatial patterns as intra-class variability is clearly observable. This variability is mainly caused by several physiographic features contributing to the runoff components of Mediterranean catchments water balance especially PC4 catchments that appeared to be the least sensitive to precipitation change, or soil and landcover as PC6 appeared the most sensitive while both classes are located in the southern CC3 region.

The sensitivity analysis conducted on the US MOPEX dataset identified that the flow generation thresholds $\lambda_s W_p$ and $\lambda_u V_p$ had a much greater control over the elasticity than the wetting W_p and vaporisation V_p potentials (Harman et al., 2011). The charts of the elasticities against the water balance parameters in Figure 5-32 endorse this observation on the Mediterranean as runoff threshold, which were determined from the interannual variability, are correlated with the flow elasticities rather than the wetting and vaporisation potentials where a higher threshold (or higher ratio to P) results with a higher elasticity.

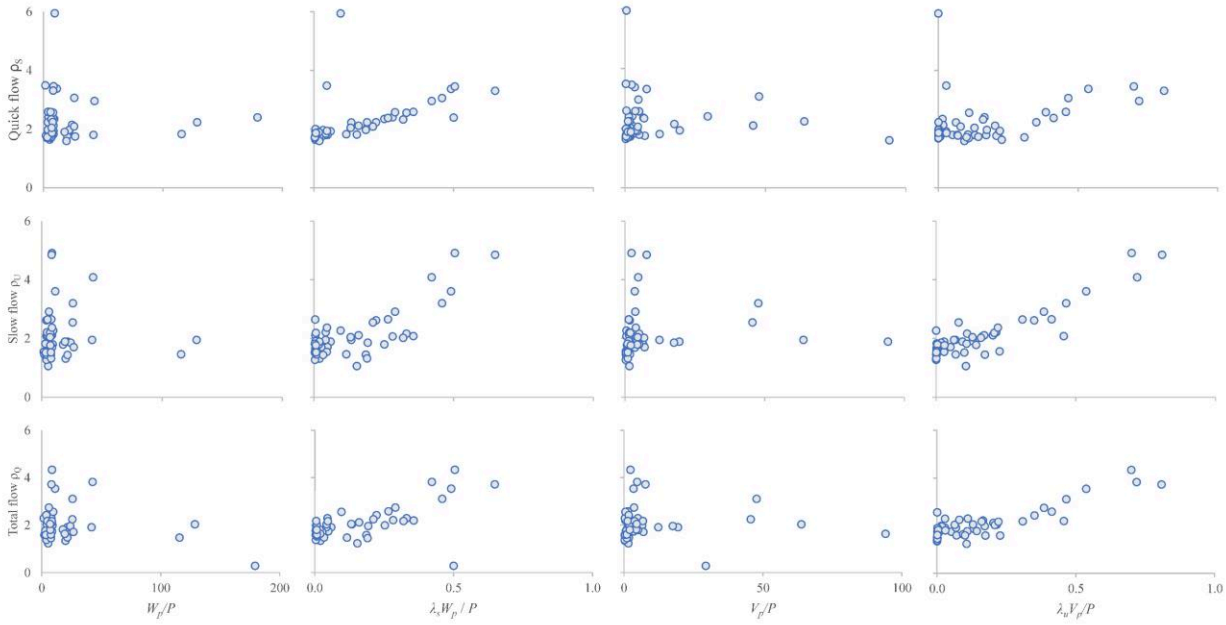

Figure 5-32: Relationships between total flow Q, quick flow S and slow flow U elasticities ρ_S, ρ_U, ρ_Q and the water balance functional parameters W_P, $\lambda_s W_p$, V_P and $\lambda_u V_p$ normalised by P.

The threshold functional parameters, normalised by mean annual precipitation, against the mean annual Horton index in Figure 5-33 shows that for CC2 semi-arid catchments (where H →1) the thresholds are a large proportion of annual precipitation, while in CC5 humid catchments (particularly where H < 0.5), the thresholds are close to 0 but with some exceptions where low precipitation yields higher $\lambda_s W_p$/P ratio.

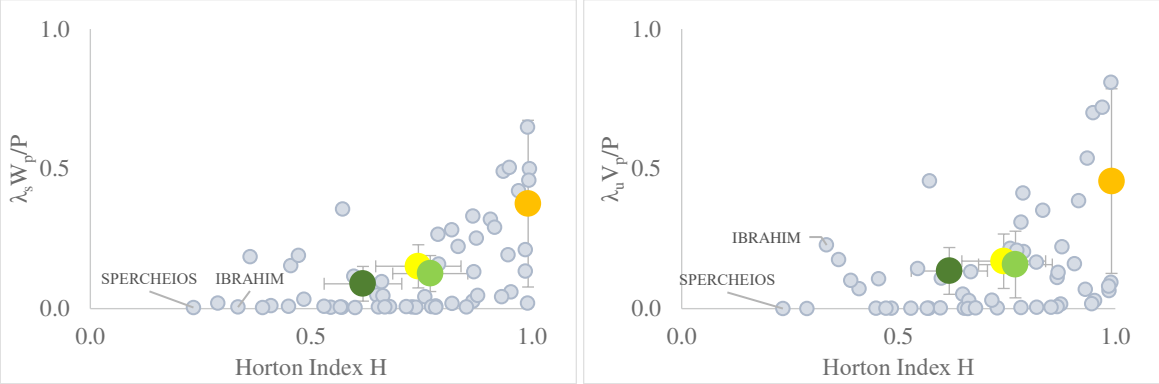

Figure 5-33: The thresholds $\lambda_s W_p$ and $\lambda_u V_p$ (normalised by P) correlated with the Horton index H=V/W.

These findings are aligned with previous observations on the runoff gain advanced in Section 5.4.3.2 where CC2 arid catchments are apt to increase their runoff coefficient with more precipitation while humid CC5 catchments are apt to decrease it with more precipitation. They are also aligned with the observations on runoff components elasticity of Harman (2011) study and consequently those of climate elasticity of streamflow in the united states which also observed that snow dominated catchments tend to have the lowest streamflow sensitivity and that arid and semiarid catchments tend to have the highest streamflow sensitivity (Sankarasubramanian et al., 2001).

5.5 CONCLUSION

The flow regimes analysis showed that group G12 dominated Northern Mediterranean catchments while group G13 dominated the Southern catchments, hence verifying the findings of Haines (1988). However, some PC4 mountainous karsitc catchments under snow influence, located between Spain and France and North Lebanon, belonged to group G14 showing a peak flow *early spring* due to snowmelt.

The water balance model of Budyko (1974) was useful in positioning all the catchments in respect to their total precipitation and evapotranspiration, hence indicating the climatic forcing on hydrology. Budyko curve can indicate the overall water availability of a catchment, but not enough to estimate the water resources. L'vovich (1979) model showed a breakdown of the annual water balance advancing more info on the surface runoff S and groundwater runoff U which indicates the physiographic forcing on hydrology. It also permitted a precise interannual comparison with precious info on water resources. Ponce and Shetty (1995a) generalized L'vovich model from annual values to continuous curves which helps in predicting the available water resources throughout the years. The model equations are dependent from runoff threshold parameters, specific for each catchment which permits more precise inter catchment comparison, highlighting Mediterranean variability. In addition, these parameters also reflect the physiographic forcing on hydrology. Sivapalan (2011) model went further with non dimensionalising Ponce and Shetty equations which permitted in addition to interannual and inter catchment comparison, an inter climatic and inter physiographic comparison, useful in our study to uncover the variability and homogeneity of Mediterranenan catchments through nondimensional metrics K_H, K_B, K_R and K_V. These metrics showed the special setting of Mediterranean catchments in correspondence to aridity index $\varphi = \tilde{V}/\tilde{P}$. Sivapalan model showed a space time symmetry where functional curves fit both to individual catchments for interannual analysis or to mean annual water balances for inter catchment analysis despite their variability.

The runoff and baseflow gain approach characterised the climatic and physiographic classes highlighting the trends of catchments to the climatic spatial distribution from wet region in the North to arid region in the south. And apparently, the runoff of CC2 catchments looks close to the semiarid north African coniferous catchments as presented by Ponce and Shetty (1995b).

In addition, Harman's elasticity analysis highlighted the role of the initial abstraction or runoff threshold in the predetermination of the elasticity of runoffs shedding the light on the ability of dry CC2 catchments to increase total flows in case of precipitation increase, found to be around 2.82, higher than the ability of humid CC5 catchments found equal to 1.86; and the ability of PC6 shrub covered catchments equal to 3.06, higher than the PC4 catchments ability, found around 1.51. The breakdown of the flow elasticity analysis

into the water balance parameters showed that the quick flow and slow flow thresholds yield the strongest control over the elasticity and are the primary determinant of any runoff gain in case of precipitation change.

All the water balance models highlighted similar Mediterranean trends following the general Mediterranean climatic setting from the wet Northern region to the arid Southern region and showed hydrological homogeneity for specific physiographic classes like PC4 mountainous snow and karst influenced catchments. However, to characterise the Mediterranean hydrological variability and homogeneity, we will rely on Ponce and Shetty (1995b) baseflow and runoff coefficients K_r and K_u which are also useful to estimate catchments' resources.

These observations and findings will be verified and completed in CHAPTER 6 with the Canonical Correlation Analysis to first discover which specific climatic and physiographic indices govern the Mediterranean hydrological behaviour, second predict the water balance coefficients values on all 1270 type II catchments and third check the climatic evolution impact on the hydrological behaviour of Mediterranean catchments in case of RCP 4.5 or RCP 8.5 scenarios, in the light of what we deduced in Section 5.4.3.1, that PC4 catchments located in CC3 regions yield the highest baseflows and runoff.

"God Rivers Duel, A Mediterranean Epic"

Fourth encounter: Adonis and Spercheios meet Tethys

ΠΟΤΑΜΙ ΕΝΑ	
Name	Ibrahim, Adonis
Country	Lebanon
Area	329 km^2
MAP	1450 mm
MAQ	1052 mm

ΠΟΤΑΜΙ ΔΥΟ	
Name	Spercheios
Country	Greece
Area	1592 km^2
MAP	701 mm
MAQ	575 mm

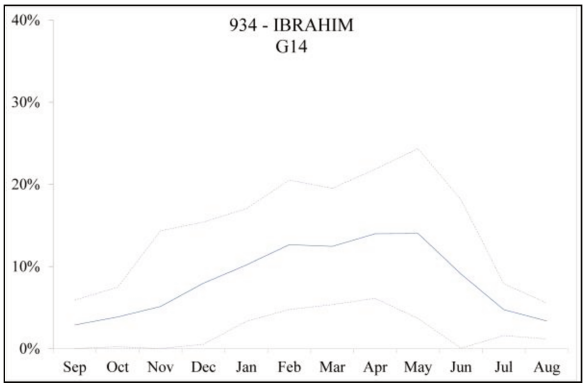

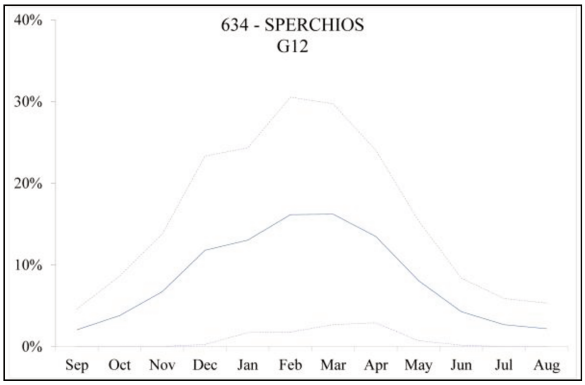

Hydrological characteristics					
Hydrological Class		HC5			
ET_p/P	0.66	E/P	0.27		
P	1450 mm	Q	1052 mm		
U	794 mm	S	258 mm		
V	399 mm	W	1193 mm		
K_r	0.73	K_u	0.67		
$\lambda_s W_p$	8 mm	$\lambda_u V_p$	330 mm		
W*	0.8	S*	0.2		
U*	0.9	V*	0.1		
$\tilde{P}$	0.2	$\tilde{V}$	0		
KH	0.1	KV	0.1		
KB	0.7	KR	0.9		
φ	0.1				
ρQ	1.6	ρS	1.6	ρU	1.6

Hydrological characteristics					
Hydrological Class		HC5			
ET_p/P	1.41	E/P	0.16		
P	701 mm	Q	572 mm		
U	421 mm	S	151 mm		
V	128 mm	W	550 mm		
K_r	0.82	K_u	0.77		
$\lambda_s W_p$	3 mm	$\lambda_u V_p$	0 mm		
W*	0.8	S*	0.2		
U*	0.8	V*	0.2		
$\tilde{P}$	0.3	$\tilde{V}$	0.1		
KH	0.2	KV	0.2		
KB	0.6	KR	0.8		
φ	0.3				
ρQ	1.4	ρS	1.7	ρU	1.3

CHAPTER 6. HYDROLOGICAL HOMOGENEITY AND VARIABILITY ANALYSIS

Chapter summary

This chapter aimed to identify hydrologically homogeneous Mediterranean catchments through the regionalisation of High and Low Flows indices and the runoff coefficients of 55 donor catchments leading to identify exactly which indices contribute the most in the definition of the Mediterranean hydrology. Based on the findings, it is believed that in the Mediterranean, climatically homogeneous catchments are more likely to have homogenous hydrological behaviour despite their physiographic variability except for karstic and snow influenced catchments which yield homogeneous hydrological behaviour despite different climates.

The regionalisation of the runoff and baseflow coefficients of type II catchments permitted the estimation of water resources, a valuable information for regional and national water management strategies, where stakeholders can easily choose which catchments to drop and which to focus on. The regionalisation has also permitted MED-CORDEX RCM climate change scenarios impact prediction on water balance coefficients. Overall, the coefficients are increasing because of the precipitation decrease, however, the projected evolution has mainly impacted the extremes, hence minimising the interclass variability and increasing catchments homogeneity. Catchments scatter and classes have drawn closer to the most Mediterranean CC3 and CC4 catchments, with PC4 staying as the highest yielding catchments.

Complementary material to Chapter 6 was added in Appendix E

APPENDIX E1 Baseflow and Runoff coefficients under MED-CORDEX RCM climate change scenario

APPENDIX E2 EGU General Assembly 2019 – Conference Poster – Determination of Hydrologically Homogeneous Mediterranean Catchments based on Multivariate Analysis

6.1 INTRODUCTION

In anthropology, identical twins who share the same DNA, appearance and behaviour can be distinguished from their biometrics like fingerprints, retina, thermogram or iris patterns (Jain et al., 2002). On the reverse, in hydrology no two identical catchments could ever be found due to the wide inter-catchment variability of area, landform, slopes, direction, landcover, soil, geological formations all affecting the river flow. However, two catchments are considered hydrologically similar if their appearance and behaviour, defined by their climatic, physiographic and hydrological indices, are close to the same clustering kernel, obtained by statistical methods, where distance measure is a function of the catchment's attributes (Blöschl, 2006). Thus, the identification of hydrologically homogeneous catchments, or equivalently the classification of catchments into homogeneous groups having the same hydrological behaviour, is the basis of all regionalisation procedures (Di Prinzio et al., 2011).

In CHAPTER 5, we analysed the water balance of 55 Mediterranean catchments that belong to different climatic and physiographic classes. The water balance characterisation shed the light on the climatic forcing, setting a general spatial trend from Southern region with low runoff catchments, coinciding with dry climate, to Northern region with high runoff catchments coinciding with wet climate, similar to the seasonality and aridity distribution over the Mediterranean and following the climatic classification obtained in CHAPTER 3. However, the characterisation also highlighted the physiographic forcing on water balances, especially for PC4 mountainous, snow and karst influenced catchments which defied the climatic setting and yielded the highest runoff and baseflow even in the South.

This chapter aims to identify hydrologically homogeneous Mediterranean catchments through the regionalisation of hydrological indices based on CCA between physioclimatic and hydrological indices of the 55 catchments as donors leading to identify exactly which indices contribute the most in the definition of the Mediterranean hydrology. The correlation of several physioclimatic indices to hydrological indices were previously identified in literature, we mainly cite catchment area correlation to flood indices, slope, mean annual precipitation, basin geology to baseflow indices (Acreman & Sinclair, 1986) and subsoil available water content to flow regimes (Oueslati et al., 2015).

It also aims to analyse the hydrological homogeneity between catchments from the same climatic and or physiographical classes. The sample constitutes only 4% of catchments, therefore we will only estimate the hydrological indices of type II catchments and identify the homogeneous catchments based on runoff and baseflow coefficients. We will also assess the climate change impact under RCP scenarios based on the projected indices calculated previously in CHAPTER 3.

The mapping of hydrologically homogeneous Mediterranean catchments is one of the basic studies to be used by researchers, laboratories, engineers, Governments, and International organizations which Mediterranean region form their target study areas. These results could help in catchment scale studies like prediction on ungauged basins or furthermore regional scale studies like global change impact prediction on Mediterranean hydrology.

This variability analysis will help in setting better management plans of gauged and ungauged basins to adapt and mitigate the expected climate change impact expressed by temperature increase, seasonal shifting, early snowmelt and anthropogenic pressures on Mediterranean runoff mainly through transformation of agriculture, land-use and touristic activities (Cudennec et al., 2007; Hreiche et al., 2007; García-Ruiz et al., 2011; Verdier & Viollet, 2015)

The proposed approach consists of first, applying Canonical Correlation Analysis (CCA) to only consider the most contributory physioclimatic indices and then the regionalisation of hydrological indices through the obtained regression equations between P-CIs and HIs of a donor set and transpose it to the target set of catchments. Finally, K-means clustering of catchments based on the regionalised HIs to determine hydrologically homogenous catchments and characterize Mediterranean hydrology. The study resulted with a hydrological cartography of Mediterranean catchments.

The climate change impact on runoff and baseflow coefficients K_r and K_u and gains K'_r and K'_u will be assessed by replacing the climatic indices in the obtained regression equations with the projected climatic indices for the period 2070-2100 under MED-CORDEX RCM ALADIN and RCM CCLM for two different RCP scenarios (RCP 4.5 and RCP 8.5). The resulting charts will form a simple follow-up tool of the climate change impact on Mediterranean hydrology.

This chapter is structured into six sections; Section 6.1 Introduction, Section 6.2 presents the approaches for the similarity regionalisation analysis; Section 6.3 presents the results of the inter-class and intra-class hydrological similarity analysis of Mediterranean catchments; Section 6.4 presents the results of the hydrological regionalisation; Section 6.5 presents the climate change impact on the water balance runoff and baseflow coefficients and gains before discussing and concluding in Section 6.6.

6.2 METHODOLOGY

Several approaches could be considered for hydrological classification and regionalisation. The adopted approach developed here, takes into consideration Blöschl's assumption on hydrological regionalisation that if catchments attributes are similar, one would expect a hydrological similarity, thus the use of similar catchment attributes for hydrological regionalisation. Defining a group of hydrologically similar catchments consists of quantifying a distance measure as a function of the catchment's attributes where classification can then be obtained by a range of statistical methods (Blöschl, 2006).

The climatic classification developed in CHAPTER 3, the physiographic classification developed in CHAPTER 4 and water balance analysis in CHAPTER 5 will serve to define the inter-class and intra-class hydrological similarity of the 55 selected catchments. The inter-class hydrological similarity will be analysed for all 55 selected catchments through a CCA between the most contributing physioclimatic indices and selected hydrological indices corresponding to either of the runoff coefficients K_r and K_u and the High and Low flows indices DH_5, FH_1, DL_5, FL_1. The intra-class similarity will be also analysed between catchments of the same physiographic cluster, here limited to the cultivated and managed catchments (PC1 and PC9), and mountainous catchments (PC4) to discover specifically which indices contribute to each of the classes and assess the hydrological similarity in regards to the climatic and physiographical ones, emphasizing the assumption that if catchments attributes are similar, one would expect a hydrological similarity (Blöschl, 2006).

The hydrological regionalisation method consists of transposing catchment characteristics from a donor to a target catchment or set of catchments. The regionalisation methods were grouped into four, mean methods, regression methods, spatial proximity methods and similarity groups of catchments attributes methods. The results of the comparison study between these methods indicated that two of them performed best, the spatial proximity kriging method and the similarity based on physiographic attributes (Parajka et al., 2005). The study area being very wide and climate being uniformly distributed, and geographical proximity is no guarantee that the distributions of normalised maximum floods are identical (Cunnane, 1986), we searched for the climatic and physiographic indices similarity based on CCA. This method was previously applied in Canada for the regionalisation of the maximum annual flood (Cavadias, 1990) and flood frequency (Ouarda et al., 2001) and for Low Flows in Massachusetts (Tsakiris et al., 2011).

6.2.1 Hydrological Indices

Several choices were discussed for the preselection of hydrological indices:

1- PCA from the complete set of 171 hydrological indices collected in the Olden's redundancy study of hydrological indices. To reduce redundancy, Olden applied PCA to examine dominant patterns of intercorrelation among 171 Hydrological Indices for each streamflow regimes and identify subsets of indices that describe the major sources of variation (Olden & Poff, 2003),
2- PCA from Richter's indices of hydrological alteration (Richter et al., 1996),
3- 90-day annual means of high and low flow magnitude and frequency indices DH_5, FH_1, DL_5, FL_1.
4- A selection of the hydrological indices according to the water balance characteristics.

We first chose to work on the water balance parameters found in CHAPTER 5 to verify what have been advanced in the chapter and to better characterise the water balance of Mediterranean catchments. We also chose, based on literature, to work on High and Low flows indices as they summarize the general hydrological behaviour of Mediterranean seasonality and the knowledge of these statistics help in setting best management practices for engineering purposes and setting operating policies (Cavadias, 1990; Ouarda et al., 2001; Tsakiris et al., 2011). The hydrological classification was only based on water balance indices. It is always interesting to consider other hydrological indices and compare with actual classification, but one can assume that catchments showing similar water balance metrics will show matching homogeneity as other indices. Furthermore, the knowledge of flow statistics is important for water resources management, for future regionalisation and PUB studies.

The 171 HIs definition were adopted from Olden's redundancy study and automatically calculated for each catchment using the Hydrological Index Tool (HIT). The HIT was developed under a joint project between the U.S. Geological Survey and several water science centres in New Jersey (Henriksen et al., 2006). The statistical summary of the hydrological indices for the selected 55 catchments shows in Table 6-2 the values of DH_5 ranging between 0.1 and 277 m^3/s and DL_5 between 0 and 45 m^3/s. These wide ranges highlight the hydrological variability between catchments while the wide difference between DH_5 and DL_5 expresses the hydrological seasonality of the Mediterranean flow regimes. The preselected HIs are shown in table II of Olden's study.

Table 6-1: Statistical summary for the selected catchments physioclimatic indices.

	A (km^2)	Z_{Mean} (m)	ZS_{Mean} (m)	T_AWC (mm)	Leptosols (%)	I_S	$P_{75\%}$	$SP_{1.5}$	I_{Hor}	$T_{25\%}$	I_{Arid}
Minimum	77	93	0	22	10.0	0.3	0.0	0	3.6	1.3	0.32
Mean	892	580	612	48	39.8	0.7	0.5	2	4.0	1.4	1.51
Maximum	3125	1572	2092	56	90.0	1.0	0.9	5	5.3	1.7	1.35
Median	634	494	0	49	37.5	0.7	0.6	1	3.8	1.4	3.29

Table 6-2: Statistical summary for the 55 selected catchments High and Low Flows indices and coefficients.

	DH_5 (m^3/s)	FH_1	DL_5 (m^3/s)	FL_1	K_r	K_u
Definition	Annual maxima of 90-day mean of daily discharge	High flood pulse count	Annual minima of 90-day mean of daily discharge	Low flood pulse count	Total Runoff Coefficient	Baseflow Coefficient
Minimum	0.1	2.9	0.0	0.0	0.34	0.28
Mean	26.7	7.9	4.4	4.8	0.01	0.01
Maximum	277.0	16.3	44.8	13.6	0.82	0.77
Median	10.3	7.3	0.4	4.6	0.22	0.21

6.2.2 CCA Multivariate Analysis

Multivariate analysis methods like Principal Component Analysis (PCA) and Canonical Correlation Analysis (CCA) are widely applied to reduce the dimensionality of datasets and keeping the most representing and uncorrelated variables. This section presents a brief description of the CCA method along with some of its applications in hydrology. For an extensive mathematical description and demonstration of these methods we advise to consult the following references : Principles of multivariate analysis: a user's perspective (Krzanowski, 1988); Principal Component Analysis (Jolliffe, 2002); and Ouarda Taha study on regional flood frequency estimation with a detailed methodology of CCA application to regional estimation on gauged and ungauged target basins (Ouarda et al., 2001).

CCA permits to establish the interrelations that may exist between two groups of variables, by identifying the linear combinations of the variables of the first group that are the most correlated to some linear combinations of the variables of the second group (Ouarda et al., 2001). CCA allows to identify the dominant linear modes of covariability between two sets of variables $X= \{X_1, X_2, \ldots, X_n\}$ and $Y = \{Y_1, Y_2, \ldots, Y_r\}$, $n \geq r$.

Let V and W be linear combinations of the X and Y respectively and C their covariance Matrix

$$V = a_1X_1 + a_1X_2 + \cdots + a_nX_n = a'X$$

$$W = b_1Y_1 + b_1Y_2 + \cdots + b_nY_n = b'Y$$

$$\lambda = corr(V,W) = \frac{cov(V,W)}{\sqrt{Var(V)}\sqrt{Var(W)}} = \frac{a'C_{XY}b}{\sqrt{a'C_{XX}a}\sqrt{b'C_{YY}b}}$$

The CCA identifies the eigenvectors a and b for which *corr(V,W)* is maximal, using Lagrange multipliers technique subject to the constraints that Var (V) = Var (W) = 1, leading to p solution-triplets (λ_i, V_i, W_i) from which results two main properties (P1): distinct Vi and Wi are uncorrelated (P2): Wi and Vj, i≠j, are uncorrelated.

If the basin physioclimatic indices appeared as good predictors, regionalisation of the hydrological indices could be carried out. CCA application and regionalisation methodology was detailed in the paper presented to the UNESCO International conference on Statistical and Bayesian Methods in Hydrological Sciences by Cavadias (1995). In brief, the hydrological canonical covariates (W_1) should be estimated based on the regression equations between V and W where $W_i = \lambda_i V_i$ with λ_i correlation coefficients; and second, regression equations should be determined between the covariates and the hydrological indices based on the inverted matrix of their coefficients obtained from CCA. Normalised values of the hydrological indices could be obtained then and if donor catchments are representative of the population and the physioclimatic indices are good predictors, accurate denormalized values could be obtained.

CCA was applied to identify main coupled circulation–rainfall patterns and to relate recent variability and trends of Mediterranean precipitation to large-scale circulation dynamics (Dünkeloh & Jacobeit, 2003). In an application to the PUB problem on a Mediterranean country, Di Prinzio classified 296 Italian catchments using a combination of PCA and CCA and Self Organization Map (SOM) (Di Prinzio et al., 2011). ACP and CCA calculation tools are widespread among statistical software such as SPSS V. 25 used in this study.

6.2.3 RCP Scenarios

For climate change impact assessment, the projected climatic indices obtained in CHAPTER 3, for the period 2070-2100 under MED-CORDEX RCM ALADIN and RCM CCLM for two different RCP scenarios (RCP 4.5 and RCP 8.5) will be replaced in the canonical regression equations obtained from the CCA of the water balance runoff and baseflow coefficients K_r and K_u. The projected precipitation will also be replaced to estimate the coefficients and gains K_r and K_u and gains K'_r and K'_u.

6.2.4 Adopted Methodology

The proposed methodology consists of a two-step physioclimatic variability – hydrological homogeneity analysis. We search to define the inter-class and intra-class hydrological similarity of the 55 selected catchments. The inter-class hydrological similarity will be analysed for all 55 selected catchments through a CCA between physioclimatic indices and water balance and High and Low Flows hydrological indices. The intra-class similarity will be analysed for catchments of the same physiographic cluster, here limited to the cultivated and managed PC1 and PC9 catchments being the most problematic in the Mediterranean and to PC4 catchments for their special behaviour and interest as freshwater resources. Then, the different hydrological characteristics will be regionalised based on the regression equations obtained from CCA to define the Mediterranean hydrological regions from K-means of the regionalised values. And climate change scenario will be carried out to assess the impact on water balance coefficients.

6.3 HYDROLOGICAL HOMOGENEITY

6.3.1 High Flows and Low Flows inter – class analysis

The inter-class hydrological homogeneity was analysed for the 55 selected catchments through CCA between physioclimatic indices listed in Table 6-1 and High and Low Flows hydrological indices listed in Table 6-2. The intra-class homogeneity of cultivated and managed PC1 and PC9 catchments and mountainous, under snow and karst influence PC4 catchments was also analysed to discover which indices contribute to each class' hydrology and if they are the same for all classes. In the following High Flows will be indicated as "HF" and Low Flows as "LF".

6.3.1.1 All catchments High Flows CCA

The canonical correlations shown in Table 6-3 highlight the clear relationship between the two groups of indices with a correlation of 0.84 for the first canonical variable and zero value for Wilks significance test. The correlation between variables showed that the most significant physioclimatic indices are A, $T_{25\%}$, MAP, T_AWC and I_{Arid} where DH_5 is highly negatively correlated (-0.95) and to a lower extend FH_1 (-0.55) both with the first canonical variable W_{HF1} which in its turn is highly correlated with A, MAP, $T_{25\%}$ and I_{Arid} with some canonical pairs of high correlation are worth noting like A – DH_5 (-0.74) and $T_{25\%}$ – DH_5 (-0.81). The flood frequency index FH_1 is highly negatively correlated (-0.83) with the second canonical correlation W_{HF2} which is highly correlated with T_AWC (0.80)

Another valuable illustration is the population representation on the canonical space based on the regression equations in Figure 6-1 and Figure 6-2. At first, the physioclimatic scatter diagram in Figure 6-1 showed no logical distribution and the hydrological diagram showed only one main distinct scattered set. But once coloured according to their climatic classes, the close clusters were well identified with limited overlap between class boundaries while the distant scattered sets in both diagrams corresponded to climatic class 5 catchments defined as low seasonal highly humid catchments. The similarity of catchments distribution between both physioclimatic and hydrological variables diagrams is observable for climatic classes, where catchments of same climatic classes are evenly positioned vis-a-vis other catchments or classes. The same observation was noticed but less intense for the scatter diagrams in Figure 6-2 coloured according to their physiographic classification. The similarity difference returns to the fact that climatic indices contribute more into catchments hydrological response than physiographic indices.

Table 6-3: Eigenvalues, Canonical Correlations and Coefficients of Variables and Covariates for High Flows CCA with the corresponding two-dimensional plot of PCIs and HIs correlations for High Flows.

HIGH FLOWS				
Canonical Variable	Eigenvalue	Pct. %	Canon Cor.	Sig. of F
1	2.47	89.01	0.84	0.00
2	0.30	10.99	0.48	0.01
	Correlation		Coefficients	
PCIs	V_{HF1}	V_{HF2}	V_{HF1}	V_{HF2}
A	-0.74	0.37	-0.55	0.41
T_AWC	0.18	-0.80	0.07	-0.76
MAP	-0.75	-0.45	-0.71	-0.19
$T_{25\%}$	-0.81	-0.28	-0.31	-0.21
I_{Arid}	0.59	0.41	-0.35	0.23
HIs	W_{HF1}	W_{HF2}	W_{HF1}	W_{HF2}
DH_5	-0.95	0.31	-0.86	0.57
FH_1	-0.55	-0.83	-0.32	-0.99

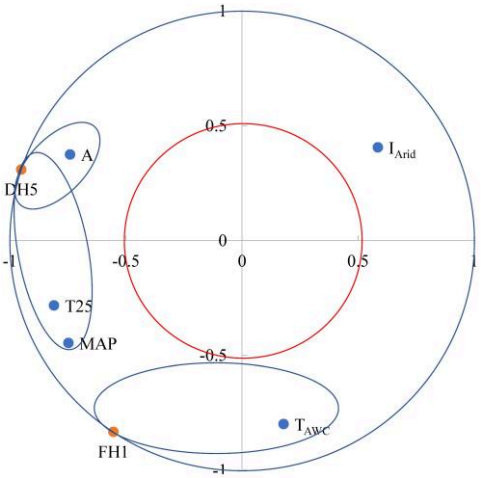

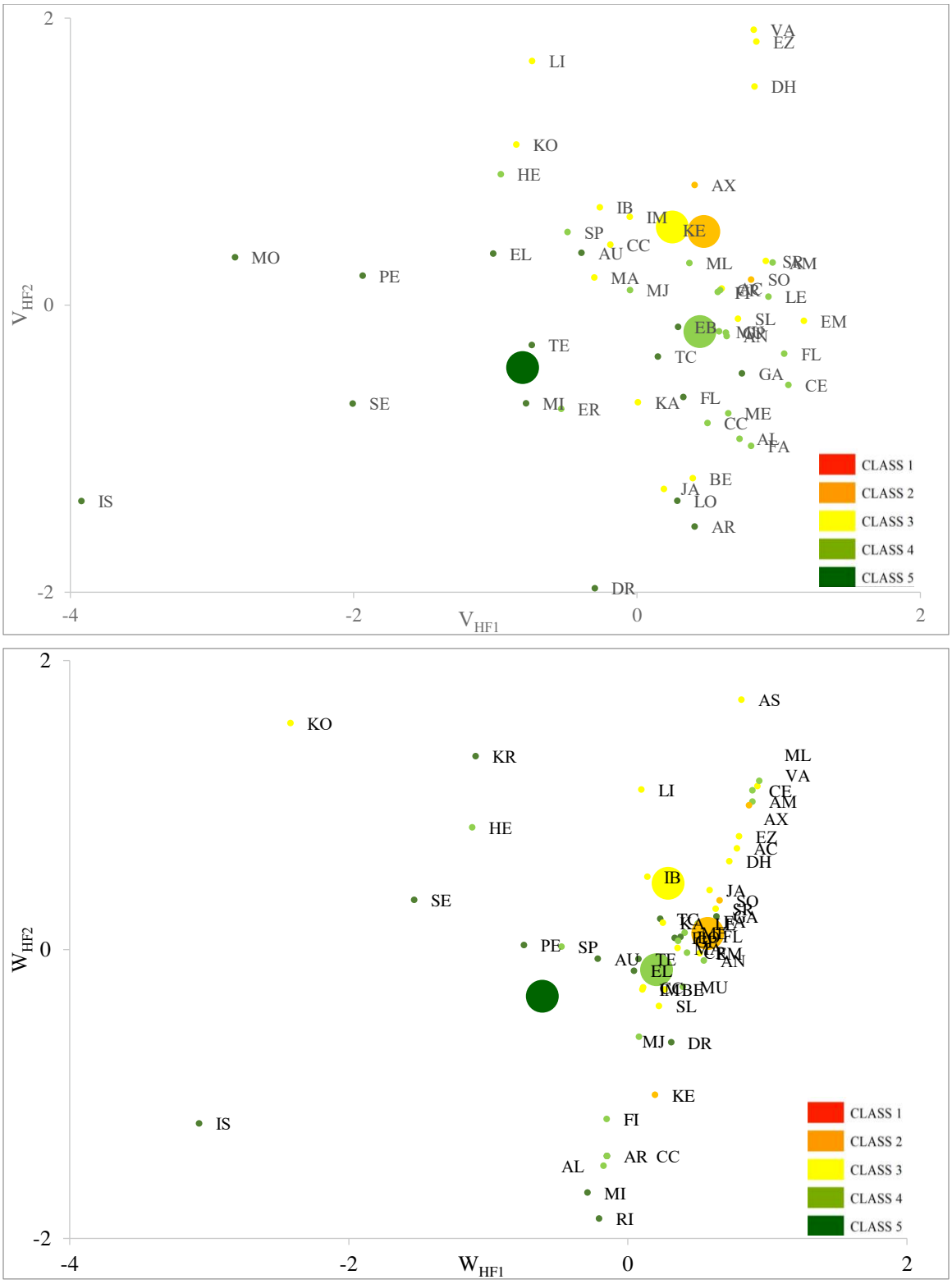

Figure 6-1: Catchments scatter diagrams for High Flows of the first two physioclimatic canonical dimensions (up) and hydrological canonical dimensions (down) with classes kernels (big circles) coloured according to climatic classes.

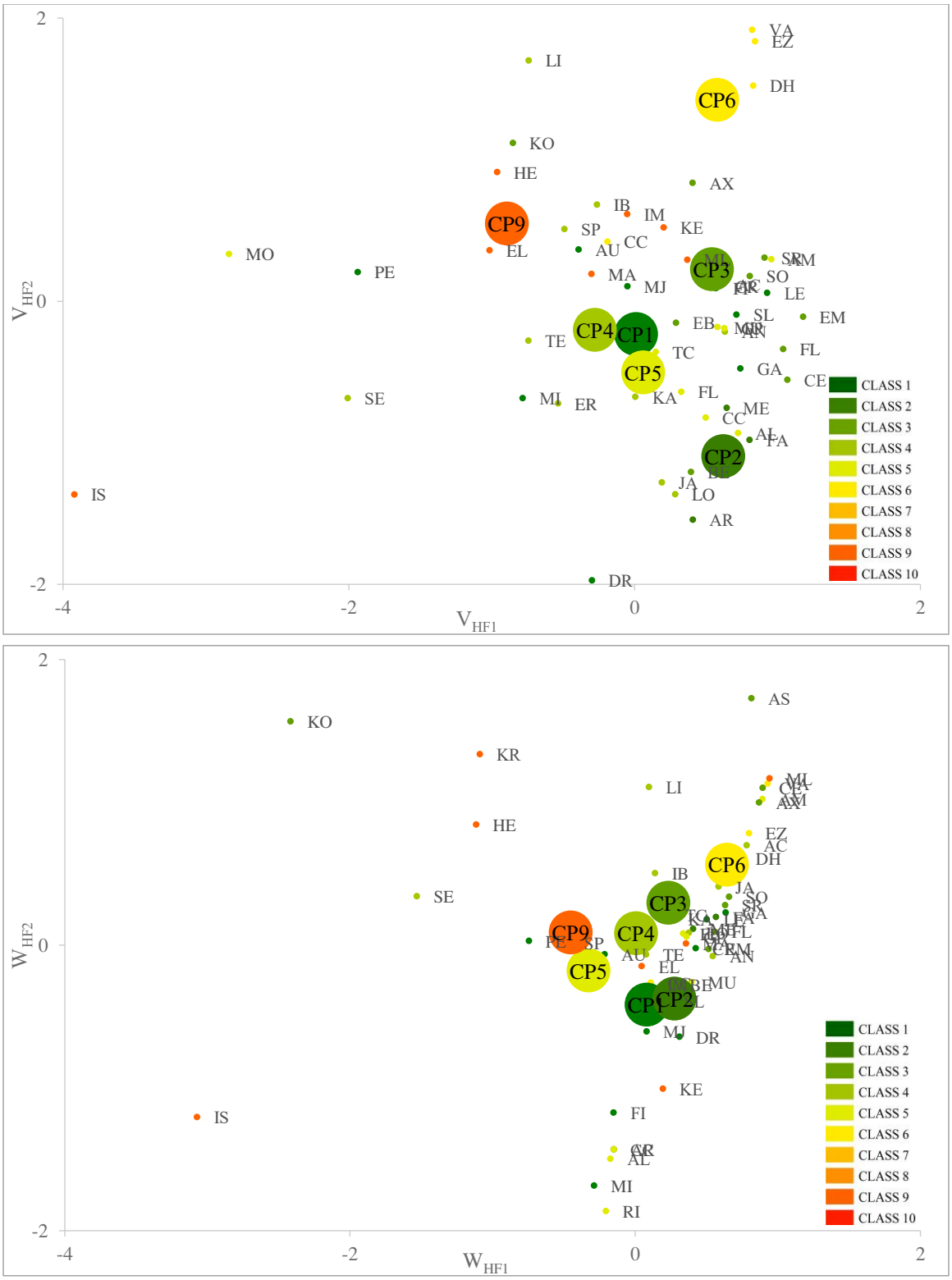

Figure 6-2: Catchments scatter diagrams for High Flows of the first two physioclimatic canonical dimensions (up) and hydrological canonical dimensions (down) with classes kernels (big circles) coloured according to physiographic classes.

6.3.1.2 *All catchments Low Flows CCA*

The Canonical correlations for Low flows also highlighted the presence of a relationship between the two groups of indices with a correlation of 0.84 for the first canonical variable and zero value for Wilks significance test. The correlation between variables showed that the most significant physioclimatic indices are A, $T_{25\%}$, MAP and I_{Arid} where DL_5 is highly negatively correlated (-0.91) and to a lower extend FL_1 (-0.67) both with the first canonical variable W_{LF1} which in its turn is highly correlated with A, MAP, $T_{25\%}$ and I_{Arid} with some canonical pairs of high correlation worth noting A – DL_5 (-0.77), $T_{25\%}$ – DH_5 (-0.82) and I_{Arid} – DL_5 (0.69). The Low flow frequency index FL_1 is highly negatively correlated (-0.75) with the second canonical correlation W_{LF2} which is highly correlated with I_{Arid} (0.64). The scatter diagrams of the canonical variables are presented in Figure 6-3 and Figure 6-4. These diagrams had shown the same homogeneous clusters as High flows. The difference between High and Low flows scatters distribution might be due to their uncorrelation with T_AWC but instead with the aridity index I_{Arid}. Low flows represent the recession period during summer at the end of the hydrological year in the Mediterranean where the only contribution into rivers comes from underground storage after percolation like springs and not from direct runoff or excess of infiltration like winter precipitation which might explain the independence from soil indices.

Table 6-4: Eigenvalues, Canonical Correlations and Coefficients of Variables and Covariates for Low Flows CCA with the corresponding two-dimensional plot of PCIs and HIs correlations for Low Flows

LOW FLOWS				
Canonical Variable	Eigenvalue	Pct. %	Canon Cor.	Sig. of F
1	2.47	83.62	0.84	0.00
2	0.48	16.37	0.57	0.00
	Correlation		Coefficients	
PCIs	V_{LF1}	V_{LF2}	V_{LF1}	V_{LF2}
A	-0.77	0.21	-0.59	0.14
MAP	-0.75	-0.28	-0.44	0.44
$T_{25\%}$	-0.82	0.05	-0.25	0.86
I_{Arid}	0.69	0.64	0.03	1.65
HIs	W_{LF1}	W_{LF2}	W_{LF1}	W_{LF2}
DL_5	-0.91	0.42	-0.78	0.69
FL_1	-0.67	-0.75	-0.44	-0.95

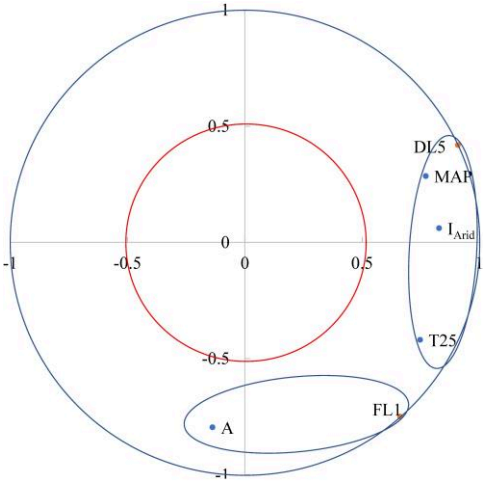

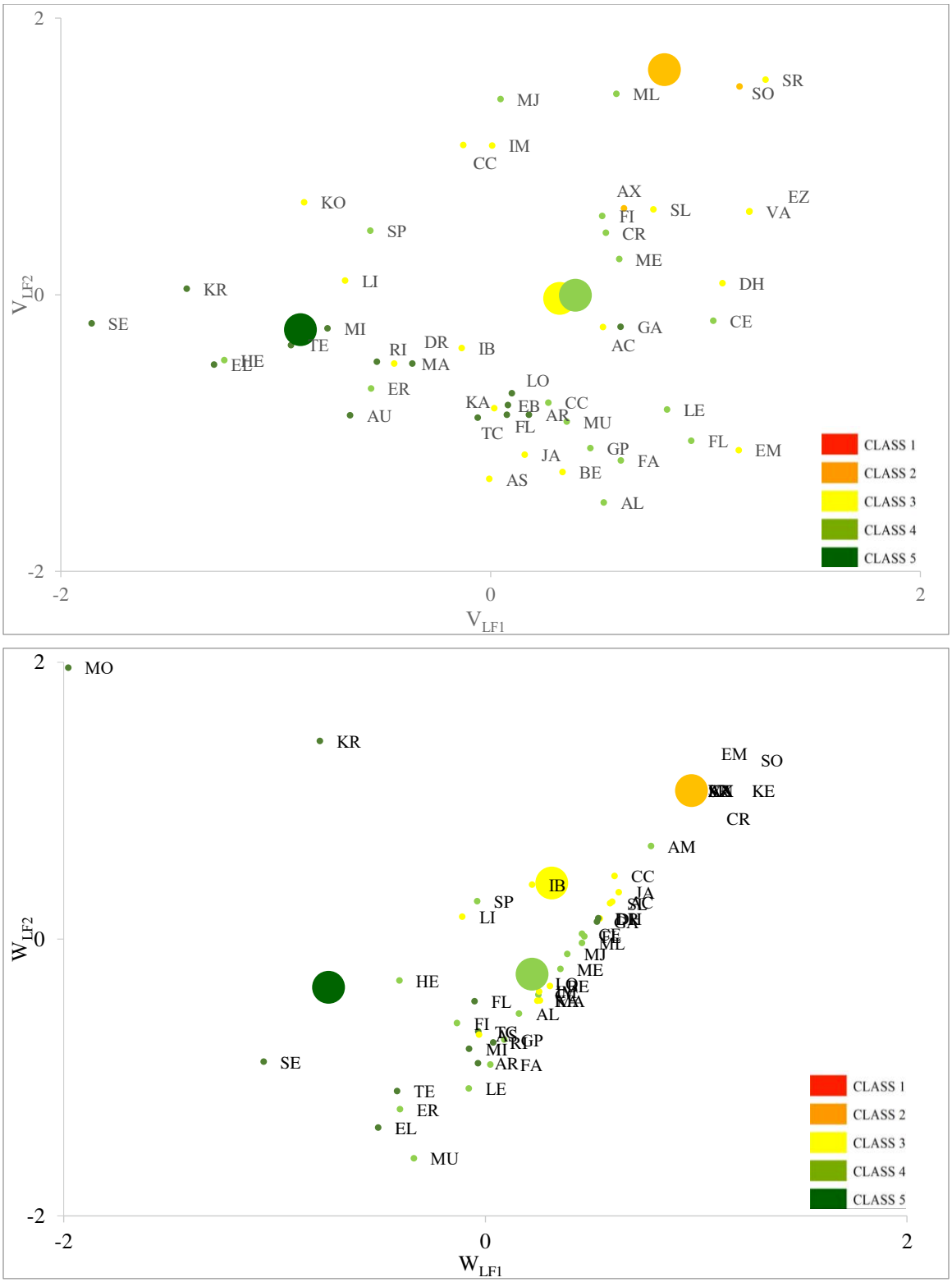

Figure 6-3: Catchments scatter diagrams for Low Flows of the first two physioclimatic canonical dimensions (up) and hydrological canonical dimensions (down) with classes kernels (big circles) coloured according to the climatic *classes.*

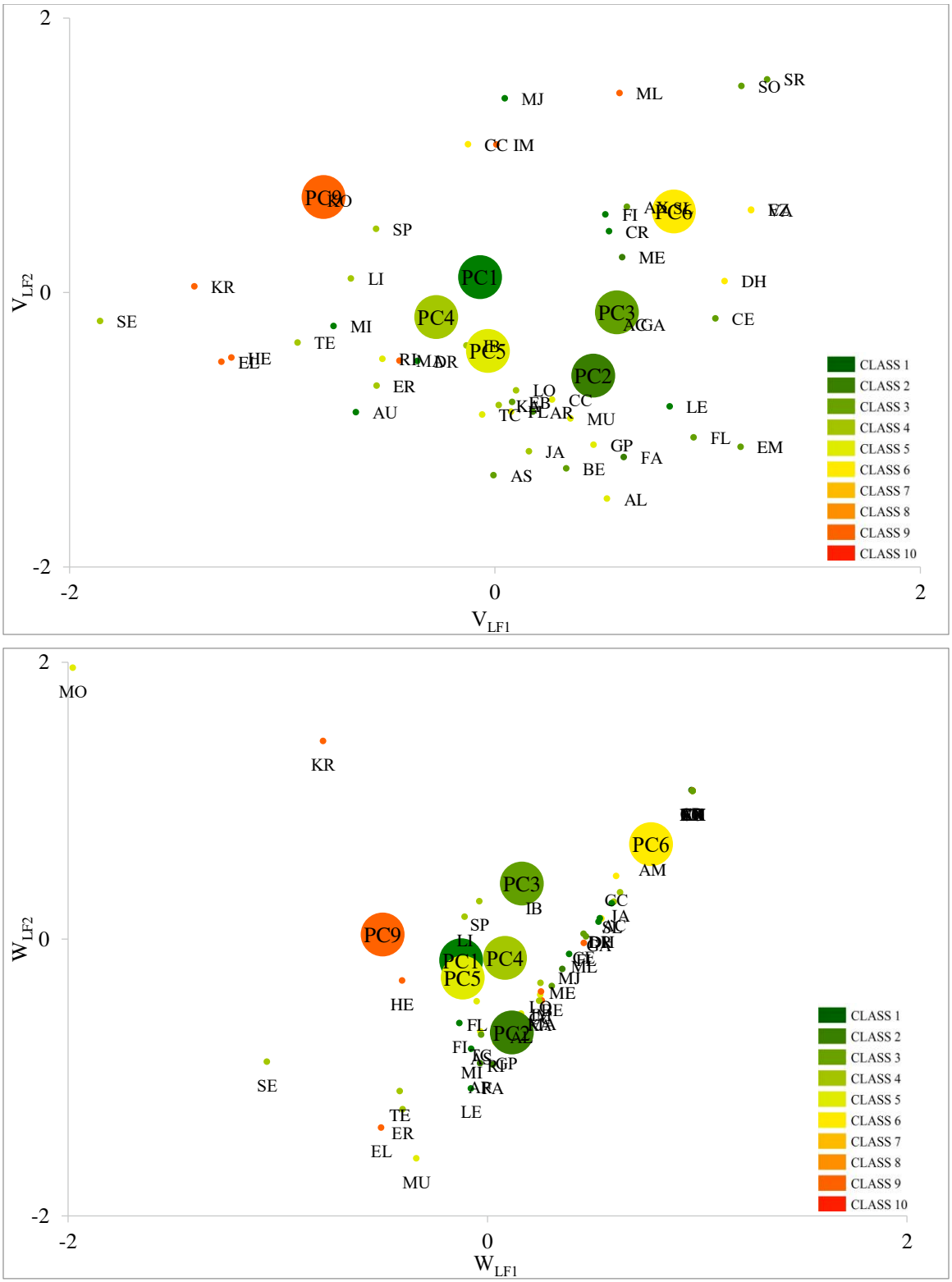

Figure 6-4: Catchments scatter diagrams for Low Flows of the first two physioclimatic canonical dimensions (up) and hydrological canonical dimensions (down) with classes kernels (big circles) coloured according to physiographic classes.

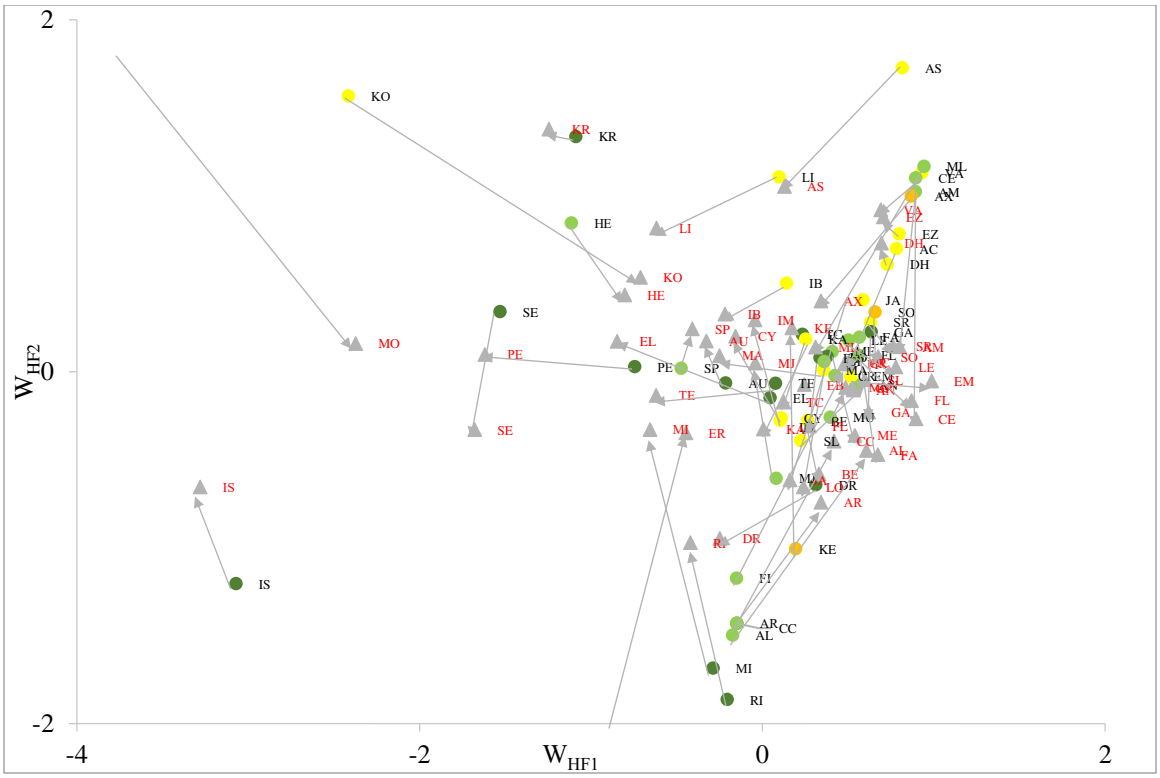

Figure 6-5: High Flows canonical variables error vector diagram between calculated canonical variables based on measured flow and estimated canonical variables based on CCA regression equations with catchment colours according to climatic classes

Figure 6-5 shows the scatter plot of the hydrological canonical variables for both CCA calculated and estimated from regression (gray triangles) including the error vectors for each basin. This plot reveals that:

a. The vertical components of the error vectors are generally larger than the horizontal components, due to the low correlation with the second canonical variable W_{HF2}
b. There are some basins with larger error vectors than other catchments explained by the drainage areas difference of the catchments and the aridity variability and temperature of basin.

6.3.1.3 Cultivated and managed PC1 and PC9 catchments intra – class analysis

To validate and highlight the similarity between catchments of the same class we repeated the CCA for the 18 catchments of classes 1 and 9 combined known to be highly cultivated and managed catchments. The correlation between physioclimatic and high flow indices increased for the first from 0.84 to 0.90 and from 0.47 to 0.71 for the second canonical variable. The correlation between variables showed that the most significant physioclimatic indices are A, $T_{25\%}$, MAP, T_AWC and ZS_{Mean}. As for the low flow indices the CCA yielded a correlation of 0.90 for the first canonical variable and 0.70 for the second variable while the most significant indices became A, $T_{25\%}$, MAP, and ZS_{Mean} only without the T_AWC. The cluster diagrams representation of the canonical variables in Figure 6-6 for High flows and Figure 6-7 for Low flows

according to both climatic and physiographic classifications indicate a similarity between both PCs and Hs components, mirroring the correlation results between both sets of indices.

Table 6-5: PC1 & PC9 Eigenvalues, Canonical Correlations and Coefficients of Variables and Covariates

	HIGH FLOWS				LOW FLOWS			
Canonical Variable	Eigenvalue	Pct. %	Canon Cor.	Sig. of F	Eigenvalue	Pct. %	Canon Cor.	Sig. of F
1	4.22	80.21	0.90	0.00	4.14	80.86	0.90	0.00
2	1.04	19.79	0.71	0.06	0.98	19.1	0.70	0.03
	Correlation		Coefficients		Correlation		Coefficients	
PCIs	V_{HF1}	V_{HF2}	V_{HF1}	V_{HF2}	V_{LF1}	V_{LF2}	V_{LF1}	V_{LF2}
A	-0.66	0.32	-0.60	-0.01	-0.61	0.05	-0.48	0.83
T_AWC	0.55	-0.58	0.35	-0.66				
ZS_{Mean}	-0.72	0.33	0.10	0.46	-0.70	-0.39	0.01	-1.27
MAP	-0.75	-0.56	-0.64	-0.59	-0.81	-0.25	-0.29	-1.31
$T_{25\%}$	-0.75	-0.42	0.00	-0.33	-0.88	0.09	-0.54	1.64
HIs	W_{HF1}	W_{HF2}	W_{HF1}	W_{HF2}	W_{LF1}	W_{LF2}	W_{LF1}	W_{LF2}
DH_5/DL_5	-1.00	-0.03	-1.01	0.40	-0.99	0.16	-0.90	0.39
FH_1/FL_1	-0.36	-0.93	0.04	-1.09	-0.61	-0.79	-0.18	-1.09

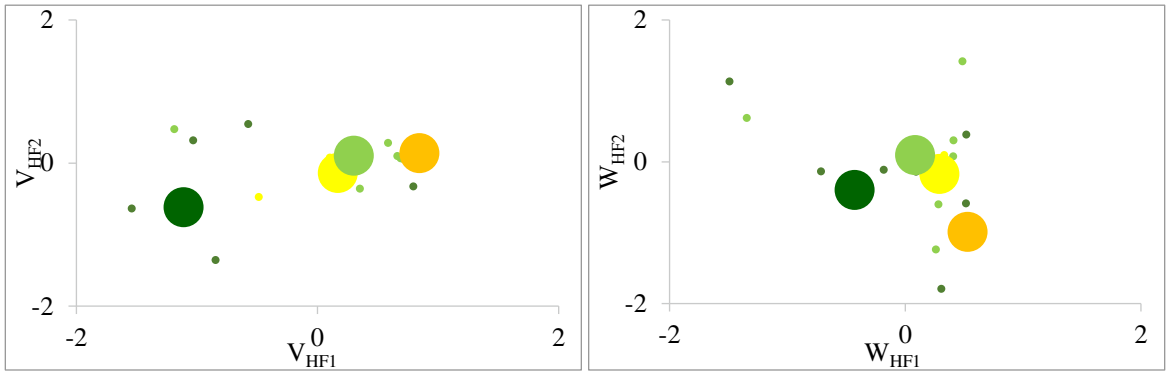

Figure 6-6: PC1 and PC9 catchments scatter diagrams for High Flows of the first two physioclimatic canonical dimensions (left) and hydrological canonical dimensions (right) with classes kernels (big circles) coloured according to climatic classes

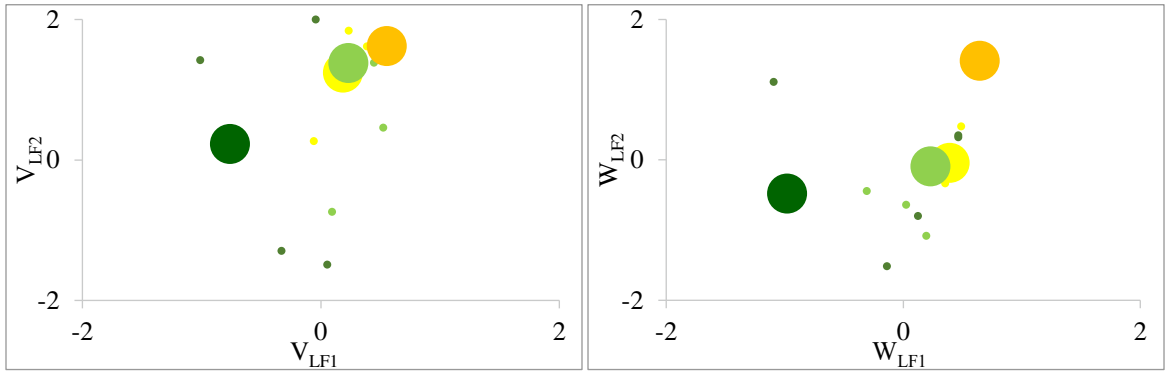

Figure 6-7: PC1 and PC9 catchments scatter diagrams for Low Flows of the first two physioclimatic canonical dimensions (left) and hydrological canonical dimensions (right) with classes kernels (big circles) coloured according to climatic classes

6.3.1.4 Mountainous, snow and karst influenced PC4 catchments intra – class analysis

To validate and highlight the similarity between catchments of PC4 we repeated the CCA for the 11 catchments known to be mountainous, highly karstic and snow influenced. The correlation between physioclimatic and hydrological indices increased for the first from 0.84 to 0.91 and for the second from 0.48 to 0.57 for the second canonical variable. The correlation between variables showed that the most significant physioclimatic indices are only A, MAP and $T_{25\%}$. As for the low flow indices, the CCA yielded a correlation of 0.99 for the first canonical variable and 0.46 for the second variable while the most significant indices stayed the same. The cluster diagrams representation of the canonical variables according to the climatic classes in Figure 6-8 and Figure 6-9 shows a disturbed distribution despite the high correlation of the first canonical variable, mainly due to the low correlation of the second variable, however the second canonical variable barely contributes to the definition with only 9% for the first and less than 1% for the second.

Table 6-6: PC4 Eigenvalues, Canonical Correlations and Coefficients of Variables and Covariates

	HIGH FLOWS				LOW FLOWS			
Canonical Variable	Eigenvalue	Pct. %	Canon Cor.	Sig. of F	Eigenvalue	Pct. %	Canon Cor.	Sig. of F
1	4.79	90.89	0.91	0.02	41.22	99.36	0.99	0.00
2	0.48	9.10	0.57	0.25	0.26	0.63	0.46	0.44
	Correlation		Coefficients		Correlation		Coefficients	
PCIs	V_{HF1}	V_{HF2}	V_{HF1}	V_{HF2}	V_{LF1}	V_{LF2}	V_{LF1}	V_{LF2}
A	0.76	0.58	0.56	0.97	-0.77	0.62	-0.58	0.77
MAP	0.71	-0.39	0.53	-0.22	-0.69	-0.69	-0.51	-0.75
$T_{25\%}$	0.73	-0.43	0.27	-0.80	-0.73	-0.04	-0.27	-0.11
HIs	W_{HF1}	W_{HF2}	W_{HF1}	W_{HF2}	W_{LF1}	W_{LF2}	W_{LF1}	W_{LF2}
DH_5/DL_5	0.99	0.11	0.96	0.37	-0.92	0.40	-0.64	1.03
FH_1/FL_1	0.36	-0.93	0.12	-1.02	-0.85	-0.53	-0.48	-1.11

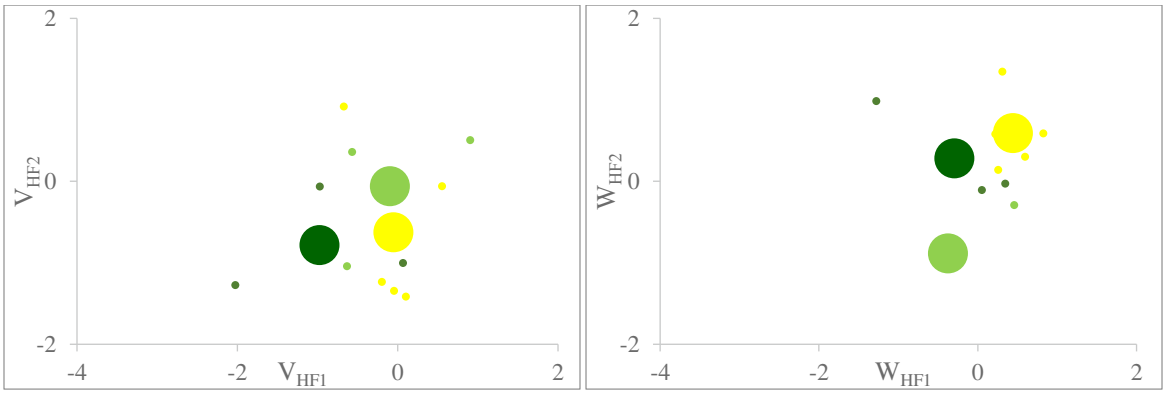

Figure 6-8: PC4 catchments scatter diagrams for High Flows of the first two physioclimatic canonical dimensions (left) and hydrological canonical dimensions (right) with classes kernels (big circles) coloured according to climatic classes.

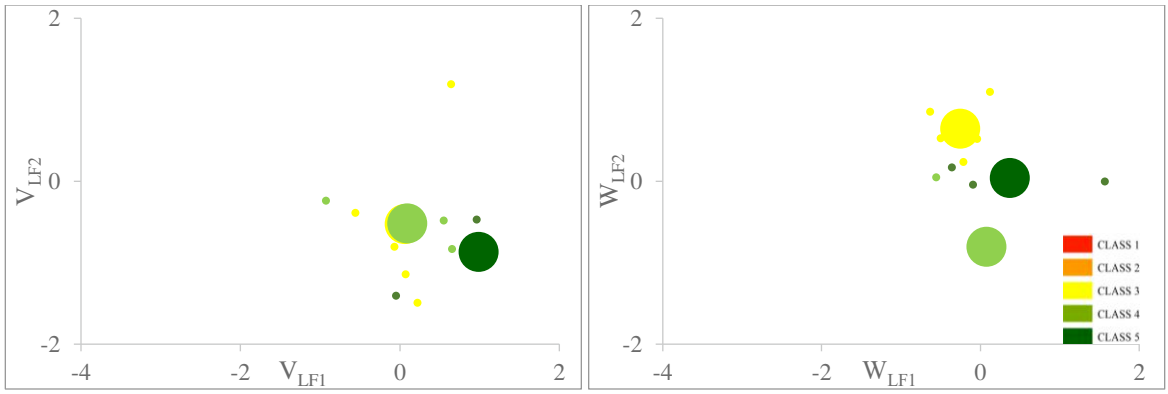

Figure 6-9: PC4 catchments scatter diagrams for Low Flows of the first two physioclimatic canonical dimensions (left) and hydrological canonical dimensions (right) with classes kernels (big circles) coloured according to climatic classes.

6.3.2 Water balance interclass hydrological homogeneity

To characterise the water balance of type II catchments, we analysed the inter-class hydrological homogeneity for the total runoff coefficient K_r and baseflow coefficient K_u of all 55 catchments through CCA between physioclimatic indices listed in Table 6-1 and water balance coefficients K_r and K_u summarised in Table 6-2. The intra-class homogeneity of cultivated and managed PC1 and PC9 catchments and mountainous, under snow and karst influence PC4 catchments was also analysed to discover which indices contribute to each class' hydrology and if they are the same for all classes.

6.3.2.1 All catchments water balance CCA

The CCA yielded a correlation of 0.78 for the first canonical variable and 0.57 for the second. The correlation between variables showed that the most significant physioclimatic indices are ZS_{Mean}, MAP, TC_BDC, $T_{25\%}$, I_{Arid} and P_{Karst}. These indices confirm the previous findings that some physiographic features mainly forest, landform and karst govern the Mediterranean water balance.

The cluster diagrams representation of the canonical variables in Figure 6-10 shows an almost perfect similarity between the first two physioclimatic and hydrological variables catchments distribution. In addition, we notice the remarkable separation of PC4 catchments from other catchments and that for different climatic classes. Another overlap between climatic classes but to a lower extent was noticed for PC2 and PC5 forest catchments. The other physiographic classes are spread according to climatic classes hence its water balance is more governed by climate than by physiography. The scatter spread is less noticeable for hydrological canonical variables than for the physioclimatic canonical variables.

Table 6-7: Water balance eigenvalues, canonical correlations and coefficients of variables and covariates

	WATER BALANCE			
Canonical Variable	Eigenvalue	Pct. %	Canon Cor.	Sig. of F
1	1.56	75.97	0.78	0.00
2	0.49	24.03	0.57	0.00
	Correlation		Coefficients	
PCIs	V_{WB1}	V_{WB2}	V_{WB1}	V_{WB2}
MAP	-0.67	-0.51	0.32	-0.42
ZS_{Mean}	-0.73	0.46	-0.40	0.72
P_{Karst}	-0.63	-0.04	-0.42	0.21
TC_BDC	-0.19	-0.70	-0.02	-0.43
$T_{25\%}$	-0.77	-0.21	-0.26	-0.05
I_{Arid}	0.81	0.47	0.55	0.33
HIs	W_{WB1}	W_{WB2}	W_{WB1}	W_{WB2}
K_r	-0.97	-0.26	0.45	-5.51
K_u	-1.00	-0.08	-1.44	5.34

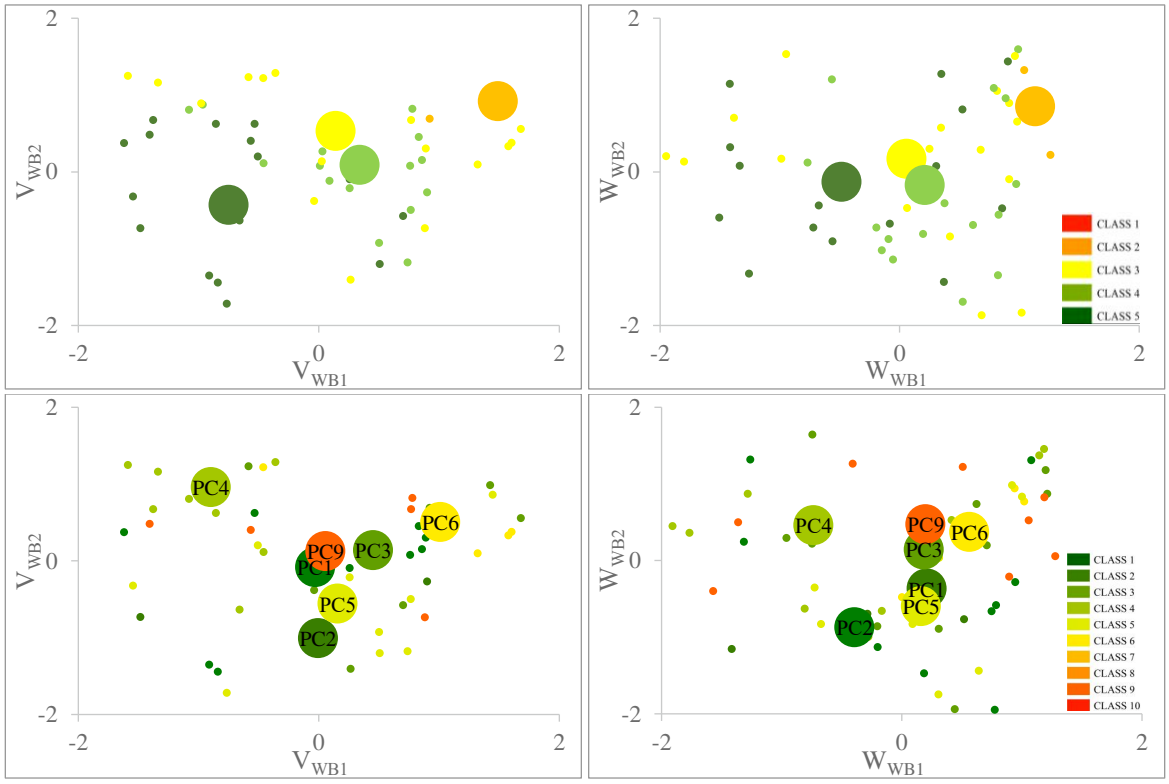

Figure 6-10: Catchments scatter diagrams for total runoff K_r and baseflow K_u of the first two physioclimatic canonical dimensions (left) and hydrological canonical dimensions (right) with classes kernels (big dots) coloured according to climatic classes (up) and physiographic classes (down)

6.3.2.2 *Cultivated and managed PC1 and PC9 catchments water balance intra – class CCA*

The CCA yielded a correlation of 0.88 for the first canonical variable and 0.52 for the second. The correlation between variables showed that the most significant physioclimatic indices are ZS_{Mean}, MAP, $T_{25\%}$, and I_{Arid} hence dropping TC_BDC and P_{Karst}.

The cluster diagrams representation of the canonical variables in Figure 6-11 shows some similarity between the first two physioclimatic and hydrological variables catchments distribution. We notice that catchments are much closer than in Figure 6-10 but still a distant CC5. The scatter spread is less noticeable for hydrological canonical variables than for the physioclimatic canonical variables.

Table 6-8: Water balance eigenvalues, canonical correlations and coefficients of variables and covariates

	WATER BALANCE			
Canonical Variable	Eigenvalue	Pct. %	Canon Cor.	Sig. of F
1	3.27	89.82	0.88	0.00
2	0.37	10.17	0.52	0.24
	Correlation		Coefficients	
PCIs	V_{WB1}	V_{WB2}	V_{WB1}	V_{WB2}
ZS_{Mean}	-0.96	0.25	-0.82	0.75
MAP	-0.54	-0.75	0.13	-0.33
$T_{25\%}$	-0.67	-0.73	-0.37	-0.64
I_{Arid}	0.69	0.56	0.05	0.17
HIs	W_{WB1}	W_{WB2}	W_{WB1}	W_{WB2}
K_r	-0.78	-0.62	2.48	-4.73
K_u	-0.89	-0.46	-3.32	4.18

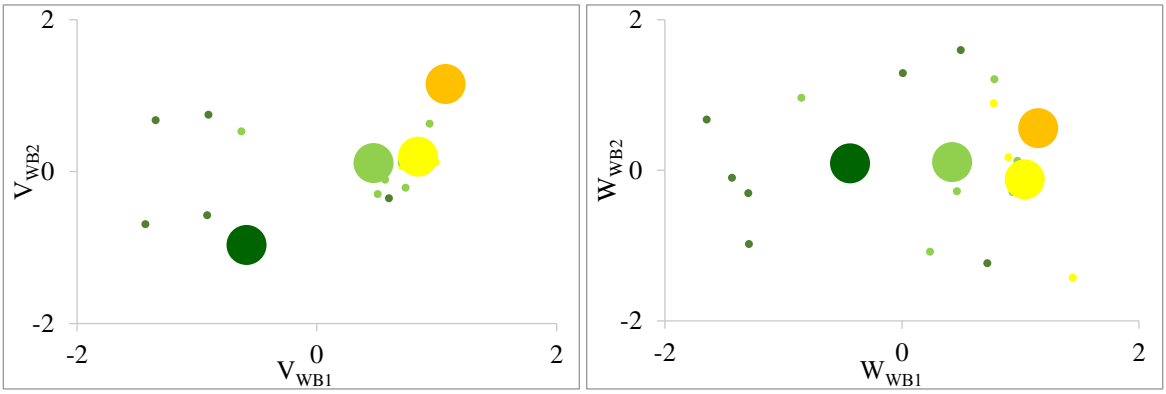

Figure 6-11: PC1 and PC9 catchments scatter diagrams for total runoff and baseflow coefficients K_r and K_u of the first two physioclimatic canonical dimensions (left) and hydrological canonical dimensions (right) with classes kernels (big dots) coloured according to climatic classes.

6.3.2.3 *Mountainous, snow and karst influenced PC4 catchments water balance intra – class CCA*

The CCA yielded a high correlation of 0.95 for the first canonical variable and 0.85 for the second. The correlation between variables showed that the most significant physioclimatic indices are P_{Karst}, MAP, $T_{25\%}$, and I_{Arid} hence dropping TC_BDC and surprisingly ZS_{Mean} although all PC4 are highly influenced by snow which could have make it non-contributing to the regression.

The cluster diagrams representation of the canonical variables in Figure 6-12 do show some similarity between the first two physioclimatic and hydrological variables catchments distribution. We notice that catchments are much closer than in Figure 6-10 showing more homogeneity between PC4 catchments.

Table 6-9: Water balance eigenvalues, canonical correlations and coefficients of variables and covariates

	WATER BALANCE			
Canonical Variable	Eigenvalue	Pct. %	Canon Cor.	Sig. of F
1	9.47	77.98	0.95	0.00
2	2.68	22.02	0.85	0.04
	Correlation		Coefficients	
PCIs	V_{WB1}	V_{WB2}	V_{WB1}	V_{WB2}
P_{Karst}	-0.69	0.31	-0.91	-0.41
MAP	-0.22	-0.88	0.52	-0.80
$T_{25\%}$	-0.47	-0.61	-0.71	-0.15
I_{Arid}	0.41	0.82	0.38	0.08
HIs	W_{WB1}	W_{WB2}	W_{WB1}	W_{WB2}
K_r	-0.95	-0.30	1.40	-7.83
K_u	-0.98	-0.17	-2.37	7.59

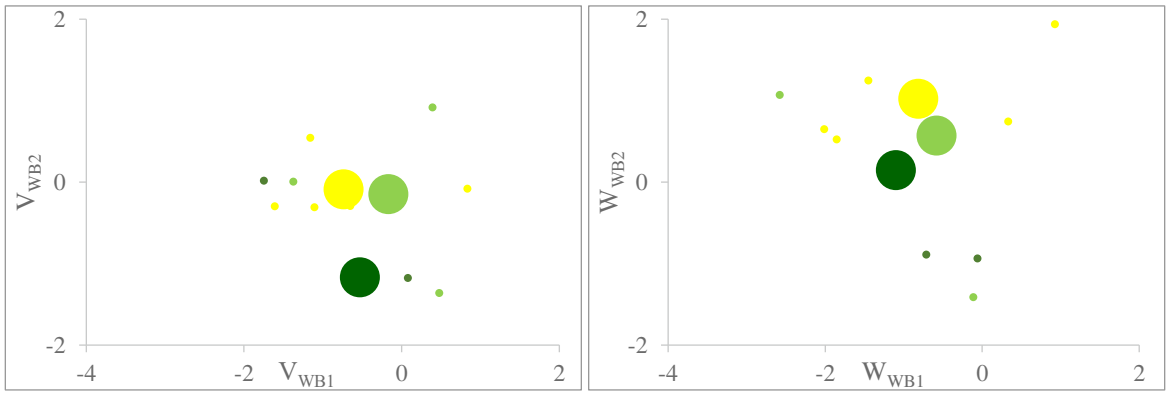

Figure 6-12: PC4 catchments scatter diagrams for total runoff and baseflow coefficients K_r and K_u of the first two physioclimatic canonical dimensions (left) and hydrological canonical dimensions (right) with classes kernels (big dots) coloured according to climatic classes.

6.3.2.4 Jack-knife validation of water balance hydrological homogeneity

To validate our results and asses the reliability of CCA method in estimating water balance coefficients of ungauged basins we applied the jack-knife cross-validation procedure also known as leave one out cross validation (LOOCV) procedure (Efron, 1982; Brath et al., 2003; Castellarin et al., 2004; Zhang & Kroll, 2007; Castiglioni et al., 2009; Tsakiris et al., 2011). This procedure is inscribed in the general framework for systematic model testing which is dated back to Klemeš (1986) and can evaluate the CCA results obtained previously since it simulates the ungauged conditions for each of the 55 gauged catchments.

The jack-knife method is adapted from Castiglioni et al. (2009) and Tsaikiris et al. (2011) and includes the following steps:

1) One of the n = 55 catchments in the study is considered ungauged, say catchment i.
2) The data for catchment i is removed from data matrices V and W, i.e., the i^{th} row of each one of these matrices is removed to obtain data matrices V_i and W_i.
3) CCA is applied to V_i and W_i to extract the regression equations for the n-1 gauged catchments and calculate the estimated values of the canonical variables V(i) and W(i) of the ungauged catchment I.
4) We repeat steps 1 to 3 n times for i = 1, 2, …, n and obtain the jack-knife values of n catchment canonical variables.
5) The estimated values of the K_r and K_u are then compared with the values that were drawn from observations. The comparison is based on multiple statistical indices: the Nash–Sutcliffe efficiency criterion E (Nash & Sutcliffe, 1970), and the root mean square error, RMSE.

$$E = \frac{\sum_{i=1}^{n}(x_i - \hat{x}_i)^2}{\sum_{i=1}^{n}(x_i - \bar{x}_i)^2} \quad 44$$

$$RMSE = \sqrt{\frac{\sum_{i=1}^{n}(x_i - \hat{x}_i)^2}{n}} \quad 45$$

where x_i denotes the i^{th} coefficient from the observed data with the mean equal to $\bar{x}_i$ and $\hat{x}_i$ is the corresponding jack-knife estimate.

The results of the jack-knife method showed that CCA was capable of correctly locating the 55 catchments hence preserving the same classes distribution as seen in Figure 6-13. It shows the scatter diagram (V_{WB1}; V_{WB2}) of the canonical variables for the 55 catchments with observed data as circles and Jack-knife estimated values of ungauged catchments as triangles.

We were also curious to test if a class specific CCA regression equation of PC1, PC9 and PC4 can improve the estimation of water balance coefficients corresponding to classes catchments.

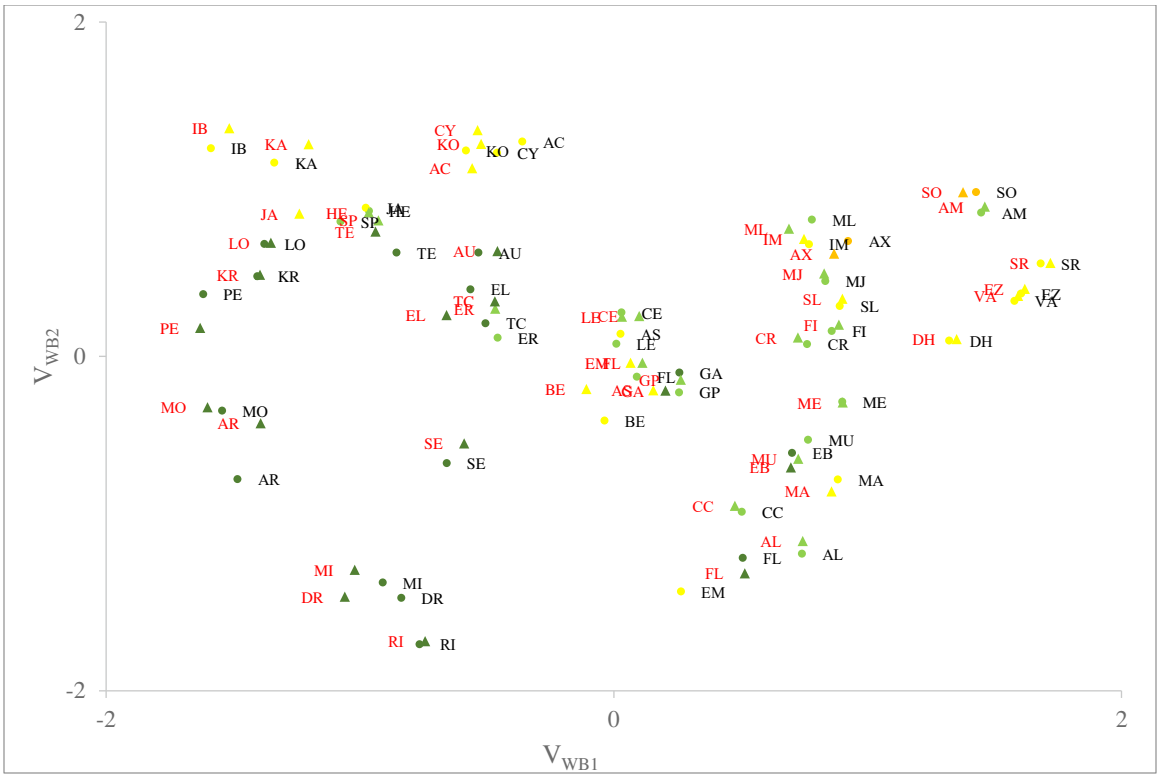

Figure 6-13: Scatter diagrams of the canonical variables (V_{WB1}; V_{WB2}) for the 55 catchments with the observed data (dots) and the Jack-knife estimated values of ungauged catchments (triangles) coloured according to climatic classes.

Therefore, we applied the Jack-knife procedure described above on all 55 catchments, then on 18 catchments of PC1 and PC9 and 11 catchments of PC4 and compared the estimated coefficients to the observed values for each class (see Table 6-10). We can notice that the high efficiency (0.89;0.92) calculated on all catchments validates the overall estimates of the water balance coefficients. However, the low efficiency (0.50 and 0.56 for K_r and 0.65 and 0.72 for K_u) calculated on different classes based on regression equations extracted from all catchments show that CCA is not "class specific" while a class specific CCA improved the efficiency to 0.79 for PC1 and PC9 and 0.90 for PC4 for K_r same as for K_u. This efficiency improvement could be caused by smaller samples however, we can still deduce that a class specific CCA is better for regionalisation of hydrological indices.

Table 6-10: Statistical indices for comparison of K_r and K_u estimates based on jack-knife data from all catchments and from PC1, PC9 and PC4 catchments with (x) number of catchments.

Criteria calculated on	*Regression based on CCA of*	*Nash Efficiency*		*RMSE*	
		K_r	K_u	K_r	K_u
All Catchments (55)	*All Catchments*	*0.89*	*0.92*	*0.17*	*0.15*
PC1 & PC9 (18)	*All Catchments*	*0.50*	*0.65*	*0.37*	*0.31*
	PC1 & PC9	*0.79*	*0.77*	*0.17*	*0.15*
PC4 (11)	*All Catchments*	*0.56*	*0.72*	*0.34*	*0.28*
	PC4	*0.90*	*0.90*	*0.17*	*0.16*

6.4 REGIONALISATION OF HYDROLOGICAL INDICES

6.4.1 Estimation of High and Low Flows indices

We estimate the hydrological canonical variables (W_{HF1}, W_{HF2}, W_{LF1} and W_{LF2}) from the regression equations between V and W where $W_i = \lambda_i V_i$ with λ_i the correlation.

For High Flows $W_{HF1} = 0.84\ V_{HF1}$ and $W_{HF2} = 0.48\ V_{HF2}$ as for Low Flows $W_{LF1} = 0.84\ V_{LF1}$ and $W_{LF2} = 0.57\ V_{LF2}$. Knowing V_{HF1} and V_{HF2} we can henceforth deduce DH_5, FH_1, DL_5 and FL_1 from the inverted matrices of the canonical coefficients.

We have for High Flows

$$\{W_{HF1}; W_{HF2}\} = \begin{bmatrix} -0.86 & 0.57 \\ -0.32 & -0.99 \end{bmatrix} \{DH_5; FH_1\}$$

$$\{DH_5; FH_1\} = \begin{bmatrix} -0.95 & -0.55 \\ 0.31 & -0.83 \end{bmatrix} \{W_{HF1}; W_{HF2}\}$$

As for Low Flows:

$$\{W_{LF1}; W_{LF2}\} = \begin{bmatrix} -0.78 & 0.69 \\ -0.44 & -0.95 \end{bmatrix} \{DL_5; FL_1\}$$

$$\{DL_5; FL_1\} = \begin{bmatrix} -0.91 & -0.67 \\ 0.42 & -0.75 \end{bmatrix} \{W_{LF1}; W_{LF2}\}$$

We show in Figure 6-14 to Figure 6-17, the regionalised physioclimatic and hydrological canonical variables for High and Low Flows.

The scatter diagrams according to the regionalised physioclimatic canonical variables in Figure 6-14 to Figure 6-17 are similar to the sample scatter distribution in Figure 6-1 and Figure 6-2 for CC2, CC3, CC4 and CC5 except for CC1 catchments illustrated in red which were not represented in the sample. The CC1 catchments are mostly PC7, PC8 and PC10 which are desertic. CC1 catchments showed a variability according to the first canonical variable V_{WB1} for High Flows and a variability according to the second canonical variable V_{WB2} for Low Flows.

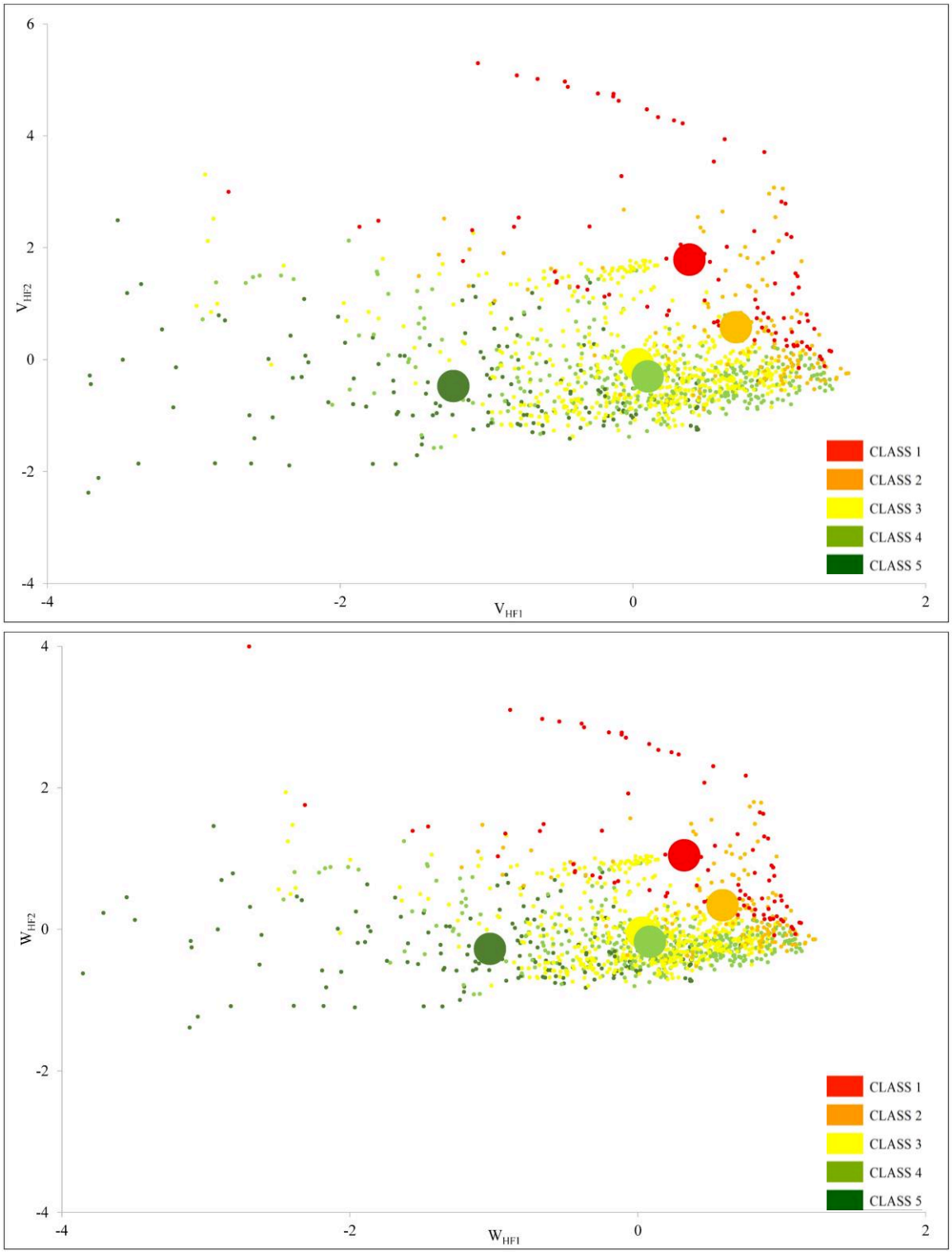

Figure 6-14: Regionalisation of High Flows canonical variables represented according to climatic classes with big dots as classes kernels.

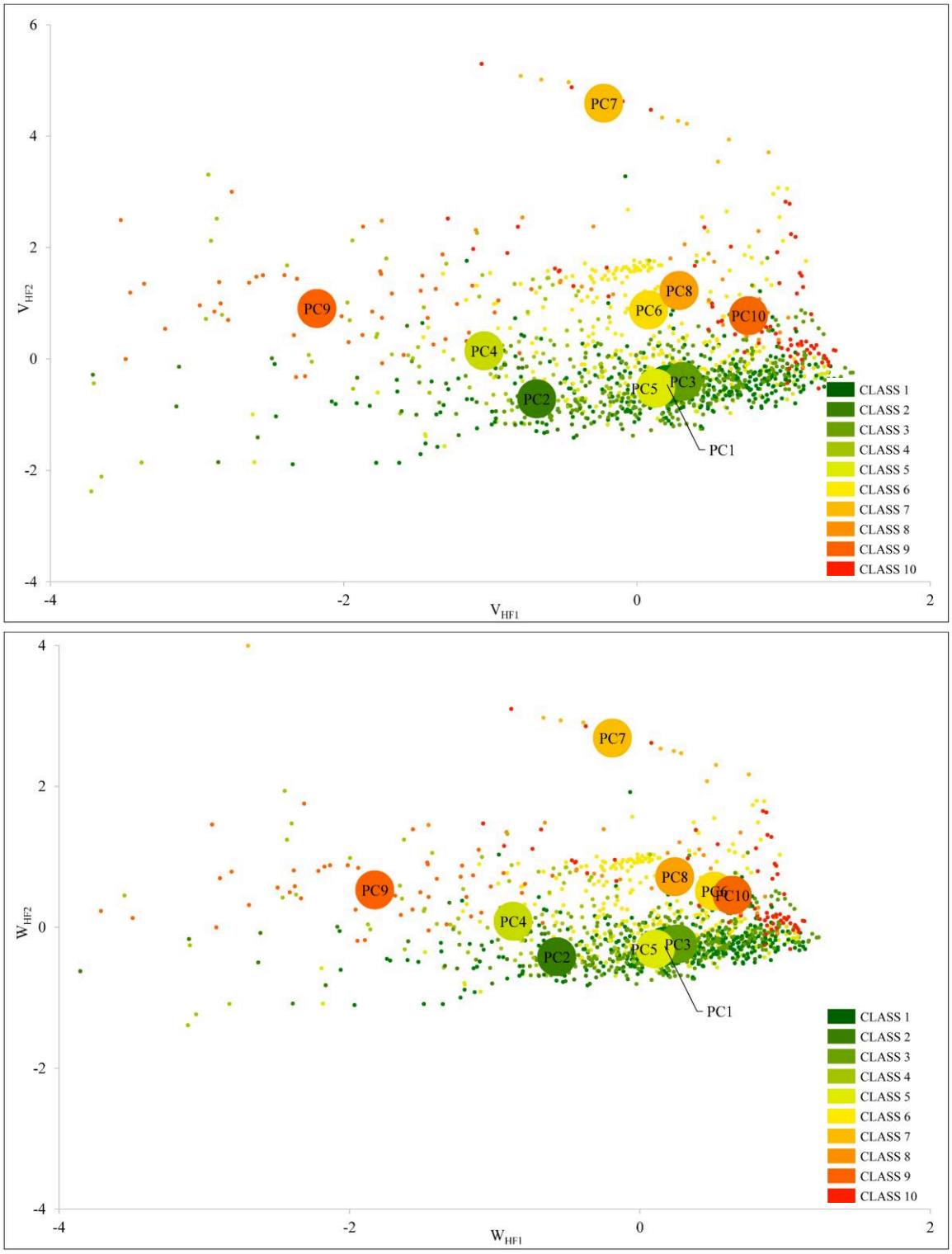

Figure 6-15: Regionalisation of High Flows canonical variables represented according to physiographic classes with big dots as classes kernels.

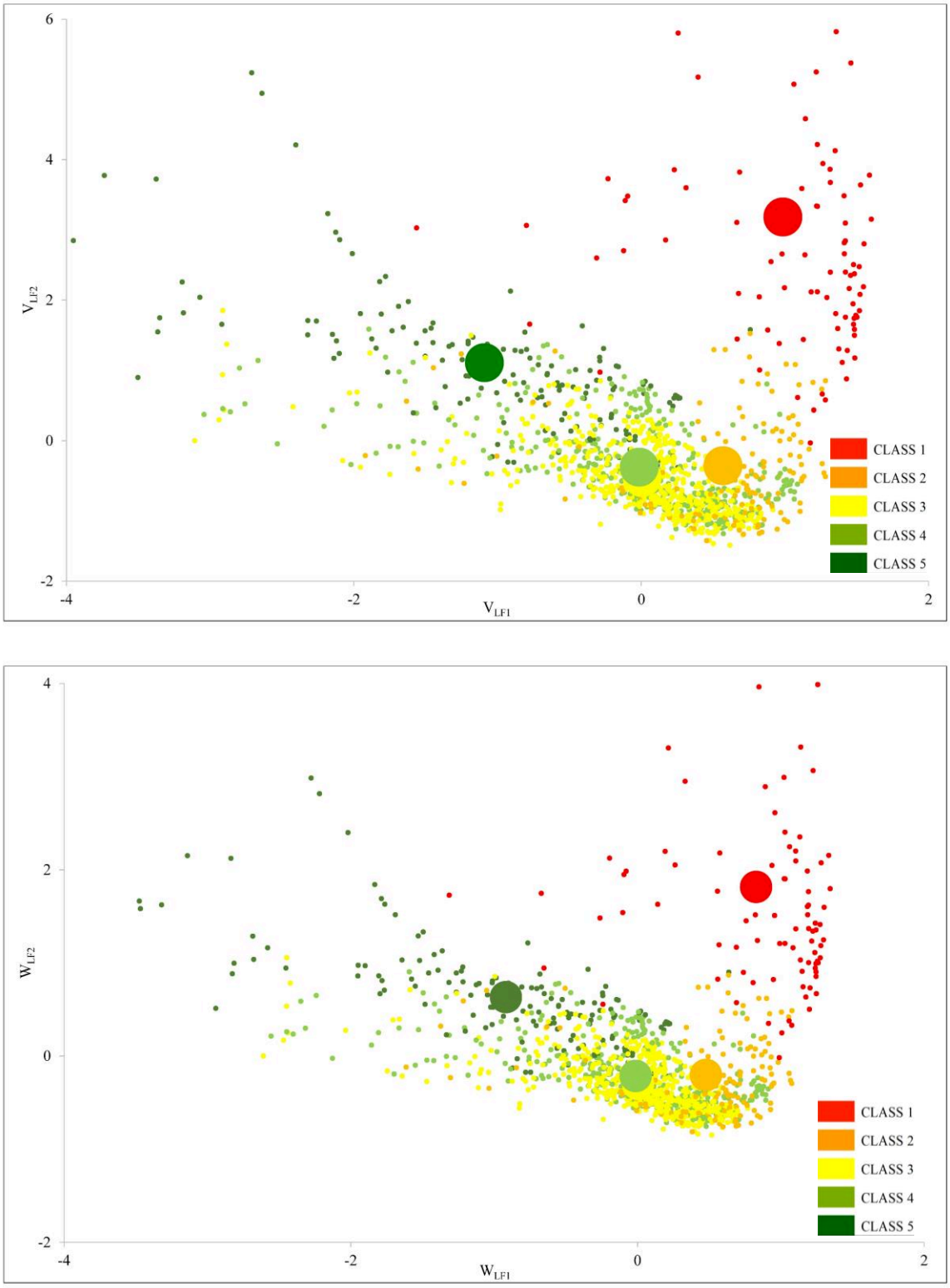

Figure 6-16: Regionalisation of Low Flows canonical variables represented according to climatic classes with big dots as classes kernels.

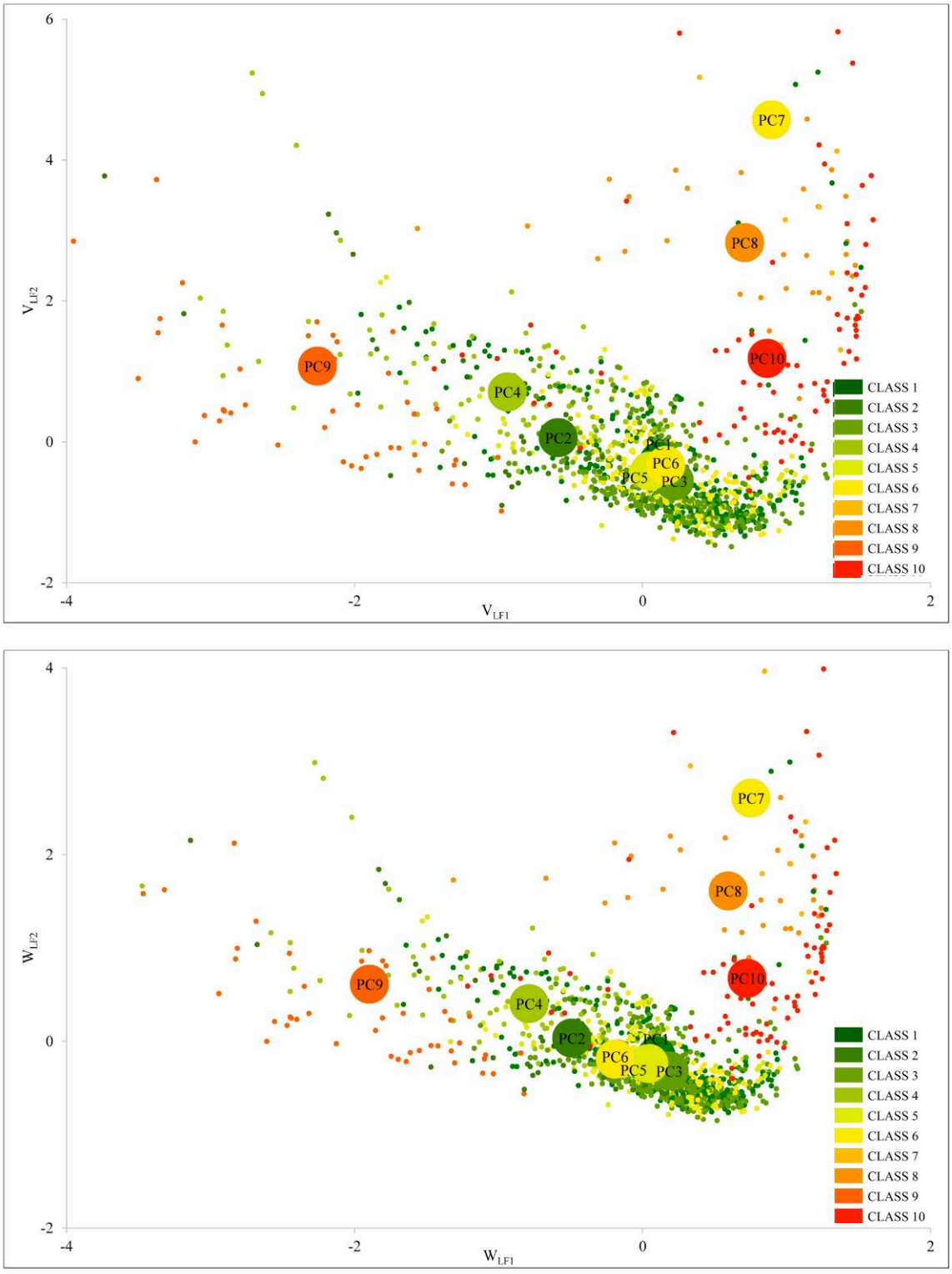

Figure 6-17: Regionalisation of Low Flows canonical variables represented according to physiographic classes with big dots as classes kernels.

6.4.2 Regionalisation of runoff K_r and baseflow K_u coefficients

We also estimated the hydrological canonical variables corresponding to the water balance (W_{WB1}, W_{WB2}) from the following regression equations. $W_{WB1} = 0.78\ V_{WB1}$ and $W_{WB2} = 0.57\ V_{WB2}$. Henceforth, knowing V_{WB1} and V_{WB2} we can deduce K_r and K_u from the following inverted matrices of the canonical coefficients

$$\{W_{WB1}; W_{WB2}\} = \begin{bmatrix} 0.45 & -5.51 \\ -1.44 & 5.34 \end{bmatrix} \{K_r; K_u\}$$

$$\{K_r; K_u\} = \begin{bmatrix} -0.97 & -1.00 \\ -0.26 & -0.08 \end{bmatrix} \{W_{WB1}; W_{WB2}\}$$

Figure 6-18 and Figure 6-19 show the regionalised canonical variables for water balance, and Figure 6-20 and Figure 6-21 show the regionalised total runoff and baseflow coefficients K_r and K_u, and gains K'_r and K'_u versus the precipitation illustrated according to climatic classes. The distribution of climatic classes verifies the findings in CHAPTER 5, where K_r and K_u increase with precipitation in line with the climatic classification. For the gains, they increase as long as the precipitation is lower than a threshold P_{rt} and P_{ut} here found around 180 mm, lower than the threshold previously found for the studied sample in Section 5.4.3.1. Once precipitation exceeds the threshold, mainly for CC3, CC4 and CC5, K_r lower boundary is 0.25 and K_u is 0.18 and K_r higher boundary reaches 0.8 and K_u 0.75. The runoff gain lower boundary is 0.00025 mm^{-1}.

CC1 catchments yielded negative coefficients and gains as no catchments were included in the sample. Although this is physically unrealistic, it could be interpreted that CC1 evapotranspiration and consequently aridity is very high that all precipitation will be evaporated before reaching runoff.

Table 6-11: Summary of runoff and baseflow coefficients and gains according to Ponce and Shetty (1995b)

Summary	K_r	K_u	K'_r (mm^{-1})	K'_u (mm^{-1})
Average	0.34	0.28	0.00056	0.00044
Minimum	-0.57	-0.54	-0.01097	-0.01044
Maximum	0.81	0.80	0.00292	0.00253
Standard Dev	0.15	0.14	0.00066	0.00063
Abs. Confidence interval	0.02	0.02	0.00003	0.00002
Rel. Confidence interval	5%	5%	5%	5%

Table 6-12: Runoff and baseflow coefficients and gains averaged by climatic classes for type II catchments.

Climatic Class (Type II *Catchments*)	K_r	K_u	K'_r (mm^{-1})	K'_u (mm^{-1})
CC1 (93)	0.03	0.01	-0.00016	-0.00029
CC2 (131)	0.26	0.21	0.00080	0.00063
CC3 (527)	0.35	0.28	0.00053	0.00042
CC4 (368)	0.38	0.31	0.00068	0.00056
CC5 (151)	0.49	0.41	0.00064	0.00054

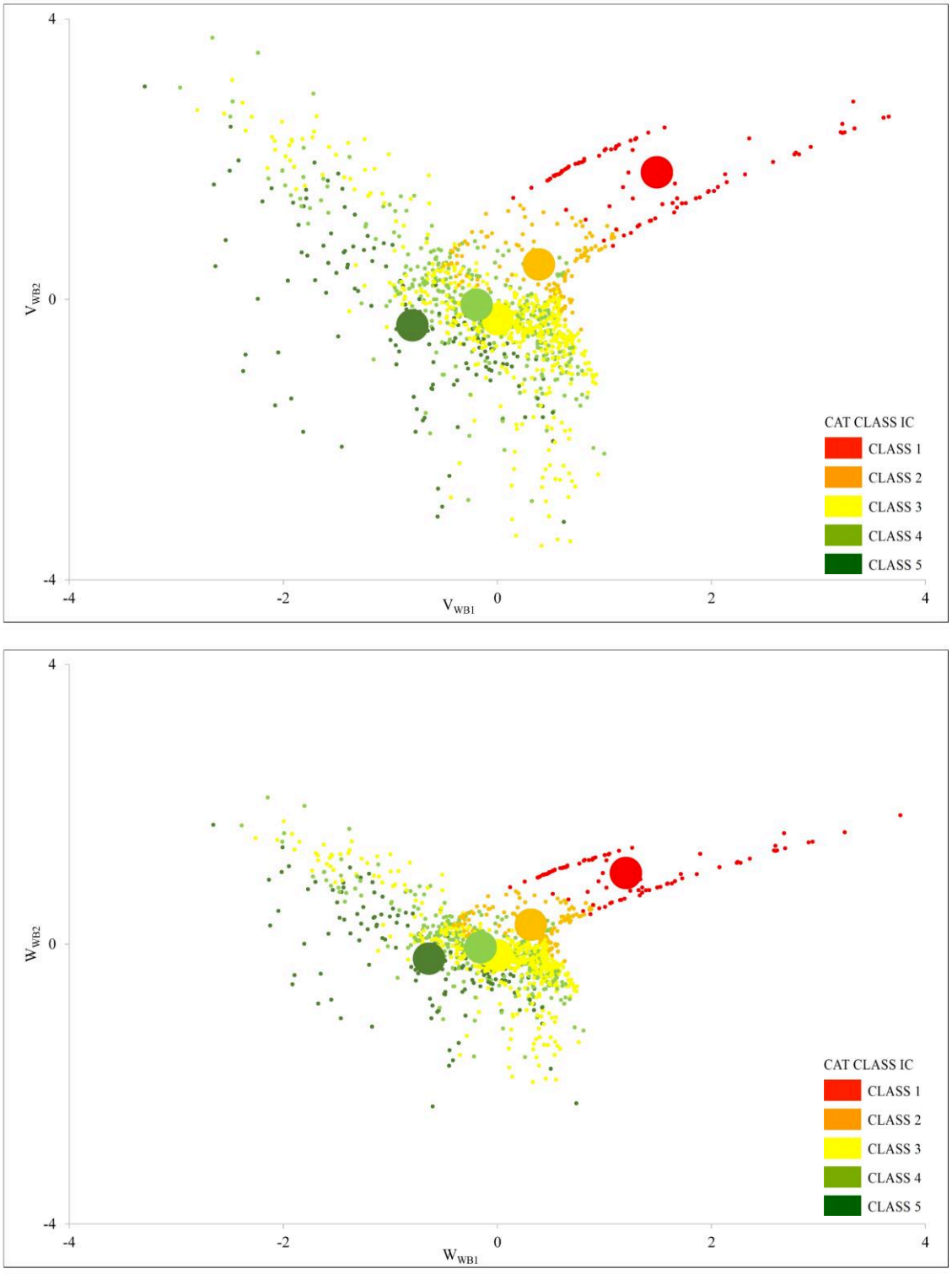

Figure 6-18: Regionalisation of water balance canonical variables represented according to climatic classes with big dots as classes kernels.

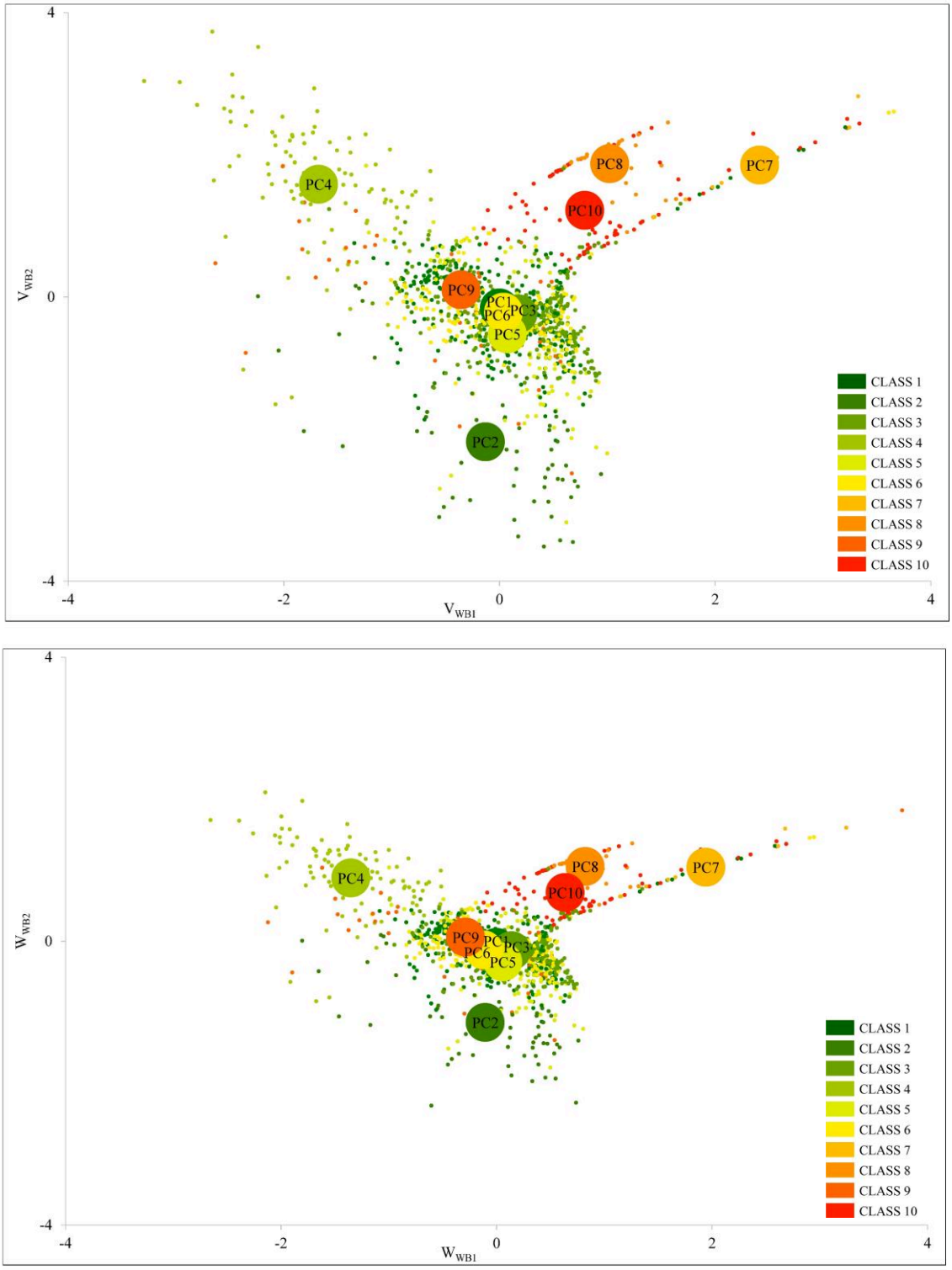

Figure 6-19: Regionalisation of water balance canonical variables represented according to physiographic classes with big dots as classes kernels.

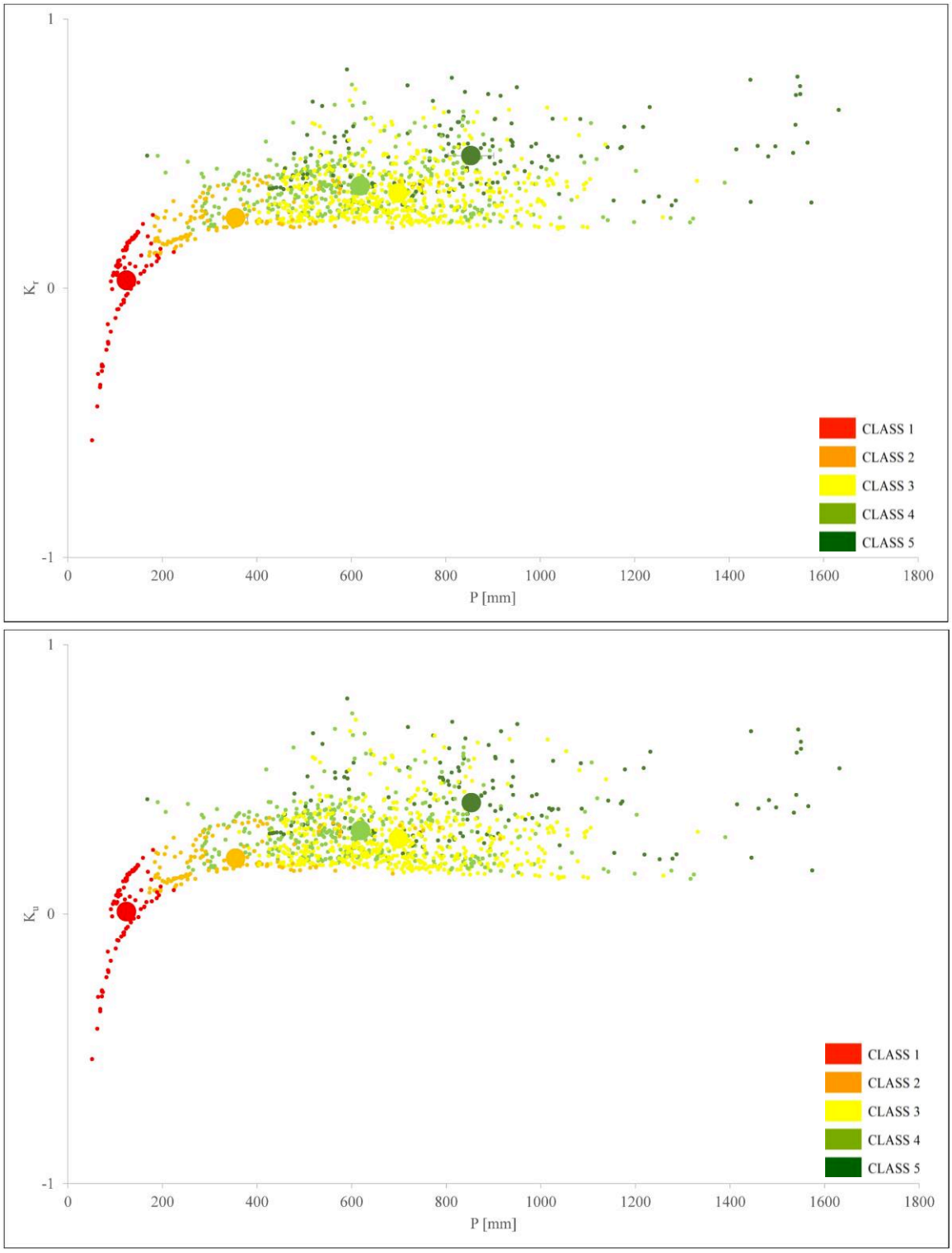

Figure 6-20: Regionalised runoff and baseflow coefficient K_r, and K_u with average values coloured according to climatic classes with big dots as classes kernels.

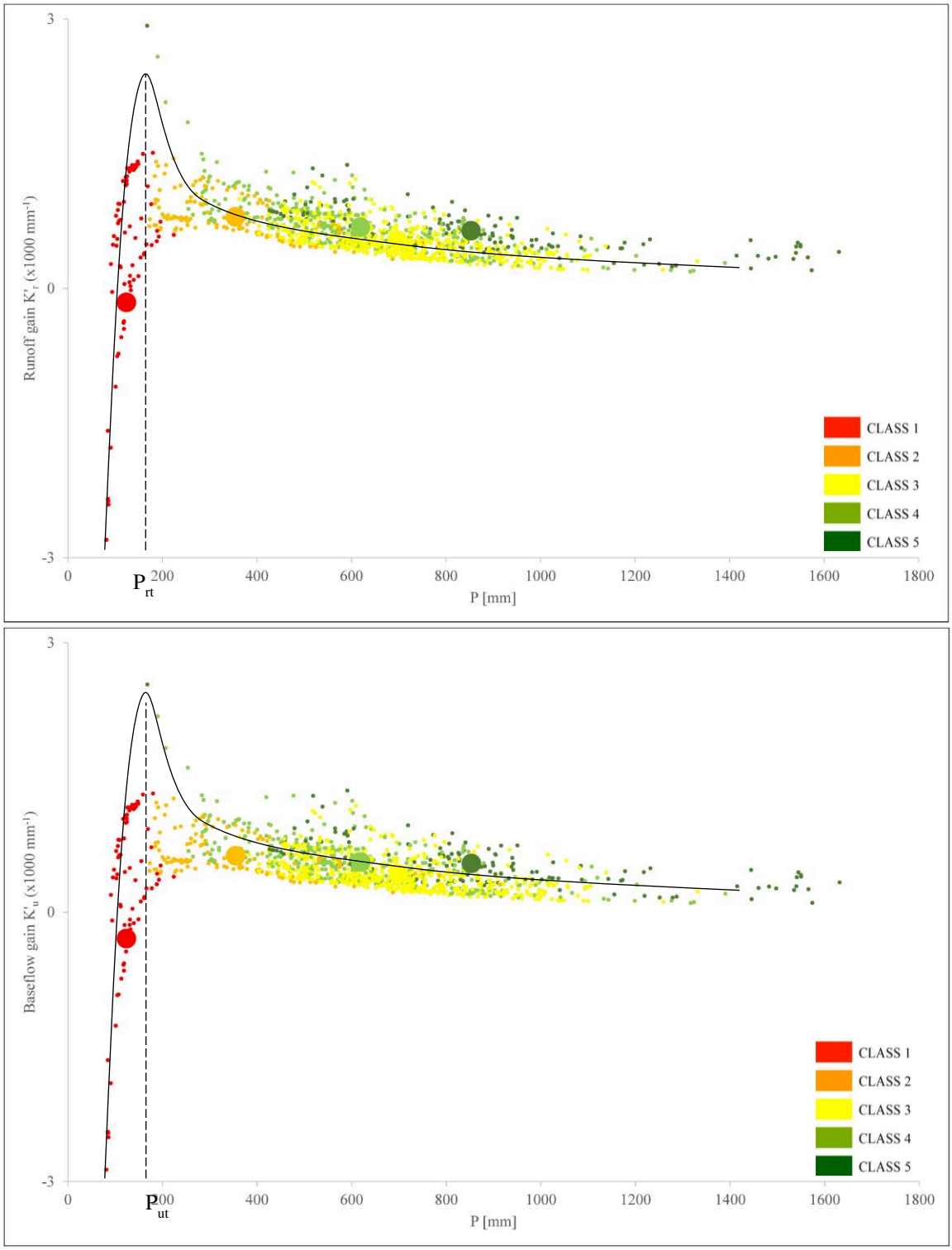

Figure 6-21: Regionalised runoff and baseflow gains K'$_r$, and K'$_u$ with average values coloured according to climatic classes with big dots as classes kernels, dashed line represents the runoff and baseflow threshold precipitation and continuous lines are theoretical trendline.

Figure 6-22 show the regionalised total runoff and baseflow coefficients K_r and K_u, and Figure 6-23 the gains K'_r and K'_u versus the precipitation illustrated according to physiographic classes. We notice that PC4 catchments yielded the highest runoff coefficients across different climatic classes. Desertic catchments PC7, PC8, and PC10 yielded the lowest coefficients but the highest gains as their mean precipitation is lower than the threshold P_{rt}. The other classes are spread according to the climatic distribution yielding almost the same class averages.

Table 6-13: Runoff and Baseflow coefficients and gains averaged by climatic classes for type II catchments.

Physiographic Class (Type II *Catchments)*	K_r	K_u	K'_r (mm^{-1})	K'_u (mm^{-1})
PC1 (304)	0.35	0.28	0.00059	0.00046
PC2 (62)	0.43	0.32	0.00057	0.00043
PC3 (351)	0.32	0.25	0.00056	0.00044
PC4 (105)	0.58	0.54	0.00077	0.00073
PC5 (88)	0.35	0.27	0.00063	0.00050
PC6 (190)	0.34	0.27	0.00050	0.00039
PC7 (10)	-0.13	-0.15	-0.00189	-0.00199
PC8 (29)	0.11	0.09	0.00086	0.00070
PC9 (49)	0.40	0.34	0.00033	0.00024
PC10 (75)	0.17	0.13	0.00089	0.00069

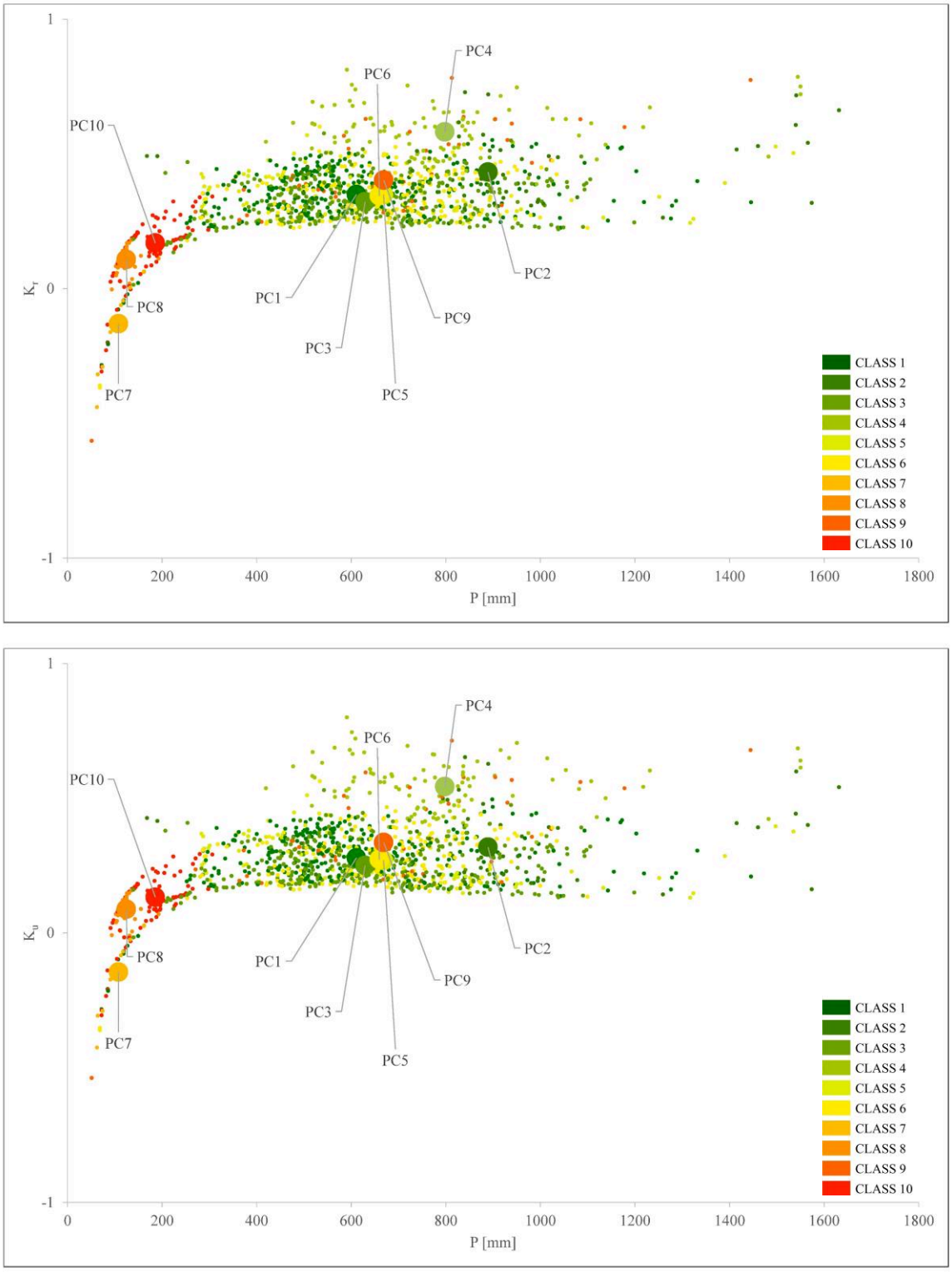

Figure 6-22: Regionalised runoff and baseflow coefficient K_r, and K_u with average values coloured according to physiographic classes.

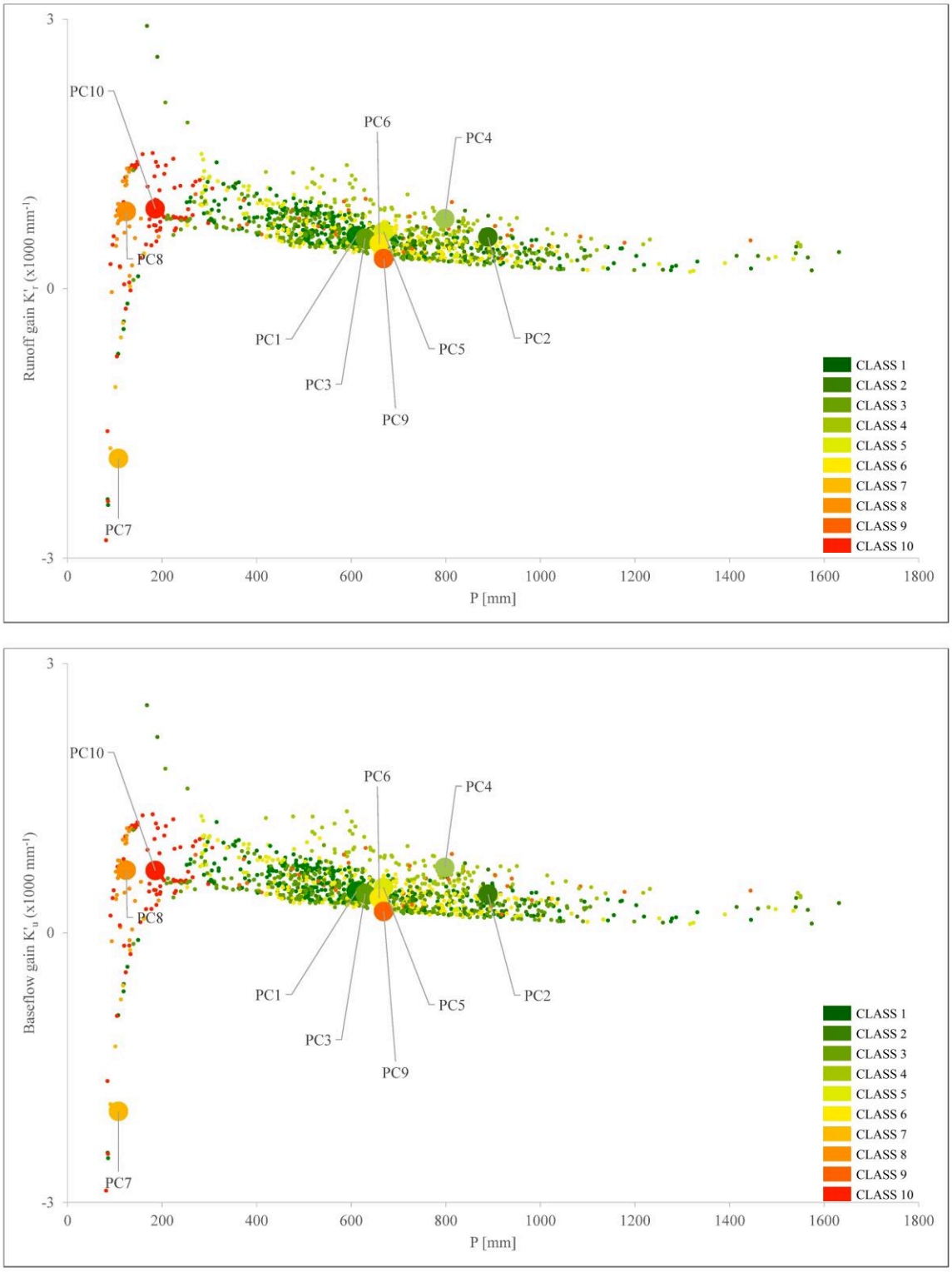

Figure 6-23: Regionalised runoff and baseflow gains K'r, and K'u with average values coloured according to physiographic classes.

6.4.3 Hydrologically homogeneous Mediterranean catchments

Figure 6-24 shows the total runoff coefficient distribution and Figure 6-25 the baseflow coefficient distribution for type II catchments. These maps show high variability across the Mediterranean even for neighbouring catchments.

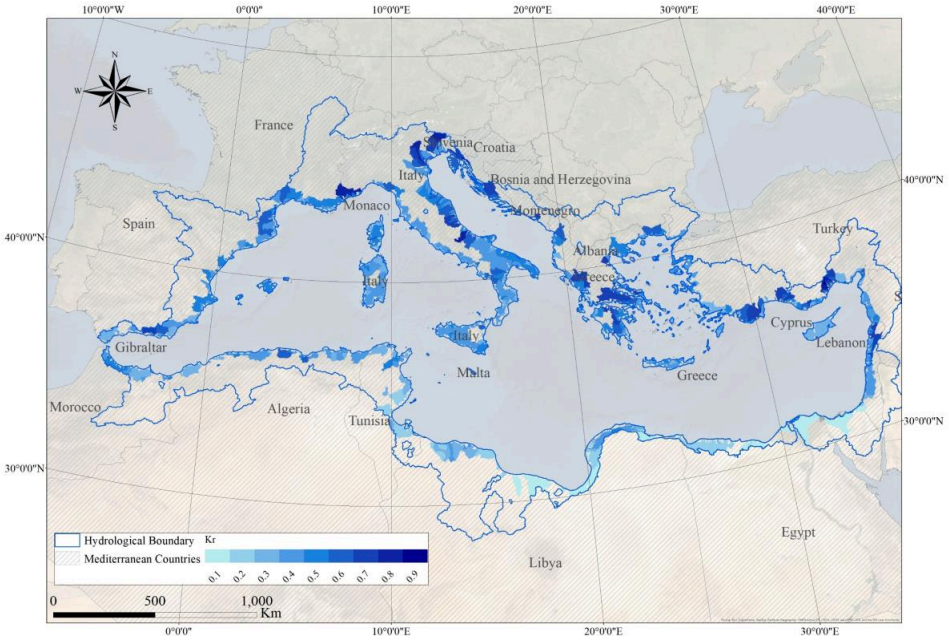

Figure 6-24: Spatial distribution of the regionalised Runoff coefficient K_r ranging between 0 (light blue) and 1 (dark blue)

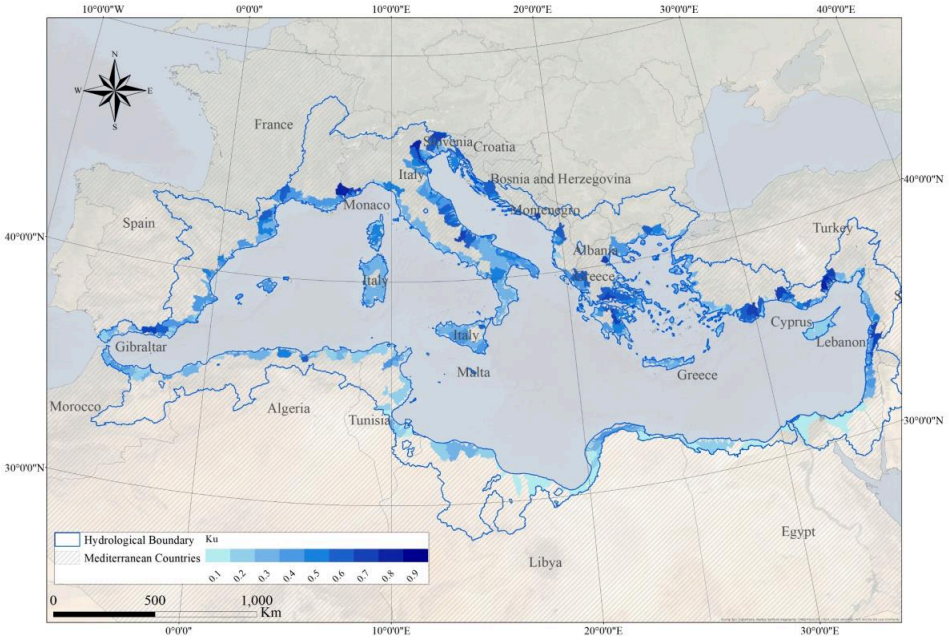

Figure 6-25: Spatial distribution of the regionalised Runoff coefficient K_u ranging between 0 (light blue) and 1 (dark blue)

To determine hydrologically homogeneous Mediterranean catchments, we applied the K-means cluster analysis on type II catchments considering as variables the most contributing physioclimatic indices I_S, I_{Arid}, ZS_{Mean}, P_{Karst}, T_AWC, TC_BDC in addition to the runoff and baseflow coefficients K_r and K_u. Although silhouette plot showed that k = 3 clusters would be the best fit, we also show the silhouette plot for k= 5 which splits the large cluster of k=3 into 3 clusters. Hence, catchments were divided into 5 clusters (see Figure 6-26).

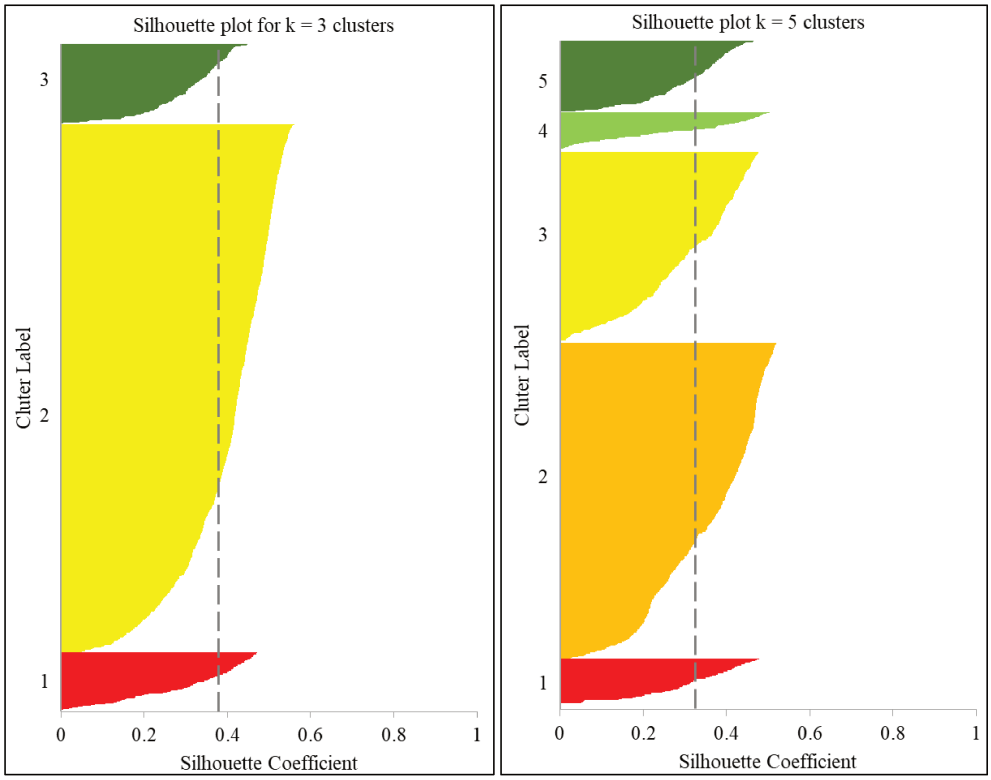

Figure 6-26: Cluster silhouette for the hydrological classification with K-means number of cluster K = 3 and 5

Furthermore, we notice from the map in Figure 6-27 that the five hydrological classes were not uniformly distributed across the Mediterranean although with adjacent catchments belong to different classes however with HC1 limited to South but the others

The summary of hydrological classes' kernels in Table 6-14 and their distribution map in Figure 6-27 show that HC1 represent the arid desertic catchments of the South, HC2 represents the non-karstic catchments, HC3 represents the highly karstic catchments (85%) but very low lands thus yielding high baseflow (K_u= 0.34), HC4 represents the highly watered forest catchments yielding moderate total runoff off (K_r= 0.42) and finally HC5 represents the Mountainous and snow influenced catchments yielding the highest runoff and baseflow (K_r = 0.57, K_u = 0.53).

Table 6-14: Summary of the hydrological classes' kernels

CLASS	MAP	I_S	I_{Arid}	Z_{Mean} (m)	ZS_{Mean} (m)	P_{Karst} (%)	T_AWC (mm)	TC_BDC (%)	K_r	K_u
HC1 (97)	126	0.99	12.27	317	0	49	45	0	0.03	0.01
HC2 (599)	610	0.81	2.17	245	3	6	46	3	0.29	0.22
HC3 (363)	631	0.80	2.06	91	2	85	45	2	0.41	0.34
HC4 (75)	910	0.75	1.27	495	225	33	50	57	0.42	0.31
HC5 (136)	798	0.71	1.27	784	1385	49	41	9	0.57	0.53

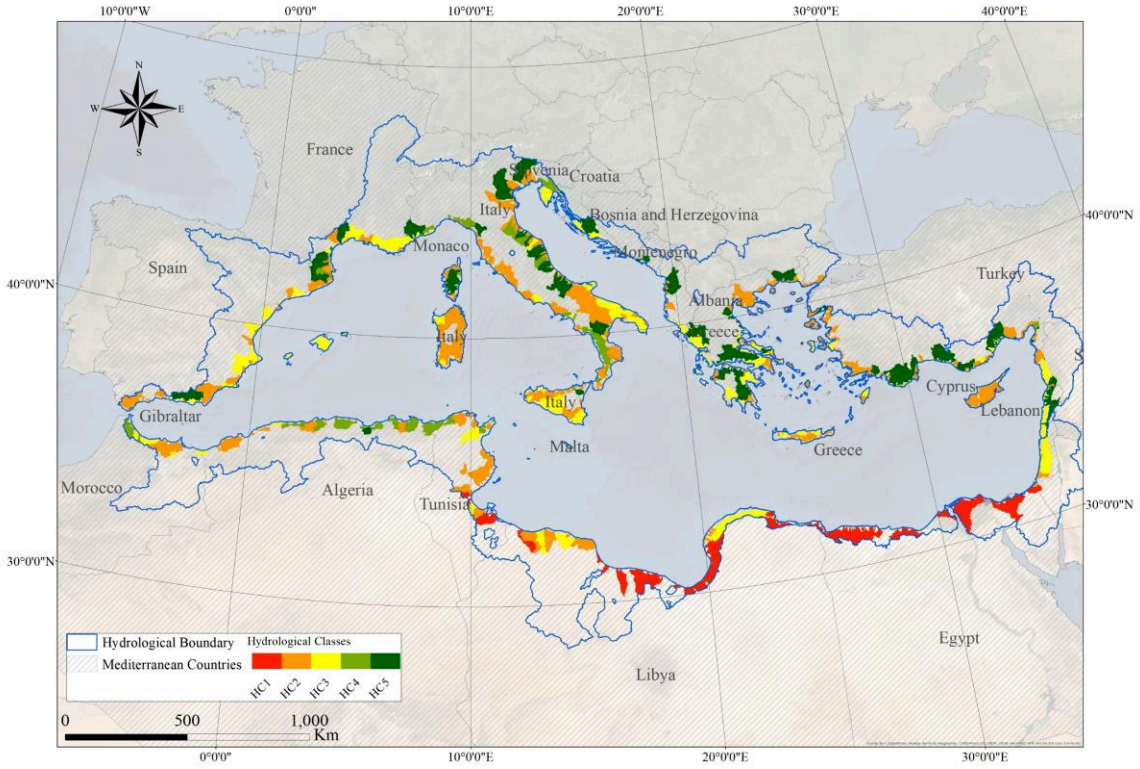

Figure 6-27: Distribution of Mediterranenan type II catchments based on the runoff and baseflow coefficients K_r K_u clustering.

6.5 RUNOFF COEFFICIENTS EVOLUTION UNDER CLIMATE CHANGE SCENARIO

The climate change impact on runoff and baseflow coefficients K_r and K_u and gains K'_r and K'_u was estimated using the projected climatic indices for the period 2070-2100 as calculated in CHAPTER 3 under MED-CORDEX RCM ALADIN and RCM CCLM or two different RCP scenarios (RCP 4.5 and RCP 8.5). The climatic indices in the canonical regression equation from the previous section were replaced by the projected values but he physiographic indices TC_BDC and P_{Karst} were kept without any change. The snow index ZS_{Mean} would absolutely change under climate change scenarios however, it was impossible for us to estimate that change, hence it was also kept without change. In this section, we will only show the charts of the projected runoff and baseflow coefficients under RCM ALADIN for RCP 8.5 (see Figure 6-28 and Figure 6-29) and the summary of the changes as included in Table 6-15. The charts and their corresponding tables for all the scenarios are included in APPENDIX E1.

The projected runoff and baseflow coefficients K_r and K_u, and gains K'_r and K'_u are plotted in Figure 6-28 and Figure 6-29 versus the precipitation and illustrated according to climatic and physiographic classes. The distribution of the coefficients follows the same trend as the baseline reference, where K_r and K_u increase with precipitation in line with the climatic classification. The overall average of K_r has increased by 2% to 7% and K_u has changed by -2% to 5% under all scenarios, but standard deviation has decreased by 37% to 42% for K_r and 28% to 31% for K_u (see Table 6-15). The runoff and baseflow coefficients have decreased for both Spercheios and Adonis rivers by -7% to -16% under all scenarios with a slight advantage for Adonis under ALADIN RCP 4.5, however it is still above 0.50 for both coefficients.

The overall increase was not expected as precipitation is projected to decrease, however, the interclass variation would reflect better analysis. The climatic classes averages have shown variable evolution, with K_r increasing by 850% to 950% for CC1 catchments, reaching 0.31, while it decreased by -15% to -18% for CC5 catchments, reaching 0.41. In its turn, K_u have increased by 2400% for CC1 catchments, reaching 0.26, and decreased by -17% to -20% for CC5 catchments, reaching 0.34.

The physiographic classes averages have also shown variable evolution with K_r of PC7, PC8 and PC10 desertic catchments increasing by 86% to 279% while other classes variations were limited between -12% to 6%. PC4 and PC9 were negatively impacted catchments as RCM scenarios projected that K_r would decrease by -11% to -12% and K_u would decrease by -10% to -12% for PC4 catchments, and K_r would decrease by -3% to -5% and K_u would decrease by -6% to -8% for PC9 catchments. For the gains K'_r and K'_u, the averages have also increased by 28% to 46% according to scenarios, and the threshold P_{rt} and P_{ut} have decreased to 80-100 mm, lower than the thresholds found in previous section.

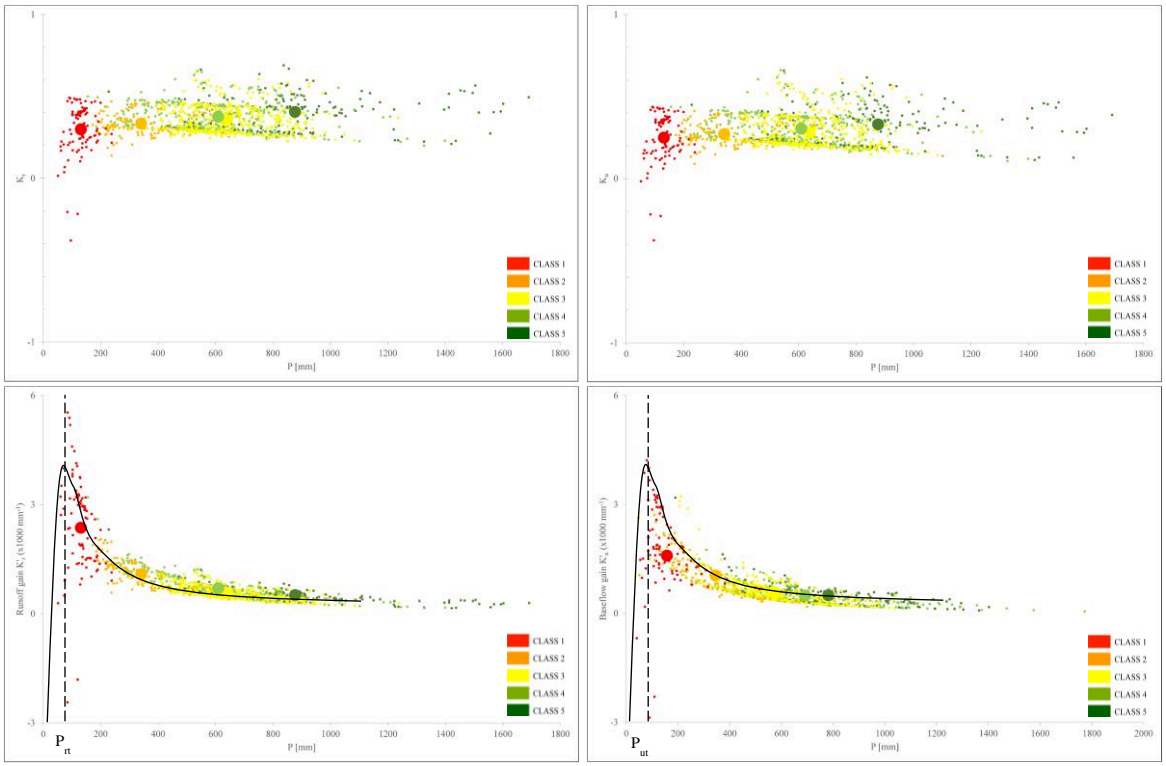

Figure 6-28: Projected regionalised runoff and baseflow coefficients K_r, and K_u and gains K'_r, and K'_u with average values coloured according to climatic classes based on projected climatic indices under ALADIN RCP8.5 scenarios for 2070-2100.

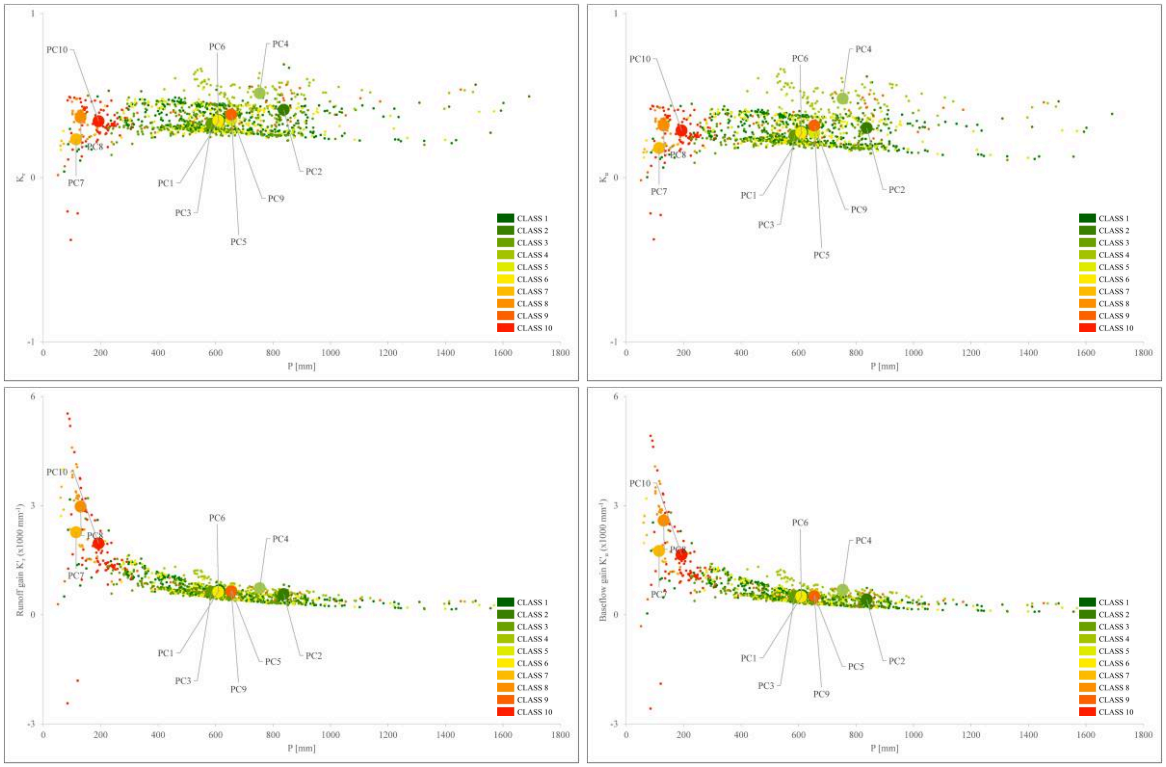

Figure 6-29: Projected regionalised runoff and baseflow coefficients K_r, and K_u and gains K'_r, and K'_u with average values coloured according to physiographic classes based on projected climatic indices under ALADIN RCP8.5 scenarios for 2070-2100.

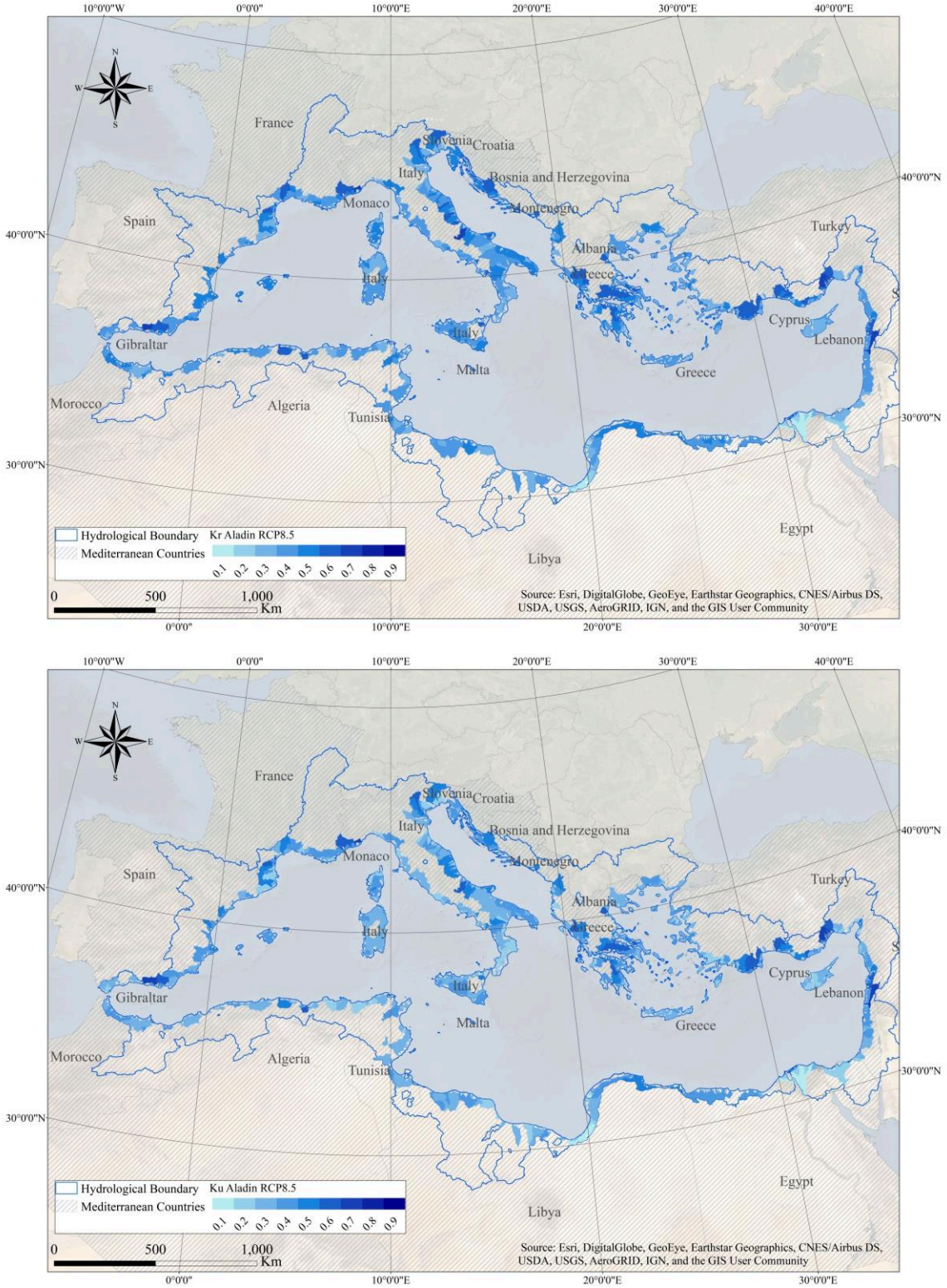

Figure 6-30: Spatial distribution of the projected regionalised runoff and baseflow coefficients K_r and K_u based on projected climatic indices under ALADIN RCP8.5 scenarios for 2070-2100.

The projected evolution under MED-CORDEX RCM scenarios has mainly impacted the extremes. The water balance coefficients are increasing in CC1 arid catchments and decreasing in humid catchments hence minimising the interclass variability and increasing catchments homogeneity. Overall, catchments scatter and classes have drawn closer to the most Mediterranean CC3 and CC4 catchments, with PC4 staying as the highest yielding catchments. However, climate change would also draw a physiographic change, mostly vegetation and landcover which was not taken into consideration but will certainly affect the water balance coefficients. The physiographic change could be considered in future studies.

Table 6-15: Water balance runoff coefficients under RCM ALADIN and CCLM RCP scenarios with evolution ratio in italic

	Summary	K_r		K_u		K'_r (mm^{-1})		K'_u (mm^{-1})	
BASELINE 1970-2000	Average	0.34		0.28		0.00056		0.00044	
	Minimum	-0.57		-0.54		-0.01097		-0.01044	
	Maximum	0.81		0.80		0.00292		0.00253	
	Standard Dev	0.15		0.14		0.00066		0.00063	
	Abs. Confidence interval	0.02		0.02		0.00003		0.00002	
	Rel. Confidence interval	5%		5%		5%		5%	
ALADIN RCP 4.5 2070-2100	Average	0.36	7%	0.29	5%	0.00075	34%	0.00061	38%
	Minimum	-0.04	92%	-0.07	87%	-0.00079	93%	-0.00125	88%
	Maximum	0.68	-16%	0.65	-19%	0.00381	31%	0.00337	33%
	Standard Dev	0.09	-41%	0.10	-31%	0.00055	-16%	0.00049	-22%
	Abs. Confidence interval	0.02	0%	0.02	-19%	0.00004	37%	0.00003	67%
	Rel. Confidence interval	5%	10%	5%	10%	5%	10%	5%	10%
ALADIN RCP 8.5 2070-2100	Average	0.36	6%	0.29	3%	0.00079	41%	0.00064	46%
	Minimum	-0.38	33%	-0.38	30%	-0.00395	64%	-0.00391	63%
	Maximum	0.69	-15%	0.66	-17%	0.00553	89%	0.00492	94%
	Standard Dev	0.09	-37%	0.10	-27%	0.00067	1%	0.00059	-6%
	Abs. Confidence interval	0.02	-1%	0.02	-20%	0.00004	45%	0.00004	77%
	Rel. Confidence interval	5%	10%	5%	10%	5%	10%	5%	10%
CCLM RCP 4.5 2070-2100	Average	0.36	6%	0.29	3%	0.00073	31%	0.00060	36%
	Minimum	0.03	105%	0.00	99%	0.00013	101%	-0.00005	100%
	Maximum	0.67	-17%	0.65	-19%	0.00338	16%	0.00297	17%
	Standard Dev	0.09	-42%	0.10	-31%	0.00053	-20%	0.00047	-26%
	Abs. Confidence interval	0.02	-1%	0.02	-21%	0.00004	35%	0.00003	64%
	Rel. Confidence interval	5%	10%	5%	10%	5%	10%	5%	10%
CCLM RCP 8.5 2070-2100	Average	0.35	2%	0.27	-2%	0.00072	28%	0.00058	31%
	Minimum	0.00	100%	-0.03	94%	-0.00004	100%	-0.00046	96%
	Maximum	0.69	-14%	0.66	-17%	0.00332	14%	0.00291	15%
	Standard Dev	0.09	-39%	0.10	-28%	0.00049	-27%	0.00043	-31%
	Abs. Confidence interval	0.02	-5%	0.02	-25%	0.00004	31%	0.00003	58%
	Rel. Confidence interval	5%	10%	5%	10%	5%	10%	5%	10%

6.6 CONCLUSION

The observation of canonical scatter diagrams permitted the discussion of Mediterranean catchments homogeneity and variability. One should ask, does physiographically similar or different but climatically different or similar catchments induce or not their hydrological similarity?

To answer these questions, we first refer to the regionalised inter-class analysis of High Flows and Low Flows scatter diagrams where we noticed in Figure 6-14 how CC1 and CC5 catchments, despite their presence within the Mediterranean hydrological boundary, were set apart from CC2, CC3 and CC4 in both physioclimatic and hydrological diagrams. In Figure 6-17, catchments scatters where only spaced from each other if they belong to either PC7, PC8 and PC10 which are desertic and located in CC1 region, or if they were PC9 which are located in CC5 region, hence physiographic features are not the major control of catchments hydrology and *we can deduce that the general Mediterranean climate influence a hydrological homogeneity despite the physiographic variability*.

Nevertheless, the intra-class hydrological analysis for High Flows in PC1 and PC9 catchments represented in Figure 6-6 showed that when all catchments share the same physiographic characteristics, CC5 catchments where closing up from CC2, CC3 and CC4 on hydrological scatter diagram while they keep the same distance for Low Flows in Figure 6-7. This might be due to flow regulation in managed catchments which is attenuating CC5 High Flows during wet season, while in dry seasons, CC5 wet catchments have naturally higher flows than the catchments in CC2 and CC3 dry regions.

As for PC4 catchments scatter diagrams, represented in Figure 6-8 according to climatic classes show a totally different distribution between physioclimatic and hydrological canonical variables. In addition, we notice in the CCA scatter diagram of water balance coefficients in Figure 6-10 the remarkable separation of PC4 catchments from the others and that for different climatic classes, which is interpreted by PC4 physiographic features taking over climatic features. Same observation with the regionalised scatter diagrams in Figure 6-19 endorsed by the charts in Figure 6-21 and Figure 6-23 and the hydrological clusters in Figure 6-27 where PC4 catchments yield the highest runoff coefficients over different climatic classes.

We deduce that some physiographic features mainly mountains, snow and karst might take over the climatic forcing features and such catchments shall yield high runoff.

Thus, to answer our earlier question we can say that climatically homogeneous catchments are more likely to have homogenous hydrological behaviour despite their physiographic variability except for mountainous, snow and karst influenced catchments which yield homogeneous hydrological behaviour despite the climatic forcing. A simple physical interpretation is that exposed karst and the top layer of the snow cover

protect the water resources from ambient climatic conditions, mainly evapotranspiration, by storing it as groundwater in direct infiltration or delayed snowmelt, while other physiographic features like landcover and soil are result of long climatic exposition making their hydrological behaviour more aligned with climate.

The regionalisation of the runoff and baseflow coefficients K_r and K_u of type II catchments permitted the estimation of water resources, a valuable information for regional and national water management strategies, where stakeholders can easily choose which catchments to drop and which to focus on. The regionalisation has also permitted MED-CORDEX RCM climate change scenarios impact prediction on type II catchments water balance coefficients.

Overall, the coefficients K_r and K_u are increasing because of the precipitation decrease, however, the projected evolution has mainly impacted the extremes, hence minimising the interclass variability and increasing catchments homogeneity. Catchments scatter and classes have drawn closer to the most Mediterranean CC3 and CC4 catchments, with PC4 staying as the highest yielding catchments.

"God Rivers Duel, A Mediterranean Epic"

The Duel Card

ΠΟΤΑΜΙ ΕΝΑ	
Name	Ibrahim, Adonis
Country	Lebanon
Area	329 km^2
MAP	1450 mm
MAQ	1052 mm

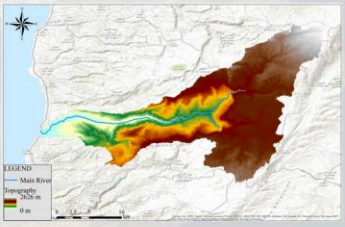

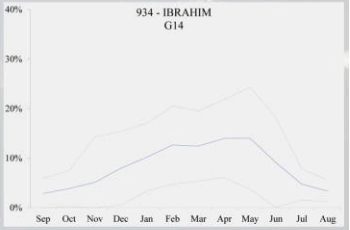

Climatic characteristics	
Climatic Class	CC3
I_S	0.99
$SP_{1.5}$	4
$P_{25\%}$	2.12
S_{Tm}	6
I_{Arid}	0.99
$T_{25\%}$	1.52
S_{PET}	5

Physiographic characteristics	
Physiographic Class	PC4
Z_{Mean}	1572 m
ZS_{Mean}	1928 m
I_{Hypso}	0.13
P_{Karst}	100%
T_AWC	34.2 mm
Leptosols	0.35
TC_MLT	0%
SC_COD	47%
BA	1.5%
CMA	0%
SHC	48.4%
TC_BDC	0%

Hydrologic characteristics					
Hydrologic Class	HC5				
ET_p/P	0.66		E/P	0.27	
P	1450 mm		Q	1052 mm	
U	794 mm		S	258 mm	
V	399 mm		W	1193 mm	
K_r	0.73		K_u	0.67	
$\lambda_s W_p$	8 mm		$\lambda_u V_p$	330 mm	
W*	0.8		S*	0.2	
U*	0.9		V*	0.1	
P¯	0.2		V¯	0	
KH	0.1		KV	0.1	
KB	0.7		KR	0.9	
φ	0.1				
ρQ	1.6	ρS	1.6	ρU	1.6

ΠΟΤΑΜΙ ΔΥΟ	
Name	Sperchios
Country	Greece
Area	1592 km^2
MAP	701 mm
MAQ	575 mm

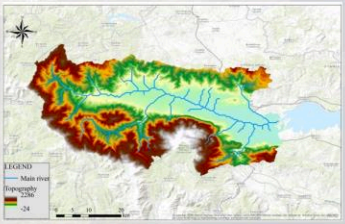

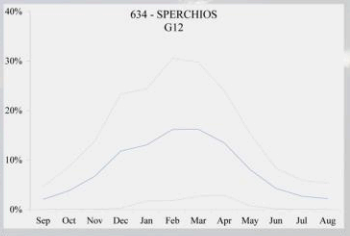

Climatic characteristics	
Climatic Class	CC4
I_S	0.75
$SP_{1.5}$	2
$P_{25\%}$	1.36
S_{Tm}	6
I_{Arid}	1.26
$T_{25\%}$	1.56
S_{PET}	6

Physiographic characteristics	
Physiographic Class	PC4
Z_{Mean}	714 m
ZS_{Mean}	1344 m
I_{Hypso}	-0.1
P_{Karst}	58%
T_AWC	42.1 mm
Leptosols	0.35
TC_MLT	9%
SC_COD	4%
BA	0%
CMA	17%
SHC	0%
TC_BDC	10%

Hydrologic characteristics					
Hydrologic Class	HC5				
ET_p/P	1.41		E/P	0.16	
P	701 mm		Q	572 mm	
U	421 mm		S	151 mm	
V	128 mm		W	550 mm	
K_r	0.82		K_u	0.77	
$\lambda_s W_p$	3 mm		$\lambda_u V_p$	0 mm	
W*	0.8		S*	0.2	
U*	0.8		V*	0.2	
P¯	0.3		V¯	0.1	
KH	0.2		KV	0.2	
KB	0.6		KR	0.8	
φ	0.3				
ρQ	1.4	ρS	1.7	ρU	1.3

GENERAL DISCUSSION

In this thesis, we carried out a comprehensive characterisation covering the climate, landscape, and hydrology of Mediterranean catchments, as we were curious if a specific hydrology might govern the region and as serious challenges face Mediterranean water resources.

We defined first in CHAPTER 1 the various boundaries of the Mediterranean region according to climatic, hydrological, agro-bioclimatic, and administrative definitions. And presented in CHAPTER 2, an overview of the collected database starting with the delineation of all Mediterranean catchments located within the hydrological boundary, the climatic characteristics derived from the gridded WorldClim-2 database, or other collected weather stations; the physiographic characteristics derived from global data sets of topography, geology, landcover, lithology, soil, snow and karst; the hydrological data of 55 catchments serving as a sample for later water balance characterisation. Despite of the extensive job performed for data collection, which required direct contact sometimes by mails and other by phones, with several hydrological services in different countries, (Greece, Turkey, Spain, etc.), it was impossible to obtain any runoff data of any Egyptian or Libyan catchment, in addition, it was very challenging to find concomitant daily timeseries for all 55 catchments, hence the first source of uncertainty, a second source lies in the influence of existing management projects which we tried to reduce to minimum by selecting lowly influenced catchments.

Climatic characterisation

We established in CHAPTER 3 a new high-resolution climatic classification for hydrology purposes based on Mediterranean specific climate indices like precipitation seasonality I_s and aridity I_{Arid} that play an important role in the hydrological mechanisms of Mediterranean catchments and flow intermittence. Upon the PCA, seven indices I_S, $P_{25\%}$, $SP_{1.5}$, I_{Arid}, $T_{25\%}$, S_{PET} and S_{Tm} were the most contributing climatic indices with 70% of total variance explained for the first two components. Statistical summaries show I_S values ranging between 0.2 and 1 with an average of 0.8 highlighting Mediterranean seasonality. The Mediterranean climate was demonstrated continuous through the indices values uniformly increasing or decreasing from North to South. I_s is highest in the South and lowest in North, same for I_{Arid}. In general, the gridded classification gradient confirms that I_s and I_{Arid} are the main contributors to the climatic classification taking over precipitation and temperature frequency indices.

In addition, to follow up the classification evolution at the end of 21st century, we carried out two climate change scenarios RCP 4.5 and 8.5 for two different RCM models CCLM and ALADIN. We found that in the North, where seasonality is low and precipitation is regular along the year, that the two scenarios for the two models are projecting a high precipitation decrease, down to -60% and a warming up to 6.8°C during dry spring and summer seasons, hence increasing I_s by +80% and I_{Arid} by +60% causing the wet seasons shortening and river regimes modification.

Physiographic characterisation

We carried out in CHAPTER 4 a physiographic classification of all catchments based on landform, landcover and soil indices to highlight Mediterranean variability. The PCA reduced the number of physiographic indices to 13 showing A, Z_{Mean}, ZS_{Mean}, I_{Hypso}, P_{Karst}, T_AWC, Leptosols, and Landcover types, Tree Cover Mixed Leaf Type (TC_MLT), Tree Cover Broadleaved Closed Deciduous (TC_BCD), Shrub Cover Closed-Open Deciduous (SC_COD), Bare Areas (BA), Sparse Herbaceous Cover (SHC) and Cultivated and Managed Areas (CMA) as the most contributing indices with 70% of total variance explained.

An insight to classification indices uncovers the physioclimatic interaction, (microclimates, landcover distribution, etc.), part of the self-organisation of the vegetation with the climate proposed by Horton (1933), and its role in shaping Mediterranean hydrology and flow regimes. Catchments areas A have the same range (300 to 500 km^2) for all classes except class 9 which was separated for landcover reasons, that means that Area does not impact much in the classification. Average altitude Z_{Mean} indicates the role of landforms as a natural boundary shaping the incidence between air masses and catchments. It sometimes provokes orographic precipitations in frontal catchments if high mountains were exposed to cold fronts while creating arid zones in their adjacent backyard catchments. On the other hand, low catchments in North Africa dissipate any possible precipitation and permit desertic influence through low corridors. This landform impact is widely observable in the Mediterranean, we cite Andarax, in Southern Spain (MAP = 240 mm), “Jabal el Akhdar” or “green mountain” reaching a maximum altitude of 875m, the only green spot between Alexandria and Tunis. It creates a natural boundary between Mediterranean Sea and desert making it more homogeneous with Eastern Mediterranean catchments of CC3 while adjacent lower catchments have dominant bare lands and lack tree and shrub cover belonging to CC1 or CC2. It is also observable in Cyprus and North Lebanon (Nahr Bared catchment MAP = 1450 mm vs Assi subcatchments his backyard catchment with MAP = 660 mm). T_AWC characterises the types of soil and conditions the type of vegetation able to grow in these conditions. It appears that only shrubs and needle leaved trees grow in leptosols, Low T_AWC and high seasonality, dominant in East Mediterranean region, while broadleaved and mixed leaf trees prefer North Eastern Mediterranean where high T_AWC and low seasonality reigns. Cultivated areas are dominant in North Mediterranean countries and Italy where lowlands and wide fields are suitable for agricultural activities.

Hydrological characterisation

To characterise the hydrological behaviour of the Mediterranean region, we collected rainfall and runoff series of 55 catchments across 15 countries. In CHAPTER 5, we studied their flow regimes according to

Haines (1988) and applied the different water balance functional models. The functional approach provided a clear and simple way to characterise each water balance component and interaction.

The water balance model of Budyko (1974) was useful in positioning all the catchments in respect to their total precipitation and evapotranspiration, hence indicating the climatic forcing on hydrology. Budyko curve can indicate the overall water availability of a catchment, but not enough to estimate the water resources. L'vovich (1979) model showed a breakdown of the annual water balance advancing more info on the surface runoff S and groundwater runoff U which indicates the physiographic forcing on hydrology. It also permitted a precise interannual comparison with precious info on water resources. Ponce and Shetty (1995a) generalized L'vovich model from annual values to continuous curves which helps in predicting the available water resources throughout the years. The model equations are dependent from runoff threshold parameters, specific for each catchment which permits more precise inter catchment comparison, highlighting Mediterranean variability. In addition, these parameters also reflect the physiographic forcing on hydrology. Sivapalan (2011) model went further with non dimensionalising Ponce and Shetty equations which permitted in addition to interannual and inter catchment comparison, an inter climatic and inter physiographic comparison, useful in our study to uncover the variability and homogeneity of Mediterranenan catchments through nondimensional metrics K_H, K_B, K_R and K_V. These metrics showed the special setting of Mediterranean catchments in correspondence to aridity index $\varphi = \tilde{V}/\tilde{P}$. Sivapalan model showed a space time symmetry where functional curves fit both to individual catchments for interannual analysis or to mean annual water balances for inter catchment analysis despite their variability.

The spatial distribution of Ponce and Shetty water balance parameters W_p, V_p, $\lambda_s W_p$ and $\lambda_u V_p$ reflected a wide geographical variability across the Mediterranean without clear indication of any patterns. We therefore applied the nondimensional formulation of Sivapalan to plot on the same chart all 55 catchments water balance components and discuss their variability in relation to their climatic and physiographic classes. The climatic illustration of $W^* = f(\tilde{P})$ and $S^* = f(\tilde{P})$ showed that the competition between surface runoff and wetting is gradually evolving from climatic CC2 in the South, where low precipitation and low quick flows dominate, to CC5 in the North where high precipitation and high quick flows dominate. The same trend could be observed for of $U^* = f(\widetilde{W})$ and $V^* = f(\widetilde{W})$ but with disturbance of CC3 due to Lebanese catchments. The physiographic illustration of the same charts did not show any inter class trend or clustering except for PC2 forest catchment yielding the highest quick flow S* and lowest wetting W* maybe because they are already located in CC5 wet region which is also related to the type of tree and their density. Another cluster is PC4 snow and karst influenced catchments which are spread across the Mediterranean but yield the highest slow flow U* with the lowest vaporisation V*, no matter the climatic positioning.

The calculation of the dimensionless water balance metrics K_H, K_B, K_V, K_R endorsed the previous findings as aridity index $\varphi = \tilde{V}/\tilde{P}$ turned to be a primary determinant of the mean annual water balance. The charts showed that K_H and K_V were increasing with aridity, suggesting that in general, the vaporisation V (energy) takes over the wetting W and consequently the slow flow component U while moving towards arid catchments. In reverse K_B and K_R were decreasing with aridity except for, once again, PC4 catchments which showed to be independent to climate variability. The same climate trends and separated position of PC4 catchments were also observed for runoff and baseflow coefficients and gains and flow elasticities in Section 5.4.3; Therefore we state that "*In the Mediterranean, the mountainous, snow and karst influenced catchments yield the highest slow flow and runoff especially if located in high seasonal region (Southern Mediterranean CC3 regions) where precipitation are concentrated in winter and runoff are concentrated in winter and spring seasons (Haines Group 13 or 14 for North Lebanon), when minimum vegetation cover the land and vaporisation (or evapotranspiration) is at lowest, part of the self-organisation of the vegetation with the climate as proposed by Horton (1933) but at the intra-annual scale.*"

In the light of what we deduced that PC4 catchments characteristics are independent from climate variability to some extent, it is highly probable that the climatic evolution impact on their hydrological behaviour, as seen in CHAPTER 3, will positively affect the hydrological regimes of PC4 catchments as aridity φ is expected to decrease because of Vaporisation V decrease when precipitation season will shorten and consequently baseflow U and wetting W are expected to increase as long as they stay under snow influence.

These observations and findings were verified and completed in CHAPTER 6 where we exported the water balance coefficients and hydrological indices to 1270 catchments ranging between 100 km^2 and 3000 km^2 using Canonical Correlation Analysis regression equations. Canonical Correlation Analysis detected which specific climatic and physiographic indices govern the Mediterranean hydrological behaviour, mainly water balance coefficients K_r and K_u and 90 days indices of High Flows (DH_5, FH_1) and Low Flows (DL_5, FL_1) for their major importance in water resources management.

Canonical Correlations Analysis detected that some physioclimatic indices showed high correlation with (DH_5; DL_5) like A, MAP, $T_{25\%}$, I_{Arid} while T_AWC showed an important correlation with FH_1. The intra – class CCA of PC1 and PC9 catchments detected an additional correlation between ZS_{Mean} and (DH_5; DL_5), as of PC4 catchments, it remarkably did not show any important correlation with I_{Arid} making (DH_5; DL_5) somehow independent from it. The CCA of water balance coefficients showed that MAP, ZS_{Mean}, TC_BDC, $T_{25\%}$, I_{Arid} are highly correlated to K_r and K_u and were validated using Jack-knife cross validation method.

The representation of canonical diagrams according to their climatic and physiographic regions helped in identifying the existence of homogeneous clusters in the canonical spaces. The contribution of climatic

indices in the CCA forced some spatial clustering despite that physiographic indices are variable across the Mediterranean, but they are also affected by climate characteristics as mentioned above.

The regionalisation of flow indices (DH_5; DL_5) showed that the general Mediterranean climate force a hydrological homogeneity despite the physiographic variability**.** However, the regionalisation of water balance coefficients K_r and K_u showed that PC4 catchments yield the highest runoff coefficients over different climatic classes, hence we deduce that some physiographic features mainly landform, snow and karst take over the climatic forcing features. Thus, we can say that *in the Mediterranean, climatically homogeneous catchments are more likely to have homogenous hydrological behaviour despite their physiographic variability except for mountainous catchments influenced by the snow and karst which yield homogeneous hydrological behaviour despite different climate*.

The regionalisation has also permitted the prediction of the climate change impact on type II catchments water balance coefficients, under MED-CORDEX RCM scenarios. Overall, the average coefficients K_r and K_u are increasing despite the precipitation decrease, however, the projected evolution has mainly impacted the extremes, hence minimising the interclass variability and increasing catchments homogeneity. Catchments scatter and classes have drawn closer to the most Mediterranean CC3 and CC4 catchments, with PC4 staying as the highest yielding catchments. Climate change would also draw a physiographic change, mostly vegetation and landcover which was not taken into consideration but will certainly affect the water balance coefficients. The physiographic change could be considered in ulterior studies.

The K-means classification of the physioclimatic indices I_S, I_{Arid}, ZS_{Mean}, P_{Karst}, T_AWC, TC_BDC with the runoff and baseflow coefficients K_r and K_u showed that the climatic dimension is responsible for highlighting the spatial proximity of some catchments that belong to HC1. However, most catchments that belong to HC2, HC3; HC4 and HC5 showed hydrological homogeneity between non-adjacent catchments.

Thus, merging all the characterisation findings, we deduce that Mediterranean hydrology is conditioned by 1st degree climatic forcing, generated by the complex of North Atlantic Oscillations, Islandic Siberian and other cyclones drifting across the Mediterranean, here expressed by the seasonality I_S and aridity I_{Arid} indices and 1st degree physiographic forcing such as landforms, generators of microclimates. Microclimates are the 2nd degree climatic forcing expressed by the amount and type of precipitation that shape the 2nd degree physiography like landcover types, T_AWC and other physiographic features which result from long climatic exposition. Such Mediterranean specific landscape-climate organization indirectly shapes hydrological processes like runoff, infiltration and evapotranspiration making them more aligned with climate.

However, an important “intruder” to this landscape-climate organisation is the elevated and exposed karst, which is also Mediterranean specific dating since the Messinian period 5.96 - 5.33 Ma when sea level dropped dramatically, causing Karstogenèse of Lapiaz, caves and other underground formations present across the Mediterranean. Karstic catchments defied the climatic aligned hydrological behaviour of other Mediterranean catchments and showed a homogeneous behaviour independent from climatic forcings. Another “intruder” is the water resources management in the case of PC1 or PC9 catchments but still aligned with climate at least for the selected catchments in this study.

Climate is indeed the major and primary determinant of Mediterranean hydrology but not the only as major contribution into flow regimes came from physiographic indices like ZS_{Mean}, TC_BDC, T_AWC. Hence, defining hydrologically homogeneous Mediterranean catchments consists of finding 1st and 2nd degree climatic and physiographic forcing.

Conclusion and Perspectives

The alerting climatic and anthropogenic impacts call for urgent adaptation and mitigation measures that should be included in future national strategies and water resources management plans and that should be more based on regional research by deepening the knowledge on the spatial and temporal variability of hydrological resources all over the Mediterranean.

The mapping of hydrologically homogeneous Mediterranean catchments is one of the basic studies to be used by researchers, laboratories, engineers, Governments, and International organizations which Mediterranean region form their target study areas. These results could help in catchment scale studies like prediction on ungauged basins or furthermore regional scale studies like global change impact prediction on Mediterranean hydrology leading to adaptation and mitigation policies and practices.

To overcome the problematic challenges facing the cultivation and freshwater resources management in the Mediterranean, we would like to elaborate some propositions to be taken into consideration in future strategies and management plans based on the findings of this thesis.

1- Perspectives for hydrological research in the Mediterranean

First, we would like to validate this study on available subcatchments to study the homogeneity and variability at both regional and local scales, and to increase precision of physioclimatic characteristics and hydrological indices. We would include additional indices like daily peak flows, interesting for flood risk studies of small catchments and an indices uncertainty analysis.

Second, this study could be replicated at the global level, to locate the Mediterranean catchments from other catchments under different climatic and physiographic forcings. We would also include other catchments under Mediterranean climate in California, South America, or South Africa.

Third, we would like to apply in addition to climate change scenarios (RCM models), some climate shifting by forcing the climate of CC5 on CC3 catchments and vis versa for catchments of same physiographic classes. Also, we would like to apply some landscape scenarios to follow up the global evolution of hydrological regimes in case of cultivation increase, urbanisation increase, deforestation, and other scenarios, while targeting specific physiographic or climatic classes. This would also be possible using the same functional approach as simple follow up tool.

2- Perspectives for water resources management

a. Optimisation of national strategies

The benefits of homogeneity analysis are not limited to the transfer of hydrological characteristics between similar catchments but exceeds it to the transfer of experiences and best management practices between national services where two water establishments in different countries managing similar catchments can share their know-how and optimise the management plans. Hence, we call for a Mediterranean "Twin catchments" project, like "Twin towns" or "sister city", to transfer successful sustainable strategies and implement it onto underdeveloped catchment. Such project shall reshape national water sector strategies in developing countries, making it scientifically grounded with custom plans for each catchment targeting water resources management, agriculture, water treatment, wastewater reuse.

b. Mitigation of freshwater shortage

This study detected the importance of mountainous catchments under snow and karst influence as they yield the highest runoff and baseflow coefficients. These catchments are main supplier of freshwater and could be game changer against shortage problems. Hence, any further management plan or national strategy should first target these catchments and benefit from their freshwater for both future Mediterranean citizen and tourist. However, these catchments are the most environmentally sensitive to contamination and pollution and one should be careful how to manage them.

c. Mitigation measures regarding climate change

Climate change impact highlighted the evolution of CC5 to CC4 and CC3 catchments with increasing seasonality and aridity provoking the evolution of spring flow regimes to extreme winter flow regimes which shortens the storage and watering seasons. Hence to mitigate this change, which will mainly affect PC1 and PC9 managed and cultivated catchments, Southern countries shall include in their national strategies the increase of storage capacities and Northern countries shall plan to move into seasonal agriculture.

[This page was left intentionally blank]

REFERENCES

Acreman, M., & Sinclair, C. (1986). Classification of drainage basins according to their physical characteristics; an application for flood frequency analysis in Scotland. *Journal of Hydrology, 84*(3), 365-380. doi:https://doi.org/10.1016/0022-1694(86)90134-4

Allam A., Moussa R., Najem W., & Bocquillon C., 2020. Specific climate classification for Mediterranean hydrology and future evolution under Med-CORDEX regional climate model scenarios. Hydrol. Earth Syst. Sci., 24(9), 4503-4521. https://hess.copernicus.org/articles/24/4503/2020/

Allam A., El Hassan J., Najem W., Bocquillon C, Moussa R., 2020. Classification climatique méditerranéenne pour l'hydrologie. La Houille Blanche Vol. 1, 60 – 69. https://doi.org/10.1051/lhb/2020008

Allam A., Moussa R., Najem W., Bocquillon C., 2020. "Chapter 1: Hydrological cycle, Mediterranean basins hydrology". In Water Resources in the Mediterranean Region, Editors Mehrez Zribi, Luca Brocca, Yves Tramblay and Francois Molle, Elsevier, pp. 1-21. https://doi.org/10.1016/B978-0-12-818086-0.00001-7

Alpert, P., Osetinsky, I., Ziv, B., & Shafir, H. (2004). Semi-objective classification for daily synoptic systems: Application to the eastern Mediterranean climate change. *International Journal of Climatology, 24*(8), 1001-1011. doi:10.1002/joc.1036

Aouad-Rizk, A., Job, J.-O., Khalil, S., Touma, T., Bitar, C., Boqcuillon, C., et al. (2005). Snow in Lebanon: a preliminary study of snow cover over Mount Lebanon and a simple snowmelt model / Etude préliminaire du couvert neigeux et modèle de fonte des neige pour le Mont Liban. *Hydrological Sciences Journal, 50*(3), null-569. doi:10.1623/hysj.50.3.555.65023

Asch, K., & Bellenberg, S. (2005). *The 1: 5 million international geological map of Europe and adjacent areas (IGME 5000)[cartographic material]*: Bundesanstalt für Geowissenschaften und Rohstoffe.

Atkinson, S., Sivapalan, M., Viney, N., & Woods, R. (2003). Predicting space–time variability of hourly streamflow and the role of climate seasonality: Mahurangi Catchment, New Zealand. *Hydrological Processes, 17*(11), 2171-2193.

Audra, P., Mocochain, L., Camus, H., Gilli, É., Clauzon, G., & Bigot, J.-y. (2004). The effect of the Messinian Deep Stage on karst development around the Mediterranean Sea. Examples from Southern France. *Geodinamica Acta, 17*(6), 389-400.

Baccour, H., Slimani, M., and Cudennec, C.: Spatial structures of reference evapotranspiration and climatic variables in Tunisia, Hydrological Sciences Journal, 57(4), 818-829, http://dx.doi.org/10.1080/02626667.2012.672986, 2012.

Barnes, B. S. (1939). The structure of discharge-recession curves. *Eos, Transactions American Geophysical Union, 20*(4), 721-725. doi:10.1029/TR020i004p00721

Barredo, J. I., Mauri, A., Caudullo, G., & Dosio, A. (2019). Assessing shifts of Mediterranean and arid climates under RCP4. 5 and RCP8. 5 climate projections in Europe. In *Meteorology and Climatology of the Mediterranean and Black Seas* (pp. 235-251): Springer.

Barry, R. G., & Chorley, R. J. (2009). *Atmosphere, weather and climate*: Routledge.

Bartholome, E., Belward, A., Achard, F., Bartalev, S., Carmona-Moreno, C., Eva, H., et al. (2002). GLC 2000: Global Land Cover mapping for the year 2000. *Project status, November*.

Beck, H. E., Zimmermann, N. E., McVicar, T. R., Vergopolan, N., Berg, A., & Wood, E. F. (2018). Present and future Köppen-Geiger climate classification maps at 1-km resolution. *Scientific data, 5*, 180214. doi:10.1038/sdata.2018.214

Beckinsale, R. P. (1969). River regimes. In *Water, Earth and Man: a Synthesis of Hydrology, Geomorphology and Socio-Economic Geography* (pp. 588). London: Methuen.

Bergeron, T. (1928). *Über die dreidimensional verknüpfende Wetteranalyse*: Cammermeyer in Komm.

Beven, K. (2000). On model uncertainty, risk and decision making. *Hydrological Processes, 14*(14), 2605-2606. doi:10.1002/1099-1085(20001015)14:14<2605::Aid-hyp400>3.0.Co;2-w

Beven, K., & Kirkby, M. (1979). A physically based, variable contributing area model of basin hydrology/Un modèle à base physique de zone d'appel variable de l'hydrologie du bassin versant. *Hydrological Sciences Journal, 24*(1), 43-69.

Bholowalia, P., & Kumar, A. (2014). EBK-means: A clustering technique based on elbow method and k-means in WSN. *International Journal of Computer Applications, 105*(9).

Blöschl, G. (2006). Rainfall-runoff modeling of ungauged catchments. *Encyclopedia of hydrological sciences*.

Bois, P. (1986). *Contrôle de séries chronologiques corrélées par étude du cumul des résidus de la corrélation.* Paper presented at the Deuxièmes journées hydrologiques de l'ORSTOM.

Boorman, D., Hollis, J. M., & Lilly, A. (1995). *Hydrology of soil types: a hydrologically-based classification of the soils of United Kingdom*: Institute of Hydrology.

Boscarello, L., Ravazzani, G., Cislaghi, A., & Mancini, M. (2015). Regionalization of flow-duration curves through catchment classification with streamflow signatures and physiographic–climate indices. *Journal of Hydrologic Engineering, 21*(3), 05015027.

Bouma, J., Droogers, P., Sonneveld, M., Ritsema, C., Hunink, J., Immerzeel, W., et al. (2011). Hydropedological insights when considering catchment classification. *Hydrology and Earth System Sciences, 15*(6), 1909-1919.

Brandimarte, L., Di Baldassarre, G., Bruni, G., D'Odorico, P., & Montanari, A. (2011). Relation between the North-Atlantic Oscillation and hydroclimatic conditions in Mediterranean areas. *Water Resources Management, 25*(5), 1269-1279.

Bras, R. L. (1999). A Brief History of Hydrology* The Robert E. Horton Lecture. *Bulletin of the American Meteorological Society, 80*(6), 1151-1164.

Brath, A., Castellarin, A., & Montanari, A. (2003). Assessing the reliability of regional depth-duration-frequency equations for gaged and ungaged sites. *Water Resources Research, 39*(12). doi:10.1029/2003wr002399

Braudel, F. (1949). *La Méditerranée et le monde méditerranéen à l'époque de Philippe II-: 1. La part du milieu* (A. Colin Ed. Neuvième Edition ed. Vol. 1). Paris, France: Le livre de poche.

Breiman, L., Friedman, J., Stone, C. J., & Olshen, R. A. (1984). *Classification and Regression Trees*: Taylor & Francis.

Buchhorn, M., Bertels, L., Smets, B., Lesiv, M., & Wur, N. (2017). Copernicus Global Land Operations "Vegetation and Energy". *Copernicus Global Land Operations "Vegetation and Energy*.

Budyko, M. I. (1974). *Climate & Life* (Vol. Volume 18). University of Wisconsin, Milwaukee, Wisconsin: Academic Press.

Buishand, T. (1984). Tests for detecting a shift in the mean of hydrological time series. *Journal of Hydrology, 73*(1-2), 51-69.

Carvalho, M. J., Melo-Gonçalves, P., Teixeira, J. C., & Rocha, A. (2016). Regionalization of Europe based on a K-Means Cluster Analysis of the climate change of temperatures and precipitation. *Physics and Chemistry of the Earth, Parts A/B/C, 94*, 22-28. doi:10.1016/j.pce.2016.05.001

Castellarin, A., Galeati, G., Brandimarte, L., Montanari, A., & Brath, A. (2004). Regional flow-duration curves: reliability for ungauged basins. *Advances in Water Resources, 27*(10), 953-965.

Castiglioni, S., Castellarin, A., & Montanari, A. (2009). Prediction of low-flow indices in ungauged basins through physiographical space-based interpolation. *Journal of Hydrology, 378*(3-4), 272-280.

Catafago, S., & Najem, W. (1976). *Contribution à l'étude de la pluviométrie Libanaise.* Thèse de Doctorat présentée à l'Université Montpellier II, France,

Cavadias, G. (1990). The canonical correlation approach to regional flood estimation. *Regionalization in hydrology, 191*, 171-178.

Cermak, R. J., Feldman, A. D., & Webb, R. P. (1979). *Hydrologic land use classification using Landsat*. Retrieved from

Champeaux, J., & Tamburini, A. (1996). Climatological zoning of France from precipitation measurements (1971-1990) of the French climatological network. *Meteorologie (France)*. doi:10.4267/2042/51183

Chapman, T. (1989). Classification of regions. *Comparative hydrology: an ecological approach to land and water resources. Paris: UNESCO*, 67-74.

Chen, Z., Auler, A. S., Bakalowicz, M., Drew, D., Griger, F., Hartmann, J., et al. (2017). The World Karst Aquifer Mapping project: concept, mapping procedure and map of Europe. *Hydrogeology Journal, 25*(3), 771-785.

Chéruy, F., & Aires, F. (2009). Cluster Analysis of Cloud Properties over the Southern European Mediterranean Area in Observations and a Model. *Monthly Weather Review, 137*(10), 3161-3176. doi:10.1175/2009mwr2882.1

Choubin, B., Solaimani, K., Habibnejad Roshan, M., & Malekian, A. (2017). Watershed classification by remote sensing indices: A fuzzy c-means clustering approach. *Journal of Mountain Science, 14*(10), 2053-2063. doi:10.1007/s11629-017-4357-4

Ciscar, J.-C., Iglesias, A., Feyen, L., Szabó, L., Van Regemorter, D., Amelung, B., et al. (2011). Physical and economic consequences of climate change in Europe. *Proceedings of the National Academy of Sciences, 108*(7), 2678-2683.

Clausen, B., & Biggs, B. (2000). Flow variables for ecological studies in temperate streams: groupings based on covariance. *Journal of Hydrology, 237*(3-4), 184-197.

Clerget, M. (1937). *Les types de temps en Méditerranée.* Paper presented at the Annales de géographie.

Cramer, W., Guiot, J., Fader, M., Garrabou, J., Gattuso, J.-P., Iglesias, A., et al. (2018). Climate change and interconnected risks to sustainable development in the Mediterranean. *Nature Climate Change, 8*(11), 972-980.

Cudennec, C., Leduc, C., & Koutsoyiannis, D. (2007). Dryland hydrology in Mediterranean regions—a review. *Hydrological Sciences Journal/Journal des Sciences Hydrologiques, 52*(6), 1077-1087.

Cunnane, C. (1986). *Review of statistical models for flood frequency estimation*. Paper presented at the International Symposium on Flood Frequency and Risk Analysis, Baton Rouge.

Davis, W. M. (1899). The geographical cycle. *The Geographical Journal, 14*(5), 481-504.

De Jager, A. L., & Vogt, J. V. (2010). Development and demonstration of a structured hydrological feature coding system for Europe. *Hydrological Sciences Journal, 55*(5), 661-675. doi:10.1080/02626667.2010.490786

Dell'Aquila, A., Mariotti, A., Bastin, S., Calmanti, S., Cavicchia, L., Deque, M., et al. (2018). Evaluation of simulated decadal variations over the Euro-Mediterranean region from ENSEMBLES to Med-CORDEX. *Climate dynamics, 51*(3), 857-876.

Desbois, M., Seze, G., & Szejwach, G. (1982). Automatic Classification of Clouds on METEOSAT Imagery: Application to High-Level Clouds. *Journal of Applied Meteorology, 21*(3), 401-412. doi:10.1175/1520-0450(1982)021<0401:Acocom>2.0.Co;2

Di Prinzio, M., Castellarin, A., & Toth, E. (2011). Data-driven catchment classification: application to the pub problem. *Hydrol. Earth Syst. Sci., 15*(6), 1921-1935. doi:10.5194/hess-15-1921-2011

Douguédroit, A., & Lionello, P. (2015). Temperature and precipitation in the Mediterranean region: Present trends and future scenarios. In *Connections, Mobilities, Urban Prospects and Environmental Threats: The Mediterranean in Transition*. Newcastle upon Tyne, UK: Cambridge Scholars.

Drobinski, P., Silva, N. D., Panthou, G., Bastin, S., Muller, C., Ahrens, B., et al. (2018). Scaling precipitation extremes with temperature in the Mediterranean: past climate assessment and projection in anthropogenic scenarios. *Climate dynamics, 51*(3), 1237-1257. doi:10.1007/s00382-016-3083-x

Dünkeloh, A., & Jacobeit, J. (2003). Circulation dynamics of Mediterranean precipitation variability 1948–98. *International Journal of Climatology, 23*(15), 1843-1866. doi:doi:10.1002/joc.973

Eagleson, P. S. (1978). Climate, soil, and vegetation: 3. A simplified model of soil moisture movement in the liquid phase. *Water Resources Research, 14*(5), 722-730. doi:10.1029/WR014i005p00722

Eagleson, P. S., & Tellers, T. E. (1982). Ecological optimality in water-limited natural soil-vegetation systems: 2. Tests and applications. *Water Resources Research, 18*(2), 341-354. doi:10.1029/WR018i002p00341

Eckhardt, K. (2005). How to construct recursive digital filters for baseflow separation. *Hydrological Processes: An International Journal, 19*(2), 507-515.

Efremides, D., & Tsakiris, G. (1994). Stochastic modelling of point rainfall in a Mediterranean island environment. *Water Resources Management, 8*(3), 171-182.

Efron, B. (1982). *The jackknife, the bootstrap, and other resampling plans* (Vol. 38): Siam.

Emberger, L. (1955). Une classification biogéographique des climats, Rec. Trav. *Fac. Sci. Montpellier Bot, 7*, 3-43.

Eveno, M., Planchon, O., Oszwald, J., Dubreuil, V., & Quénol, H. (2016). Variabilité et changement climatique en France de 1951 à 2010 : analyse au moyen de la classification de Köppen et des « types de climats annuels ». *Climatologie*(Volume 13). doi:10.4267/climatologie.1203

Falkenmark, M., & Chapman, T. (1989). *Comparative hydrology: An ecological approach to land and water resources*: Unesco.

FAO, I., & ISRIC, I. (2012). JRC: Harmonized World Soil Database (version 1.2). *FAO, Rome, Italy and IIASA, Laxenburg, Austria*.

Feki, H., Slimani, M., and Cudennec, C.: Incorporating elevation in rainfall interpolation in Tunisia using geostatistical methods, *Hydrological Sciences Journal, 57*(7), 1294-1314, https://doi.org/10.1080/02626667.2012.710334, 2012.

Fick, S. E., & Hijmans, R. J. (2017). WorldClim 2: new 1-km spatial resolution climate surfaces for global land areas. *International Journal of Climatology, 37*(12), 4302-4315.

Forgy, E. W. (1965). Cluster analysis of multivariate data: efficiency versus interpretability of classifications. *biometrics, 21*, 768-769.

Fraga, H., Pinto, J. G., Viola, F., & Santos, J. A. (2019). Climate change projections for olive yields in the Mediterranean Basin. *International Journal of Climatology*.

García-Ruiz, J. M., López-Moreno, J. I., Vicente-Serrano, S. M., Lasanta–Martínez, T., & Beguería, S. (2011). Mediterranean water resources in a global change scenario. *Earth-Science Reviews, 105*(3-4), 121-139.

Gaucherel, C., Frelat, R., Salomon, L., Rouy, B., Pandey, N., & Cudennec, C. (2017). Regional watershed characterization and classification with river network analyses. *Earth Surface Processes and Landforms, 42*(13), 2068-2081. doi:10.1002/esp.4172

Gentilli, J. (1952). *Seasonal river regimes in Australia.* Paper presented at the Proceedings Eighth General Assembly and Seventeenth International Congress, International Geographical Union.

Giorgi, F. (2006). *Regional climate modeling: Status and perspectives.* Paper presented at the Journal de Physique IV (Proceedings).

Giorgi, F., Jones, C., & Asrar, G. R. (2009). Addressing climate information needs at the regional level: the CORDEX framework. *World Meteorological Organization (WMO) Bulletin, 58*(3), 175.

Gray, D. M. (1970). *Handbook on the Principles of Hydrology: with special emphasis directed to Canadian conditions in the discussions, applications and presentation of data*: Secretariat, Canadian National Committee for the International Hydrological ….

Haines, A., Finlayson, B., & McMahon, T. (1988). A global classification of river regimes. *Applied Geography, 8*(4), 255-272.

Hall, D., & Riggs, G. (2016). Modis/Terra Snow Cover 8-Day L3 Global 0.05 Deg CMG. In: Version 6.

Hall, M. J., & Minns, A. W. (1999). The classification of hydrologically homogeneous regions. *Hydrological Sciences Journal, 44*(5), 693-704. doi:10.1080/02626669909492268

Hannah, D. M., Smith, B. P., Gurnell, A. M., & McGregor, G. R. (2000). An approach to hydrograph classification. *Hydrological Processes, 14*(2), 317-338.

Harman, C., Troch, P. A., & Sivapalan, M. (2011). Functional model of water balance variability at the catchment scale: 2. Elasticity of fast and slow runoff components to precipitation change in the continental United States. *Water Resources Research, 47*(2).

Harrison, S. P., Prentice, I. C., Barboni, D., Kohfeld, K. E., Ni, J., & Sutra, J. P. (2010). Ecophysiological and bioclimatic foundations for a global plant functional classification. *Journal of Vegetation Science, 21*(2), 300-317.

Hartmann, J., & Moosdorf, N. (2012). The new global lithological map database GLiM: A representation of rock properties at the Earth surface. *Geochemistry, Geophysics, Geosystems, 13*(12).

Henriksen, J. A., Heasley, J., Kennen, J. G., & Nieswand, S. (2006). *Users' manual for the Hydroecological Integrity Assessment Process software(including the New Jersey Assessment Tools)*. Retrieved from

Hiederer, R. (2013). Mapping soil properties for Europe—spatial representation of soil database attributes. *Publications Office of the European Union, EUR26082EN Scientific and Technical Research series. Luxembourg*.

Hijmans, R. J., Cameron, S. E., Parra, J. L., Jones, P. G., & Jarvis, A. (2005). Very high resolution interpolated climate surfaces for global land areas. *International Journal of Climatology, 25*(15), 1965-1978.

Holdridge, L. R. (1947). Determination of world plant formations from simple climatic data. *Science, 105*(2727), 367-368.

Horton, R. E. (1933). The Rôle of infiltration in the hydrologic cycle. *Eos, Transactions American Geophysical Union, 14*(1), 446-460. doi:10.1029/TR014i001p00446

Host, G. E., Polzer, P. L., Mladenoff, D. J., White, M. A., & Crow, T. R. (1996). A Quantitative Approach to Developing Regional Ecosystem Classifications. *Ecological Applications, 6*(2), 608-618. doi:10.2307/2269395

Hotelling, H. (1933). Analysis of a complex of statistical variables into principal components. *Journal of educational psychology, 24*(6), 417.

Hreiche, A. (2003). *Modélisation conceptuelle de la transformation pluie-débit dans le contexte méditerranéen.* Université Montpellier II-Sciences et Techniques du Languedoc,

Hreiche, A., Najem, W., & Bocquillon, C. (2007). Hydrological impact simulations of climate change on Lebanese coastal rivers/Simulations des impacts hydrologiques du changement climatique sur les fleuves côtiers Libanais. *Hydrological Sciences Journal/Journal des Sciences Hydrologiques, 52*(6), 1119-1133.

Hsü, K. J., Montadert, L., Bernoulli, D., Cita, M. B., Erickson, A., Garrison, R. E., et al. (1977). History of the Mediterranean salinity crisis. *Nature, 267*(5610), 399.

Hubert, P., Carbonnel, J. P., & Chaouche, A. (1989). Segmentation des séries hydrométéorologiques—application à des séries de précipitations et de débits de l'Afrique de l'ouest. *Journal of Hydrology, 110*(3-4), 349-367.

IPCC. (2013). *Climate Change 2013: The Physical Science Basis: Working Group I contribution to the Fifth assessment report of the Intergovernmental Panel on Climate Change*. Cambridge, United Kingdom and New York, NY, USA: Cambridge University Press.

Jain, A. K., Prabhakar, S., & Pankanti, S. (2002). On the similarity of identical twin fingerprints. *Pattern Recognition, 35*(11), 2653-2663.

Jang, G., Sudduth, K., Sadler, E., & Lerch, R. (2009). Watershed-scale crop type classification using seasonal trends in remote sensing-derived vegetation indices. *Transactions of the ASABE, 52*(5), 1535-1544.

Jarvis, A., Reuter, H. I., Nelson, A., & Guevara, E. (2008). Hole-filled SRTM for the globe Version 4.

Jensen, M. E., & Allen, R. G. (2016). *Evaporation, evapotranspiration, and irrigation water requirements*.

Jolliffe, I. T. (2002). *Principal Component Analysis*: Springer.
Kirkby, M. (1975). Hydrograph modeling strategies. *Process in physical and human geography*, 69-90.
Klemeš, V. (1986). Operational testing of hydrological simulation models. *Hydrological Sciences Journal, 31*(1), 13-24.
Kodinariya, T. M., & Makwana, P. R. (2013). Review on determining number of Cluster in K-Means Clustering. *International Journal, 1*(6), 90-95.
Köppen, W. (1936). *Das geographische System der Klimate*: Borntraeger.
Kotlarski, S., Keuler, K., Christensen, O., Colette, A., Déqué, M., Gobiet, A., et al. (2014). Regional climate modeling on European scales: a joint standard evaluation of the EURO-CORDEX RCM ensemble, Geosci. Model Dev., 7, 1297–1333. In: gmd-7-1297-2014.
Koutroulis, A. G. (2019). Dryland changes under different levels of global warming. *Science of The Total Environment, 655*, 482-511.
Krijgsman, W., Hilgen, F., Raffi, I., Sierro, F. J., & Wilson, D. (1999). Chronology, causes and progression of the Messinian salinity crisis. *Nature, 400*(6745), 652.
Krzanowski, W. J. (1988). *Principles of multivariate analysis: a user's perspective*: Clarendon Press.
L'vovich, M. I. (1979). World water resources, present and future. *GeoJournal, 3*(5), 423-433. doi:10.1007/bf00455981
Lane, E. W. (1957). Study of the shape of channels formed by natural streams flowing in erodible material, A. *MRD sediment series; no. 9*.
Langbein, W. B. (1947). Topographic characteristics of drainage basins.
Lehner, B., & Grill, G. (2013). Global river hydrography and network routing: baseline data and new approaches to study the world's large river systems. *Hydrological Processes, 27*(15), 2171-2186.
Linnaeus, C. (1748). Hortus upsaliensis. *Stockholm: Laurentius Salvius*.
Lionello, P., Malanotte-Rizzoli, P., Boscolo, R., Alpert, P., Artale, V., Li, L., et al. (2006). The Mediterranean climate: an overview of the main characteristics and issues. In: Elsevier.
Lionello, P., & Scarascia, L. (2018). The relation between climate change in the Mediterranean region and global warming. *Regional environmental change, 18*(5), 1481-1493.
Llasat, M., Llasat-Botija, M., Petrucci, O., Pasqua, A., Rosselló, J., Vinet, F., et al. (2013). Towards a database on societal impact of Mediterranean floods within the framework of the HYMEX project. *Natural Hazards and Earth System Sciences, 13*(5), 1337-1350.
Lucian, Strong, H. A., & Garstang, J. (1913). The Syrian goddess : being a translation of Lucian's "De dea Syria," : with a life of Lucian. London: Constable.
Lyne, V., & Hollick, M. (1979). *Stochastic time-variable rainfall-runoff modelling*. Paper presented at the Institute of Engineers Australia National Conference.
MacQueen, J. (1967). *Some methods for classification and analysis of multivariate observations.* Paper presented at the Proceedings of the fifth Berkeley symposium on mathematical statistics and probability.
Mather, J. R., & Yoshioka, G. A. (1968). The role of climate in the distribution of vegetation. *Annals of the Association of American Geographers, 58*(1), 29-41.
McDonnell, J. J., & Woods, R. (2004). On the need for catchment classification. *Journal of Hydrology, 299*, 2-3.
McMillan, H. K., Westerberg, I. K., & Krueger, T. (2018). Hydrological data uncertainty and its implications. *Wiley Interdisciplinary Reviews: Water, 5*(6), e1319.
Menne, M. J., Durre, I., Korzeniewski, B., McNeal, S., Thomas, K., Yin, X., et al. (2012). Global historical climatology network-daily (GHCN-Daily), Version 3. *NOAA National Climatic Data Center, 10*, V5D21VHZ.
Merheb, M., Moussa, R., Abdallah, C., Colin, F., Perrin, C., & Baghdadi, N. (2016). Hydrological response characteristics of Mediterranean catchments at different time scales: a meta-analysis. *Hydrological Sciences Journal, 61*(14), 2520-2539. doi:10.1080/02626667.2016.1140174
Mhanna, M., & Bauwens, W. (2009). *Assessment of a single-site daily rainfall generator in the Middle East.* Paper presented at the 2009 Second International Conference on Environmental and Computer Science.
Milano, M. (2012). Face aux changements globaux les demandes en eau toujours satisfaites en Méditerranée à l'horizon 2050 ? In: Plan Bleu.
Milano, M., Ruelland, D., Fernandez, S., Dezetter, A., Fabre, J., Servat, E., et al. (2013). Current state of Mediterranean water resources and future trends under climatic and anthropogenic changes. *Hydrological Sciences Journal, 58*(3), 498-518. doi:10.1080/02626667.2013.774458
Milligan, G. W., & Cooper, M. C. (1985). An examination of procedures for determining the number of clusters in a data set. *Psychometrika, 50*(2), 159-179.

Milly, P. (1994a). Climate, interseasonal storage of soil water, and the annual water balance. *Advances in Water Resources, 17*(1-2), 19-24.

Milly, P. (1994b). Climate, soil water storage, and the average annual water balance. *Water Resources Research, 30*(7), 2143-2156.

Moreno, J. A. O. (2014). *Modelización del ciclo fenológico reproductor del olivo (Olea europaea L.).* Universidad de Córdoba,

Morin, E., Georgakakos, K. P., Shamir, U., Garti, R., & Enzel, Y. (2002). Objective, observations-based, automatic estimation of the catchment response timescale. *Water Resources Research, 38*(10), 30-31-30-16.

Moron, V., Robertson, A. W., Ward, M. N., & Ndiaye, O. (2008). Weather types and rainfall over Senegal. Part I: Observational analysis. *Journal of Climate, 21*(2), 266-287.

Musy, A. (2001). Cours d'Hydrologie générale. *Ecole Polytechnique Fédérale de Lausanne,(EPFL), Suisse*.

Najem, W. (1988). A continous point process model for daily rainfall. *Stochastic Hydrology and Hydraulics, 2*(3), 189-200.

Nash, J. E., & Sutcliffe, J. V. (1970). River flow forecasting through conceptual models part I—A discussion of principles. *Journal of Hydrology, 10*(3), 282-290.

Nathan, R. J., & McMahon, T. A. (1990). Identification of homogeneous regions for the purposes of regionalisation. *Journal of Hydrology, 121*(1), 217-238. doi:https://doi.org/10.1016/0022-1694(90)90233-N

Olden, J. D., Kennard, M. J., & Pusey, B. J. (2012). A framework for hydrologic classification with a review of methodologies and applications in ecohydrology. *Ecohydrology, 5*(4), 503-518. doi:10.1002/eco.251

Olden, J. D., & Poff, N. L. (2003). Redundancy and the choice of hydrologic indices for characterizing streamflow regimes. *River Research and Applications, 19*(2), 101-121. doi:doi:10.1002/rra.700

Ouarda, T. B., Girard, C., Cavadias, G. S., & Bobée, B. (2001). Regional flood frequency estimation with canonical correlation analysis. *Journal of Hydrology, 254*(1-4), 157-173.

Oueslati, O., De Girolamo, A. M., Abouabdillah, A., Kjeldsen, T. R., & Lo Porto, A. (2015). Classifying the flow regimes of Mediterranean streams using multivariate analysis. *Hydrological Processes, 29*(22), 4666-4682. doi:10.1002/hyp.10530

Panagos, P., Van Liedekerke, M., Jones, A., & Montanarella, L. (2012). European Soil Data Centre: Response to European policy support and public data requirements. *Land Use Policy, 29*(2), 329-338.

Parajka, J., Merz, R., & Blöschl, G. (2005). A comparison of regionalisation methods for catchment model parameters. *Hydrology and Earth System Sciences, 9*(3), 157-171.

Pearson, K. (1901). Principal components analysis. *The London, Edinburgh, and Dublin Philosophical Magazine and Journal of Science, 6*(2), 559.

Peel, M. C., Finlayson, B. L., & McMahon, T. A. (2007). Updated world map of the Köppen-Geiger climate classification. *Hydrology and earth system sciences discussions, 4*(2), 439-473.

Pettitt, A. (1979). A non-parametric approach to the change-point problem. *Journal of the Royal Statistical Society: Series C (Applied Statistics), 28*(2), 126-135.

Poff, N. L., Allan, J. D., Bain, M. B., Karr, J. R., Prestegaard, K. L., Richter, B. D., et al. (1997). The natural flow regime. *BioScience, 47*(11), 769-784.

Ponce, V. M., & Shetty, A. V. (1995a). A conceptual model of catchment water balance: 1. Formulation and calibration. *Journal of Hydrology, 173*(1), 27-40. doi:http://dx.doi.org/10.1016/0022-1694(95)02739-C

Ponce, V. M., & Shetty, A. V. (1995b). A conceptual model of catchment water balance: 2. Application to runoff and baseflow modeling. *Journal of Hydrology, 173*(1–4), 41-50. doi:https://doi.org/10.1016/0022-1694(95)02745-B

Potter, N., Zhang, L., Milly, P., McMahon, T. A., & Jakeman, A. (2005). Effects of rainfall seasonality and soil moisture capacity on mean annual water balance for Australian catchments. *Water Resources Research, 41*(6).

Praskievicz, S. (2018). River classification as a geographic tool in the age of big data and global change. *Geographical review, 108*(1), 120-137.

Ramírez-Cobo, P., Marzo, X., Olivares-Nadal, A. V., Francoso, J. Á., Carrizosa, E., & Pita, M. F. (2014). The Markovian arrival process: A statistical model for daily precipitation amounts. *Journal of Hydrology, 510*, 459-471.

Raymond, F., Ullmann, A., Camberlin, P., Drobinski, P., & Smith, C. C. (2016). Extreme dry spell detection and climatology over the Mediterranean Basin during the wet season. *Geophysical Research Letters, 43*(13), 7196-7204.

Reggiani, P., Sivapalan, M., & Hassanizadeh, S. M. (2000). Conservation equations governing hillslope responses: Exploring the physical basis of water balance. *Water Resources Research, 36*(7), 1845-1863.

Resh, V. H., Brown, A. V., Covich, A. P., Gurtz, M. E., Li, H. W., Minshall, G. W., et al. (1988). The role of disturbance in stream ecology. *Journal of the North American benthological society, 7*(4), 433-455.

Richter, B., Baumgartner, J., Wigington, R., & Braun, D. (1997). How much water does a river need? *Freshwater biology, 37*(1), 231-249.

Richter, B. D., Baumgartner, J. V., Braun, D. P., & Powell, J. (1998). A spatial assessment of hydrologic alteration within a river network. *Regulated Rivers: Research & Management: An International Journal Devoted to River Research and Management, 14*(4), 329-340.

Richter, B. D., Baumgartner, J. V., Powell, J., & Braun, D. P. (1996). A Method for Assessing Hydrologic Alteration within Ecosystems. *Conservation biology, 10*(4), 1163-1174. doi:doi:10.1046/j.1523-1739.1996.10041163.x

Risbey, J. S., & Entekhabi, D. (1996). Observed Sacramento Basin streamflow response to precipitation and temperature changes and its relevance to climate impact studies. *Journal of Hydrology, 184*(3-4), 209-223.

Rivoire, P., Tramblay, Y., Neppel, L., Hertig, E., & Vicente-Serrano, S. M. (2019). Impact of the dry-day definition on Mediterranean extreme dry-spell analysis. *Natural Hazards and Earth System Science, 19*(8), 1629-1638. doi:10.5194/nhess-19-1629-2019

Rockel, B., Will, A., & Hense, A. (2008). The regional climate model COSMO-CLM (CCLM). *Meteorologische Zeitschrift, 17*(4), 347-348.

Rodwell, M. J., & Hoskins, B. J. (1996). Monsoons and the dynamics of deserts. *Quarterly Journal of the Royal Meteorological Society, 122*(534), 1385-1404.

Romera, R., Sánchez, E., Domínguez, M., Gaertner, M. Á., & Gallardo, C. (2015). Evaluation of present-climate precipitation in 25 km resolution regional climate model simulations over Northwest Africa. *Climate Research, 66*(2), 125-139.

Ruti, P. M., Somot, S., Giorgi, F., Dubois, C., Flaounas, E., Obermann, A., et al. (2016). MED-CORDEX initiative for Mediterranean climate studies. *Bulletin of the American Meteorological Society, 97*(7), 1187-1208.

Sankarasubramanian, A., Vogel, R. M., & Limbrunner, J. F. (2001). Climate elasticity of streamflow in the United States. *Water Resources Research, 37*(6), 1771-1781.

Sauquet, E., Richard, B., Devers, A., & Prudhomme, C. (2018). Water restrictions under climate change: a Rhone-Mediterranean perspective combining 'bottom up' and 'top- down' approaches. *Hydrol. Earth Syst. Sci. Discuss., 2018*, 1-40. doi:10.5194/hess-2018-456

Schaake, J., Cong, S., & Duan, Q. (2006). US MOPEX data set (No. UCRL-JRNL-221228). Lawrence Livermore National Lab.(LLNL), Livermore, CA (United States).

Schröder, B. (2006). Pattern, process, and function in landscape ecology and catchment hydrology – how can quantitative landscape ecology support predictions in ungauged basins? *Hydrol. Earth Syst. Sci., 10*(6), 967-979. doi:10.5194/hess-10-967-2006

Servat, E. (2003). *Hydrology of Mediterranean and Semiarid Regions: Papers Selected for the International Conference on Hydrology of the Mediterranean and Semi-Arid Regions, Held in Montpellier, France from 1 to 4 April 2003*: International Assn of Hydrological Sciences.

Shamir, E., Imam, B., Gupta, H. V., & Sorooshian, S. (2005a). Application of temporal streamflow descriptors in hydrologic model parameter estimation. *Water Resources Research, 41*(6).

Shamir, E., Imam, B., Morin, E., Gupta, H. V., & Sorooshian, S. (2005b). The role of hydrograph indices in parameter estimation of rainfall–runoff models. *Hydrological Processes: An International Journal, 19*(11), 2187-2207.

Sivakumar, B., Singh, V. P., Berndtsson, R., & Khan, S. K. (2015). Catchment Classification Framework in Hydrology: Challenges and Directions. *Journal of Hydrologic Engineering, 20*(1), A4014002. doi:doi:10.1061/(ASCE)HE.1943-5584.0000837

Sivapalan, M. (2005). Encyclopedia of hydrological sciences. *Encyclopedia of Hydrological Sciences, edited by MG Anderson, chap. Pattern, process and function: elements of a unified theory of hydrology at the catchment scale*, 193-219.

Slimani, M., Cudennec, C., and Feki, H.: Structure of the rainfall gradient in the Mediterranean–Sahara transition in Tunisia: geographical determinants and seasonality, http://dx.doi.org/10.1623/hysj.52.6.1088, 2007.

Sivapalan, M., Yaeger, M. A., Harman, C. J., Xu, X., & Troch, P. A. (2011). Functional model of water balance variability at the catchment scale: 1. Evidence of hydrologic similarity and space-time symmetry. *Water Resources Research, 47*(2), n/a-n/a. doi:10.1029/2010WR009568

Sönmez, İ., & Kömüşcü, A. Ü. (2011). Reclassification of rainfall regions of Turkey by K-means methodology and their temporal variability in relation to North Atlantic Oscillation (NAO). *Theoretical and Applied Climatology, 106*(3-4), 499-510. doi:10.1007/s00704-011-0449-1

Spearman, C. (1904). The Proof and Measurement of Association between Two Things. *The American Journal of Psychology, 15*(1), 72-101. doi:10.2307/1412159

Sposito, G. (2017). Understanding the Budyko Equation. *Water, 9*(4), 236.
Suess, E. (1893). Are ocean depths permanent? Natural Science: A Monthly Review of Scientific Progress, 2, 180-187.
Thiébault, S., & Moatti, J.-P. (2016). *The Mediterranean region under climate change: a scientific update*.
Thornthwaite, C. W. (1948). An approach toward a rational classification of climate. *Geographical review, 38*(1), 55-94.
Toth, E. (2013). Catchment classification based on characterisation of streamflow and precipitation time series. *Hydrology and Earth System Sciences, 17*(3), 1149-1159.
Trajković, S., & Kolaković, S. (2009). Evaluation of Reference Evapotranspiration Equations Under Humid Conditions. Water Resources Management, 23(14), 3057. doi:10.1007/s11269-009-9423-4
Trajković, S., & Stojnić, V. (2007). Effect of wind speed on accuracy of Turc method in a humid climate. Facta universitatis-series: Architecture and Civil Engineering, 5(2), 107-113.
Tramblay, Y., Ruelland, D., Somot, S., Bouaicha, R., & Servat, E. (2013). High-resolution Med-CORDEX regional climate model simulations for hydrological impact studies: a first evaluation of the ALADIN-Climate model in Morocco. *Hydrology & Earth System Sciences, 17*(10).
Tramblay, Y., & Somot, S. (2018). Future evolution of extreme precipitation in the Mediterranean. *Climatic Change, 151*(2), 289-302. doi:10.1007/s10584-018-2300-5
Trigo, I. F., Davies, T. D., & Bigg, G. R. (1999). Objective climatology of cyclones in the Mediterranean region. *Journal of Climate, 12*(6), 1685-1696.
Trigo, R. M., Pozo-Vázquez, D., Osborn, T. J., Castro-Díez, Y., Gámiz-Fortis, S., & Esteban-Parra, M. J. (2004). North Atlantic Oscillation influence on precipitation, river flow and water resources in the Iberian Peninsula. *International Journal of Climatology: A Journal of the Royal Meteorological Society, 24*(8), 925-944.
Troch, P. A., Martinez, G. F., Pauwels, V. R. N., Durcik, M., Sivapalan, M., Harman, C., et al. (2009). Climate and vegetation water use efficiency at catchment scales. *Hydrological Processes, 23*(16), 2409-2414. doi:10.1002/hyp.7358
Tsakiris, G., Nalbantis, I., & Cavadias, G. (2011). Regionalization of low flows based on Canonical Correlation Analysis. *Advances in Water Resources, 34*(7), 865-872. https://doi.org/10.1016/j.advwatres.2011.04.007
Turc, L. (1961). Estimation of irrigation water requirements, potential evapotranspiration: a simple climatic formula evolved up to date. *Ann. Agron, 12*(1), 13-49.
Unal, Y., Kindap, T., & Karaca, M. (2003). Redefining the climate zones of Turkey using cluster analysis. *International Journal of Climatology, 23*(9), 1045-1055.
Verdier, J., & Viollet, P.-L. (2015). Les tensions sur l'eau en Europe et dans le bassin méditerranéen. Des crises de l'eau d'ici 2050. *La Houille Blanche*(6), 102-107.
Wagener, T., Sivapalan, M., Troch, P., & Woods, R. (2007). Catchment Classification and Hydrologic Similarity. *Geography Compass, 1*(4), 901-931. doi:10.1111/j.1749-8198.2007.00039.x
Wainwright, J., & Thornes, J. B. (2004). *Environmental issues in the Mediterraean* (Vol. null).
Wardrop, D. H., Bishop, J. A., Easterling, M., Hychka, K., Myers, W., Patil, G. P., et al. (2005). Use of landscape and land use parameters for classification and characterization of watersheds in the mid-Atlantic across five physiographic provinces. *Environmental and Ecological Statistics, 12*(2), 209-223. doi:10.1007/s10651-005-1042-5
Westerberg, I. K., & McMillan, H. K. (2015). Uncertainty in hydrological signatures. *Hydrol. Earth Syst. Sci., 19*(9), 3951-3968. doi:10.5194/hess-19-3951-2015
Westerberg, I. K., Wagener, T., Coxon, G., McMillan, H. K., Castellarin, A., Montanari, A., et al. (2016). Uncertainty in hydrological signatures for gauged and ungauged catchments. *Water Resources Research, 52*(3), 1847-1865.
Winter, T. C. (2001). The concept of hydrologic landscapes 1. *JAWRA Journal of the American Water Resources Association, 37*(2), 335-349.
WMO. (2012). *International Glossary of Hydrology*.
Wolock, D. M., Winter, T. C., & McMahon, G. (2004). Delineation and evaluation of hydrologic-landscape regions in the United States using geographic information system tools and multivariate statistical analyses. *Environmental Management, 34*(1), S71-S88.
Woods, R. (2003). The relative roles of climate, soil, vegetation and topography in determining seasonal and long-term catchment dynamics. *Advances in Water Resources, 26*(3), 295-309.
Woods, R. (2005). Hydrologic concepts of variability and scale. *Encyclopedia of hydrological sciences*.
Woods, R. (2006). *Global similarity indices for mean and seasonal hydrology of ungauged basins.* Paper presented at the Presentation at USA PUB Workshop.

World Tourism Organization. (2019). International Tourism Highlights. In (2019 ed.). Madrid: UNWTO.
Yadav, M., Wagener, T., & Gupta, H. (2006). *Regionalization of dynamic watershed behavior.* Paper presented at the Large sample basin experiments for hydrological model parameterization Results of the Model Parameter Estimation Experiment (MOPEX) Paris (2004) and Foz de Iguaçu (2005) workshops. Wallingford, UK: IAHS Redbook Publication.
Yadav, M., Wagener, T., & Gupta, H. (2007). Regionalization of constraints on expected watershed response behavior for improved predictions in ungauged basins. *Advances in Water Resources, 30*(8), 1756-1774.
Yokoo, Y., Sivapalan, M., & Oki, T. (2008). Investigating the roles of climate seasonality and landscape characteristics on mean annual and monthly water balances. *Journal of Hydrology, 357*(3-4), 255-269.
Yu, P.-S., & Yang, T.-C. (2000). Fuzzy multi-objective function for rainfall-runoff model calibration. *Journal of Hydrology, 238*(1-2), 1-14.
Zhang, Z., & Kroll, C. (2007). The baseflow correlation method with multiple gauged sites. *Journal of Hydrology, 347*(3-4), 371-380.
Zittis, G. (2018). Observed rainfall trends and precipitation uncertainty in the vicinity of the Mediterranean, Middle East and North Africa. *Theoretical and Applied Climatology, 134*(3-4), 1207-1230.

FURTHER READING

Andréassian, V., Coron, L., Lerat, J., & Le Moine, N. (2016). Climate elasticity of streamflow revisited – an elasticity index based on long-term hydrometeorological records. *Hydrol. Earth Syst. Sci., 20*(11), 4503-4524. doi:10.5194/hess-20-4503-2016
Andréassian, V., Mander, Ü., & Pae, T. (2016). The Budyko hypothesis before Budyko: The hydrological legacy of Evald Oldekop. *Journal of Hydrology, 535*, 386-391. doi:https://doi.org/10.1016/j.jhydrol.2016.02.002
Andréassian, V., & Perrin, C. (2012). On the ambiguous interpretation of the Turc-Budyko nondimensional graph. *Water Resources Research, 48*(10). doi:https://doi.org/10.1029/2012WR012532
Andréassian, V., & Sari, T. (2019). Technical Note: On the puzzling similarity of two water balance formulas – Turc–Mezentsev vs. Tixeront–Fu. *Hydrol. Earth Syst. Sci., 23*(5), 2339-2350. doi:10.5194/hess-23-2339-2019
Beven, K. (1991). *Hydrograph separation.* Paper presented at the Proceedings of the 3rd National Hydrology Symposium.
Brigode, P., Lilas, D., Andreassian, V., Nicolle, P., Le Moine, N., Perrin, C., . . . Augeard, B. (2019). Une cartographie de l'écoulement des rivières de Corse. *La Houille Blanche*(1), 68-77.
Coron, L., Andréassian, V., Perrin, C., & Le Moine, N. (2015). Graphical tools based on Turc-Budyko plots to detect changes in catchment behaviour. *Hydrological Sciences Journal, 60*(7-8), 1394-1407.
de Lavenne, A., & Andréassian, V. (2018). Impact of climate seasonality on catchment yield: A parameterization for commonly-used water balance formulas. *Journal of Hydrology, 558*, 266-274.
Fu, B. (1981). On the calculation of the evaporation from land surface. *Sci. Atmos. Sin, 5*(1), 23-31.
Hewlett, J. D., & Hibbert, A. R. (1967). Factors affecting the response of small watersheds to precipitation in humid areas. *Forest hydrology, 1*, 275-290.
Klemeš, V. (1986). Dilettantism in hydrology: Transition or destiny? *Water Resources Research, 22*(9S), 177S-188S.
Lebecherel, L., Andréassian, V., & Perrin, C. (2013). On regionalizing the Turc-Mezentsev water balance formula. *Water Resources Research, 49*(11), 7508-7517.
Margat, J. (2004). *Atlas de l'eau dans le bassin méditerranéen*: Plan bleu Commission de la carte geologique du monde Unesco.
Mezentsev, V. (1955). Back to the computation of total evaporation. *Meteorologia i Gidrologia, 5*, 24-26.
Moussa, R., & Lhomme, J.-P. (2016). The Budyko functions under non-steady-state conditions. *Hydrology and Earth System Sciences, 20*(12), 4867-4879.
Pelletier, A., & Andréassian, V. (2020). Hydrograph separation: an impartial parametrisation for an imperfect method. *Hydrology and Earth System Sciences, 24*(3), 1171-1187.
Tixeront, J. (1964). *Prévision des apports des cours d'eau.* Paper presented at the Symposium sur les Eau de surface, Assemblée générale de l'IUGG, Berkeley.
Turc, L. (1954). The water balance of soils. Relation between precipitation, evaporation and flow. *Ann. Agron, 5*, 491-569.

APPENDICES

APPENDIX A to CHAPTER 2

APPENDIX A1 (Allam et al., 2020b)

Allam A., Moussa R., Najem W., Bocquillon C., 2020. "Chapter 1: Hydrological cycle, Mediterranean basins hydrology". In Water Resources in the Mediterranean Region, Editors Mehrez Zribi, Luca Brocca, Yves Tramblay and Francois Molle, Elsevier, pp. 1-21.

APPENDIX A2 Complementary information about the Mediterranean research programs

APPENDIX A3 Hydrometric data quality check

APPENDIX B to CHAPTER 3

APPENDIX B1 (Allam et al., 2020a)

Allam A., El Hassan J., Najem W., Bocquillon C, Moussa R., 2020. Classification climatique méditerranéenne pour l'hydrologie. La Houille Blanche Vol. 1, 60 – 69. https://doi.org/10.1051/lhb/2020008

APPENDIX B2 (Allam et al., 2020c)

Allam A., Moussa R., Najem W., & Bocquillon C., 2020. Specific climate classification for Mediterranean hydrology and future evolution under Med-CORDEX regional climate model scenarios. Hydrol. Earth Syst. Sci., 24(9), 4503-4521. https://hess.copernicus.org/articles/24/4503/2020/

APPENDIX B3 Climatic Indices of the selected catchments

APPENDIX C to CHAPTER 4

APPENDIX C1 Physiographic Indices of the selected catchments

APPENDIX D to CHAPTER 5

APPENDIX D1 Flow regime types for all catchments according to the classification of Haines (1988)

APPENDIX D2 Summary table of all water balance parameters

APPENDIX D3 The water balance partitioning model of L'vovich and fitting curves of Ponce & Shetty

APPENDIX D4 The nondimensional water balance curves of Sivapalan

APPENDIX E to CHAPTER 6

APPENDIX E1 Baseflow and Runoff coefficients under MED-CORDEX RCM climate change scenario

APPENDIX E2 EGU General Assembly 2019 Conference Poster

APPENDIX A1

(Allam et al., 2020b)

Allam A., Moussa R., Najem W., Bocquillon C., 2020. “Chapter 1: Hydrological cycle, Mediterranean basins hydrology”. In Water Resources in the Mediterranean Region, Editors Mehrez Zribi, Luca Brocca, Yves Tramblay and Francois Molle, Elsevier, pp. 1-21. https://doi.org/10.1016/B978-0-12-818086-0.00001-7

Note: Only the first page was included in the appendix due to copyright restriction.

CHAPTER 1

Hydrological cycle, Mediterranean basins hydrology

Antoine Allam[a,b], Roger Moussa[b], Wajdi Najem[a], Claude Bocquillon[a]
[a]CREEN, ESIB, Univ. Saint-Joseph, Beirut, Lebanon
[b]UMR LISAH, Univ. Montpellier, INRA, Montpellier, France

1.1 Introduction

The Mediterranean climate is characterized by seasonal rainfall patterns, high spatio-temporal variability of precipitation, summer drought, and intense rainfall events. These climatic factors are generating several water challenges across the Mediterranean. Water resources become scarcer due to climate change and the increasing demands on water by various economic sectors [1]. Moreover, the irregular spatial distribution of precipitation leads to disproportional water availability across territories with long periods of drought. Furthermore, high intensity but short rainfall events cause intense flooding. Mediterranean catchments are therefore characterized by three main features: limited water resources, dry summers, and high-intensity rainfall events that generate flash floods.

Many attempts have been made to provide an overview on the hydrology of the Mediterranean region. Reviews have already detailed specific aspects of the hydrology of Mediterranean catchments, such as rainfall interception [2], the impact of the Mediterranean forest on catchment responses [3], the dryland hydrology [4], the impact of human activities on fluvial systems [5], erosion processes [6, 7], the hydrology of mountainous catchments [8], and more recently the review and the metaanalysis of hydrological response characteristics of Mediterranean catchments at different time scales [9].

This chapter aims to present an overview of the hydrological response characteristics of Mediterranean catchments. It starts by defining the study area, then the physical and hydro-climatic characteristics, followed by a synthesis of studies related to annual water balance, flood events, and droughts.

1.2 Mediterranean catchments

1.2.1 Boundary of the Mediterranean region

From the Latin word *Mediterranĕus* meaning "middle land," the Mediterranean refers to the sea and bordering region located in the middle of the Ecumene between the European, African, and Asiatic continents. With Köppen's classification [10], the definition designates

Water Resources in the Mediterranean Region
https://doi.org/10.1016/B978-0-12-818086-0.00001-7

APPENDIX A2

Complementary information about the Mediterranean research programs

Several international research programs tried to improve the knowledge on Mediterranean hydrology by establishing or enhancing hydrological information systems across the Mediterranean, discussing water resources assessment and management challenges and organizing international conferences; Despite that all these programs shared the main objective of data collection, there still a huge work before we obtain a common Mediterranean hydrological database at the example of the US MOPEX dataset (Schaake et al., 2006)[1], that all researchers working in the field of Water sector could easily use; here below we mentioned the main Mediterranean programs.

PLAN BLEU; In 1976, the Mediterranean-rim countries and the European Community adopted the Barcelona Convention to protect marine environment and its coastal areas, (amended later in 1995). The necessity to address collectively development and environment in order to build a sustainable future for the Mediterranean is already fully integrated by signatory countries.

Plan Bleu is one of the Regional Activity Centres of the Mediterranean Action Plan (MAP) of United Nations Environment Programme (UNEP), put in place by France since 1977.

Plan Bleu produces studies and future scenarios in order to raise awareness of Mediterranean stakeholders and decision-makers regarding environment and sustainable development issues in the region, with focus activities on water, aiming to support the implementation of the Mediterranean Strategy for Sustainable Development (MSSD) and more specifically, to help Mediterranean countries ensure water security in the face of overall changes. They are structured around four strategic goals:

- Facilitate information exchange and data collection,
- Promote integrated management of water resources, in particular water demand management;
- Contribute to the definition and implementation of climate change adaptation strategies,
- Protect and improve water quality.

MEDFRIEND; launched in 1991 by Cemagref as FRIEND - AMHY, one of the eight "Flow Regime from International Experimental and Network Data" – FRIEND programs of the UNESCO International Hydrological Program – IHP, an international collaborative research study intended to develop, through the mutual exchange of data, knowledge and techniques at a regional level and a better understanding of hydrological variability and similarity across time and space. It covered topics like extreme events, erosion and solid transport, flow regimes and water resources, assessment of global changes, karstic hydrogeology and coastal ecohydrology.

[1] Schaake, J., Cong, S., & Duan, Q. (2006). US MOPEX data set (No. UCRL-JRNL-221228). Lawrence Livermore National Lab.(LLNL), Livermore, CA (United States).

POEM; the international POEM (Physical Oceanography of the Eastern Mediterranean) is an international cooperative research program (Malanotte-Rizzoli and Robinson, 1988) It was established to determine the circulation of that sea, to research associated fundamental processes, and to construct realistic models for physical, biological and chemical studies and applications. Scientific activities included field work and multiple-ship surveys (1985-1987), data analysis and modelling. Scientific workshops for communication, planning, intercalibration and syntheses were held in Erdemli (Turkey), Trieste (Italy), Cambridge (Massachusetts) and Venice (Italy). Scientists from Cyprus, Croatia, Egypt, England, France, Germany, Greece, Israel, Italy, Turkey, the United Kingdom and the United States of America have participated.

PRIMO, WMGE, EU/MAST/MTP I and EU/MAST/MTP II) ; Mediterranean Targeted Project I (MTP I, 1993-1996) and the MTP II (1196-1999), Established by the European Commission in 1993 through the Marine Science and Technology Programme (MAST), represents a major effort in the understanding of the overall functioning of the Mediterranean Sea.

MEDHYCOS; launched in 1995 and terminated in 2001, with 24 participating countries, the first regional component of the World Hydrological Cycle Observation System – WHYCOS, promoted by the World Meteorological Organization – WMO, with the support of the World Bank and hosted by the Institute of Research for Development – IRD in a pilot regional centre in Montpellier. MED-HYCOS contributed to water resources assessment and management by strengthening the National Hydrological Services capacities with the installation of several meteorological stations and promoting the exchange of information and skills among the participating countries. The program main achievements were:

- the development of the Mediterranean Hydrological Information System.
- the establishment of a network of hydrometeorological of 50 stations composed of Data Collecting Platforms DCP and Near Real Time Stations – NRTS.
- the implementation of training events and expertise exchange between countries.
- the development of a co-operation infrastructure with other programs.

EMWIS; in 1996, Euro-Mediterranean Information System on Know-How in the Water Sector, an initiative of the Euro-Mediterranean Partnership. It provides a strategic tool for exchanging information and knowledge in the water sector between and within the 43 Euro Mediterranean partnership countries. Its task is to make an inventory and gather all available information, providing easy access to everyone. The EMWIS initiative is based on active participation and on the sharing of information and experience acquired by the partner countries at local, regional and national levels. EMWIS has three main targets

- To provide easy access to information, with special emphasis on institutions, documentation, Training, Research and development and Data administration

- To develop the sharing of information
- To work together on common products and cooperation programmes.

HyMEX; Hydrological cycle in the Mediterranean EXperiment launched in 2007 in the objective of identifying the main scientific challenges regarding the Mediterranean water cycle and making suggestions on how to address them. HyMeX has since extended to the international community, produced an International Science Plan (ISP), and is currently working at its International Implementation Plan (IIP). HyMeX aims at a better understanding, quantification and modelling of the hydrological cycle in the Mediterranean, with emphasis on the predictability and evolution of extreme weather events, inter-annual to decadal variability of the Mediterranean coupled system, and associated trends in the context of global change. The multidisciplinary research and associated database developed within HyMeX aim to improve the observational and modelling systems, better predict extreme events, simulate the long-term water-cycle, and provide guidelines for adaptation measures. HyMeX Science is organised along five major research topics, each addressed in a dedicated Working Group (WG):

- The water budget of the Mediterranean Sea (WG1)
- The continental hydrological cycle and related water resources (WG2)
- Heavy rainfalls, flash floods and floods (WG3)
- Intense sea-atmosphere interactions (WG4)
- Societal and economic impacts (WG5)

The topics "Water budget of the Mediterranean Sea" and "Hydrological continental cycle" aim at better understanding and simulating the long-term water cycle over the Mediterranean basin through budget and trend analyses. The general underlying question for both topics pertains to the variability of the water cycle components in the context of global climate change and how it will impact water resources.

The topics "Heavy rainfalls, flash-floods and floods" and "Intense sea-atmosphere interactions" aim at improving the knowledge and predictability of intense events. The process studies carried out within these topics will aim to identify the components as well as their interactions needed to produce extreme events. To which extent and how such extreme events will evolve with global climate change will also be addressed.

The topic "Societal and economic impacts" addresses vulnerability questions and adaptation strategies in societies facing high-impact weather events through the monitoring of relevant factors. How to reduce the impacts of extreme events and climate change is the key issue in this topic.

Several international conferences and related works have also focused on Mediterranean hydrology to increase the scientific knowledge in face of water resources management challenges, we mention:

- Hydrology of Mediterranean Regions, International seminar, Montpellier, 11-13 October 2000, IHP-V Project/ Technical Documents in Hydrology/ N° 51, UNESCO, Paris, UMR 5569 HydroSciences Montpellier, 2001. A joint conference between FRIEND-AMHY and HYDROMED that tackled several topics of Mediterranean hydrology mainly droughts, erosion, Rainfall Runoff modelling, IWRM, hydrological flow regimes, variability and Extreme events.
- Hydrology of Mediterranean and Semi-Arid Region, 2003, IAHS Red Book, (Servat, 2003)[2], selected papers from the conference held in Montpellier, France, from 1 to 4 April 2003 and which focused on surface and groundwater hydrology, Climatic variability and hydrological consequences, Extreme Phenomena (Floods and Droughts) and Integrated Water Resources Management, Erosion and Sediment Transport and Consequences of Human Activity and Coastal Areas
- More recently within the HyMEX project, a special issue "Hydrological cycle in the Mediterranean" is jointly organised between six journals - ACP/AMT/GMD/HESS/NHESS/OS (April 01, 2018 - December 31, 2021), and aims at gathering contributions to the areas of understanding, modelling, and predicting at various timescales and spatial scales of the Mediterranean water cycle and its related extreme events, including cyclones, heavy precipitation, flash floods and impacts, drought and water resources, strong winds, and dense water formation.

The scientific research at the faculty of engineering of Saint Joseph University also focused on Mediterranean hydrology especially that USJ launched in 1906 the Ksara observatory whose mission was the monitoring of the Lebanese Meteorological Network. One hydrology thesis in 1976 consisted on the definition of a specific Lebanese precipitation that respects a Markovian stochastic model and which was later verified for all Mediterranean rim countries. The Mediterranean research program was expanded in 1998, with the establishment of the Regional Centre for Water and Environment (CREEN) at USJ and the establishment of the first Lebanese snow monitoring service and which resulted with the characterisation of Lebanese snow, the estimation of Snow Water Equivalent and the estimation of snow contribution into Lebanese water resources. A second project consisted on the characterisation of Lebanese Karstic aquifers, and a third project which consisted on the development of a 4-parameter conceptual rainfall - runoff model that considers the stochastic structure of rainfall and the soil moisture in its production function. This work was subsequently used to assess the impact of climate change in the Mediterranean.

[2] Servat, E. (2003). *Hydrology of Mediterranean and Semiarid Regions: Papers Selected for the International Conference on Hydrology of the Mediterranean and Semi-Arid Regions, Held in Montpellier, France from 1 to 4 April 2003*: International Assn of Hydrological Sciences.

APPENDIX A3

Hydrometric data quality check

Analyse de séries chronologiques

D:\These\Donnees\Controle des Donnees\Hypothesis Tests\4.ksi

Identification 4_MELAH
Variable étudiée Debit annuel
Unité m3s
Chronique de 1979 ***à*** 1995

Valeurs

Tests de vérification du caractère aléatoire

Test de corrélation sur le RANG

Hypothèse nulle (série chronologique aléatoire) **acceptée** au seuil de confiance de 99%
Hypothèse nulle (série chronologique aléatoire) **acceptée** au seuil de confiance de 95%
Hypothèse nulle (série chronologique aléatoire) **acceptée** au seuil de confiance de 90%

Valeur de la variable de calcul: **-0.1648**

Tests de détection de rupture

Test de BUISHAND et ellipse de BOIS

Hypothèse nulle (absence de rupture) **acceptée** au seuil de confiance de 99%
Hypothèse nulle (absence de rupture) **acceptée** au seuil de confiance de 95%
Hypothèse nulle (absence de rupture) **acceptée** au seuil de confiance de 90%

Méthode non paramétrique de PETTITT

Hypothèse nulle (absence de rupture) **acceptée** au seuil de confiance de 99%
Hypothèse nulle (absence de rupture) **acceptée** au seuil de confiance de 95%
Hypothèse nulle (absence de rupture) **acceptée** au seuil de confiance de 90%

Méthode bayésienne de LEE et HEGHINIAN

Mode de la fonction densité de probabilité *a posteriori* de la position du point de rupture: **0.0909** en **1979**

Segmentation de HUBERT

Niveau de signification du test de Scheffé: **1%**

Début	Fin	Moyenne	Ecart type
1979	1995	3.053	2.126

Analyse de séries chronologiques

D:\These\Donnees\Controle des Donnees\Hypothesis Tests\5.ksi

Identification 5_MAZAFRAN
Variable étudiée Debit annuel
Unité m3s
Chronique de 1979 ***à*** 1994

Valeurs

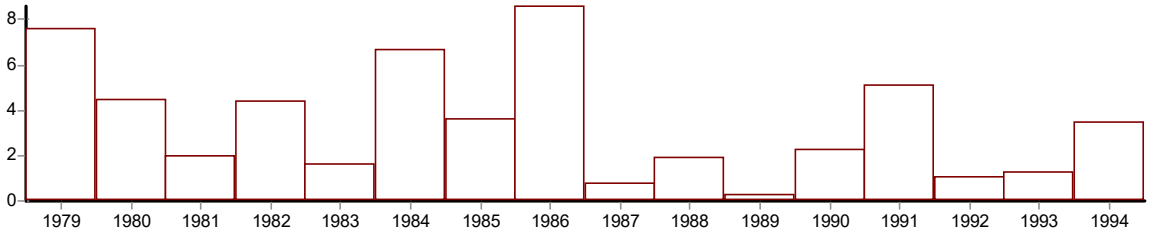

Tests de vérification du caractère aléatoire

Test de corrélation sur le RANG

Hypothèse nulle (série chronologique aléatoire) **acceptée** au seuil de confiance de 99%
Hypothèse nulle (série chronologique aléatoire) **acceptée** au seuil de confiance de 95%
Hypothèse nulle (série chronologique aléatoire) **acceptée** au seuil de confiance de 90%

Valeur de la variable de calcul: **-1.5308**

Tests de détection de rupture

Test de BUISHAND et ellipse de BOIS

Hypothèse nulle (absence de rupture) **acceptée** au seuil de confiance de 99%
Hypothèse nulle (absence de rupture) **acceptée** au seuil de confiance de 95%
Hypothèse nulle (absence de rupture) **acceptée** au seuil de confiance de 90%

Méthode non paramétrique de PETTITT

Hypothèse nulle (absence de rupture) **acceptée** au seuil de confiance de 99%
Hypothèse nulle (absence de rupture) **acceptée** au seuil de confiance de 95%
Hypothèse nulle (absence de rupture) **acceptée** au seuil de confiance de 90%

Méthode bayésienne de LEE et HEGHINIAN

Mode de la fonction densité de probabilité *a posteriori* de la position du point de rupture: **0.3030** en **1986**

Segmentation de HUBERT

Niveau de signification du test de Scheffé: **1%**

Début	Fin	Moyenne	Ecart type
1979	1994	3.456	2.522

Analyse de séries chronologiques

D:\These\Donnees\Controle des Donnees\Hypothesis Tests\15.ksi

Identification 15_ERZENIT
Variable étudiée Debit annuel
Unité m3s
Chronique de 1954 ***à*** 1993

Valeurs

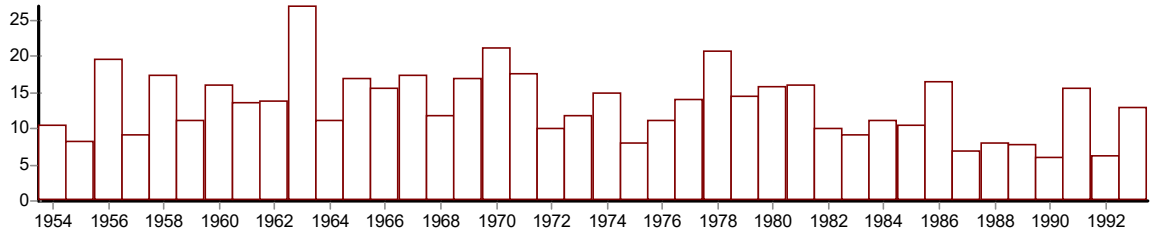

Tests de vérification du caractère aléatoire

Test de corrélation sur le RANG

Hypothèse nulle (série chronologique aléatoire) **acceptée** au seuil de confiance de 99%
Hypothèse nulle (série chronologique aléatoire) **rejetée** au seuil de confiance de 95%
Hypothèse nulle (série chronologique aléatoire) **rejetée** au seuil de confiance de 90%

Valeur de la variable de calcul: **-1.9807**

Tests de détection de rupture

Test de BUISHAND et ellipse de BOIS

Hypothèse nulle (absence de rupture) **acceptée** au seuil de confiance de 99%
Hypothèse nulle (absence de rupture) **rejetée** au seuil de confiance de 95%
Hypothèse nulle (absence de rupture) **rejetée** au seuil de confiance de 90%

Méthode non paramétrique de PETTITT

Hypothèse nulle (absence de rupture) **acceptée** au seuil de confiance de 99%
Hypothèse nulle (absence de rupture) **rejetée** au seuil de confiance de 95%
Hypothèse nulle (absence de rupture) **rejetée** au seuil de confiance de 90%

Probabilité de dépassement de la valeur critique du test: **3.41E-02** en **1981**

Méthode bayésienne de LEE et HEGHINIAN

Mode de la fonction densité de probabilité *a posteriori* de la position du point de rupture: **0.2083** en **1981**

Segmentation de HUBERT

Niveau de signification du test de Scheffé: **1%**

Début	Fin	Moyenne	Ecart type
1954	1981	14.682	4.302
1982	1993	10.058	3.478

Analyse de séries chronoloqiques

D:\These\Donnees\Controle des Donnees\Hypothesis Tests\47.ksi

Identification 47_SERRAKHIS
Variable étudiée Debit annuel
Unité m3s
Chronique de 1966 ***à*** 1995

Valeurs

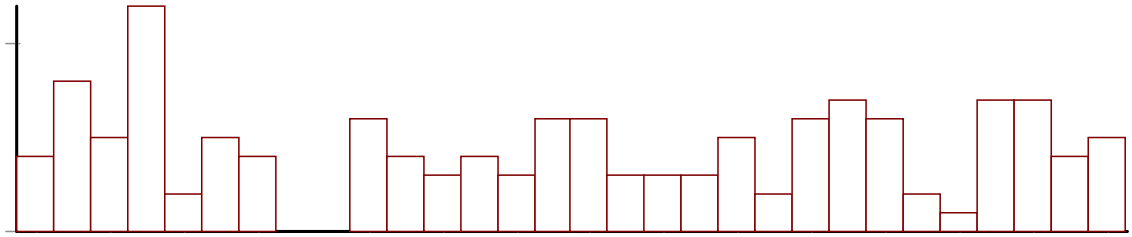

Tests de vérification du caractère aléatoire

Test de corrélation sur le RANG

Hypothèse nulle (série chronologique aléatoire) **acceptée** au seuil de confiance de 99%
Hypothèse nulle (série chronologique aléatoire) **acceptée** au seuil de confiance de 95%
Hypothèse nulle (série chronologique aléatoire) **acceptée** au seuil de confiance de 90%

Valeur de la variable de calcul: **0.5137**

Tests de détection de rupture

Test de BUISHAND et ellipse de BOIS

Hypothèse nulle (absence de rupture) **acceptée** au seuil de confiance de 99%
Hypothèse nulle (absence de rupture) **acceptée** au seuil de confiance de 95%
Hypothèse nulle (absence de rupture) **acceptée** au seuil de confiance de 90%

Méthode non paramétrique de PETTITT

Hypothèse nulle (absence de rupture) **acceptée** au seuil de confiance de 99%
Hypothèse nulle (absence de rupture) **acceptée** au seuil de confiance de 95%
Hypothèse nulle (absence de rupture) **acceptée** au seuil de confiance de 90%

Méthode bayésienne de LEE et HEGHINIAN

Mode de la fonction densité de probabilité *a posteriori* de la position du point de rupture: **0.3646** en **1969**

Segmentation de HUBERT

Niveau de signification du test de Scheffé: **1%**

Début	Fin	Moyenne	Ecart type
1966	1995	0.475	0.229

Analyse de séries chronologiques

D:\These\Donnees\Controle des Donnees\Hypothesis Tests\51.ksi

Identification 51_VASILIKOS
Variable étudiée Debit annuel
Unité m3s
Chronique de 1966 ***à*** 2003

Valeurs

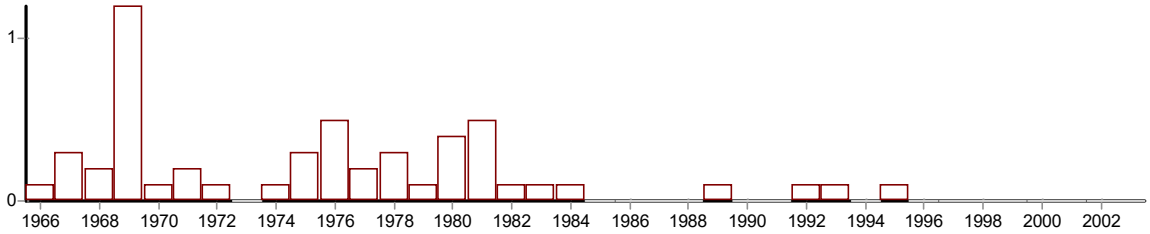

Tests de vérification du caractère aléatoire

Test de corrélation sur le RANG

Hypothèse nulle (série chronologique aléatoire) **acceptée** au seuil de confiance de 99%
Hypothèse nulle (série chronologique aléatoire) **acceptée** au seuil de confiance de 95%
Hypothèse nulle (série chronologique aléatoire) **rejetée** au seuil de confiance de 90%

Valeur de la variable de calcul: **-1.6469**

Tests de détection de rupture

Test de BUISHAND et ellipse de BOIS

RE

Méthode non paramétrique de PETTITT

Hypothèse nulle (absence de rupture) **rejetée** au seuil de confiance de 99%
Hypothèse nulle (absence de rupture) **rejetée** au seuil de confiance de 95%
Hypothèse nulle (absence de rupture) **rejetée** au seuil de confiance de 90%

Probabilité de dépassement de la valeur critique du test: **9.30E-05** en **1984**

Méthode bayésienne de LEE et HEGHINIAN

RE

Segmentation de HUBERT

Niveau de signification du test de Scheffé: **1%**

Début	Fin	Moyenne	Ecart type
1966	1968	1.200	0.100
1969	1969	2.200	0.000
1970	1974	1.100	0.071
1975	1981	1.329	0.150
1982	2003	1.032	0.048

Analyse de séries chronoloqiques

D:\These\Donnees\Controle des Donnees\Hypothesis Tests\56.ksi

Identification	56_EZOUSAS
Variable étudiée	Debit annuel
Unité	m3s
Chronique de	1966 ***à*** 2002

Valeurs

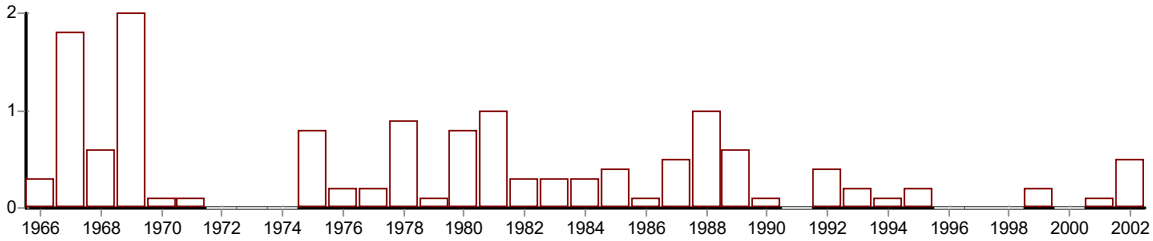

Tests de vérification du caractère aléatoire

Test de corrélation sur le RANG

Hypothèse nulle (série chronologique aléatoire) **acceptée** au seuil de confiance de 99%
Hypothèse nulle (série chronologique aléatoire) **acceptée** au seuil de confiance de 95%
Hypothèse nulle (série chronologique aléatoire) **acceptée** au seuil de confiance de 90%

Valeur de la variable de calcul: **-0.7847**

Tests de détection de rupture

Test de BUISHAND et ellipse de BOIS

RE

Méthode non paramétrique de PETTITT

Hypothèse nulle (absence de rupture) **acceptée** au seuil de confiance de 99%
Hypothèse nulle (absence de rupture) **acceptée** au seuil de confiance de 95%
Hypothèse nulle (absence de rupture) **rejetée** au seuil de confiance de 90%

Probabilité de dépassement de la valeur critique du test: **9.34E-02** en **1989**

Méthode bayésienne de LEE et HEGHINIAN

RE

Segmentation de HUBERT

Niveau de signification du test de Scheffé: **1%**

Début	Fin	Moyenne	Ecart type
1966	1969	2.175	0.850
1970	2002	1.288	0.310

Analyse de séries chronoloqiques

D:\These\Donnees\Controle des Donnees\Hypothesis Tests\63.ksi

Identification 63_DHIARIZOS
Variable étudiée Debit annuel
Unité m3s
Chronique de 1966 ***à*** 1996

Valeurs

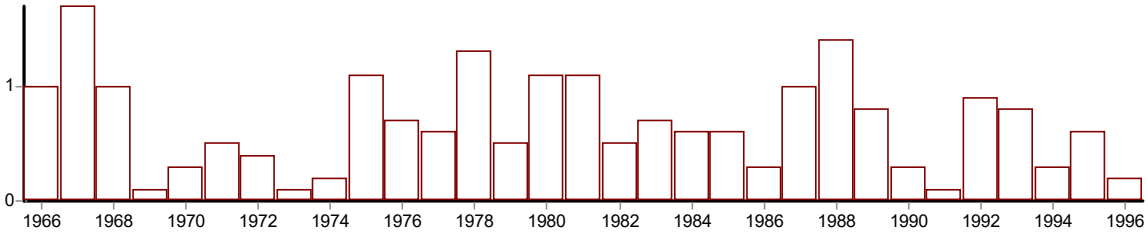

Tests de vérification du caractère aléatoire

Test de corrélation sur le RANG

Hypothèse nulle (série chronologique aléatoire) **acceptée** au seuil de confiance de 99%
Hypothèse nulle (série chronologique aléatoire) **acceptée** au seuil de confiance de 95%
Hypothèse nulle (série chronologique aléatoire) **acceptée** au seuil de confiance de 90%

Valeur de la variable de calcul: **-0.0850**

Tests de détection de rupture

Test de BUISHAND et ellipse de BOIS

Hypothèse nulle (absence de rupture) **acceptée** au seuil de confiance de 99%
Hypothèse nulle (absence de rupture) **acceptée** au seuil de confiance de 95%
Hypothèse nulle (absence de rupture) **acceptée** au seuil de confiance de 90%

Méthode non paramétrique de PETTITT

Hypothèse nulle (absence de rupture) **acceptée** au seuil de confiance de 99%
Hypothèse nulle (absence de rupture) **acceptée** au seuil de confiance de 95%
Hypothèse nulle (absence de rupture) **acceptée** au seuil de confiance de 90%

Méthode bayésienne de LEE et HEGHINIAN

Mode de la fonction densité de probabilité *a posteriori* de la position du point de rupture: **0.3161** en **1968**

Segmentation de HUBERT

Niveau de signification du test de Scheffé: **1%**

Début	Fin	Moyenne	Ecart type
1966	1996	0.671	0.412

Analyse de séries chronoloqiques

D:\These\Donnees\Controle des Donnees\Hypothesis Tests\88.ksi

Identification 88_CENIA
Variable étudiée Debit annuel
Unité m3s
Chronique de 1951 ***à*** 2015

Valeurs

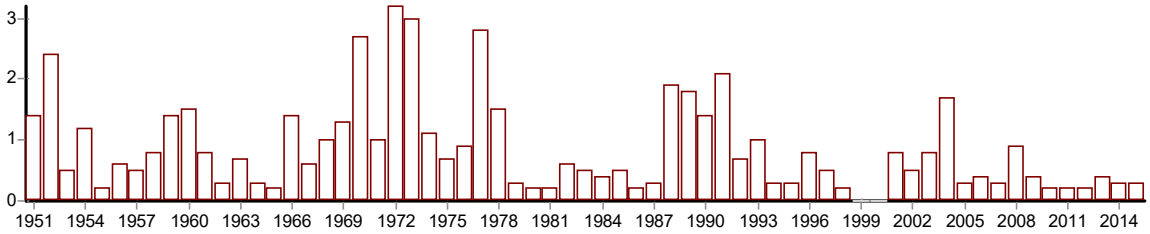

Tests de vérification du caractère aléatoire

Test de corrélation sur le RANG

Hypothèse nulle (série chronologique aléatoire) **acceptée** au seuil de confiance de 99%
Hypothèse nulle (série chronologique aléatoire) **rejetée** au seuil de confiance de 95%
Hypothèse nulle (série chronologique aléatoire) **rejetée** au seuil de confiance de 90%

Valeur de la variable de calcul: **-2.2079**

Tests de détection de rupture

Test de BUISHAND et ellipse de BOIS

RE

Méthode non paramétrique de PETTITT

Hypothèse nulle (absence de rupture) **rejetée** au seuil de confiance de 99%
Hypothèse nulle (absence de rupture) **rejetée** au seuil de confiance de 95%
Hypothèse nulle (absence de rupture) **rejetée** au seuil de confiance de 90%

Probabilité de dépassement de la valeur critique du test: **4.96E-03** en **1978**

Méthode bayésienne de LEE et HEGHINIAN

RE

Segmentation de HUBERT

Niveau de signification du test de Scheffé: **1%**

Début	Fin	Moyenne	Ecart type
1951	1969	0.900	0.572
1970	1978	1.878	1.024
1979	1987	0.356	0.151
1988	1991	1.800	0.294
1992	2015	0.479	0.378

Analyse de séries chronoloqiques

D:\These\Donnees\Controle des Donnees\Hypothesis Tests\103.ksi

Identification 103_AMADORIO
Variable étudiée Debit annuel
Unité m3s
Chronique de 1949 ***à*** 1987

Valeurs

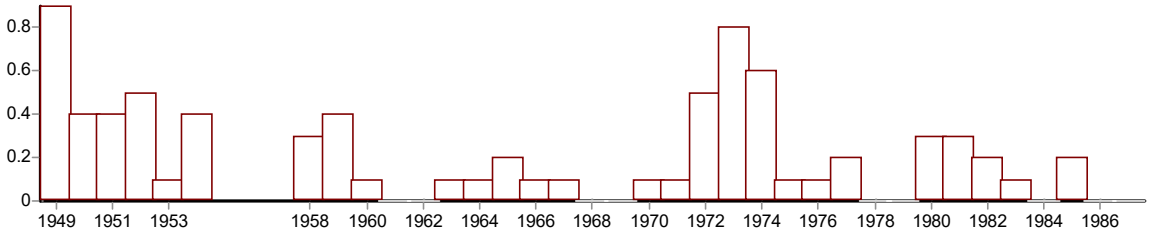

Tests de vérification du caractère aléatoire

Test de corrélation sur le RANG

Hypothèse nulle (série chronologique aléatoire) **acceptée** au seuil de confiance de 99%
Hypothèse nulle (série chronologique aléatoire) **acceptée** au seuil de confiance de 95%
Hypothèse nulle (série chronologique aléatoire) **acceptée** au seuil de confiance de 90%

Valeur de la variable de calcul: **-0.6538**

Tests de détection de rupture

Test de BUISHAND et ellipse de BOIS

RE

Méthode non paramétrique de PETTITT

Hypothèse nulle (absence de rupture) **acceptée** au seuil de confiance de 99%
Hypothèse nulle (absence de rupture) **acceptée** au seuil de confiance de 95%
Hypothèse nulle (absence de rupture) **rejetée** au seuil de confiance de 90%

Probabilité de dépassement de la valeur critique du test: **8.46E-02** en **1959**

Méthode bayésienne de LEE et HEGHINIAN

RE

Segmentation de HUBERT

Niveau de signification du test de Scheffé: **1%**

Début	Fin	Moyenne	Ecart type
1949	1949	1.900	0.000
1950	1956	1.357	0.127
1957	1968	1.075	0.062
1969	1971	1.633	0.153
1972	1984	1.115	0.114

Analyse de séries chronoloqiques

D:\These\Donnees\Controle des Donnees\Hypothesis Tests\162.ksi

Identification 162_FLUVIA
Variable étudiée Debit annuel
Unité m3s
Chronique de 1990 ***à*** 2017

Valeurs

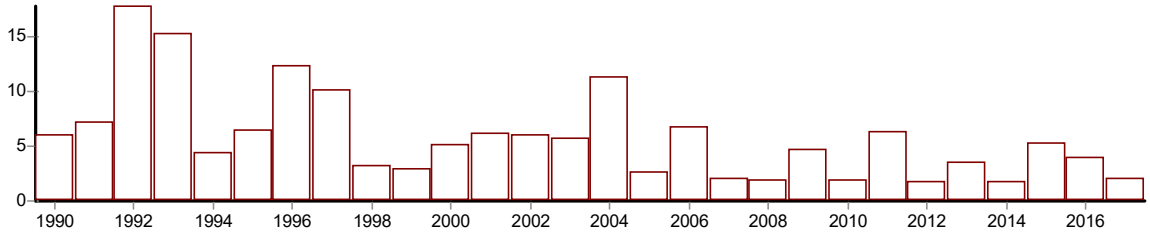

Tests de vérification du caractère aléatoire

Test de corrélation sur le RANG

Hypothèse nulle (série chronologique aléatoire) **rejetée** au seuil de confiance de 99%
Hypothèse nulle (série chronologique aléatoire) **rejetée** au seuil de confiance de 95%
Hypothèse nulle (série chronologique aléatoire) **rejetée** au seuil de confiance de 90%

Valeur de la variable de calcul: **-3.2401**

Tests de détection de rupture

Test de BUISHAND et ellipse de BOIS

Hypothèse nulle (absence de rupture) **rejetée** au seuil de confiance de 99%
Hypothèse nulle (absence de rupture) **rejetée** au seuil de confiance de 95%
Hypothèse nulle (absence de rupture) **rejetée** au seuil de confiance de 90%

Méthode non paramétrique de PETTITT

Hypothèse nulle (absence de rupture) **acceptée** au seuil de confiance de 99%
Hypothèse nulle (absence de rupture) **rejetée** au seuil de confiance de 95%
Hypothèse nulle (absence de rupture) **rejetée** au seuil de confiance de 90%

Probabilité de dépassement de la valeur critique du test: **1.22E-02** en **2006**

Méthode bayésienne de LEE et HEGHINIAN

Mode de la fonction densité de probabilité *a posteriori* de la position du point de rupture: **0.3081** en **2004**

Segmentation de HUBERT

Niveau de signification du test de Scheffé: **1%**

Début	Fin	Moyenne	Ecart type
1990	1991	6.600	0.849
1992	1993	16.550	1.768
1994	2017	4.946	2.992

Analyse de séries chronoloqiques

D:\These\Donnees\Controle des Donnees\Hypothesis Tests\165.ksi

Identification 165_LAMUGA
Variable étudiée Debit annuel
Unité m3s
Chronique de 1943 ***à*** 2017

Valeurs

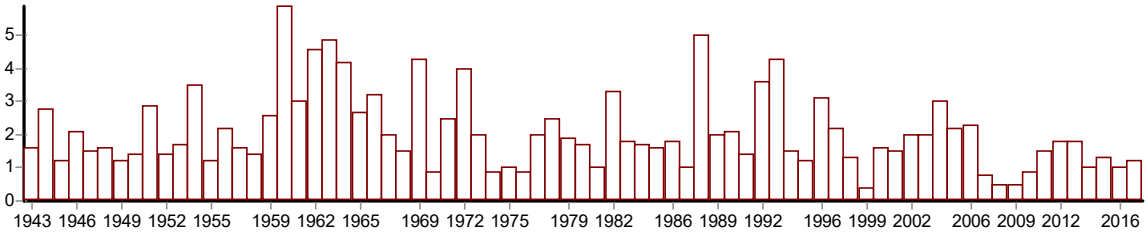

Tests de vérification du caractère aléatoire

Test de corrélation sur le RANG

Hypothèse nulle (série chronologique aléatoire) **acceptée** au seuil de confiance de 99%
Hypothèse nulle (série chronologique aléatoire) **acceptée** au seuil de confiance de 95%
Hypothèse nulle (série chronologique aléatoire) **rejetée** au seuil de confiance de 90%

Valeur de la variable de calcul: **-1.7245**

Tests de détection de rupture

Test de BUISHAND et ellipse de BOIS

Hypothèse nulle (absence de rupture) **rejetée** au seuil de confiance de 99%
Hypothèse nulle (absence de rupture) **rejetée** au seuil de confiance de 95%
Hypothèse nulle (absence de rupture) **rejetée** au seuil de confiance de 90%

Méthode non paramétrique de PETTITT

Hypothèse nulle (absence de rupture) **acceptée** au seuil de confiance de 99%
Hypothèse nulle (absence de rupture) **acceptée** au seuil de confiance de 95%
Hypothèse nulle (absence de rupture) **rejetée** au seuil de confiance de 90%

Probabilité de dépassement de la valeur critique du test: **7.27E-02** en **1997**

Méthode bayésienne de LEE et HEGHINIAN

Mode de la fonction densité de probabilité *a posteriori* de la position du point de rupture: **0.3391** en **2006**

Segmentation de HUBERT

Niveau de signification du test de Scheffé: **1%**

Début	Fin	Moyenne	Ecart type
1943	1959	1.876	0.692
1960	1964	4.520	1.057
1965	2017	1.909	1.027

Analyse de séries chronologiques

D:\These\Donnees\Controle des Donnees\Hypothesis Tests\169.ksi

Identification 169_ELTER
Variable étudiée Debit annuel
Unité m3s
Chronique de 1990 ***à*** 2017

Valeurs

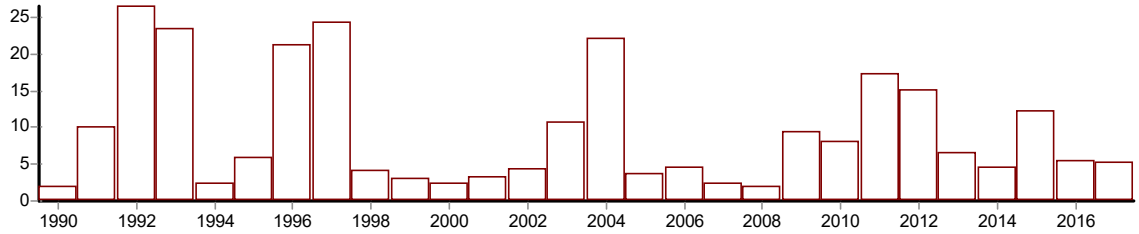

Tests de vérification du caractère aléatoire

Test de corrélation sur le RANG

Hypothèse nulle (série chronologique aléatoire) **acceptée** au seuil de confiance de 99%
Hypothèse nulle (série chronologique aléatoire) **acceptée** au seuil de confiance de 95%
Hypothèse nulle (série chronologique aléatoire) **acceptée** au seuil de confiance de 90%

Valeur de la variable de calcul: **0.0395**

Tests de détection de rupture

Test de BUISHAND et ellipse de BOIS

Hypothèse nulle (absence de rupture) **acceptée** au seuil de confiance de 99%
Hypothèse nulle (absence de rupture) **acceptée** au seuil de confiance de 95%
Hypothèse nulle (absence de rupture) **acceptée** au seuil de confiance de 90%

Méthode non paramétrique de PETTITT

Hypothèse nulle (absence de rupture) **acceptée** au seuil de confiance de 99%
Hypothèse nulle (absence de rupture) **acceptée** au seuil de confiance de 95%
Hypothèse nulle (absence de rupture) **acceptée** au seuil de confiance de 90%

Méthode bayésienne de LEE et HEGHINIAN

Mode de la fonction densité de probabilité *a posteriori* de la position du point de rupture: **0.1748** en **1990**

Segmentation de HUBERT

Niveau de signification du test de Scheffé: **1%**

Début	Fin	Moyenne	Ecart type
1990	2017	9.404	7.799

Analyse de séries chronologiques

D:\These\Donnees\Controle des Donnees\Hypothesis Tests\174.ksi

Identification 174_ELBESOS
Variable étudiée Debit annuel
Unité m3s
Chronique de 2003 ***à*** 2017

Valeurs

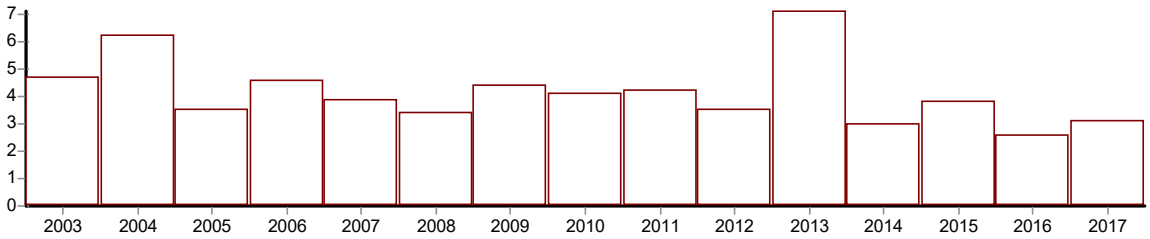

Tests de vérification du caractère aléatoire

Test de corrélation sur le RANG

Hypothèse nulle (série chronologique aléatoire) **acceptée** au seuil de confiance de 99%
Hypothèse nulle (série chronologique aléatoire) **rejetée** au seuil de confiance de 95%
Hypothèse nulle (série chronologique aléatoire) **rejetée** au seuil de confiance de 90%

Valeur de la variable de calcul: **-2.1279**

Tests de détection de rupture

Test de BUISHAND et ellipse de BOIS

Hypothèse nulle (absence de rupture) **acceptée** au seuil de confiance de 99%
Hypothèse nulle (absence de rupture) **acceptée** au seuil de confiance de 95%
Hypothèse nulle (absence de rupture) **acceptée** au seuil de confiance de 90%

Méthode non paramétrique de PETTITT

Hypothèse nulle (absence de rupture) **acceptée** au seuil de confiance de 99%
Hypothèse nulle (absence de rupture) **acceptée** au seuil de confiance de 95%
Hypothèse nulle (absence de rupture) **acceptée** au seuil de confiance de 90%

Méthode bayésienne de LEE et HEGHINIAN

Mode de la fonction densité de probabilité *a posteriori* de la position du point de rupture: **0.2658** en **2013**

Segmentation de HUBERT

Niveau de signification du test de Scheffé: **1%**

Début	Fin	Moyenne	Ecart type
2003	2017	4.140	1.192

Analyse de séries chronologiques

D:\These\Donnees\Controle des Donnees\Hypothesis Tests\175.ksi

Identification 175_GAIA
Variable étudiée Debit annuel
Unité m3s
Chronique de 2000 ***à*** 2017

Valeurs

Tests de vérification du caractère aléatoire

Test de corrélation sur le RANG

Hypothèse nulle (série chronologique aléatoire) **acceptée** au seuil de confiance de 99%
Hypothèse nulle (série chronologique aléatoire) **acceptée** au seuil de confiance de 95%
Hypothèse nulle (série chronologique aléatoire) **acceptée** au seuil de confiance de 90%

Valeur de la variable de calcul: **0.9469**

Tests de détection de rupture

Test de BUISHAND et ellipse de BOIS

RE

Méthode non paramétrique de PETTITT

Hypothèse nulle (absence de rupture) **acceptée** au seuil de confiance de 99%
Hypothèse nulle (absence de rupture) **acceptée** au seuil de confiance de 95%
Hypothèse nulle (absence de rupture) **acceptée** au seuil de confiance de 90%

Méthode bayésienne de LEE et HEGHINIAN

RE

Segmentation de HUBERT

Niveau de signification du test de Scheffé: **1%**

Début	Fin	Moyenne	Ecart type
2000	2017	0.228	0.227

Analyse de séries chronoloqiques

D:\These\Donnees\Controle des Donnees\Hypothesis Tests\194.ksi

Identification 194_ANDARRAX
Variable étudiée Debit annuel
Unité m3s
Chronique de 1998 ***à*** 2017

Valeurs

Tests de vérification du caractère aléatoire

Test de corrélation sur le RANG

Hypothèse nulle (série chronologique aléatoire) **rejetée** au seuil de confiance de 99%
Hypothèse nulle (série chronologique aléatoire) **rejetée** au seuil de confiance de 95%
Hypothèse nulle (série chronologique aléatoire) **rejetée** au seuil de confiance de 90%

Valeur de la variable de calcul: **5.1911**

Tests de détection de rupture

Test de BUISHAND et ellipse de BOIS

RE

Méthode non paramétrique de PETTITT

Hypothèse nulle (absence de rupture) **acceptée** au seuil de confiance de 99%
Hypothèse nulle (absence de rupture) **acceptée** au seuil de confiance de 95%
Hypothèse nulle (absence de rupture) **acceptée** au seuil de confiance de 90%

Méthode bayésienne de LEE et HEGHINIAN

RE

Segmentation de HUBERT

Niveau de signification du test de Scheffé: **1%**

Début	Fin	Moyenne	Ecart type
1998	2017	0.020	0.052

Analyse de séries chronoloqiques

D:\These\Donnees\Controle des Donnees\Hypothesis Tests\206.ksi

Identification	206_FIUM_ALTO
Variable étudiée	Debit annuel
Unité	m3s
Chronique de	1969 ***à*** 2012

Valeurs

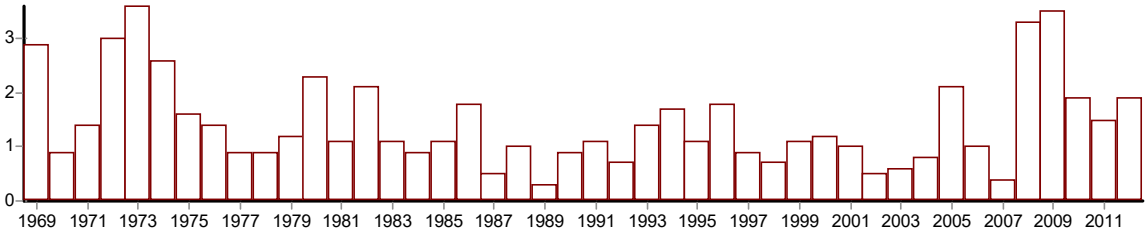

Tests de vérification du caractère aléatoire

Test de corrélation sur le RANG

Hypothèse nulle (série chronologique aléatoire) **acceptée** au seuil de confiance de 99%
Hypothèse nulle (série chronologique aléatoire) **acceptée** au seuil de confiance de 95%
Hypothèse nulle (série chronologique aléatoire) **acceptée** au seuil de confiance de 90%

Valeur de la variable de calcul: **-0.6878**

Tests de détection de rupture

Test de BUISHAND et ellipse de BOIS

Hypothèse nulle (absence de rupture) **acceptée** au seuil de confiance de 99%
Hypothèse nulle (absence de rupture) **acceptée** au seuil de confiance de 95%
Hypothèse nulle (absence de rupture) **rejetée** au seuil de confiance de 90%

Méthode non paramétrique de PETTITT

Hypothèse nulle (absence de rupture) **acceptée** au seuil de confiance de 99%
Hypothèse nulle (absence de rupture) **acceptée** au seuil de confiance de 95%
Hypothèse nulle (absence de rupture) **acceptée** au seuil de confiance de 90%

Méthode bayésienne de LEE et HEGHINIAN

Mode de la fonction densité de probabilité *a posteriori* de la position du point de rupture: **0.1238** en **1975**

Segmentation de HUBERT

Niveau de signification du test de Scheffé: **1%**

Début	Fin	Moyenne	Ecart type
1969	1974	2.400	1.033
1975	2007	1.127	0.498
2008	2012	2.420	0.912

Analyse de séries chronoloqiques

D:\These\Donnees\Controle des Donnees\Hypothesis Tests\297.ksi

Identification	297_LEZ
Variable étudiée	Debit annuel
Unité	m3s
Chronique de	1999 ***à*** 2016

Valeurs

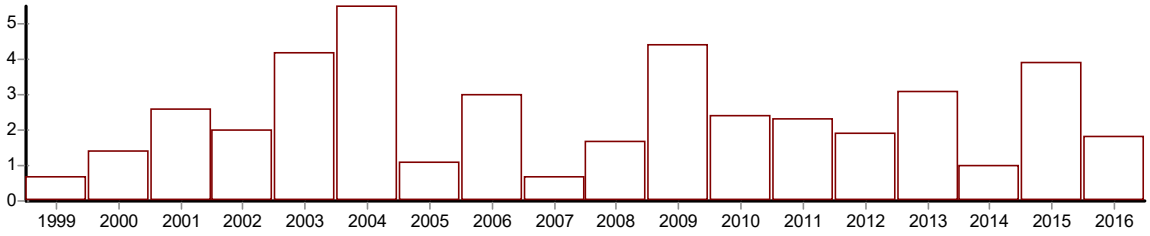

Tests de vérification du caractère aléatoire

Test de corrélation sur le RANG

Hypothèse nulle (série chronologique aléatoire) **acceptée** au seuil de confiance de 99%
Hypothèse nulle (série chronologique aléatoire) **acceptée** au seuil de confiance de 95%
Hypothèse nulle (série chronologique aléatoire) **acceptée** au seuil de confiance de 90%

Valeur de la variable de calcul: **0.4924**

Tests de détection de rupture

Test de BUISHAND et ellipse de BOIS

Hypothèse nulle (absence de rupture) **acceptée** au seuil de confiance de 99%
Hypothèse nulle (absence de rupture) **acceptée** au seuil de confiance de 95%
Hypothèse nulle (absence de rupture) **acceptée** au seuil de confiance de 90%

Méthode non paramétrique de PETTITT

Hypothèse nulle (absence de rupture) **acceptée** au seuil de confiance de 99%
Hypothèse nulle (absence de rupture) **acceptée** au seuil de confiance de 95%
Hypothèse nulle (absence de rupture) **acceptée** au seuil de confiance de 90%

Méthode bayésienne de LEE et HEGHINIAN

Mode de la fonction densité de probabilité *a posteriori* de la position du point de rupture: **0.1569** en **2000**

Segmentation de HUBERT

Niveau de signification du test de Scheffé: **1%**

Début	Fin	Moyenne	Ecart type
1999	2016	2.428	1.365

Analyse de séries chronologiques

D:\These\Donnees\Controle des Donnees\Hypothesis Tests\319.ksi

Identification 319_LE_LOUP
Variable étudiée Debit annuel
Unité m3s
Chronique de 1980 ***à*** 2017

Valeurs

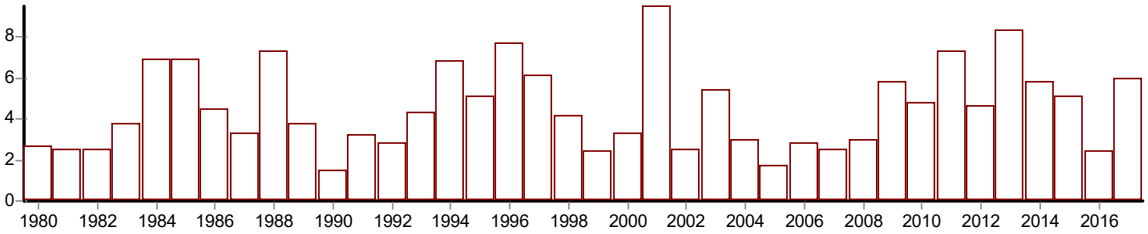

Tests de vérification du caractère aléatoire

Test de corrélation sur le RANG

Hypothèse nulle (série chronologique aléatoire) **acceptée** au seuil de confiance de 99%
Hypothèse nulle (série chronologique aléatoire) **acceptée** au seuil de confiance de 95%
Hypothèse nulle (série chronologique aléatoire) **acceptée** au seuil de confiance de 90%

Valeur de la variable de calcul: **1.0686**

Tests de détection de rupture

Test de BUISHAND et ellipse de BOIS

Hypothèse nulle (absence de rupture) **acceptée** au seuil de confiance de 99%
Hypothèse nulle (absence de rupture) **acceptée** au seuil de confiance de 95%
Hypothèse nulle (absence de rupture) **acceptée** au seuil de confiance de 90%

Méthode non paramétrique de PETTITT

Hypothèse nulle (absence de rupture) **acceptée** au seuil de confiance de 99%
Hypothèse nulle (absence de rupture) **acceptée** au seuil de confiance de 95%
Hypothèse nulle (absence de rupture) **acceptée** au seuil de confiance de 90%

Méthode bayésienne de LEE et HEGHINIAN

Mode de la fonction densité de probabilité *a posteriori* de la position du point de rupture: **0.1007** en **1982**

Segmentation de HUBERT

Niveau de signification du test de Scheffé: **1%**

Début	Fin	Moyenne	Ecart type
1980	2017	4.529	2.032

Analyse de séries chronoloqiques

D:\These\Donnees\Controle des Donnees\Hypothesis Tests\531.ksi

Identification 531_HERAULT
Variable étudiée Debit annuel
Unité m3s
Chronique de 1953 ***à*** 2016

Valeurs

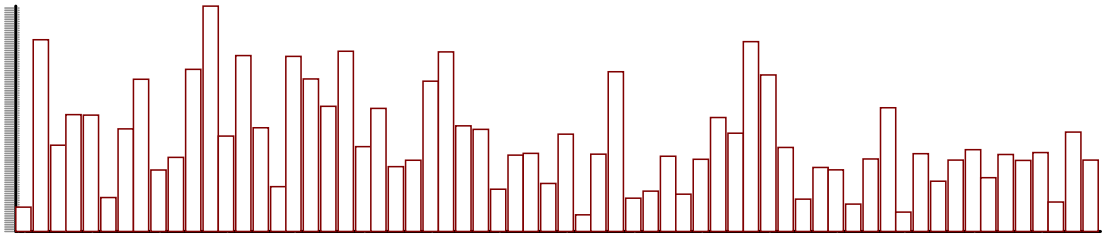

Tests de vérification du caractère aléatoire

Test de corrélation sur le RANG

Hypothèse nulle (série chronologique aléatoire) **rejetée** au seuil de confiance de 99%
Hypothèse nulle (série chronologique aléatoire) **rejetée** au seuil de confiance de 95%
Hypothèse nulle (série chronologique aléatoire) **rejetée** au seuil de confiance de 90%

Valeur de la variable de calcul: **-2.7694**

Tests de détection de rupture

Test de BUISHAND et ellipse de BOIS

Hypothèse nulle (absence de rupture) **rejetée** au seuil de confiance de 99%
Hypothèse nulle (absence de rupture) **rejetée** au seuil de confiance de 95%
Hypothèse nulle (absence de rupture) **rejetée** au seuil de confiance de 90%

Méthode non paramétrique de PETTITT

Hypothèse nulle (absence de rupture) **rejetée** au seuil de confiance de 99%
Hypothèse nulle (absence de rupture) **rejetée** au seuil de confiance de 95%
Hypothèse nulle (absence de rupture) **rejetée** au seuil de confiance de 90%

Probabilité de dépassement de la valeur critique du test: **5.44E-03** en **1980**

Méthode bayésienne de LEE et HEGHINIAN

Mode de la fonction densité de probabilité *a posteriori* de la position du point de rupture: **0.2058** en **1980**

Segmentation de HUBERT

Niveau de signification du test de Scheffé: **1%**

Début	Fin	Moyenne	Ecart type
1953	1980	52.468	23.027
1981	2016	33.089	17.401

Analyse de séries chronologiques

D:\These\Donnees\Controle des Donnees\Hypothesis Tests\541.ksi

Identification 541_AUDE
Variable étudiée Debit annuel
Unité m3s
Chronique de 1969 ***à*** 2016

Valeurs

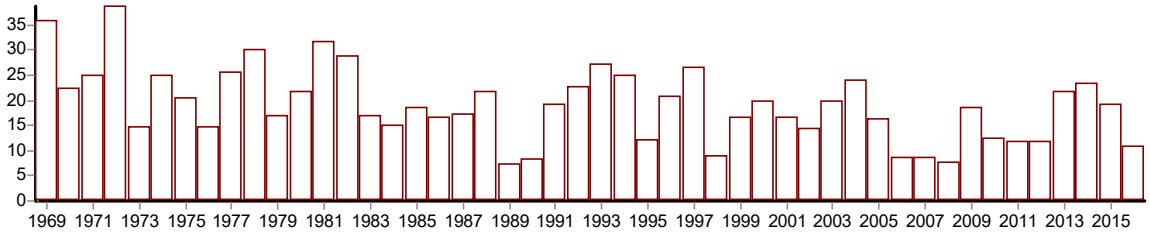

Tests de vérification du caractère aléatoire

Test de corrélation sur le RANG

Hypothèse nulle (série chronologique aléatoire) **rejetée** au seuil de confiance de 99%
Hypothèse nulle (série chronologique aléatoire) **rejetée** au seuil de confiance de 95%
Hypothèse nulle (série chronologique aléatoire) **rejetée** au seuil de confiance de 90%

Valeur de la variable de calcul: **-3.0575**

Tests de détection de rupture

Test de BUISHAND et ellipse de BOIS

Hypothèse nulle (absence de rupture) **rejetée** au seuil de confiance de 99%
Hypothèse nulle (absence de rupture) **rejetée** au seuil de confiance de 95%
Hypothèse nulle (absence de rupture) **rejetée** au seuil de confiance de 90%

Méthode non paramétrique de PETTITT

Hypothèse nulle (absence de rupture) **acceptée** au seuil de confiance de 99%
Hypothèse nulle (absence de rupture) **rejetée** au seuil de confiance de 95%
Hypothèse nulle (absence de rupture) **rejetée** au seuil de confiance de 90%

Probabilité de dépassement de la valeur critique du test: **1.90E-02** en **1982**

Méthode bayésienne de LEE et HEGHINIAN

Mode de la fonction densité de probabilité *a posteriori* de la position du point de rupture: **0.3401** en **1982**

Segmentation de HUBERT

Niveau de signification du test de Scheffé: **1%**

Début	Fin	Moyenne	Ecart type
1969	1982	25.186	7.370
1983	2016	16.744	5.704

Analyse de séries chronoloqiques

D:\These\Donnees\Controle des Donnees\Hypothesis Tests\550.ksi

Identification 550_GAPEAU
Variable étudiée Debit annuel
Unité m3s
Chronique de 1961 ***à*** 2017

Valeurs

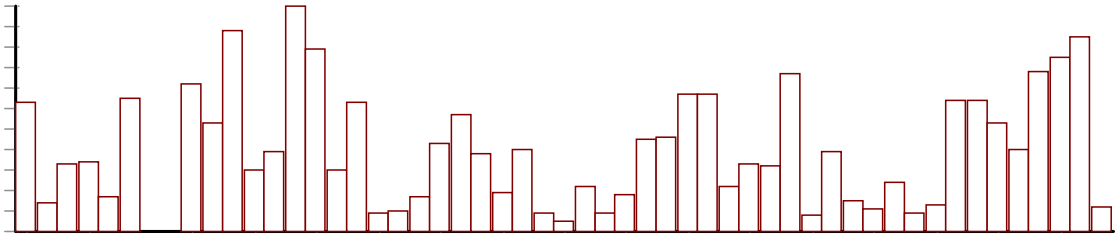

Tests de vérification du caractère aléatoire

Test de corrélation sur le RANG

Hypothèse nulle (série chronologique aléatoire) **acceptée** au seuil de confiance de 99%
Hypothèse nulle (série chronologique aléatoire) **acceptée** au seuil de confiance de 95%
Hypothèse nulle (série chronologique aléatoire) **acceptée** au seuil de confiance de 90%

Valeur de la variable de calcul: **0.0731**

Tests de détection de rupture

Test de BUISHAND et ellipse de BOIS

Hypothèse nulle (absence de rupture) **acceptée** au seuil de confiance de 99%
Hypothèse nulle (absence de rupture) **acceptée** au seuil de confiance de 95%
Hypothèse nulle (absence de rupture) **acceptée** au seuil de confiance de 90%

Méthode non paramétrique de PETTITT

Hypothèse nulle (absence de rupture) **acceptée** au seuil de confiance de 99%
Hypothèse nulle (absence de rupture) **acceptée** au seuil de confiance de 95%
Hypothèse nulle (absence de rupture) **acceptée** au seuil de confiance de 90%

Méthode bayésienne de LEE et HEGHINIAN

Mode de la fonction densité de probabilité *a posteriori* de la position du point de rupture: **0.0991** en **2008**

Segmentation de HUBERT

Niveau de signification du test de Scheffé: **1%**

Début	Fin	Moyenne	Ecart type
1961	2016	4.127	2.771

Analyse de séries chronoloqiques

D:\These\Donnees\Controle des Donnees\Hypothesis Tests\559.ksi

Identification	559_TECH
Variable étudiée	Debit annuel
Unité	m3s
Chronique de	1985 ***à*** 2017

Valeurs

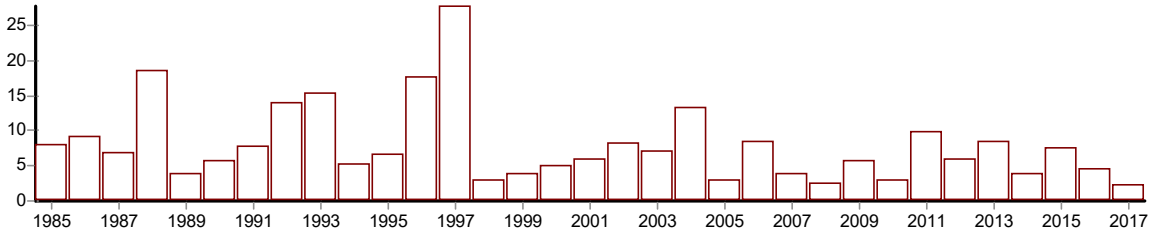

Tests de vérification du caractère aléatoire

Test de corrélation sur le RANG

Hypothèse nulle (série chronologique aléatoire) **acceptée** au seuil de confiance de 99%
Hypothèse nulle (série chronologique aléatoire) **acceptée** au seuil de confiance de 95%
Hypothèse nulle (série chronologique aléatoire) **rejetée** au seuil de confiance de 90%

Valeur de la variable de calcul: **-1.9213**

Tests de détection de rupture

Test de BUISHAND et ellipse de BOIS

Hypothèse nulle (absence de rupture) **acceptée** au seuil de confiance de 99%
Hypothèse nulle (absence de rupture) **rejetée** au seuil de confiance de 95%
Hypothèse nulle (absence de rupture) **rejetée** au seuil de confiance de 90%

Méthode non paramétrique de PETTITT

Hypothèse nulle (absence de rupture) **acceptée** au seuil de confiance de 99%
Hypothèse nulle (absence de rupture) **acceptée** au seuil de confiance de 95%
Hypothèse nulle (absence de rupture) **rejetée** au seuil de confiance de 90%

Probabilité de dépassement de la valeur critique du test: **6.63E-02** en **1997**

Méthode bayésienne de LEE et HEGHINIAN

Mode de la fonction densité de probabilité *a posteriori* de la position du point de rupture: **0.3647** en **1997**

Segmentation de HUBERT

Niveau de signification du test de Scheffé: **1%**

Début	Fin	Moyenne	Ecart type
1985	1995	9.264	4.699
1996	1997	22.750	7.142
1998	2017	5.800	2.880

Analyse de séries chronologiques

D:\These\Donnees\Controle des Donnees\Hypothesis Tests\561.ksi

Identification 561_TET
Variable étudiée Debit annuel
Unité m3s
Chronique de 1970 ***à*** 2015

Valeurs

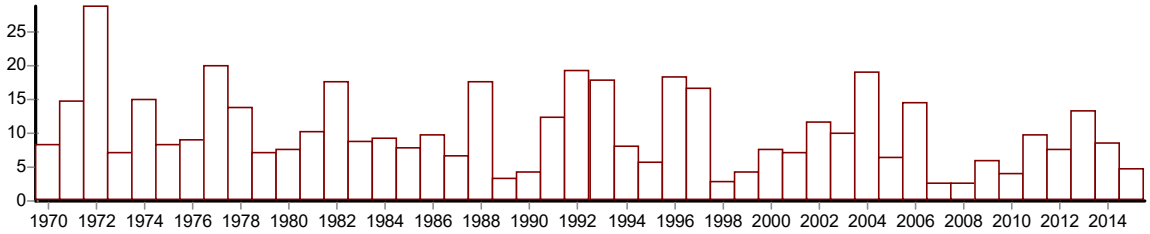

Tests de vérification du caractère aléatoire

Test de corrélation sur le RANG

Hypothèse nulle (série chronologique aléatoire) **acceptée** au seuil de confiance de 99%
Hypothèse nulle (série chronologique aléatoire) **rejetée** au seuil de confiance de 95%
Hypothèse nulle (série chronologique aléatoire) **rejetée** au seuil de confiance de 90%

Valeur de la variable de calcul: **-1.9978**

Tests de détection de rupture

Test de BUISHAND et ellipse de BOIS

Hypothèse nulle (absence de rupture) **acceptée** au seuil de confiance de 99%
Hypothèse nulle (absence de rupture) **rejetée** au seuil de confiance de 95%
Hypothèse nulle (absence de rupture) **rejetée** au seuil de confiance de 90%

Méthode non paramétrique de PETTITT

Hypothèse nulle (absence de rupture) **acceptée** au seuil de confiance de 99%
Hypothèse nulle (absence de rupture) **acceptée** au seuil de confiance de 95%
Hypothèse nulle (absence de rupture) **acceptée** au seuil de confiance de 90%

Méthode bayésienne de LEE et HEGHINIAN

Mode de la fonction densité de probabilité *a posteriori* de la position du point de rupture: **0.1296** en **2006**

Segmentation de HUBERT

Niveau de signification du test de Scheffé: **1%**

Début	Fin	Moyenne	Ecart type
1970	2015	10.313	5.683

Analyse de séries chronoloqiques

D:\These\Donnees\Controle des Donnees\Hypothesis Tests\634.ksi

Identification	634_SPERCHIOS
Variable étudiée	Debit annuel
Unité	m3s
Chronique de	1960 ***à*** 2005

Valeurs

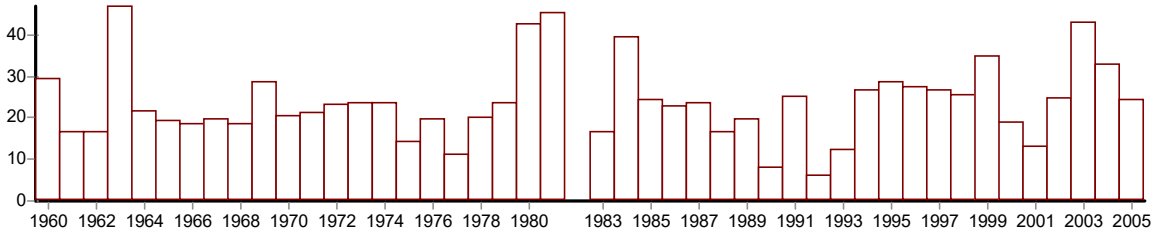

Tests de vérification du caractère aléatoire

Test de corrélation sur le RANG

Hypothèse nulle (série chronologique aléatoire) **acceptée** au seuil de confiance de 99%
Hypothèse nulle (série chronologique aléatoire) **acceptée** au seuil de confiance de 95%
Hypothèse nulle (série chronologique aléatoire) **acceptée** au seuil de confiance de 90%

Valeur de la variable de calcul: **1.5065**

Tests de détection de rupture

Test de BUISHAND et ellipse de BOIS

Hypothèse nulle (absence de rupture) **acceptée** au seuil de confiance de 99%
Hypothèse nulle (absence de rupture) **acceptée** au seuil de confiance de 95%
Hypothèse nulle (absence de rupture) **acceptée** au seuil de confiance de 90%

Méthode non paramétrique de PETTITT

Hypothèse nulle (absence de rupture) **acceptée** au seuil de confiance de 99%
Hypothèse nulle (absence de rupture) **acceptée** au seuil de confiance de 95%
Hypothèse nulle (absence de rupture) **acceptée** au seuil de confiance de 90%

Méthode bayésienne de LEE et HEGHINIAN

Mode de la fonction densité de probabilité *a posteriori* de la position du point de rupture: **0.1161** en **2002**

Segmentation de HUBERT

Niveau de signification du test de Scheffé: **1%**

Début	Fin	Moyenne	Ecart type
1960	2005	23.747	9.191

Analyse de séries chronologiques

D:\These\Donnees\Controle des Donnees\Hypothesis Tests\677.ksi

Identification 677_MIRNA
Variable étudiée Debit annuel
Unité m3s
Chronique de 1955 ***à*** 2017

Valeurs

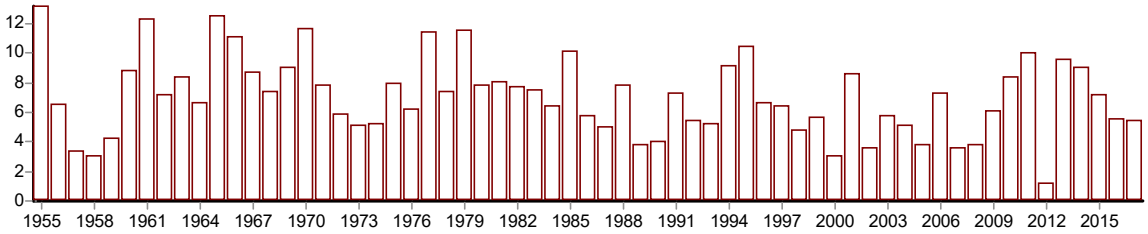

Tests de vérification du caractère aléatoire

Test de corrélation sur le RANG

Hypothèse nulle (série chronologique aléatoire) **acceptée** au seuil de confiance de 99%
Hypothèse nulle (série chronologique aléatoire) **rejetée** au seuil de confiance de 95%
Hypothèse nulle (série chronologique aléatoire) **rejetée** au seuil de confiance de 90%

Valeur de la variable de calcul: **-2.2479**

Tests de détection de rupture

Test de BUISHAND et ellipse de BOIS

Hypothèse nulle (absence de rupture) **acceptée** au seuil de confiance de 99%
Hypothèse nulle (absence de rupture) **rejetée** au seuil de confiance de 95%
Hypothèse nulle (absence de rupture) **rejetée** au seuil de confiance de 90%

Méthode non paramétrique de PETTITT

Hypothèse nulle (absence de rupture) **acceptée** au seuil de confiance de 99%
Hypothèse nulle (absence de rupture) **rejetée** au seuil de confiance de 95%
Hypothèse nulle (absence de rupture) **rejetée** au seuil de confiance de 90%

Probabilité de dépassement de la valeur critique du test: **2.70E-02** en **1985**

Méthode bayésienne de LEE et HEGHINIAN

Mode de la fonction densité de probabilité *a posteriori* de la position du point de rupture: **0.1200** en **1985**

Segmentation de HUBERT

Niveau de signification du test de Scheffé: **1%**

Début	Fin	Moyenne	Ecart type
1955	1985	8.087	2.658
1986	2017	6.091	2.250

Analyse de séries chronologiques

D:\These\Donnees\Controle des Donnees\Hypothesis Tests\681.ksi

Identification	681_KRKA
Variable étudiée	Debit annuel
Unité	m3s
Chronique de	1947 ***à*** 2017

Valeurs

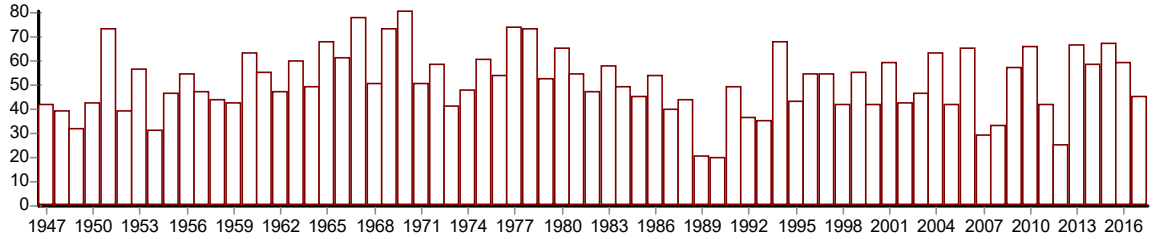

Tests de vérification du caractère aléatoire

Test de corrélation sur le RANG

Hypothèse nulle (série chronologique aléatoire) **acceptée** au seuil de confiance de 99%
Hypothèse nulle (série chronologique aléatoire) **acceptée** au seuil de confiance de 95%
Hypothèse nulle (série chronologique aléatoire) **acceptée** au seuil de confiance de 90%

Valeur de la variable de calcul: **0.0546**

Tests de détection de rupture

Test de BUISHAND et ellipse de BOIS

Hypothèse nulle (absence de rupture) **acceptée** au seuil de confiance de 99%
Hypothèse nulle (absence de rupture) **acceptée** au seuil de confiance de 95%
Hypothèse nulle (absence de rupture) **acceptée** au seuil de confiance de 90%

Méthode non paramétrique de PETTITT

Hypothèse nulle (absence de rupture) **acceptée** au seuil de confiance de 99%
Hypothèse nulle (absence de rupture) **acceptée** au seuil de confiance de 95%
Hypothèse nulle (absence de rupture) **acceptée** au seuil de confiance de 90%

Méthode bayésienne de LEE et HEGHINIAN

Mode de la fonction densité de probabilité *a posteriori* de la position du point de rupture: **0.0526** en **1950**

Segmentation de HUBERT

Niveau de signification du test de Scheffé: **1%**

Début	Fin	Moyenne	Ecart type
1947	2017	51.262	13.294

Analyse de séries chronoloqiques

D:\These\Donnees\Controle des Donnees\Hypothesis Tests\692.ksi

Identification	692_ALEXANDER
Variable étudiée	Debit annuel
Unité	m3s
Chronique de	1968 ***à*** 1993

Valeurs

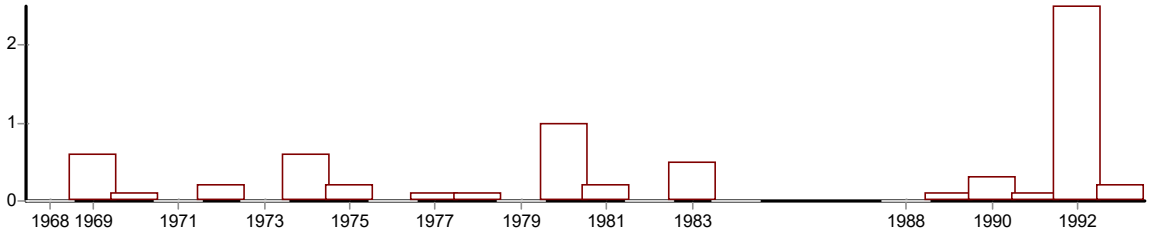

Tests de vérification du caractère aléatoire

Test de corrélation sur le RANG

Hypothèse nulle (série chronologique aléatoire) **acceptée** au seuil de confiance de 99%
Hypothèse nulle (série chronologique aléatoire) **rejetée** au seuil de confiance de 95%
Hypothèse nulle (série chronologique aléatoire) **rejetée** au seuil de confiance de 90%

Valeur de la variable de calcul: **1.9808**

Tests de détection de rupture

Test de BUISHAND et ellipse de BOIS

RE

Méthode non paramétrique de PETTITT

Hypothèse nulle (absence de rupture) **acceptée** au seuil de confiance de 99%
Hypothèse nulle (absence de rupture) **acceptée** au seuil de confiance de 95%
Hypothèse nulle (absence de rupture) **acceptée** au seuil de confiance de 90%

Méthode bayésienne de LEE et HEGHINIAN

RE

Segmentation de HUBERT

Niveau de signification du test de Scheffé: **1%**

Début	Fin	Moyenne	Ecart type
1968	1988	1.195	0.267
1989	1989	3.500	0.000
1990	1990	1.200	0.000

Analyse de séries chronoloqiques

D:\These\Donnees\Controle des Donnees\Hypothesis Tests\693.ksi

Identification 693_SOREQ
Variable étudiée Debit annuel
Unité m3s
Chronique de 1961 ***à*** 1992

Valeurs

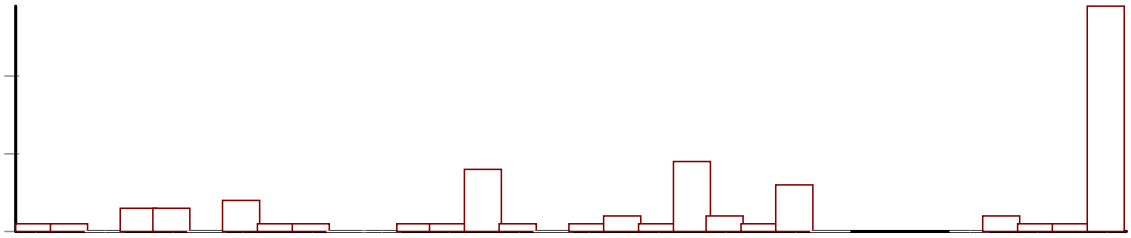

Tests de vérification du caractère aléatoire

Test de corrélation sur le RANG

Hypothèse nulle (série chronologique aléatoire) **rejetée** au seuil de confiance de 99%
Hypothèse nulle (série chronologique aléatoire) **rejetée** au seuil de confiance de 95%
Hypothèse nulle (série chronologique aléatoire) **rejetée** au seuil de confiance de 90%

Valeur de la variable de calcul: **2.5886**

Tests de détection de rupture

Test de BUISHAND et ellipse de BOIS

RE

Méthode non paramétrique de PETTITT

Hypothèse nulle (absence de rupture) **acceptée** au seuil de confiance de 99%
Hypothèse nulle (absence de rupture) **acceptée** au seuil de confiance de 95%
Hypothèse nulle (absence de rupture) **acceptée** au seuil de confiance de 90%

Méthode bayésienne de LEE et HEGHINIAN

RE

Segmentation de HUBERT

Niveau de signification du test de Scheffé: **1%**

Début	Fin	Moyenne	Ecart type
1961	1988	1.182	0.233
1989	1989	3.900	0.000

Analyse de séries chronologiques

D:\These\Donnees\Controle des Donnees\Hypothesis Tests\710.ksi

Identification 710_FIORA
Variable étudiée Debit annuel
Unité m3s
Chronique de 1964 ***à*** 1994

Valeurs

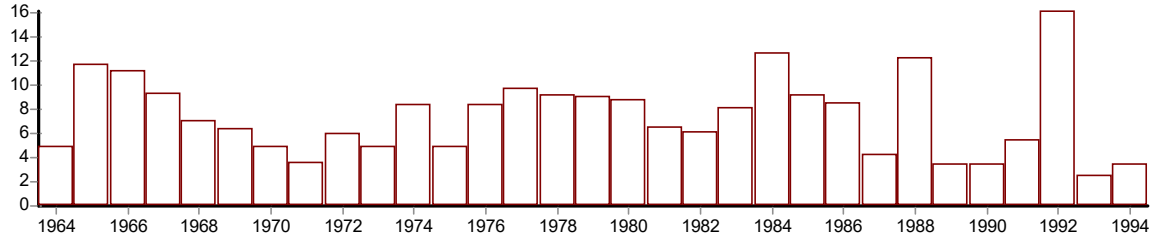

Tests de vérification du caractère aléatoire

Test de corrélation sur le RANG

Hypothèse nulle (série chronologique aléatoire) **acceptée** au seuil de confiance de 99%
Hypothèse nulle (série chronologique aléatoire) **acceptée** au seuil de confiance de 95%
Hypothèse nulle (série chronologique aléatoire) **acceptée** au seuil de confiance de 90%

Valeur de la variable de calcul: **-0.9348**

Tests de détection de rupture

Test de BUISHAND et ellipse de BOIS

Hypothèse nulle (absence de rupture) **acceptée** au seuil de confiance de 99%
Hypothèse nulle (absence de rupture) **acceptée** au seuil de confiance de 95%
Hypothèse nulle (absence de rupture) **acceptée** au seuil de confiance de 90%

Méthode non paramétrique de PETTITT

Hypothèse nulle (absence de rupture) **acceptée** au seuil de confiance de 99%
Hypothèse nulle (absence de rupture) **acceptée** au seuil de confiance de 95%
Hypothèse nulle (absence de rupture) **acceptée** au seuil de confiance de 90%

Méthode bayésienne de LEE et HEGHINIAN

Mode de la fonction densité de probabilité *a posteriori* de la position du point de rupture: **0.2400** en **1992**

Segmentation de HUBERT

Niveau de signification du test de Scheffé: **1%**

Début	Fin	Moyenne	Ecart type
1964	1994	7.481	3.247

Analyse de séries chronoloqiques

D:\These\Donnees\Controle des Donnees\Hypothesis Tests\722.ksi

Identification	722_ALCANTARA
Variable étudiée	Debit annuel
Unité	m3s
Chronique de	1981 ***à*** 1999

Valeurs

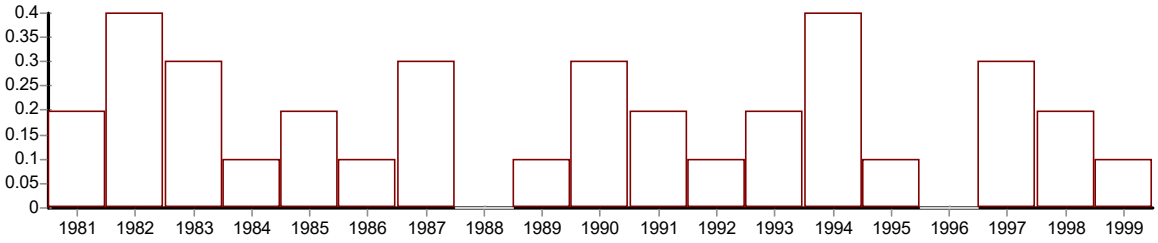

Tests de vérification du caractère aléatoire

Test de corrélation sur le RANG

Hypothèse nulle (série chronologique aléatoire) **acceptée** au seuil de confiance de 99%
Hypothèse nulle (série chronologique aléatoire) **acceptée** au seuil de confiance de 95%
Hypothèse nulle (série chronologique aléatoire) **acceptée** au seuil de confiance de 90%

Valeur de la variable de calcul: **0.3149**

Tests de détection de rupture

Test de BUISHAND et ellipse de BOIS

RE

Méthode non paramétrique de PETTITT

Hypothèse nulle (absence de rupture) **acceptée** au seuil de confiance de 99%
Hypothèse nulle (absence de rupture) **acceptée** au seuil de confiance de 95%
Hypothèse nulle (absence de rupture) **acceptée** au seuil de confiance de 90%

Méthode bayésienne de LEE et HEGHINIAN

RE

Segmentation de HUBERT

Niveau de signification du test de Scheffé: **1%**

Début	Fin	Moyenne	Ecart type
1981	1999	0.189	0.120

Analyse de séries chronoloqiques

D:\These\Donnees\Controle des Donnees\Hypothesis Tests\725.ksi

Identification 725_FLUMINIMAGGIORE
Variable étudiée Debit annuel
Unité m3s
Chronique de 1985 ***à*** 2005

Valeurs

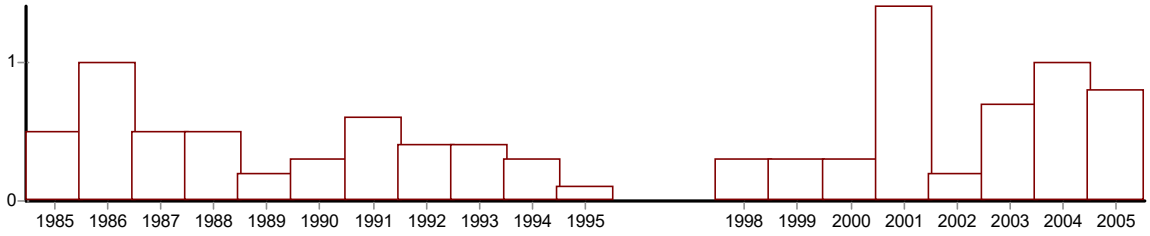

Tests de vérification du caractère aléatoire

Test de corrélation sur le RANG

Hypothèse nulle (série chronologique aléatoire) **acceptée** au seuil de confiance de 99%
Hypothèse nulle (série chronologique aléatoire) **acceptée** au seuil de confiance de 95%
Hypothèse nulle (série chronologique aléatoire) **acceptée** au seuil de confiance de 90%

Valeur de la variable de calcul: **0.5248**

Tests de détection de rupture

Test de BUISHAND et ellipse de BOIS

Hypothèse nulle (absence de rupture) **acceptée** au seuil de confiance de 99%
Hypothèse nulle (absence de rupture) **acceptée** au seuil de confiance de 95%
Hypothèse nulle (absence de rupture) **acceptée** au seuil de confiance de 90%

Méthode non paramétrique de PETTITT

Hypothèse nulle (absence de rupture) **acceptée** au seuil de confiance de 99%
Hypothèse nulle (absence de rupture) **acceptée** au seuil de confiance de 95%
Hypothèse nulle (absence de rupture) **acceptée** au seuil de confiance de 90%

Méthode bayésienne de LEE et HEGHINIAN

Mode de la fonction densité de probabilité *a posteriori* de la position du point de rupture: **0.1727** en **2002**

Segmentation de HUBERT

Niveau de signification du test de Scheffé: **1%**

Début	Fin	Moyenne	Ecart type
1985	2005	0.516	0.334

Analyse de séries chronoloqiques

D:\These\Donnees\Controle des Donnees\Hypothesis Tests\800.ksi

Identification	800_SERCHIO
Variable étudiée	Debit annuel
Unité	m3s
Chronique de	1999 ***à*** 2015

Valeurs

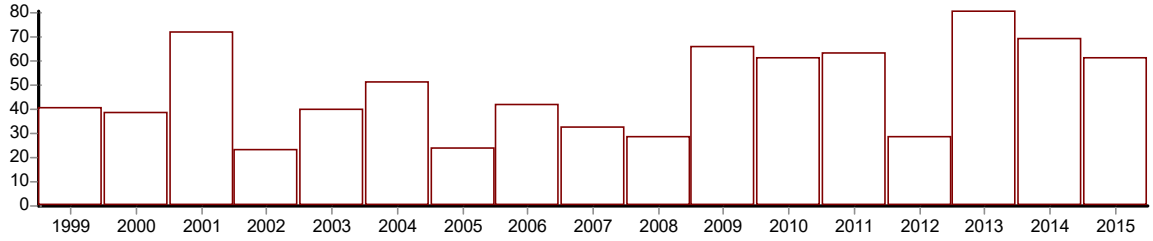

Tests de vérification du caractère aléatoire

Test de corrélation sur le RANG

Hypothèse nulle (série chronologique aléatoire) **acceptée** au seuil de confiance de 99%
Hypothèse nulle (série chronologique aléatoire) **acceptée** au seuil de confiance de 95%
Hypothèse nulle (série chronologique aléatoire) **acceptée** au seuil de confiance de 90%

Valeur de la variable de calcul: **1.4829**

Tests de détection de rupture

Test de BUISHAND et ellipse de BOIS

Hypothèse nulle (absence de rupture) **acceptée** au seuil de confiance de 99%
Hypothèse nulle (absence de rupture) **acceptée** au seuil de confiance de 95%
Hypothèse nulle (absence de rupture) **rejetée** au seuil de confiance de 90%

Méthode non paramétrique de PETTITT

Hypothèse nulle (absence de rupture) **acceptée** au seuil de confiance de 99%
Hypothèse nulle (absence de rupture) **acceptée** au seuil de confiance de 95%
Hypothèse nulle (absence de rupture) **acceptée** au seuil de confiance de 90%

Méthode bayésienne de LEE et HEGHINIAN

Mode de la fonction densité de probabilité *a posteriori* de la position du point de rupture: **0.3097** en **2008**

Segmentation de HUBERT

Niveau de signification du test de Scheffé: **1%**

Début	Fin	Moyenne	Ecart type
1999	2008	39.320	14.464
2009	2015	61.429	16.052

Analyse de séries chronologiques

D:\These\Donnees\Controle des Donnees\Hypothesis Tests\803.ksi

Identification 803_ARGENTINA
Variable étudiée Debit annuel
Unité m3s
Chronique de 1925 ***à*** 1996

Valeurs

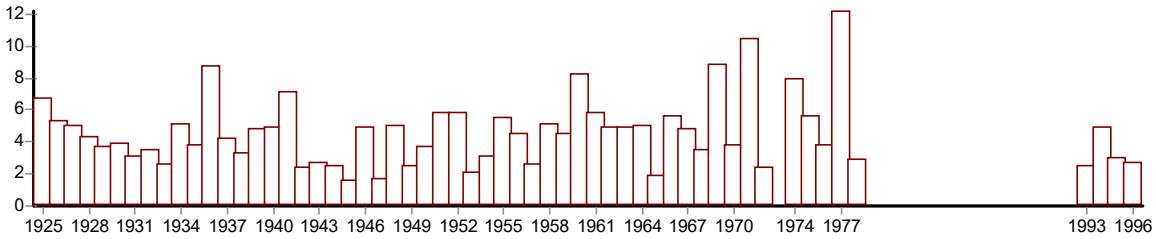

Tests de vérification du caractère aléatoire

Test de corrélation sur le RANG

Hypothèse nulle (série chronologique aléatoire) **acceptée** au seuil de confiance de 99%
Hypothèse nulle (série chronologique aléatoire) **acceptée** au seuil de confiance de 95%
Hypothèse nulle (série chronologique aléatoire) **acceptée** au seuil de confiance de 90%

Valeur de la variable de calcul: **0.4819**

Tests de détection de rupture

Test de BUISHAND et ellipse de BOIS

Hypothèse nulle (absence de rupture) **acceptée** au seuil de confiance de 99%
Hypothèse nulle (absence de rupture) **acceptée** au seuil de confiance de 95%
Hypothèse nulle (absence de rupture) **acceptée** au seuil de confiance de 90%

Méthode non paramétrique de PETTITT

Hypothèse nulle (absence de rupture) **acceptée** au seuil de confiance de 99%
Hypothèse nulle (absence de rupture) **acceptée** au seuil de confiance de 95%
Hypothèse nulle (absence de rupture) **acceptée** au seuil de confiance de 90%

Méthode bayésienne de LEE et HEGHINIAN

Mode de la fonction densité de probabilité *a posteriori* de la position du point de rupture: **0.0528** en **1925**

Segmentation de HUBERT

Niveau de signification du test de Scheffé: **1%**

Début	Fin	Moyenne	Ecart type
1925	1996	4.600	2.163

Analyse de séries chronologiques

D:\These\Donnees\Controle des Donnees\Hypothesis Tests\822.ksi

Identification	822_CECINA
Variable étudiée	Debit annuel
Unité	m3s
Chronique de	1953 ***à*** 2006

Valeurs

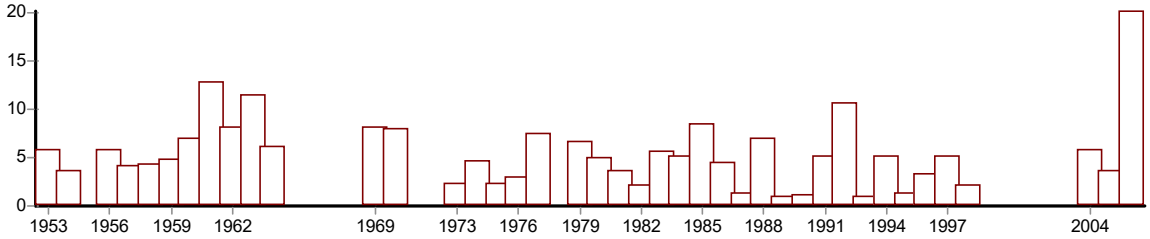

Tests de vérification du caractère aléatoire

Test de corrélation sur le RANG

Hypothèse nulle (série chronologique aléatoire) **acceptée** au seuil de confiance de 99%
Hypothèse nulle (série chronologique aléatoire) **acceptée** au seuil de confiance de 95%
Hypothèse nulle (série chronologique aléatoire) **acceptée** au seuil de confiance de 90%

Valeur de la variable de calcul: **-1.3029**

Tests de détection de rupture

Test de BUISHAND et ellipse de BOIS

Hypothèse nulle (absence de rupture) **acceptée** au seuil de confiance de 99%
Hypothèse nulle (absence de rupture) **acceptée** au seuil de confiance de 95%
Hypothèse nulle (absence de rupture) **acceptée** au seuil de confiance de 90%

Méthode non paramétrique de PETTITT

Hypothèse nulle (absence de rupture) **acceptée** au seuil de confiance de 99%
Hypothèse nulle (absence de rupture) **acceptée** au seuil de confiance de 95%
Hypothèse nulle (absence de rupture) **acceptée** au seuil de confiance de 90%

Méthode bayésienne de LEE et HEGHINIAN

Mode de la fonction densité de probabilité *a posteriori* de la position du point de rupture: **0.9802** en **2005**

Segmentation de HUBERT

Niveau de signification du test de Scheffé: **1%**

Début	Fin	Moyenne	Ecart type
1953	1992	5.125	2.824
1993	1993	20.100	0.000

Analyse de séries chronoloqiques

D:\These\Donnees\Controle des Donnees\Hypothesis Tests\845 - Copy.ksi

Identification	845_PESCARA
Variable étudiée	Debit annuel
Unité	m3s
Chronique de	1982 ***à*** 2013

Valeurs

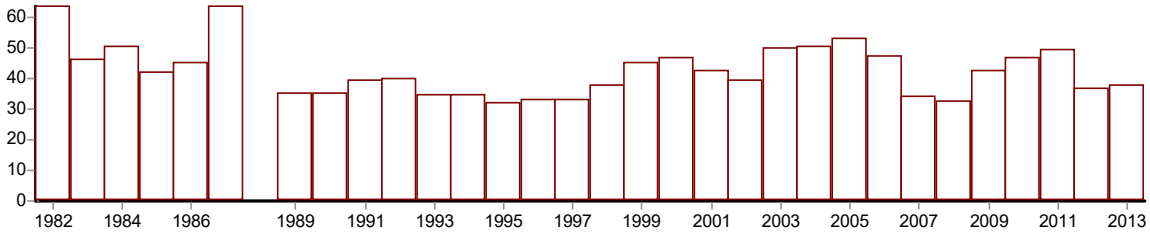

Tests de vérification du caractère aléatoire

Test de corrélation sur le RANG

Hypothèse nulle (série chronologique aléatoire) **acceptée** au seuil de confiance de 99%
Hypothèse nulle (série chronologique aléatoire) **acceptée** au seuil de confiance de 95%
Hypothèse nulle (série chronologique aléatoire) **acceptée** au seuil de confiance de 90%

Valeur de la variable de calcul: **-0.4589**

Tests de détection de rupture

Test de BUISHAND et ellipse de BOIS

Hypothèse nulle (absence de rupture) **acceptée** au seuil de confiance de 99%
Hypothèse nulle (absence de rupture) **acceptée** au seuil de confiance de 95%
Hypothèse nulle (absence de rupture) **acceptée** au seuil de confiance de 90%

Méthode non paramétrique de PETTITT

Hypothèse nulle (absence de rupture) **acceptée** au seuil de confiance de 99%
Hypothèse nulle (absence de rupture) **acceptée** au seuil de confiance de 95%
Hypothèse nulle (absence de rupture) **acceptée** au seuil de confiance de 90%

Méthode bayésienne de LEE et HEGHINIAN

Mode de la fonction densité de probabilité *a posteriori* de la position du point de rupture: **0.4721** en **1987**

Segmentation de HUBERT

Niveau de signification du test de Scheffé: **1%**

Début	Fin	Moyenne	Ecart type
1982	1987	51.950	9.442
1988	2012	40.520	6.522

Analyse de séries chronologiques

D:\These\Donnees\Controle des Donnees\Hypothesis Tests\887.ksi

Identification 887_ALENTO
Variable étudiée Debit annuel
Unité m3s
Chronique de 1961 ***à*** 1981

Valeurs

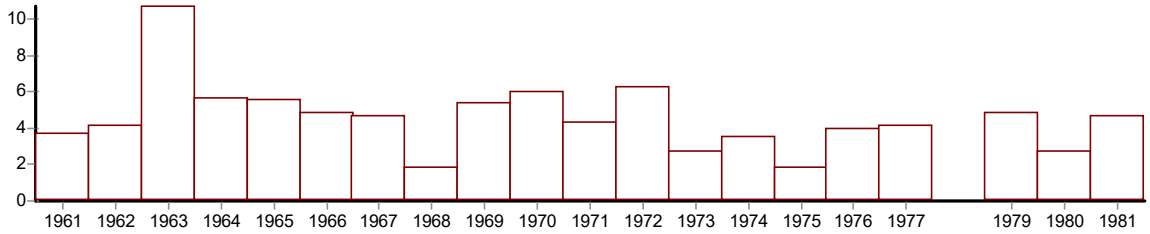

Tests de vérification du caractère aléatoire

Test de corrélation sur le RANG

Hypothèse nulle (série chronologique aléatoire) **acceptée** au seuil de confiance de 99%
Hypothèse nulle (série chronologique aléatoire) **acceptée** au seuil de confiance de 95%
Hypothèse nulle (série chronologique aléatoire) **acceptée** au seuil de confiance de 90%

Valeur de la variable de calcul: **-1.1031**

Tests de détection de rupture

Test de BUISHAND et ellipse de BOIS

Hypothèse nulle (absence de rupture) **acceptée** au seuil de confiance de 99%
Hypothèse nulle (absence de rupture) **acceptée** au seuil de confiance de 95%
Hypothèse nulle (absence de rupture) **acceptée** au seuil de confiance de 90%

Méthode non paramétrique de PETTITT

Hypothèse nulle (absence de rupture) **acceptée** au seuil de confiance de 99%
Hypothèse nulle (absence de rupture) **acceptée** au seuil de confiance de 95%
Hypothèse nulle (absence de rupture) **acceptée** au seuil de confiance de 90%

Méthode bayésienne de LEE et HEGHINIAN

Mode de la fonction densité de probabilité *a posteriori* de la position du point de rupture: **0.1329** en **1972**

Segmentation de HUBERT

Niveau de signification du test de Scheffé: **1%**

Début	Fin	Moyenne	Ecart type
1961	1981	4.600	1.915

Analyse de séries chronologiques

D:\These\Donnees\Controle des Donnees\Hypothesis Tests\903.ksi

Identification 903_SAN_LEONARDO
Variable étudiée Debit annuel
Unité m3s
Chronique de 1951 ***à*** 1980

Valeurs

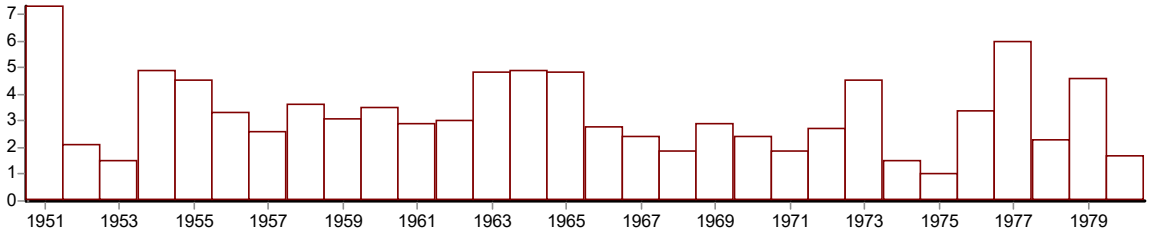

Tests de vérification du caractère aléatoire

Test de corrélation sur le RANG

Hypothèse nulle (série chronologique aléatoire) **acceptée** au seuil de confiance de 99%
Hypothèse nulle (série chronologique aléatoire) **acceptée** au seuil de confiance de 95%
Hypothèse nulle (série chronologique aléatoire) **acceptée** au seuil de confiance de 90%

Valeur de la variable de calcul: **-1.4808**

Tests de détection de rupture

Test de BUISHAND et ellipse de BOIS

Hypothèse nulle (absence de rupture) **acceptée** au seuil de confiance de 99%
Hypothèse nulle (absence de rupture) **acceptée** au seuil de confiance de 95%
Hypothèse nulle (absence de rupture) **acceptée** au seuil de confiance de 90%

Méthode non paramétrique de PETTITT

Hypothèse nulle (absence de rupture) **acceptée** au seuil de confiance de 99%
Hypothèse nulle (absence de rupture) **acceptée** au seuil de confiance de 95%
Hypothèse nulle (absence de rupture) **acceptée** au seuil de confiance de 90%

Méthode bayésienne de LEE et HEGHINIAN

Mode de la fonction densité de probabilité *a posteriori* de la position du point de rupture: **0.7749** en **1951**

Segmentation de HUBERT

Niveau de signification du test de Scheffé: **1%**

Début	Fin	Moyenne	Ecart type
1951	1951	7.300	0.000
1952	1980	3.155	1.266

Analyse de séries chronoloqiques

D:\These\Donnees\Controle des Donnees\Hypothesis Tests\908.ksi

Identification 908_IMERA_MERIDIONALE
Variable étudiée Debit annuel
Unité m3s
Chronique de 1963 ***à*** 2001

Valeurs

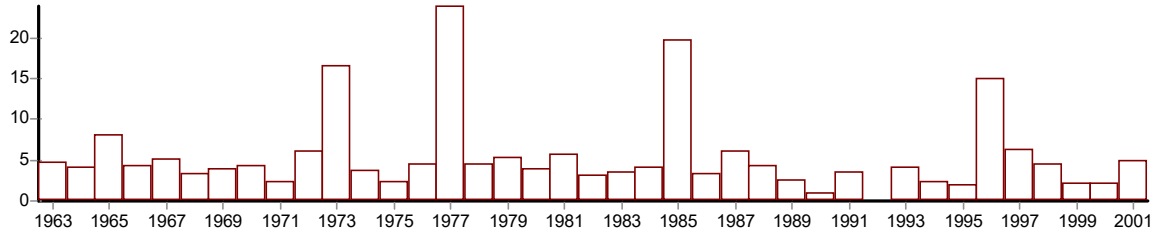

Tests de vérification du caractère aléatoire

Test de corrélation sur le RANG

Hypothèse nulle (série chronologique aléatoire) **acceptée** au seuil de confiance de 99%
Hypothèse nulle (série chronologique aléatoire) **acceptée** au seuil de confiance de 95%
Hypothèse nulle (série chronologique aléatoire) **acceptée** au seuil de confiance de 90%

Valeur de la variable de calcul: **-1.2698**

Tests de détection de rupture

Test de BUISHAND et ellipse de BOIS

RE

Méthode non paramétrique de PETTITT

Hypothèse nulle (absence de rupture) **acceptée** au seuil de confiance de 99%
Hypothèse nulle (absence de rupture) **acceptée** au seuil de confiance de 95%
Hypothèse nulle (absence de rupture) **acceptée** au seuil de confiance de 90%

Méthode bayésienne de LEE et HEGHINIAN

RE

Segmentation de HUBERT

Niveau de signification du test de Scheffé: **1%**

Début	Fin	Moyenne	Ecart type
1963	2001	5.605	4.927

Analyse de séries chronologiques

D:\These\Donnees\Controle des Donnees\Hypothesis Tests\913.ksi

Identification 913_CERVARO
Variable étudiée Debit annuel
Unité m3s
Chronique de 1966 ***à*** 1997

Valeurs

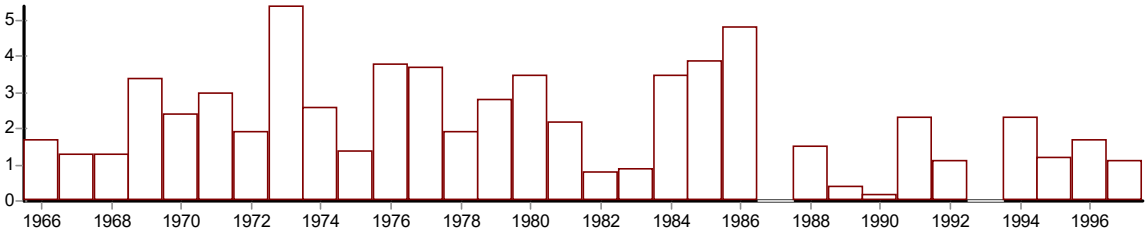

Tests de vérification du caractère aléatoire

Test de corrélation sur le RANG

Hypothèse nulle (série chronologique aléatoire) **acceptée** au seuil de confiance de 99%
Hypothèse nulle (série chronologique aléatoire) **acceptée** au seuil de confiance de 95%
Hypothèse nulle (série chronologique aléatoire) **acceptée** au seuil de confiance de 90%

Valeur de la variable de calcul: **-1.5892**

Tests de détection de rupture

Test de BUISHAND et ellipse de BOIS

Hypothèse nulle (absence de rupture) **acceptée** au seuil de confiance de 99%
Hypothèse nulle (absence de rupture) **rejetée** au seuil de confiance de 95%
Hypothèse nulle (absence de rupture) **rejetée** au seuil de confiance de 90%

Méthode non paramétrique de PETTITT

Hypothèse nulle (absence de rupture) **acceptée** au seuil de confiance de 99%
Hypothèse nulle (absence de rupture) **rejetée** au seuil de confiance de 95%
Hypothèse nulle (absence de rupture) **rejetée** au seuil de confiance de 90%

Probabilité de dépassement de la valeur critique du test: **1.89E-02** en **1986**

Méthode bayésienne de LEE et HEGHINIAN

Mode de la fonction densité de probabilité *a posteriori* de la position du point de rupture: **0.6127** en **1986**

Segmentation de HUBERT

Niveau de signification du test de Scheffé: **1%**

Début	Fin	Moyenne	Ecart type
1966	1986	3.676	1.271
1987	1997	2.073	0.844

Analyse de séries chronologiques

D:\These\Donnees\Controle des Donnees\Hypothesis Tests\928.ksi

Identification	928_NAHR_JAWZ
Variable étudiée	Debit annuel
Unité	m3s
Chronique de	1966 ***à*** 2016

Valeurs

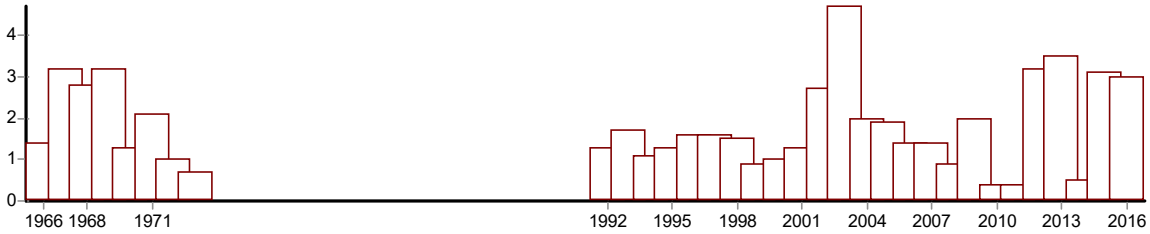

Tests de vérification du caractère aléatoire

Test de corrélation sur le RANG

Hypothèse nulle (série chronologique aléatoire) **acceptée** au seuil de confiance de 99%
Hypothèse nulle (série chronologique aléatoire) **acceptée** au seuil de confiance de 95%
Hypothèse nulle (série chronologique aléatoire) **acceptée** au seuil de confiance de 90%

Valeur de la variable de calcul: **0.1859**

Tests de détection de rupture

Test de BUISHAND et ellipse de BOIS

Hypothèse nulle (absence de rupture) **acceptée** au seuil de confiance de 99%
Hypothèse nulle (absence de rupture) **acceptée** au seuil de confiance de 95%
Hypothèse nulle (absence de rupture) **acceptée** au seuil de confiance de 90%

Méthode non paramétrique de PETTITT

Hypothèse nulle (absence de rupture) **acceptée** au seuil de confiance de 99%
Hypothèse nulle (absence de rupture) **acceptée** au seuil de confiance de 95%
Hypothèse nulle (absence de rupture) **acceptée** au seuil de confiance de 90%

Méthode bayésienne de LEE et HEGHINIAN

Mode de la fonction densité de probabilité *a posteriori* de la position du point de rupture: **0.1096** en **2014**

Segmentation de HUBERT

Niveau de signification du test de Scheffé: **1%**

Début	Fin	Moyenne	Ecart type
1966	2016	1.821	1.033

Analyse de séries chronologiques

D:\These\Donnees\Controle des Donnees\Hypothesis Tests\929.ksi

Identification 929_NAHR_BEYROUTH
Variable étudiée Debit annuel
Unité m3s
Chronique de 1966 ***à*** 2015

Valeurs

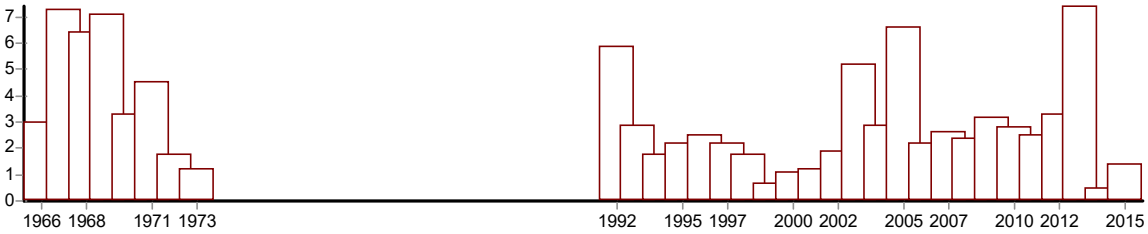

Tests de vérification du caractère aléatoire

Test de corrélation sur le RANG

Hypothèse nulle (série chronologique aléatoire) **acceptée** au seuil de confiance de 99%
Hypothèse nulle (série chronologique aléatoire) **acceptée** au seuil de confiance de 95%
Hypothèse nulle (série chronologique aléatoire) **acceptée** au seuil de confiance de 90%

Valeur de la variable de calcul: **-0.9406**

Tests de détection de rupture

Test de BUISHAND et ellipse de BOIS

Hypothèse nulle (absence de rupture) **acceptée** au seuil de confiance de 99%
Hypothèse nulle (absence de rupture) **acceptée** au seuil de confiance de 95%
Hypothèse nulle (absence de rupture) **acceptée** au seuil de confiance de 90%

Méthode non paramétrique de PETTITT

Hypothèse nulle (absence de rupture) **acceptée** au seuil de confiance de 99%
Hypothèse nulle (absence de rupture) **acceptée** au seuil de confiance de 95%
Hypothèse nulle (absence de rupture) **acceptée** au seuil de confiance de 90%

Méthode bayésienne de LEE et HEGHINIAN

Mode de la fonction densité de probabilité *a posteriori* de la position du point de rupture: **0.1983** en **2013**

Segmentation de HUBERT

Niveau de signification du test de Scheffé: **1%**

Début	Fin	Moyenne	Ecart type
1966	1969	5.950	2.004
1970	1997	2.786	1.716

Analyse de séries chronologiques

D:\These\Donnees\Controle des Donnees\Hypothesis Tests\930.ksi

Identification 930_NAHR_KALB
Variable étudiée Debit annuel
Unité m3s
Chronique de 1950 ***à*** 2015

Valeurs

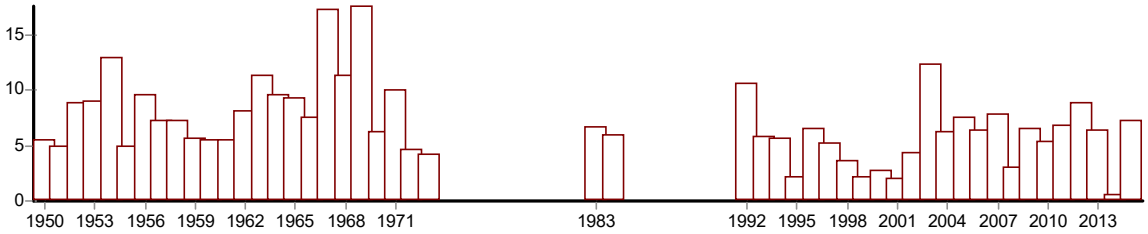

Tests de vérification du caractère aléatoire

Test de corrélation sur le RANG

Hypothèse nulle (série chronologique aléatoire) **acceptée** au seuil de confiance de 99%
Hypothèse nulle (série chronologique aléatoire) **acceptée** au seuil de confiance de 95%
Hypothèse nulle (série chronologique aléatoire) **acceptée** au seuil de confiance de 90%

Valeur de la variable de calcul: **-1.6311**

Tests de détection de rupture

Test de BUISHAND et ellipse de BOIS

Hypothèse nulle (absence de rupture) **acceptée** au seuil de confiance de 99%
Hypothèse nulle (absence de rupture) **rejetée** au seuil de confiance de 95%
Hypothèse nulle (absence de rupture) **rejetée** au seuil de confiance de 90%

Méthode non paramétrique de PETTITT

Hypothèse nulle (absence de rupture) **acceptée** au seuil de confiance de 99%
Hypothèse nulle (absence de rupture) **rejetée** au seuil de confiance de 95%
Hypothèse nulle (absence de rupture) **rejetée** au seuil de confiance de 90%

Probabilité de dépassement de la valeur critique du test: **1.35E-02** en **1971**

Méthode bayésienne de LEE et HEGHINIAN

Mode de la fonction densité de probabilité *a posteriori* de la position du point de rupture: **0.2508** en **1971**

Segmentation de HUBERT

Niveau de signification du test de Scheffé: **1%**

Début	Fin	Moyenne	Ecart type
1950	1966	7.835	2.312
1967	1969	15.433	3.496
1970	1999	5.810	2.636

Analyse de séries chronologiques

D:\These\Donnees\Controle des Donnees\Hypothesis Tests\934.ksi

Identification 934_NAHR_IBRAHIM
Variable étudiée Debit annuel
Unité m3s
Chronique de 1966 ***à*** 2015

Valeurs

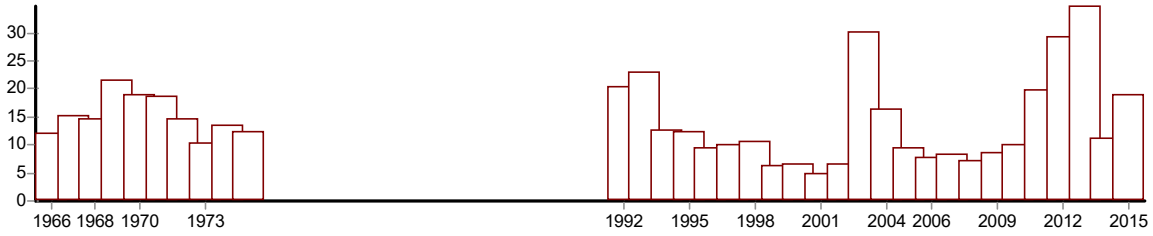

Tests de vérification du caractère aléatoire

Test de corrélation sur le RANG

Hypothèse nulle (série chronologique aléatoire) **acceptée** au seuil de confiance de 99%
Hypothèse nulle (série chronologique aléatoire) **acceptée** au seuil de confiance de 95%
Hypothèse nulle (série chronologique aléatoire) **acceptée** au seuil de confiance de 90%

Valeur de la variable de calcul: **-1.0229**

Tests de détection de rupture

Test de BUISHAND et ellipse de BOIS

Hypothèse nulle (absence de rupture) **acceptée** au seuil de confiance de 99%
Hypothèse nulle (absence de rupture) **acceptée** au seuil de confiance de 95%
Hypothèse nulle (absence de rupture) **acceptée** au seuil de confiance de 90%

Méthode non paramétrique de PETTITT

Hypothèse nulle (absence de rupture) **acceptée** au seuil de confiance de 99%
Hypothèse nulle (absence de rupture) **acceptée** au seuil de confiance de 95%
Hypothèse nulle (absence de rupture) **acceptée** au seuil de confiance de 90%

Méthode bayésienne de LEE et HEGHINIAN

Mode de la fonction densité de probabilité *a posteriori* de la position du point de rupture: **0.3724** en **2010**

Segmentation de HUBERT

Niveau de signification du test de Scheffé: **1%**

Début	Fin	Moyenne	Ecart type
1966	1994	12.866	5.857
1995	1999	22.880	9.276

Analyse de séries chronologiques

D:\These\Donnees\Controle des Donnees\Hypothesis Tests\936.ksi

Identification	936_NAHR_ASSI
Variable étudiée	Debit annuel
Unité	m3s
Chronique de	1956 ***à*** 2011

Valeurs

Tests de vérification du caractère aléatoire

Test de corrélation sur le RANG

Hypothèse nulle (série chronologique aléatoire) **acceptée** au seuil de confiance de 99%
Hypothèse nulle (série chronologique aléatoire) **acceptée** au seuil de confiance de 95%
Hypothèse nulle (série chronologique aléatoire) **acceptée** au seuil de confiance de 90%

Valeur de la variable de calcul: **0.7669**

Tests de détection de rupture

Test de BUISHAND et ellipse de BOIS

Hypothèse nulle (absence de rupture) **acceptée** au seuil de confiance de 99%
Hypothèse nulle (absence de rupture) **acceptée** au seuil de confiance de 95%
Hypothèse nulle (absence de rupture) **acceptée** au seuil de confiance de 90%

Méthode non paramétrique de PETTITT

Hypothèse nulle (absence de rupture) **acceptée** au seuil de confiance de 99%
Hypothèse nulle (absence de rupture) **acceptée** au seuil de confiance de 95%
Hypothèse nulle (absence de rupture) **acceptée** au seuil de confiance de 90%

Méthode bayésienne de LEE et HEGHINIAN

Mode de la fonction densité de probabilité *a posteriori* de la position du point de rupture: **0.1336** en **1961**

Segmentation de HUBERT

Niveau de signification du test de Scheffé: **1%**

Début	Fin	Moyenne	Ecart type
1956	2011	5.697	2.336

Analyse de séries chronoloqiques

D:\These\Donnees\Controle des Donnees\Hypothesis Tests\937.ksi

Identification	937_NAHR_LITANI
Variable étudiée	Debit annuel
Unité	m3s
Chronique de	1939 ***à*** 2015

Valeurs

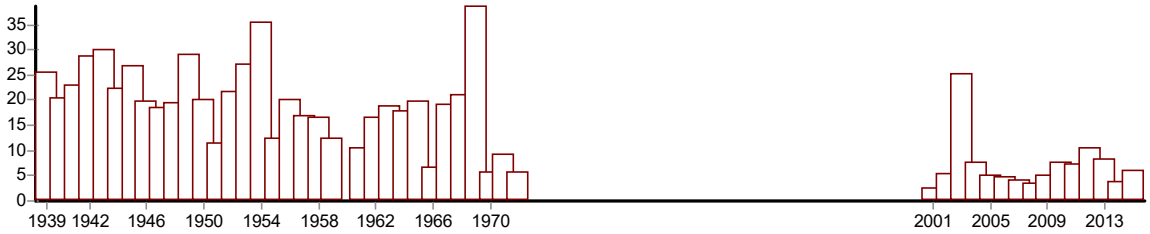

Tests de vérification du caractère aléatoire

Test de corrélation sur le RANG

Hypothèse nulle (série chronologique aléatoire) **rejetée** au seuil de confiance de 99%
Hypothèse nulle (série chronologique aléatoire) **rejetée** au seuil de confiance de 95%
Hypothèse nulle (série chronologique aléatoire) **rejetée** au seuil de confiance de 90%

Valeur de la variable de calcul: **-5.3506**

Tests de détection de rupture

Test de BUISHAND et ellipse de BOIS

RE

Méthode non paramétrique de PETTITT

Hypothèse nulle (absence de rupture) **rejetée** au seuil de confiance de 99%
Hypothèse nulle (absence de rupture) **rejetée** au seuil de confiance de 95%
Hypothèse nulle (absence de rupture) **rejetée** au seuil de confiance de 90%

Probabilité de dépassement de la valeur critique du test: **8.25E-06** en **1969**

Méthode bayésienne de LEE et HEGHINIAN

RE

Segmentation de HUBERT

Niveau de signification du test de Scheffé: **1%**

Début	Fin	Moyenne	Ecart type
1939	1954	23.819	5.763
1955	1967	16.100	4.283
1968	1968	38.700	0.000
1969	1986	7.128	5.024

Analyse de séries chronoloqiques

D:\These\Donnees\Controle des Donnees\Hypothesis Tests\938.ksi

Identification 938_MORACA
Variable étudiée Debit annuel
Unité m3s
Chronique de 1948 ***à*** 1991

Valeurs

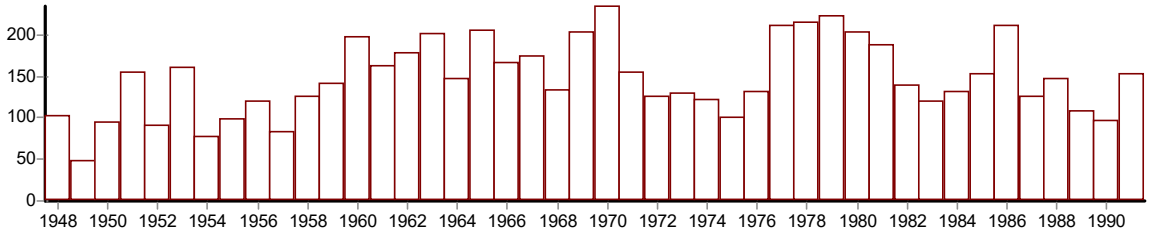

Tests de vérification du caractère aléatoire

Test de corrélation sur le RANG

Hypothèse nulle (série chronologique aléatoire) **acceptée** au seuil de confiance de 99%
Hypothèse nulle (série chronologique aléatoire) **acceptée** au seuil de confiance de 95%
Hypothèse nulle (série chronologique aléatoire) **acceptée** au seuil de confiance de 90%

Valeur de la variable de calcul: **1.6183**

Tests de détection de rupture

Test de BUISHAND et ellipse de BOIS

Hypothèse nulle (absence de rupture) **acceptée** au seuil de confiance de 99%
Hypothèse nulle (absence de rupture) **rejetée** au seuil de confiance de 95%
Hypothèse nulle (absence de rupture) **rejetée** au seuil de confiance de 90%

Méthode non paramétrique de PETTITT

Hypothèse nulle (absence de rupture) **acceptée** au seuil de confiance de 99%
Hypothèse nulle (absence de rupture) **rejetée** au seuil de confiance de 95%
Hypothèse nulle (absence de rupture) **rejetée** au seuil de confiance de 90%

Probabilité de dépassement de la valeur critique du test: **1.59E-02** en **1959**

Méthode bayésienne de LEE et HEGHINIAN

Mode de la fonction densité de probabilité *a posteriori* de la position du point de rupture: **0.3219** en **1958**

Segmentation de HUBERT

Niveau de signification du test de Scheffé: **1%**

Début	Fin	Moyenne	Ecart type
1948	1958	105.455	33.523
1959	1991	161.915	38.777

Analyse de séries chronologiques

D:\These\Donnees\Controle des Donnees\Hypothesis Tests\949.ksi

Identification 949_KERT
Variable étudiée Debit annuel
Unité m3s
Chronique de 1971 ***à*** 1988

Valeurs

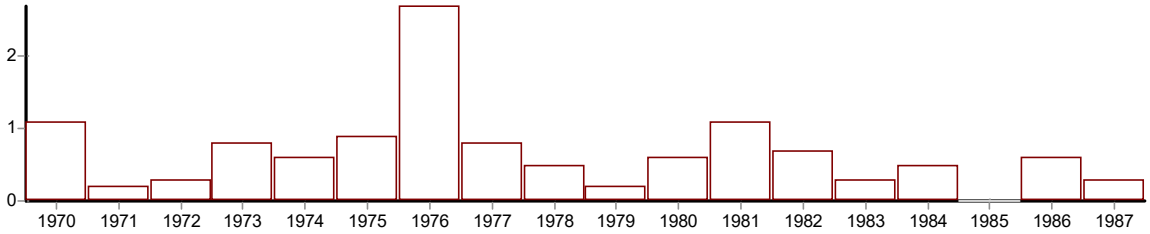

Tests de vérification du caractère aléatoire

Test de corrélation sur le RANG

Hypothèse nulle (série chronologique aléatoire) **acceptée** au seuil de confiance de 99%
Hypothèse nulle (série chronologique aléatoire) **acceptée** au seuil de confiance de 95%
Hypothèse nulle (série chronologique aléatoire) **acceptée** au seuil de confiance de 90%

Valeur de la variable de calcul: **-0.8712**

Tests de détection de rupture

Test de BUISHAND et ellipse de BOIS

RE

Méthode non paramétrique de PETTITT

Hypothèse nulle (absence de rupture) **acceptée** au seuil de confiance de 99%
Hypothèse nulle (absence de rupture) **acceptée** au seuil de confiance de 95%
Hypothèse nulle (absence de rupture) **acceptée** au seuil de confiance de 90%

Méthode bayésienne de LEE et HEGHINIAN

RE

Segmentation de HUBERT

Niveau de signification du test de Scheffé: **1%**

Début	Fin	Moyenne	Ecart type
1971	1987	0.678	0.592

Analyse de séries chronologiques

D:\These\Donnees\Controle des Donnees\Hypothesis Tests\949.ksi

Identification 951_EMSA
Variable étudiée Debit annuel
Unité m3s
Chronique de 1971 ***à*** 1988

Valeurs

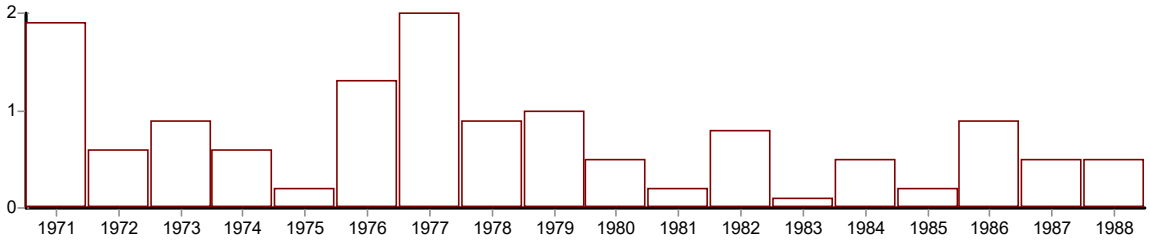

Tests de vérification du caractère aléatoire

Test de corrélation sur le RANG

Hypothèse nulle (série chronologique aléatoire) **acceptée** au seuil de confiance de 99%
Hypothèse nulle (série chronologique aléatoire) **acceptée** au seuil de confiance de 95%
Hypothèse nulle (série chronologique aléatoire) **acceptée** au seuil de confiance de 90%

Valeur de la variable de calcul: **-1.3257**

Tests de détection de rupture

Test de BUISHAND et ellipse de BOIS

Hypothèse nulle (absence de rupture) **acceptée** au seuil de confiance de 99%
Hypothèse nulle (absence de rupture) **acceptée** au seuil de confiance de 95%
Hypothèse nulle (absence de rupture) **acceptée** au seuil de confiance de 90%

Méthode non paramétrique de PETTITT

Hypothèse nulle (absence de rupture) **acceptée** au seuil de confiance de 99%
Hypothèse nulle (absence de rupture) **acceptée** au seuil de confiance de 95%
Hypothèse nulle (absence de rupture) **rejetée** au seuil de confiance de 90%

Probabilité de dépassement de la valeur critique du test: **8.43E-02** en **1979**

Méthode bayésienne de LEE et HEGHINIAN

Mode de la fonction densité de probabilité *a posteriori* de la position du point de rupture: **0.1868** en **1979**

Segmentation de HUBERT

Niveau de signification du test de Scheffé: **1%**

Début	Fin	Moyenne	Ecart type
1971	1988	0.756	0.539

Analyse de séries chronoloqiques

D:\These\Donnees\Controle des Donnees\Hypothesis Tests\959.ksi

Identification 959_RIZANA
Variable étudiée Debit annuel
Unité m3s
Chronique de 1965 ***à*** 2015

Valeurs

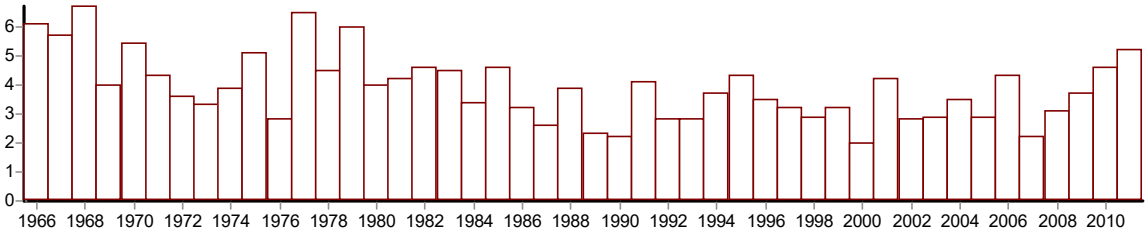

Tests de vérification du caractère aléatoire

Test de corrélation sur le RANG

Hypothèse nulle (série chronologique aléatoire) **rejetée** au seuil de confiance de 99%
Hypothèse nulle (série chronologique aléatoire) **rejetée** au seuil de confiance de 95%
Hypothèse nulle (série chronologique aléatoire) **rejetée** au seuil de confiance de 90%

Valeur de la variable de calcul: **-2.7363**

Tests de détection de rupture

Test de BUISHAND et ellipse de BOIS

Hypothèse nulle (absence de rupture) **rejetée** au seuil de confiance de 99%
Hypothèse nulle (absence de rupture) **rejetée** au seuil de confiance de 95%
Hypothèse nulle (absence de rupture) **rejetée** au seuil de confiance de 90%

Méthode non paramétrique de PETTITT

Hypothèse nulle (absence de rupture) **rejetée** au seuil de confiance de 99%
Hypothèse nulle (absence de rupture) **rejetée** au seuil de confiance de 95%
Hypothèse nulle (absence de rupture) **rejetée** au seuil de confiance de 90%

Probabilité de dépassement de la valeur critique du test: **1.18E-03** en **1985**

Méthode bayésienne de LEE et HEGHINIAN

Mode de la fonction densité de probabilité *a posteriori* de la position du point de rupture: **0.2154** en **1983**

Segmentation de HUBERT

Niveau de signification du test de Scheffé: **1%**

Début	Fin	Moyenne	Ecart type
1965	1967	6.167	0.503
1968	1984	4.394	0.955
1985	2010	3.312	0.810

Analyse de séries chronologiques

D:\These\Donnees\Controle des Donnees\Hypothesis Tests\960.ksi

Identification 960_DRAGONJA
Variable étudiée Debit annuel
Unité m3s
Chronique de 1979 ***à*** 2015

Valeurs

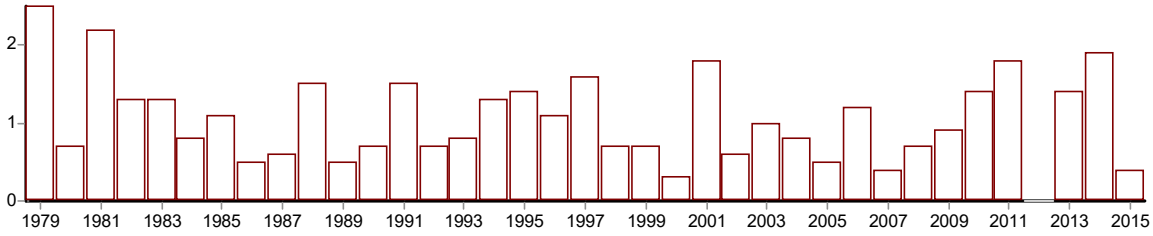

Tests de vérification du caractère aléatoire

Test de corrélation sur le RANG

Hypothèse nulle (série chronologique aléatoire) **acceptée** au seuil de confiance de 99%
Hypothèse nulle (série chronologique aléatoire) **acceptée** au seuil de confiance de 95%
Hypothèse nulle (série chronologique aléatoire) **acceptée** au seuil de confiance de 90%

Valeur de la variable de calcul: **-0.3924**

Tests de détection de rupture

Test de BUISHAND et ellipse de BOIS

Hypothèse nulle (absence de rupture) **acceptée** au seuil de confiance de 99%
Hypothèse nulle (absence de rupture) **acceptée** au seuil de confiance de 95%
Hypothèse nulle (absence de rupture) **acceptée** au seuil de confiance de 90%

Méthode non paramétrique de PETTITT

Hypothèse nulle (absence de rupture) **acceptée** au seuil de confiance de 99%
Hypothèse nulle (absence de rupture) **acceptée** au seuil de confiance de 95%
Hypothèse nulle (absence de rupture) **acceptée** au seuil de confiance de 90%

Méthode bayésienne de LEE et HEGHINIAN

Mode de la fonction densité de probabilité *a posteriori* de la position du point de rupture: **0.4123** en **1979**

Segmentation de HUBERT

Niveau de signification du test de Scheffé: **1%**

Début	Fin	Moyenne	Ecart type
1979	1979	2.500	0.000
1980	2015	1.003	0.511

Analyse de séries chronologiques

D:\These\Donnees\Controle des Donnees\Hypothesis Tests\962.ksi

Identification	962_ISONZO
Variable étudiée	Debit annuel
Unité	m3s
Chronique de	1980 ***à*** 2016

Valeurs

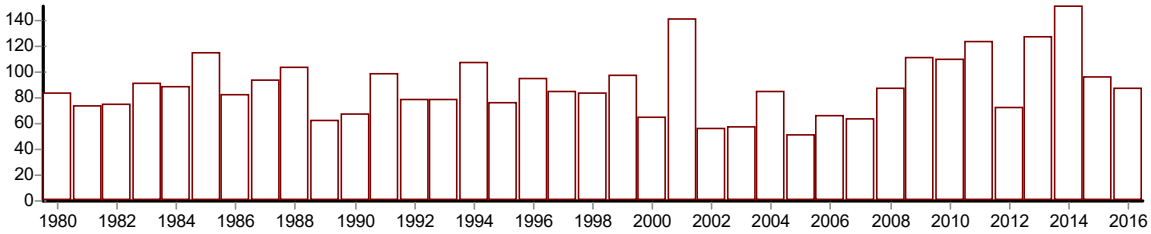

Tests de vérification du caractère aléatoire

Test de corrélation sur le RANG

Hypothèse nulle (série chronologique aléatoire) **acceptée** au seuil de confiance de 99%
Hypothèse nulle (série chronologique aléatoire) **acceptée** au seuil de confiance de 95%
Hypothèse nulle (série chronologique aléatoire) **acceptée** au seuil de confiance de 90%

Valeur de la variable de calcul: **1.0463**

Tests de détection de rupture

Test de BUISHAND et ellipse de BOIS

Hypothèse nulle (absence de rupture) **acceptée** au seuil de confiance de 99%
Hypothèse nulle (absence de rupture) **acceptée** au seuil de confiance de 95%
Hypothèse nulle (absence de rupture) **acceptée** au seuil de confiance de 90%

Méthode non paramétrique de PETTITT

Hypothèse nulle (absence de rupture) **acceptée** au seuil de confiance de 99%
Hypothèse nulle (absence de rupture) **acceptée** au seuil de confiance de 95%
Hypothèse nulle (absence de rupture) **acceptée** au seuil de confiance de 90%

Méthode bayésienne de LEE et HEGHINIAN

Mode de la fonction densité de probabilité *a posteriori* de la position du point de rupture: **0.3086** en **2008**

Segmentation de HUBERT

Niveau de signification du test de Scheffé: **1%**

Début	Fin	Moyenne	Ecart type
1980	2008	83.162	19.431
2009	2016	110.000	24.807

Analyse de séries chronoloqiques

D:\These\Donnees\Controle des Donnees\Hypothesis Tests\1035.ksi

Identification	1035_KOEPRUE
Variable étudiée	Debit annuel
Unité	m3s
Chronique de	1978 ***à*** 1988

Valeurs

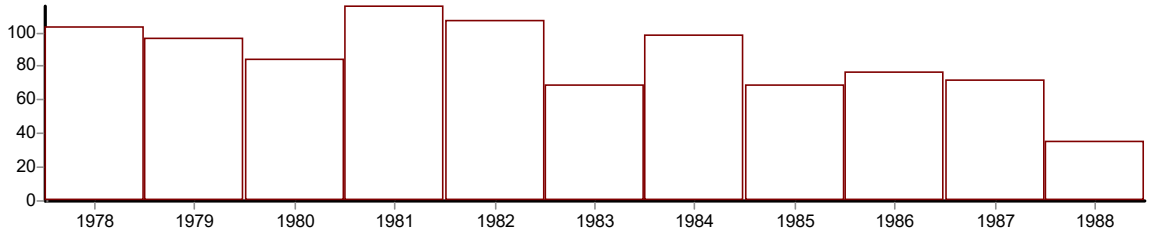

Tests de vérification du caractère aléatoire

Test de corrélation sur le RANG

Hypothèse nulle (série chronologique aléatoire) **acceptée** au seuil de confiance de 99%
Hypothèse nulle (série chronologique aléatoire) **rejetée** au seuil de confiance de 95%
Hypothèse nulle (série chronologique aléatoire) **rejetée** au seuil de confiance de 90%

Valeur de la variable de calcul: **-2.1019**

Tests de détection de rupture

Test de BUISHAND et ellipse de BOIS

Hypothèse nulle (absence de rupture) **acceptée** au seuil de confiance de 99%
Hypothèse nulle (absence de rupture) **rejetée** au seuil de confiance de 95%
Hypothèse nulle (absence de rupture) **rejetée** au seuil de confiance de 90%

Méthode non paramétrique de PETTITT

Hypothèse nulle (absence de rupture) **acceptée** au seuil de confiance de 99%
Hypothèse nulle (absence de rupture) **acceptée** au seuil de confiance de 95%
Hypothèse nulle (absence de rupture) **acceptée** au seuil de confiance de 90%

Méthode bayésienne de LEE et HEGHINIAN

Mode de la fonction densité de probabilité *a posteriori* de la position du point de rupture: **0.2802** en **1987**

Segmentation de HUBERT

Niveau de signification du test de Scheffé: **1%**

Début	Fin	Moyenne	Ecart type
1978	1988	84.464	22.918

Analyse de séries chronologiques

D:\These\Donnees\Controle des Donnees\Hypothesis Tests\1042.ksi

Identification 1042_KOEPRUE
Variable étudiée Debit annuel
Unité m3s
Chronique de 1978 ***à*** 1987

Valeurs

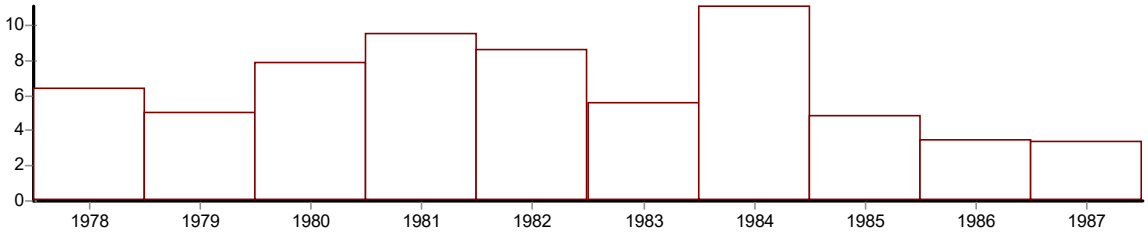

Tests de vérification du caractère aléatoire

Test de corrélation sur le RANG

Hypothèse nulle (série chronologique aléatoire) **acceptée** au seuil de confiance de 99%
Hypothèse nulle (série chronologique aléatoire) **acceptée** au seuil de confiance de 95%
Hypothèse nulle (série chronologique aléatoire) **acceptée** au seuil de confiance de 90%

Valeur de la variable de calcul: **-1.3416**

Tests de détection de rupture

Test de BUISHAND et ellipse de BOIS

Hypothèse nulle (absence de rupture) **acceptée** au seuil de confiance de 99%
Hypothèse nulle (absence de rupture) **acceptée** au seuil de confiance de 95%
Hypothèse nulle (absence de rupture) **acceptée** au seuil de confiance de 90%

Méthode non paramétrique de PETTITT

Hypothèse nulle (absence de rupture) **acceptée** au seuil de confiance de 99%
Hypothèse nulle (absence de rupture) **acceptée** au seuil de confiance de 95%
Hypothèse nulle (absence de rupture) **acceptée** au seuil de confiance de 90%

Méthode bayésienne de LEE et HEGHINIAN

Mode de la fonction densité de probabilité *a posteriori* de la position du point de rupture: **0.4344** en **1984**

Segmentation de HUBERT

Niveau de signification du test de Scheffé: **1%**

Début	Fin	Moyenne	Ecart type
1978	1987	6.590	2.597

Analyse de séries chronoloqiques

D:\These\Donnees\Controle des Donnees\Hypothesis Tests\1048_A.ksi

Identification 1048_MEJERDA
Variable étudiée Debit annuel
Unité m3s
Chronique de 1950 ***à*** 1996

Valeurs

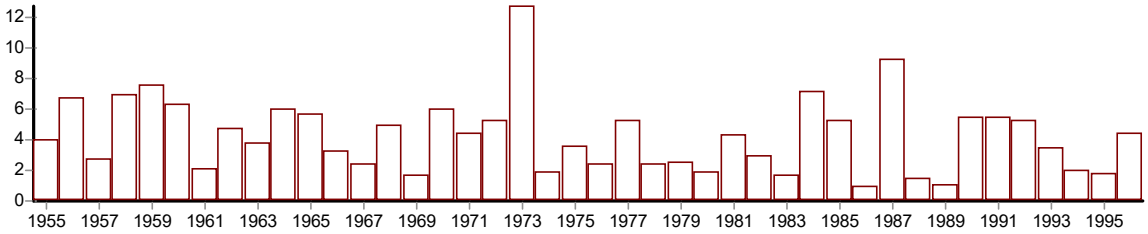

Tests de vérification du caractère aléatoire

Test de corrélation sur le RANG

Hypothèse nulle (série chronologique aléatoire) **acceptée** au seuil de confiance de 99%
Hypothèse nulle (série chronologique aléatoire) **acceptée** au seuil de confiance de 95%
Hypothèse nulle (série chronologique aléatoire) **rejetée** au seuil de confiance de 90%

Valeur de la variable de calcul: **-1.8098**

Tests de détection de rupture

Test de BUISHAND et ellipse de BOIS

Hypothèse nulle (absence de rupture) **acceptée** au seuil de confiance de 99%
Hypothèse nulle (absence de rupture) **acceptée** au seuil de confiance de 95%
Hypothèse nulle (absence de rupture) **rejetée** au seuil de confiance de 90%

Méthode non paramétrique de PETTITT

Hypothèse nulle (absence de rupture) **acceptée** au seuil de confiance de 99%
Hypothèse nulle (absence de rupture) **acceptée** au seuil de confiance de 95%
Hypothèse nulle (absence de rupture) **acceptée** au seuil de confiance de 90%

Méthode bayésienne de LEE et HEGHINIAN

Mode de la fonction densité de probabilité *a posteriori* de la position du point de rupture: **0.1042** en **1973**

Segmentation de HUBERT

Niveau de signification du test de Scheffé: **1%**

Début	Fin	Moyenne	Ecart type
1950	1996	4.262	2.407

Analyse de séries chronoloqiques

D:\These\Donnees\Controle des Donnees\Hypothesis Tests\1074.ksi

Identification 1074_MILIANE
Variable étudiée Debit annuel
Unité m3s
Chronique de 1970 ***à*** 2005

Valeurs

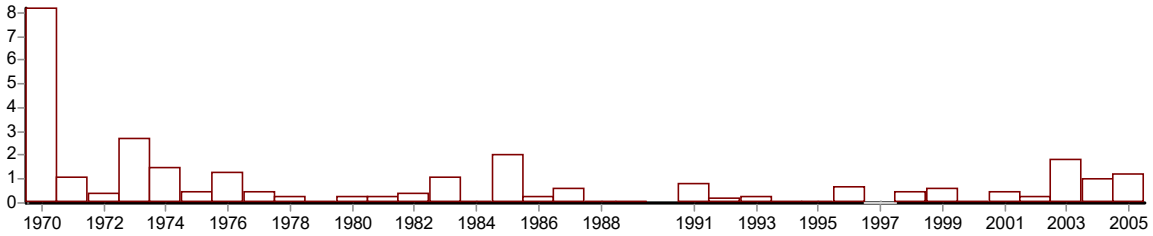

Tests de vérification du caractère aléatoire

Test de corrélation sur le RANG

Hypothèse nulle (série chronologique aléatoire) **acceptée** au seuil de confiance de 99%
Hypothèse nulle (série chronologique aléatoire) **acceptée** au seuil de confiance de 95%
Hypothèse nulle (série chronologique aléatoire) **acceptée** au seuil de confiance de 90%

Valeur de la variable de calcul: **-0.6959**

Tests de détection de rupture

Test de BUISHAND et ellipse de BOIS

RE

Méthode non paramétrique de PETTITT

Hypothèse nulle (absence de rupture) **acceptée** au seuil de confiance de 99%
Hypothèse nulle (absence de rupture) **acceptée** au seuil de confiance de 95%
Hypothèse nulle (absence de rupture) **acceptée** au seuil de confiance de 90%

Méthode bayésienne de LEE et HEGHINIAN

RE

Segmentation de HUBERT

Niveau de signification du test de Scheffé: **1%**

Début	Fin	Moyenne	Ecart type
1970	1970	8.200	0.000
1971	2004	0.644	0.629

APPENDIX B1

(Allam et al., 2020a)

Allam A., El Hassan J., Najem W., Bocquillon C., Moussa R., 2020. Classification climatique méditerranéenne pour l'hydrologie. La Houille Blanche Vol. 1, 60 – 69. https://doi.org/10.1051/lhb/2020008

La Houille Blanche 2020, 1, 60–69

https://doi.org/10.1051/lhb/2020008

Disponible en ligne :
www.shf-lhb.org

ARTICLE DE RECHERCHE / RESEARCH ARTICLE

Classification climatique méditerranéenne pour l'hydrologie

Antoine Allam[1,2,*], Jinane El Hassan[1], Wajdi Najem[1], Claude Bocquillon[1] et Roger Moussa[2]

[1] CREEN, ESIB, Univ. Saint Joseph, Beyrouth, Liban
[2] UMR LISAH, Univ. Montpellier, INRA, Montpellier, France

Reçu le 31 juillet 2018 / Accepté le 5 février 2020

Résumé – La Méditerranée est une zone tempérée occupée par diverses populations la rendant une des régions les plus sensibles aux changements anthropiques et climatiques. L'objectif de ce travail est d'établir une classification climatique pour l'hydrologie qui met en évidence la continuité climatique d'un lieu à un autre et pourrait évaluer les tendances des changements. La démarche proposée comporte une Analyse en Composantes Principales pour réduire le nombre des indices climatiques et ne considérer que les plus contributaires, une classification en *K*-moyennes pour distribuer les stations en un certain nombre de classes, ici 5 et finalement la construction d'un arbre de décision à partir des distances aux noyaux des classes climatiques pour déterminer si un lieu quelconque possède ou non un climat méditerranéen et à quel type appartient-il. Les données de 144 stations au pas de temps mensuel dans 20 pays méditerranéens sont utilisées pour caler la classification, 36 autres stations pour vérifier cette classification en Méditerranée et 21 stations pour la vérifier au Chili et en Afrique du Sud connus pour leur climat à caractère Méditerranéen. Les résultats montrent que la distribution en 5 classes coïncide avec une distribution géographique en Méditerranée et l'analyse de la connexité interclasse montre que l'évolution du climat se fait de façon continue, puisqu'une même station peut obéir aux critères d'appartenance de plusieurs classes.

Mots clés : climatologie méditerranéenne / hydrologie / classification climatique / *K*-moyennes / ACP

Abstract – Mediterranean climatic classification for hydrology. The Mediterranean region is a temperate zone where various populations live, making it one of the most sensitive regions to anthropic and climatic changes. The objective of this study is to establish a fine climate classification in the Mediterranean region that highlights the climatic continuity from one place to another and could evaluate changes trends. The proposed approach includes a Principal Component Analysis to reduce the number of climate indices to consider only the most contributory, a classification in *K*-means to distribute the stations into 5 classes here and finally the construction of a decision tree based on the distances to the climatic classes kernels to determine whether a place belongs to a Mediterranean climate or not, and to which type it belongs to if so. Data from 144 stations at monthly time steps in 20 Mediterranean countries, inside and outside the watersheds periphery are used to calibrate the classification, 36 stations to verify it within Mediterranean region and 21 stations to verify it on regions known for their Mediterranean climate as Chile and South Africa. The results show that the distribution into 5 classes coincides with a geographical distribution in the Mediterranean and the interclass connectivity analysis shows that the evolution of the climate is done in a continuous way, since the same station can obey the criteria of membership of several classes.

Keywords: mediterranean climatology / hydrology / climatic classification / *K*-means / PCA

1 Introduction

Le climat Méditerranéen est le résultat du fonctionnement complexe d'un bassin évaporatoire important situé dans une zone balayée par les perturbations cycloniques. La répartition des masses d'air maritimes et terrestres crée un système complexe de zones « permanentes » de basses pressions provenant de l'Islande et du Golfe Persique, et de hautes pressions provenant des Açores et de Sibérie (Clerget, 1937).

Les déplacements saisonniers de ces zones « permanentes » sont amplifiés par des mécanismes de plus grande échelle, l'Oscillation Nord Atlantique (ONA), l'El Niño Southern Oscillation (ENSO) et les Moussons (Lionello *et al.*, 2006) qui jouent un rôle important dans la formation du climat

*Correspondance : antoine.allam@net.usj.edu.lb

méditerranéen. Ce climat est variable spatialement et temporellement, avec en général des hivers humides et froids entre septembre et avril et des étés chauds et secs entre mai et août. De ce fait, le climat méditerranéen a permis depuis plus de 4000 ans, l'évolution des systèmes culturaux et sociaux qui ont mené à l'expansion démographique avec plus de 510 millions d'habitants des pays méditerranéens (PlanBleu, 2018) et 400 Millions de touristes annuellement (World Tourism Organization, 2019) ainsi que l'activité agricole qui constituait en 2005 12 % du PIB des pays du Sud et 3 % des pays du Nord (Mediterra, 2008). Cette alternance continue de basses et hautes pressions fait de la Méditerranée une zone tempérée occupée par diverses populations la rendant une des régions les plus sensibles aux pressions anthropiques causées par le développement agricole, industriel, touristique, urbain et démographique avec l'amélioration du niveau de vie (PlanBleu, 2012). Les pressions anthropiques sont amplifiées par les pressions dues au changement climatique et auront plusieurs conséquences sur le climat avec la baisse des précipitations et la hausse des températures en Méditerranée (IPCC, 2013). Ceci va mener à la diminution des débits des sources et cours d'eau, la baisse des niveaux de nappes augmentant ainsi le risque de pénuries d'eau (Hreiche *et al.*, 2007 ; Fernandez *et al.*, 2014). Une classification fine qui décompose la région méditerranéenne en plusieurs classes, basée sur des indices hydroclimatiques telle la saisonnalité des précipitations permet de mieux connaître le milieu, de suivre les activités hydrologiques (gestion des ressources, crues et étiages) et les activités éco-hydrologiques telles l'agriculture, afin de prévoir l'évolution future.

La science des classifications ou taxonomie vise à séparer un ensemble d'individus en groupes présentant des caractères semblables. Elle a été surtout développée par les naturalistes (Linné, 1748). Mais Thornthwaite (1948) remarque que le problème de la classification des climats ne relève pas de la même approche, puisqu'on passe d'un climat à un autre de façon continue alors que les diverses espèces de poissons par exemple sont tout à fait individualisées. Cette continuité peut être mise en évidence à l'aide d'une classification d'un nombre de stations rapprochées. Pour aboutir à cette classification fine, il est indispensable d'introduire des indices numériques assurant une échelle de variation continue.

Les méthodes de classification automatique essaient de construire une partition d'un ensemble d'objets en connaissant les distances deux à deux de façon que les classes formées soient les plus homogènes possible tout en restant distinctes entre elles. Comme toute classification, la méthode dépend de l'objectif recherché et de la spécificité du sujet. On distingue plusieurs modes de classifications des climats :

1 Les classifications génétiques liées aux causes météorologiques et à l'origine des masses d'air (Tor Bergeron, 1928) ;
2 Les classifications bioclimatologiques basées sur l'interrelation entre type de végétation et climat (Holdridge, 1947 ; Mather et Yoshioka, 1968) ;
3 Les méthodes agro-climatiques basées sur l'évaluation du bilan pluie-évapotranspiration potentielle (Thornthwaite, 1948) en vue d'une estimation de la productivité agricole ;
4 Les méthodes climatiques basées sur les variables de pluies et de températures telle la classification de Köppen (1936) qui reste la plus utilisée. Elle répartit le globe terrestre en trente zones climatiques et s'appuie sur une hiérarchie de partition. Les climats méditerranéens sont classés en (Csa) et (Csb) ; (Csa) correspond à un été chaud avec la température du mois le plus chaud qui dépasse 22 °C et (Csb) correspond à un été tempéré avec le nombre de mois qui dépasse une température mensuelle de 10 °C, supérieur ou égal à 4 mois.

Sur la zone côtière du pourtour méditerranéen, où le climat (Cs) prédomine, il existe d'autres climats tels que celui en Egypte et en Libye au climat désertique de classe (BWh), celui au Sud-Est de l'Espagne de classe aride froid (Bsk) où la température moyenne annuelle ne dépasse pas 18 °C et celui des régions de Thessalonique et de Vénétie où la saisonnalité disparaît avec la classification (Cf) puisqu'aucune saison sèche n'existe. En revanche, il y a quelques régions du globe en dehors de la Méditerranée où la classe (Cs) domine, principalement en Californie, Chili et Afrique du Sud indiquant l'indépendance de (Cs) de la zone géographique.

Il existe plusieurs études de classification climatique en Méditerranée. Parmi ces études on cite la classification des systèmes synoptiques en Méditerranée (Trigo *et al.*, 1999 ; Alpert *et al.*, 2004), celle des nuages (Chéruy et Aires, 2009) et la décomposition en régions climatiques à partir des séries de précipitations et de températures au niveau national en France, en Turquie et dans d'autres pays (Erinç, 1984 ; Champeaux et Tamburini, 1996 ; Ünal *et al.*, 2003 ; Sönmez et Kömüscü, 2011 ; Eveno *et al.*, 2016). Néanmoins, aucune classification basée sur des indices dédiés à l'hydrologie, à partir des séries de précipitations et de températures, n'a encore traité la région méditerranéenne en tant qu'une région homogène climatiquement.

L'objectif de ce travail est alors d'établir une classification climatique fine qui décompose la région méditerranéenne en plusieurs classes et qui met en évidence la continuité climatique d'un lieu à un autre et pourrait évaluer les tendances des changements en simulant l'effet des scénarios de hausse de température et la variabilité des précipitations sur les indices choisis et leurs conséquences sur les régions classées. Cette classification nécessite l'examen des indices des séries mensuelles moyennes de précipitations et de températures. La démarche proposée comporte une Analyse en Composantes Principales pour réduire le nombre des indices climatiques et ne considérer que les plus significatifs, une classification en *K*-moyennes (nuées dynamiques) pour distribuer les stations en classes et finalement la construction d'un arbre de décision à partir des distances aux noyaux des classes climatiques pour déterminer si un lieu quelconque possède ou non un climat méditerranéen et à quel type il appartient.

2 Méthodologie

2.1 Indices climatiques

Les indices climatiques considérés dans cette étude sont en relation directe ou indirecte avec les différents éléments du climat comme la pluie et la température. Le caractère saisonnier des variables climatiques fait que ces indices sont issus d'un ensemble de douze valeurs mensuelles ordonnées avec le début de l'année hydrologique choisi au 1er septembre en Méditerranée.

En général, les indices climatiques permettent de mettre en relief les similarités entre les différentes régions et de réaliser dans la suite une certaine classification climatique. Il est

évident qu'un certain nombre d'indices représentent des propriétés climatiques voisines. Ils seront triés ultérieurement par l'Analyse en Composantes Principales. Les indices proposés sont répertoriés en quatre groupes et résumés dans le tableau 1 ci-dessous.

2.2 Méthodologie de classification

2.2.1 Analyse en composantes principales

Le nombre optimal d'indices climatiques a été déterminé à partir d'une Analyse en Composantes Principales (ACP). L'ACP a été introduite par Pearson (1901) et développée dans la suite par Hotelling (1933). L'ensemble des données forme un « nuage de n points » représentés dans un espace à *p* dimensions. Le principe de l'ACP est d'obtenir une représentation approchée du nuage dans un sous-espace à *k* dimensions, avec *k* inférieur à p, par projection sur des axes nommés composantes principales (Jolliffe, 2002). L'ACP construit ainsi de nouvelles variables et des représentations graphiques permettant de visualiser les relations entre variables initiales, et de mettre en évidence l'existence éventuelle de groupes d'observations et de groupes de variables. L'ACP est disponible dans plusieurs logiciels statistiques, en particulier XLSTAT Ver. 2016 utilisé pour cette étude.

2.2.2 Méthode des *K*-moyennes

La méthode des *K*-moyennes permet de répartir un ensemble de données en *k* classes homogènes. Elle a été introduite par Forgy (1965) et McQueen (1967). Cette méthode a gagné en réputation ces dernières décennies dans les études d'analyse des nuages dans les images satellites (Desbois *et al.*, 1982) et de la classification et régionalisation climatologique à partir de séries chronologiques mesurées de température et de précipitations ou simulées en cas d'étude de changement climatique (Fovell et Fovell, 1993 ; Moron *et al.*, 2008 ; Carvalho *et al.*, 2016).

Les méthodes de classifications non supervisées consistent à partitionner l'espace en classes isolées les unes des autres. Dans cette optique, la méthode des *K*-moyennes vise à minimiser la distance euclidienne du point au noyau de sa classe et à maximiser la distance vers d'autres classes. Les étapes de l'optimisation commencent par (1) l'initialisation des noyaux, le noyau étant un point virtuel qui représente le centre statistique d'une classe, (2) la mise à jour des classes, (3) la réévaluation des noyaux et (4) la répétition des étapes (2) et (3) jusqu'à la stabilisation des noyaux. Cet algorithme vise à réduire au minimum la fonction objectif erreur carrée. La qualité de la solution ainsi trouvée dépend fortement des noyaux initiaux. De plus, la sensibilité à l'initialisation est d'autant plus grande que l'écart des données est grand. Par ailleurs, l'application des *K*-moyennes demande de définir le nombre de classes, sinon l'algorithme de minimisation conduit à construire autant de classes que d'individus. La méthode des *K*-moyennes a été appliquée à l'aide du logiciel STATISTICA Ver. 13.

Concernant le nombre de classes à retenir, nous cherchons une classification qui repartit la zone côtière intermédiaire en 3 classes au moins auxquelles nous ajoutons la délimitation des régions Nord (Paris, Nantes, Lille) et Sud (désert Libye, Algérie) sans dépasser un trop grand nombre de classes qui produirait une zonation morcelée ininterprétable, d'où le choix de 5 classes.

2.2.3 Arbre de décision et classification de nouvelles stations

La construction d'un arbre de décision tel proposé par Breiman *et al.* (1984), repose sur la détermination de critères de distance aux divers noyaux de classes. Ces critères sont développés sous forme d'une hiérarchie de questions qui conduit à un diagnostic connu. Pour la construction de l'arbre de décision on procède ainsi :

- calcul des indices bruts obtenus après réduction du nombre d'indices par ACP, à normaliser suivant les moyennes et écart-types issus du traitement de toutes les stations ;
- calcul des distances d_k aux centres de gravité des noyaux de chaque classe ;
- détermination des critères d'appartenance à chaque classe.

Pour ajouter de nouvelles stations, il n'est pas nécessaire de reprendre la classification mais il suffit de suivre la procédure détaillée ci-dessus qui répartira les stations selon leurs distances aux noyaux.

3 Base de données

L'étude a porté sur 144 stations réparties sur les pays ayant une côte sur la Méditerranée pour le calage de la classification. Parmi les 144 stations en Méditerranée, 105 sont à l'intérieur de la limite hydrologique et 39 hors de cette limite. 102 stations sont dans les limites des classes de Köppen du climat méditerranéen (Csa) et (Csb) et 42 à l'extérieur. La longueur moyenne des séries climatiques est de 60 ans au pas de temps mensuel, dont 4 stations de 30 ans de données, 50 stations de plus de 60 ans de données et 6 stations de plus de 100 ans de données. La période 1960–1990 est commune à l'ensemble des stations considérées. La qualité des données (*i.e.* ellipse de Bois ; Bois, 1986) a été vérifiée pays par pays en raison des différences de traitement liées aux habitudes des différents services nationaux sachant que seules les années hydrologiques complètes ont été conservées pour le calcul des indices. L'ensemble des indices climatiques constitue une population de variables qui sera traitée par diverses méthodes d'analyse. Une analyse (non présentée ici) a montré que les distributions des indices suivent une distribution normale indiquant le phénomène naturel issu d'évènements aléatoires, à l'exception de quelques indices qui seront rejetés à la suite de l'ACP. Pour vérifier cette classification par l'arbre de décision on a considéré 36 autres stations en Méditerranée et 21 stations en Afrique du Sud et au Chili où un climat méditerranéen existe (Fig. 1). Toutes les stations font partie de l'ensemble des stations considérées par l'Organisation Météorologie Mondiale (OMM) et disponibles en accès libre sur le portail de l'Administration Nationale des Océans et de l'Atmosphère des États-Unis (NOAA). Ces données ont été utilisées dans 3 étapes successives :

- calcul de l'ACP ;
- classification en *K*-moyennes des 144 stations en Méditerranée ;
- construction de l'arbre de décision et vérification de la classification sur les 36 stations en Méditerranée et 21 stations en Afrique du Sud et au Chili.

Tableau 1. Liste des 19 indices climatiques utilisés dans cette étude.

Groupe	Type	Indice climatique	Description
I	Indices climatiques fonctions de la pluie moyenne mensuelle	Indice de saisonnalité I_S	Écart de pluie entre la saison pluvieuse et la saison sèche avec P_i pluie mensuelle (mm). I_s tend vers 1 quand les saisons sont bien définies $I_s = 1 - \frac{min\ C_i}{\max\ C_i}$ avec $C_i = \sum_i^{i+2} P_i$
		Indices adimensionnels de pluie $P_{25\%}$ et $P_{75\%}$	Régularité de la pluviosité à partir de la courbe des pluies mensuelles adimensionnelles classées $\frac{P_i}{\overline{p}}$ dépassées durant 25 % et 75 % du temps avec $\overline{p}$ moyenne des pluies mensuelles (mm)
		Indices seuils de pointe $S_{P1,5}$, $S_{P1,7}$ et S_{P2} (mois)	Nombre de mois dépassant la moyenne des pluies mensuelles $\overline{p}$ par un facteur de 1,5, 1,7 et 2.
		Indice d'Inertie Horizontale I_{Hor}	Dispersion des valeurs de la pluie mensuelle par rapport à la moyenne des pluies mensuelles $\overline{p}$ $I_{Hor} = \sqrt{\sum_{i=1}^{12} \left(\frac{P_i}{\overline{p}} - 1\right)^2}$
		Indice d'Inertie Verticale I_{Ver}	Regroupement de la pluie autour de la date $\overline{t}$ où l'on atteint la médiane de la pluie moyenne annuelle P $I_{Ver} = \sqrt{\sum_{i=1}^{12} \left(\frac{t_i - \overline{t}}{(\overline{t})}\right)^2 \times \frac{p_i}{P}}$
II	Indices climatiques fonctions de la température moyenne mensuelle	Amplitude de l'écart thermique ΔT_1 (°C)	Écart thermique entre le mois le plus froid et le mois le plus chaud $\Delta T_1 = T_{\max} - T_{\min}$
		Amplitude de l'écart thermique ΔT_2 (°C)	Écart thermique entre les trois mois consécutifs les plus chauds et les trois mois consécutifs les plus froids
		Indices de température adimensionnelle $T_{25\%}$ et $T_{75\%}$	Régularité de la température à partir de la courbe des températures mensuelles adimensionnelles classées $\frac{T_i}{\overline{t}}$ dépassées durant 25 % et 75 % du temps avec $\overline{T}$ moyenne des températures mensuelles (°C)
		Indices seuils S_{T1} et $S_{T1,2}$ (mois)	Nombre de mois dépassant la température moyenne par un facteur de 1 et 1,2
		Indice degrés jour D_J	Décomposition des régions en zones suivant la nécessité de chauffage de l'habitat pour un seuil de température mensuelle de 18 °C $D_l = \sum_{i=1}^{12} n_i \times (18 - T_i)$ Avec T_i la température mensuelle moyenne du mois et n_i le nombre de jour
		Indice seuil moyenne S_{Tm} (mois)	S_{Tm} est le nombre de mois de l'année ayant une température moyenne supérieure à la température moyenne annuelle T_m
III	Indices climatiques mixtes	Indices de décalage temporel I_{Decal} (mois)	Décalage temporel entre le mois le plus froid et le mois le plus pluvieux
IV	Indices climatiques fonctions de l'Evapotranspiration	Indice d'aridité I_{Arid}	Rapport de l'ETP annuelle à la pluie annuelle $I_{arid} = \frac{ETP}{P}$; ETP calculée selon Turc (1961)
		Indice seuil S_{ETP}	Nombre de mois pendant lesquels la précipitation mensuelle dépasse l'ETP mensuelle

4 Résultats

4.1 ACP

La matrice de corrélation des indices climatiques permet d'éliminer les indices fortement corrélés (corrélations supérieures à 0,9) et qui peuvent fausser les résultats de l'ACP dans la suite :

- I_s et $P_{25\%}$ sont fortement corrélés en sens inverse (−0,937). I_s est retenu ;
- ΔT_1 et ΔT_2 sont fortement corrélés (0,997). ΔT_1 est retenu ;

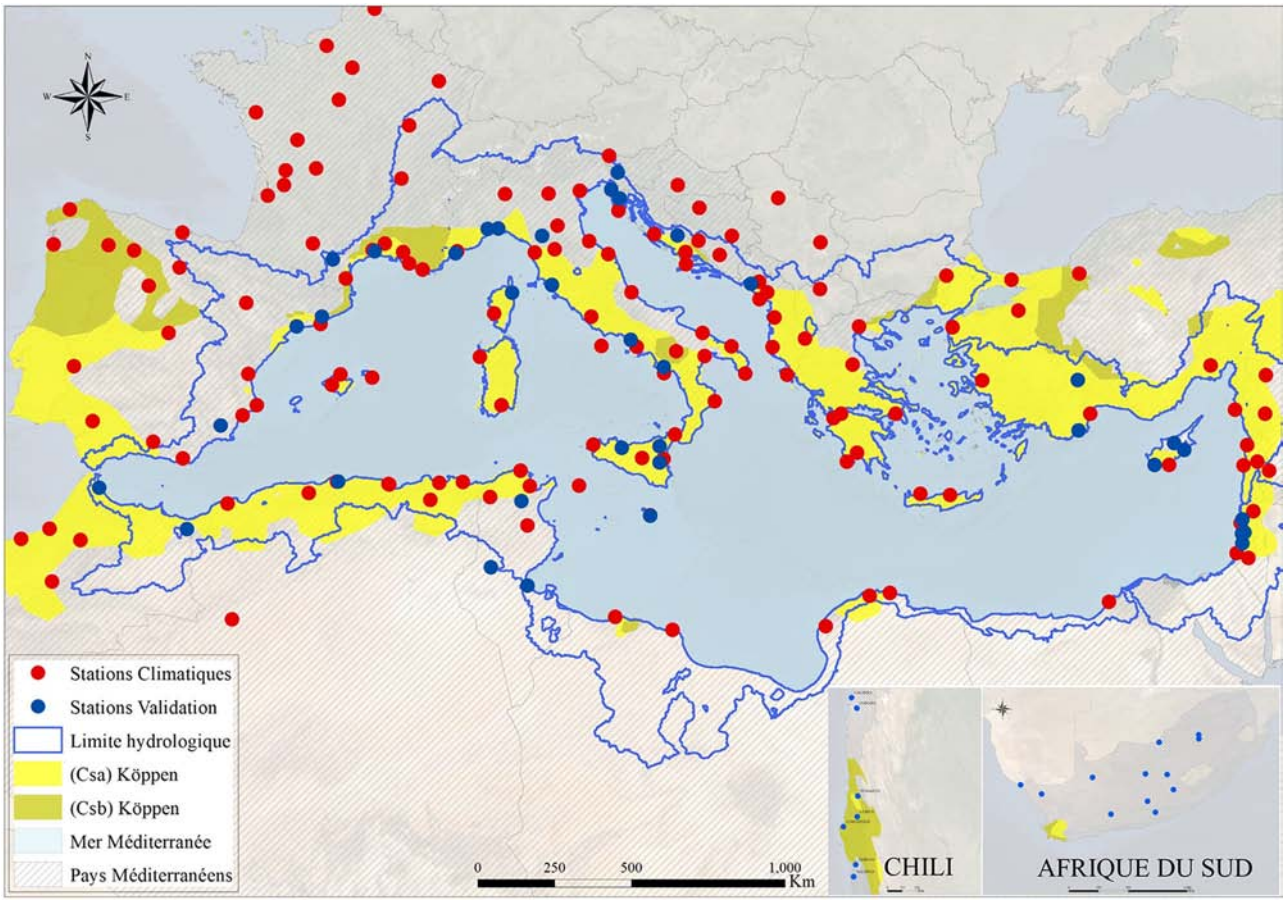

Fig. 1. Carte de localisation des 144 stations de calage (rouge), des 36 stations en Méditerranée et 21 stations au Chili et en Afrique du Sud de validation (bleu).

– $T_{25\%}$ et $T_{75\%}$ sont fortement corrélés en sens inverse (−0,976). $T_{25\%}$ est retenu ;
– D_j et $T_{25\%}$ sont fortement corrélés (0,917). $T_{25\%}$ est retenu.

La première opération a donc permis d'éliminer les 4 indices $P_{25\%}$, ΔT_2, $T_{75\%}$ et D_j et de ne retenir que 15 indices sur les 19 présentés dans le tableau 1. La matrice de corrélation transformée en une matrice diagonale permet de trouver les valeurs propres représentant la qualité de la projection en passant de p (15 indices) à *k* dimensions (ici 2 composantes). La matrice des vecteurs propres est l'expression linéaire des indices par rapport aux composantes principales (Fig. 2).

La première valeur propre 10,9 représente 57 % de la variance et la seconde 2,8 représente 15 %. Les deux premiers facteurs F1 et F2 représentent les deux plus grandes variances et 72 % de la variance totale est donc préservée avec ce choix de conserver les deux premiers facteurs.

Le cercle des corrélations présenté à la figure 3, correspond à une projection des variables initiales sur un plan constitué par les deux premiers facteurs F1 et F2. Seuls les indices qui ont marqué des corrélations supérieures à 0,85 sur l'un des axes ont été retenus. Ceci a réduit le nombre des indices de 15 à 6 indices peu corrélés entre eux et qui ont une contribution significative d'où le choix de I_s, $P_{75\%}$, $S_{P1,5}$, I_{Hor}, $T_{25\%}$ et S_{Tm}.

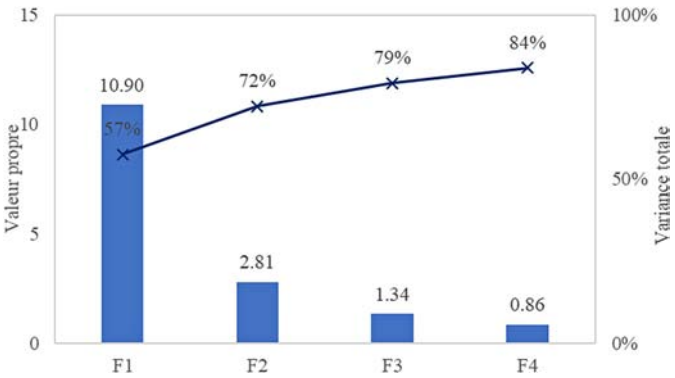

Fig. 2. Valeurs propres et variance totale.

4.2 *K*-moyennes

4.2.1 Les noyaux des classes

Une classification des 144 stations en 5 classes a été retenue puisqu'elle montre une répartition optimale qui sépare les climats méditerranéens du Nord, des climats méditerranéens de la zone côtière classifiés en 4 classes et qui met en relief la variabilité climatique tout en restant continue. Les coordonnées des noyaux des cinq classes obtenues sont

Indices	F1	F2
I_s	0.92	0.12
P_{75}	-0.92	-0.25
$S_{P1.5}$	0.87	0.19
$S_{P1.7}$	0.83	0.30
S_{P2}	0.77	0.32
I_{Hor}	0.94	0.27
I_{Ver}	-0.35	-0.58
ΔT_1	-0.59	0.72
T_{25}	-0.85	0.43
S_{T1}	-0.26	0.32
$S_{T1.2}$	-0.68	0.53
I_{Decal}	-0.64	-0.25
S_{ETP}	-0.64	-0.18
S_{Tm}	0.87	0.08
I_{Arid}	0.62	0.23

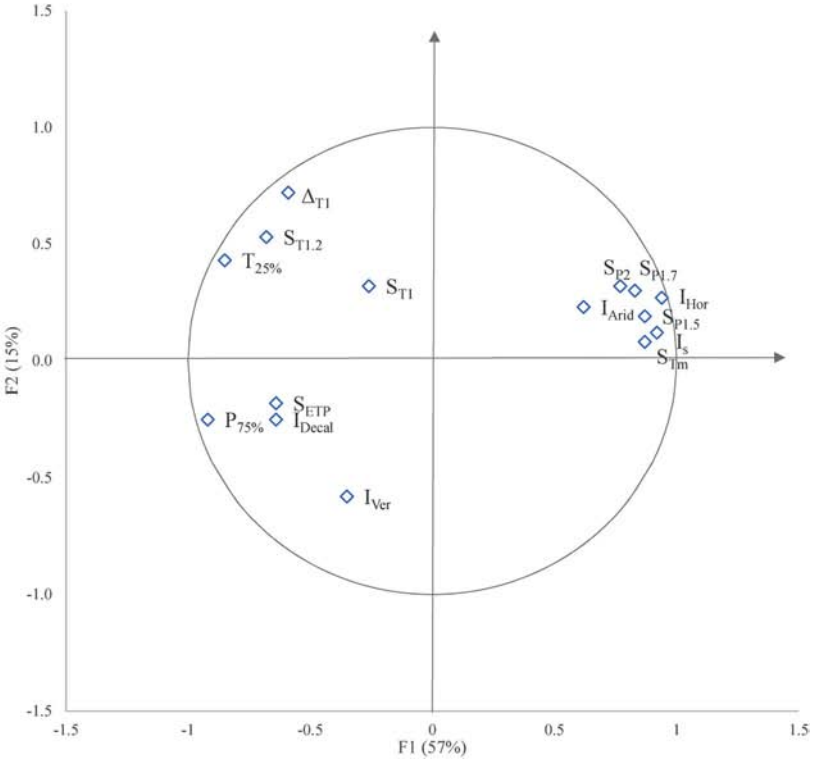

Fig. 3. Cercle et tableau des corrélations aux deux premiers facteurs F1 et F2.

représentées dans la figure 4 et la cartographie géographique des stations classées en figure 5.

Cette cartographie marque un certain regroupement géographique des stations. En sommaire :

- les classes 1 et 2 regroupent les stations de la zone centrale, depuis l'Espagne jusqu'en Grèce ;
- la classe 3 regroupe les stations du Sud et de l'Est de la Méditerranée ;
- la classe 4 regroupe les stations côtières du Nord-Ouest de la Méditerranée ;
- la classe 5 regroupe les stations du Nord : Paris, Lyon, Milan...

On remarque dans cette cartographie que la totalité des stations situées dans les régions climatiques (Csa) et (Csb) sont de classes 1, 2, 3 ou 4 et toutes les stations de classe 5 se trouvent à l'extérieur de ces régions ce qui valide la nouvelle classification par rapport à celle de Köppen. En contrepartie, les stations situées à l'extérieur de (Csa) et (Csb) mais à l'intérieur de la limite des bassins versants méditerranéens sont de toutes les classes et principalement les stations du Sud de l'Espagne situées dans un climat aride froid (Bsk).

La diversité des classes des stations situées au sein de (Csa) ou (Csb) indiquent une variabilité intra climatique. Cette variabilité est claire dans le profil indiciel des noyaux des classes (voir Fig. 4). Elle est principalement due à la variabilité et la complexité de la saisonnalité sur le pourtour méditerranéen. Cette complexité, qui a été identifiée par les différents indices présentés au début, est supérieure à celle définie par Köppen et limitée aux critères simples d'un hiver humide et un été sec ou tempéré.

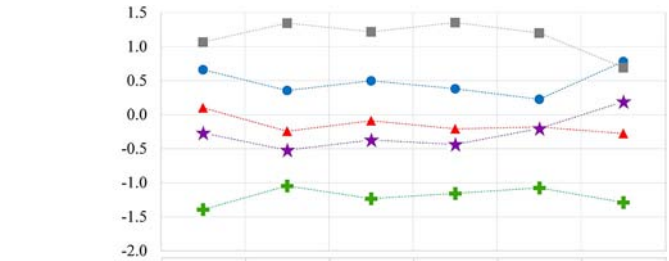

CLASSE	I_s	$P_{75\%}$	$S_{P1.5}$	I_{Hor}	S_{Tm}	$T_{25\%}$
▲CLASSE1	0.10	-0.24	-0.09	-0.21	-0.18	-0.28
●CLASSE2	0.66	0.36	0.50	0.38	0.23	0.78
■CLASSE3	1.07	1.35	1.22	1.36	1.20	0.69
★CLASSE4	-0.27	-0.52	-0.37	-0.44	-0.20	0.19
✚CLASSE5	-1.39	-1.05	-1.23	-1.16	-1.07	-1.29

Fig. 4. Coordonnées et profil indiciel des noyaux des classes.

4.2.2 Analyse de la connexité

La méthode des *K*-moyennes agglomère les stations en classes disjointes avec un certain flou lié à la continuité du climat. Néanmoins, des incertitudes interclasses peuvent toujours exister ; à titre d'exemple la station Potenza au Sud d'Italie groupée avec la classe 1 plutôt que la classe 4 prédominante dans la région. Pour avoir une vue plus nuancée de l'appartenance aux diverses classes, on a analysé classe par classe les distances aux noyaux les plus proches et l'ensemble de ces liaisons est résumé dans le tableau et le graphe de connexité associé à la figure 6. On remarque que :

- les classes 1, 2 et 4 sont connectées entre elles 2 à 2 et représentent la Méditerranée centrale ;

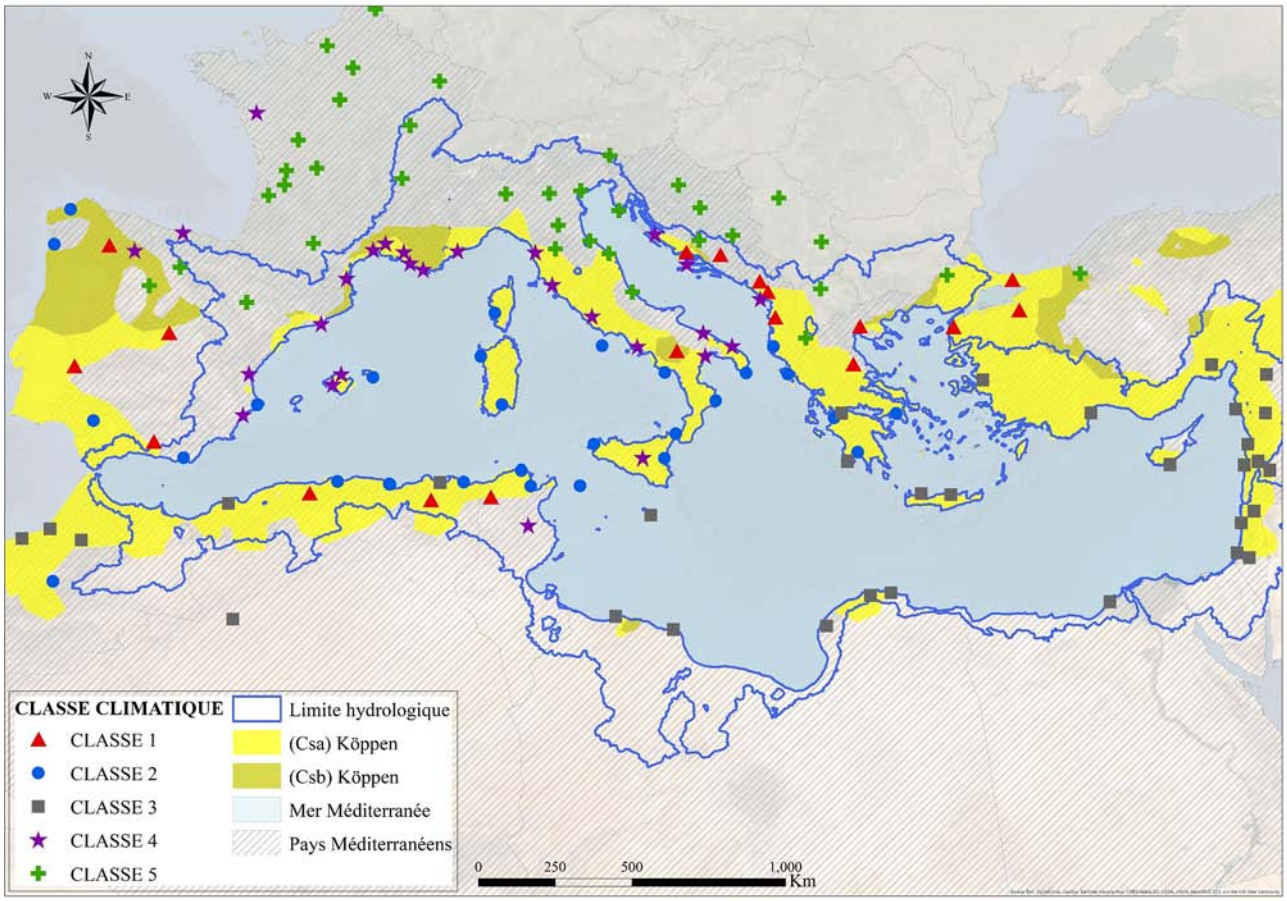

Fig. 5. Carte de classification des stations méditerranéennes.

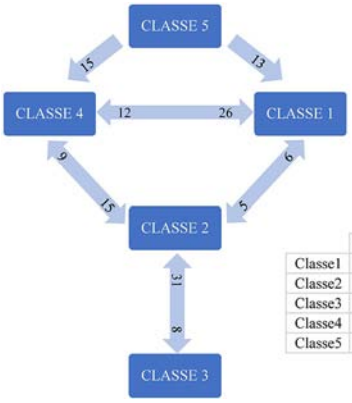

	Classe1	Classe2	Classe3	Classe4	Classe5
Classe1	18	5	1	12	0
Classe2	6	29	8	15	0
Classe3	2	31	33	0	0
Classe4	26	9	0	35	0
Classe5	13	0	1	15	29

Fig. 6. Graphe de connexité interclasses.

– la classe 3 ne présente de connexion qu'avec la classe 2. Cette classe exprime une borne de la classification correspondant à un climat extrême ;
– aucune station des classes 1, 2, 3, 4 ne présente en deuxième classification la classe 5 ; ceci confirme que les stations de la classe 5 sont hors du climat méditerranéen.

La connexité interclasses montre que la méthode des *K*-moyennes est robuste pour distinguer 5 classes distinctes. Le climat reste une variable continue, cette zonation est cependant utile pour éviter une estimation ponctuelle impossible.

Tableau 2. Table de normalisation des indices des nouvelles stations.

	I_s	$P_{75\%}$	$S_{P1,5}$	I_{Hor}	S_{Tm}	$T_{25\%}$
Moyenne	0,72	1,49	2,08	1,83	5,95	0,55
Écart-type	0,24	0,29	1,51	0,94	1,58	0,16

4.2.3 Construction de l'arbre de décision et classement d'une nouvelle station

On a construit l'arbre de décision hiérarchique à partir des distances euclidiennes de l'échantillon initial aux 5 noyaux produisant ainsi des critères d'appartenances. Cette méthode a donné une nouvelle répartition de l'échantillon avec une bonne concordance de 86 % à la classification initiale. Les cas de non-concordance correspondent aux stations situées à la frontière de deux classes. Pour classer une nouvelle station n'appartenant pas à l'échantillon initial, on calcule les 6 indices bruts de la nouvelle station Ij = (Is, P75 %, SP1,5, IHor, T25 % et STm), on les normalise suivant les moyennes et écart-types issus du traitement et fournis dans le tableau 2 et on applique les critères d'appartenance suivants, avec d_x la distance au noyau de la classe x (voir Fig. 7).

– si $d_3 > 4{,}29$ et $d_2 > 4{,}13 \rightarrow$ Classe 5 ;

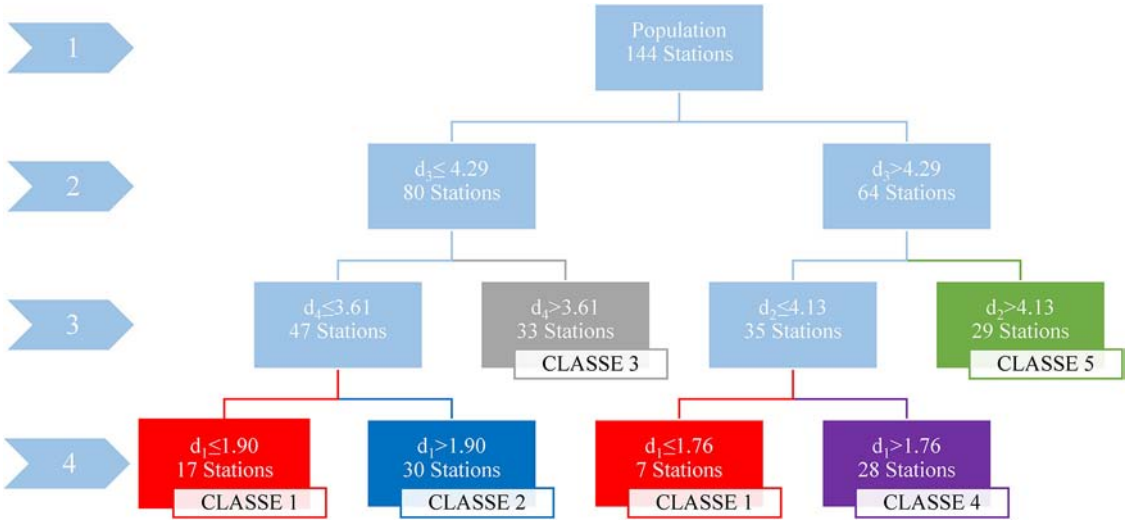

Fig. 7. Arbre de décision de la classification.

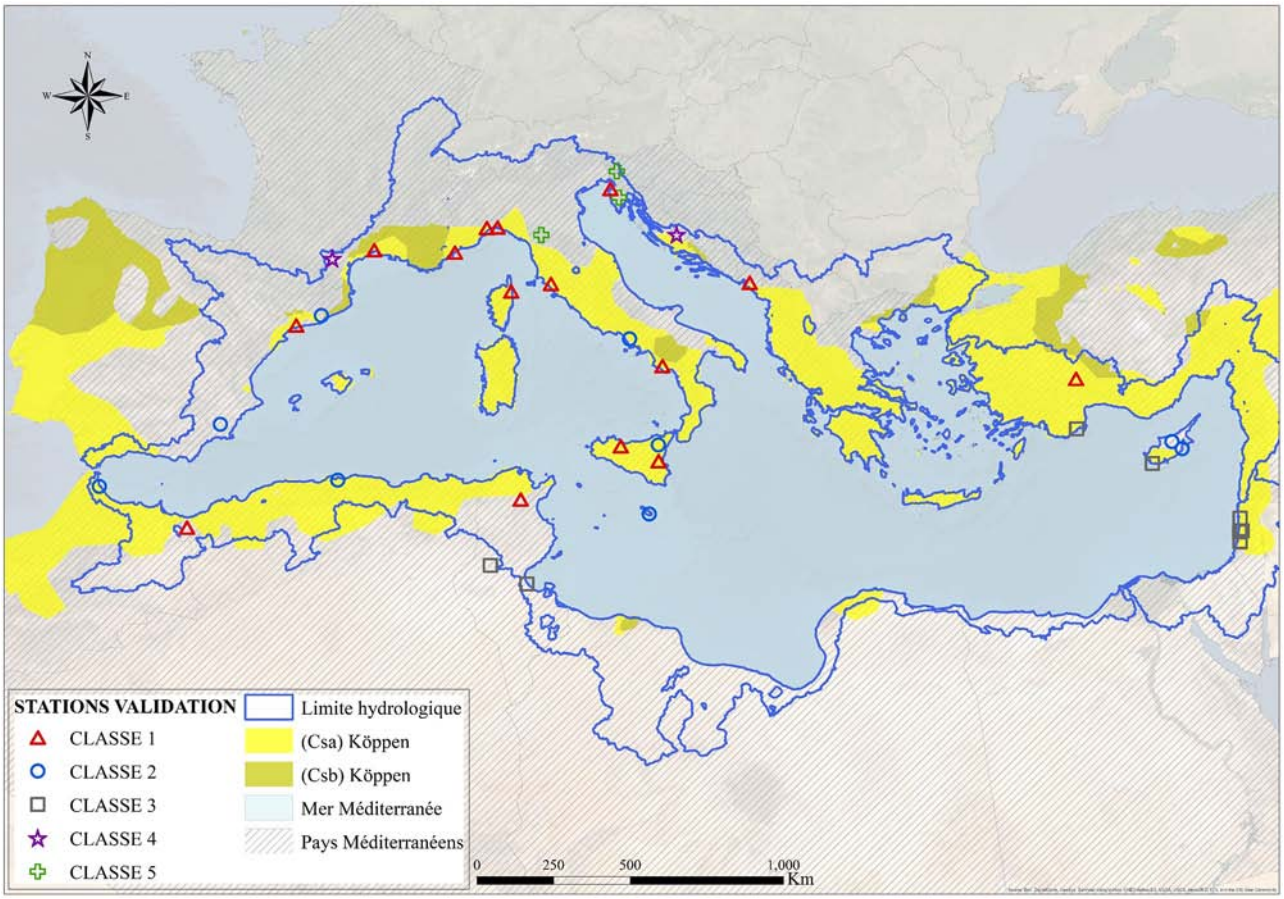

Fig. 8. Vérification de la classification climatique en Méditerranée.

- si $d_3 > 4{,}29$ et $d_2 \leq 4{,}13$ et $d_1 \leq 1{,}76 \rightarrow$ Classe 1 ou $d_3 \leq 4{,}29$ et $d_4 \leq 3{,}61$ et $d_1 \leq 1{,}90 \rightarrow$ Classe 1 ;
- si $d_3 \leq 4{,}29$ et $d_4 \leq 3{,}61$ et $d_1 > 1{,}90 \rightarrow$ Classe 2 ;
- si $d_3 \leq 4{,}29$ et $d_4 > 3{,}61 \rightarrow$ Classe 3 ;
- si $d_3 > 4{,}29$ et $d_2 \leq 4{,}13$ et $d_1 > 1{,}76 \rightarrow$ Classe 4.

L'applicabilité de cette classification a été vérifiée sur 36 stations en Méditerranée et 21 stations en Afrique du Sud et au Chili, connus pour leur climat à caractère méditerranéen. Les cartes de classification obtenues sont présentées dans les figures 8 et 9.

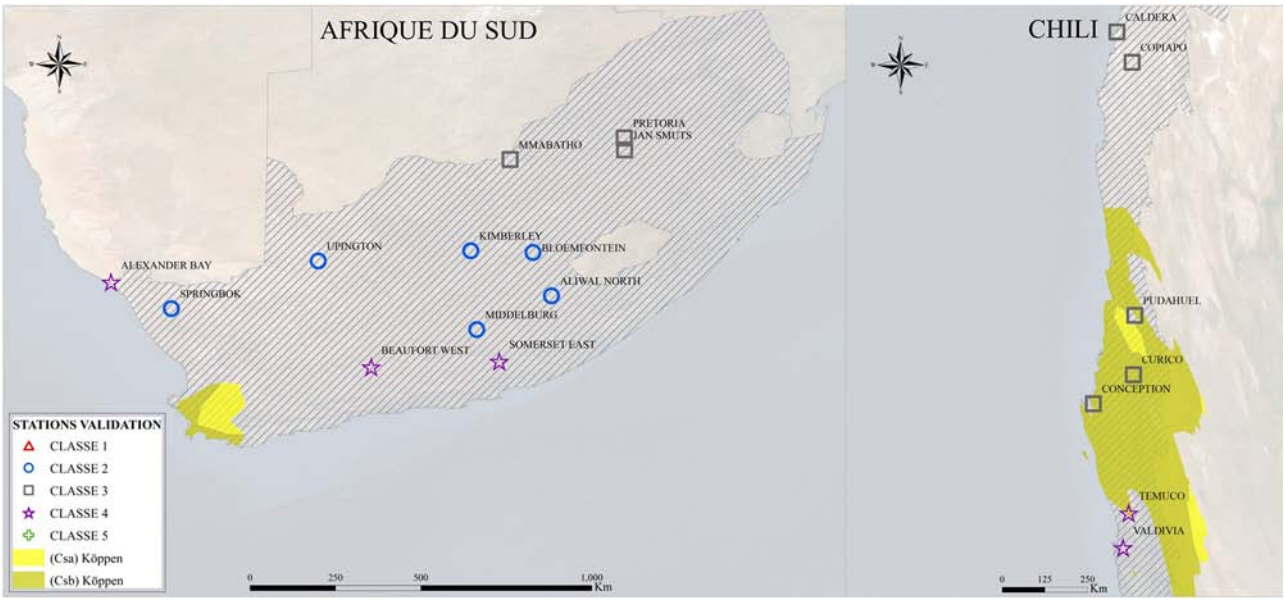

Fig. 9. Vérification de la classification climatique en Afrique du Sud et au Chili.

On observe en figure 8 qu'en Méditerranée la répartition reste similaire à celle obtenue en *K*-moyennes en figure 5 avec les stations des classes 1 et 2 situées dans la zone centrale, avec celles de la classe 3 situées au Sud et Sud-Est, avec celles de la classe 4 situées dans des zones côtières du Nord, à l'exception des stations de la côte française qui se sont classées en classe 1 et finalement celles de la classe 5 situées au Nord d'Italie.

En Afrique du Sud, figure 9, on observe que les caractéristiques climatiques de classe 2 prédominent avec la présence des classes 3 et 4. Alors que la classe 3 prédomine au Chili. L'absence de la classe 5 dans ces deux zones valide le caractère méditerranéen d'une part et la classification d'autre part, puisque les stations sont plutôt rapprochées des noyaux des classes 2, 3 et 4 que de la classe 5 non méditerranéenne.

5 Conclusion

La méthode des *K*-moyennes a défini 5 classes climatiques à partir d'indices climatiques des séries de pluies et de températures mensuelles moyennes de 144 stations. L'analyse de la connexité interclasse montre que l'évolution du climat se fait de façon continue d'un lieu à un autre, puisqu'une même station peut obéir aux critères d'appartenance de plusieurs classes. Un arbre de décision permet de définir à partir des distances aux noyaux des classes, si un lieu quelconque possède un climat méditerranéen ou non, et à quel type de climat méditerranéen il appartient. Cet arbre de décision a été appliqué avec succès à des régions connues pour leurs climats à caractère méditerranéen telles le Chili et l'Afrique du sud.

Les caractéristiques climatiques spécifiques à la Méditerranée, la saisonnalité des précipitations en premier degré, contributeur principal à la classification climatique selon l'ACP, jouent un rôle important dans les mécanismes hydrologiques des cours d'eau méditerranéens et dans la saisonnalité des débits. La classification climatique réalisée dans cette étude sera valorisée ultérieurement dans le cadre d'une classification des bassins versants à partir des bilans hydrologiques et des caractéristiques physiques pour identifier les zones hydrologiquement homogènes, la prévision sur les bassins non jaugés, l'étude des tendances et l'aide à la décision pour une meilleure gestion des ressources en eau en Méditerranée.

Références

Alpert P, Osetinsky I, Ziv B, Shafir H. 2004. Semi-objective classification for daily synoptic systems: Application to the eastern Mediterranean climate change. *Int J Climatol* 24(8): 1001–1011.

Bergeron T. 1928. Dissertation. Université de Bergen.

Bois P. 1986. Contrôle de séries chronologiques corrélées par étude du cumul des résidus de la corrélation. In : *Deuxièmes journées hydrologiques de l'ORSTOM*, pp. 89–100.

Breiman L, Friedman J, Stone CJ, Olshen RA. 1984. Classification and regression trees. Taylor and Francis.

Carvalho MJ, Melo-Gonçalves P, Teixeira JC, Rocha A. 2016. Regionalization of Europe based on a *K*-means cluster analysis of the climate change of temperatures and precipitation. *Phys Chem Earth* Parts A/B/C 94: 22–28.

Champeaux JL, Tamburini A. 1996. Zonage climatique de la France à partir des séries de précipitations (1971–1990) du réseau climatologique d'État. Météo-France. *La Météorologie* 8e série 14: 44–54.

Chéruy F, Aires F. 2009. Cluster analysis of cloud properties over the southern European Mediterranean area in observations and a model. *Mon Weather Rev* 137: 3161–3176.

Clerget M. 1937. Les types de temps en Méditerranée. Paper presented at the *Annales de géographie*.

Desbois M, Seze G, Szejwach G. 1982. Automatic classification of clouds on METEOSAT imagery: Application to high-level clouds. *J Appl Meteorol* 21(3): 401–412.

Erinç S. 1984. Climatology and its methods, 3rd ed. Istanbul, Turkey: Marine Science, Institute of Geography, Istanbul University Press (in Turkish).

Eveno M, Planchon O, Oszwald J, Dubreuil V, Quénol H. 2016. Variabilité et changement climatique en France de 1951 à 2010 : analyse au moyen de la classification de Köppen et des « types de climats annuels ». *Climatologie* 13: 47–70.

Fernandez S, Martin MA, Troy B, Verdier J, Viollet PL. 2014. Prospective et tensions sur l'eau. Des crises de l'eau en 2050 ? In : *Note de synthèse, SHF, AFEID et Académie de l'Eau*.

Forgy E. 1965. Cluster analysis of multivariate data: Efficiency *vs.* interpretability of classifications. *Biometrics* 21(3): 768.

Fovell RG, Fovell MYC. 1993. Climate zones of the conterminous United States defined using cluster analysis. *J Climat* 6(11): 2103–2135.

Holdridge L. 1947. Determination of world formations from simple climate data. *Science* 105: 367–368.

Hotelling H. 1933. Analysis of a complex of statistical variables into principal components. *J Educ Psychol* 24(7): 498–520.

Hreiche A, Najem W, Bocquillon C. 2007. Hydrological impact simulations of climate change on Lebanese coastal rivers. *Hydrol Sci J* 52(6): 1119–1133.

IPCC. 2013. Climate change 2013: The physical science basis. In : Stocker TF, Qin D, Plattner G-K, Tignor M, Allen SK, Boschung J *et al.*, eds. *Contribution of Working Group I to the Fifth Assessment Report of the Intergovernmental Panel on Climate Change*. Cambridge, United Kingdom and New York, NY, USA: Cambridge University Press, 1535 p.

Jolliffe I. 2002. Principal component analysis, 2nd ed. Springer.

Köppen W. 1936. Das geographische System der climate. In : *Handbuch der Klimatologie*. Berlin: Gedruder Borntrager.

Linné C. 1748. *Systema Naturae*, ed. Stocklom: Keisewetter.

Lionello P, Malanotte-Rizzoli P, Boscolo R, *et al*. 2006. The Mediterranean climate: an overview of the main characteristics and issues. *Develop Earth Environ Sci*, Elsevier 4: 1–26.

Mather J, Yoshioka G. 1968. The role of climate in the distribution of vegetation. *Annal Assoc Am Geograph* 58: 29–41.

McQueen J. 1967. Some methods for classification and analysis of multivariate observations. In : *Proceeding of the 5th Berkeley Symposium on Mathematical Statistics and Probability*, pp. 281–97.

Mediterra. 2008. Les futurs agricoles et alimentaires en Méditerranée. Paris : Centre International de Hautes Etudes Agronomiques Méditerranéennes (CIHEAM), Presses de Sciences Po.

Moron V, Robertson AW, Ward MN, Ndiaye O. 2008. Weather types and rainfall over Senegal. Part I: Observational analysis. *J Climate* 21(2): 266–287.

Pearson K. 1901. Principal components analysis. *Edinburgh Dublin Philosoph Mag J*, London 6(2): 566.

PlanBleu. 2012. Les demandes en eau toujours satisfaites en Méditerranée à l'horizon 2050 ? *Les Notes du Plan Bleu.– Sophia Antipolis, Plan Bleu PNUE/PAM*, Vol. 25.

PlanBleu. 2018. Rapport d'activités. Sophia Antipolis : PlanBleu.

Sönmez İ, Kömüscü AO. 2011. Reclassification of rainfall regions of Turkey by *K*-means methodology and their temporal variability in relation to North Atlantic Oscillation (NAO). *Theor Appl Climatol* 106(3): 499–510.

Thornthwaite CW. 1948. An approach toward a rational classification of climate. *Geograph Rev* 38: 55–94.

Trigo IF, Davies TD, Bigg GR. 1999. Objective climatology of cyclones in the Mediterranean region. *J Climat Am Meteorol Soc* 12: 1685–1696.

Turc L. 1961. Estimation of irrigation water requirements, potential evapotranspiration: A simple climatic formula evolved up to date. *Annales Agronomiques* 12(1): 13–49.

Ünal Y, Kindap T, Karaca M. 2003. Redefining the climate zones of Turkey using cluster analysis. *Int J Climatol* 23: 1045–1055.

World Tourism Organization. 2019. Madrid: International Tourism Highlights, UNWTO.

Citation de l'article : Allam A, El Hassan J, Najem W, Bocquillon C, Moussa R. 2020. Classification climatique méditerranéenne pour l'hydrologie. *La Houille Blanche* 1: 60–69.

APPENDIX B2

(Allam et al., 2020c)

Allam A., Moussa R., Najem W., & Bocquillon C., 2020. Specific climate classification for Mediterranean hydrology and future evolution under Med-CORDEX regional climate model scenarios. Hydrol. Earth Syst. Sci., 24(9), 4503-4521. https://hess.copernicus.org/articles/24/4503/2020/

Hydrol. Earth Syst. Sci., 24, 4503–4521, 2020
https://doi.org/10.5194/hess-24-4503-2020

Hydrology and Earth System Sciences
Open Access
EGU

Specific climate classification for Mediterranean hydrology and future evolution under Med-CORDEX regional climate model scenarios

Antoine Allam[1,2], **Roger Moussa**[2], **Wajdi Najem**[1], **and Claude Bocquillon**[1]

[1]CREEN, Saint-Joseph University, Beirut, 1107 2050, Lebanon
[2]LISAH, Univ. Montpellier, INRAE, IRD, SupAgro, Montpellier, France

Correspondence: Antoine Allam (antoine_allam@hotmail.com)

Received: 18 February 2020 – Discussion started: 25 March 2020
Accepted: 27 July 2020 – Published: 16 September 2020

Abstract. The Mediterranean region is one of the most sensitive regions to anthropogenic and climatic changes, mostly affecting its water resources and related practices. With multiple studies raising serious concerns about climate shifts and aridity expansion in the region, this one aims to establish a new high-resolution classification for hydrology purposes based on Mediterranean-specific climate indices. This classification is useful in following up on hydrological (water resource management, floods, droughts, etc.) and ecohydrological applications such as Mediterranean agriculture. Olive cultivation is the characteristic agricultural practice of the Mediterranean region. The proposed approach includes the use of classic climatic indices and the definition of new climatic indices, mainly precipitation seasonality index I_s or evapotranspiration threshold S_{PET}, both in line with river flow regimes, a principal component analysis to reduce the number of indices, K-means classification to distribute them into classes, and finally the construction of a decision tree based on the distances to class kernels to reproduce the classification without having to repeat the whole process. The classification was set and validated by WorldClim-2 at 1 km high-resolution gridded data for the 1970–2000 baseline period and 144 stations' data over 30 to 120 years, both at monthly time steps. Climatic classes coincided with a geographical distribution in the Mediterranean ranging from the most seasonal and driest class 1 in the south to the least seasonal and most humid class 5 in the north, showing the climatic continuity from one place to another and enhancing the visibility of change trends. The MED-CORDEX ALADIN and CCLM historical and projected data at 12 and 50 km resolution simulated under the RCP4.5 and 8.5 scenarios for the 2070–2100 period served to assess the climate change impact on this classification by superimposing the projected changes on the baseline grid-based classification. RCP scenarios increase the seasonality index I_s by +80 % and the aridity index I_{Arid} by +60 % in the north and I_{Arid} by +10 % without I_s change in the south, hence causing the wet season shortening and river regime modification with the migration north of moderate and extreme winter regimes instead of early spring regimes. The ALADIN and CCLM regional climate models (RCMs) have demonstrated an evolution of the Mediterranean region towards arid climate. The classes located to the north are slowly evolving towards moderate coastal classes, which might affect hydrologic regimes due to shorter humid seasons and earlier snowmelts. These scenarios might look favourable for Mediterranean cultivation; however, the expected impact on water resources and flow regimes will surely expand and directly hit ecosystems, food, health, and tourism, as risk is interconnected between domains. This kind of classification might be reproduced at the global scale, using the same or other climatic indices specific to each region, highlighting their physiographic characteristics and hydrological responses.

1 Introduction

Mediterranean climate is a result of a complicated global cyclonic system swiping a large evaporative basin. The distribution of marine and continental air masses creates an alternation of low-pressure zones coming over from Iceland and

the Persian Gulf or high-pressure zones from Siberia and the Azores (Clerget, 1937). The seasonal shifts of these zones are magnified by the North Atlantic Oscillation (NAO) that plays an important role in shaping Mediterranean climate and influencing the evolution of farming and social activities in the long term (Rodwell and Hoskins, 1996). During the positive phases of the NAO, oceanic disturbances bring the most humid to northern Europe and the less humid to northern Africa and the Middle East (Douguédroit and Lionello, 2015). This continuous alternation of high- and low-pressure, cold and humid winters followed by hot and dry summers marks the Mediterranean seasonality, which makes the region attractive for social activities, hence its sensitivity to climate change and anthropogenic pressures (PlanBleu, 2012). A north–south general precipitation and evapotranspiration gradient has been identified in Tunisia through the analysis of directional variograms that results from partial gradients evolving through seasons (Slimani et al., 2007; Baccour et al., 2012; Feki et al., 2012). These spatial gradients mainly depend on topographic structures through the interception of rainfall-generating air masses. The climatic classification will try to identify the general spatial gradients across the Mediterranean. Hydrologically, the precipitation seasonality characterizing the Mediterranean climate is reflected in the flow regimes of Mediterranean rivers, as pointed out by Haines (1988), who classified the Mediterranean rivers under Group 12 Winter Moderate hydrologic regimes, Group 13 Extreme Winter, and Group 14 Early Spring and found a clear relation to the Köppen Csa and Csb climates and a close equivalent of the "Mediterranean Seasonal" categories of Gentilli (Haines et al., 1988). Seasonality is the main factor in the Mediterranean, but to our knowledge its use is still limited as a characterizing index for climatic and hydrological classification. Climate change is expected to have severe consequences for Mediterranean runoff, with a serious risk of freshwater availability decrease of 2 % to 15 % for 2 °C of warming (Cramer et al., 2018) and a significant increase in drought periods, particularly in the south and east (Hreiche et al., 2007; Cudennec et al., 2007; Garcia-Ruiz et al., 2011; Verdier and Viollet, 2015). The CMIP5 simulations (Coupled Model Intercomparison Project, Phase 5) expected a mean precipitation decrease of $-4\,\%\,^{\circ}\mathrm{C}^{-1}$ and a temperature increase of 20 %, more than the global average, with a maximum precipitation reduction reaching $-7\,\%\,^{\circ}\mathrm{C}^{-1}$ in winter in the southern Mediterranean region and $-9\,\%\,^{\circ}\mathrm{C}^{-1}$ in the summer in the northern region (Lionello and Scarascia, 2018). At 1.5 °C global warming, some Mediterranean areas are under aridification while moving to drier states due to the decrease in precipitation combined with a potential evapotranspiration (PET) increase leading to an expansion of drylands, thus affecting more people (Koutroulis, 2019).

Automatic classification methods partition a set of objects, knowing their distances by pairs in a way to keep the classes as homogeneous as possible while remaining distinct from each other. Like any classification, the adopted method depends on the objective and its specificity. There are several modes of climatic classification: (a) genetic classifications related to meteorological causes and the origin of air masses (Bergeron, 1928; Barry and Chorley, 2009); (b) bioclimatic classifications based on the interrelation between vegetation type and climate (Holdridge, 1947; Mather and Yoshioka, 1968; Harrison et al., 2010); (c) an agroclimatic method based on the assessment of the rainfall–evapotranspiration balance for the estimation of agricultural productivity (Thornthwaite, 1948); and (d) climatic methods based on precipitation and temperature indices similarly to the classification of Köppen (1936) updated by Peel in 2007 (Peel et al., 2007) and which remains the most used.

There are several climate classification studies of the Mediterranean region; among these we cite Köppen–Geiger classification at the global scale in which the Mediterranean climate is very distinctive (Köppen, 1936; Peel et al., 2007; Eveno et al., 2016). Köppen's classification divides the globe into 30 climate zones and relies on a partition hierarchy. It is based on precipitation and temperature indices where Mediterranean climate corresponds to dry hot or dry warm summer where the precipitation in the driest month in summer is either below 40 mm or below the third of the precipitation in the wettest month in winter (Cs) and the air temperature of the warmest month is above 22 °C (Csa) or the number of months with air temperature above 10 °C exceeds 4 (Csb). The (Cs) climate does not reign all over the Mediterranean region, as Köppen (B) classes are also observable. (B) classes correspond to arid climate in general, with (BWh) the desertic and hot climate that dominates Egypt and Libya characterized by very low precipitation ($\mathrm{MAP} < 5 \times P_{\mathrm{threshold}}$ with $P_{\mathrm{threshold}} = 2 \times \mathrm{MAT}$) and high temperature ($\mathrm{MAT} \geq 18\,^{\circ}\mathrm{C}$), (BSk) the arid steppe cold climate that dominates south-eastern Spain characterized by low precipitation ($5 \times P_{\mathrm{threshold}} > \mathrm{MAP} > 10 \times P_{\mathrm{threshold}}$) and low temperature ($\mathrm{MAT} < 18\,^{\circ}\mathrm{C}$), (Cf) the temperate climate without any dry season in the regions of Thessaloniki and Veneto, and finally (D) cold climate present further north. On the other hand, and at a global scale, some regions share a similar Mediterranean (Cs) climate, such as California, Chile, South Africa, and Australia (Fig. 1). Rivoire et al. (2019) classified 160 Mediterranean rain gauges according to monthly net precipitation ($P - \mathrm{ET}_0$). The classification showed a marked distinction between two clusters, with northern stations having a precipitation deficit from April to September and southern stations having a precipitation deficit from March to October. Other climatic classifications were also carried out in the Mediterranean but at the national scale like in France, using ascending hierarchical automatic classification based on a 1976-rain-gauge network for the 1971–1990 period (Champeaux and Tamburini, 1996). In Turkey seven different climate zones were identified by using Ward's hierarchical cluster analysis based on data from 113 climate stations for the 1951–1998 period (Unal et al., 2003). Another reclassification of rainfall re-

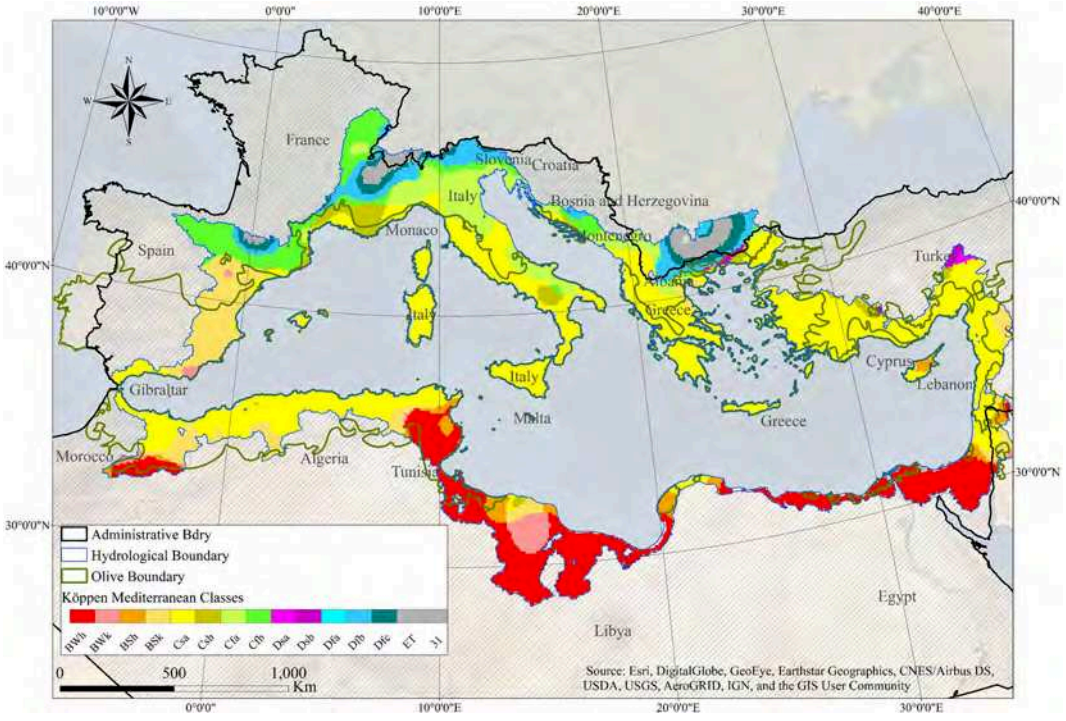

Figure 1. Four Mediterranean region boundaries (Merheb et al., 2016); first administrative, second topographic (Milano, 2013), third olive cultivation (Moreno, 2014), and fourth climatic (Peel et al., 2007).

gions of Turkey was also carried out in 2011 by K-means based on 148 stations covering the 1977–2006 period (Sönmez and Kömüşcü, 2011). We also mention the classification of cyclonic trajectory information using K-means clustering for an 18-year period over the Mediterranean (Trigo et al., 1999). Synoptic meteorology uses discriminant analysis over the eastern Mediterranean for 1948–2000 (Alpert et al., 2004). Cloud physical property classification at the pixel level uses K-means applied over the European Mediterranean region (Chéruy and Aires, 2009). The hydrological classification of 40 Mediterranean streams' natural flow regimes uses principal component analysis (PCA) to identify the most representative Richter hydrological indices and agglomerative cluster analysis (Oueslati et al., 2015). However, no specific classification based on precipitation and temperature series has yet treated the Mediterranean region as a climatic or hydrological unit, hence the aim of our study.

The objective of this study is first to establish a Mediterranean-specific climatic classification for hydrology purposes based on a set of indices, mainly seasonality and aridity, and second to estimate the future evolution of this classification based on Radiative Concentration Pathway (RCP) scenarios with an easy follow-up tool using olive cultivation evolution in the Mediterranean.

Through the classification of the Mediterranean catchments climatically and, in a second step, physiographically, we will be able to characterize their hydrological patterns and identify homogeneous regions which will be useful for the prediction of ungauged basins (Wagener et al., 2007; Hrachowitz et al., 2013). This study is a contribution to the HyMeX (HYdrological cycle in the Mediterranean Experiment) programme and to the Med-CORDEX initiative. The HyMeX programme aims at a better understanding of the Mediterranean hydrology, with emphasis on the predictability and evolution of decadal variability in the context of global change. Med-CORDEX, a HyMeX initiative (Ruti et al., 2016), is part of the COordinated Regional Downscaling EXperiment specific to the Mediterranean that aims at improving our understanding of climate change through high-resolution atmosphere regional climate models (RCMs). RCMs were introduced in the late 1980s as a nested technique in global climate models (GCMs) to consider regional-scale climatic forcings caused by the complex physiographic features and small-scale circulation features (Giorgi, 2006). The primary application of RCMs has been in the development of climate change scenarios, of which we mention the ALADIN RCM (Aire Limitée Adaptation dynamique Développement InterNational) developed by Météo France and the CCLM (Cosmo Climate Limited-area Model) developed by the German Weather Service (DWD), both applied for the EURO-CORDEX and MED-CORDEX projects (Rockel et al., 2008; Tramblay et al., 2013). We aim in this study to discuss the results of the individual models and not to compare their performances; such a study was carried out for EURO-CORDEX with 17 RCM models for the represen-

tation of the basic spatiotemporal patterns of the European climate for the period 1989–2008 (Kotlarski et al., 2014).

This paper is structured into six sections: Sect. 1 Introduction; Sect. 2 presents the Mediterranean limits and the database; Sect. 3 the classification approach based on PCA, K-means, and the decision tree with the presentation of MED-CORDEX atmosphere-RCM climate change scenarios; Sect. 4 the results of WorldClim-2 classification of gridded indices, verification of stations and comparison to catchment indices, and classification projection and impacts under MED-CORDEX scenarios; followed by a discussion in Sect. 5 before concluding with Sect. 6.

2 Study area and database

2.1 Defining the Mediterranean region boundaries

From the Latin word "Mediterranĕus" meaning "in the middle of lands", the Mediterranean refers to the sea and bordering region located in the middle of the ecumene between the European, African, and Asiatic continents. With Köppen's classification (Köppen, 1936), the definition designated henceforth a moderate climate and extended geographically beyond the limits of the Mediterranean Sea. The question that arises is how the Mediterranean boundary would be defined. Several definitions of the Mediterranean boundary have been previously mentioned by Merheb et al. (2016) as collected from the literature; a hydrological boundary was adopted for this study as shown in Fig. 1.

- The climatic boundary could be defined according to Köppen's classification where a set of regions shares similar temperature and precipitation characteristics and is known for their warm and dry summers and cold and humid winters. It is limited by the African desert to the south and the temperate European countries to the north. This boundary might change according to the definition of this similarity.

- The hydrological boundary is defined by the set of catchments draining towards the Mediterranean Sea (Milano, 2013). This definition neglects some Mediterranean climate regions like Portugal and western Spain and favours geographically adjacent regions like Egypt and Libya.

- The agricultural–bioclimatic boundary consists of the set of regions sharing the same types of vegetation considered to be indicators of the Mediterranean region, such as olives (Moreno, 2014). This definition is linked to human activity with the same nuances as the climatic limit.

- The administrative boundaries of countries adjacent to the Mediterranean Sea have a problematic definition independent of any natural basis (Wainwright and Thornes, 2004). These boundaries include several climatic classes and cover larger areas than the topographical limits.

2.2 Catchments

Since the geographic extent of the study is very wide, the delimitation of catchments was imported from international references. The European Commission, using the Joint Research Centre (JRC), has done extensive and elaborate work on the delimitation of catchments in Europe and some adjacent countries as part of the Catchment Characterization and Modelling (CMM) project (de Jager and Vogt, 2010). For catchments in the Middle East and northern Africa, catchments from HydroSHEDS, the World Wildlife Fund's project, were used (Lehner and Grill, 2013). According to these databases, the total number of catchments extracted at their main stem outlet to the Mediterranean coastline and exceeding 1 km^2 is 3681, covering a total area of 1 781 645 km^2. It should be noted that the Nile was omitted for its extent 3500 km to the south of the Mediterranean. Catchment surface distribution is shown in Table 1, where middle-range catchments, between 100 and 3000 km^2, constitute 35 % of the total and cover 28 % of the total area.

2.3 Climatic data

Three types of monthly climatic data were used in this study: (1) WorldClim-2 new 1 km spatial resolution climate surface data (Fick and Hijmans, 2017), (2) time series of 144 stations from the NOAA database of 20 different Mediterranean countries covering a period of 30 to 120 years used for validation purposes, and (3) MED-CORDEX historical and projected data simulated under the RCP4.5 and 8.5 scenarios for future projections (Tramblay et al., 2013).

1. WorldClim-2 new 1 km spatial resolution climate surface data, which consist of long-term average monthly temperature and precipitation, solar radiation, vapour pressure, and wind speed data, aggregated across a target temporal range of 1970–2000, using data from 9000 to 60 000 weather stations (Fick and Hijmans, 2017). The WorldClim-2 database is a refined and expanded version of the 2005 WorldClim-1 database (Hijmans et al., 2005). This database covers the whole study area; thus, climatic classification of Mediterranean catchments was possible. The WorldClim-2 database was built over 23 regions with different coverage for each parameter. For the precipitation an overlap of three regions covered the Mediterranean area, with a total of 10 410 stations for the three regions (western Europe $n = 3730$; eastern Europe $n = 3632$; northern Africa $n = 3048$). For average temperature, the Mediterranean was covered by one region (eu1) with number of stations $n = 1760$; $n = 1627$ for maximum temperature and $n = 1626$ for minimum temperature;

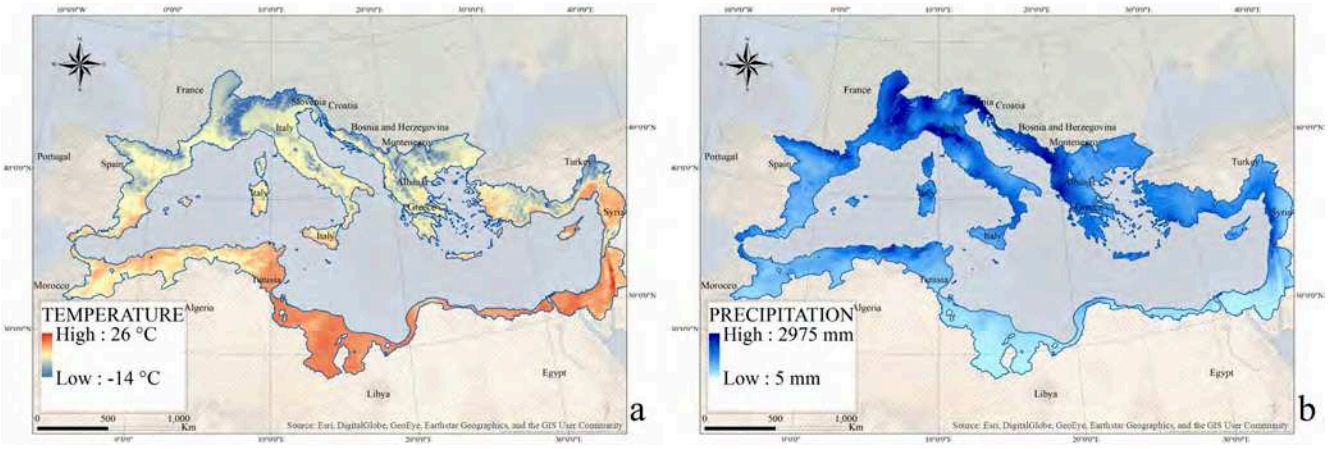

Figure 2. WorldClim-2 gridded mean annual temperature in °C **(a)** and mean annual precipitation in mm **(b)** from Fick and Hijmans (2017).

Table 1. Catchment distribution per area and ratio to total area.

Area range	Number of catchments	Number of catchments ratio	Total area (km^2)	Ratio area
$A < 100\,km^2$	2333	63 %	80 157	4 %
$100\,km^2 < A < 3000\,km^2$	1270	35 %	498 614	28 %
$A > 3000\,km^2$	78	2 %	1 202 874	68 %

refer to Figs. S1 and S2 in the supporting information of the Fick and Hijmans (2017) article. Monthly precipitation and temperature were averaged for each catchment and then climatic indices calculated at both grid and catchment scale. Climatic characteristics of a Mediterranean catchment are summarized and illustrated in Table 2 and Fig. 2, reflecting the wide variability of mean annual precipitation ranging between 5 ("Jabal el Aswad desert in Libya") and 3000 mm (Kobarid in Slovenia) and mean annual temperature ranging between −14 °C (Mont Blanc, Alps, France) and +26 °C (Karak, Jordan), where some catchments receive 50 times the amount of precipitation more than others while being 4 times colder.

2. 144 ground weather station data covering the whole study area served to validate the Mediterranean climate classification, with 105 stations located within catchment boundaries and 39 outside. Also, 102 of these stations were located within Köppen's (Csa) and (Csb) Mediterranean climate, and 42 outside. These stations belong to the Global Historical Climatology Network – GHCN (Menne et al., 2012) – and are recognized by the World Meteorological Organization (WMO); they are available for free access on the portal of the National Administration of Oceans and Atmosphere of the United States (NOAA). The average length of data series is 60 years and ranges between 30 and 120 years at a monthly time step. The 1960–1990 period is common to all stations. The data quality was verified (i.e. ellipse of Bois, 1987), and only complete hydrological years were retained for indices calculation.

3. MED-CORDEX simulations of the regional climate models (RCMs) ALADIN-Climate v5.2 at 12 km and CCLM at a 50 km spatial resolution grid were used to analyse the climate change impacts on the climatic classification for the end of the century projection period 2070–2100 and for two different RCP4.5 and 8.5 scenarios in comparison to the historical 1970–2000 baseline period (Rockel et al., 2008; Tramblay et al., 2013). We limited the climate change study to the ALADIN and CCLM models since when the article was written those were the only MED-CORDEX models to present the simulation results for RCP4.5 and 8.5 for the 2070–2100 period with the three required variables available (average temperature – tas, average precipitation – pr, and average radiation – rlds).

RCP or Radiative Concentration Pathway is a greenhouse gas (GHG) concentration trajectory adopted by the International Panel for Climate Change (IPCC) for its fifth Assessment Report (AR5) in 2014. RCP4.5 and 8.5 were chosen between four available scenarios, being the most focused on in the literature. RCP4.5 assumes that global annual emissions measured in CO_2 equivalents peak around 2040,

Table 2. Statistical summaries for the catchment climatic parameters maximum altitude (Z_{Max}), mean altitude (Z_{Mean}), mean annual precipitation (MAP), mean annual temperature (MAT), and mean potential evapotranspiration (MPET).

	Area (km^2)	Z_{Max} (m)	Z_{Mean} (m)	MAP (mm)	MAT (°C)	MPET (mm)
Minimum	0.01	−2	−4	39	5.1	444
Mean	467.5	737	255	595	16.5	1136
Maximum	96 619.0	4783	1727	2004	21.7	1498
Median	54.4	598	185	592	16.5	1127

with emissions declining substantially thereafter, while under RCP8.5, emissions continue to rise throughout the 21st century. RCP4.5 (RCP8.5) means that the GHG and aerosol concentrations evolve in a way that leads to an additional radiative forcing equal to $+4.5\,W\,m^{-2}$ ($+8.5\,W\,m^{-2}$) at the end of the 21st century with respect to the pre-industrial climate. Consequently, RCP4.5 can be considered an optimistic scenario, whereas RCP8.5 is a more pessimistic option (Giorgi et al., 2009; IPCC, 2013; Ruti et al., 2016).

While temperature increase and precipitation decrease have already been observed (IPCC, 2013), MED-CORDEX RCP4.5 scenario projections, as simulated by ALADIN v5.2 for the 2071–2100 period (Tramblay et al., 2013; Dell'Aquila et al., 2018; Drobinski et al., 2018; Tramblay et al., 2018), estimate a spatially distributed temperature increase of 1.4 to 3.5 °C and a precipitation evolution of ±10 %, while RCP8.5 projects an increase of 2.2 to 6.4 °C and a precipitation evolution of ±20 % compared with the baseline period 1970–2000 with expected shifts of Mediterranean climate and expansion of arid regions (Beck et al., 2018; Barredo et al., 2019) and related water restrictions and legal decision-making processes (Sauquet et al., 2019).

The use of ground-based station time series or gridded observational data is limited by several uncertainties, mainly density and interpolation processing methods, especially in the Mediterranean region, where northern African and Levantine countries are poorly covered (Raymond et al., 2016; Zittis, 2018). Nevertheless, the use of specific indices like seasonality and aridity, which are averaged on 30-year periods and based on monthly and annual values, while avoiding extreme event indices, reduces data quality uncertainties. On the other hand, several studies have revealed the uncertainties connected to the resolution of RCM-simulated gridded data in the Mediterranean complex domain (Romera et al., 2015), hence the use of high-resolution data like MED-CORDEX 12 and 50 km grids and WorldClim-2 1 km, and overall, the regional aspect of this study makes it less sensitive to local errors.

3 Methodology

The suggested methodology includes first the definition of the climatic indices, of which some are classic, like the frequency indices, and others are specific to the Mediterranean climate, like precipitation seasonality. Second, there is a PCA to reduce the number of climate indices and consider only the most contributing ones. Third, there are K-means classification according to the most contributing indices and finally the construction of a decision tree based on distances to class kernels to determine whether or not a place has a Mediterranean climate and to which type it belongs. This approach was applied at grid scale, verified on a set of ground stations, and then compared to a catchment-scale classification where indices are calculated from averaged climatic variables of each catchment. Each class was described and characterized by its corresponding climatic indices. The Mediterranean climatic class evolution was assessed according to indices variation based on simulated RCP scenarios and by following up the olive tree cultivation boundary as an example of a historical Mediterranean-specific bioindicator. The olive reproductive cycle displays considerable variations due to climate evolution among others, influencing flowering intensity mainly affected by seasonal temperature and water availability (Moreno, 2014).

3.1 Hydrology-driven climatic indices

The hydrology-driven independent climatic indices were chosen subjectively and developed at the grid and catchment scales from WorldClim-2 monthly average data and divided into four groups to highlight the Mediterranean seasonality and precipitation intermittence hypothesis of the climate and its corresponding hydrological response. The climatic indices were inspired by Köppen's definition of Mediterranean climates to emphasize the precipitation and temperature variability between seasons and from the components of the water balance in its general form $P = S + U + V$ (P: precipitation, S: surface runoff, U: underground runoff, V: evapotranspiration) to highlight the link between climate and hydrology. Hence Group I and II indices I_s, $P_{25\,\%}$, $P_{75\,\%}$, and I_{Decal} characterize Mediterranean precipitation P in its seasonality and monthly distribution. Group II and IV indices S_{PET}, I_{Arid}, $T_{25\,\%}$, and $T_{75\,\%}$ characterize the hydrological loss to evapotranspiration in the Mediterranean. While the flow seasonality is clearly affected by the precipitation seasonality, the other indices help in fine-tuning this theory, like monthly temperature and potential evapotranspiration variation. A complete list of indices with a description of each is in Table 3.

– Group I: indices based on monthly precipitation, of which we mention seasonality index I_s, peak indices $P_{1.5}$, P_2, and frequency indices $P_{25\,\%}$, $P_{75\,\%}$. I_s is directly linked to Mediterranean flow regimes for expressing the precipitation ratio between the 3 most hu-

Table 3. Climatic indices definition.

Group	Type	Climatic indices	Description
I	Climatic indices based on average monthly rainfall	Seasonality index I_s	One minus the precipitation ratio of the 3 driest months over the 3 humid months.
		Precipitation index $P_{25\,\%}$ and $P_{75\,\%}$	Rain value exceeded 25 % or 75 % of the time
		Peak index $S_{P1.5}$ $S_{P1.7}$ S_{P2}	Number of months exceeding the average monthly precipitation by 1.5, 1.7, and 2 times
		Horizontal inertia index I_{Hor}	Dispersion of monthly rainfall compared to the annual average
II	Climatic indices based on average monthly temperature	ΔT_1	Temperature lag between the coldest and warmest months
		ΔT_2	Temperature lag between the coldest and warmest 3 consecutive months
		Temperature index $T_{25\,\%}$ and $T_{75\,\%}$	Temperature value exceeded 25 % and 75 % of the time
		Peak index $S_{T1.2}$	Number of months exceeding the average temperature by 1.2 times
		Degree day D_j	Decomposition according to the need for habitat heating
		Mean temperature index S_{T_m}	Number of months exceeding the Mediterranean monthly average temperature T_m 16.4 °C
III	Climatic indices based on precipitation and temperature	Time-lag index I_{Decal}	Time lag between the coldest and most humid month
IV	Climatic indices of Evapotranspiration	Aridity index I_{Arid}	Annual evapotranspiration over annual precipitation $I_{Arid} = PET/P$
		Threshold index S_{PET}	Number of months where precipitation P exceeds evapotranspiration PET, formula PET calculated using Turc (1961)

mid months and the 3 driest months, with values ranging from 0 to 1 (Hreiche, 2003). I_s values tending towards 0 express uniform distribution of precipitation along the year with a hydrological response lacking flood and drought seasons, while I_s values tending towards 1 correspond to a normal distribution of precipitation with a hydrological response more likely to show flood and drought seasons.

- Group II: indices based on monthly temperature expressed by the temperature lag between the coldest and warmest months ΔT_1, frequency indices $T_{25\,\%}$, and number of months exceeding the average Mediterranean temperature S_{T_m}.
- Group III: indices based on both temperature and precipitation expressed by I_{Decal}, the time lag between the coldest and most humid months.
- Group IV: indices based on precipitation and evapotranspiration expressed by aridity index I_{Arid}. The evapotranspiration was estimated according to Turc's formula (Turc, 1961), chosen for its application simplicity and adequacy for Mediterranean humid areas in southern European countries, as it was originally developed for southern France and northern African countries (Trajković and Stojnić, 2007; Trajković and Kolaković, 2009; Jensen and Allen, 2016). Turc's formula is mainly based on temperature and radiation, two stable parameters on the regional scale which reduce the uncertainties when using a regionalized dataset such as WorldClim-2. Group II and IV indices describe the seasonality and variability of evapotranspiration and intermittence of wet and dry seasons.

3.2 Principle component analysis

Principal component analysis is widely applied to reduce the dimensionality of datasets and keep the most representative and uncorrelated variables. This section presents a brief description of the method along with some of their applications in hydrology. For an extensive mathematical description and demonstration of these methods, we advise the reader to consult Krzanowski (1988) and Jollife (2002).

PCA was first introduced by Karl Pearson (Pearson, 1901) and then developed by Harold Hotelling (Hotelling, 1933). Hotelling's (1933) motivation is that there may be a smaller *fundamental set of independent variables which determine the values* and conserve the maximum amount of information of the original variables (Jolliffe, 2002). This is achieved by transforming a vector of p random variables to a new set of variables, named principal components (PCs), by looking for a linear function of the elements with maximum variance and next looking for another linear function uncorrelated with the first and having maximum variance and so on up to p PCs. It is hoped in general that most of the variation will be accounted for by m PCs, where $m < p$.

The number of indices is reduced at two steps. The first step is based on the correlation matrix, where strongly correlated indices were eliminated (a threshold of 0.85 was chosen for this study). The second is based on PCA results, where indices that do not contribute to the principal components that represent the greatest variabilities are eliminated.

3.3 K-means clustering technique

Cluster analysis consists of data points partitioning into isolated groups while minimizing the distance between the same cluster data points and maximizing it between different clusters. One of the most popular clustering methods is the K-means method introduced by Edward Forgy (Forgy, 1965) and MacQueen (1967). It aims to minimize the square error objective function for distance optimization. The optimization steps begin with (1) kernel initialization, the kernel being a virtual point representing the statistical centre of a class, (2) updating classes, (3) re-evaluation of kernels, and (4) repetition of steps (2) and (3) until stabilization. The quality of the solution thus found strongly depends on the initial kernels. In its turn, kernel initialization is sensitive to the data dimensionality. Classification gives a deterministic result where each point should belong to one of the classes, a result of a set of decision rules based on its distances to class kernels.

The application of K-means requires the setting of a number of classes; otherwise, the optimization leads to as many classes as individuals. The optimum number of classes K could be defined according to the elbow method (Bholowalia and Kumar, 2014).

K-means has gained in reputation in the last decades and has been widely applied in the hydrology field for cloud classification from satellite imagery (Desbois et al., 1982) and for climatic classification using measured and simulated time series (Moron et al., 2008; Carvalho et al. 2016) for catchment classification based on streamflow characterization and precipitation (Toth, 2013). K-means classification was applied, and indices were distributed into five classes of kernels to determine whether they belong, or not, to a Mediterranean climate and to which type they belong, if so. We hoped for a classification that delimits the Mediterranean climate from the south and north and divides the intermediate coastal zone. Therefore, a distribution into five classes was chosen despite three classes being optimal as per the elbow method, in detail, one class that covers the southern desertic region, another class that covers the northern continental region of non-Mediterranean climate, and three classes that cover the intermediate coastal region. A larger number of classes would produce an uninterpretable fragmented classification.

3.4 Decision tree

A decision tree is a set of distance criteria or questions in the form of a hierarchy that leads to an intended classification (Breiman, 1984). To classify new points or stations or to reproduce the classification on another dataset, it suffices to define the distance criterion to the various kernels of the climatic classes by predicting values of a dependent variable based on values of predictor variables from a reference classification. This procedure provides validation tools for exploratory and confirmatory classification analysis.

We generated a decision tree based on the distances to the clusters' kernels obtained from the gridded indices classification. The aim of this decision tree is to easily reproduce the classification with the same kernels rather than to repeat the whole classification process, which will modify the clusters and their kernels. By conserving the same kernels, the decision tree will permit us to follow up the climate evolution and its impact on the classification under other scenarios.

In our case, the dependent variables are the climatic classes obtained from K-means clustering, while the predictor variables are the distances to each cluster's kernels. This procedure was done for both gridded and catchment classification. The decision tree generates a set of classification rules usually used to classify new stations based on their distances to class kernels. In this study, these rules were used in Sect. 5 to classify the projected indices. This has fixed the class kernel indices of the 1970–2000 baseline period and calculated the distances to the baseline of the 2070–2100 projected grid to compare both the classification indices and the spatial evolution.

3.5 RCP scenarios

For climate change impact assessment, temperature and precipitation delta change were calculated between both baseline period 1970–2000 and projected period 2070–2100 for the MED-CORDEX RCM ALADIN and RCM CCLM grids and for two different RCP scenarios (RCP4.5 and RCP8.5). Those delta changes were then superimposed on the WorldClim-2 grid, based on the nearest Euclidean distance between MED-CORDEX grid cells and WorldClim-2 grid cells using the GIS spatial join toolbox. The indices were then recalculated using the projected values of monthly temperatures and precipitation. The decision tree rules from Table 6 were then applied for the projected period and the

climate change under RCP was illustrated in Fig. 7 and expressed by indices evolution between classes in Table 7.

3.6 Adopted methodology

The proposed methodology consisted first in calculating the grid-based climatic indices using WorldClim-2 monthly data, second in reducing the number of indices with the PCA, and third in classifying it using K-means clustering. The gridded indices classification was later verified on the ground station indices and then compared to the catchment-scale-averaged data for future hydrological applications. In addition, a hierarchical decision tree was constructed to avoid repeating the whole process when classifying projected indices. All PCAs, K-means, and decision trees were calculated using SPSS software. Projected indices under RCP scenarios were calculated and classification evolutions were then deduced.

4 Results

This section details the climatic indices derived from the collected database, the results of PCA/K-means classification of the gridded indices, and their validation on the stations and catchment indices with a decision tree for replicating the classification on new stations or grids.

4.1 PCA results for WorldClim-2 grid-based indices

The number of indices was reduced the first time based on the correlation matrix and the second based on PCA results. We eliminated the strongly correlated indices (correlation higher than 0.85), and 10 indices were kept upon the first step.

- I_s and $P_{75\,\%}$ are strongly inversely correlated (-0.947). I_s was kept.
- ΔT_1 and ΔT_2 are strongly correlated (0.992). ΔT_1 was kept.
- $T_{25\,\%}$ and $T_{75\,\%}$ are strongly inversely correlated (-0.999). $T_{25\,\%}$ was kept.
- $P_{25\,\%}$, $SP_{1.7}$, and SP_2 are strongly correlated (0.885, 0.852). $P_{25\,\%}$ was kept.
- I_{Hor} and I_{Arid} are strongly correlated (0.856). I_{Arid} was kept.
- S_{T_m} and D_j are strongly inversely correlated (-0.949). S_{T_m} was kept.

Once the correlation matrix transformed into a diagonal one, it was possible to find the eigenvalues representing the projection from p to k dimensions. The eigenvector matrix is the linear expression of the indices with respect to the principal components. The first eigenvalue 4.8 represents 48 % of the variability, the second 1.09 represents 11 %, and the third 1.02 represents 10 %. The first three factors represent the three greatest variabilities with respect to the following factors, and 68 % of the total variability is thus preserved with this choice. Upon PCA, the number of indices was reduced to 7, showing that I_s, $S_{P1.5}$, $P_{25\,\%}$, S_{T_m}, I_{Arid}, $T_{25\,\%}$, and S_{PET} were the most contributing climatic indices, with 68 % of the total variance explained. Statistical summaries are shown in Table 4, with I_s values ranging between 0.06 and 1 with an average of 0.7 highlighting Mediterranean seasonality.

Table 4. Statistical summaries of the PCA-selected grid-based climatic indices using WorldClim-2 monthly data.

	I_s	$S_{P1.5}$	$P_{25\,\%}$	S_{T_m}	I_{Arid}	$T_{25\,\%}$	S_{PET}
Minimum	0.1	0.0	1.0	0.0	0.1	1.2	0.0
Mean	0.7	1.9	1.5	5.9	4.8	1.6	4.3
Maximum	1.0	6.0	2.8	12.0	76.3	43.7	12.0
Median	0.8	2.0	1.4	6.0	1.7	1.5	5.0

4.2 Grid-based classification

The K-means classification shown in Fig. 3 is distributed into five classes.

- Class 1: present between Egypt and Libya, highlighting a desertic influence with few rain episodes registered per year, if any, expressed by $I_s = 0.99$ and $I_{Arid} = 39.8$ on average. Precipitation never exceeds evapotranspiration in this region, hence $S_{PET} = 0$.
- Class 2: mainly present in the south and east of the Mediterranean, characterized by a high seasonality $I_s = 0.98$ and high aridity $I_{Arid} = 9.27$.
- Class 3: dominates the central region from the southern tip of Spain to Syria with an average seasonality $I_s = 0.87$.
- Class 4: covers mainly coastal catchments in north-western countries, south-eastern Italy, and western Greece and present discontinuously in the south-west. $I_s = 0.62$ in this class.
- Class 5: only present in northern non-coastal catchments and characterized by a low seasonality $I_s = 0.42$.

In comparison to Köppen's, classes 2–4 match with (Csa), while classes 1 and 5 are mainly outside (Csa) and (Csb), henceforth defined as non-Mediterranean climate. The main difference with Köppen's Mediterranean classes is in southern Spain, defined as an arid climate (Bsk), while in the present classification it varies between classes 2 and 4. This new distribution indicates climate variability within (Csa) or (Csb), hence the importance of a fine gridded classification. This variability is highlighted in the class kernel indices

(Fig. 4) and is mainly due to the complex seasonality across the Mediterranean. This complexity is shown here more delicately than the one defined by Köppen, which is climate-oriented only and limited to the simple criteria of a wet winter and dry or temperate summer. Therefore, we think that a hydrology-oriented climatic classification should account for an intra-climate characteristic expressed by specific indices like the one shown here, specific to the Mediterranean and expressed by I_s.

Olive is one of the best Mediterranean-specific physiographic indices, and we noticed that its cultivation boundary is limited by those of classes 1 and 5, where 13 % is in class 2, 49 % in class 3, and 34 % in class 4. This observation gives an accurate idea of suitable climate conditions for olive cultivation, deducing that extreme seasonality combined with very high aridity (south) or very low seasonality combined with high humidity (north) are avoided by olive trees. In a similar way, other tree types like pine trees also characterize Mediterranean landscapes, putting forward the need for a physiographic classification to interpret in parallel to this climatic classification under the umbrella of hydrological characterization. The future of Mediterranean cultivation in the case of climate change will be checked under the RCP4.5 and 8.5 scenarios in the next section.

4.3 Verification on station indices

The 144 stations were also K-means clustered based on the selected indices from the PCA. The resulting geographical distribution differed only by some shifting due to averaging and normalization as the sample is much less than the gridded cells. There is no coverage of class 1 as no weather station was found in that region (Fig. 5). Despite the shifting, there is an 82 % accuracy rate or 86 out of 105 stations that matched the gridded distribution; the rest is located within the adjacent class boundaries. As for the olive boundary, there was only one class 5 station corresponding to Florence that was located within the boundary.

4.4 Comparison to catchment-based classification

The K-means clustering of the catchment indices classification resulted in a spatial distribution similar to the WoldClim-2 grid-based classification, where class 1 catchments dominate the south, class 5 the north, and classes 2–4 the central region (Fig. 6). This classification has shown lower resolution and revealed the shifts of some regions to adjacent classes. Class 1 dominated Egypt and Libya, class 5 climate disappeared from northern Spanish coasts, class 3 climate from Sardinia and Greece, and class 2 from Syria, and the limited spread of classes 4 and 5 also disappeared from eastern Turkey. However, climate continuity is conserved in this classification for indices gradually increasing or decreasing from north to south.

We believe that this classification is useful both for hydrological and ecohydrological applications like cultivation and other related environmental practices affected by water resources and river flows.

4.5 Decision tree analysis

A decision tree was generated based on the gridded indices and their distances to a cluster's kernels. The total population of gridded indices was divided randomly into two equal subsets, one for training and the second for testing. The predicted class values of both sets were then compared to the original classification of the gridded indices obtained in Sect. 4.3, and both yielded an overall 93 % accuracy (Table 5). We notice that some grids have joined one of the adjacent classes due to interclass connectivity; this confirms once more the continuity of climate. The generated decision tree of three levels includes 75 nodes in total due to the high population number with 75 classification rules sampled in Table 6. As an example, for class 1, if the distance to kernel 1 (D1) is below 3.5 and the distance to kernel 2 (D2) is above 2.2, then the grid cell belongs to class 1. This decision tree permits us to follow up the climate evolution and its impact on the classification applied in Sect. 5.

4.6 MED-CORDEX ALADIN RCP scenario climate evolution

The climate change under the RCP was illustrated in Fig. 7 and expressed by indices evolution between classes in Table 7. Under the RCP4.5 scenario, temperature increases by 1.4 to 3.5 °C (average 2.2 °C), with the lowest rates during winter and the highest during summer. In the south, on average, precipitation increases by 25 % during winter and by 70 % during summer and decreases by 15 % during spring and by 5 % during autumn. In the north it increases by 10 % during winter, spring, and autumn while staying stable along the year in the central region. No major area changes occur between classes. In detail, class 5 reduces its extent in Greece and Albania in favour of classes 3 and 4 but compensates in central Spain; class 3 extent decreases in Turkey and Corsica in favour of class 4 in Lebanon and class 2 in Cyprus. Classes 1–3 seasonality indices I_s are stable, while classes 4 and 5 increase by 7 % and 9 %. Also for classes 4 and 5, $S_{P1.5}$ is highly increasing (70 %), with $P_{25\,\%}$ staying almost the same (3 %), which means that precipitation change is temporally distributed in a way that more months exceed the average monthly precipitation by 1.5 times and that the humid season has shortened, enhancing seasonality variation. Another remarkable change is the class 5 I_{Arid} 20 % increase, pushing it towards class 4.

Under the RCP8.5 scenario, the case is accentuated for temperature, which increases evenly across the Mediterranean by 2.5 to 5.6 °C (average 3.8 °C), with the lowest rates during winter and the highest during summer. In the

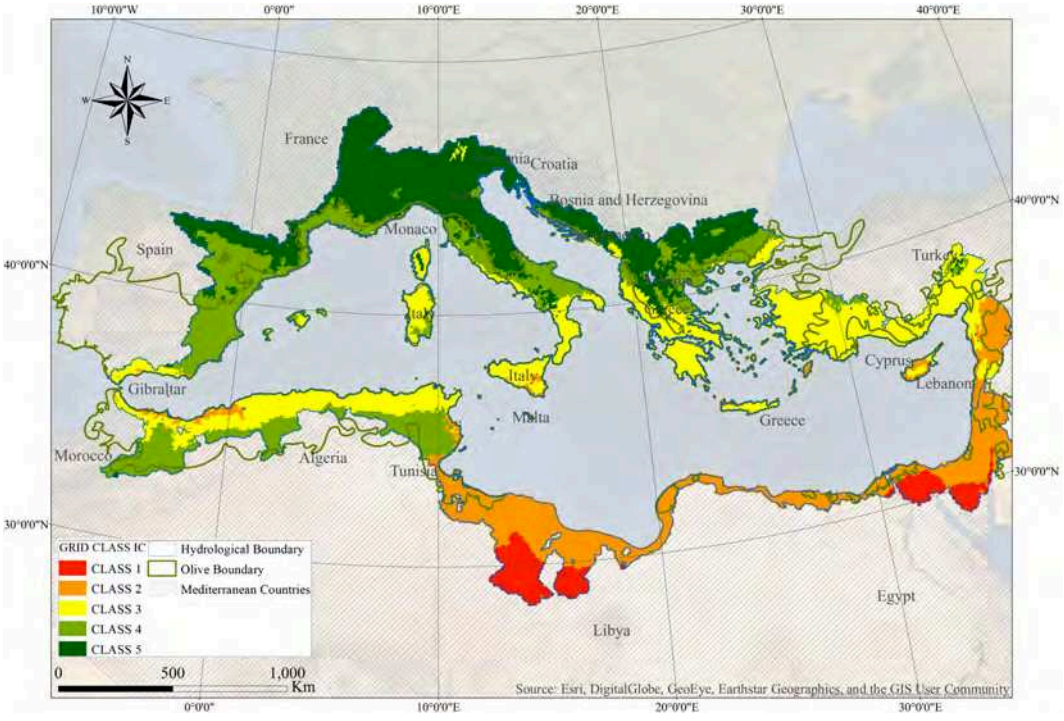

Figure 3. Geographical distribution of the Mediterranean climatic classes based on gridded indices using WorldClim-2 monthly data.

Table 5. Gridded classification decision tree accuracy table. The accuracy rate is calculated in comparison to the K-means classification of the gridded indices in Sect. 4.4.1.

	Sample	1	2	3	4	5	Accuracy
Training	1	636	26	1	1	2	95.5 %
	2	86	1915	131	0	0	89.8 %
	3	0	118	3537	186	17	91.7 %
	4	1	0	135	2860	68	93.3 %
	5	0	0	1	72	3511	98.0 %
	Overall percentage	5.4 %	15.5 %	28.6 %	23.4 %	27.0 %	93.6 %
Test	1	637	33	2	2	0	94.5 %
	2	71	1889	166	0	0	88.9 %
	3	1	124	3635	197	11	91.6 %
	4	0	0	167	2912	69	92.5 %
	5	0	0	0	83	3389	97.6 %
	Overall percentage	5.3 %	15.3 %	29.7 %	23.9 %	25.9 %	93.1 %

south, on average, precipitation increases by 60 % during summer and decreases by 10 % during winter. In the north it increases by 5 % during spring and summer while staying almost stable along the year in the central region. The area also did not change much under RCP8.5; in detail, class 3 takes over the south-eastern coast of Spain but retreats in favour of class 4 from north-western Africa and Turkey. The difference with the RCP4.5 scenario is first in the indices evolution, where I_s increases by 9 % in class 5 and $S_{P1.5}$ highly increases by 96 %. This has caused an area change of 2 % towards class 4, mainly in Spain, Greece, and Albania. Another change is class 3 I_{Arid} increasing by 19 % and S_{PET} decreasing by 10 %, which means that this moderate region is pushing towards a more arid climate.

4.7 MED-CORDEX CCLM RCP scenario climate evolution

Under the RCP4.5 scenario, temperature increases by 1.9 to 3.5 °C (average 2.9 °C), with the lowest rates in the south during winter and the highest in the north during summer. In the south, on average, precipitation increases by 20 % during

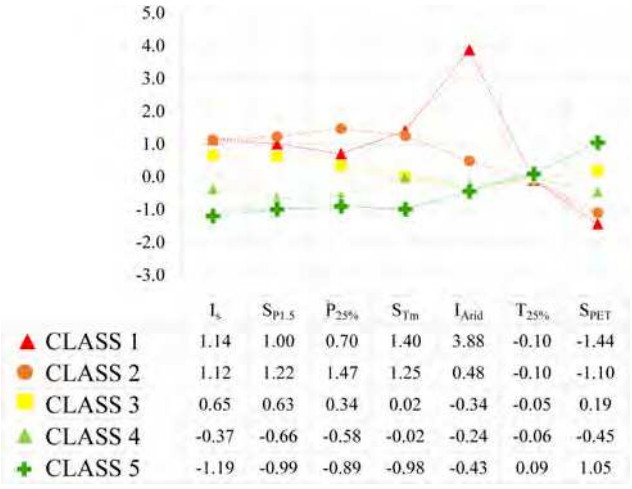

	I_s	$S_{P1.5}$	$P_{25\%}$	S_{Tm}	I_{Arid}	$T_{25\%}$	S_{PET}
▲ CLASS 1	1.14	1.00	0.70	1.40	3.88	-0.10	-1.44
● CLASS 2	1.12	1.22	1.47	1.25	0.48	-0.10	-1.10
■ CLASS 3	0.65	0.63	0.34	0.02	-0.34	-0.05	0.19
▲ CLASS 4	-0.37	-0.66	-0.58	-0.02	-0.24	-0.06	-0.45
✚ CLASS 5	-1.19	-0.99	-0.89	-0.98	-0.43	0.09	1.05

Figure 4. Normalized indices values of the five climatic class kernels from the Mediterranean catchment's classification using WorldClim-2 data.

Table 6. Sample of the decision tree set of rules for the gridded classification (D1–D5 correspond to distance to kernel of classes 1–5). As an example, for class 1, if the distance to kernel 1 (D1) is below 3.5 and the distance to kernel 2 (D2) is above 2.2, then the grid cell belongs to class 1.

Class 1 (4 rules)	(D1) < 3.5 and (D2) > 2.2
Class 2 (13 rules)	(D1) < 3.5 and 1.9 < (D2) < 2.2 3.5 < (D1) < 4.2 and 2.4 < (D4) < 2.8 and (D2) < 2.2 3.5 < (D1) < 4.2 and 2.8 < (D4) < 3.4 4.7 < (D1) < 4.8 and (D4) > 3.4 4.8 < (D1) < 5.1 and (D4) > 3.4
Class 3 (23 rules)	3.5 < (D1) < 4.2 and 1.8 < (D4) < 2.1 and (D2) < 2.2 3.5 < (D1) < 4.2 and 2.1 < (D4) < 2.4 5.1 < (D1) < 5.5 and 1.5 < (D4) < 1.8 and (D5) > 1.7 5.1 < (D1) < 5.5 and 1.5 < (D4) > 1.8
Class 4 (23 rules)	3.5 < (D1) < 4.2 and (D4) < 1.8 3.5 < (D1) < 4.2 and 1.8 < (D4) < 2.1 and (D2) > 2.2 5.5 < (D1) < 5.9 and 1.3 < (D5) < 1.7 and 1.2 < (D4) < 1.5 5.5 < (D1) < 5.9 and (D5) > 1.7
Class 5 (12 rules)	5.1 < (D1) < 5.5 and 1 < (D4) < 1.2 and (D5) < 1.3 5.1 < (D1) < 5.5 and 1.5 < (D4) < 1.5 and (D5) < 1.7 5.9 < (D1) < 6.5 and 1.5 < (D4) < 2.4 and (D5) > 1.7 5.9 < (D1) < 6.5 and (D4) > 2.4 (D1) > 6.5

winter and by 10 % during autumn and decreases by 10 % during summer but is stable during spring. In the north it increases by up to 10 % during autumn and winter and decreases to 30 % during spring and summer. The spatial extent of class 5 increases by 4 %, mostly in northern Spain, Albania, Morocco, and Algeria in favour of class 4, which decreases by 5 %; class 3 appeared between Italy and France on the Ligurian Sea, at San Marino, and on the Spanish coast; class 2 expanded over the Turkish coast and in Morocco; class 1 remained almost unchanged. Classes 1 and 2 seasonality indices I_s are constant, while classes 3–5 increase by 4 %, 27 %, and 42 %. Also, $S_{P1.5}$ increases by 14 %, 120 %, and 320 % for classes 3–5, with a little change in $P_{25\,\%}$ (less than 10 %), the same observation as the ALADIN RCP4.5 scenario but more accentuated. I_{Arid} increases by 56 % in class 5, while S_{PET} increases by 25 %.

Under the RCP8.5 scenario, temperature increases by 3.6 to 6.4 °C (average 5.1 °C), with the lowest rates in the south during winter and the highest in the north during summer. In the south, on average, precipitation increases by 30 % during winter and by 10 % during autumn and decreases to 25% during summer but is stable during spring. In the north it increases by 10 % during autumn and winter and decreases to 60 % during spring and summer. Spatially, class 3 increases by 9 %, mostly in Italy, France, Spain, northern Greece, and Algeria in favour of class 4, which decreases by 7 %; classes 1, 2, and 5 remained almost unchanged. Class 3–5 seasonality indices I_s increase by 8 %, 39 %, and 80 %. $S_{P1.5}$ increases by 17 %, 215 %, and 516 % for classes 3–5, with a change in $P_{25\,\%}$ of a maximum of 17 %. Aridity indices increase by 24 % to 50 % for classes 3–5, while S_{PET} decreases between 13 % and 26 % for the same classes. In summary, the Mediterranean is evolving towards an arid region under both the CCLM RCP4.5 and 8.5 scenarios.

5 Discussion

The objective of this study is first to establish a Mediterranean-specific climatic classification for hydrology purposes based on a set of indices, mainly seasonality and aridity, and second to estimate the future evolution of this classification based on RCP scenarios.

In this study, the climatic classification was applied and verified on three datasets of different resolutions; the grid-based, the station-based, and catchment-based classification using the same climatic indices. We can clearly notice that the grid-based classification yielded the best resolution; however, despite the variability of the class boundaries between classifications, where some regions shift from class to another, the continuous evolution of climate across the Mediterranean was demonstrated by the indices values uniformly increasing or decreasing from north to south in all classifications. In general, precipitation seasonality is highest in the south and lowest in the north, the same for other precipitation indices and aridity; hence, the overall classification gradient was maintained from class 1 in the south to class 5 in the north, which confirms that I_s and I_{Arid} are the main contributors to the classification taking over precipitation and temperature frequency indices (Figs. 4–6).

The catchment-based classification put the whole catchment within the same class despite the intra-climatic diversity which mostly affected wide catchments (above 10 000 km^2) like the Rhône, Ebro, and Po and, to a lesser

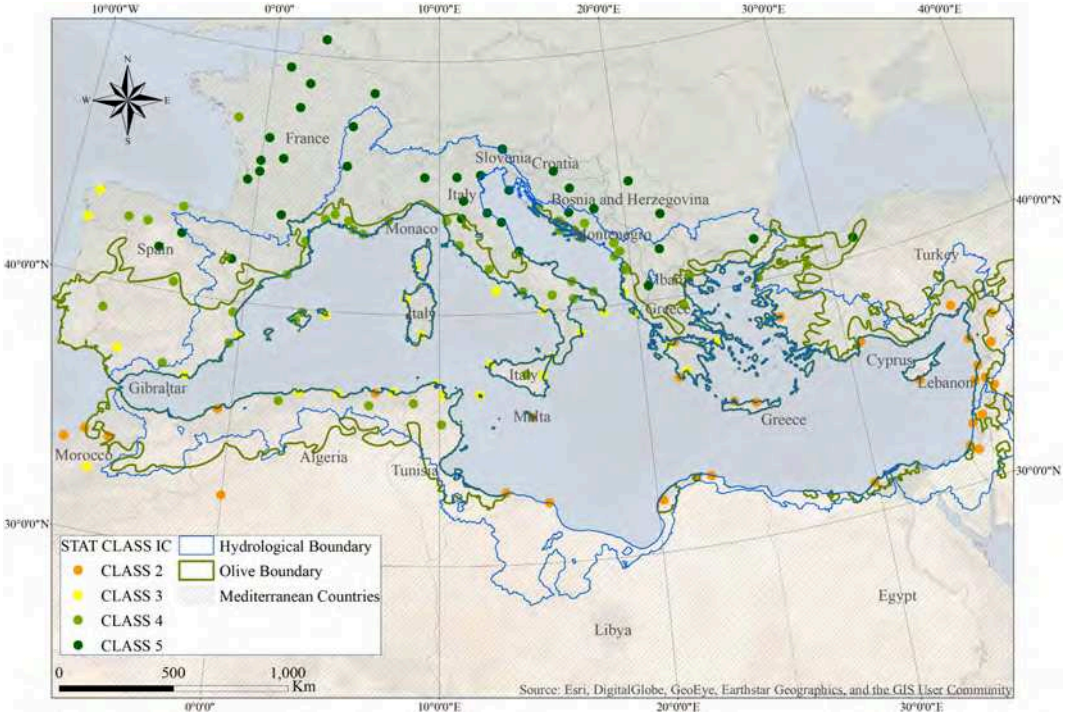

Figure 5. Geographical distribution of the Mediterranean climatic classes based on 144 stations' climatic indices.

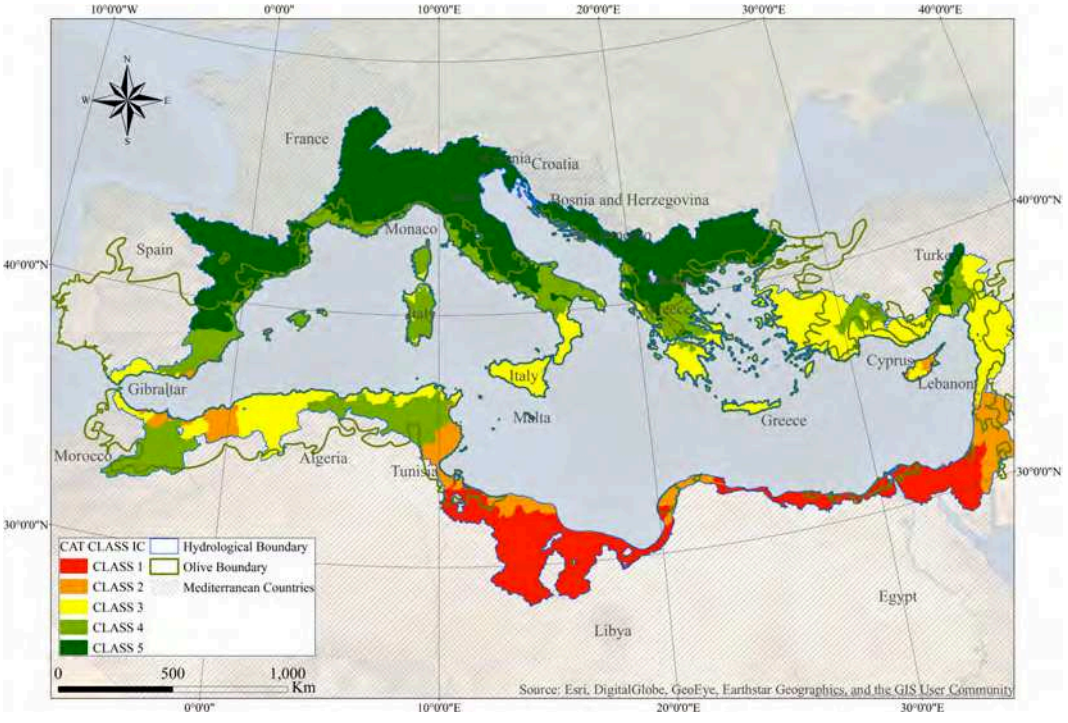

Figure 6. Geographical distribution of the Mediterranean climatic classes based on average catchment indices using WorldClim-2 monthly data.

https://doi.org/10.5194/hess-24-4503-2020

Table 7. Climatic indices values under the RCM ALADIN and CCLM RCP scenarios, with the *evolution ratio* in italic.

	Area		T		P		I_s		$S_{P1.5}$		$P_{25\,\%}$		S_{T_m}		I_{Arid}		$T_{25\,\%}$		S_{PET}	
Baseline 1970–2000																				
Class 1	5 %				0.99		3.53		1.70		9.10		39.80		1.33		0.00	
Class 2	18 %				0.98		3.88		1.94		8.76		9.18		1.32		1.00	
Class 3	27 %				0.87		2.90		1.58		5.98		1.75		1.48		4.85	
Class 4	22 %				0.61		0.77		1.29		5.81		2.58		1.47		3.05	
Class 5	28 %				0.41		0.29		1.20		3.66		0.89		1.94		7.56	
ALADIN RCP4.5 2070–2100																				
Class 1	4 %	*0 %*	2.13	19 %	0.99	*0 %*	3.45	*–2 %*	1.79	*6 %*	9.00	*–1 %*	39.46	*–1 %*	1.32	*–1 %*	0.00	*0 %*
Class 2	19 %	*1 %*	2.14	12 %	0.98	*0 %*	3.65	*–6 %*	1.99	*3 %*	8.43	*–4 %*	9.94	*8 %*	1.31	*–1 %*	0.99	*–1 %*
Class 3	26 %	*–1 %*	2.26	1 %	0.87	*0 %*	2.90	*0 %*	1.60	*1 %*	5.91	*–1 %*	2.01	*15 %*	1.44	*–3 %*	4.51	*–7 %*
Class 4	23 %	*0 %*	2.14	2 %	0.66	*9 %*	1.31	*70 %*	1.32	*3 %*	5.64	*–3 %*	2.73	*6 %*	1.44	*–2 %*	2.80	*–8 %*
Class 5	28 %	*0 %*	2.21	7 %	0.45	*7 %*	0.50	*71 %*	1.22	*2 %*	3.67	*0 %*	1.06	*20 %*	1.87	*–4 %*	7.11	*–6 %*
ALADIN RCP8.5 2070–2100																				
Class 1	4 %	*0 %*	3.80	11 %	0.99	*0 %*	3.44	*–3 %*	1.83	*8 %*	8.90	*–2 %*	38.43	*–3 %*	1.32	*–1 %*	0.00	*0 %*
Class 2	19 %	*1 %*	3.79	8 %	0.98	*0 %*	3.60	*–7 %*	1.98	*2 %*	8.45	*–4 %*	10.11	*10 %*	1.31	*–1 %*	1.02	*2 %*
Class 3	26 %	*–1 %*	3.84	−3 %	0.86	*0 %*	2.79	*–4 %*	1.58	*0 %*	5.92	*–1 %*	2.08	*19 %*	1.44	*–3 %*	4.38	*–10 %*
Class 4	24 %	*2 %*	3.76	−2 %	0.65	*7 %*	1.33	*74 %*	1.34	*4 %*	5.57	*–4 %*	2.66	*3 %*	1.44	*–2 %*	2.95	*–3 %*
Class 5	26 %	*–2 %*	3.67	3 %	0.45	*9 %*	0.57	*96 %*	1.23	*3 %*	3.62	*–1 %*	0.93	*4 %*	1.89	*–3 %*	7.32	*–3 %*
CCLM RCP4.5 2070–2100																				
Class 1	5 %	*0 %*	2.67	6 %	0.99	*0 %*	3.51	*–1 %*	1.72	*2 %*	9.06	*0 %*	38.26	*–4 %*	1.30	*–2 %*	0.00	*0 %*
Class 2	19 %	*1 %*	2.58	6 %	0.99	*0 %*	3.87	*0 %*	2.02	*4 %*	8.43	*–4 %*	9.01	*–2 %*	1.28	*–3 %*	1.05	*5 %*
Class 3	27 %	*–1 %*	2.89	−3 %	0.90	*4 %*	3.31	*14 %*	1.68	*6 %*	5.97	*0 %*	1.96	*12 %*	1.39	*–6 %*	4.59	*–5 %*
Class 4	17%	*0 %*	3.00	−7 %	0.77	*27 %*	1.69	*120 %*	1.37	*7 %*	5.86	*1 %*	2.89	*12 %*	1.40	*–5 %*	2.97	*–3 %*
Class 5	32 %	*0 %*	3.07	−7 %	0.59	*42 %*	1.22	*316 %*	1.31	*9 %*	3.93	*8 %*	1.39	*56 %*	1.69	*–13 %*	5.70	*–25 %*
CCLM RCP8.5 2070–2100																				
Class 1	5 %	*0 %*	4.66	6 %	0.99	*0 %*	3.57	*1 %*	1.85	*9 %*	8.48	*–7 %*	36.64	*–8 %*	1.27	*–4 %*	0.00	*0 %*
Class 2	17 %	*1 %*	4.61	1 %	0.99	*1 %*	3.89	*0 %*	2.09	*8 %*	8.10	*–8 %*	9.49	*3 %*	1.26	*–4 %*	1.00	*0 %*
Class 3	36 %	*–1 %*	5.22	−11 %	0.93	*8 %*	3.40	*17 %*	1.76	*11 %*	5.82	*–3 %*	2.19	*25 %*	1.36	*–8 %*	4.02	*–17 %*
Class 4	15 %	*2 %*	5.31	−18 %	0.84	*39 %*	2.41	*215 %*	1.50	*17 %*	5.60	*–4 %*	3.20	*24 %*	1.38	*–6 %*	2.64	*–13 %*
Class 5	28 %	*–2 %*	5.36	−23 %	0.75	*80 %*	1.79	*514 %*	1.39	*16 %*	3.69	*1 %*	1.40	*58 %*	1.48	*–24 %*	5.61	*–26 %*

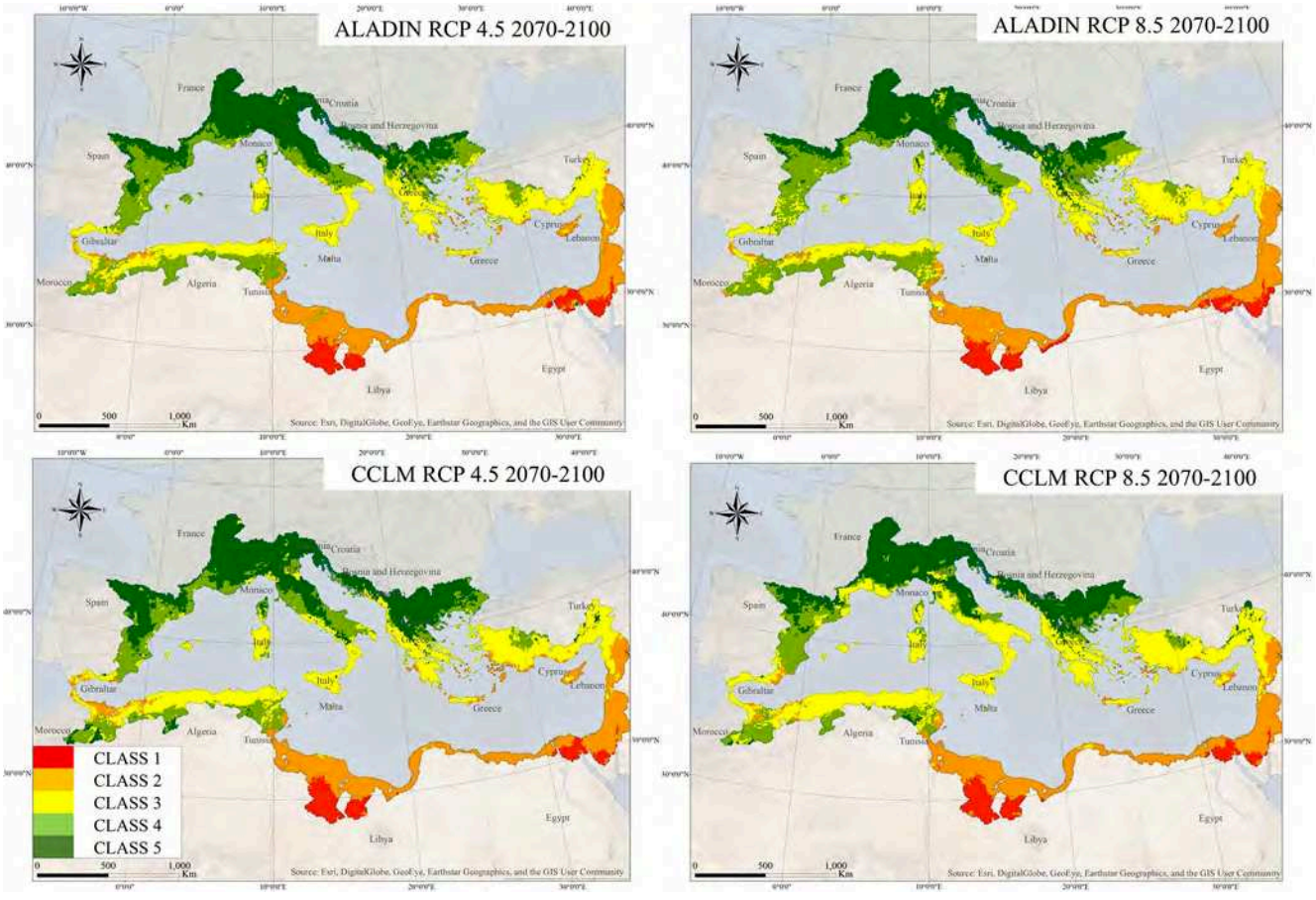

Figure 7. Projected geographical distribution of the Mediterranean climatic classes based on WorldClim-2 gridded climatic indices using projected data under the ALADIN and CCLM RCP4.5 and 8.5 scenarios for the 2070–2100 period.

extent, smaller catchments (less than 3000 km^2) as climatic diversity decreases with area and spatial spread. The grid-based classification refined the catchment-based classification showing different climatic classes within the same catchment mainly between coastal lowland areas, valleys, and mountainous highland areas. However, we could still notice in Fig. 5 that the Alps and the Po Valley are still in the same class according to our classification approach as they both share close seasonality index ($I_s \approx 0.47$) and aridity index ($I_{Arid} \approx 1.06$). Nevertheless, class 3 spots were seen in northern Italian mountains at the boundary with Austria which upon checking appeared to have a higher seasonality and aridity ($I_s \approx 0.70$; $I_{Arid} \approx 0.98$) than the surrounding region ($I_s \approx 0.61$; $I_{Arid} \approx 0.78$), an anomaly that might be caused by variables interpolations in the area. It is interesting to cross-analyse this classification with a catchment-based physiographic classification (article in preparation) which both classifications will be used for a hydrological characterization of Mediterranean catchments.

In the north, where seasonality is low and precipitation is regular along the year, RCP4.5 and 8.5 scenario impacts on hydrology are more accentuated for CCLM than ALADIN, as the first projects a high precipitation decrease, down to −30 % and −60 % and a warming of 3.8 and 6.8 °C for RCP4.5 and 8.5 consequently during dry spring and summer seasons, hence increasing I_s by +80 % and I_{Arid} by +60 %, causing the wet season shortening and river regime modification with the migration north of Group 12 Winter Moderate regimes instead of Group 14 Early Spring regimes. ALADIN projects a moderate precipitation variation of ±10 % with a warming of 2.7 and 4.5 °C and increasing I_s by only +9 % and I_{Arid} by +20 % (see Table 7).

In the south, where seasonality is very high already and precipitation is limited to autumn and winter, models have projected little to no modification. RCP4.5 and 8.5 scenario impacts on hydrology are more accentuated for ALADIN than CCLM as the first is projecting a precipitation change between −5 % and +25 % for RCP4.5 and between −12 % and −2 % for RCP8.5 during autumn and winter consequently with I_{Arid} change reaching 10 %; CCLM is projecting a precipitation increase between +8 % and +22 % for RCP4.5 and between +5 % and +32 % for RCP8.5 with only +3 % I_{Arid} change, while I_s did not change for both. A mod-

ification of hydrologic regime from Group 14 Early Spring to Group 13 Extreme Winter is expected.

Looking to the maps in Fig. 7, we can easily notice that classes 2 and 3 are expanding to the north for RCM CCLM, while this change is limited for RCM ALADIN; looking south, we do not see much change on the maps, thus confirming our previous observations.

The use of the ALADIN and CCLM models is not enough to fully assess the uncertainties, which is beyond the scope of this paper. Nevertheless, the seasonal variability between models and scenarios, despite the general trend towards warming, aridity and accentuated seasonality, incited us to address the main reasons behind. This uncertainty usually depends on adopted climate variables, the region, seasons (Lionello and Scarascia, 2018). In addition, the adopted models in this study are atmosphere-RCM and not fully coupled models, as they are not yet achieved by the MED-CORDEX, which could have returned different results.

The ALADIN and CCLM RCM models have demonstrated an evolution of the Mediterranean region towards arid climates, more emphasized with CCLM, especially for RCP8.5. These scenarios might look Mediterranean friendly as class 4 and 5 seasonality indices are evolving towards class 3 in addition to some spatial expansion which might look favourable for Mediterranean cultivation. However, the expected impact on water resources and flow regimes will surely expand and directly hit ecosystems, food, health, and tourism, as risk is interconnected between domains (Cramer et al., 2018).

6 Conclusion

The Mediterranean climate characteristics, and specifically precipitation seasonality, the main contributor according to PCA, play an important role in the hydrological mechanisms of Mediterranean catchments and flow intermittence. A decision tree makes it possible to define, from distances to class kernels, whether any place has a Mediterranean climate or not and to which type of Mediterranean climate it belongs, for present and future scenarios. On the other hand, the superposition of the olive cultivation boundary as a Mediterranean-specific physiographic index highlighted the utility and importance of physiographic–climatic coupled scenario models that could be extended to other Mediterranean physiographic or bio-climatic indices. The climatic classification and corresponding indices evolution under RCP scenarios helped in identifying the general climate change impact on Mediterranean seasonality that might uncover valuable findings about water balance, floods, and droughts for water sector stakeholders. Both the ALADIN and CCLM scenarios showed an increase in the average seasonality and aridity indices affecting hydrologic regimes due to shorter humid seasons and earlier snowmelts. The results of this study are useful for future water resources and cultivation management policies to identify the most impacted zones and propose preventive and adaptative measures for a more resilient and sustainable region. This kind of classification might be reproduced at the global scale, using the same or other region-specific climatic indices highlighting their physiographic characteristics and hydrological response.

Data availability. All the climatic data are freely available online. The WorldClim-2 data are available from the WorldClim website at https://www.worldclim.org/data/worldclim21.html (last access: 8 September 2020, WorldClim, 2020). The ground weather station data are available from the Global Historical Climatology Network website at https://www.ncdc.noaa.gov/ghcn-daily-description (last access: 8 September 2020, NCEI, 2020). The ALADIN and CCLM simulations used in the current work can be downloaded from the Med-CORDEX database at https://www.medcordex.eu/ (last access: 8 September 2020).

Author contributions. All the authors (AA, RM, WN and CB) contributed to the conceptualization and methodology of the study as well as drafting, reviewing, and editing the article. AA developed the climatic classification for the 1970–2000 baseline period and for the 2070–2100 projected period under Med-CORDEX scenarios. AA, RM, WN and CB carried out the validation and analysis of the results.

Competing interests. The authors declare that they have no conflict of interest.

Special issue statement. This article is part of the special issue "Hydrological cycle in the Mediterranean (ACP/AMT/GMD/HESS/NHESS/OS inter-journal SI)". It is not associated with a conference.

Acknowledgements. The authors would like to thank the editor Giuseppe Tito Aronica, first reviewer Christophe Cudennec, and anonymous second reviewer for their constructive comments. We would also like to thank the Med-CORDEX providers for making their Regional Climate Data available.

Thanks to the HESS Executive Editor for granting the authors a full APC waiver for this paper.

Review statement. This paper was edited by Giuseppe Tito Aronica and reviewed by Christophe Cudennec and one anonymous referee.

References

Alpert, P., Osetinsky, I., Ziv, B., and Shafir, H.: Semi-objective classification for daily synoptic systems: Application to the eastern Mediterranean climate change, Int. J. Climatol., 24, 1001–1011, https://doi.org/10.1002/joc.1036, 2004.

Baccour, H., Slimani, M., and Cudennec, C.: Spatial structures of reference evapotranspiration and climatic variables in Tunisia, Hydrolog. Sci. J., 57, 818–829, https://doi.org/10.1080/02626667.2012.672986, 2012.

Barredo, J. I., Mauri, A., Caudullo, G., and Dosio, A.: Assessing shifts of Mediterranean and arid climates under RCP4.5 and RCP8.5 climate projections in Europe, in: Meteorology and Climatology of the Mediterranean and Black Seas, Springer, 235–251, 2019.

Barry, R. G. and Chorley, R. J.: Atmosphere, weather and climate, Routledge, 2009.

Beck, H. E., Zimmermann, N. E., McVicar, T. R., Vergopolan, N., Berg, A., and Wood, E. F.: Present and future Köppen-Geiger climate classification maps at 1-km resolution, Scient. Data, 5, 180214, https://doi.org/10.1038/sdata.2018.214, 2018.

Bergeron, T.: Über die dreidimensional verknüpfende Wetteranalyse: Cammermeyer in Komm., Oslo Cammermeyers Boghandel, 1928.

Bholowalia, P. and Kumar, A.: EBK-means: A clustering technique based on elbow method and k-means in WSN, Int. J. Comput. Appl., 105, 17–24, https://doi.org/10.5120/18405-9674, 2014.

Bois, P.: Contrôle de séries chronologiques corrélées par étude du cumul des résidus de la corrélation, in: Deuxièmes journées hydrologiques de l'ORSTOM à Montpellier, Paris, ORSTOM, 89–99, Colloques et Séminaires, Journées Hydrologiques de l'ORSTOM à Montpellier, 2, Montpellier (FRA), 16–17 September 1986, ISBN 2-7099-0865-4, 1987.

Breiman, L., Friedman, J., Stone, C. J., and Olshen, R. A.: Classification and Regression Trees, Taylor & Francis, 1984.

Carvalho, M. J., Melo-Gonçalves, P., Teixeira, J. C., and Rocha, A.: Regionalization of Europe based on a K-Means Cluster Analysis of the climate change of temperatures and precipitation, Phys. Chem. Earth Pt. A/B/C, 94, 22–28, https://doi.org/10.1016/j.pce.2016.05.001, 2016.

Champeaux, J. and Tamburini, A.: Climatological zoning of France from precipitation measurements (1971–1990) of the French climatological network, Meteorologie (France), 14, 44-54, https://doi.org/10.4267/2042/51183, 1996.

Chéruy, F. and Aires, F.: Cluster Analysis of Cloud Properties over the Southern European Mediterranean Area in Observations and a Model, Mon. Weather Rev., 137, 3161–3176, https://doi.org/10.1175/2009MWR2882.1, 2009.

Clerget, M.: Les types de temps en Méditerranée, Paper presented at the Annales de géographie, Armand Colin, 1937.

Cramer, W., Guiot, J., Fader, M., Garrabou, J., Gattuso, J.-P., Iglesias, A., Lange, M. A., Lionello, P., Llasat, M. C., and Paz, S.: Climate change and interconnected risks to sustainable development in the Mediterranean, Nat. Clim. Change, 8, 972–980, https://doi.org/10.1038/s41558-018-0299-2, 2018.

Cudennec, C., Leduc, C., and Koutsoyiannis, D.: Dryland hydrology in Mediterranean regions – a review, Hydrolog. Sci. J./Journal des Sciences Hydrologiques, 52, 1077–1087, https://doi.org/10.1623/hysj.52.6.1077, 2007.

De Jager, A. L. and Vogt, J. V.: Development and demonstration of a structured hydrological feature coding system for Europe, Hydrolog. Sci. J., 55, 661–675, https://doi.org/10.1080/02626667.2010.490786, 2010.

Dell'Aquila, A., Mariotti, A., Bastin, S., Calmanti, S., Cavicchia, L., Deque, M., Djurdjevic, V., Dominguez, M., Gaertner, M., and Gualdi, S.: Evaluation of simulated decadal variations over the Euro-Mediterranean region from ENSEMBLES to Med-CORDEX, Clim. Dynam., 51, 857–876, https://doi.org/10.1007/s00382-016-3143-2, 2018.

Desbois, M., Seze, G., and Szejwach, G.: Automatic Classification of Clouds on METEOSAT Imagery: Application to High-Level Clouds, J. Appl. Meteorol., 21, 401–412, https://doi.org/10.1175/1520-0450(1982)021<0401:ACOCOM>2.0.CO;2, 1982.

Douguédroit, A. and Lionello, P.: Temperature and precipitation in the Mediterranean region: Present trends and future scenarios, in: Connections, Mobilities, Urban Prospects and Environmental Threats: The Mediterranean in Transition, Cambridge Scholars, Newcastle upon Tyne, UK, 2015.

Drobinski, P., Silva, N. D., Panthou, G., Bastin, S., Muller, C., Ahrens, B., Borga, M., Conte, D., Fosser, G., Giorgi, F., Güttler, I., Kotroni, V., Li, L., Morin, E., Önol, B., Quintana-Segui, P., Romera, R., and Torma, C. Z.: Scaling precipitation extremes with temperature in the Mediterranean: past climate assessment and projection in anthropogenic scenarios, Clim. Dynam., 51, 1237–1257, https://doi.org/10.1007/s00382-016-3083-x, 2018.

Eveno, M., Planchon, O., Oszwald, J., Dubreuil, V., and Quénol, H.: Variabilité et changement climatique en France de 1951 à 2010: analyse au moyen de la classification de Köppen et des "types de climats annuels", Climatologie, 13, 47–70, https://doi.org/10.4267/climatologie.1203, 2016.

Feki, H., Slimani, M., and Cudennec, C.: Incorporating elevation in rainfall interpolation in Tunisia using geostatistical methods, Hydrolog. Sci. J., 57, 1294–1314, https://doi.org/10.1080/02626667.2012.710334, 2012.

Fick, S. E. and Hijmans, R. J.: WorldClim 2: new 1-km spatial resolution climate surfaces for global land areas, Int. J. Climatol., 37, 4302–4315, https://doi.org/10.1002/joc.5086, 2017.

Forgy, E. W.: Cluster analysis of multivariate data: efficiency versus interpretability of classifications, Biometrics, 21, 768–769, 1965.

García-Ruiz, J. M., López-Moreno, J. I., Vicente-Serrano, S. M., Lasanta-Martínez, T., and Beguería, S.: Mediterranean water resources in a global change scenario, Earth-Sci. Rev., 105, 121–139, https://doi.org/10.1016/j.earscirev.2011.01.006, 2011.

Giorgi, F., Regional climate modeling: Status and perspectives, Paper presented at the Journal de Physique IV (Proceedings), EDP sciences, 2006.

Giorgi, F., Jones, C., and Asrar, G. R.: Addressing climate information needs at the regional level: the CORDEX framework, World Meteorol. Organiz. Bull., 58, 175–183, 2009.

Haines, A., Finlayson, B., and McMahon, T.: A global classification of river regimes, Appl. Geogr., 8, 255–272, https://doi.org/10.1016/0143-6228(88)90035-5, 1988.

Harrison, S. P., Prentice, I. C., Barboni, D., Kohfeld, K. E., Ni, J., and Sutra, J. P.: Ecophysiological and bioclimatic foundations for a global plant functional classification, J. Veg. Sci., 21, 300–317, https://doi.org/10.1111/j.1654-1103.2009.01144.x, 2010.

Hijmans, R. J., Cameron, S. E., Parra, J. L., Jones, P. G., and Jarvis, A.: Very high resolution interpolated climate surfaces for global land areas, Int. J. Climatol., 25, 1965–1978, https://doi.org/10.1002/joc.1276, 2005.

Holdridge, L. R.: Determination of world plant formations from simple climatic data, Science, 105, 367–368, https://doi.org/10.1126/science.105.2727.367, 1947.

Hotelling, H.: Analysis of a complex of statistical variables into principal components, J. Educ. Psychol., 24, 417–441, https://doi.org/10.1037/h0071325, 1933.

Hrachowitz, M., Savenije, H. H. G., Blöschl, G., McDonnell, J. J., Sivapalan, M., Pomeroy, J. W., Arheimer, B., Blume, T., Clark, M. P., Ehret, U., Fenicia, F., Freer, J. E., Gelfan, A., Gupta, H. V., Hughes, D. A., Hut, R. W., Montanari, A., Pande, S., Tetzlaff, D., Troch, P. A., Uhlenbrook, S., Wagener, T., Winsemius, H. C., Woods, R. A., Zehe, E., and Cudennec, C.: A decade of Predictions in Ungauged Basins (PUB) – a review, Hydrolog. Sci. J., 58, 1198–1255, https://doi.org/10.1080/02626667.2013.803183, 2013.

Hreiche, A.: Modélisation conceptuelle de la transformation pluie-débit dans le contexte méditerranéen, Université Montpellier II – Sciences et Techniques du Languedoc, Montpellier, 2003.

Hreiche, A., Najem, W., and Bocquillon, C.: Hydrological impact simulations of climate change on Lebanese coastal rivers/Simulations des impacts hydrologiques du changement climatique sur les fleuves côtiers Libanais, Hydrolog. Sci. J./Journal des Sciences Hydrologiques, 52, 1119–1133, https://doi.org/10.1623/hysj.52.6.1119, 2007.

IPCC: Climate Change 2013: The Physical Science Basis: Working Group I contribution to the Fifth assessment report of the Intergovernmental Panel on Climate Change, Cambridge University Press, Cambridge, UK and New York, NY, USA, 2013.

Jolliffe, I. T.: Principal Component Analysis, Springer, 2002.

Köppen, W.: Das geographische System der Klimate, Borntraeger, 1936.

Kotlarski, S., Keuler, K., Christensen, O. B., Colette, A., Déqué, M., Gobiet, A., Goergen, K., Jacob, D., Lüthi, D., van Meijgaard, E., Nikulin, G., Schär, C., Teichmann, C., Vautard, R., Warrach-Sagi, K., and Wulfmeyer, V.: Regional climate modeling on European scales: a joint standard evaluation of the EURO-CORDEX RCM ensemble, Geosci. Model Dev., 7, 1297–1333, https://doi.org/10.5194/gmd-7-1297-2014, 2014.

Koutroulis, A. G.: Dryland changes under different levels of global warming, Sci. Total Environ., 655, 482–511, https://doi.org/10.1016/j.scitotenv.2018.11.215, 2019.

Krzanowski, W. J.: Principles of multivariate analysis: a user's perspective, Clarendon Press, 1988.

Lehner, B. and Grill, G.: Global river hydrography and network routing: baseline data and new approaches to study the world's large river systems, Hydrol. Process., 27, 2171–2186, 2013.

Lionello, P. and Scarascia, L.: The relation between climate change in the Mediterranean region and global warming, Reg. Environ. Change, 18, 1481–1493, https://doi.org/10.1007/s10113-018-1290-1, 2018.

MacQueen, J.: Some methods for classification and analysis of multivariate observations, in: Proceedings of the fifth Berkeley symposium on mathematical statistics and probability, Univ. of Calif. Press, 1967.

Mather, J. R. and Yoshioka, G. A.: The role of climate in the distribution of vegetation, Ann. Assoc. Am. Geogr., 58, 29–41, https://doi.org/10.1111/j.1467-8306.1968.tb01634.x, 1968.

Menne, M. J., Durre, I., Korzeniewski, B., McNeal, S., Thomas, K., Yin, X., Anthony, S., Ray, R., Vose, R. S., and Gleason, B. E.: Global historical climatology network-daily (GHCN-Daily), Version 3, 10, V5D21VHZ, NOAA National Climatic Data Center, 2012.

Merheb, M., Moussa, R., Abdallah, C., Colin, F., Perrin, C., and Baghdadi, N.: Hydrological response characteristics of Mediterranean catchments at different time scales: a meta-analysis, Hydrolog. Sci. J., 61, 2520–2539, https://doi.org/10.1080/02626667.2016.1140174, 2016.

Milano, M., Ruelland, D., Fernandez, S., Dezetter, A., Fabre, J., Servat, E., Fritsch, J.-M., Ardoin-Bardin, S., and Thivet, G.: Current state of Mediterranean water resources and future trends under climatic and anthropogenic changes, Hydrolog. Sci. J., 58, 498–518, https://doi.org/10.1080/02626667.2013.774458, 2013.

Moreno, J. A. O.: Modelización del ciclo fenológico reproductor del olivo (Olea europaea L.), Universidad de Córdoba, Córdoba, 2014.

Moron, V., Robertson, A. W., Ward, M. N., and Ndiaye, O.: Weather types and rainfall over Senegal. Part I: Observational analysis, J. Climate, 21, 266–287, https://doi.org/10.1175/2007JCLI1601.1, 2008.

NCEI: Ground weather station data, Global Historical Climatology Network, National Centers for Environmental Information, available at: https://www.ncdc.noaa.gov/ghcn-daily-description, last access: 8 September 2020.

Oueslati, O., De Girolamo, A. M., Abouabdillah, A., Kjeldsen, T. R., and Lo Porto, A.: Classifying the flow regimes of Mediterranean streams using multivariate analysis, Hydrol. Process., 29, 4666–4682, https://doi.org/10.1002/hyp.10530, 2015.

Pearson, K.: Principal components analysis, London Edinburgh Dublin Philos. Mag. J. Sci., 6, 559–572, 1901.

Peel, M. C., Finlayson, B. L., and McMahon, T. A.: Updated world map of the Köppen–Geiger climate classification, Hydrol. Earth Syst. Sci., 11, 1633–1644, https://doi.org/10.5194/hess-11-1633-2007, 2007.

PlanBleu: Les demandes en eau toujours satisfaites en Méditerranée à l'horizon 2050? In Les Notes du Plan Bleu, in: Vol. #25, Plan Bleu PNUE/PAM, Sophia Antipolis, 2012.

Raymond, F., Ullmann, A., Camberlin, P., Drobinski, P., and Smith, C. C.: Extreme dry spell detection and climatology over the Mediterranean Basin during the wet season, Geophys. Res. Lett., 43, 7196–7204, https://doi.org/10.1002/2016GL069758, 2016.

Rivoire, P., Tramblay, Y., Neppel, L., Hertig, E., and Vicente-Serrano, S. M.: Impact of the dry-day definition on Mediterranean extreme dry-spell analysis, Nat. Hazards Earth Syst. Sci., 19, 1629–1638, https://doi.org/10.5194/nhess-19-1629-2019, 2019.

Rockel, B., Will, A., and Hense, A.: The regional climate model COSMO-CLM (CCLM), Meteorol. Z., 17, 347–348, https://doi.org/10.1127/0941-2948/2008/0309, 2008.

Rodwell, M. J. and Hoskins, B. J.: Monsoons and the dynamics of deserts, Q. J. Roy. Meteorol. Soc., 122, 1385–1404, https://doi.org/10.1002/qj.49712253408, 1996.

Romera, R., Sánchez, E., Domínguez, M., Gaertner, M. Á., and Gallardo, C.: Evaluation of present-climate precipitation in 25 km resolution regional climate model simulations over Northwest Africa, Clim. Res., 66, 125–139, https://doi.org/10.3354/cr01330, 2015.

Ruti, P. M., Somot, S., Giorgi, F., Dubois, C., Flaounas, E., Obermann, A., Dell'Aquila, A., Pisacane, G., Harzallah, A., and Lombardi, E.: MED-CORDEX initiative for Mediterranean climate studies, B. Am. Meteorol. Soc., 97, 1187–1208, https://doi.org/10.1175/BAMS-D-14-00176.1, 2016.

Sauquet, E., Richard, B., Devers, A., and Prudhomme, C.: Water restrictions under climate change: a Rhône–Mediterranean perspective combining bottom-up and top-down approaches, Hydrol. Earth Syst. Sci., 23, 3683–3710, https://doi.org/10.5194/hess-23-3683-2019, 2019.

Slimani, M., Cudennec, C., and Feki, H.: Structure of the rainfall gradient in the Mediterranean–Sahara transition in Tunisia: geographical determinants and seasonality, Hydrol. Sci. J., 52, 1088–1102, https://doi.org/10.1623/hysj.52.6.1088, 2007.

Sönmez, Ý. and Kömüþcü, A. Ü.: Reclassification of rainfall regions of Turkey by K-means methodology and their temporal variability in relation to North Atlantic Oscillation (NAO), Theor. Appl. Climatol., 106, 499–510, https://doi.org/10.1007/s00704-011-0449-1, 2011.

Thornthwaite, C. W.: An approach toward a rational classification of climate, Geogr. Rev., 38, 55–94, https://doi.org/10.2307/210739, 1948.

Toth, E.: Catchment classification based on characterisation of streamflow and precipitation time series, Hydrol. Earth Syst. Sci., 17, 1149–1159, https://doi.org/10.5194/hess-17-1149-2013, 2013.

Tramblay, Y. and Somot, S.: Future evolution of extreme precipitation in the Mediterranean, Climatic Change, 151, 289–302, https://doi.org/10.1007/s10584-018-2300-5, 2018.

Tramblay, Y., Ruelland, D., Somot, S., Bouaicha, R., and Servat, E.: High-resolution Med-CORDEX regional climate model simulations for hydrological impact studies: a first evaluation of the ALADIN-Climate model in Morocco, Hydrol. Earth Syst. Sci., 17, 3721–3739, https://doi.org/10.5194/hess-17-3721-2013, 2013.

Trigo, I. F., Davies, T. D., and Bigg, G. R.: Objective climatology of cyclones in the Mediterranean region, J. Climate, 12, 1685–1696, https://doi.org/10.1175/1520-0442(1999)012<1685:OCOCIT>2.0.CO;2, 1999.

Turc, L.: Estimation of irrigation water requirements, potential evapotranspiration: a simple climatic formula evolved up to date, Ann. Agron., 12, 13–49, 1961.

Unal, Y., Kindap, T., and Karaca, M.: Redefining the climate zones of Turkey using cluster analysis, Int. J. Climatol., 23, 1045–1055, https://doi.org/10.1002/joc.910, 2003.

Verdier, J. and Viollet, P.-L.: Les tensions sur l'eau en Europe et dans le bassin méditerranéen. Des crises de l'eau d'ici 2050, La Houille Blanche, 6, 102–107, https://doi.org/10.1051/lhb/20150075, 2015.

Vicente-Serrano, S. M., González-Hidalgo, J. C., de Luis, M., and Raventós, J.: Drought patterns in the Mediterranean area: the Valencia region (eastern Spain), Clim. Res., 26, 5–15, https://doi.org/10.3354/cr026005, 2004.

Wagener, T., Sivapalan, M., Troch, P., and Woods, R.: Catchment Classification and Hydrologic Similarity, Geogr. Compass, 1, 901–931, https://doi.org/10.1111/j.1749-8198.2007.00039.x, 2007.

Wainwright, J. and Thornes, J. B.: Environmental issues in the Mediterraean, 1st edn., Routledge, London, 512 pp., https://doi.org/10.4324/9780203495490, 2004.

WorldClim: Worldclim-2 data, available at: https://www.worldclim.org/data/worldclim21.html, last access: 8 September 2020.

Zittis, G.: Observed rainfall trends and precipitation uncertainty in the vicinity of the Mediterranean, Middle East and North Africa, Theor. Appl. Climatol., 134, 1207–1230, https://doi.org/10.1007/s00704-017-2333-0, 2018.

APPENDIX B3

Climatic Indices of the selected catchments

Table B3 - 1 : Climatic Indices of the selected catchments

OID	PAYS	NOM ADOPTE	I_s	$P_{25\%}$	$SP_{1.5}$	ST_m	$T_{25\%}$	S_{PET}	I_{Arid}
4	AG	MELAH	0.84	1.50	2	6	1.41	4	1.86
5	AG	MAZAFRAN	0.91	1.75	3	6	1.35	5	1.61
15	AL	ERZENIT	0.66	1.32	1	6	1.49	7	0.86
47	CY	SERRAKHIS	0.96	1.79	3	6	1.36	3	2.66
51	CY	VASILIKOS	0.96	1.77	3	6	1.33	3	2.35
56	CY	EZOUSAS	0.96	1.82	3	6	1.33	3	2.38
63	CY	DHIARIZOS	0.96	1.82	3	6	1.35	5	2.03
88	ES	CENIA	0.46	1.28	0	6	1.43	4	1.83
103	ES	AMADORIO	0.59	1.42	1	6	1.39	0	2.81
162	ES	FLUVIA	0.31	1.23	0	6	1.44	6	1.20
165	ES	LA MUGA	0.43	1.10	1	6	1.39	5	1.43
169	ES	ELTER	0.29	1.15	0	6	1.48	6	1.04
174	ES	EL BESÒS	0.37	1.25	0	6	1.41	5	1.35
175	ES	GAIA	0.40	1.30	0	6	1.44	4	1.57
194	ES	ANDARAX	0.80	1.44	1	6	1.44	4	2.58
206	FR	FIUM-ALTO	0.74	1.39	2	6	1.42	6	1.17
297	FR	LEZ	0.57	1.19	1	6	1.41	5	1.44
319	FR	LOUP	0.61	1.20	1	6	1.51	7	0.96
531	FR	HERAULT	0.53	1.20	1	6	1.44	5	1.23
541	FR	AUDE	0.40	1.19	0	6	1.44	6	1.11
550	FR	GAPEAU	0.68	1.33	1	6	1.39	5	1.31
559	FR	TECH	0.35	1.13	0	6	1.48	7	1.01
561	FR	TET	0.37	1.18	0	6	1.56	8	0.82
634	GR	SPERCHIOS	0.75	1.36	2	6	1.56	6	1.26
677	HR	MIRNA	0.36	1.13	0	6	1.59	8	0.67
681	HR	KRKA	0.46	1.23	0	6	1.56	7	0.96
692	IS	ALEXANDER	1.00	2.12	4	6	1.32	4	2.35
693	IS	SOREQ	1.00	2.17	5	6	1.30	3	2.85
710	IT	FIORA	0.61	1.18	1	6	1.44	4	1.95
722	IT	ALCANTARA	0.86	1.57	4	6	1.44	6	1.54
725	IT	FLUMINIMAGGIORE	0.86	1.45	2	6	1.36	6	1.49
800	IT	SERCHIO	0.59	1.24	1	6	1.56	8	0.53
803	IT	ARGENTINA	0.58	1.20	1	6	1.50	7	0.93
822	IT	CECINA	0.55	1.22	1	6	1.44	6	1.27
845	IT	PESCARA	0.41	1.25	0	6	1.62	7	1.00
887	IT	ALENTO	0.76	1.43	1	6	1.37	6	1.17
903	IT	S.LEONARDO	0.88	1.63	3	6	1.41	4	2.07
908	IT	F.IMERA MERIDIONALE	0.90	1.69	4	6	1.38	4	2.31
913	IT	CERVARO	0.53	1.24	1	6	1.46	4	1.82
928	LB	NAHR EL JAOUZ	0.99	2.14	4	6	1.41	5	1.04
929	LB	NAHR BEYROUTH	0.99	2.23	4	6	1.37	5	1.16
930	LB	NAHR EL KALB	0.99	2.18	4	6	1.46	5	1.00
934	LB	NAHR IBRAHIM	0.99	2.12	4	6	1.52	5	0.99
936	LB	NAHR ASSI	0.99	2.04	4	6	1.35	5	1.36
937	LB	NAHR LITANI	1.00	2.26	4	6	1.44	5	1.50
938	ME	MORACA	0.63	1.31	1	6	1.64	8	0.61
949	MO	KERT	0.88	1.62	4	6	1.32	2	3.29
951	MO	EMSA	0.97	1.83	4	6	1.28	5	1.76
959	SI	RIŽANA	0.36	1.14	0	6	1.57	8	0.63
960	SI	DRAGONJA	0.37	1.13	0	6	1.57	8	0.69
962	SI	ISONZO	0.41	1.14	0	6	1.74	12	0.32
1035	TR	KOEPRUE	0.89	1.60	3	6	1.51	5	1.50
1042	TR	CINE CAYI	0.86	1.60	3	6	1.55	5	1.64
1048	TS	MEJERDA	0.77	1.42	2	6	1.41	3	2.31
1074	TS	MILIANE	0.82	1.43	2	6	1.35	3	2.60

APPENDIX C1

Physiographic Indices of the selected catchments

Table C1 - 1 : Physiographic Indices of the selected catchments

OID	PAYS	NOM ADOPTE	A	Z_{Mean}	ZS_{Mean}	I_{Hypso}	P_{Karst}	T_AWC	TC_BDC	TC_MLT	SC_COD	SHC	CMA	BA	Leptosols
4	AG	MELAH	6334	677	0	0.17	9	56	16	0	34	14	34	0	0
5	AG	MAZAFRAN	2039	391	0	-0.20	19	54	30	0	22	0	39	0	0
15	AL	ERZENIT	868	396	1479	-0.34	19	49	5	4	36	0	47	0	0
47	CY	SERRAKHIS	740	379	0	-0.30	0	48	0	0	64	0	23	0	18
51	CY	VASILIKOS	150	433	0	-0.06	0	33	0	0	84	0	5	0	51
56	CY	EZOUSAS	225	486	0	-0.10	0	34	0	0	42	0	18	0	49
63	CY	DHIARIZOS	264	660	0	-0.05	0	34	0	0	43	0	4	0	45
88	ES	CENIA	205	559	0	0.05	100	49	14	7	13	0	33	0	66
103	ES	AMADORIO	218	619	0	-0.02	16	49	0	14	28	0	58	0	67
162	ES	FLUVIA	962	506	0	-0.07	0	53	35	19	1	2	6	0	52
165	ES	LA MUGA	762	288	0	-0.29	0	51	12	13	5	4	17	0	32
169	ES	ELTER	2955	730	1743	-0.10	2	49	25	22	1	4	9	0	37
174	ES	EL BESÒS	1035	376	0	-0.25	0	51	10	4	5	8	19	0	14
175	ES	GAIA	422	468	0	0.06	43	51	8	0	13	2	53	0	42
194	ES	ANDARAX	2161	988	1786	-0.05	28	54	0	25	2	54	9	0	11
206	FR	FIUM-ALTO	127	590	0	-0.04	0	53	74	6	1	0	0	0	0
297	FR	LEZ	989	93	0	-0.29	72	45	0	3	0	0	75	0	69
319	FR	LOUP	289	830	1288	0.15	100	54	7	6	0	0	54	0	48
531	FR	HERAULT	2625	364	1168	-0.21	85	47	8	15	0	0	50	0	61
541	FR	AUDE	5226	431	1458	-0.37	26	48	12	15	0	0	52	0	23
550	FR	GAPEAU	566	304	0	-0.13	50	49	1	18	0	0	28	0	26
559	FR	TECH	725	752	1625	-0.07	0	48	29	36	0	3	9	0	34
561	FR	TET	1380	1046	1845	-0.11	0	47	1	9	1	5	13	0	42
634	GR	SPERCHIOS	1385	714	1344	-0.07	58	42	10	9	4	0	17	0	31
677	HR	MIRNA	579	289	0	-0.11	100	45	22	2	2	0	73	0	70
681	HR	KRKA	2549	406	1082	-0.22	100	22	6	1	3	0	72	0	82
692	IS	ALEXANDER	572	211	0	-0.37	71	47	0	0	3	0	22	1	0
693	IS	SOREQ	782	298	0	-0.47	55	53	0	0	22	7	4	1	20
710	IT	FIORA	826	360	0	-0.11	1	50	3	6	8	0	65	0	0
722	IT	ALCANTARA	555	916	2019	-0.01	0	46	19	17	8	0	8	2	0
725	IT	FLUMINIMAGGIORE	125	360	0	-0.04	83	49	14	3	3	0	0	0	0
800	IT	SERCHIO	1435	697	1408	-0.02	35	48	9	4	2	0	7	2	90
803	IT	ARGENTINA	209	876	1317	-0.02	100	55	84	3	0	0	8	0	0
822	IT	CECINA	909	288	0	-0.10	6	54	25	28	7	0	34	0	70
845	IT	PESCARA	3153	917	1298	-0.03	84	52	24	7	18	0	16	4	15
887	IT	ALENTO	414	381	0	-0.19	5	54	29	19	2	0	12	0	0
903	IT	S.LEONARDO	505	579	0	-0.03	21	51	0	3	0	0	82	0	12
908	IT	F.IMERA MERID	2013	494	0	-0.07	55	52	1	1	4	0	9	2	10
913	IT	CERVARO	673	402	0	-0.06	0	48	0	2	3	0	87	0	0
928	LB	NAHR EL JAOUZ	195	1050	1557	-0.04	100	54	0	0	95	5	0	0	0
929	LB	NAHR BEYROUTH	237	931	0	-0.02	99	55	0	0	75	12	5	0	0
930	LB	NAHR EL KALB	259	1406	1856	-0.02	100	48	0	0	70	28	0	0	70
934	LB	NAHR IBRAHIM	329	1572	1928	0.13	100	34	0	0	47	48	0	1	35
936	LB	NAHR ASSI	250	361	0	-0.32	74	56	0	0	78	0	8	0	0
937	LB	NAHR LITANI	2179	1098	2092	-0.07	100	37	0	0	22	25	22	1	33
938	ME	MORACA	6056	681	1257	-0.04	100	43	12	5	9	0	62	0	38
949	MO	KERT	2622	563	0	-0.07	6	56	1	0	2	73	4	3	0
951	MO	EMSA	34	285	0	-0.20	100	50	97	0	0	0	4	0	0
959	SI	RIŽANA	78	235	0	-0.19	96	55	35	15	6	0	43	0	10
960	SI	DRAGONJA	147	231	0	0.07	100	55	28	1	0	0	70	0	0
962	SI	ISONZO	3334	593	1026	-0.10	88	48	59	7	1	0	28	0	49
1035	TR	KOEPRUE	3003	967	1568	0.08	30	42	0	0	45	2	12	2	28
1042	TR	CINE CAYI	27383	848	1491	0.04	18	43	0	0	39	1	39	1	20
1048	TS	MEJERDA	23176	583	0	0.02	43	55	6	0	4	29	33	0	12
1074	TS	MILIANE	2313	262	0	-0.17	82	53	9	0	50	1	37	0	60

APPENDIX D1

Flow regime types for all catchments according to the classification of Haines (1988)

Note: for each river, the average monthly runoff was calculated and converted into the ratio from annual runoff, then ranked from June to May as recommended for the North Hemisphere.

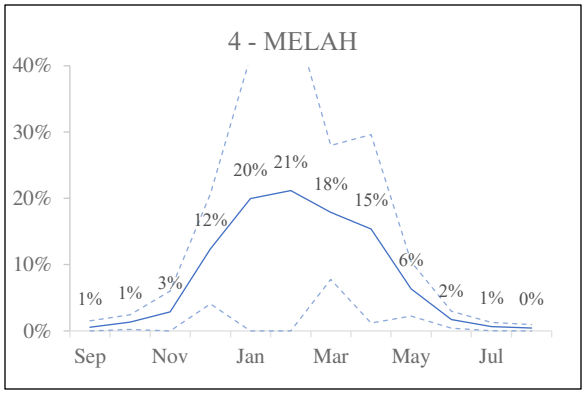
4 - MELAH
40%
30%
20%
10%
0%
1% 1% 3% 12% 20% 21% 18% 15% 6% 2% 1% 0%
Sep Nov Jan Mar May Jul

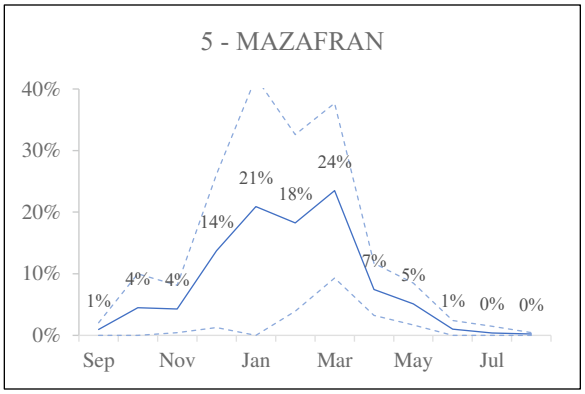
5 - MAZAFRAN
40%
30%
20%
10%
0%
1% 4% 4% 14% 21% 18% 24% 7% 5% 1% 0% 0%
Sep Nov Jan Mar May Jul

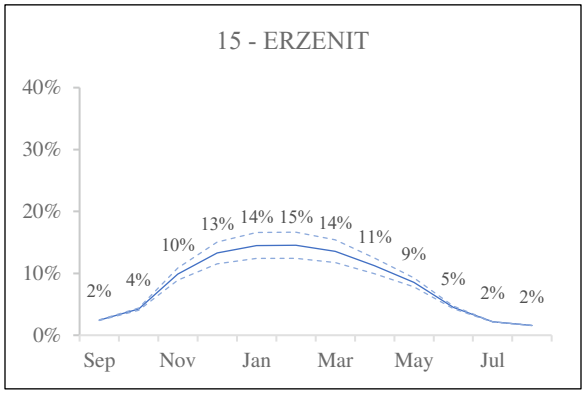
15 - ERZENIT
40%
30%
20%
10%
0%
2% 4% 10% 13% 14% 15% 14% 11% 9% 5% 2% 2%
Sep Nov Jan Mar May Jul

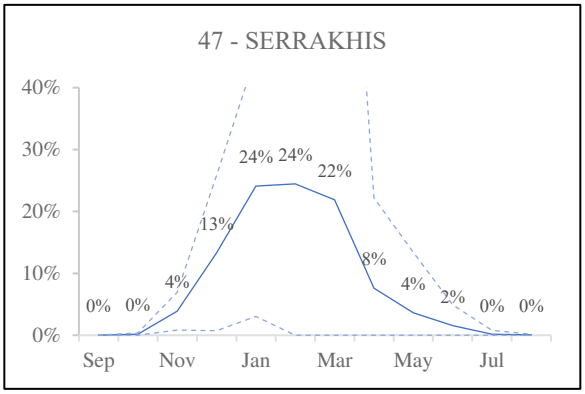
47 - SERRAKHIS
40%
30%
20%
10%
0%
0% 0% 4% 13% 24% 24% 22% 8% 4% 2% 0% 0%
Sep Nov Jan Mar May Jul

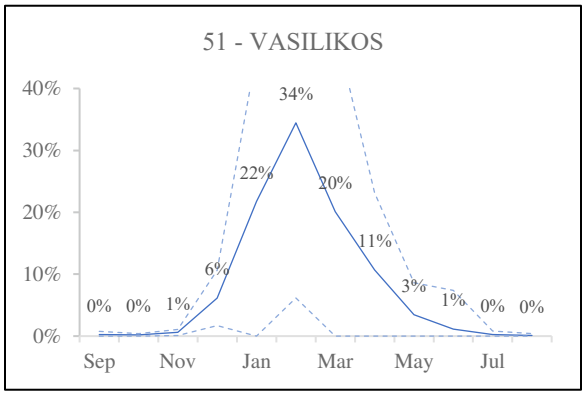
51 - VASILIKOS
40%
30%
20%
10%
0%
0% 0% 1% 6% 22% 34% 20% 11% 3% 1% 0% 0%
Sep Nov Jan Mar May Jul

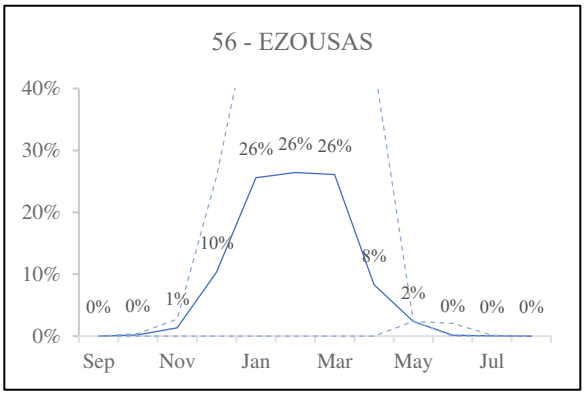
56 - EZOUSAS
40%
30%
20%
10%
0%
0% 0% 1% 10% 26% 26% 26% 8% 2% 0% 0% 0%
Sep Nov Jan Mar May Jul

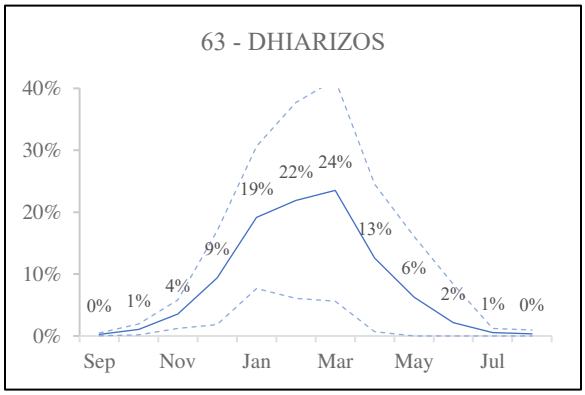
63 - DHIARIZOS
40%
30%
20%
10%
0%
0% 1% 4% 9% 19% 22% 24% 13% 6% 2% 1% 0%
Sep Nov Jan Mar May Jul

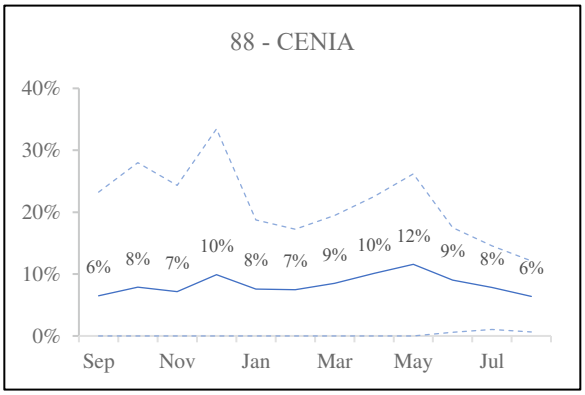
88 - CENIA
40%
30%
20%
10%
0%
6% 8% 7% 10% 8% 7% 9% 10% 12% 9% 8% 6%
Sep Nov Jan Mar May Jul

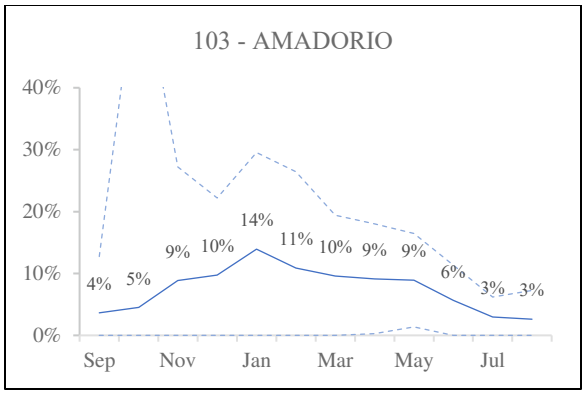
103 - AMADORIO
40%
30%
20%
10%
0%
4% 5% 9% 10% 14% 11% 10% 9% 9% 6% 3% 3%
Sep Nov Jan Mar May Jul

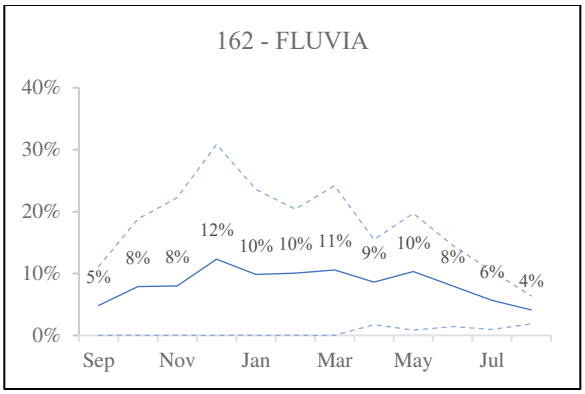
162 - FLUVIA
40%
30%
20%
10%
0%
5% 8% 8% 12% 10% 10% 11% 9% 10% 8% 6% 4%
Sep Nov Jan Mar May Jul

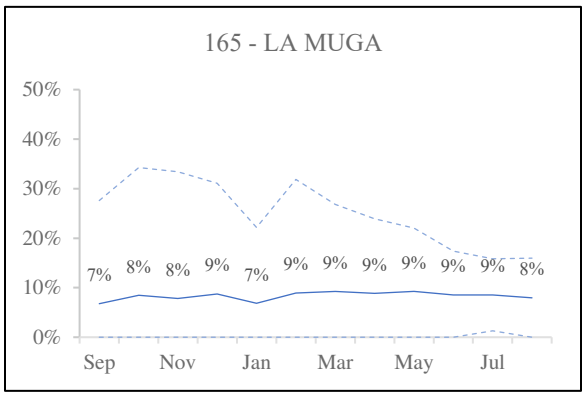
165 - LA MUGA
50%
40%
30%
20%
10%
0%
7% 8% 8% 9% 7% 9% 9% 9% 9% 9% 9% 8%
Sep Nov Jan Mar May Jul

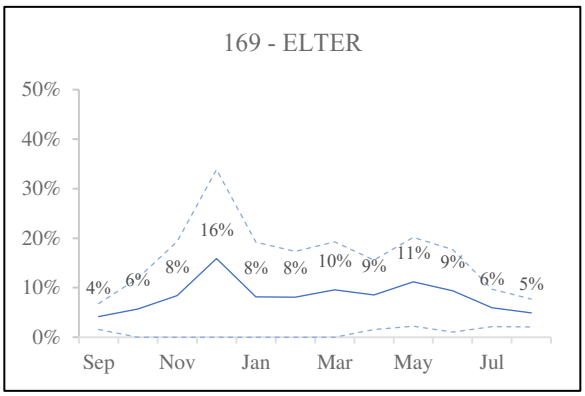
169 - ELTER
50%
40%
30%
20%
10%
0%
4% 6% 8% 16% 8% 8% 10% 9% 11% 9% 6% 5%
Sep Nov Jan Mar May Jul

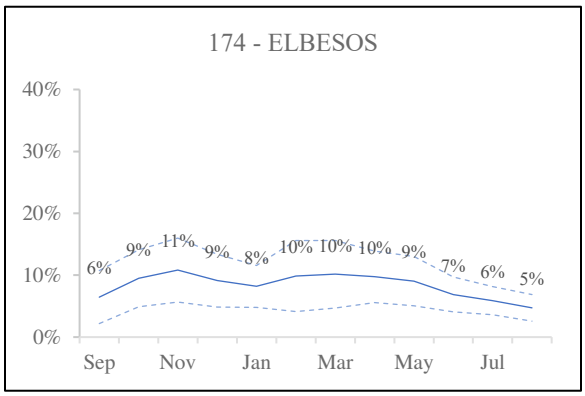
174 - ELBESOS
40%
30%
20%
10%
0%
6% 9% 11% 9% 8% 10% 10% 10% 9% 7% 6% 5%
Sep Nov Jan Mar May Jul

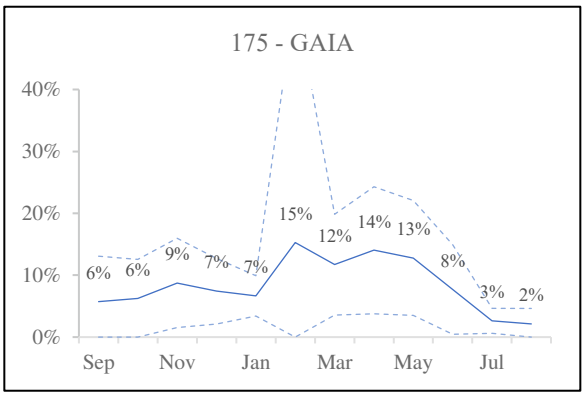
175 - GAIA
40%
30%
20%
10%
0%
6% 6% 9% 7% 7% 15% 12% 14% 13% 8% 3% 2%
Sep Nov Jan Mar May Jul

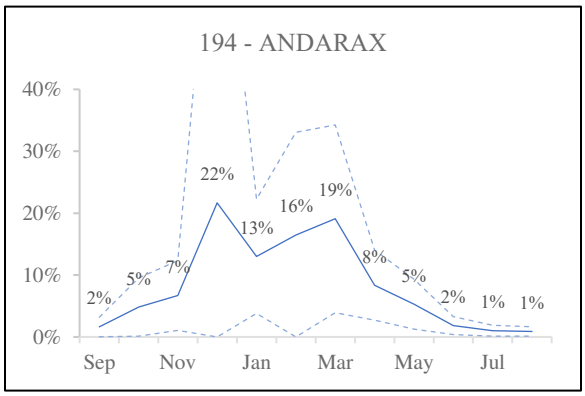
194 - ANDARAX
40%
30%
20%
10%
0%
2% 5% 7% 22% 13% 16% 19% 8% 5% 2% 1% 1%
Sep Nov Jan Mar May Jul

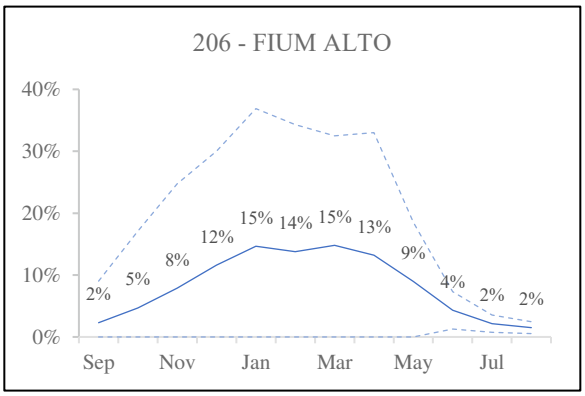
206 - FIUM ALTO
40%
30%
20%
10%
0%
2% 5% 8% 12% 15% 14% 15% 13% 9% 4% 2% 2%
Sep Nov Jan Mar May Jul

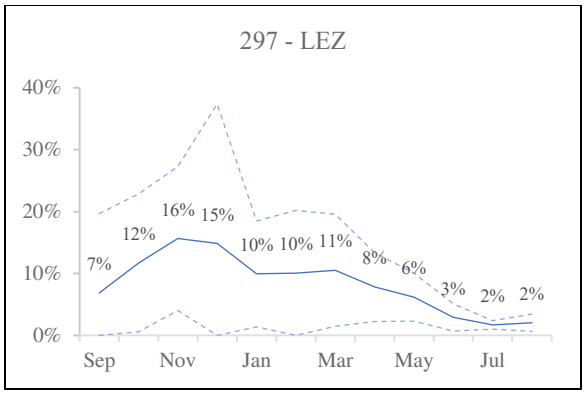
297 - LEZ
40%
30%
20%
10%
0%
7%
12%
16%
15%
10%
10%
11%
8%
6%
3%
2%
2%
Sep
Nov
Jan
Mar
May
Jul

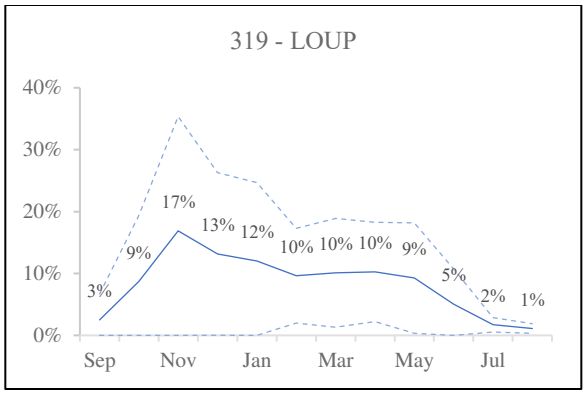
319 - LOUP
40%
30%
20%
10%
0%
3%
9%
17%
13%
12%
10%
10%
10%
9%
5%
2%
1%
Sep
Nov
Jan
Mar
May
Jul

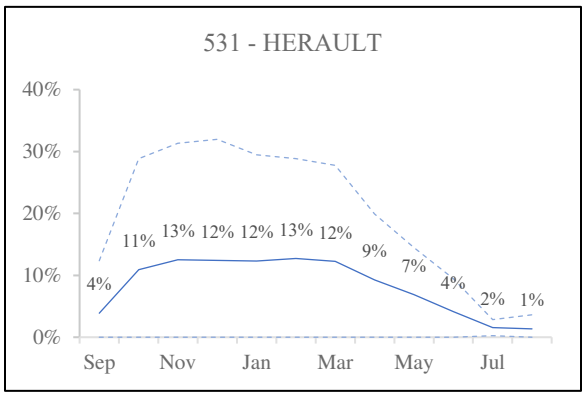
531 - HERAULT
40%
30%
20%
10%
0%
4%
11%
13%
12%
12%
13%
12%
9%
7%
4%
2%
1%
Sep
Nov
Jan
Mar
May
Jul

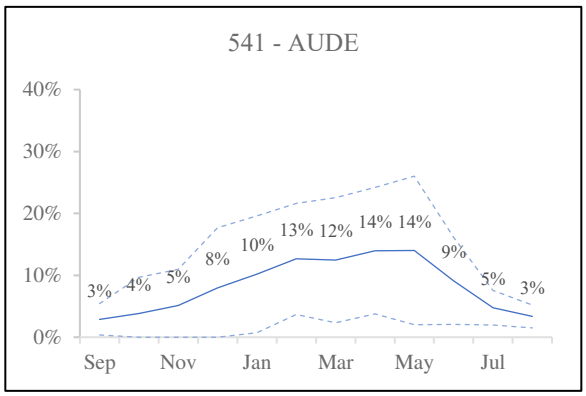
541 - AUDE
40%
30%
20%
10%
0%
3%
4%
5%
8%
10%
13%
12%
14%
14%
9%
5%
3%
Sep
Nov
Jan
Mar
May
Jul

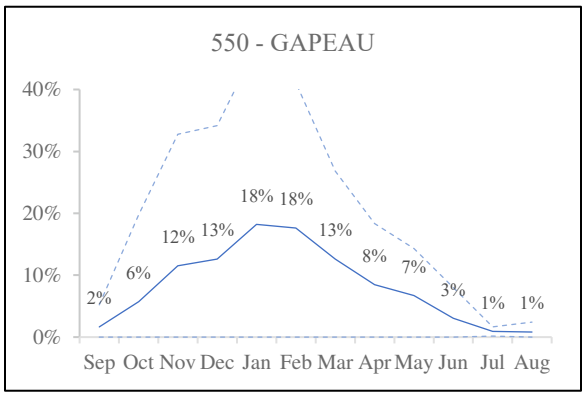
550 - GAPEAU
40%
30%
20%
10%
0%
2%
6%
12%
13%
18%
18%
13%
8%
7%
3%
1%
1%
Sep
Oct
Nov
Dec
Jan
Feb
Mar
Apr
May
Jun
Jul
Aug

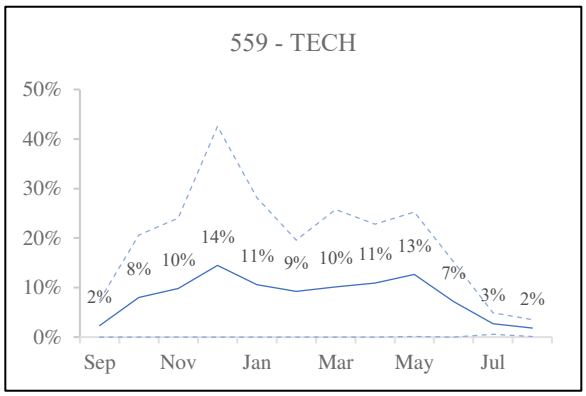
559 - TECH
50%
40%
30%
20%
10%
0%
2%
8%
10%
14%
11%
9%
10%
11%
13%
7%
3%
2%
Sep
Nov
Jan
Mar
May
Jul

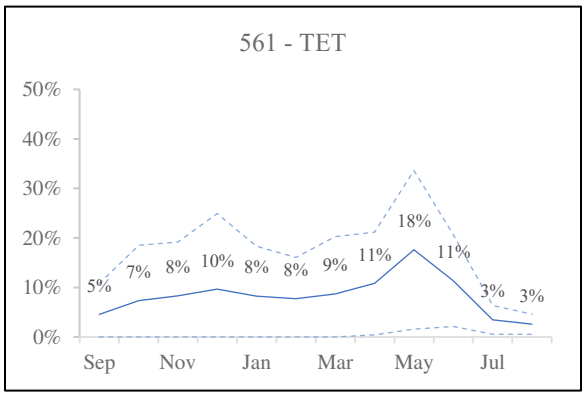
561 - TET
50%
40%
30%
20%
10%
0%
5%
7%
8%
10%
8%
8%
9%
11%
18%
11%
3%
3%
Sep
Nov
Jan
Mar
May
Jul

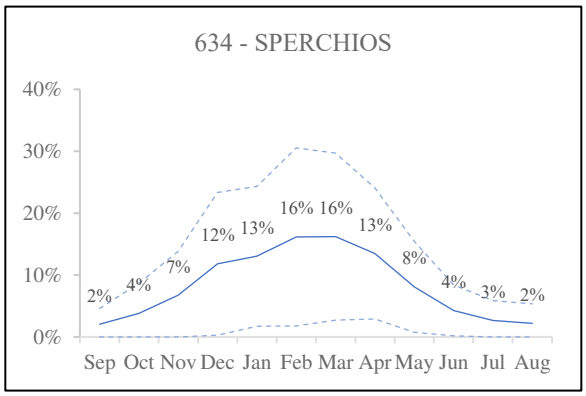
634 - SPERCHIOS
40%
30%
20%
10%
0%
2%
4%
7%
12%
13%
16%
16%
13%
8%
4%
3%
2%
Sep
Oct
Nov
Dec
Jan
Feb
Mar
Apr
May
Jun
Jul
Aug

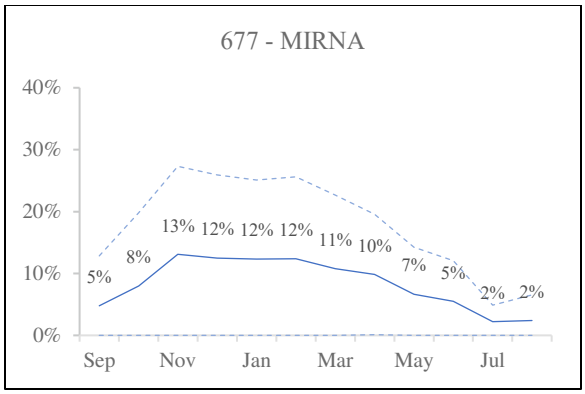
677 - MIRNA
40%
30%
20%
10%
0%
5% 8% 13% 12% 12% 12% 11% 10% 7% 5% 2% 2%
Sep Nov Jan Mar May Jul

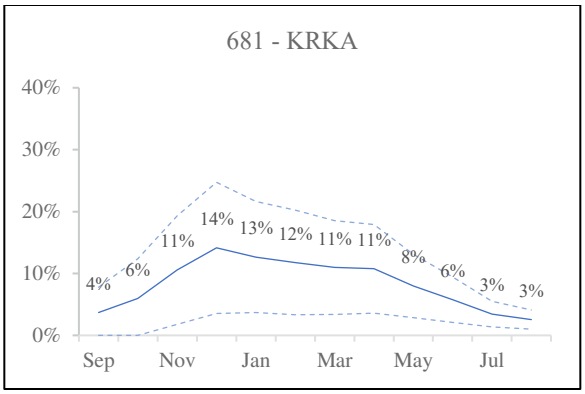
681 - KRKA
40%
30%
20%
10%
0%
4% 6% 11% 14% 13% 12% 11% 11% 8% 6% 3% 3%
Sep Nov Jan Mar May Jul

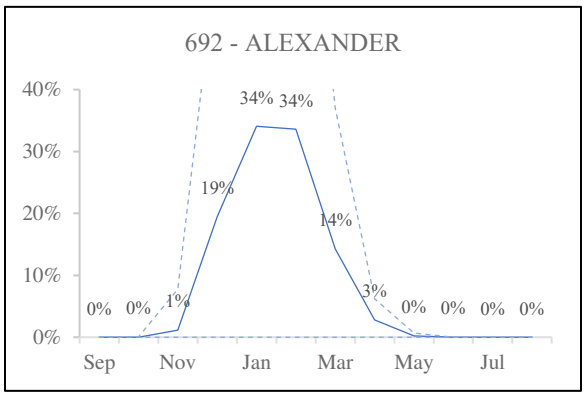
692 - ALEXANDER
40%
30%
20%
10%
0%
0% 0% 1% 19% 34% 34% 14% 3% 0% 0% 0% 0%
Sep Nov Jan Mar May Jul

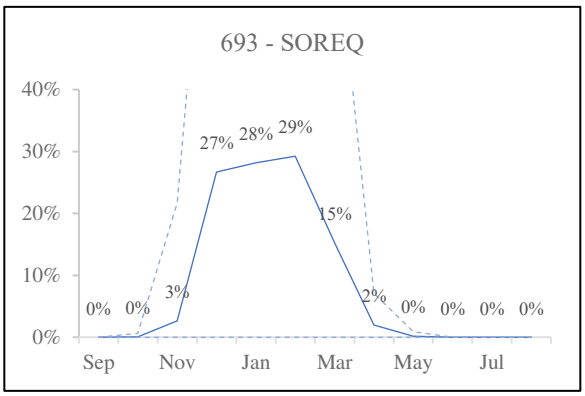
693 - SOREQ
40%
30%
20%
10%
0%
0% 0% 3% 27% 28% 29% 15% 2% 0% 0% 0% 0%
Sep Nov Jan Mar May Jul

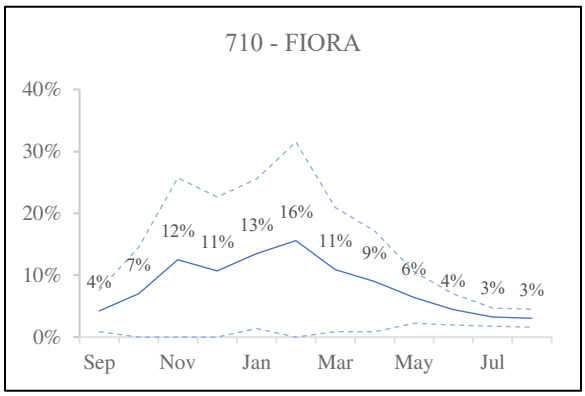
710 - FIORA
40%
30%
20%
10%
0%
4% 7% 12% 11% 13% 16% 11% 9% 6% 4% 3% 3%
Sep Nov Jan Mar May Jul

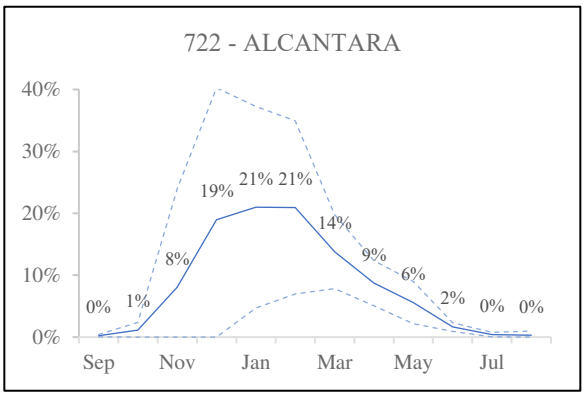
722 - ALCANTARA
40%
30%
20%
10%
0%
0% 1% 8% 19% 21% 21% 14% 9% 6% 2% 0% 0%
Sep Nov Jan Mar May Jul

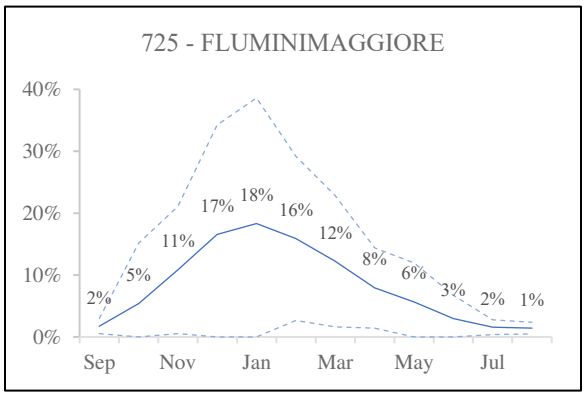
725 - FLUMINIMAGGIORE
40%
30%
20%
10%
0%
2% 5% 11% 17% 18% 16% 12% 8% 6% 3% 2% 1%
Sep Nov Jan Mar May Jul

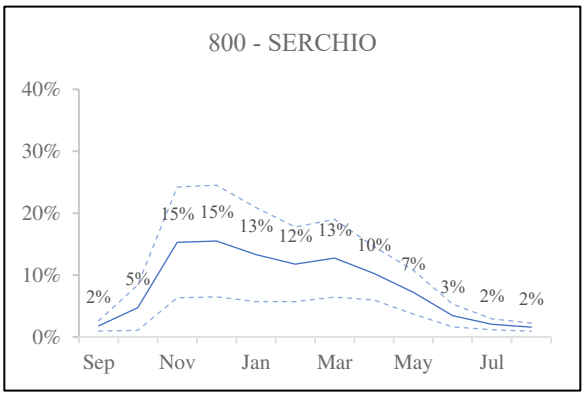
800 - SERCHIO
40%
30%
20%
10%
0%
2% 5% 15% 15% 13% 12% 13% 10% 7% 3% 2% 2%
Sep Nov Jan Mar May Jul

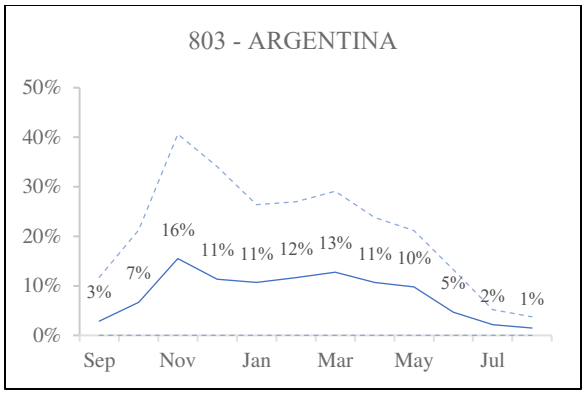
803 - ARGENTINA
50%
40%
30%
20%
10%
0%
3% 7% 16% 11% 11% 12% 13% 11% 10% 5% 2% 1%
Sep Nov Jan Mar May Jul

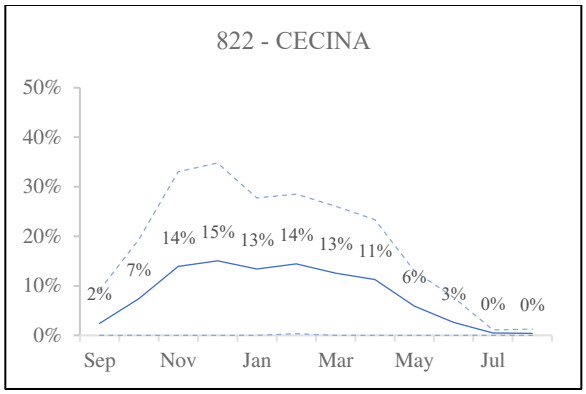
822 - CECINA
50%
40%
30%
20%
10%
0%
2% 7% 14% 15% 13% 14% 13% 11% 6% 3% 0% 0%
Sep Nov Jan Mar May Jul

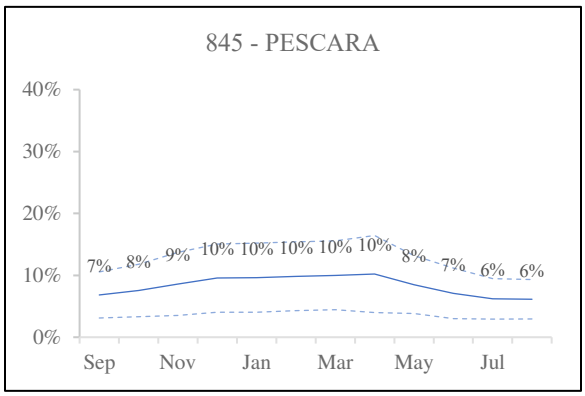
845 - PESCARA
40%
30%
20%
10%
0%
7% 8% 9% 10% 10% 10% 10% 10% 8% 7% 6% 6%
Sep Nov Jan Mar May Jul

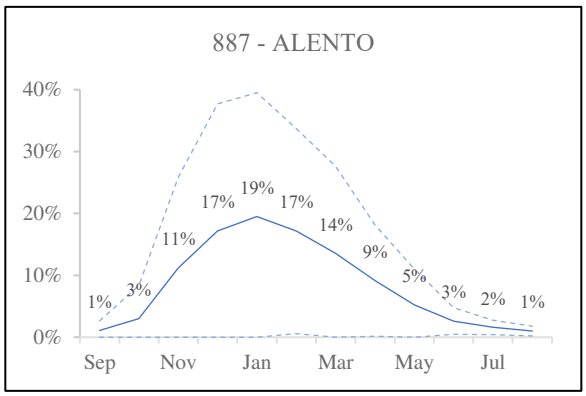
887 - ALENTO
40%
30%
20%
10%
0%
1% 3% 11% 17% 19% 17% 14% 9% 5% 3% 2% 1%
Sep Nov Jan Mar May Jul

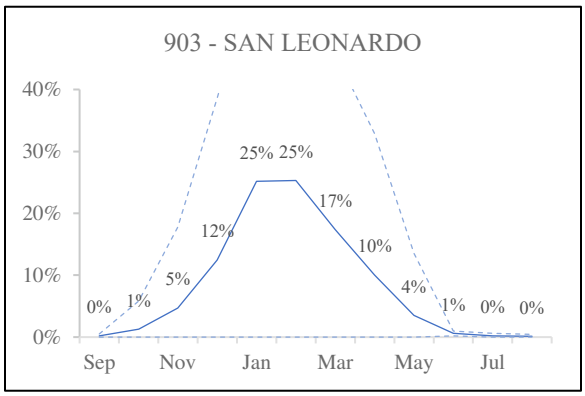
903 - SAN LEONARDO
40%
30%
20%
10%
0%
0% 1% 5% 12% 25% 25% 17% 10% 4% 1% 0% 0%
Sep Nov Jan Mar May Jul

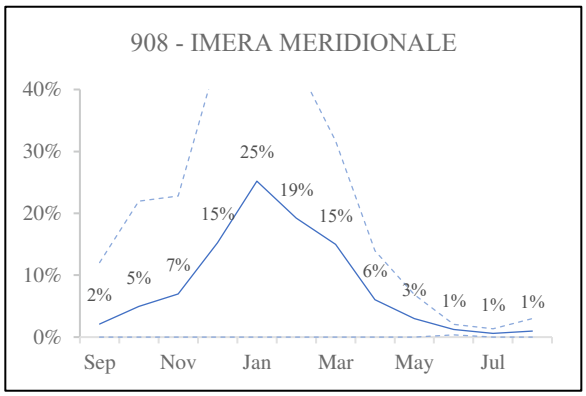
908 - IMERA MERIDIONALE
40%
30%
20%
10%
0%
2% 5% 7% 15% 25% 19% 15% 6% 3% 1% 1% 1%
Sep Nov Jan Mar May Jul

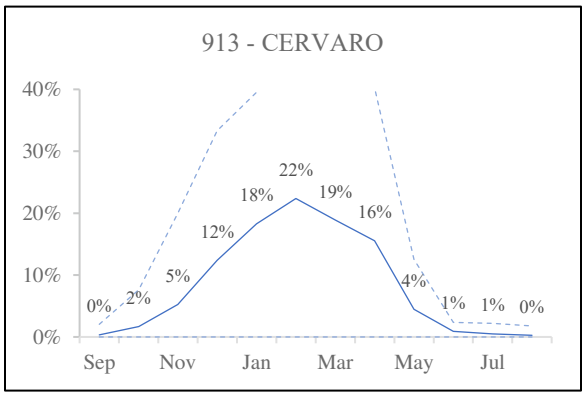
913 - CERVARO
40%
30%
20%
10%
0%
0% 2% 5% 12% 18% 22% 19% 16% 4% 1% 1% 0%
Sep Nov Jan Mar May Jul

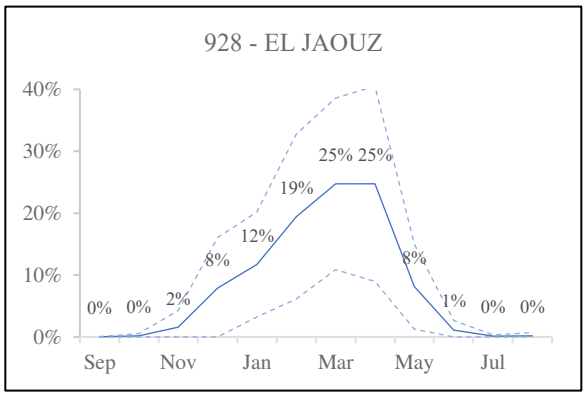
928 - EL JAOUZ
40%
30%
20%
10%
0%
0% 0% 2% 8% 12% 19% 25% 25% 8% 1% 0% 0%
Sep Nov Jan Mar May Jul

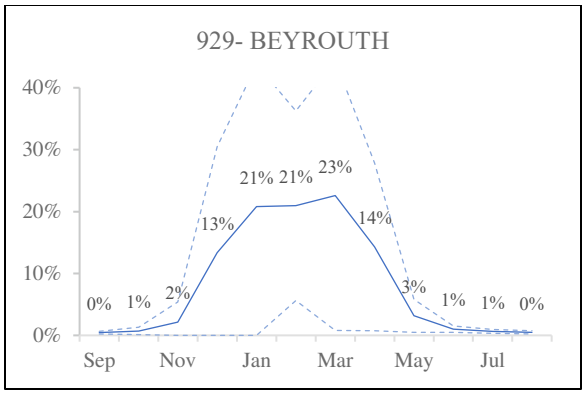
929- BEYROUTH
40%
30%
20%
10%
0%
0% 1% 2% 13% 21% 21% 23% 14% 3% 1% 1% 0%
Sep Nov Jan Mar May Jul

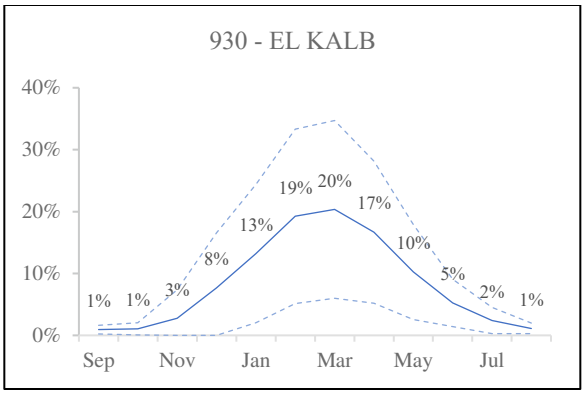
930 - EL KALB
40%
30%
20%
10%
0%
1% 1% 3% 8% 13% 19% 20% 17% 10% 5% 2% 1%
Sep Nov Jan Mar May Jul

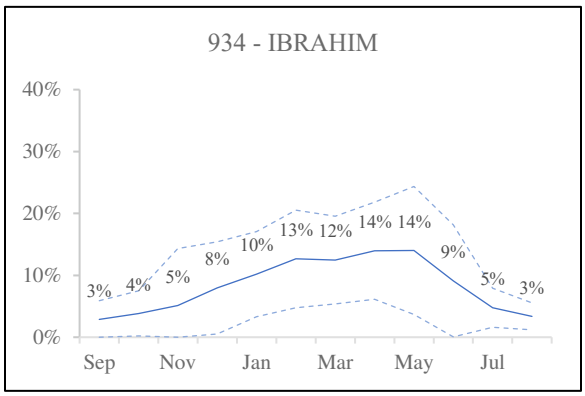
934 - IBRAHIM
40%
30%
20%
10%
0%
3% 4% 5% 8% 10% 13% 12% 14% 14% 9% 5% 3%
Sep Nov Jan Mar May Jul

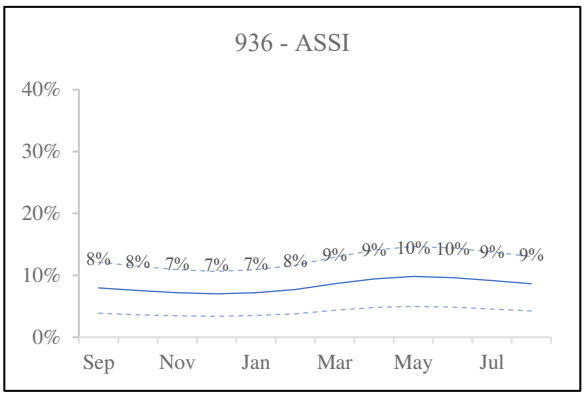
936 - ASSI
40%
30%
20%
10%
0%
8% 8% 7% 7% 7% 8% 9% 9% 10% 10% 9% 9%
Sep Nov Jan Mar May Jul

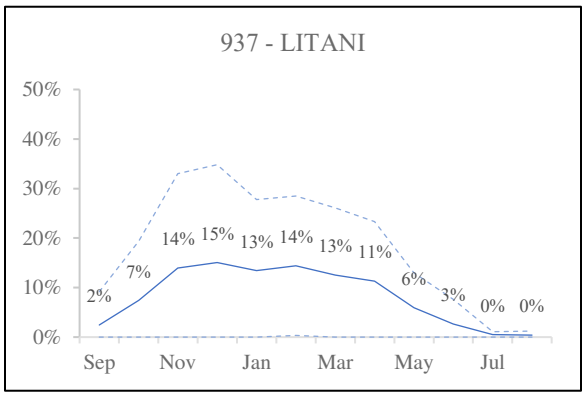
937 - LITANI
50%
40%
30%
20%
10%
0%
2% 7% 14% 15% 13% 14% 13% 11% 6% 3% 0% 0%
Sep Nov Jan Mar May Jul

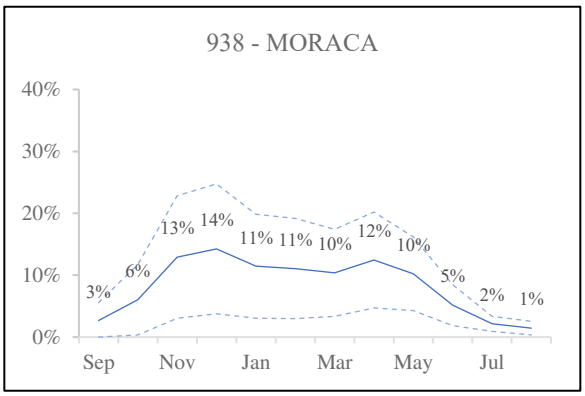
938 - MORACA
40%
30%
20%
10%
0%
3% 6% 13% 14% 11% 11% 10% 12% 10% 5% 2% 1%
Sep Nov Jan Mar May Jul

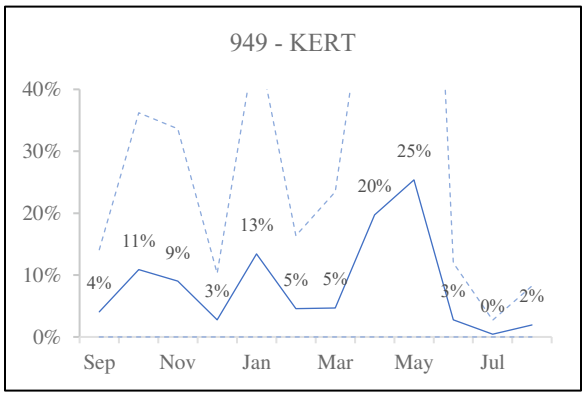
949 - KERT
40%
30%
20%
10%
0%
4% 11% 9% 3% 13% 5% 5% 20% 25% 3% 0% 2%
Sep Nov Jan Mar May Jul

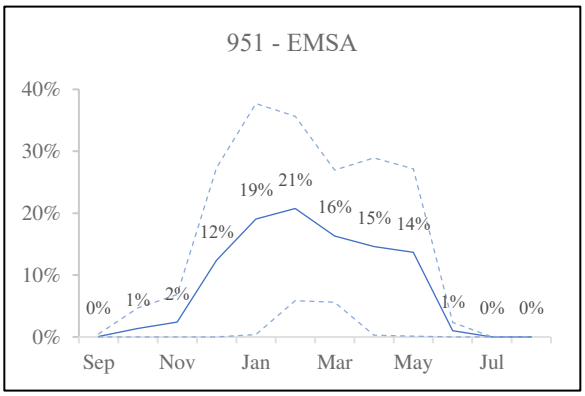
951 - EMSA
40%
30%
20%
10%
0%
0% 1% 2% 12% 19% 21% 16% 15% 14% 1% 0% 0%
Sep Nov Jan Mar May Jul

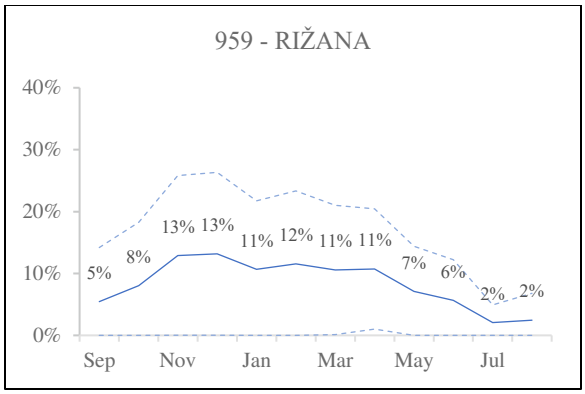
959 - RIŽANA
40%
30%
20%
10%
0%
5% 8% 13% 13% 11% 12% 11% 11% 7% 6% 2% 2%
Sep Nov Jan Mar May Jul

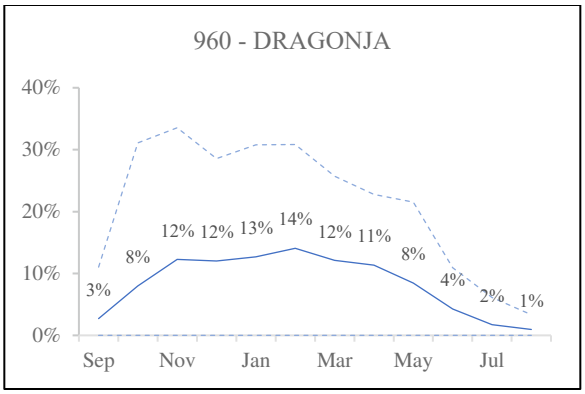
960 - DRAGONJA
40%
30%
20%
10%
0%
3% 8% 12% 12% 13% 14% 12% 11% 8% 4% 2% 1%
Sep Nov Jan Mar May Jul

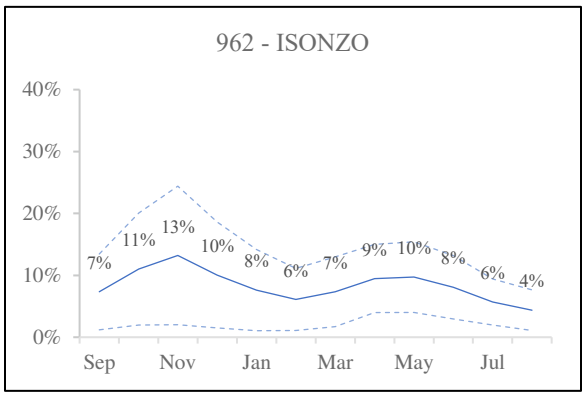
962 - ISONZO
40%
30%
20%
10%
0%
7% 11% 13% 10% 8% 6% 7% 9% 10% 8% 6% 4%
Sep Nov Jan Mar May Jul

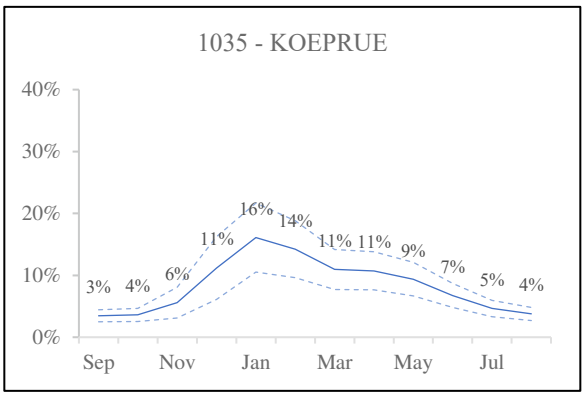
1035 - KOEPRUE
40%
30%
20%
10%
0%
3% 4% 6% 11% 16% 14% 11% 11% 9% 7% 5% 4%
Sep Nov Jan Mar May Jul

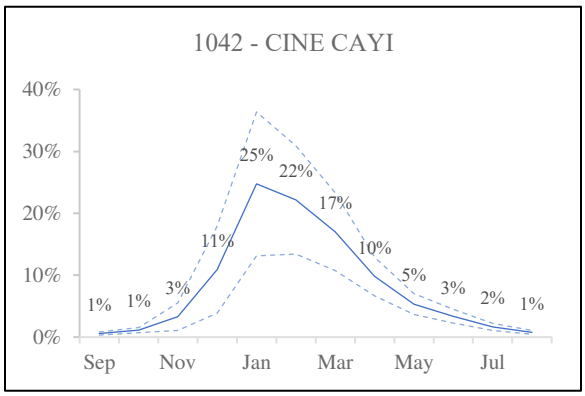
1042 - CINE CAYI
40%
30%
20%
10%
0%
1% 1% 3% 11% 25% 22% 17% 10% 5% 3% 2% 1%
Sep Nov Jan Mar May Jul

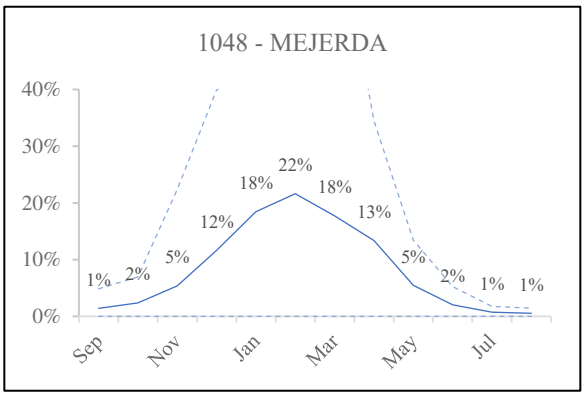
1048 - MEJERDA
40%
30%
20%
10%
0%
1% 2% 5% 12% 18% 22% 18% 13% 5% 2% 1% 1%
Sep Nov Jan Mar May Jul

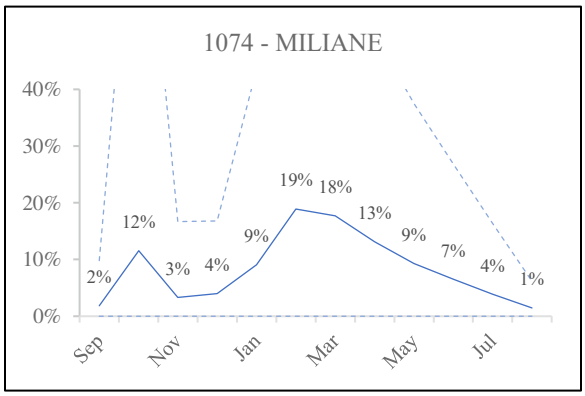
1074 - MILIANE
40%
30%
20%
10%
0%
2% 12% 3% 4% 9% 19% 18% 13% 9% 7% 4% 1%
Sep Nov Jan Mar May Jul

APPENDIX D2

Summary table of all water balance parameters

Note: To be printed on A3

Table D2 - 1: Summary of the water balance parameters of the selected catchments

OID	4	5	15	47	51	56	63	88	103	162	165	169	174	175	194	206	297	319
Country	AG	AG	AL	CY	CY	CY	CY	ES	ES	ES	ES	ES	ES	ES	ES	FR	FR	FR
Name	MELAH	MAZAFRAN	ERZENIT	SERRAKHIS	VASILIKOS	EZOUSAS	DHIARIZOS	CENIA	AMADORIO	FLUVIA	LA MUGA	ELTER	EL BESÒS	GAIA	ANDARAX	FIUM-ALTO	LEZ	LOUP
Area (km^2)	552	1912	760	77	150	210	125	97	185	842	854	2350	1036	424	490	114	150	264
PC	2	9	4	3	6	6	6	3	5	5	5	9	3	1	4	2	1	4
CC	4	3	4	3	3	3	3	5	4	5	4	5	5	5	4	4	4	5
HAINES	G13	G13	G12	G14	G13	G13	G13	G1	G12	G12	G1	G12	G14	G14	G12	G12	G12	G12
I_s	0.84	0.91	0.66	0.96	0.96	0.96	0.96	0.43	0.59	0.31	0.43	0.29	0.37	0.40	0.80	0.74	0.57	0.61
I_{Arid}	1.86	1.61	0.86	2.66	2.35	2.38	2.03	1.83	2.81	1.20	1.43	1.04	1.35	1.57	2.58	1.17	1.44	0.96
P(mm)	583	574	1202	1006	629	669	675	537	361	802	699	709	607	468	233	809	1131	762
U (mm)	93	26	351	118	40	33	133	205	24	155	37	89	78	14	1	239	316	513
S(mm)	68	25	203	64	16	22	47	59	9	66	21	42	24	4	1	121	195	40
Q(mm)	162	51	554	183	56	55	181	264	33	221	58	117	102	18	2	360	511	553
W(mm)	514	549	999	941	613	648	627	478	352	736	678	595	583	463	232	689	936	722
V(mm)	421	523	648	823	573	615	494	273	328	581	641	516	505	450	231	449	620	209
Kr	0.28	0.09	0.46	0.18	0.09	0.08	0.27	0.49	0.09	0.28	0.08	0.17	0.17	0.04	0.01	0.44	0.45	0.73
Ku	0.18	0.05	0.35	0.13	0.06	0.05	0.21	0.43	0.07	0.21	0.05	0.15	0.13	0.03	0.01	0.35	0.34	0.71
Wp(mm)	2489	12326	5814	9151	7092	5722	5359	2100	15132	6874	16811	5765	16193	19992	41767	4373	1897	15181
Vp(mm)	1510	11155	1720	6583	2188	1566	918	280	4451	1798	12258	3559	4266	2217	6855	1232	366	282
λs	0.07	0.00	0.01	0.03	0.04	0.06	0.03	0.09	0.00	0.02	0.01	0.04	0.00	0.01	0.00	0.00	0.03	0.00
λu	0.06	0.00	0.04	0.00	0.15	0.30	0.30	0.88	0.01	0.09	0.00	0.02	0.00	0.15	0.04	0.00	0.09	0.00
λsWp(mm)	164	34	58	253	309	338	179	191	15	128	135	235	16	197	116	4	52	15
λuVp(mm)	96	16	62	16	338	469	279	245	25	163	12	79	4	336	244	1	33	0
S-RMSE	23	14	35	26	12	10	11	43	7	34	11	27	11	2	0	67	22	13
W-RMSE	23	14	35	26	12	10	11	43	7	34	11	27	11	2	0	67	22	13
U-RMSE	29	17	61	28	30	18	26	125	20	70	19	54	34	7	1	102	52	114
V-RMSE	17	28	49	25	18	12	33	107	12	46	15	37	22	3	0	92	44	78
P~	0.2	0.0	0.2	0.1	0.1	0.1	0.1	0.2	0.0	0.1	0.0	0.1	0.0	0.0	0.0	0.0	0.3	0.1
V~	0.6	0.9	0.3	0.7	0.3	0.2	0.1	0.0	0.3	0.2	0.7	0.6	0.3	0.1	0.2	0.3	0.2	0.0
S*	0.1	0.0	0.2	0.1	0.0	0.1	0.1	0.2	0.0	0.1	0.0	0.1	0.0	0.0	0.0	0.2	0.2	0.1
W*	0.9	1.0	0.8	0.9	1.0	0.9	0.9	0.8	1.0	0.9	1.0	0.9	1.0	1.0	1.0	0.8	0.8	0.9
U*	0.3	0.0	0.4	0.1	0.1	0.2	0.6	1.1	0.1	0.3	0.1	0.1	0.1	0.1	-0.1	0.4	0.6	0.7
V*	0.7	1.0	0.6	0.9	0.9	0.8	0.4	-0.1	0.9	0.7	0.9	0.9	0.9	0.9	1.1	0.6	0.4	0.3
K	0.0	0.0	0.0	0.0	0.0	0.0	0.0	0.0	0.0	0.0	0.0	0.0	0.0	0.0	0.0	0.0	0.0	0.0
φ	2.1	20.6	1.4	8.7	5.8	3.3	3.7	0.1	14.6	2.4	21.7	7.3	7.2	7.0	56.7	1.7	0.6	0.4
KH	0.7	1.0	0.6	0.9	0.9	0.8	0.8	0.2	0.9	0.7	0.9	0.8	0.9	0.9	1.1	0.6	0.4	0.3
KB	0.2	0.0	0.3	0.1	0.1	0.2	0.2	0.7	0.1	0.2	0.1	0.1	0.1	0.1	-0.1	0.3	0.4	0.7
KV	0.6	0.9	0.5	0.8	0.8	0.7	0.7	0.1	0.9	0.7	0.9	0.8	0.8	0.9	1.2	0.5	0.3	0.3
KR	0.4	0.1	0.5	0.2	0.2	0.3	0.3	0.9	0.1	0.3	0.1	0.2	0.2	0.1	-0.2	0.5	0.7	0.7
ρ_Q	2.2	1.9	1.7	2.0	3.5	4.3	2.6	2.2	1.9	2.1	2.0	2.3	1.7	3.8	0.3	1.7	2.3	1.3
ρ_S	2.4	1.9	1.8	2.3	3.4	3.5	2.4	2.6	1.8	2.1	2.1	2.6	1.7	3.0	2.4	1.9	3.5	1.8
ρ_U	2.1	1.9	1.7	1.8	3.6	4.9	2.6	2.1	1.9	2.1	1.9	2.2	1.7	4.1	-0.7	1.7	1.5	1.3

OID	531	541	550	559	561	634	677	681	692	693	710	722	725	800	803	822	845	887	903
Country	FR	FR	FR	FR	FR	GR	HR	HR	IS	IS	IT	IT	IT	IT	IT	IT	IT	IT	IT
Name	HERAULT	AUDE	GAPEAU	TECH	TET	SPERCHIOS	MIRNA	KRKA	ALEXANDER	SOREQ	FIORA	ALCANTARA	FLUMINIMAGGIORE	SERCHIO	ARGENTINA	CECINA	PESCARA	ALENTO	SAN LEONARDO
Area (km^2)	2625	1754	517	729	1371	1282	579	2103	953	492	818	475	83	1525	209	634	3125	285	522
PC	9	1	5	5	4	4	1	9	3	3	1	4	3	4	2	5	1	5	1
CC	4	5	4	5	5	4	5	5	2	2	4	3	4	5	5	4	5	4	3
HAINES	G12	G14	G13	G12	G14	G12	G12	G12	G13	G13	G12	G13	G13	G12	G12	G12	G1	G13	G13
I_s	0.53	0.40	0.68	0.35	0.37	0.75	0.36	0.46	1.00	1.00	0.61	0.86	0.86	0.59	0.58	0.55	0.41	0.76	0.88
I_{Arid}	1.23	1.11	1.31	1.01	0.82	1.26	0.67	0.96	2.35	2.85	1.95	1.54	1.49	0.53	0.93	1.27	1.00	1.17	2.07
P(mm)	1276	556	536	554	557	701	1164	1057	655	534	959	613	744	1799	983	876	768	1208	658
U (mm)	422	260	125	194	154	421	254	512	4	5	186	9	209	673	408	125	379	240	81
S(mm)	36	79	74	102	78	151	199	129	9	14	103	4	115	321	292	129	33	218	110
Q(mm)	457	339	199	296	233	572	453	640	13	19	289	13	325	994	700	254	413	458	191
W(mm)	1241	477	462	452	479	550	964	928	646	520	856	610	629	1478	690	747	735	990	548
V(mm)	819	217	336	258	324	128	711	416	642	515	670	601	419	805	283	622	356	750	467
Kr	0.36	0.61	0.37	0.53	0.42	0.82	0.39	0.61	0.02	0.04	0.30	0.02	0.44	0.55	0.71	0.29	0.54	0.38	0.29
Ku	0.34	0.55	0.27	0.43	0.32	0.77	0.26	0.55	0.01	0.01	0.22	0.01	0.33	0.46	0.59	0.17	0.52	0.24	0.15
Wp(mm)	12222	3015	3028	2699	3740	2757	5751	8049	16966	4409	8219	78982	4173	8778	2139	3285	16499	5219	3386
Vp(mm)	647	875	1067	645	1067	182	1766	782	31250	4131	3381	39167	933	1292	353	1483	758	1818	3329
λs	0.01	0.03	0.00	0.00	0.00	0.00	0.00	0.00	0.02	0.08	0.00	0.00	0.00	0.00	0.00	0.06	0.00	0.01	0.00
λu	0.00	0.07	0.00	0.00	0.00	0.00	0.11	0.00	0.01	0.10	0.00	0.00	0.10	0.20	0.20	0.21	0.00	0.14	0.00
λsWp(mm)	122	85	3	3	4	3	6	8	300	347	8	82	4	9	10	194	25	51	3
λuVp(mm)	1	59	1	1	1	0	200	1	305	432	3	39	98	258	69	307	1	260	3
S-RMSE	14	31	47	30	29	60	40	25	5	6	37	3	47	44	98	56	8	63	47
W-RMSE	14	31	47	30	29	60	40	25	5	6	37	3	47	44	98	56	8	63	47
U-RMSE	96	61	73	49	62	133	55	67	4	8	49	6	67	80	106	45	80	92	29
V-RMSE	43	54	74	45	54	120	49	64	4	6	32	3	59	39	99	43	37	61	36
P~	0.0	0.2	0.2	0.2	0.2	0.3	0.2	0.1	0.0	0.1	0.1	0.0	0.2	0.2	0.5	0.2	0.1	0.2	0.2
V~	0.1	0.3	0.4	0.2	0.3	0.1	0.3	0.1	1.9	0.9	0.4	0.5	0.2	0.1	0.1	0.4	0.1	0.3	1.0
S*	0.1	0.2	0.1	0.2	0.1	0.2	0.2	0.1	0.0	0.1	0.1	0.0	0.2	0.2	0.3	0.2	0.0	0.2	0.2
W*	0.9	0.8	0.9	0.8	0.9	0.8	0.8	0.9	1.0	0.9	0.9	1.0	0.8	0.8	0.7	0.8	1.0	0.8	0.8
U*	0.5	0.4	0.3	0.4	0.3	0.8	0.3	0.5	0.0	0.0	0.2	0.0	0.4	0.5	0.7	0.3	0.5	0.3	0.2
V*	0.5	0.6	0.7	0.6	0.7	0.2	0.7	0.5	1.0	1.0	0.8	1.0	0.6	0.5	0.3	0.7	0.5	0.7	0.8
K	0.0	0.0	0.0	0.0	0.0	0.0	0.0	0.0	0.0	0.0	0.0	0.0	0.0	0.0	0.0	0.0	0.0	0.0	0.0
φ	1.3	1.7	2.3	1.3	1.9	0.3	1.4	0.7	87.3	19.7	3.6	73.6	1.1	0.6	0.3	1.7	1.0	1.3	5.1
KH	0.5	0.6	0.7	0.6	0.7	0.2	0.7	0.4	1.0	0.9	0.8	1.0	0.6	0.4	0.3	0.7	0.5	0.7	0.9
KB	0.5	0.3	0.2	0.3	0.3	0.6	0.3	0.5	0.0	0.0	0.2	0.0	0.3	0.4	0.4	0.2	0.5	0.3	0.1
KV	0.5	0.5	0.6	0.5	0.6	0.2	0.5	0.4	1.0	0.8	0.7	1.0	0.5	0.4	0.2	0.6	0.5	0.5	0.7
KR	0.5	0.5	0.4	0.5	0.4	0.8	0.5	0.6	0.0	0.2	0.3	0.0	0.5	0.6	0.8	0.4	0.5	0.5	0.3
ρ_Q	2.6	1.2	1.9	1.6	1.7	1.4	2.0	1.5	3.1	3.7	1.7	2.0	1.9	1.8	1.6	2.4	1.5	2.0	1.8
ρ_S	5.9	1.8	2.0	1.7	1.7	1.7	1.8	1.8	3.1	3.3	1.8	2.2	1.8	1.7	1.8	2.2	2.0	1.8	1.8
ρ_U	2.3	1.1	1.8	1.6	1.7	1.3	2.1	1.5	3.2	4.8	1.7	1.9	1.9	1.8	1.5	2.6	1.4	2.2	1.8

OID	908	913	928	929	930	934	936	937	938	949	951	959	960	962	1035	1042	1048	1074
Country	IT	IT	LB	LB	LB	LB	LB	LB	ME	MO	MO	SI	SI	SI	TR	TR	TS	TS
Name	F. IMERA MERIDIONALE	CERVARO	NAHR EL JAOUZ	NAHR BEYROUTH	NAHR EL KALB	NAHR IBRAHIM	NAHR ASSI	NAHR LITANI	MORACA	KERT	EMSA	RIŽANA	DRAGONJA	ISONZO	KOEPRUE	CINE CAYI	MEJERDA	MILIANE
Area (km^2)	1725	657	189	217	249	326	1507	1808	2628	1353	110	205	147	1800	1942	948	1490	1070
PC	9	1	4	3	4	4	3	4	5	9	3	5	1	9	3	6	1	9
CC	3	4	3	3	3	3	3	3	5	2	3	5	5	5	3	3	4	4
HAINES	G13	G13	G14	G13	G13	G14	G13	G1	G12	G14	G13	G12	G12	G11	G12	G13	G13	G14
I_s	0.90	0.53	0.99	0.99	0.99	0.99	0.99	1.00	0.63	0.88	0.97	0.36	0.37	0.41	0.89	0.86	0.77	0.82
I_{Arid}	2.31	1.82	1.04	1.16	1.00	0.99	1.36	1.50	0.61	3.29	1.76	0.63	0.69	0.32	1.50	1.64	2.31	2.60
P(mm)	633	713	1584	1190	1440	1450	661	637	3383	230	572	941	956	2254	632	632	449	413
U (mm)	55	55	271	235	761	794	264	309	1245	2	102	281	106	1051	263	158	53	6
S(mm)	50	58	85	157	248	258	5	53	511	14	105	239	95	532	72	77	47	12
Q(mm)	105	113	356	392	1009	1052	270	361	1756	16	207	520	200	1582	336	234	100	18
W(mm)	584	655	1499	1033	1192	1193	655	585	2872	217	467	702	861	1722	559	555	403	402
V(mm)	529	600	1228	799	431	399	391	276	1627	215	366	421	756	672	296	397	350	396
Kr	0.17	0.16	0.22	0.33	0.70	0.73	0.41	0.57	0.52	0.07	0.36	0.55	0.21	0.70	0.53	0.37	0.22	0.04
Ku	0.09	0.08	0.18	0.23	0.64	0.67	0.40	0.53	0.43	0.01	0.22	0.40	0.12	0.61	0.47	0.28	0.13	0.01
Wp(mm)	4240	4289	28176	8291	5348	7695	76560	4930	21036	4454	2725	2898	8149	7530	4874	4569	3129	10651
Vp(mm)	4319	2604	6947	2233	494	425	1175	663	4053	21671	761	806	3682	874	637	1313	2050	18857
λs	0.05	0.05	0.00	0.00	0.05	0.00	0.00	0.02	0.00	0.00	0.00	0.00	0.01	0.00	0.00	0.00	0.02	0.01
λu	0.02	0.11	0.00	0.11	0.51	0.78	0.00	0.00	0.00	0.00	0.23	0.13	0.06	0.26	0.00	0.01	0.03	0.00
λsWp(mm)	202	207	28	8	267	8	77	121	21	4	3	3	45	8	5	5	59	87
λuVp(mm)	102	275	7	248	251	330	1	1	4	22	177	102	211	228	1	19	58	33
S-RMSE	35	23	24	94	74	75	2	11	167	14	47	55	34	81	7	24	22	6
W-RMSE	35	23	24	94	74	75	2	11	167	14	47	55	34	81	7	24	22	6
U-RMSE	34	21	96	110	163	124	88	65	311	2	59	50	34	117	21	51	22	5
V-RMSE	32	19	40	98	99	55	89	30	221	6	35	49	32	94	17	19	26	6
P~	0.1	0.1	0.1	0.1	0.2	0.2	0.0	0.1	0.2	0.1	0.2	0.3	0.1	0.3	0.1	0.1	0.1	0.0
V~	1.0	0.6	0.2	0.2	0.1	0.0	0.0	0.1	0.2	4.9	0.2	0.2	0.4	0.1	0.1	0.3	0.7	1.8
S*	0.1	0.1	0.1	0.1	0.2	0.2	0.0	0.1	0.2	0.1	0.2	0.3	0.1	0.2	0.1	0.1	0.1	0.0
W*	0.9	0.9	0.9	0.9	0.8	0.8	1.0	0.9	0.8	0.9	0.8	0.7	0.9	0.8	0.9	0.9	0.9	1.0
U*	0.1	0.1	0.2	0.3	0.8	0.9	0.4	0.5	0.4	0.0	0.3	0.5	0.2	0.7	0.4	0.3	0.1	0.0
V*	0.9	0.9	0.8	0.7	0.2	0.1	0.6	0.5	0.6	1.0	0.7	0.5	0.8	0.3	0.6	0.7	0.9	1.0
K	0.0	0.0	0.0	0.0	0.0	0.0	0.0	0.0	0.0	0.0	-0.1	0.0	0.0	0.0	0.0	0.0	0.0	0.0
φ	9.8	4.6	4.7	1.7	0.2	0.1	2.1	1.3	1.2	95.8	1.0	0.7	3.8	0.3	1.0	2.1	5.1	57.7
KH	0.9	0.9	0.8	0.7	0.2	0.1	0.6	0.5	0.6	1.0	0.7	0.5	0.8	0.3	0.5	0.7	0.8	1.0
KB	0.1	0.1	0.2	0.2	0.6	0.7	0.4	0.5	0.4	0.0	0.3	0.3	0.1	0.5	0.4	0.3	0.1	0.0
KV	0.8	0.7	0.8	0.6	0.2	0.1	0.6	0.4	0.5	0.9	0.5	0.4	0.7	0.2	0.5	0.6	0.7	1.0
KR	0.2	0.3	0.2	0.4	0.8	0.9	0.4	0.6	0.5	0.1	0.5	0.6	0.3	0.8	0.5	0.4	0.3	0.0
ρ_Q	2.2	2.7	1.8	2.0	1.6	1.6	1.5	1.5	1.6	1.6	2.2	1.8	2.2	1.6	1.6	1.8	2.0	2.2
ρ_S	2.3	2.6	1.9	1.8	2.0	1.6	1.8	2.2	1.7	1.6	1.7	1.7	1.9	1.7	1.9	1.9	2.0	2.1
ρ_U	2.0	2.9	1.8	2.2	1.4	1.6	1.5	1.3	1.6	1.9	2.6	1.8	2.4	1.5	1.5	1.8	2.0	2.5

APPENDIX D3

The water balance partitioning model of L'vovich and fitting curves of Ponce & Shetty

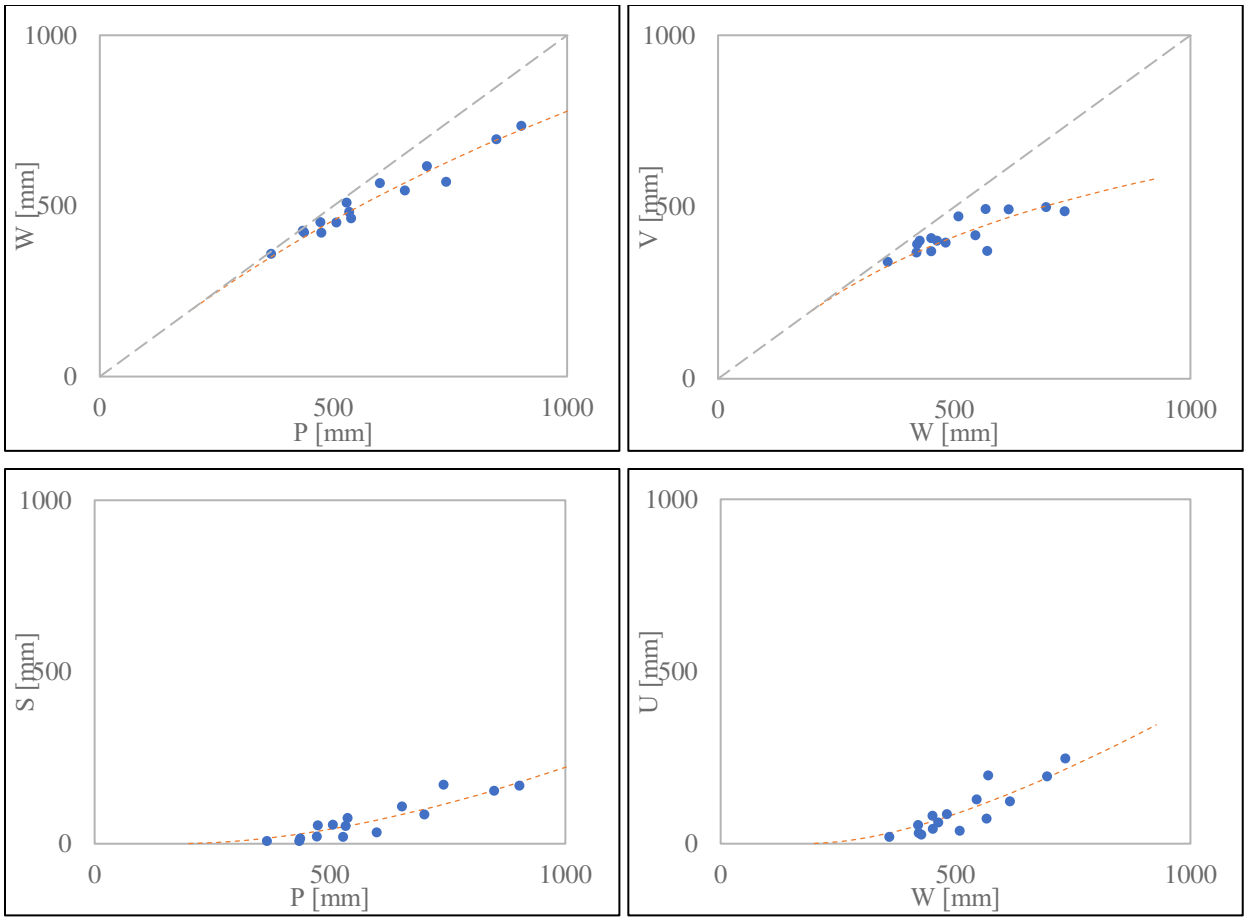

*Figure D3 - 1 : L'Vovich water balance relationships extracted for **Melah, Algeria**; Wetting W= f(P), Vaporization V=f(W), Quick flow S=f(P) and slow flow U = f(W); Points represent data (equations 14,15,16 and 17), and the dashed lines are Ponce and Shetty mathematical formulations (equations 18b and 19b)*

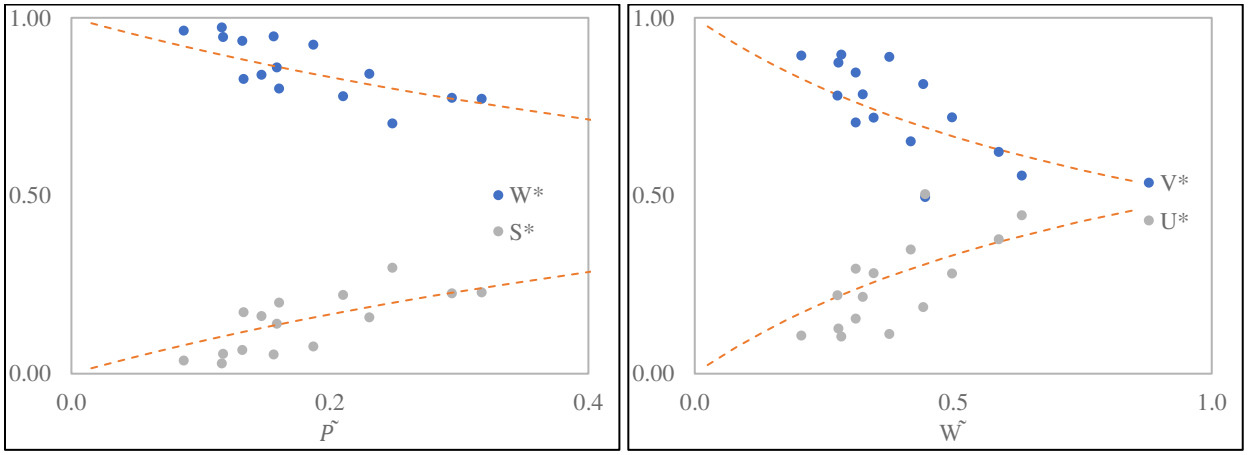

Figure D3 - 2 : Interannual variability of nondimensional annual estimates of (left) W and S* and (right) U* and V* versus annual climatic drivers $\tilde{P}$ and $\tilde{W}$ for **Melah, Algeria**; Points represent data (equations 22 and 23), and the dashed lines are theoretical (equations 25 and 26).*

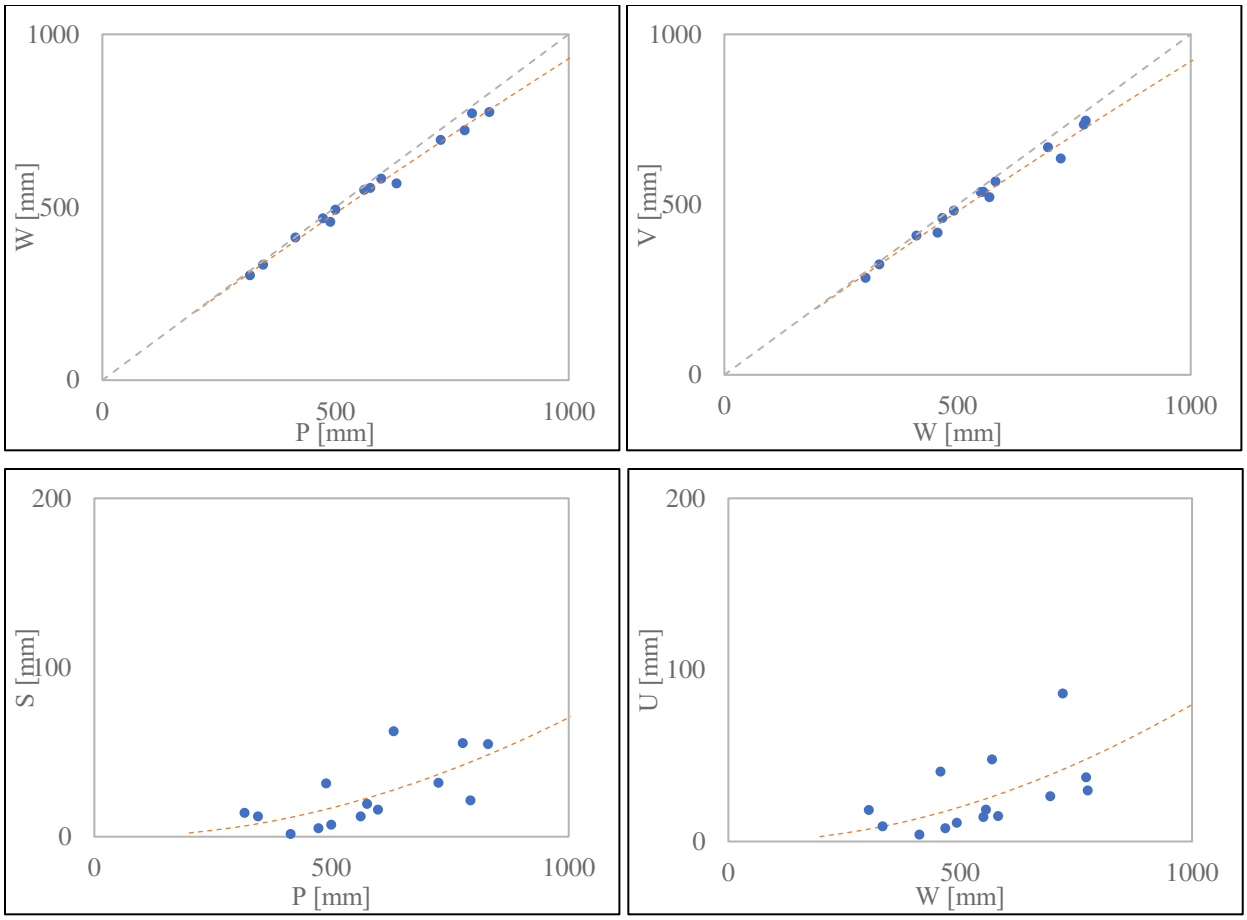

*Figure D3 - 3 : L'Vovich water balance relationships extracted for **Mazafran, Algeria**; Wetting W= f(P), Vaporization V=f(W), Quick flow S=f(P) and slow flow U = f(W); Points represent data (equations 14,15,16 and 17), and the dashed lines are Ponce and Shetty mathematical formulations (equations 18b and 19b)*

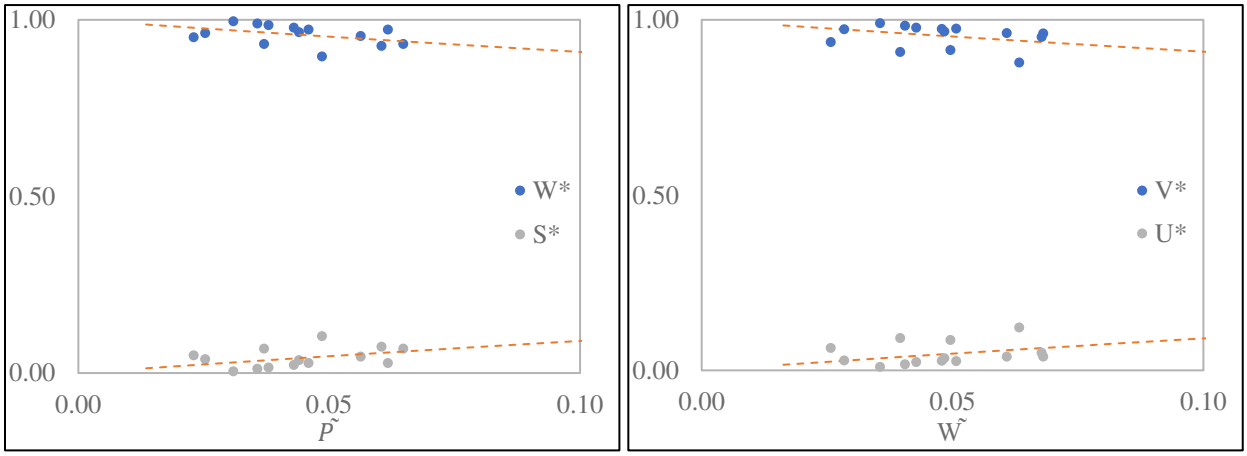

Figure D3 - 4 : Interannual variability of nondimensional annual estimates of (left) W and S* and (right) U* and V* versus annual climatic drivers $\tilde{P}$ and $\tilde{W}$ for **Mazafran, Algeria**; Points represent data (equations 22 and 23), and the dashed lines are theoretical (equations 25 and 26).*

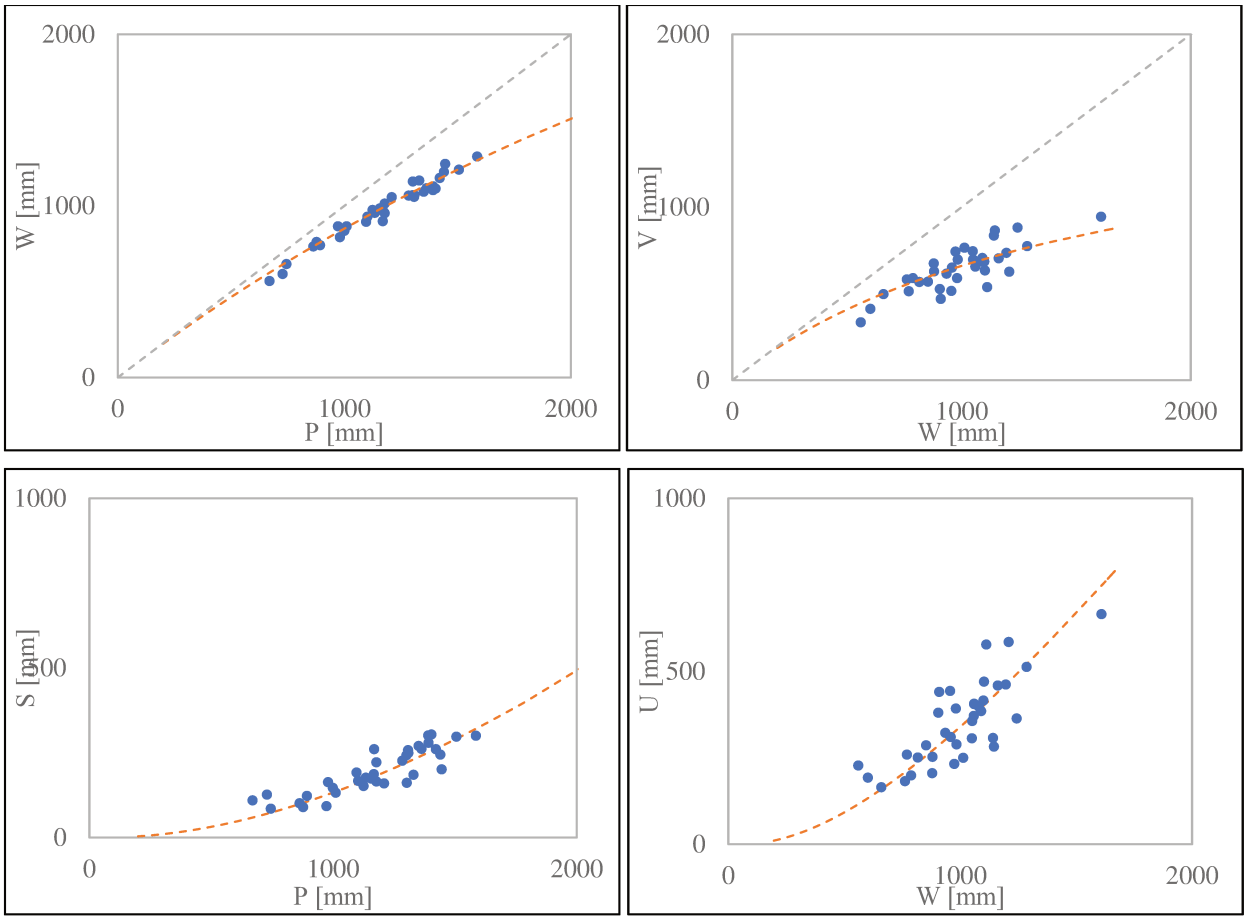

Figure D3 - 5 : L'Vovich water balance relationships extracted for ***Erzenit, Albania****; Wetting W= f(P), Vaporization V=f(W), Quick flow S=f(P) and slow flow U = f(W); Points represent data (equations 14,15,16 and 17), and the dashed lines are Ponce and Shetty mathematical formulations (equations 18b and 19b)*

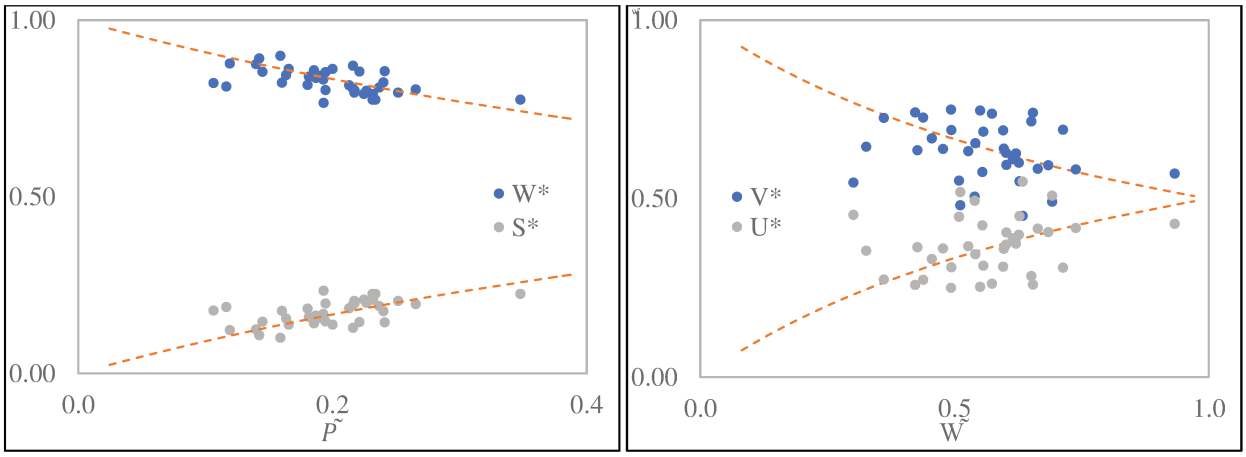

Figure D3 - 6 : Interannual variability of nondimensional annual estimates of (left) W and S* and (right) U* and V* versus annual climatic drivers* $\tilde{P}$ *and* $\tilde{W}$ *for* ***Erzenit, Albania****; Points represent data (equations 22 and 23), and the dashed lines are theoretical (equations 25 and 26).*

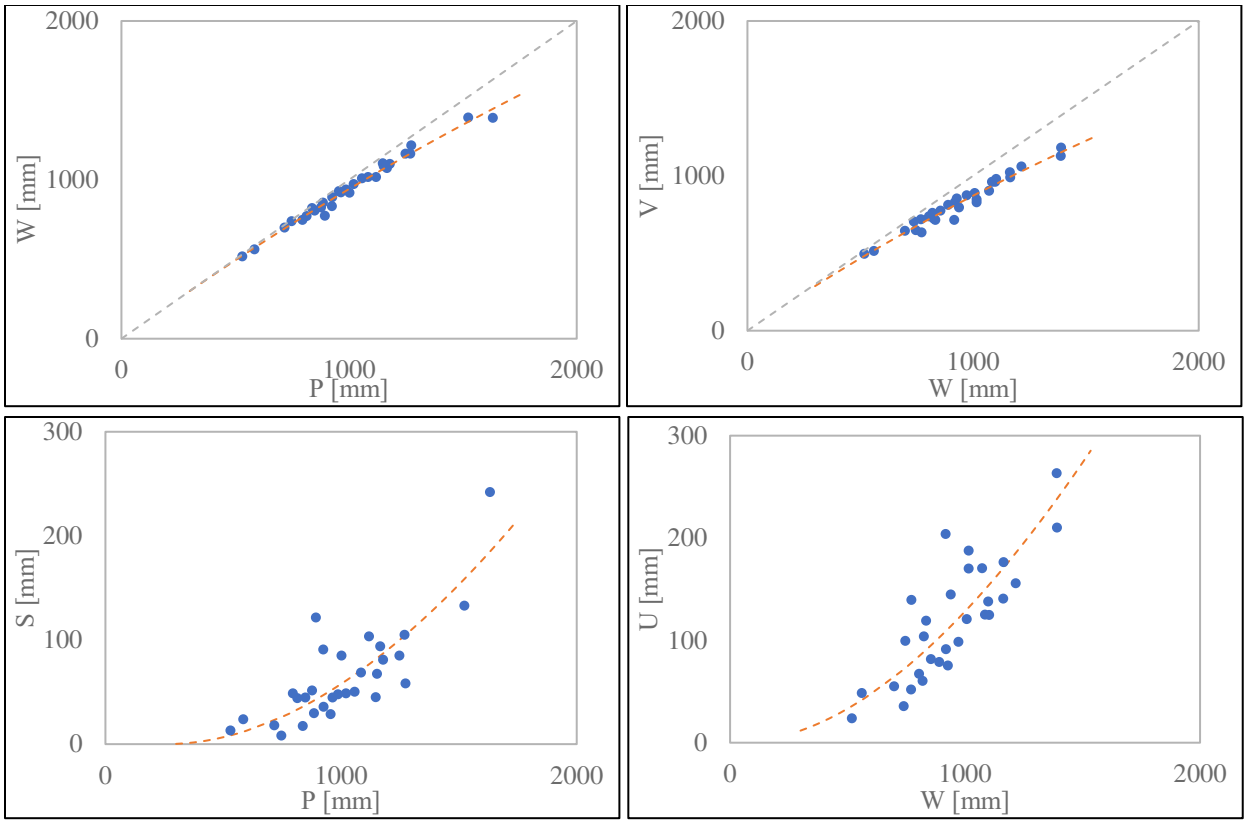

*Figure D3 - 7 : L'Vovich water balance relationships extracted for **Serrakhis, Cyprus**; Wetting W= f(P), Vaporization V=f(W), Quick flow S=f(P) and slow flow U = f(W); Points represent data (equations 14,15,16 and 17), and the dashed lines are Ponce and Shetty mathematical formulations (equations 18b and 19b)*

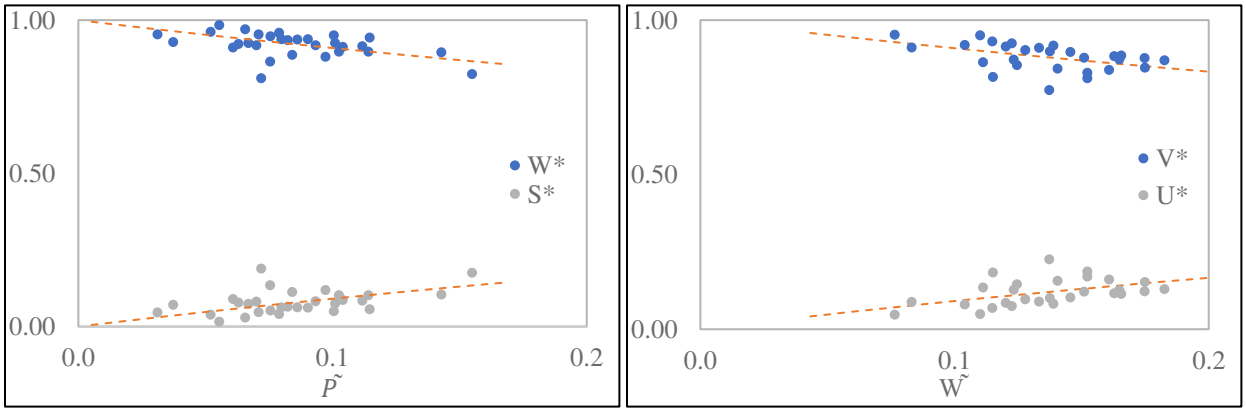

Figure D3 - 8 : Interannual variability of nondimensional annual estimates of (left) W and S* and (right) U* and V* versus annual climatic drivers $\tilde{P}$ and $\tilde{W}$ for **Serrakhis, Cyprus**; Points represent data (equations 22 and 23), and the dashed lines are theoretical (equations 25 and 26).*

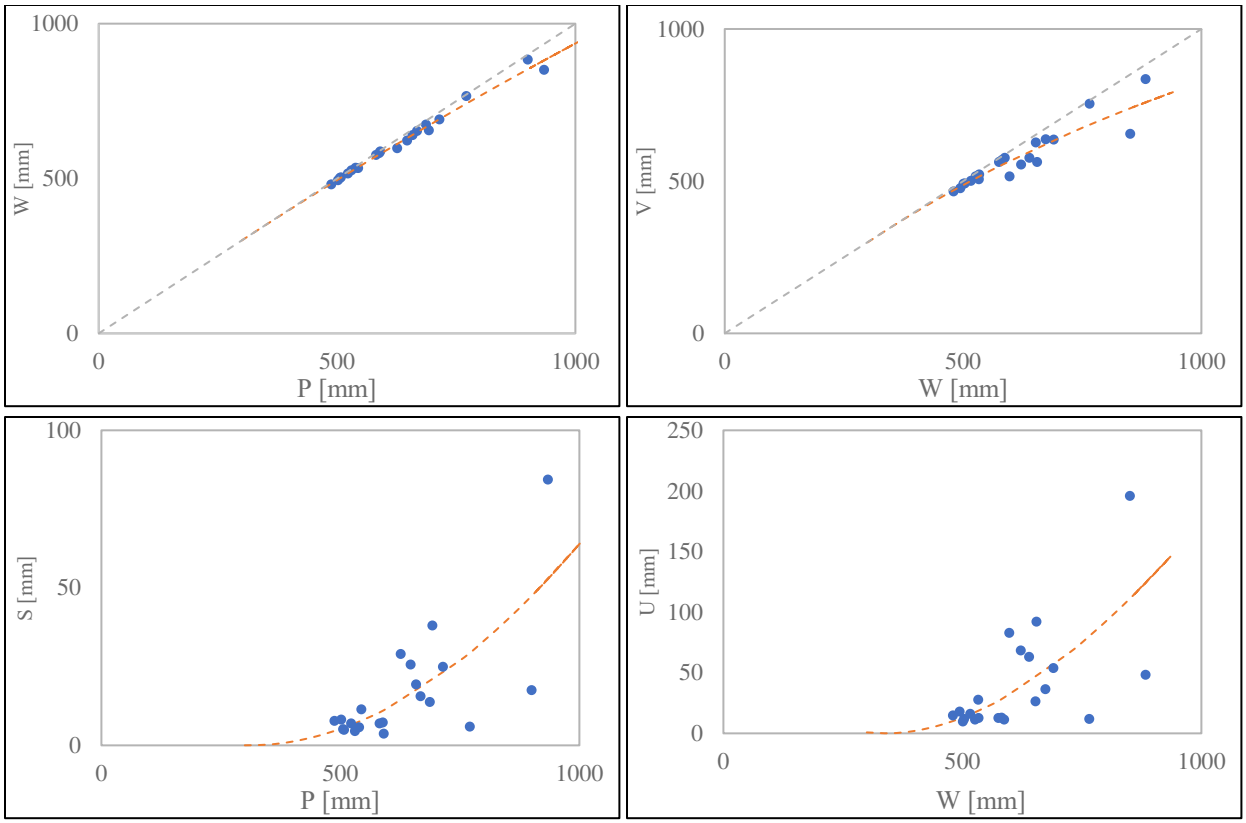

*Figure D3 - 9 : L'Vovich water balance relationships extracted for **Vasilikos, Cyprus**; Wetting W= f(P), Vaporization V=f(W), Quick flow S=f(P) and slow flow U = f(W); Points represent data (equations 14,15,16 and 17), and the dashed lines are Ponce and Shetty mathematical formulations (equations 18b and 19b)*

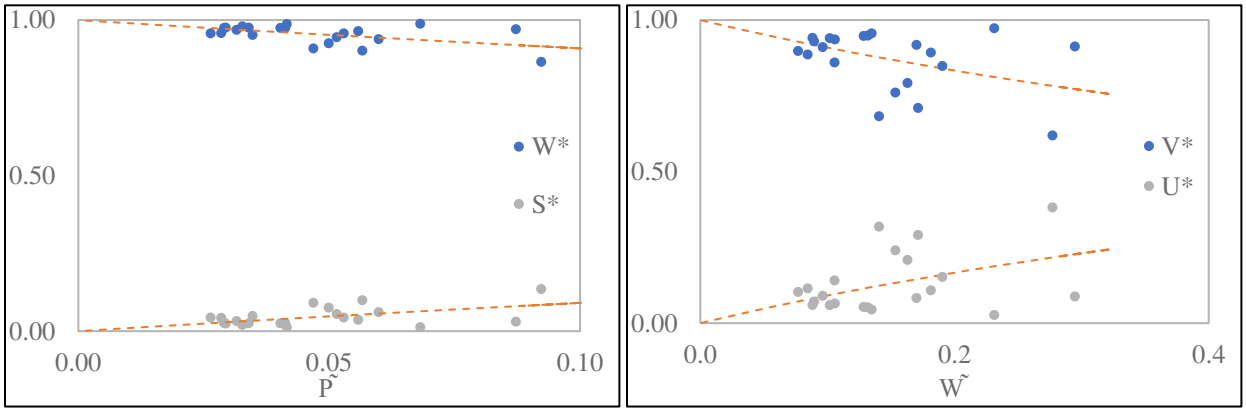

Figure D3 - 10 : Interannual variability of nondimensional annual estimates of (left) W and S* and (right) U* and V* versus annual climatic drivers $\tilde{P}$ and $\tilde{W}$ for **Vasilikos, Cyprus**; Points represent data (equations 22 and 23), and the dashed lines are theoretical (equations 25 and 26).*

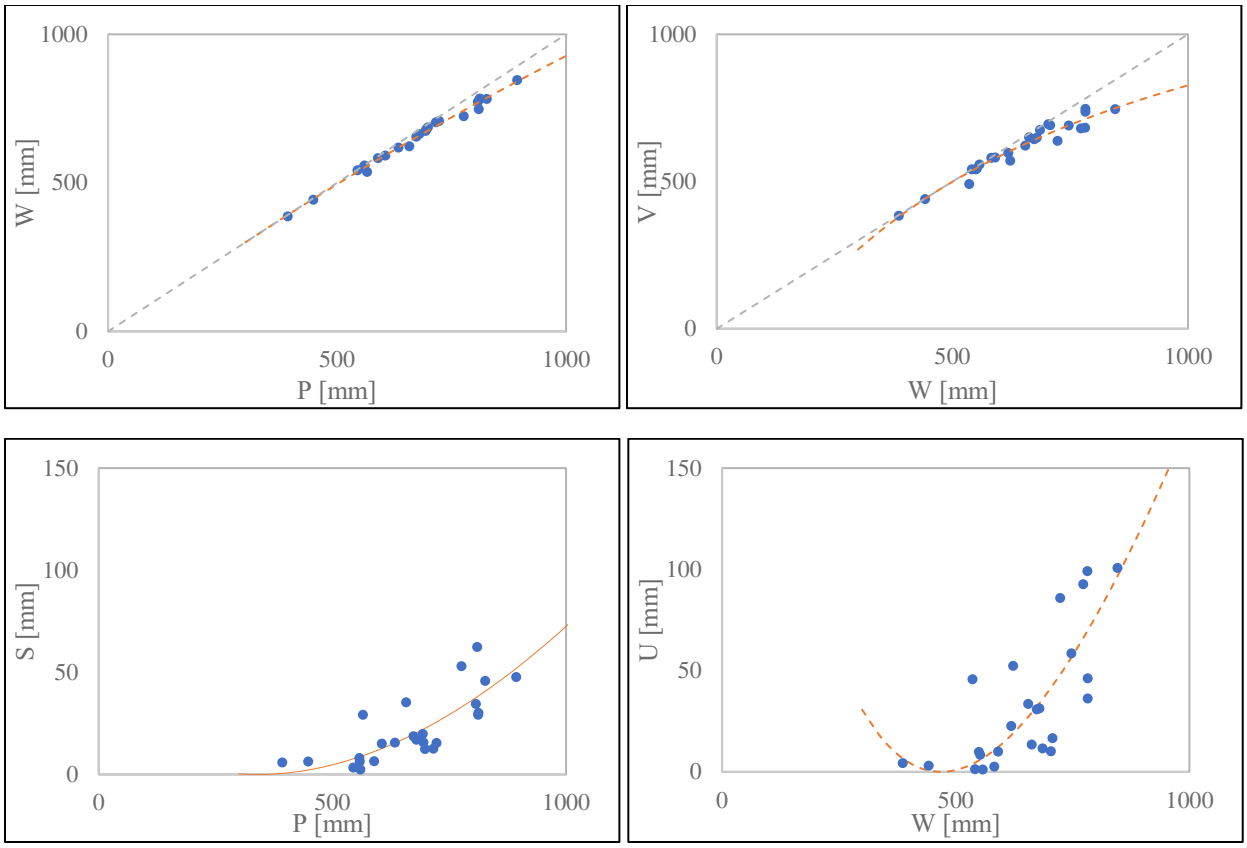

*Figure D3 - 11 : L'Vovich water balance relationships extracted for **Ezousas, Cyprus**; Wetting W= f(P), Vaporization V=f(W), Quick flow S=f(P) and slow flow U = f(W); Points represent data (equations 14,15,16 and 17), and the dashed lines are Ponce and Shetty mathematical formulations (equations 18b and 19b)*

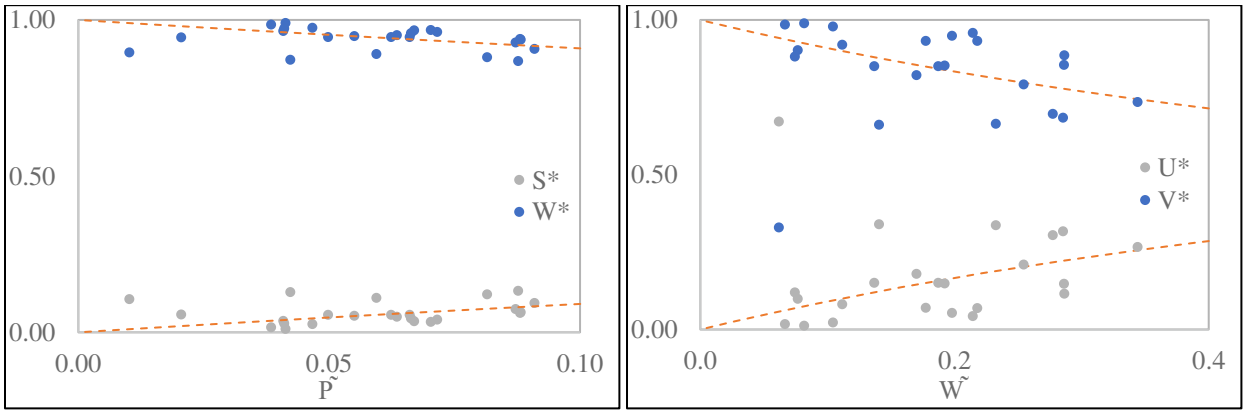

Figure D3 - 12 : Interannual variability of nondimensional annual estimates of (left) W and S* and (right) U* and V* versus annual climatic drivers $\tilde{P}$ and $\tilde{W}$ for **Ezousas, Cyprus**; Points represent data (equations 22 and 23), and the dashed lines are theoretical (equations 25 and 26).*

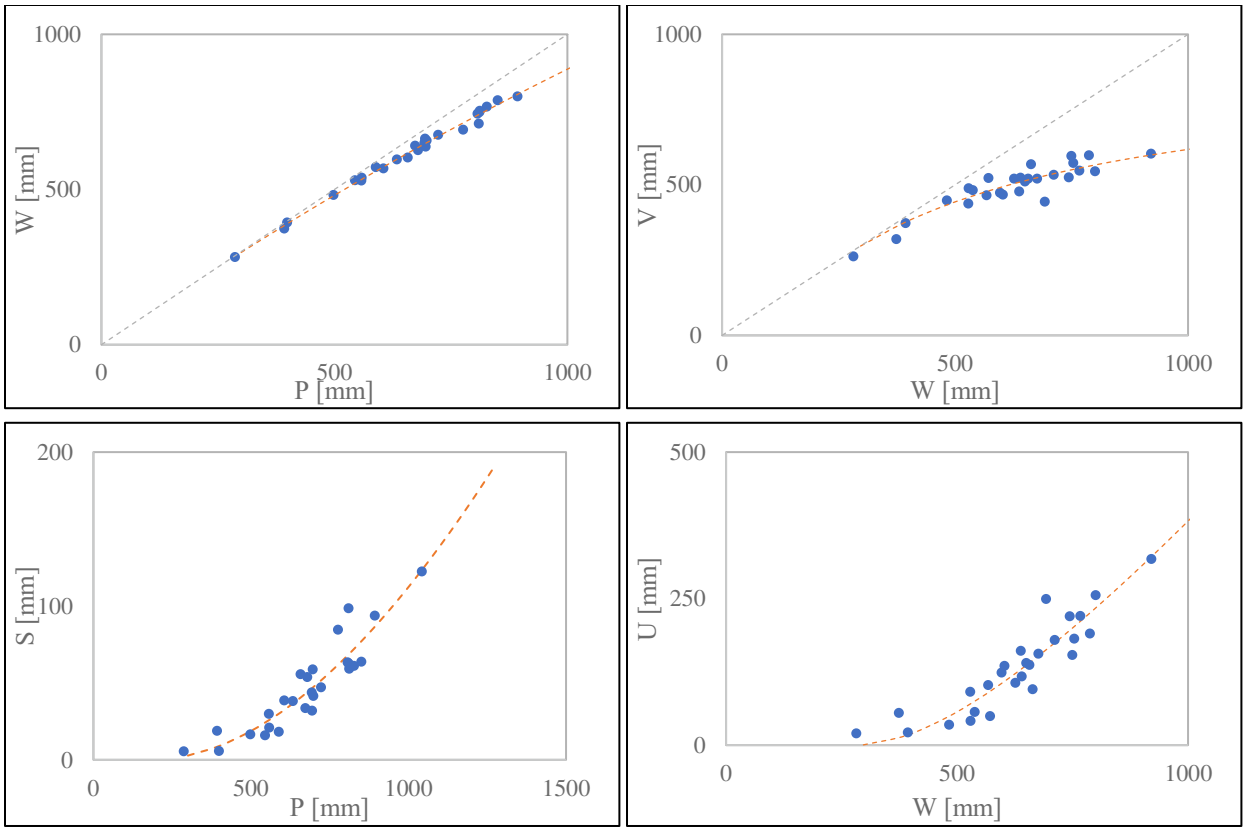

*Figure D3 - 13 : L'Vovich water balance relationships extracted for **Dhiarizos, Cyprus**; Wetting W= f(P), Vaporization V=f(W), Quick flow S=f(P) and slow flow U = f(W); Points represent data (equations 14,15,16 and 17), and the dashed lines are Ponce and Shetty mathematical formulations (equations 18b and 19b)*

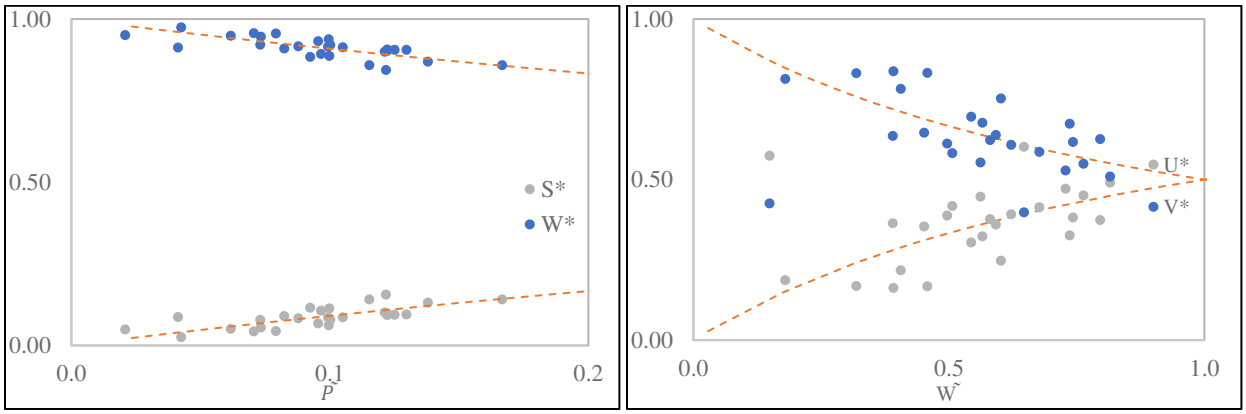

Figure D3 - 14 : Interannual variability of nondimensional annual estimates of (left) W and S* and (right) U* and V* versus annual climatic drivers $\tilde{P}$ and $\tilde{W}$ for **Dhiarizos, Cyprus**; Points represent data (equations 22 and 23), and the dashed lines are theoretical (equations 25 and 26).*

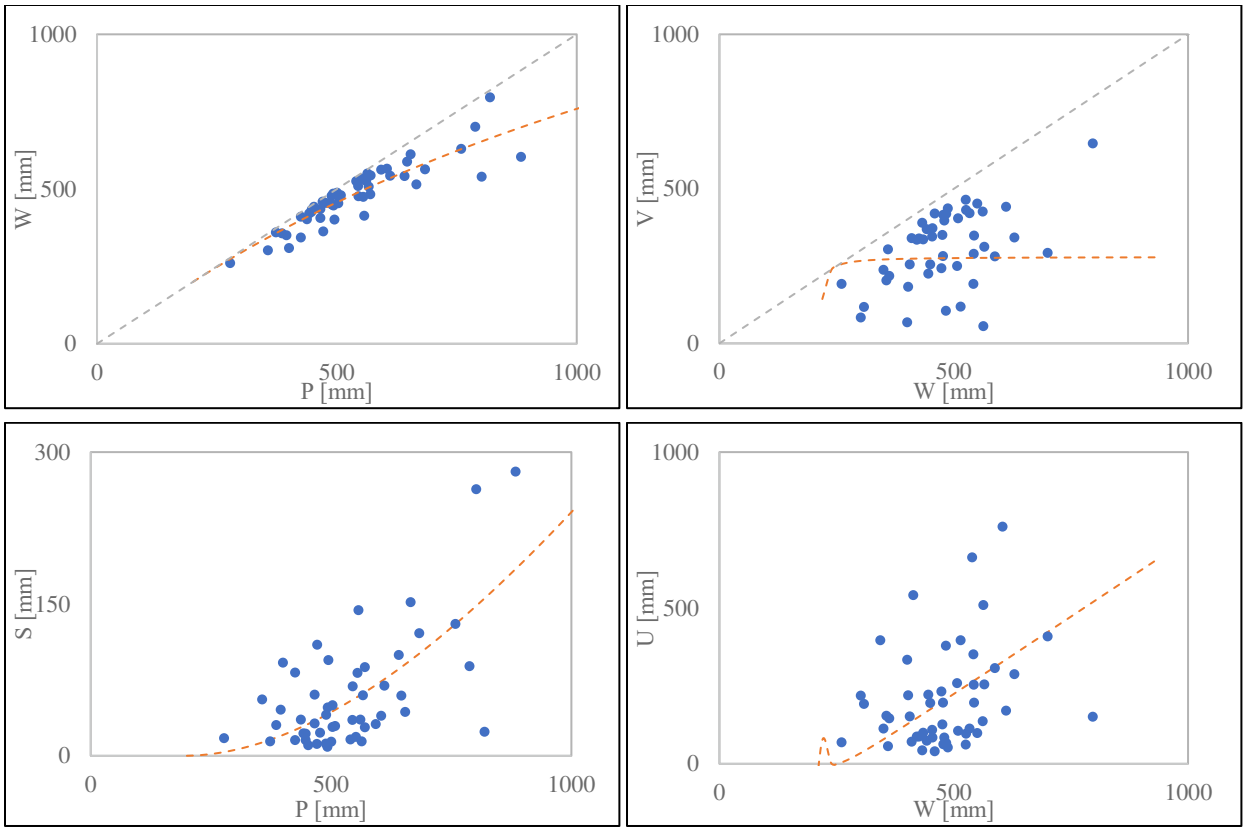

*Figure D3 - 15 : L'Vovich water balance relationships extracted for **Cenia, Spain**; Wetting W= f(P), Vaporization V=f(W), Quick flow S=f(P) and slow flow U = f(W); Points represent data (equations 14,15,16 and 17), and the dashed lines are Ponce and Shetty mathematical formulations (equations 18b and 19b)*

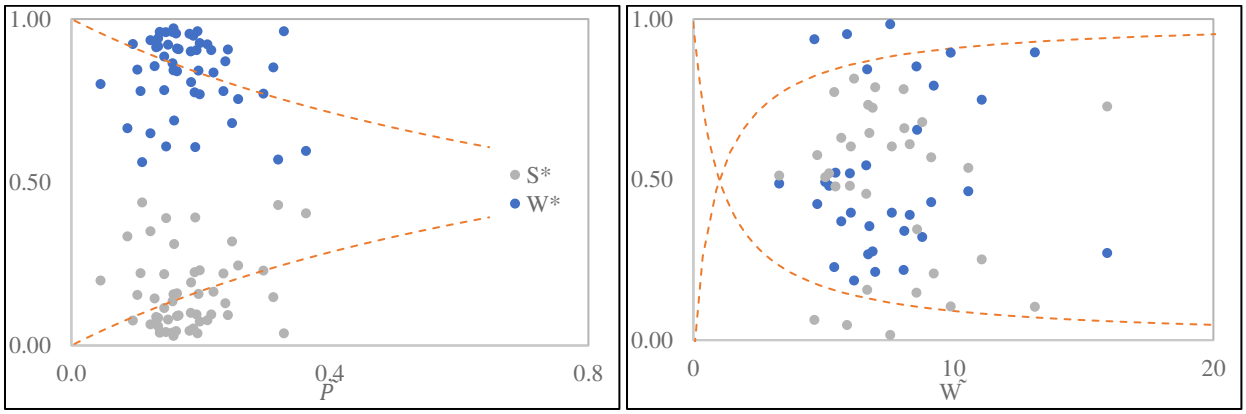

Figure D3 - 16 : Interannual variability of nondimensional annual estimates of (left) W and S* and (right) U* and V* versus annual climatic drivers $\tilde{P}$ and $\tilde{W}$ for **Cenia, Spain**; Points represent data (equations 22 and 23), and the dashed lines are theoretical (equations 25 and 26).*

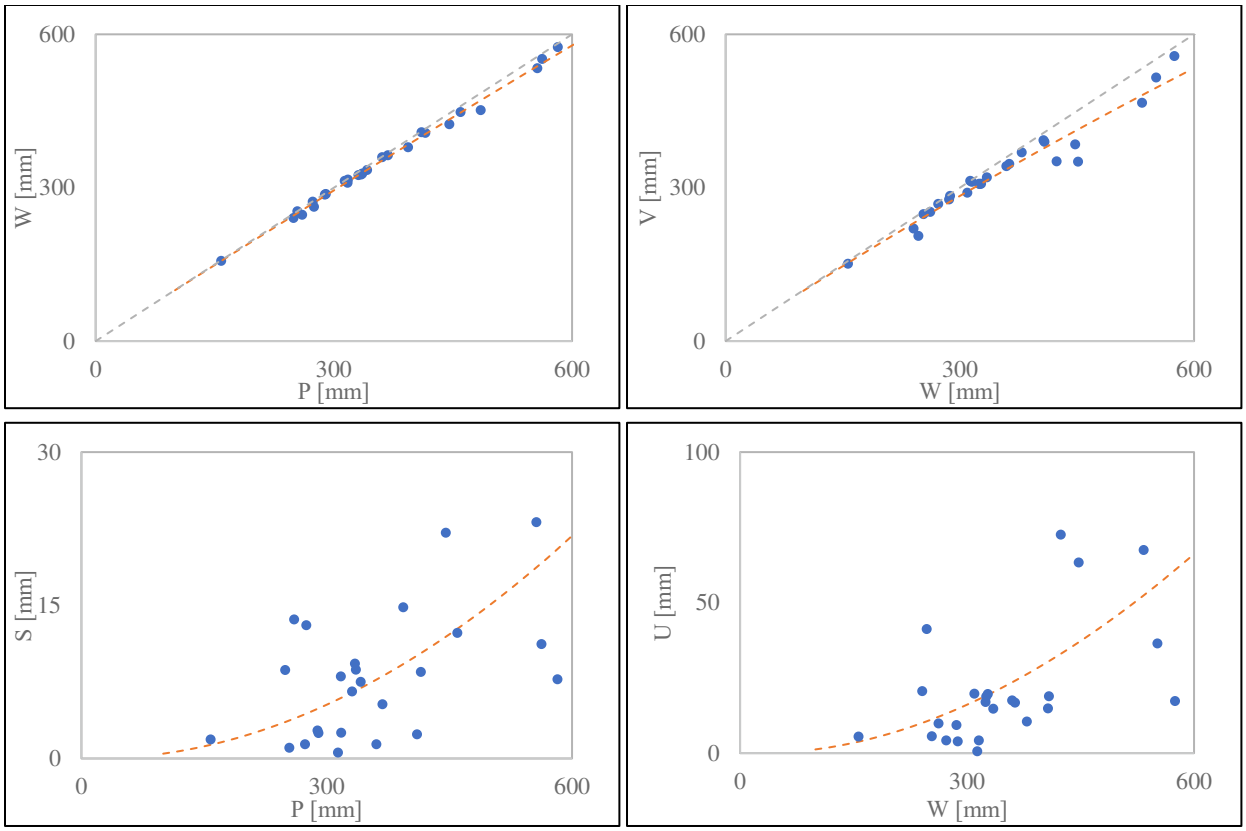

*Figure D3 - 17 : L'Vovich water balance relationships extracted for **Amadorio, Spain**; Wetting W= f(P), Vaporization V=f(W), Quick flow S=f(P) and slow flow U = f(W); Points represent data (equations 14,15,16 and 17), and the dashed lines are Ponce and Shetty mathematical formulations (equations 18b and 19b)*

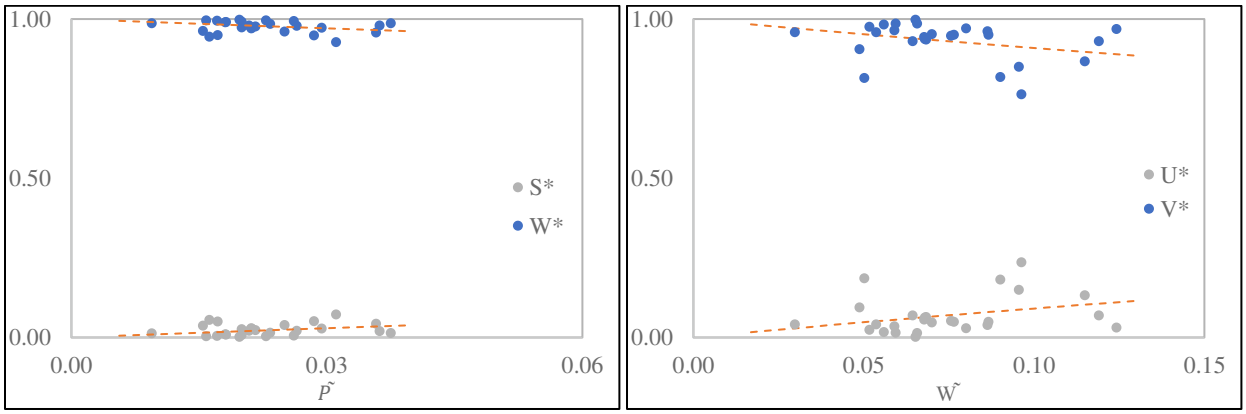

Figure D3 - 18 : Interannual variability of nondimensional annual estimates of (left) W and S* and (right) U* and V* versus annual climatic drivers $\tilde{P}$ and $\tilde{W}$ for **Amadorio, Spain**; Points represent data (equations 22 and 23), and the dashed lines are theoretical (equations 25 and 26).*

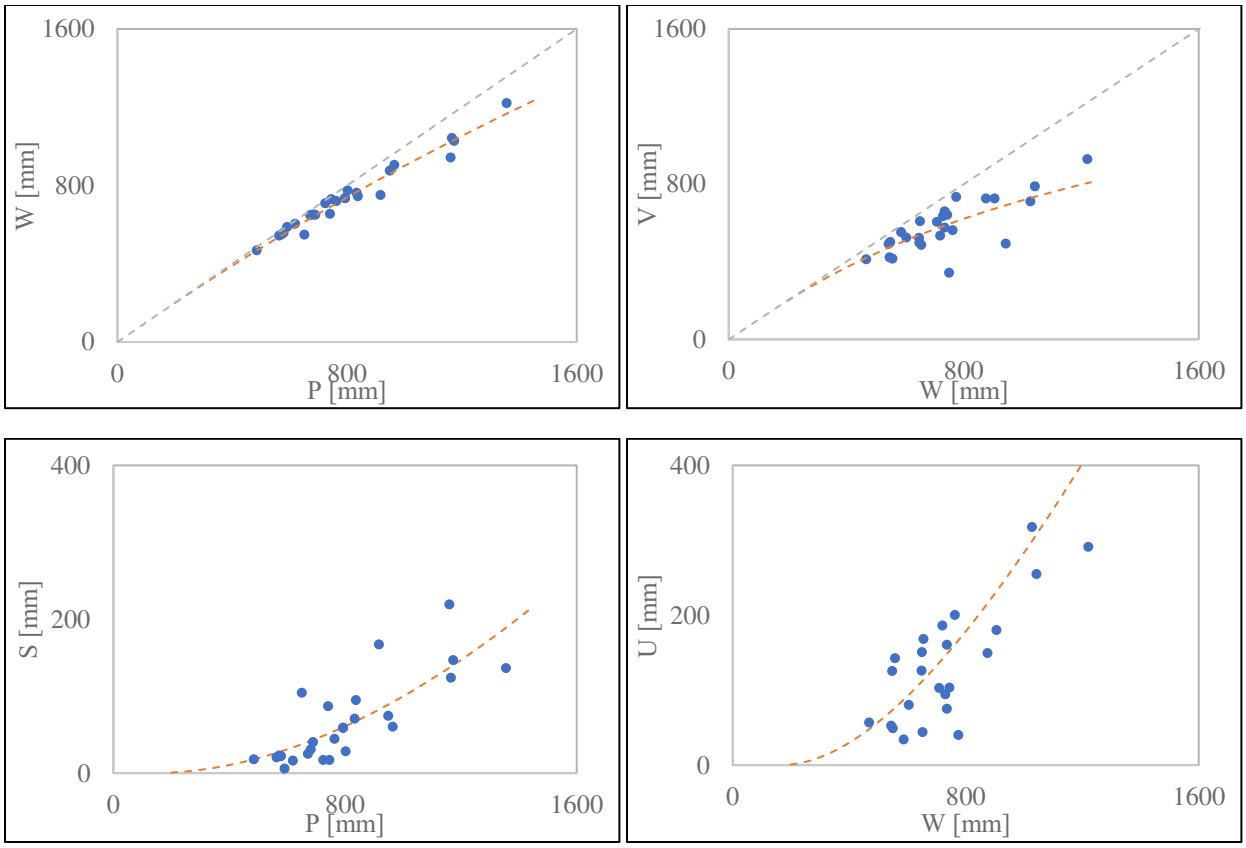

*Figure D3 - 19 : L'Vovich water balance relationships extracted for **Fluvia, Spain**; Wetting W= f(P), Vaporization V=f(W), Quick flow S=f(P) and slow flow U = f(W); Points represent data (equations 14,15,16 and 17), and the dashed lines are Ponce and Shetty mathematical formulations (equations 18b and 19b)*

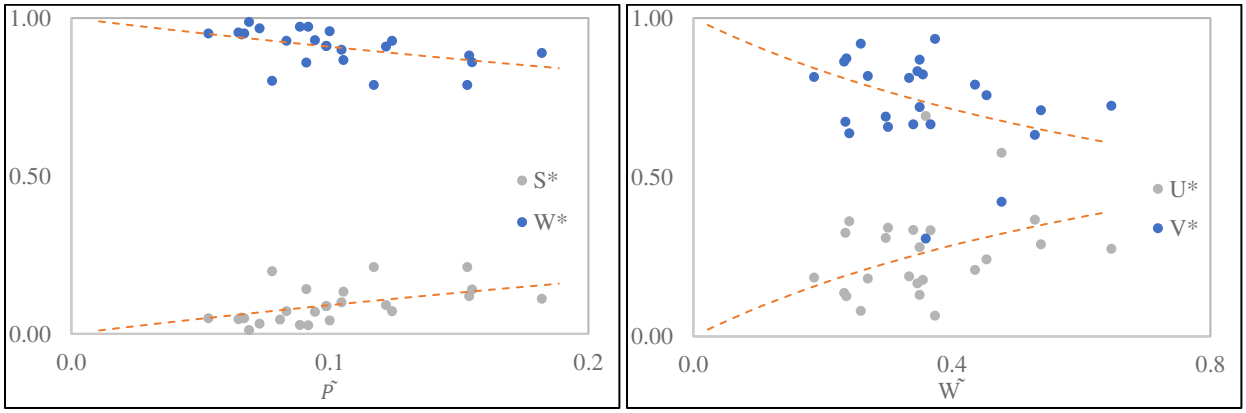

Figure D3 - 20 : Interannual variability of nondimensional annual estimates of (left) W and S* and (right) U* and V* versus annual climatic drivers $\tilde{P}$ and $\tilde{W}$ for **Fluvia, Spain**; Points represent data (equations 22 and 23), and the dashed lines are theoretical (equations 25 and 26).*

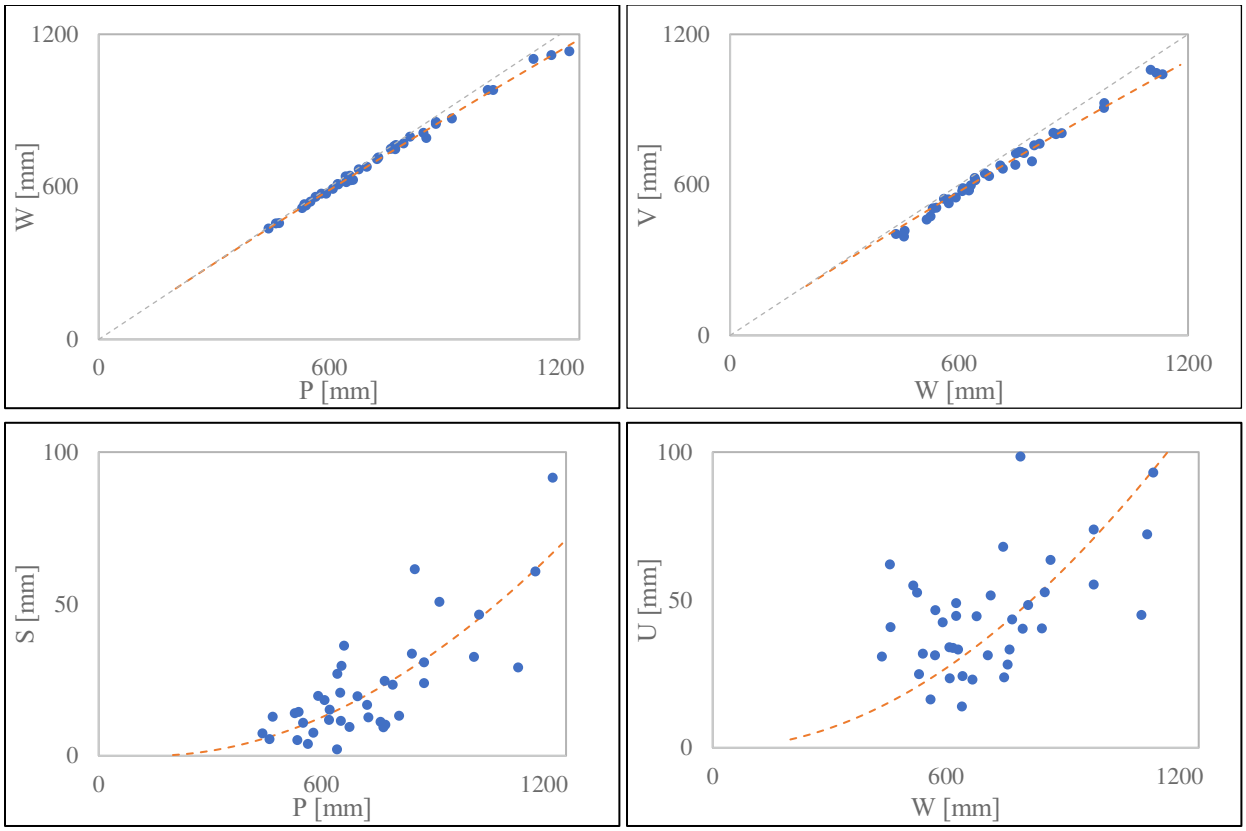

*Figure D3 - 21 : L'Vovich water balance relationships extracted for **La Muga, Spain**; Wetting W= f(P), Vaporization V=f(W), Quick flow S=f(P) and slow flow U = f(W); Points represent data (equations 14,15,16 and 17), and the dashed lines are Ponce and Shetty mathematical formulations (equations 18b and 19b)*

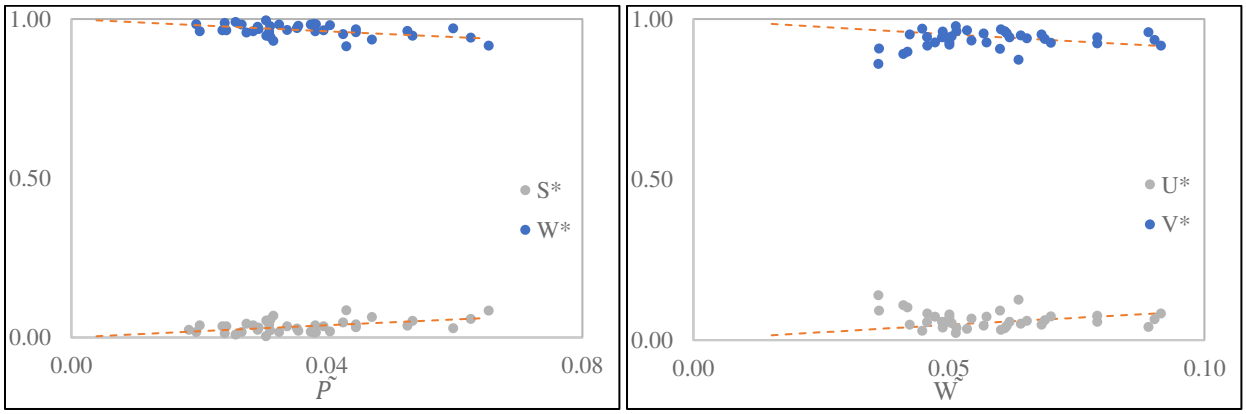

Figure D3 - 22 : Interannual variability of nondimensional annual estimates of (left) W and S* and (right) U* and V* versus annual climatic drivers $\tilde{P}$ and $\tilde{W}$ for **La Muga, Spain**; Points represent data (equations 22 and 23), and the dashed lines are theoretical (equations 25 and 26).*

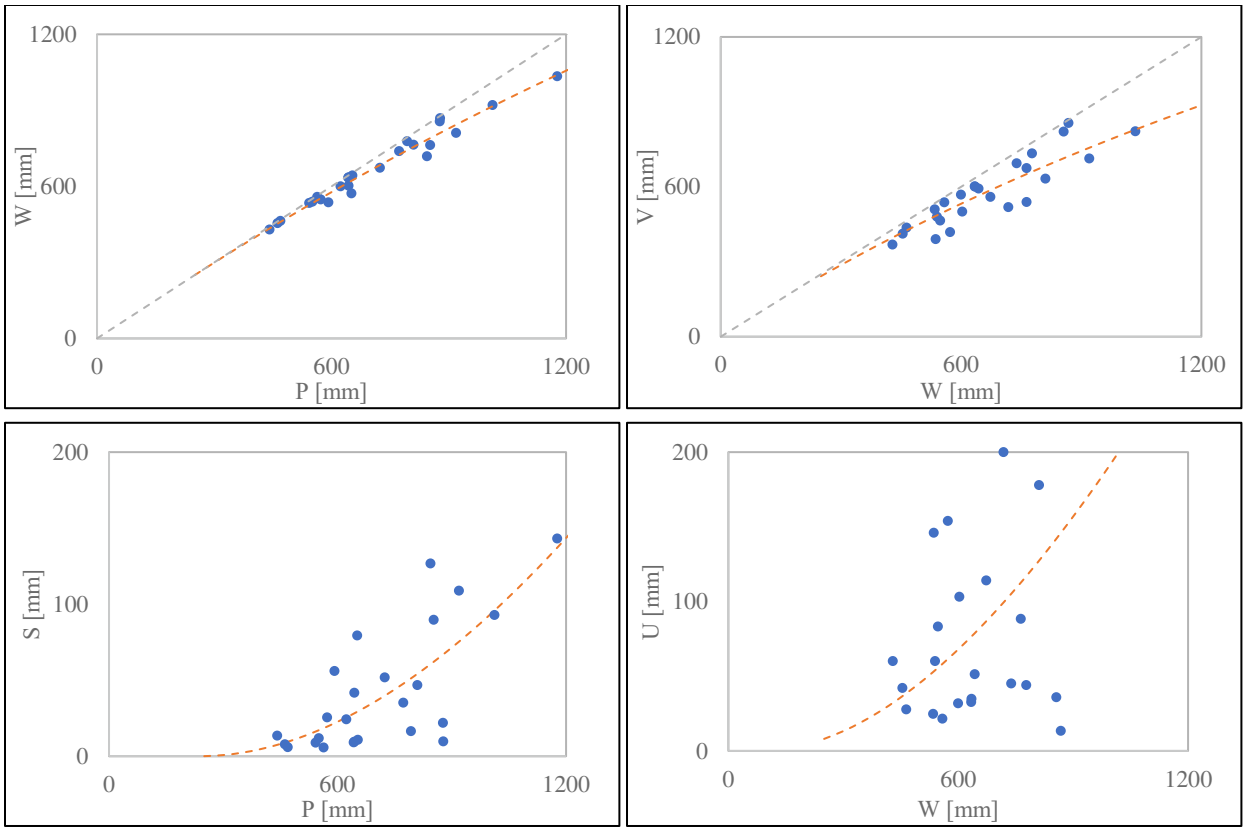

*Figure D3 - 23 : L'Vovich water balance relationships extracted for **El Ter, Spain**; Wetting W= f(P), Vaporization V=f(W), Quick flow S=f(P) and slow flow U = f(W); Points represent data (equations 14,15,16 and 17), and the dashed lines are Ponce and Shetty mathematical formulations (equations 18b and 19b)*

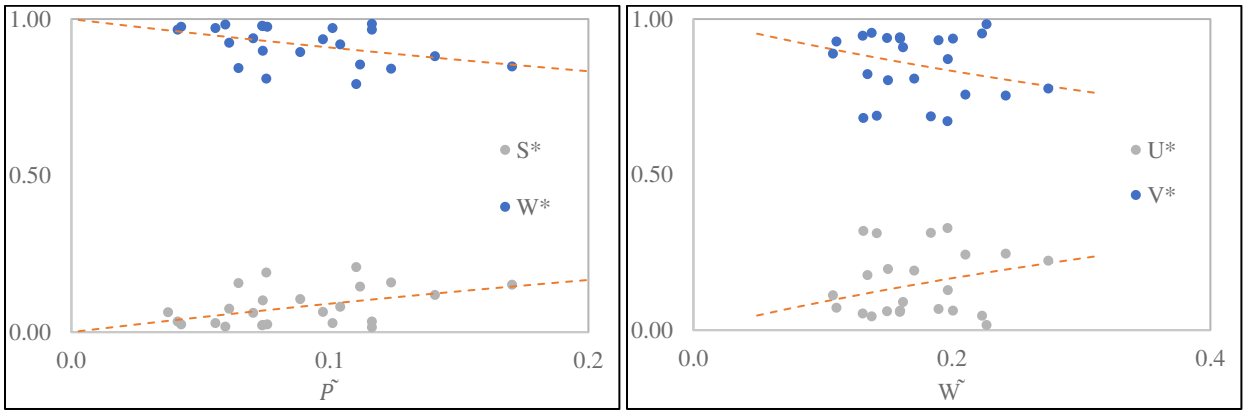

Figure D3 - 24 : Interannual variability of nondimensional annual estimates of (left) W and S* and (right) U* and V* versus annual climatic drivers $\tilde{P}$ and $\tilde{W}$ for **El Ter, Spain**; Points represent data (equations 22 and 23), and the dashed lines are theoretical (equations 25 and 26).*

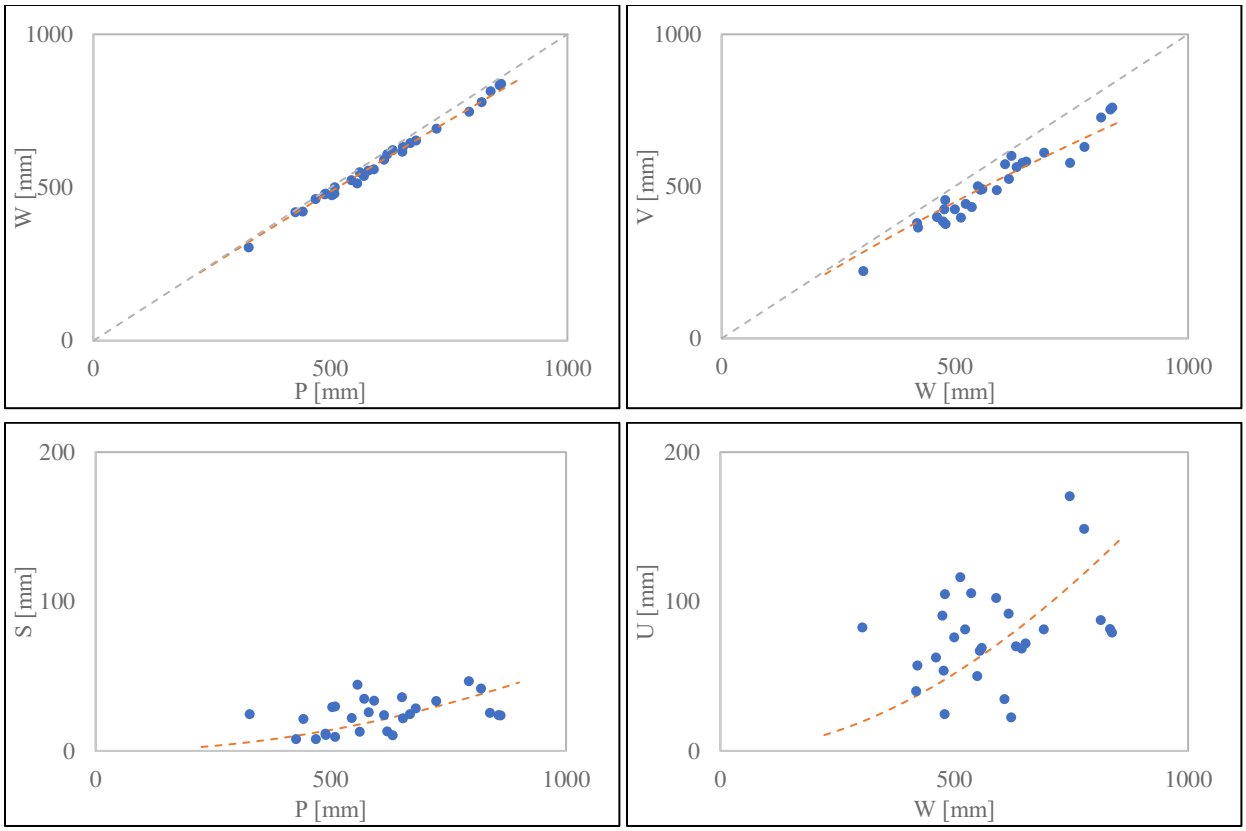

*Figure D3 - 25 : L'Vovich water balance relationships extracted for **El Besòs, Spain**; Wetting W= f(P), Vaporization V=f(W), Quick flow S=f(P) and slow flow U = f(W); Points represent data (equations 14,15,16 and 17), and the dashed lines are Ponce and Shetty mathematical formulations (equations 18b and 19b)*

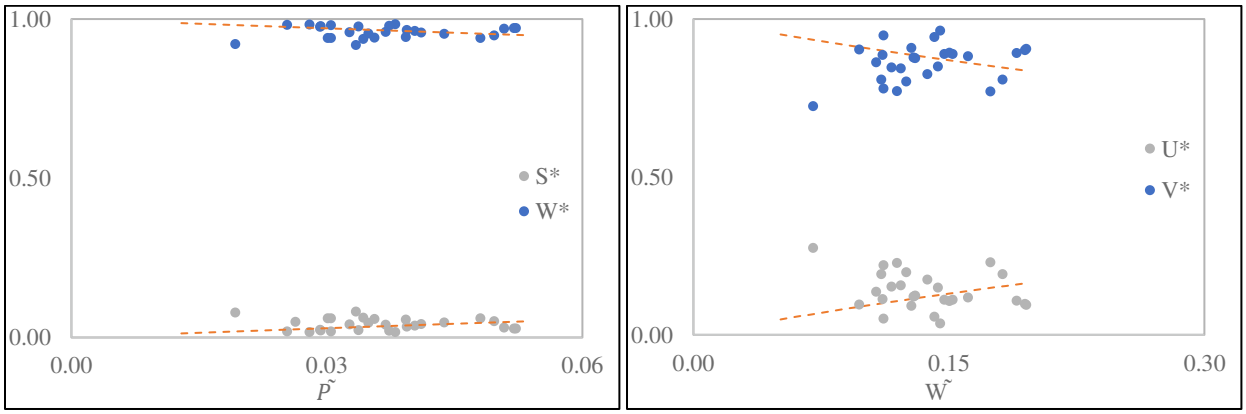

Figure D3 - 26 : Interannual variability of nondimensional annual estimates of (left) W and S* and (right) U* and V* versus annual climatic drivers $\tilde{P}$ and $\tilde{W}$ for **El Besòs, Spain**; Points represent data (equations 22 and 23), and the dashed lines are theoretical (equations 25 and 26).*

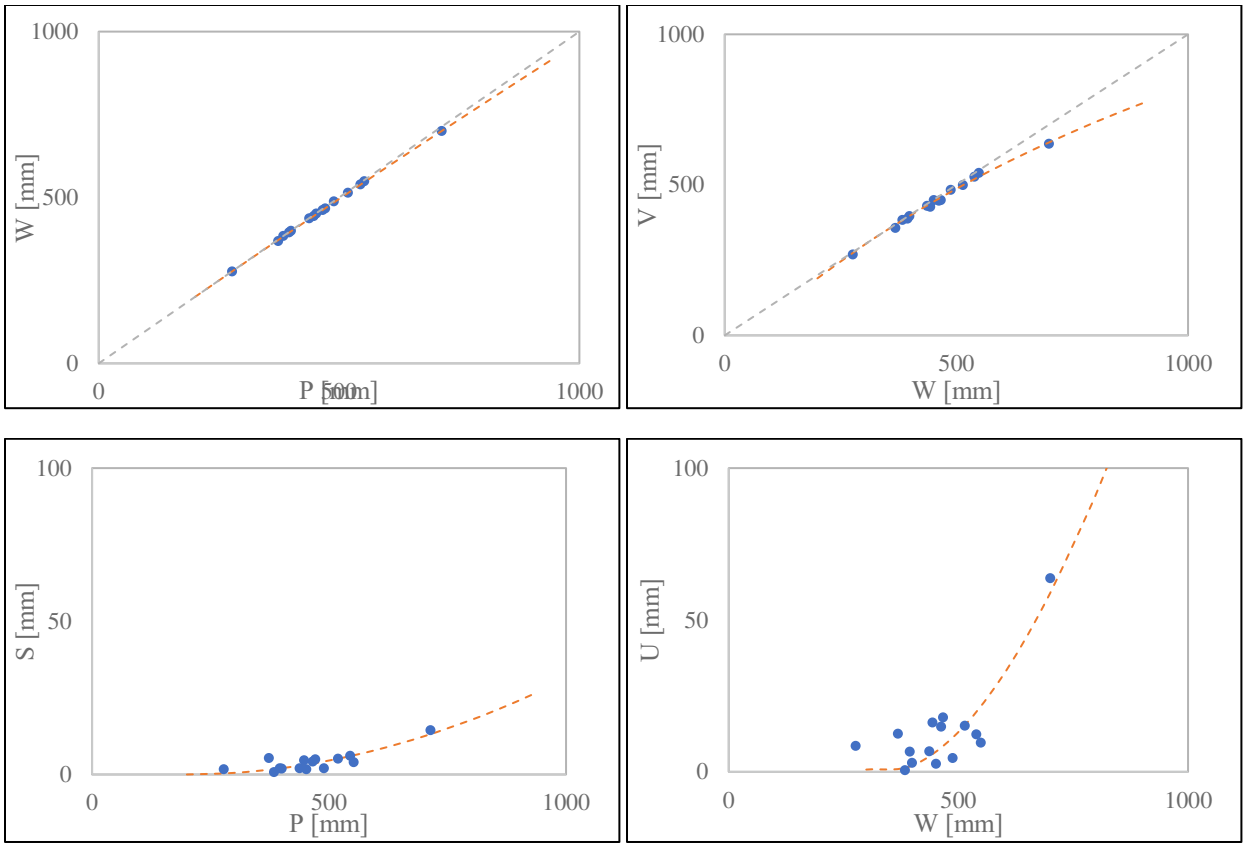

*Figure D3 - 27 : L'Vovich water balance relationships extracted for **Gaia, Spain**; Wetting W= f(P), Vaporization V=f(W), Quick flow S=f(P) and slow flow U = f(W); Points represent data (equations 14,15,16 and 17), and the dashed lines are Ponce and Shetty mathematical formulations (equations 18b and 19b)*

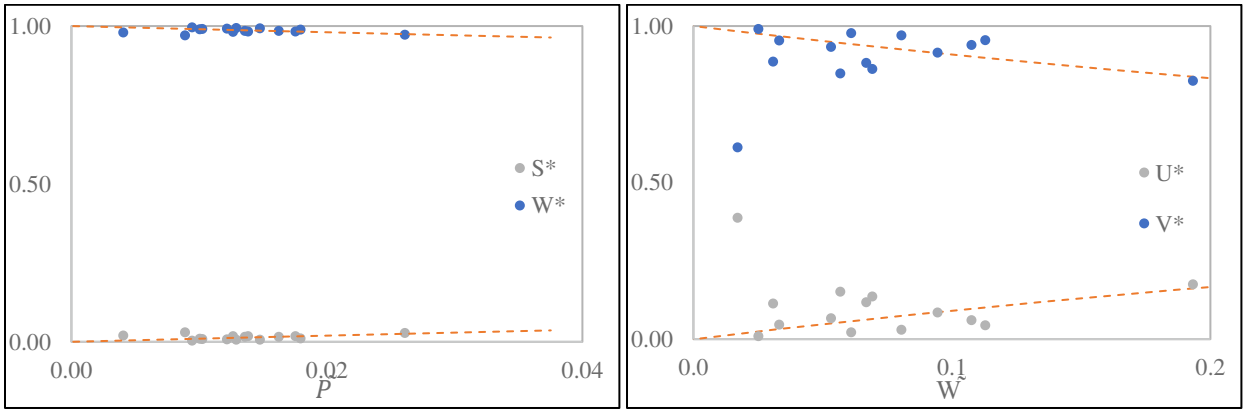

Figure D3 - 28 : Interannual variability of nondimensional annual estimates of (left) W and S* and (right) U* and V* versus annual climatic drivers $\tilde{P}$ and $\tilde{W}$ for **Gaia, Spain**; Points represent data (equations 22 and 23), and the dashed lines are theoretical (equations 25 and 26).*

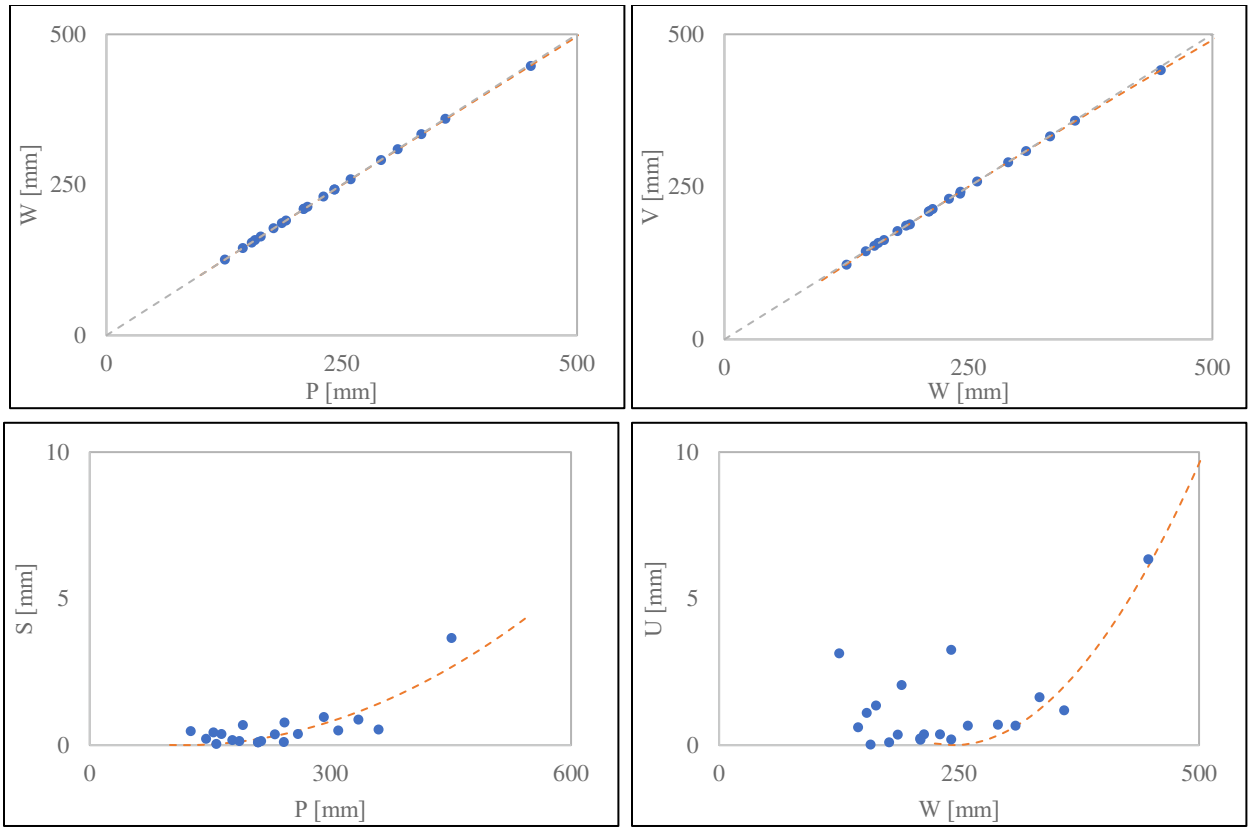

*Figure D3 - 29 : L'Vovich water balance relationships extracted for **Andarax, Spain**; Wetting W= f(P), Vaporization V=f(W), Quick flow S=f(P) and slow flow U = f(W); Points represent data (equations 14,15,16 and 17), and the dashed lines are Ponce and Shetty mathematical formulations (equations 18b and 19b)*

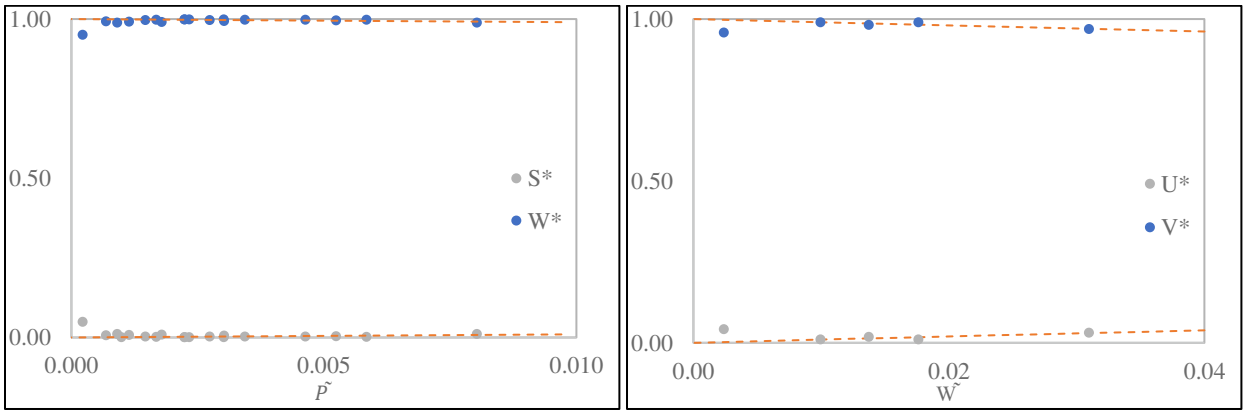

Figure D3 - 30 : Interannual variability of nondimensional annual estimates of (left) W and S* and (right) U* and V* versus annual climatic drivers $\tilde{P}$ and $\tilde{W}$ for **Andarax, Spain**; Points represent data (equations 22 and 23), and the dashed lines are theoretical (equations 25 and 26).*

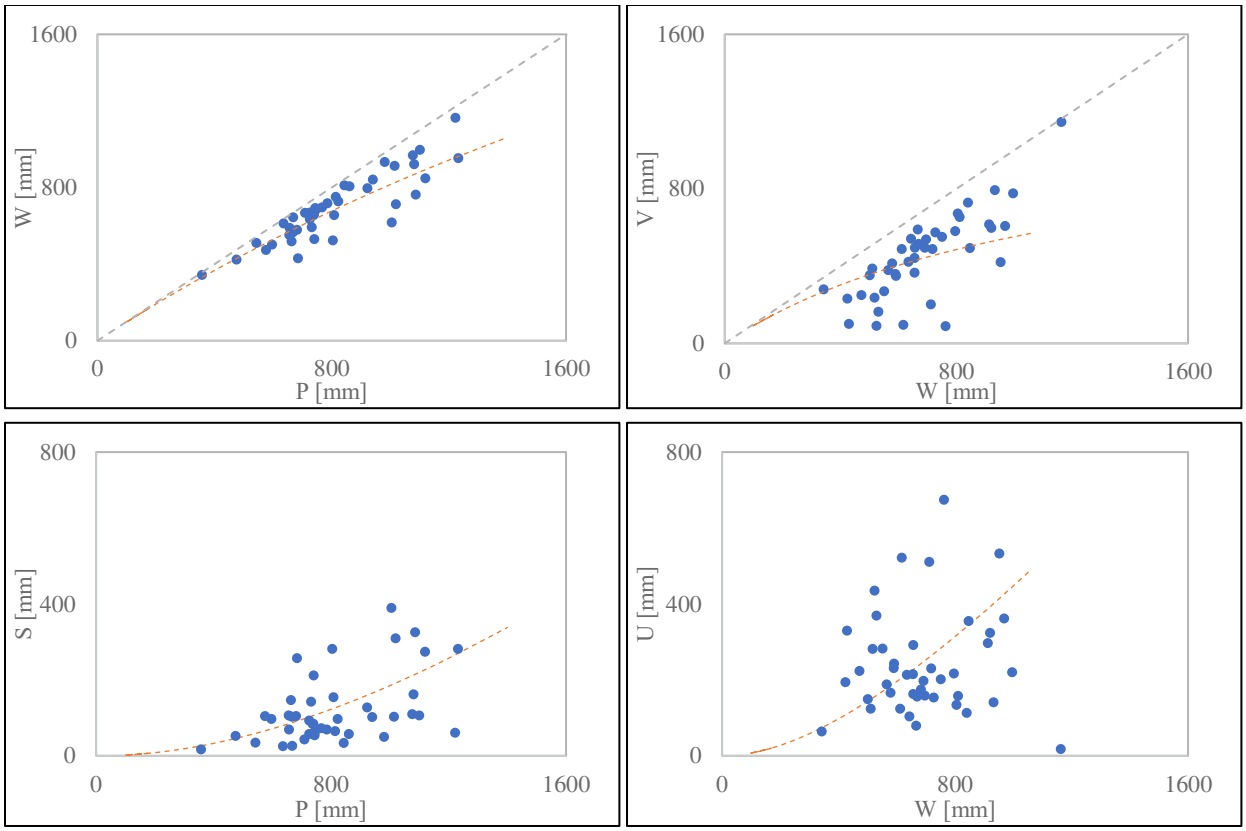

*Figure D3 - 31 : L'Vovich water balance relationships extracted for **Fium Alto, France**; Wetting W= f(P), Vaporization V=f(W), Quick flow S=f(P) and slow flow U = f(W); Points represent data (equations 14,15,16 and 17), and the dashed lines are Ponce and Shetty mathematical formulations (equations 18b and 19b)*

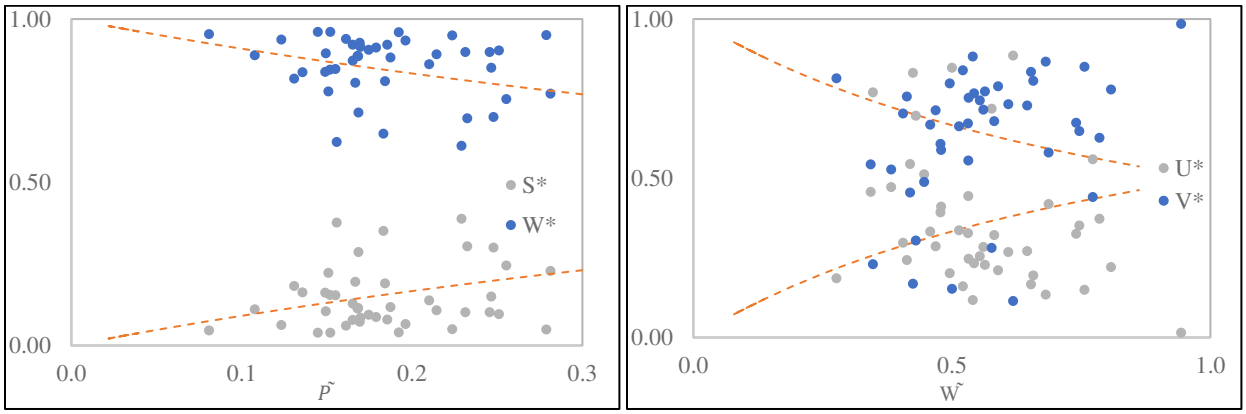

Figure D3 - 32 : Interannual variability of nondimensional annual estimates of (left) W and S* and (right) U* and V* versus annual climatic drivers $\tilde{P}$ and $\tilde{W}$ for **Fium Alto, France**; Points represent data (equations 22 and 23), and the dashed lines are theoretical (equations 25 and 26).*

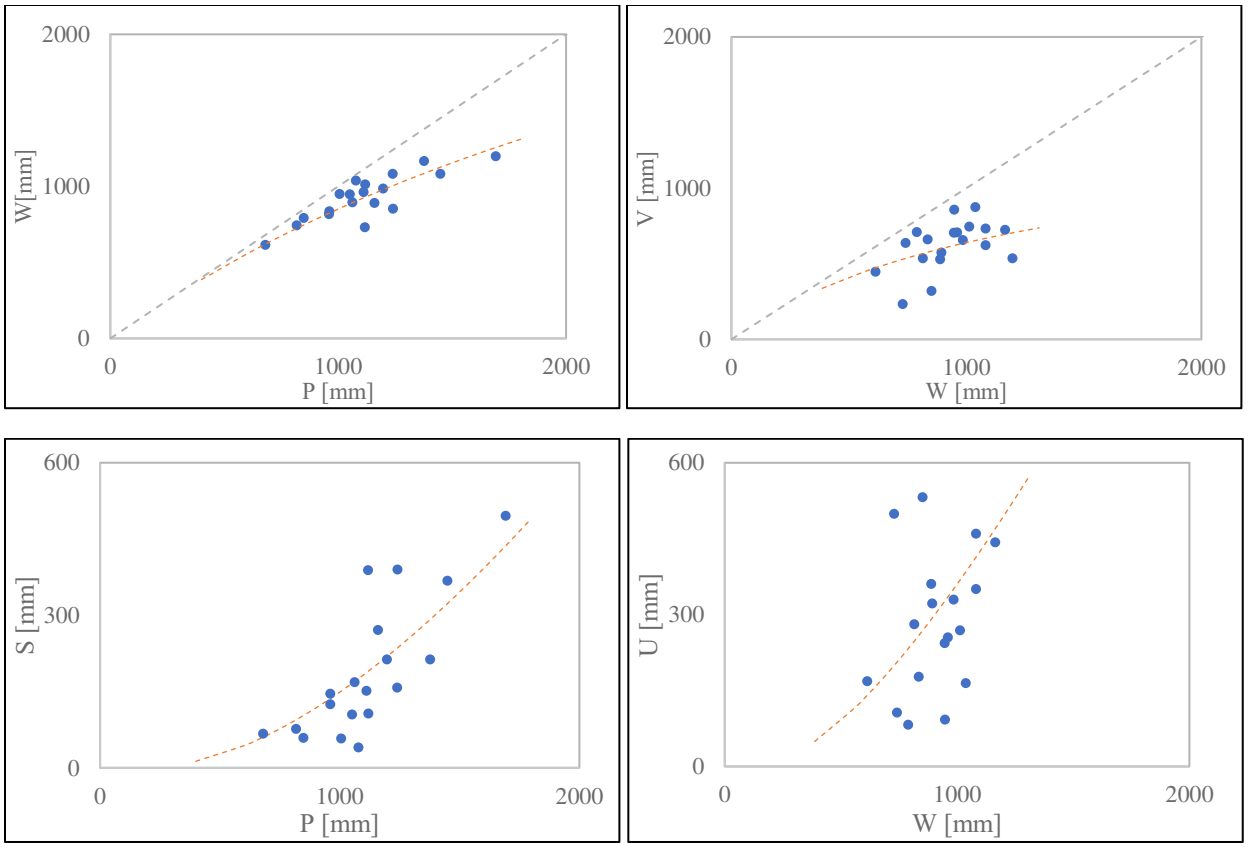

*Figure D3 - 33 : L'Vovich water balance relationships extracted for **Lez, France**; Wetting W= f(P), Vaporization V=f(W), Quick flow S=f(P) and slow flow U = f(W); Points represent data (equations 14,15,16 and 17), and the dashed lines are Ponce and Shetty mathematical formulations (equations 18b and 19b)*

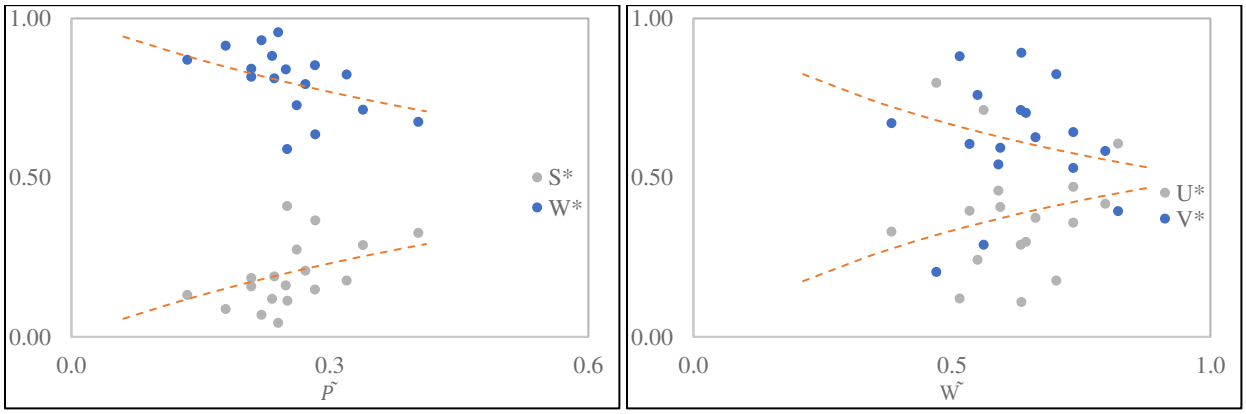

Figure D3 - 34 : Interannual variability of nondimensional annual estimates of (left) W and S* and (right) U* and V* versus annual climatic drivers $\tilde{P}$ and $\tilde{W}$ for **Lez, France**; Points represent data (equations 22 and 23), and the dashed lines are theoretical (equations 25 and 26).*

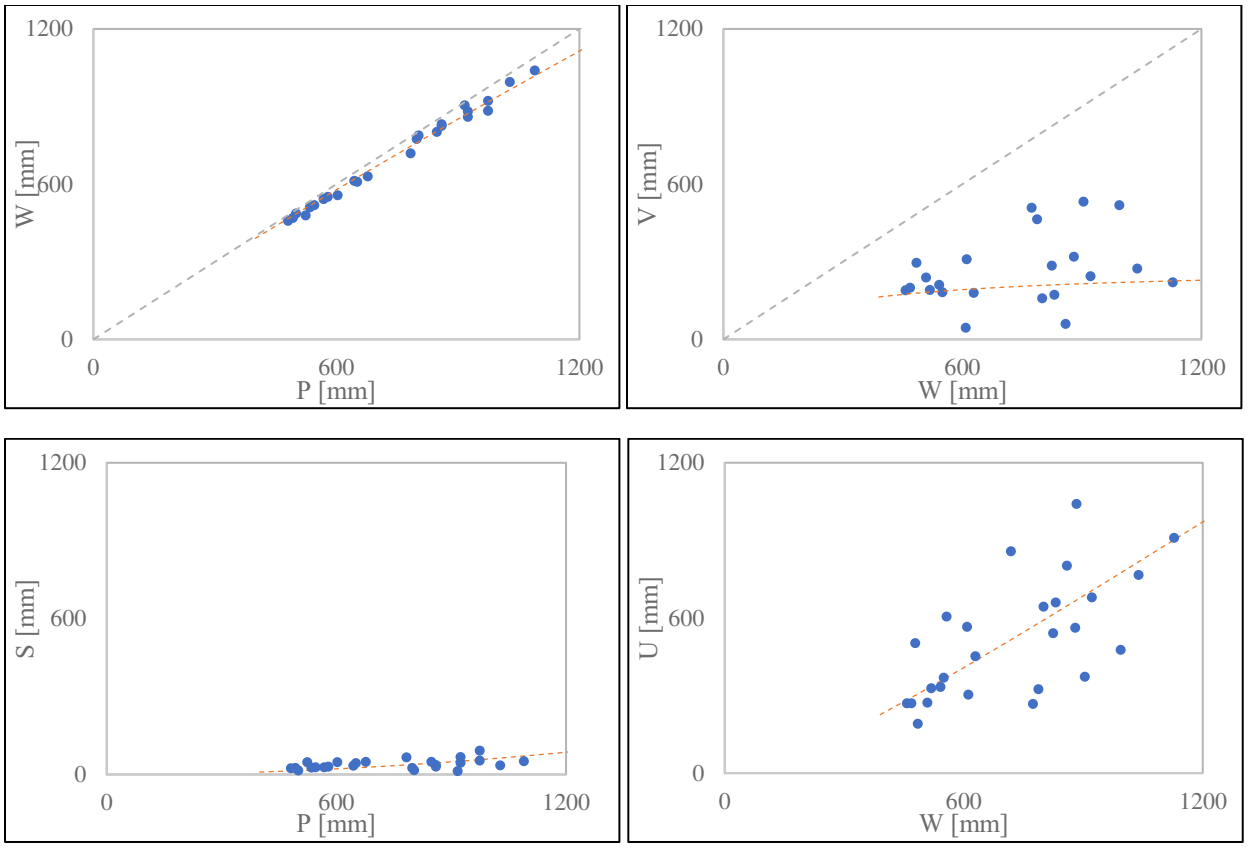

*Figure D3 - 35 : L'Vovich water balance relationships extracted for **Loup, France**; Wetting W= f(P), Vaporization V=f(W), Quick flow S=f(P) and slow flow U = f(W); Points represent data (equations 14,15,16 and 17), and the dashed lines are Ponce and Shetty mathematical formulations (equations 18b and 19b)*

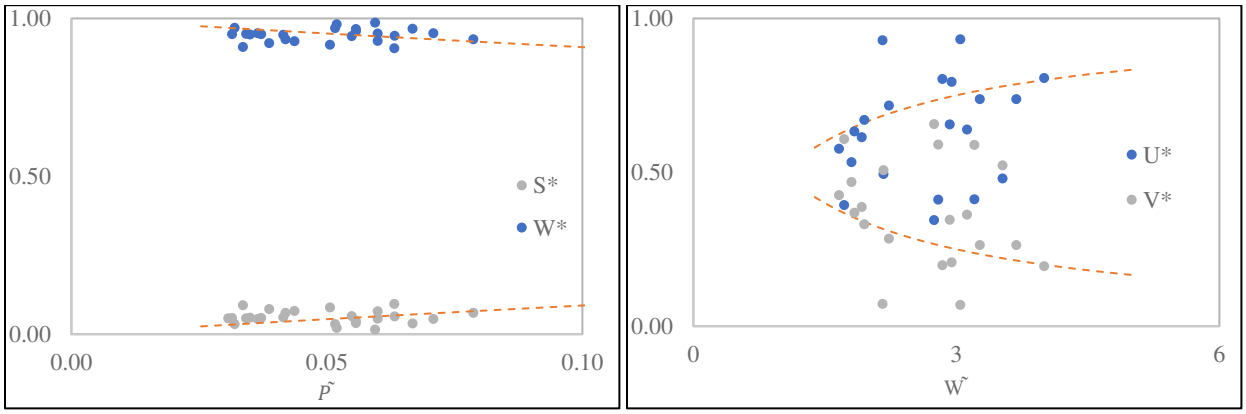

Figure D3 - 36 : Interannual variability of nondimensional annual estimates of (left) W and S* and (right) U* and V* versus annual climatic drivers $\tilde{P}$ and $\tilde{W}$ for **Loup, France**; Points represent data (equations 22 and 23), and the dashed lines are theoretical (equations 25 and 26).*

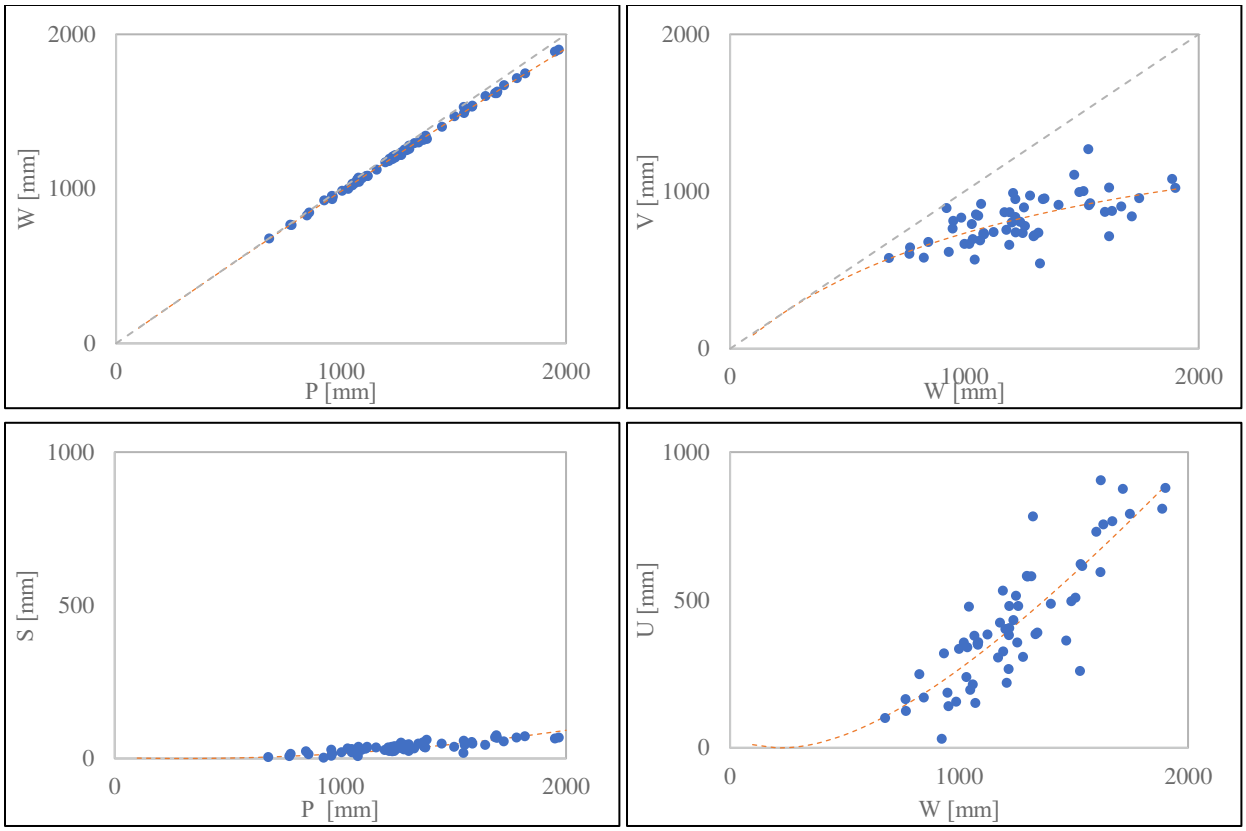

*Figure D3 - 37 : L'Vovich water balance relationships extracted for **Herault, France**; Wetting W= f(P), Vaporization V=f(W), Quick flow S=f(P) and slow flow U = f(W); Points represent data (equations 14,15,16 and 17), and the dashed lines are Ponce and Shetty mathematical formulations (equations 18b and 19b)*

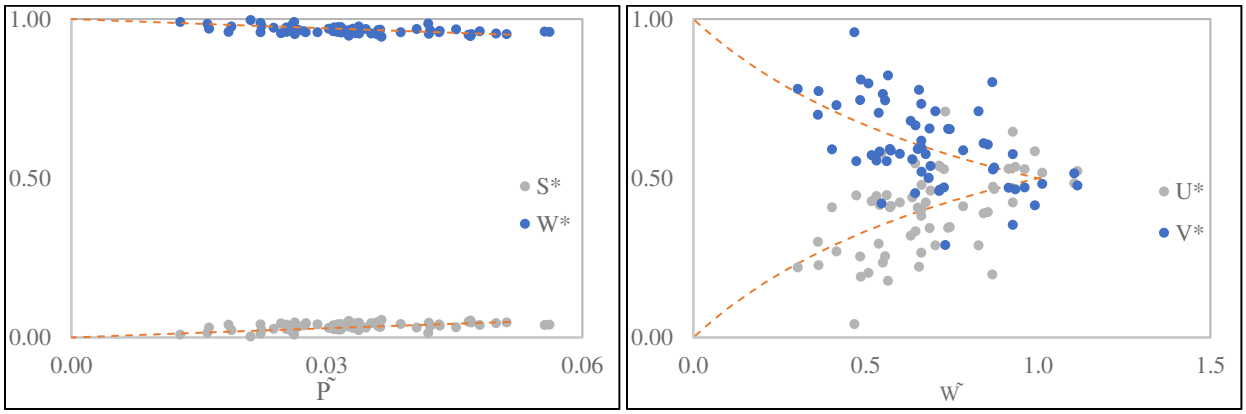

Figure D3 - 38 : Interannual variability of nondimensional annual estimates of (left) W and S* and (right) U* and V* versus annual climatic drivers $\tilde{P}$ and $\tilde{W}$ for **Herault, France**; Points represent data (equations 22 and 23), and the dashed lines are theoretical (equations 25 and 26).*

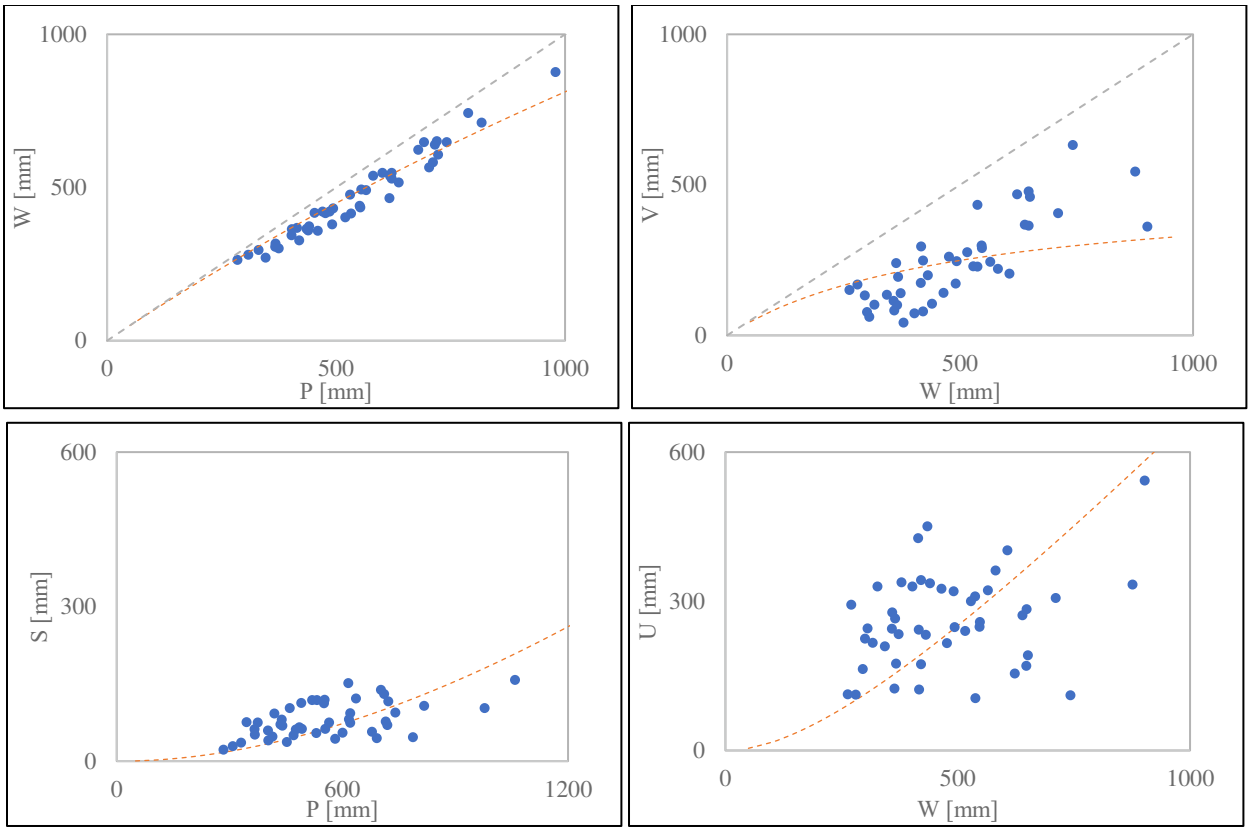

*Figure D3 - 39 : L'Vovich water balance relationships extracted for **Aude, France**; Wetting W= f(P), Vaporization V=f(W), Quick flow S=f(P) and slow flow U = f(W); Points represent data (equations 14,15,16 and 17), and the dashed lines are Ponce and Shetty mathematical formulations (equations 18b and 19b)*

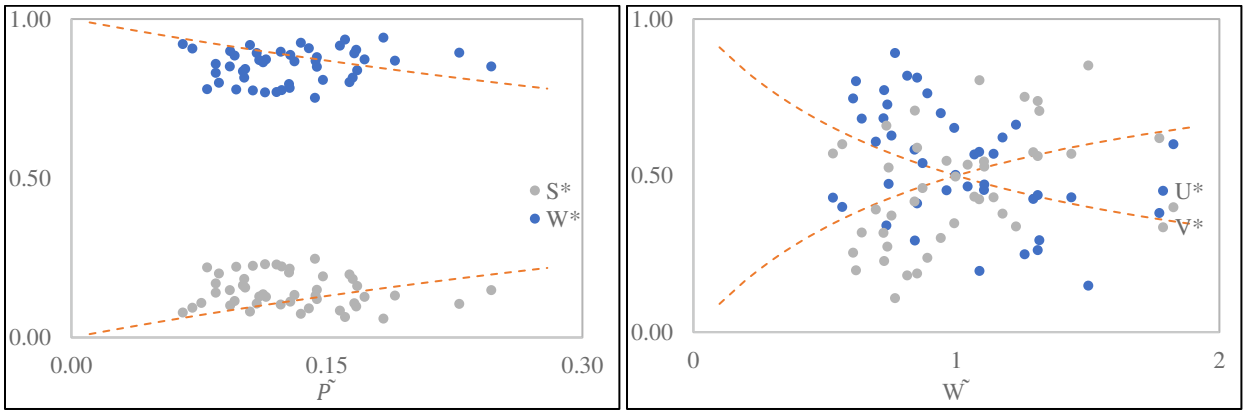

Figure D3 - 40 : Interannual variability of nondimensional annual estimates of (left) W and S* and (right) U* and V* versus annual climatic drivers $\tilde{P}$ and $\tilde{W}$ for **Aude, France**; Points represent data (equations 22 and 23), and the dashed lines are theoretical (equations 25 and 26).*

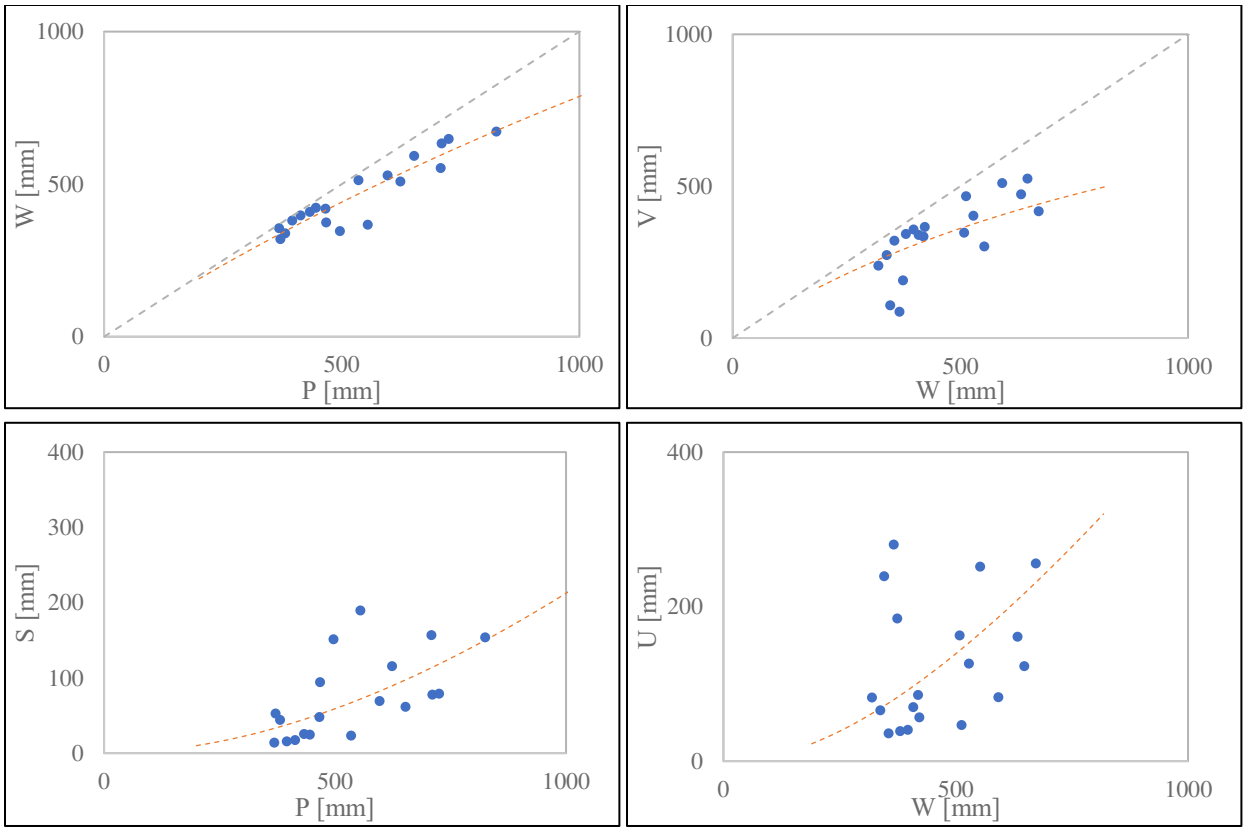

*Figure D3 - 41 : L'Vovich water balance relationships extracted for **Gapeau, France**; Wetting W= f(P), Vaporization V=f(W), Quick flow S=f(P) and slow flow U = f(W); Points represent data (equations 14,15,16 and 17), and the dashed lines are Ponce and Shetty mathematical formulations (equations 18b and 19b)*

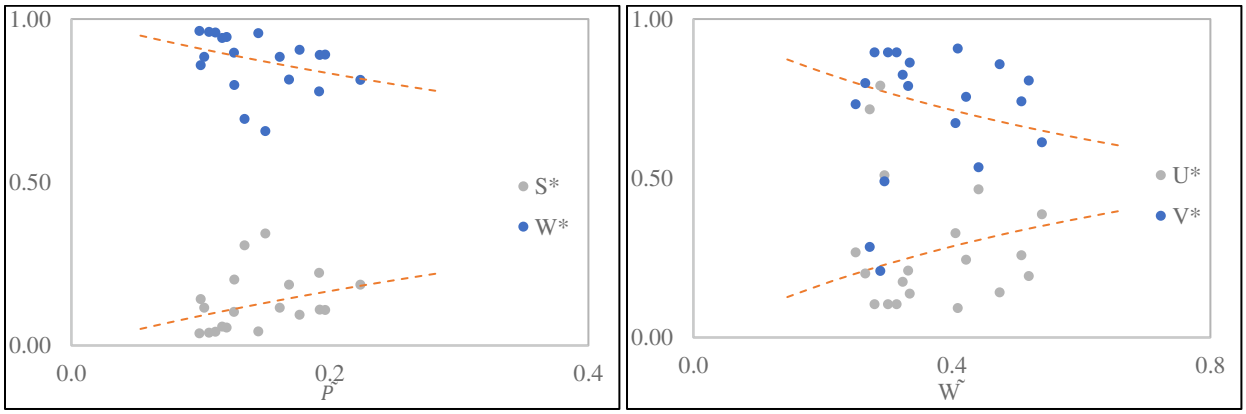

Figure D3 - 42 : Interannual variability of nondimensional annual estimates of (left) W and S* and (right) U* and V* versus annual climatic drivers $\tilde{P}$ and $\tilde{W}$ for **Gapeau, France**; Points represent data (equations 22 and 23), and the dashed lines are theoretical (equations 25 and 26).*

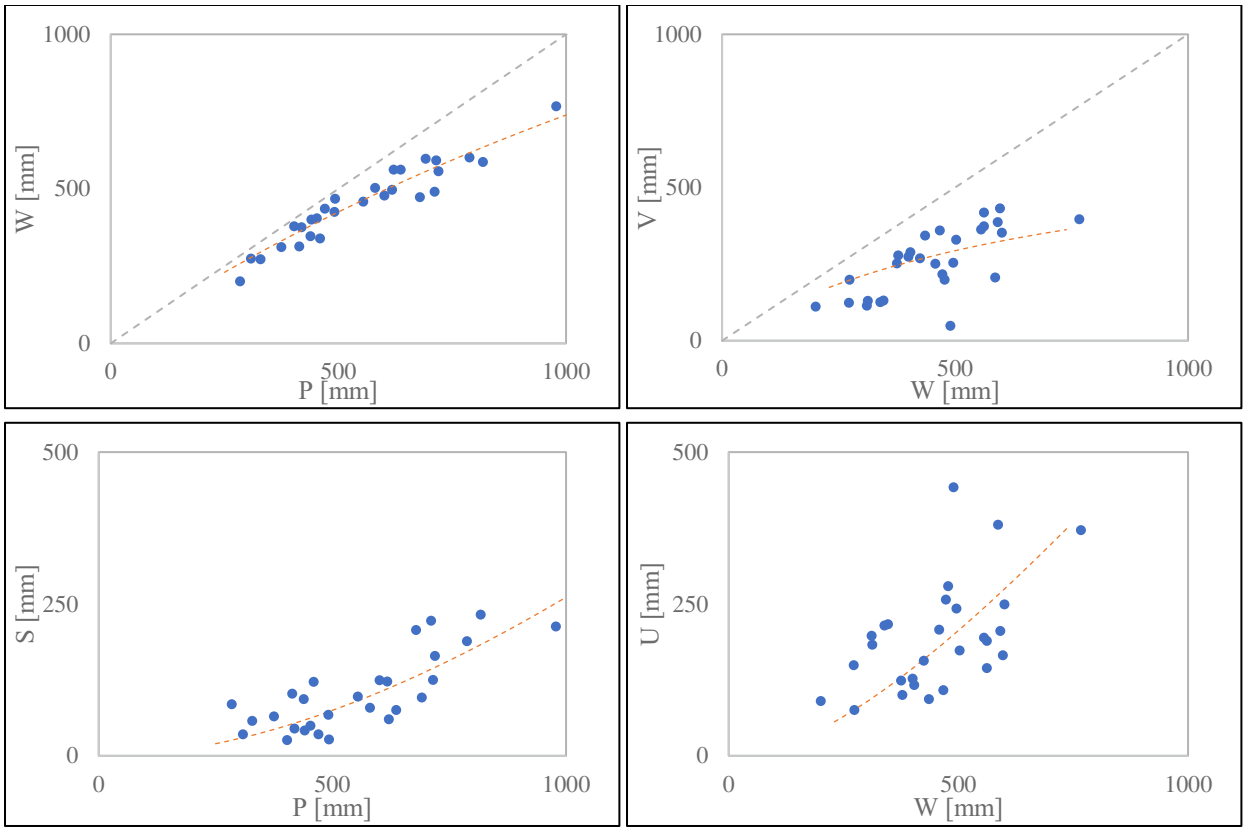

*Figure D3 - 43 : L'Vovich water balance relationships extracted for **Tech, France**; Wetting W= f(P), Vaporization V=f(W), Quick flow S=f(P) and slow flow U = f(W); Points represent data (equations 14,15,16 and 17), and the dashed lines are Ponce and Shetty mathematical formulations (equations 18b and 19b)*

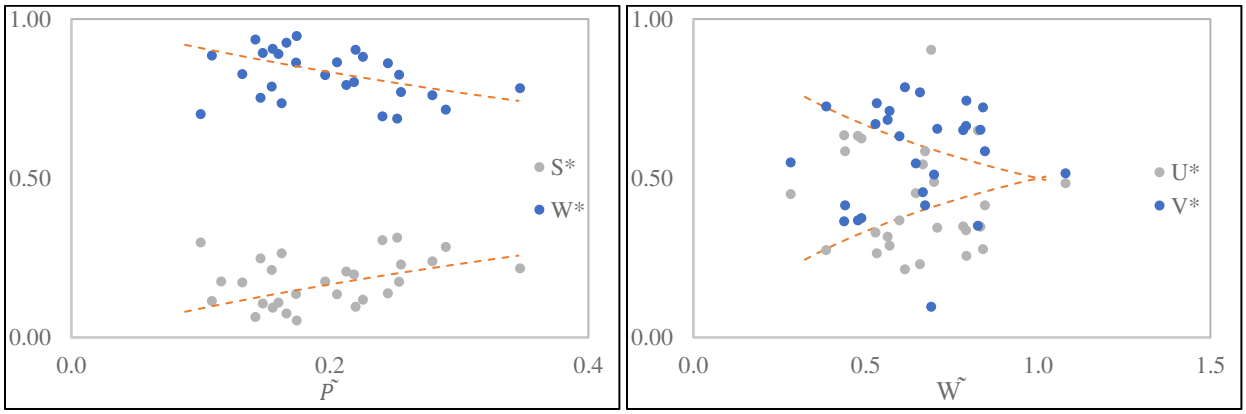

Figure D3 - 44 : Interannual variability of nondimensional annual estimates of (left) W and S* and (right) U* and V* versus annual climatic drivers $\tilde{P}$ and $\tilde{W}$ for **Tech, France**; Points represent data (equations 22 and 23), and the dashed lines are theoretical (equations 25 and 26).*

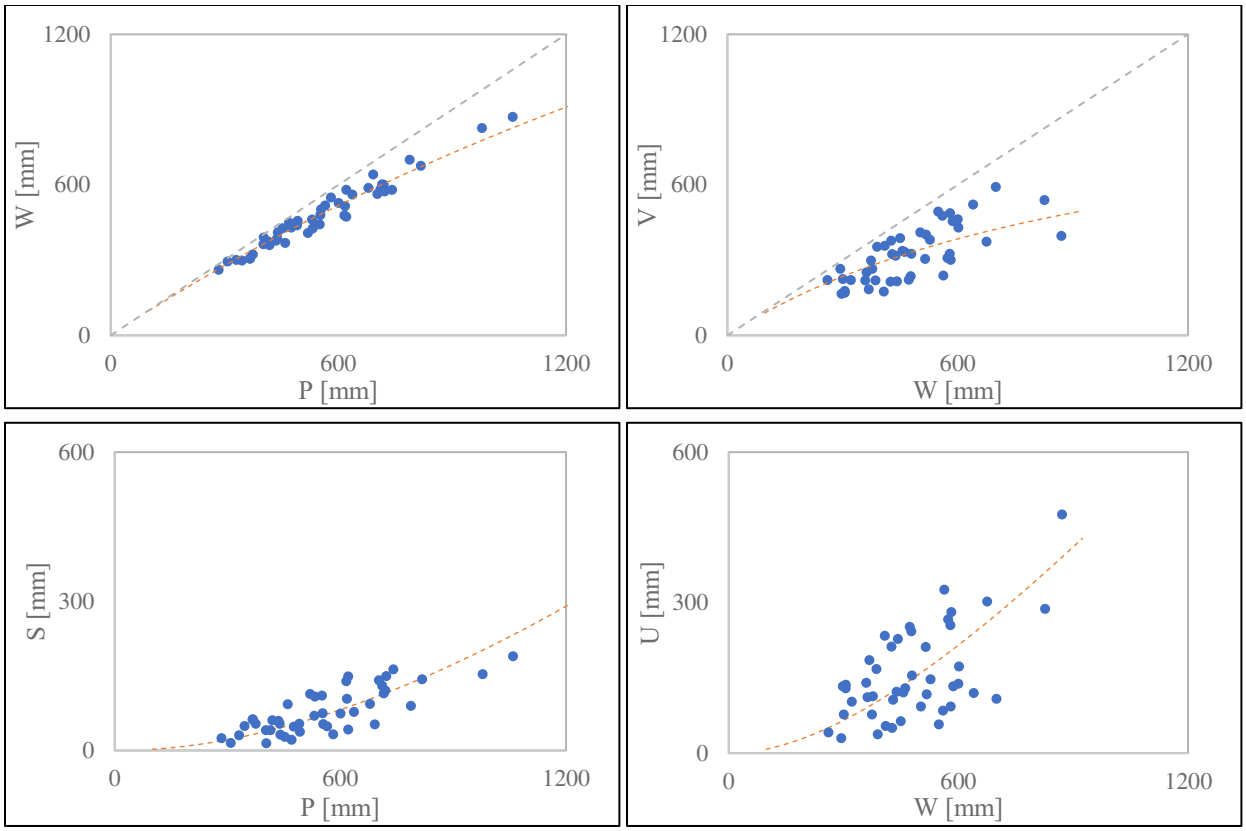

*Figure D3 - 45 : L'Vovich water balance relationships extracted for **Tet, France**; Wetting W= f(P), Vaporization V=f(W), Quick flow S=f(P) and slow flow U = f(W); Points represent data (equations 14,15,16 and 17), and the dashed lines are Ponce and Shetty mathematical formulations (equations 18b and 19b)*

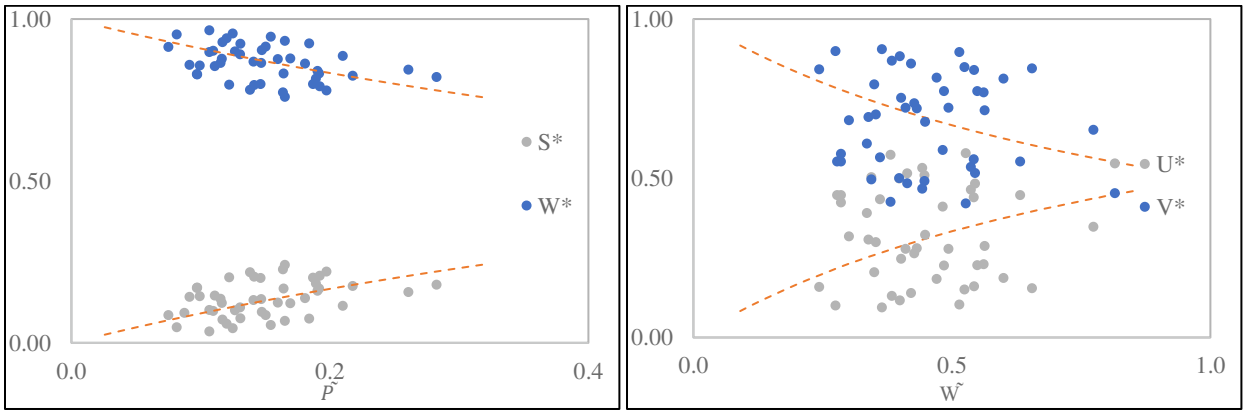

Figure D3 - 46 : Interannual variability of nondimensional annual estimates of (left) W and S* and (right) U* and V* versus annual climatic drivers $\tilde{P}$ and $\tilde{W}$ for **Tet, France**; Points represent data (equations 22 and 23), and the dashed lines are theoretical (equations 25 and 26).*

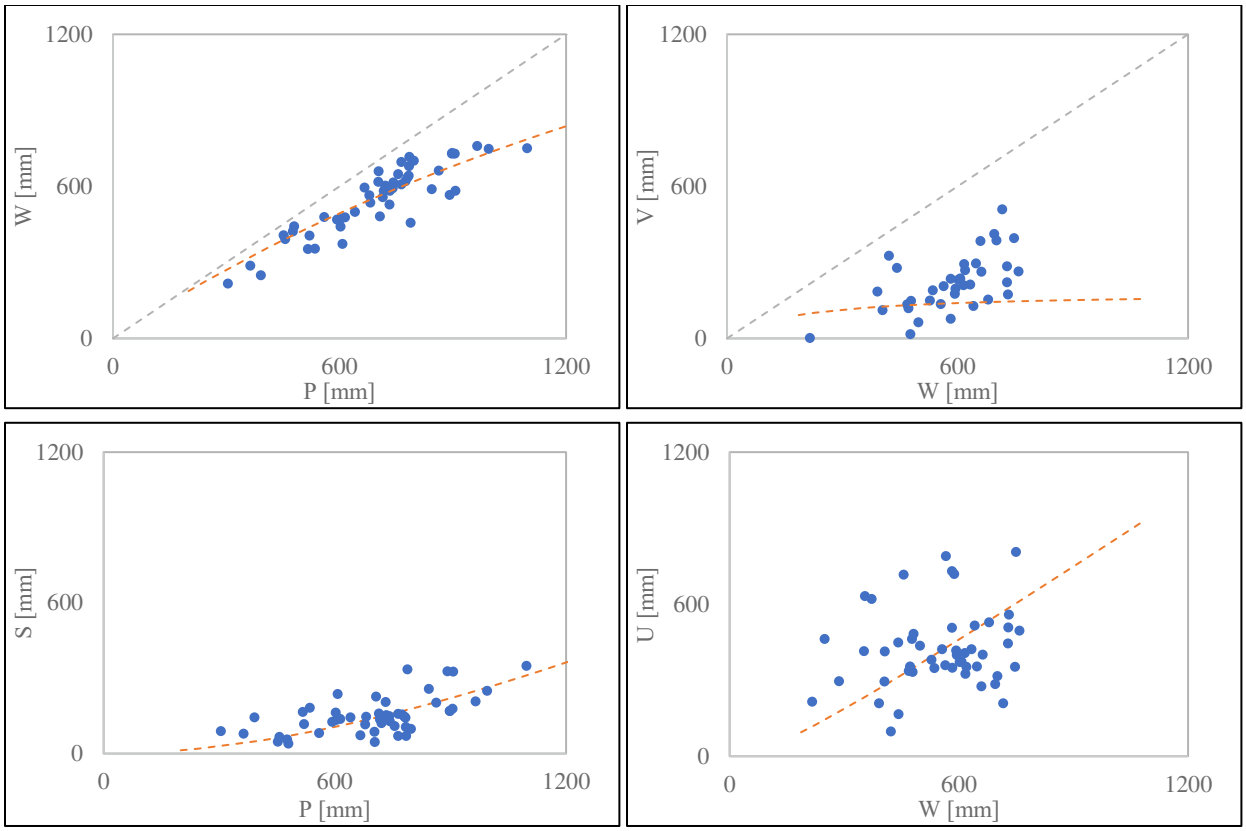

*Figure D3 - 47 : L'Vovich water balance relationships extracted for **Sperchios, Greece**; Wetting W= f(P), Vaporization V=f(W), Quick flow S=f(P) and slow flow U = f(W); Points represent data (equations 14,15,16 and 17), and the dashed lines are Ponce and Shetty mathematical formulations (equations 18b and 19b)*

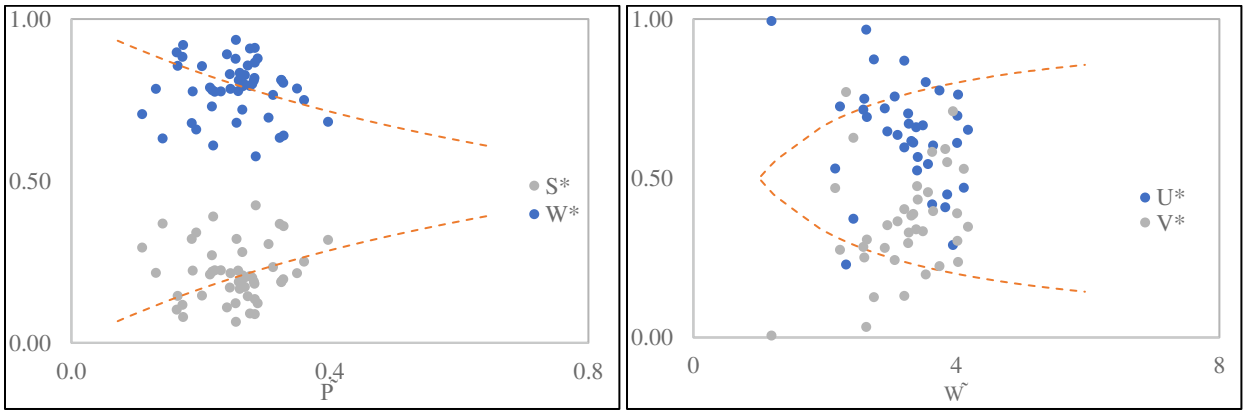

Figure D3 - 48 : Interannual variability of nondimensional annual estimates of (left) W and S* and (right) U* and V* versus annual climatic drivers $\tilde{P}$ and $\tilde{W}$ for **Sperchios, Greece**; Points represent data (equations 22 and 23), and the dashed lines are theoretical (equations 25 and 26).*

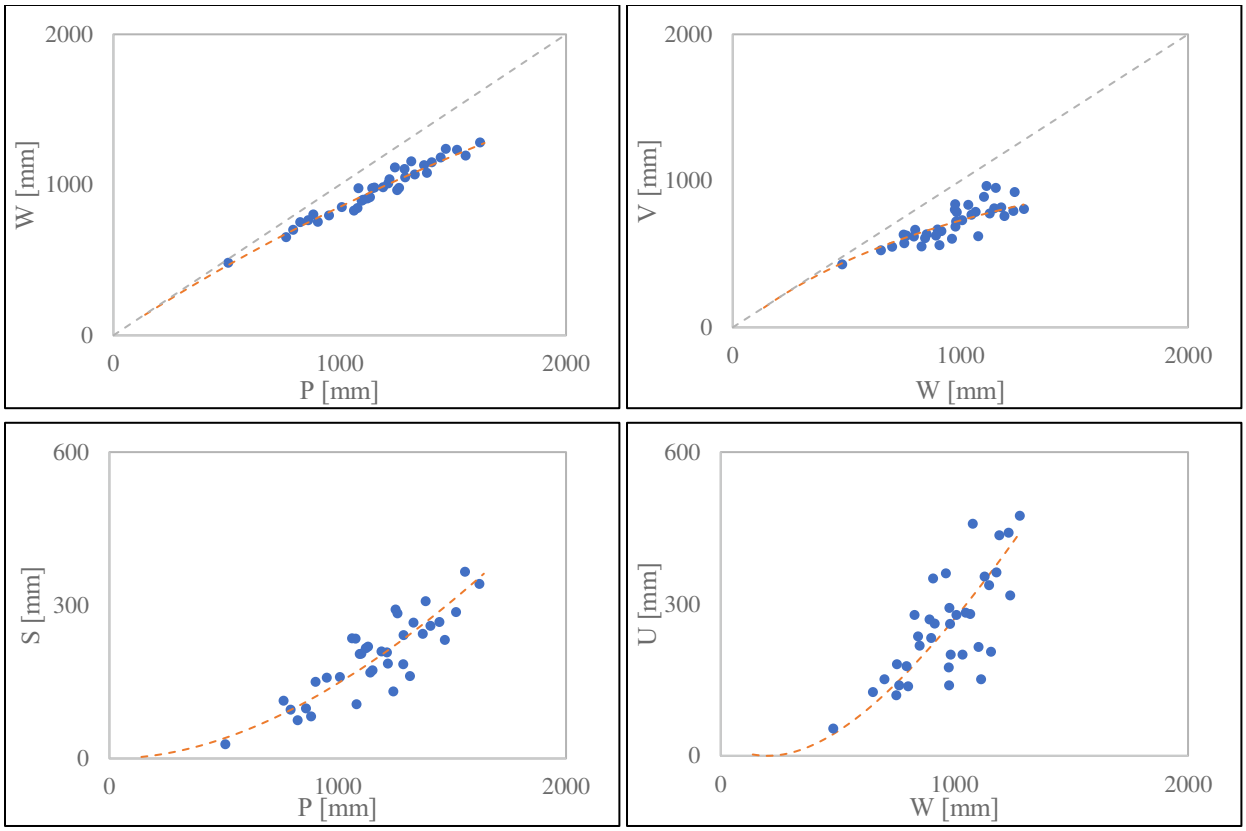

*Figure D3 - 49 : L'Vovich water balance relationships extracted for **Mirna, Croatia**; Wetting W= f(P), Vaporization V=f(W), Quick flow S=f(P) and slow flow U = f(W); Points represent data (equations 14,15,16 and 17), and the dashed lines are Ponce and Shetty mathematical formulations (equations 18b and 19b)*

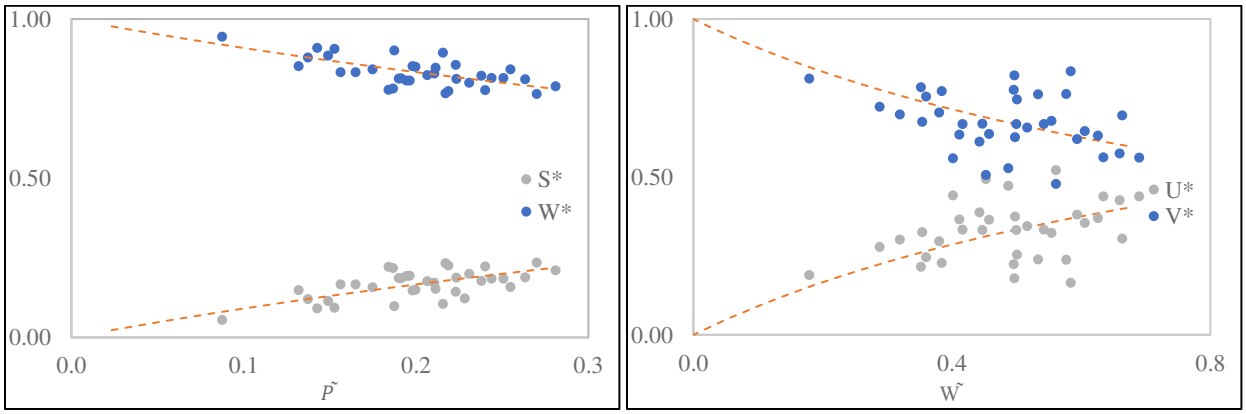

Figure D3 - 50 : Interannual variability of nondimensional annual estimates of (left) W and S* and (right) U* and V* versus annual climatic drivers $\tilde{P}$ and $\tilde{W}$ for **Mirna, Croatia**; Points represent data (equations 22 and 23), and the dashed lines are theoretical (equations 25 and 26).*

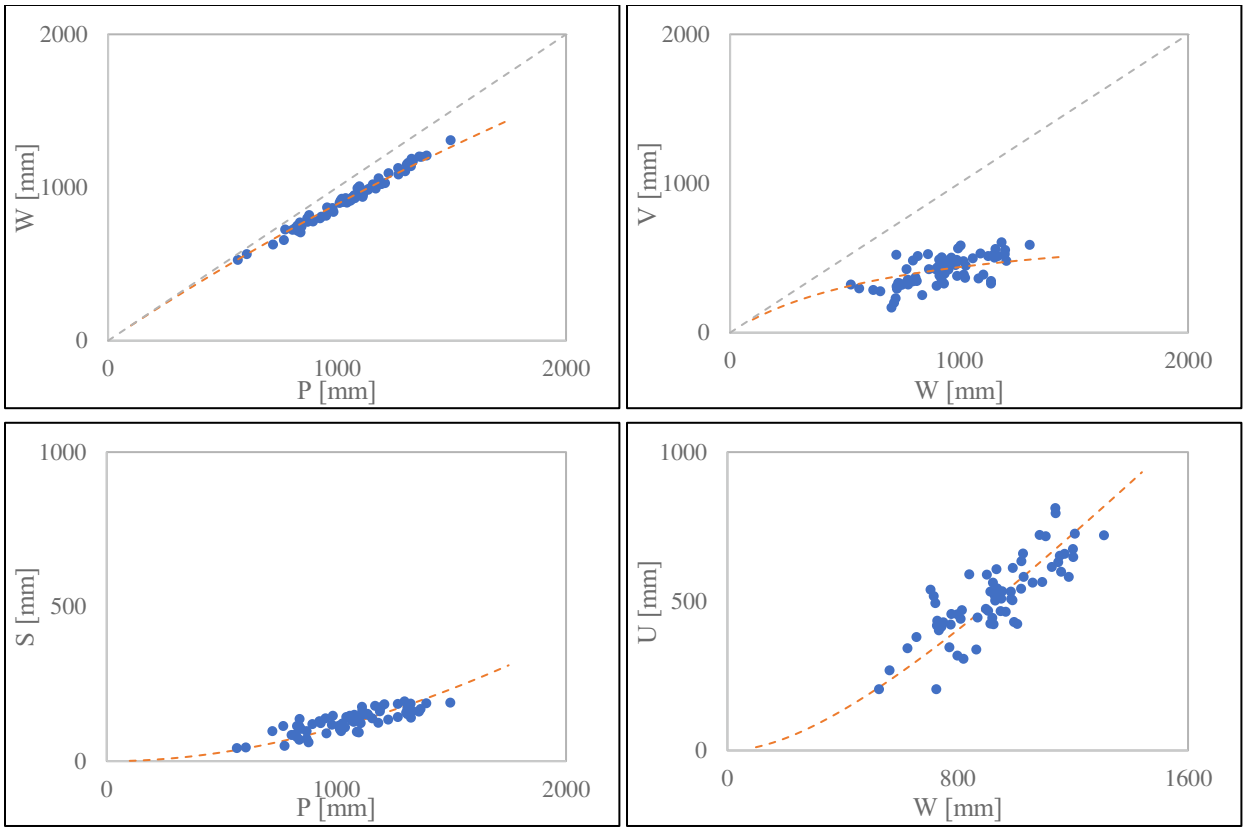

*Figure D3 - 51 : L'Vovich water balance relationships extracted for **Krka, Croatia**; Wetting W= f(P), Vaporization V=f(W), Quick flow S=f(P) and slow flow U = f(W); Points represent data (equations 14,15,16 and 17), and the dashed lines are Ponce and Shetty mathematical formulations (equations 18b and 19b)*

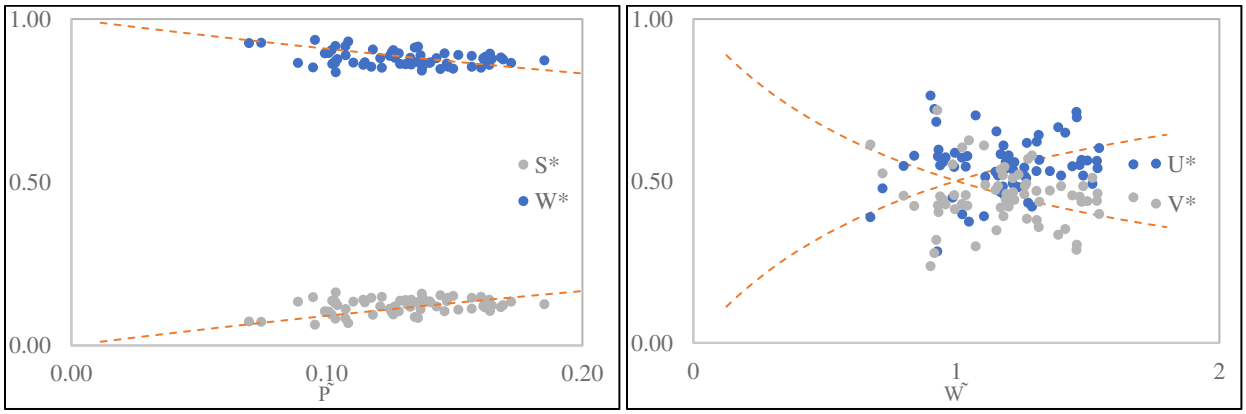

Figure D3 - 52 : Interannual variability of nondimensional annual estimates of (left) W and S* and (right) U* and V* versus annual climatic drivers $\tilde{P}$ and $\tilde{W}$ for **Krka, Croatia**; Points represent data (equations 22 and 23), and the dashed lines are theoretical (equations 25 and 26).*

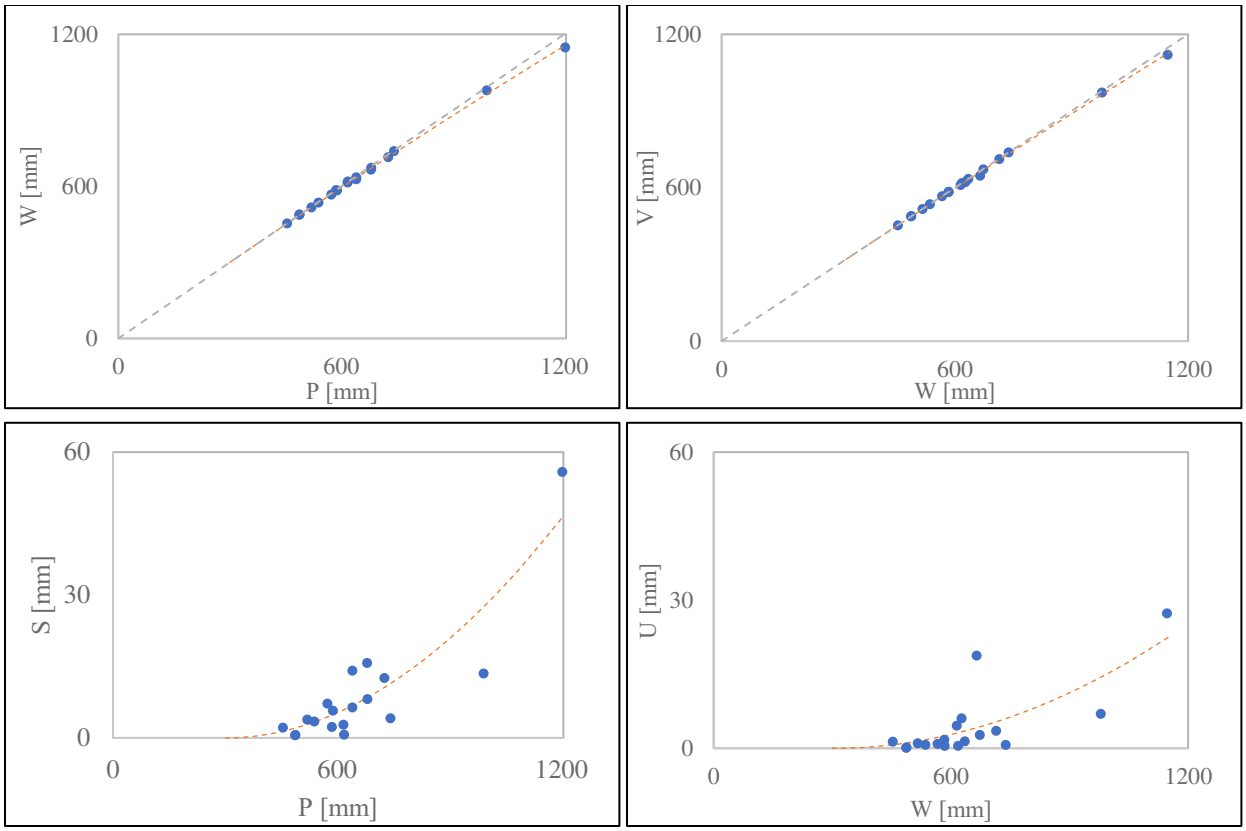

*Figure D3 - 53 : L'Vovich water balance relationships extracted for **Alexander, Israel**; Wetting W= f(P), Vaporization V=f(W), Quick flow S=f(P) and slow flow U = f(W); Points represent data (equations 14,15,16 and 17), and the dashed lines are Ponce and Shetty mathematical formulations (equations 18b and 19b)*

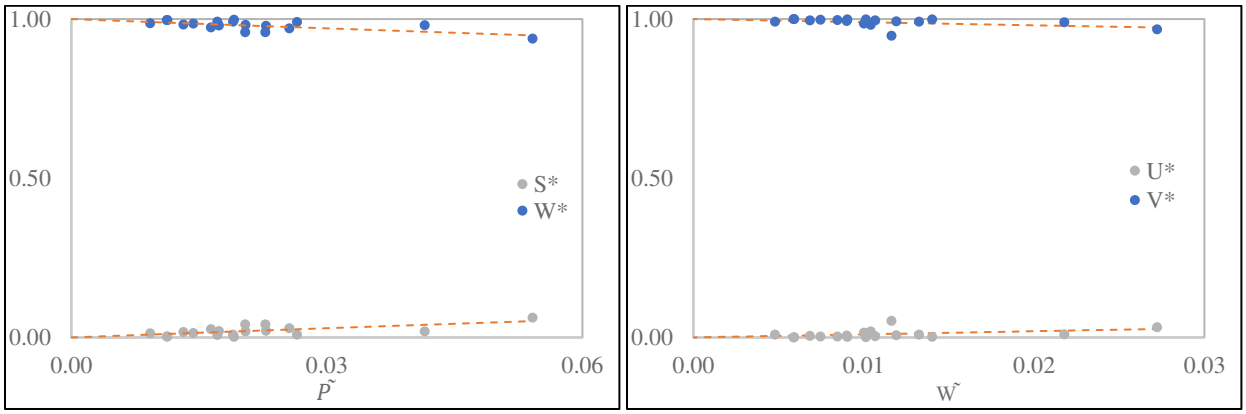

Figure D3 - 54 : Interannual variability of nondimensional annual estimates of (left) W and S* and (right) U* and V* versus annual climatic drivers $\tilde{P}$ and $\tilde{W}$ for **Alexander, Israel**; Points represent data (equations 22 and 23), and the dashed lines are theoretical (equations 25 and 26).*

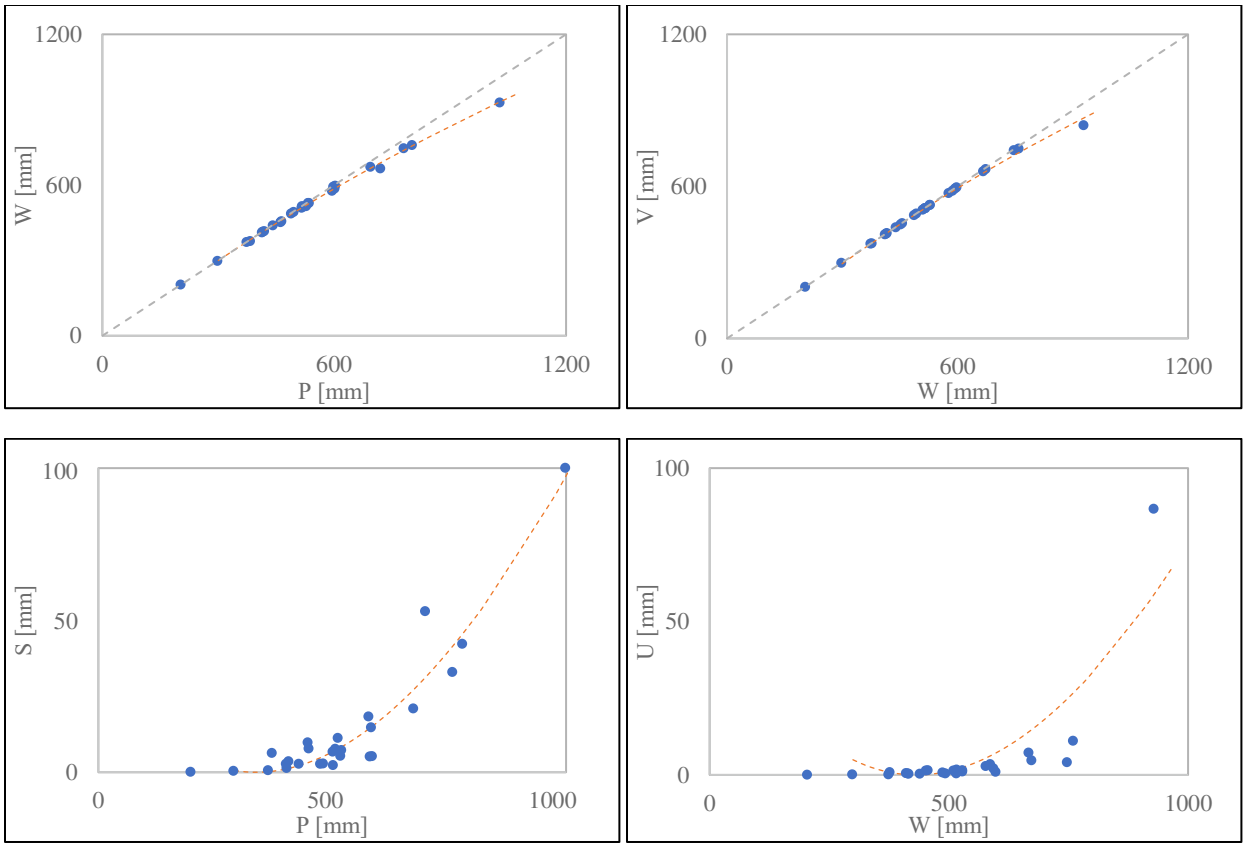

*Figure D3 - 55 : L'Vovich water balance relationships extracted for **Soreq, Israel**; Wetting W= f(P), Vaporization V=f(W), Quick flow S=f(P) and slow flow U = f(W); Points represent data (equations 14,15,16 and 17), and the dashed lines are Ponce and Shetty mathematical formulations (equations 18b and 19b)*

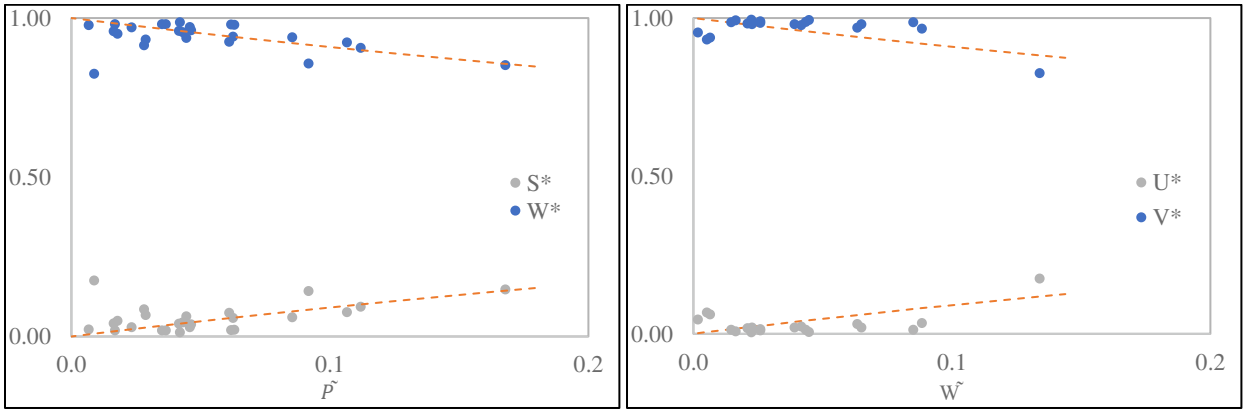

Figure D3 - 56 : Interannual variability of nondimensional annual estimates of (left) W and S* and (right) U* and V* versus annual climatic drivers $\tilde{P}$ and $\widetilde{W}$ for **Soreq, Israel**; Points represent data (equations 22 and 23), and the dashed lines are theoretical (equations 25 and 26).*

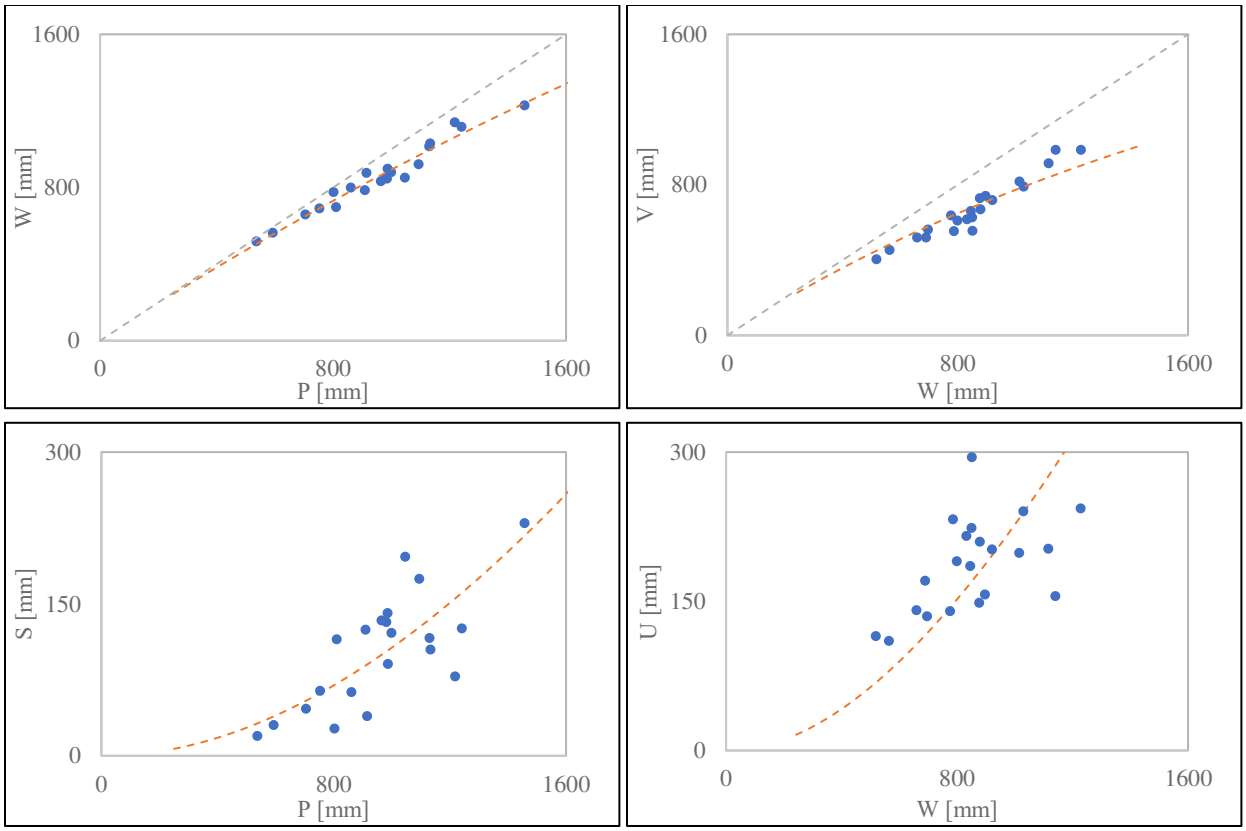

*Figure D3 - 57 : L'Vovich water balance relationships extracted for **Fiora, Italy**; Wetting W= f(P), Vaporization V=f(W), Quick flow S=f(P) and slow flow U = f(W); Points represent data (equations 14,15,16 and 17), and the dashed lines are Ponce and Shetty mathematical formulations (equations 18b and 19b)*

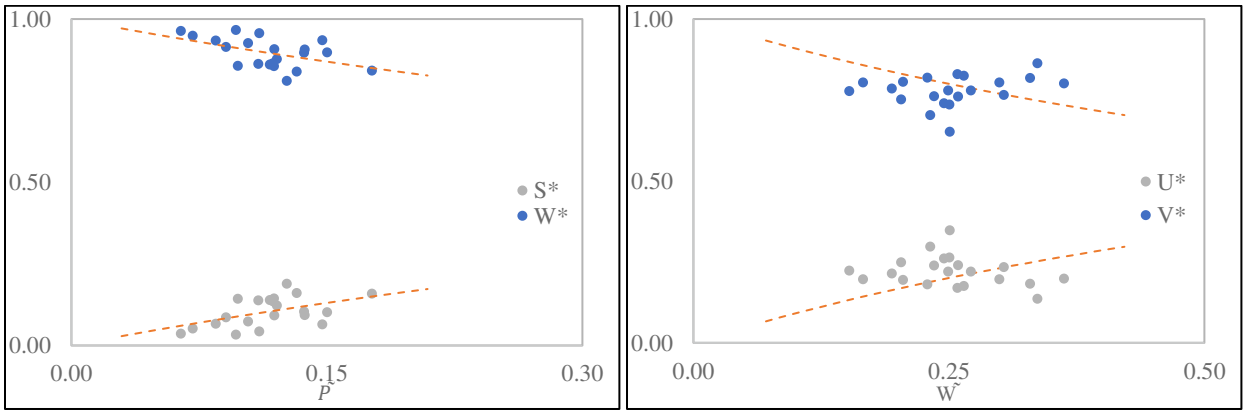

Figure D3 - 58 : Interannual variability of nondimensional annual estimates of (left) W and S* and (right) U* and V* versus annual climatic drivers $\tilde{P}$ and $\tilde{W}$ for **Fiora, Italy**; Points represent data (equations 22 and 23), and the dashed lines are theoretical (equations 25 and 26).*

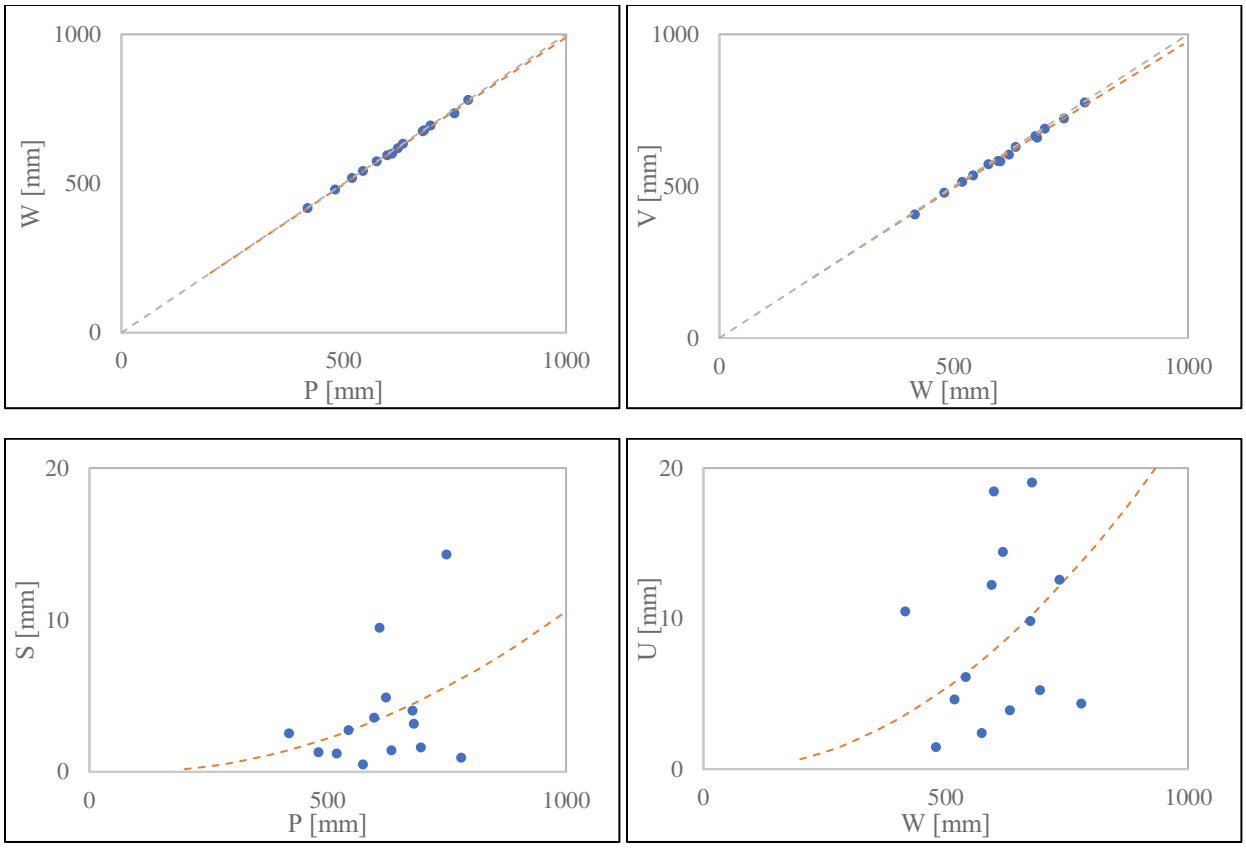

*Figure D3 - 59 : L'Vovich water balance relationships extracted for **Alcantara, Italy**; Wetting W= f(P), Vaporization V=f(W), Quick flow S=f(P) and slow flow U = f(W); Points represent data (equations 14,15,16 and 17), and the dashed lines are Ponce and Shetty mathematical formulations (equations 18b and 19b)*

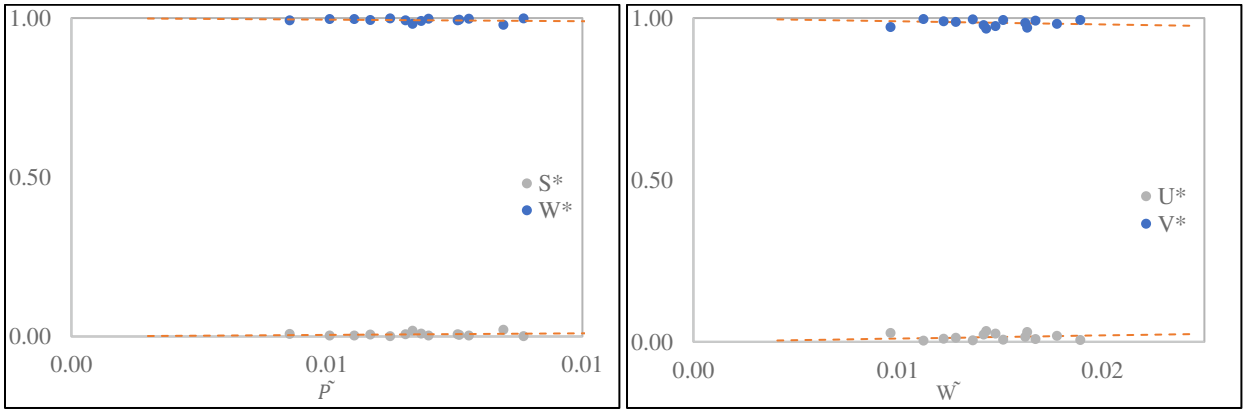

Figure D3 - 60 : Interannual variability of nondimensional annual estimates of (left) W and S* and (right) U* and V* versus annual climatic drivers $\tilde{P}$ and $\tilde{W}$ for **Alcantara, Italy**; Points represent data (equations 22 and 23), and the dashed lines are theoretical (equations 25 and 26).*

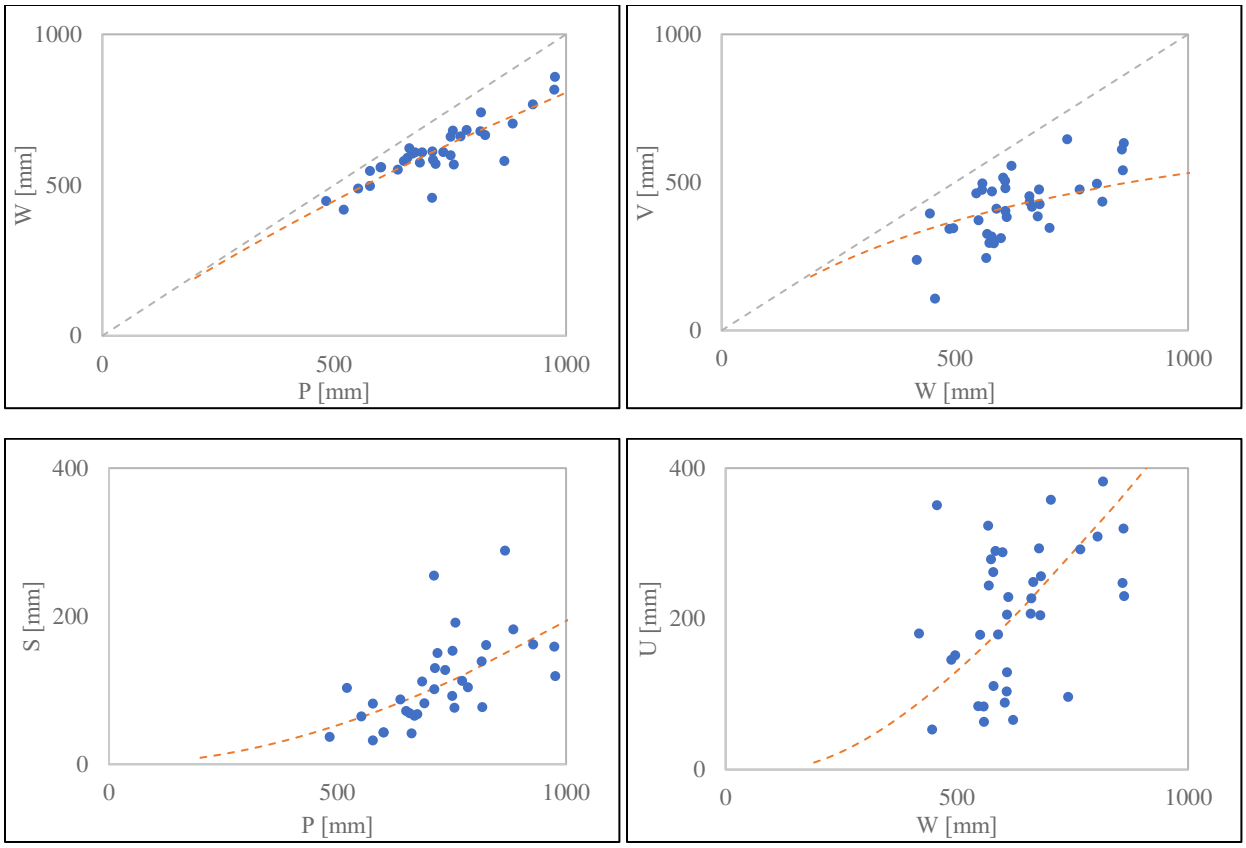

*Figure D3 - 61 : L'Vovich water balance relationships extracted for **Fluminimaggiore, Italy**; Wetting W= f(P), Vaporization V=f(W), Quick flow S=f(P) and slow flow U = f(W); Points represent data (equations 14,15,16 and 17), and the dashed lines are Ponce and Shetty mathematical formulations (equations 18b and 19b)*

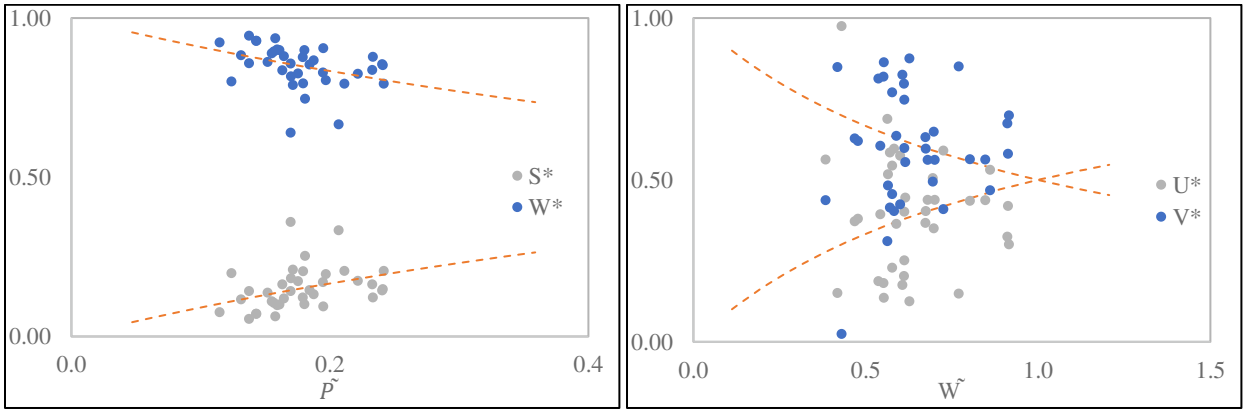

Figure D3 - 62 : Interannual variability of nondimensional annual estimates of (left) W and S* and (right) U* and V* versus annual climatic drivers $\tilde{P}$ and $\tilde{W}$ for **Fluminimaggiore, Italy**; Points represent data (equations 22 and 23), and the dashed lines are theoretical (equations 25 and 26).*

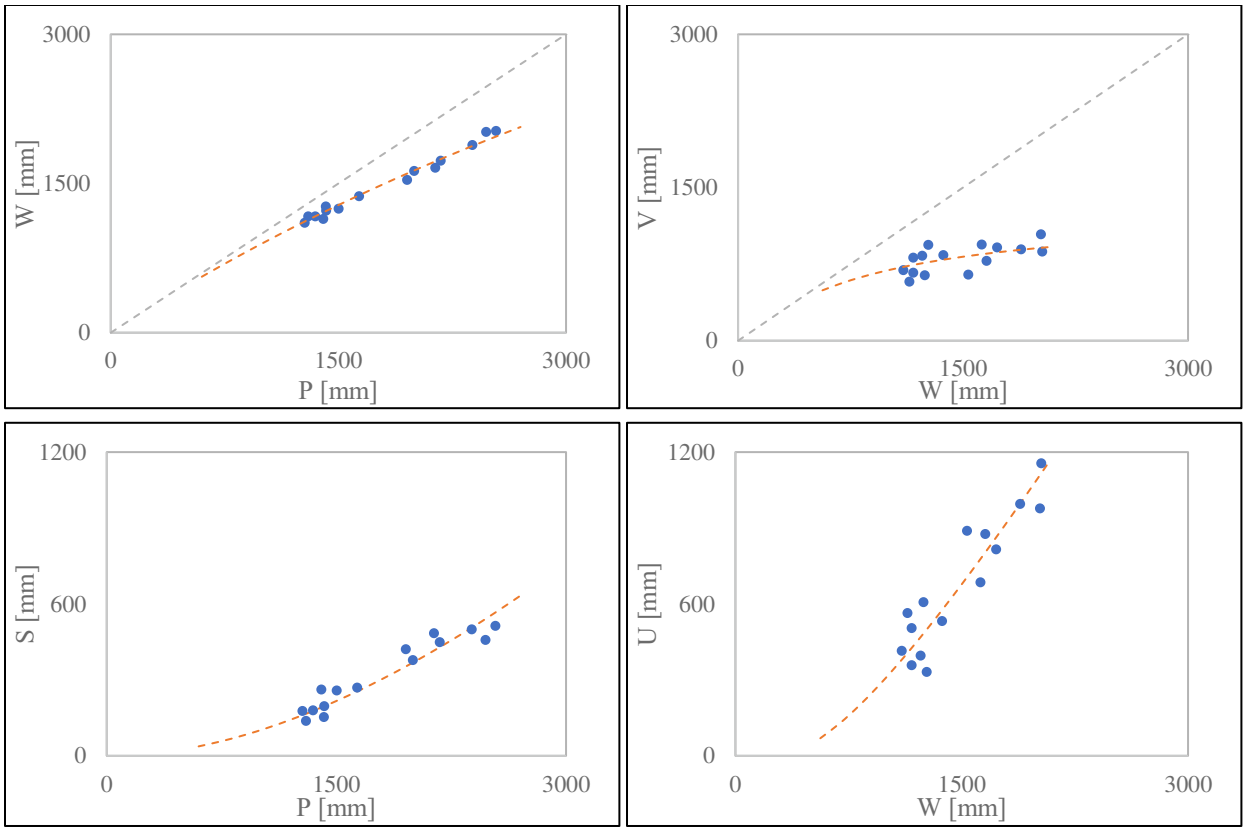

Figure D3 - 63 : L'Vovich water balance relationships extracted for ***Serchio, Italy****; Wetting W= f(P), Vaporization V=f(W), Quick flow S=f(P) and slow flow U = f(W); Points represent data (equations 14,15,16 and 17), and the dashed lines are Ponce and Shetty mathematical formulations (equations 18b and 19b)*

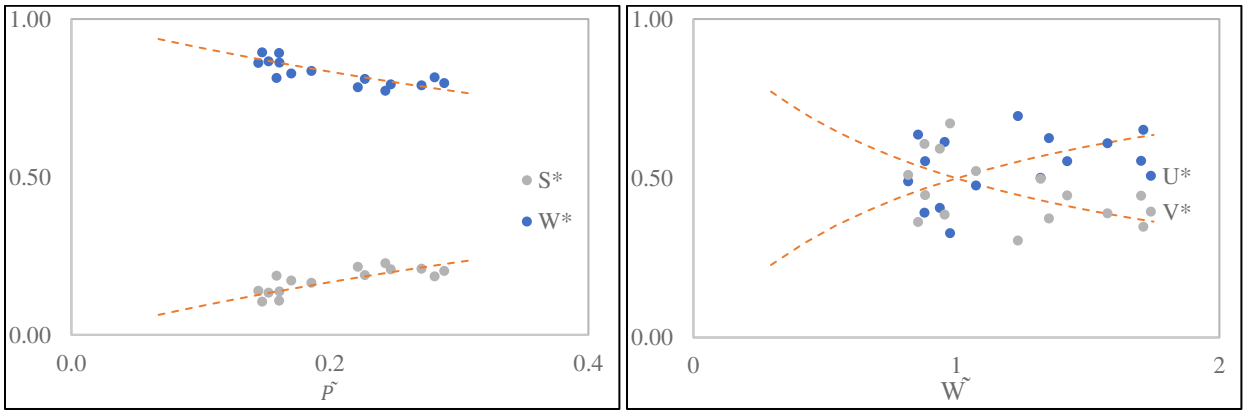

Figure D3 - 64 : Interannual variability of nondimensional annual estimates of (left) W and S* and (right) U* and V* versus annual climatic drivers* $\tilde{P}$ *and* $\tilde{W}$ *for* ***Serchio, Italy****; Points represent data (equations 22 and 23), and the dashed lines are theoretical (equations 25 and 26).*

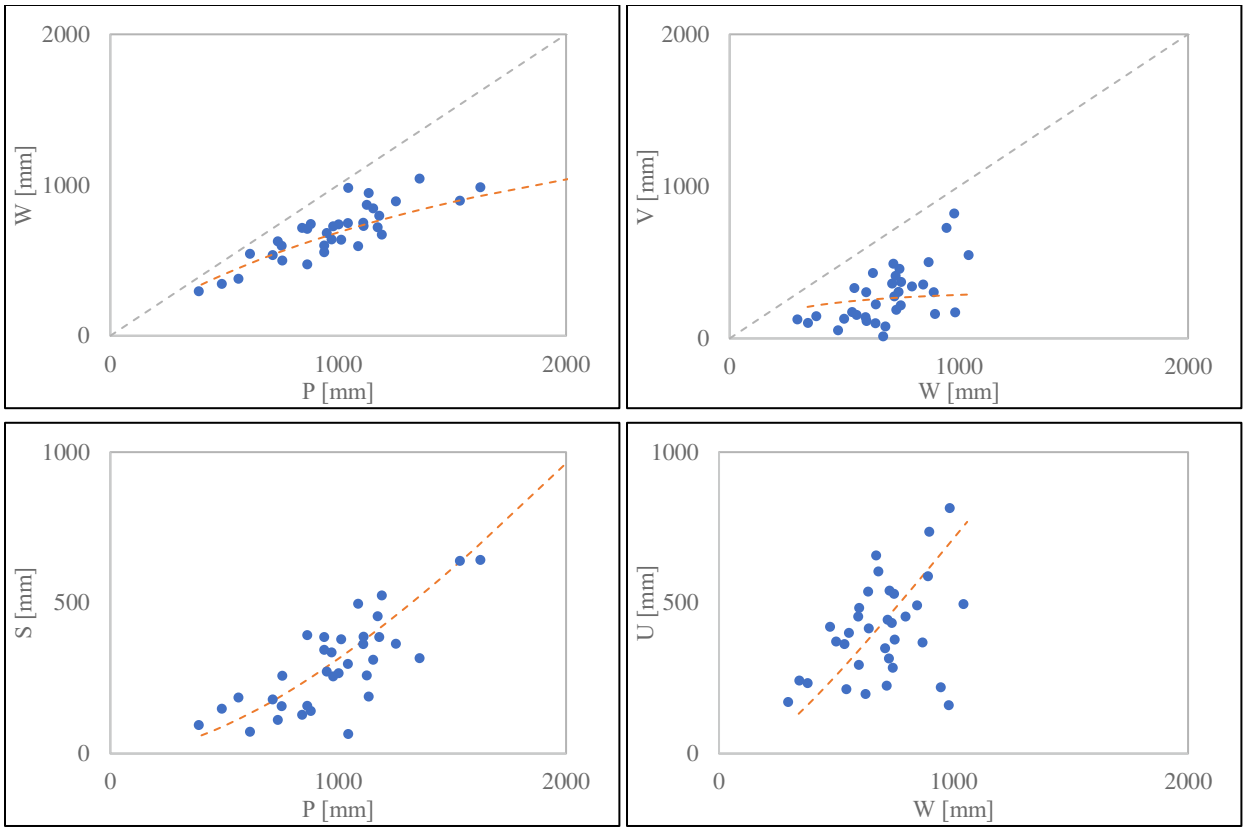

*Figure D3 - 65 : L'Vovich water balance relationships extracted for **Argentina, Italy**; Wetting W= f(P), Vaporization V=f(W), Quick flow S=f(P) and slow flow U = f(W); Points represent data (equations 14,15,16 and 17), and the dashed lines are Ponce and Shetty mathematical formulations (equations 18b and 19b)*

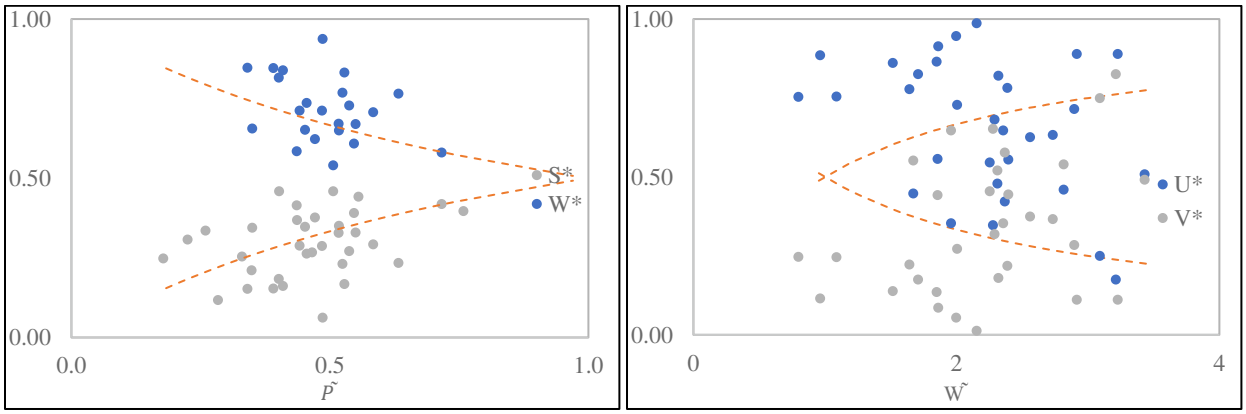

Figure D3 - 66 : Interannual variability of nondimensional annual estimates of (left) W and S* and (right) U* and V* versus annual climatic drivers $\tilde{P}$ and $\tilde{W}$ for **Argentina, Italy**; Points represent data (equations 22 and 23), and the dashed lines are theoretical (equations 25 and 26).*

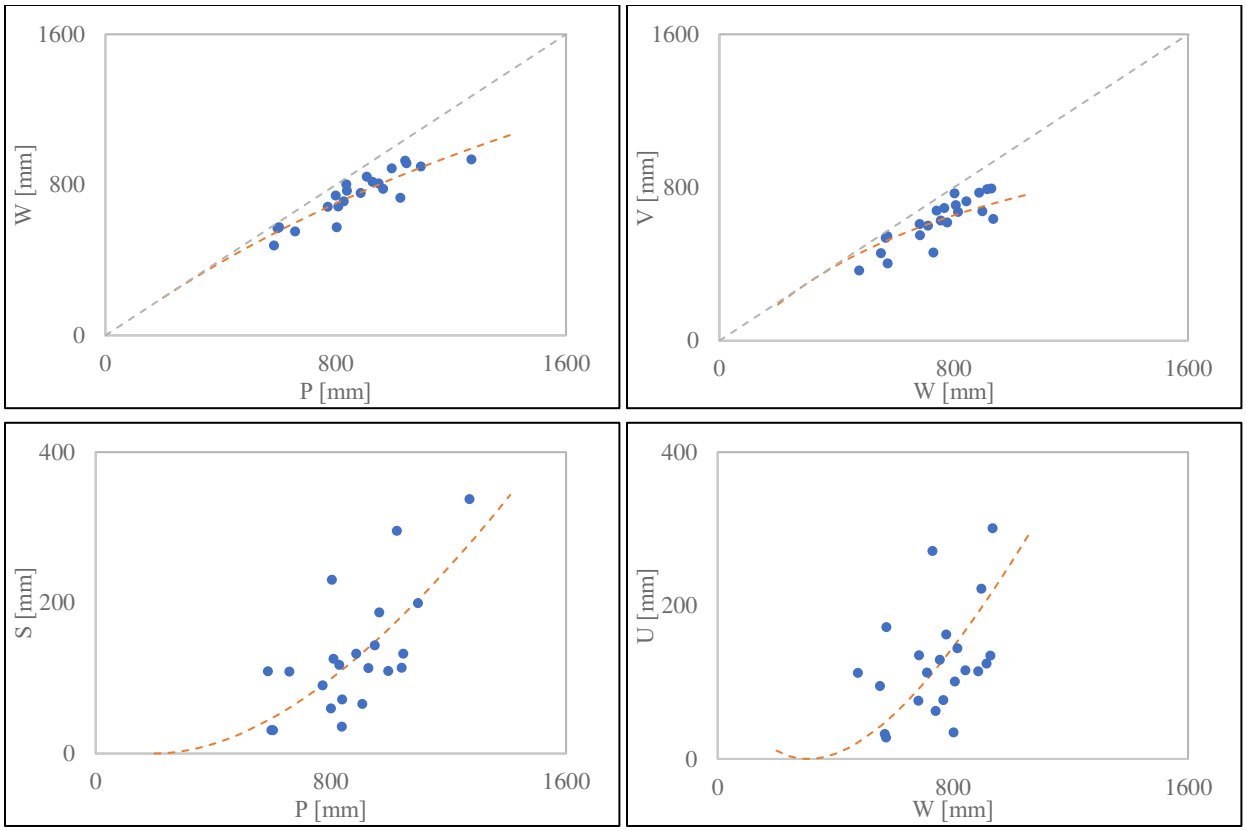

*Figure D3 - 67 : L'Vovich water balance relationships extracted for **Cecina, Italy**; Wetting W= f(P), Vaporization V=f(W), Quick flow S=f(P) and slow flow U = f(W); Points represent data (equations 14,15,16 and 17), and the dashed lines are Ponce and Shetty mathematical formulations (equations 18b and 19b)*

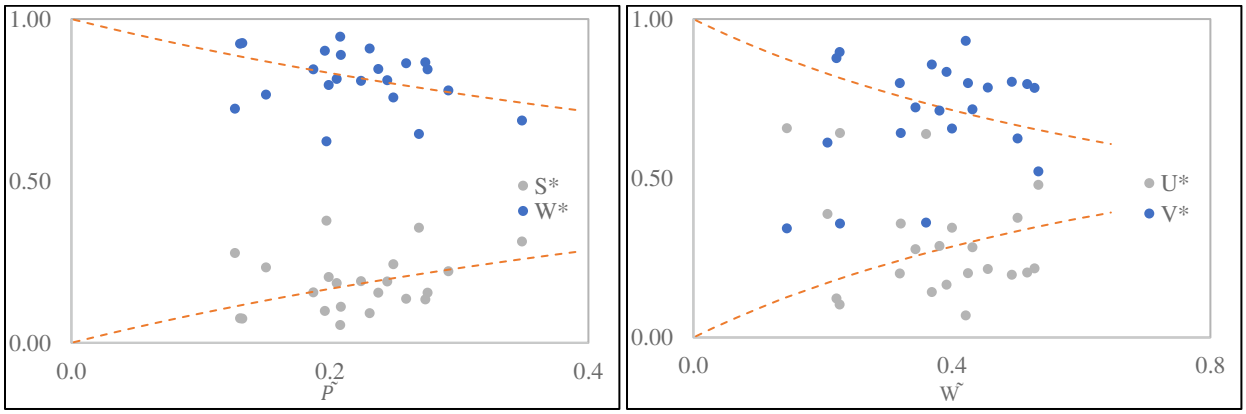

Figure D3 - 68 : Interannual variability of nondimensional annual estimates of (left) W and S* and (right) U* and V* versus annual climatic drivers $\tilde{P}$ and $\widetilde{W}$ for **Cecina, Italy**; Points represent data (equations 22 and 23), and the dashed lines are theoretical (equations 25 and 26).*

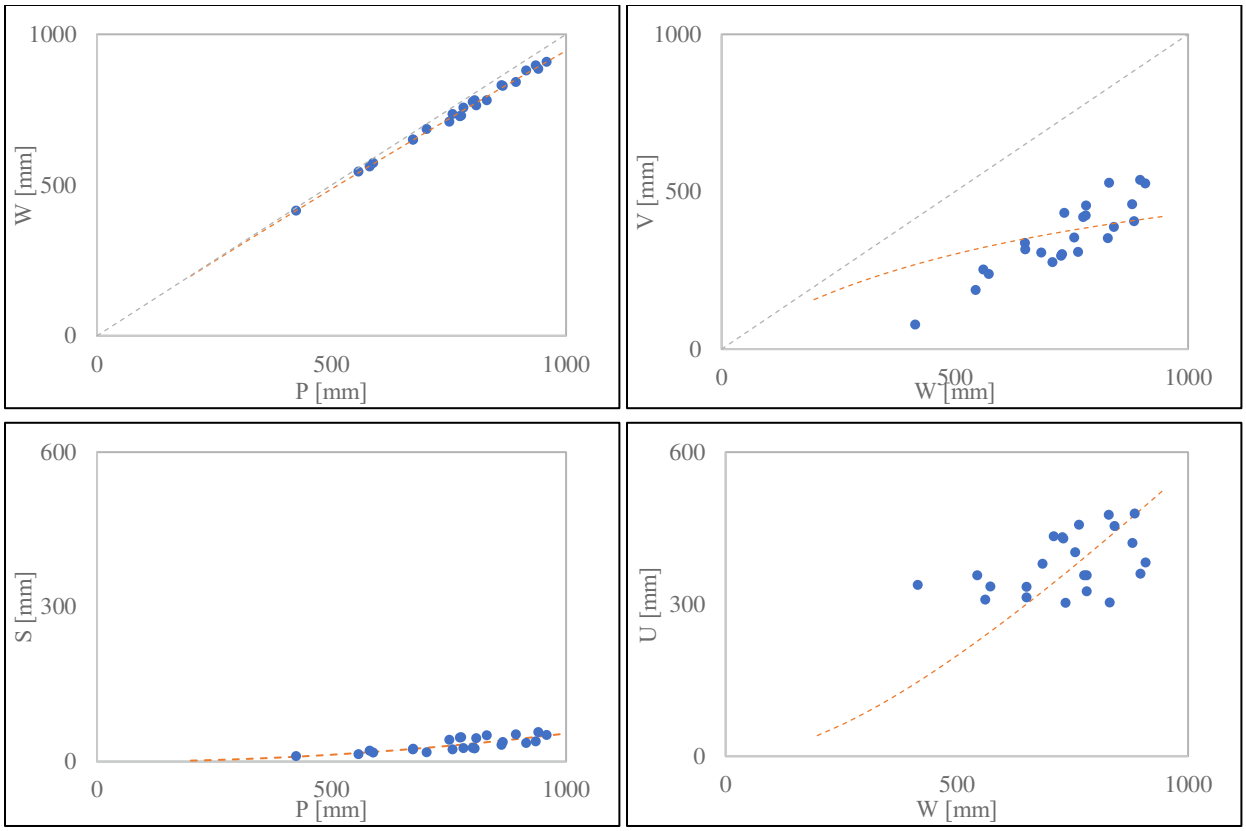

*Figure D3 - 69 : L'Vovich water balance relationships extracted for **Pescara, Italy**; Wetting W= f(P), Vaporization V=f(W), Quick flow S=f(P) and slow flow U = f(W); Points represent data (equations 14,15,16 and 17), and the dashed lines are Ponce and Shetty mathematical formulations (equations 18b and 19b)*

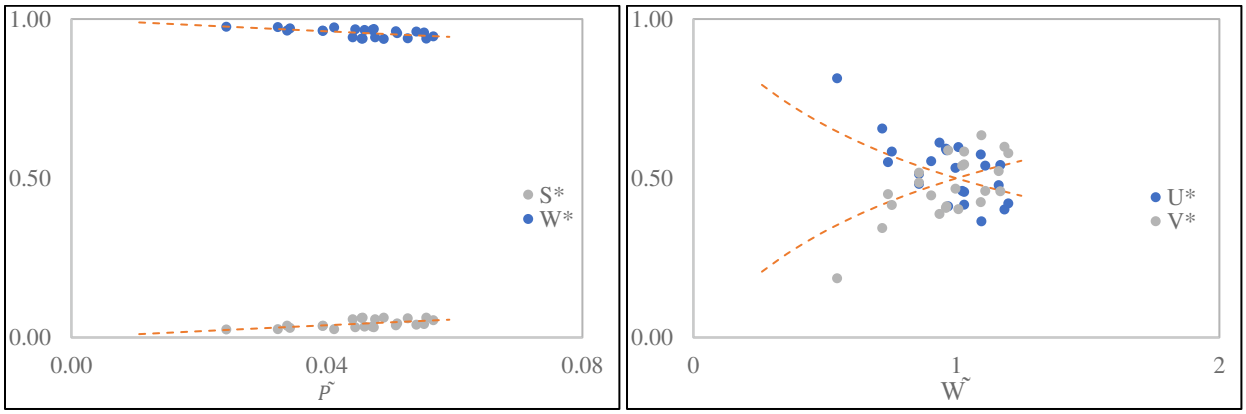

Figure D3 - 70 : Interannual variability of nondimensional annual estimates of (left) W and S* and (right) U* and V* versus annual climatic drivers $\tilde{P}$ and $\tilde{W}$ for **Pescara, Italy**; Points represent data (equations 22 and 23), and the dashed lines are theoretical (equations 25 and 26).*

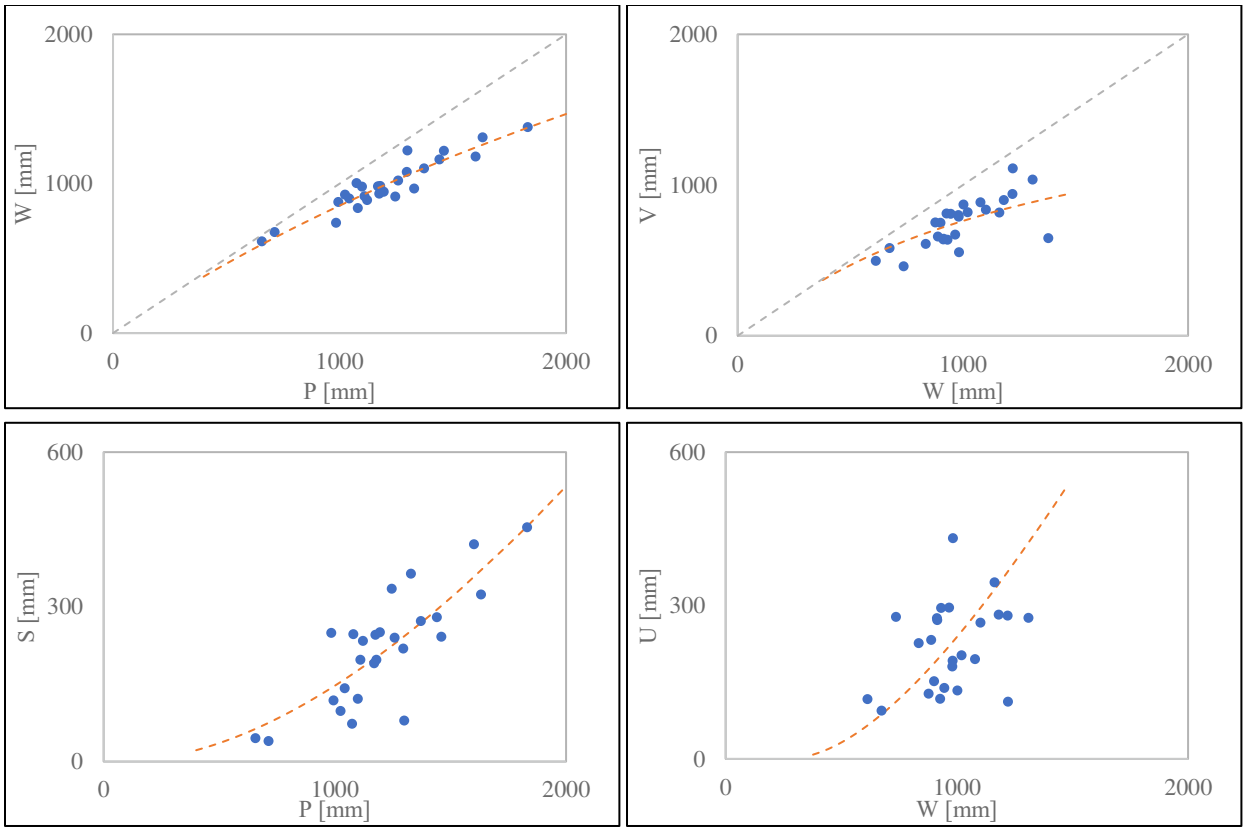

*Figure D3 - 71 : L'Vovich water balance relationships extracted for **Alento, Italy**; Wetting W= f(P), Vaporization V=f(W), Quick flow S=f(P) and slow flow U = f(W); Points represent data (equations 14,15,16 and 17), and the dashed lines are Ponce and Shetty mathematical formulations (equations 18b and 19b)*

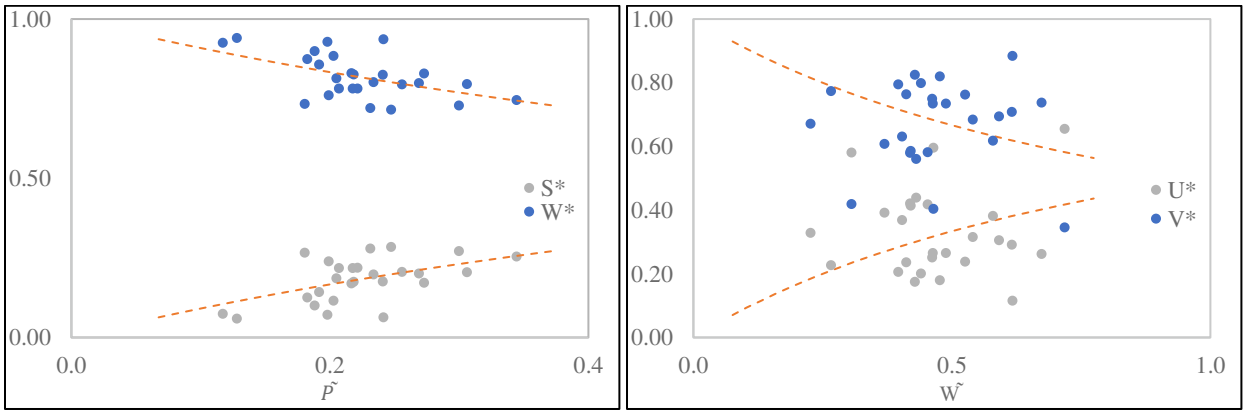

Figure D3 - 72 : Interannual variability of nondimensional annual estimates of (left) W and S* and (right) U* and V* versus annual climatic drivers $\tilde{P}$ and $\widetilde{W}$ for **Alento, Italy**; Points represent data (equations 22 and 23), and the dashed lines are theoretical (equations 25 and 26).*

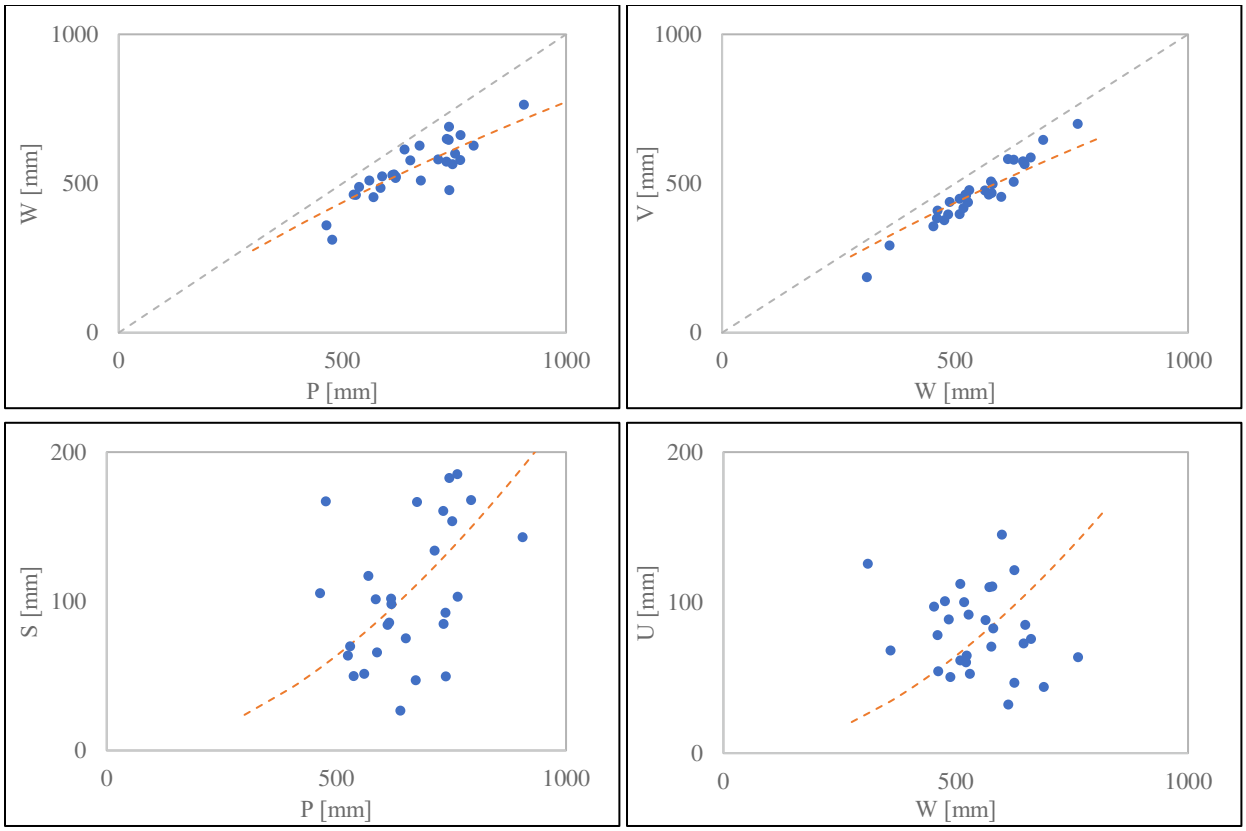

*Figure D3 - 73 : L'Vovich water balance relationships extracted for **San Leonardo, Italy**; Wetting W= f(P), Vaporization V=f(W), Quick flow S=f(P) and slow flow U = f(W); Points represent data (equations 14,15,16 and 17), and the dashed lines are Ponce and Shetty mathematical formulations (equations 18b and 19b)*

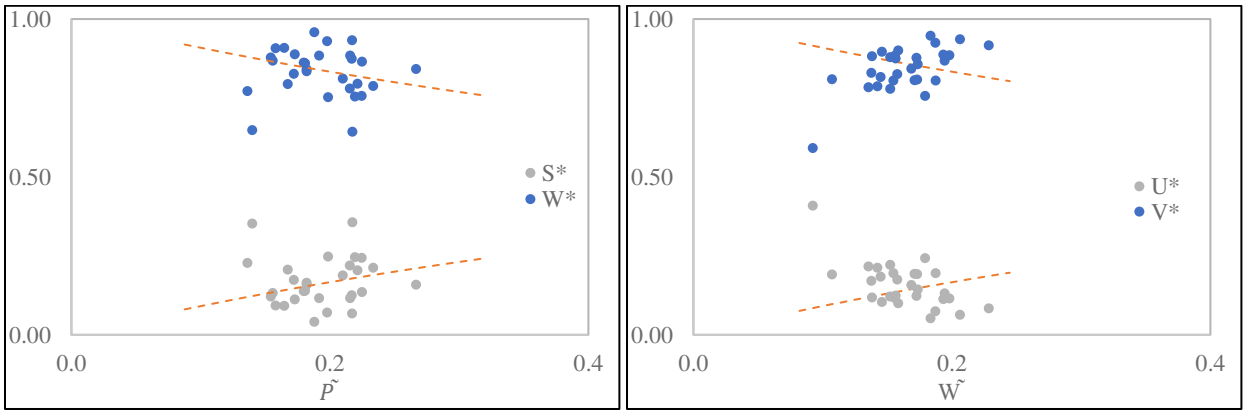

Figure D3 - 74 : Interannual variability of nondimensional annual estimates of (left) W and S* and (right) U* and V* versus annual climatic drivers $\tilde{P}$ and $\tilde{W}$ for **San Leonardo, Italy**; Points represent data (equations 22 and 23), and the dashed lines are theoretical (equations 25 and 26).*

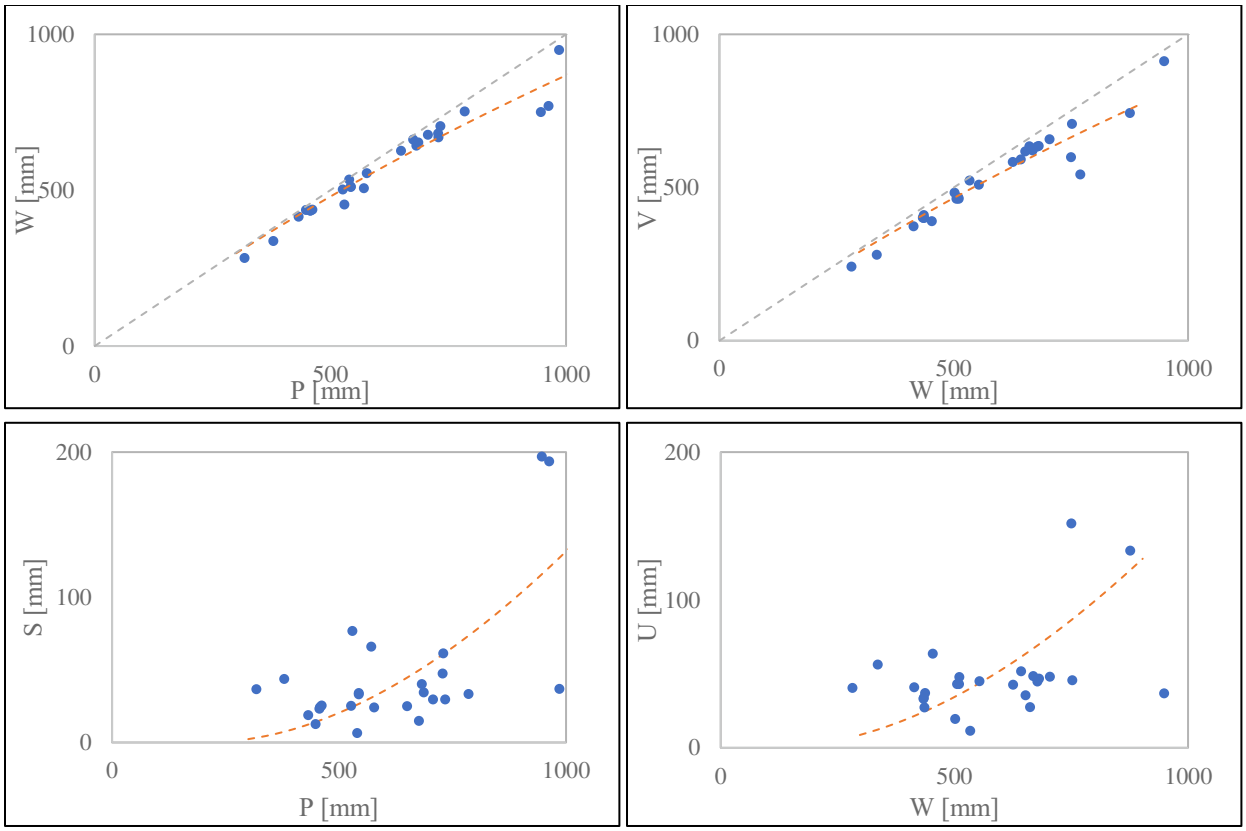

*Figure D3 - 75 : L'Vovich water balance relationships extracted for **Fiume Imera Meridionale, Italy**; Wetting W= f(P), Vaporization V=f(W), Quick flow S=f(P) and slow flow U = f(W); Points represent data (equations 14,15,16 and 17), and the dashed lines are Ponce and Shetty mathematical formulations (equations 18b and 19b)*

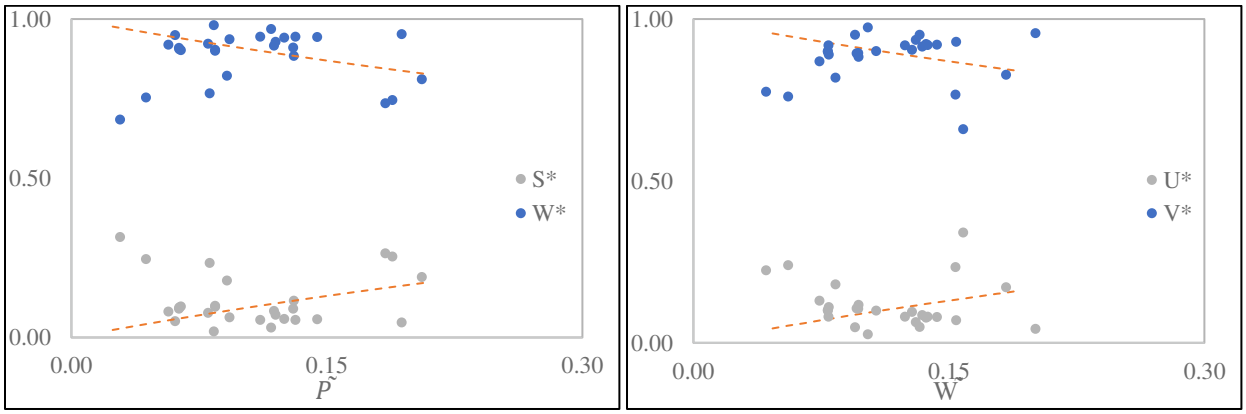

Figure D3 - 76 : Interannual variability of nondimensional annual estimates of (left) W and S* and (right) U* and V* versus annual climatic drivers $\tilde{P}$ and $\tilde{W}$ for **Fiume Imera Meridionale, Italy**; Points represent data (equations 22 and 23), and the dashed lines are theoretical (equations 25 and 26).*

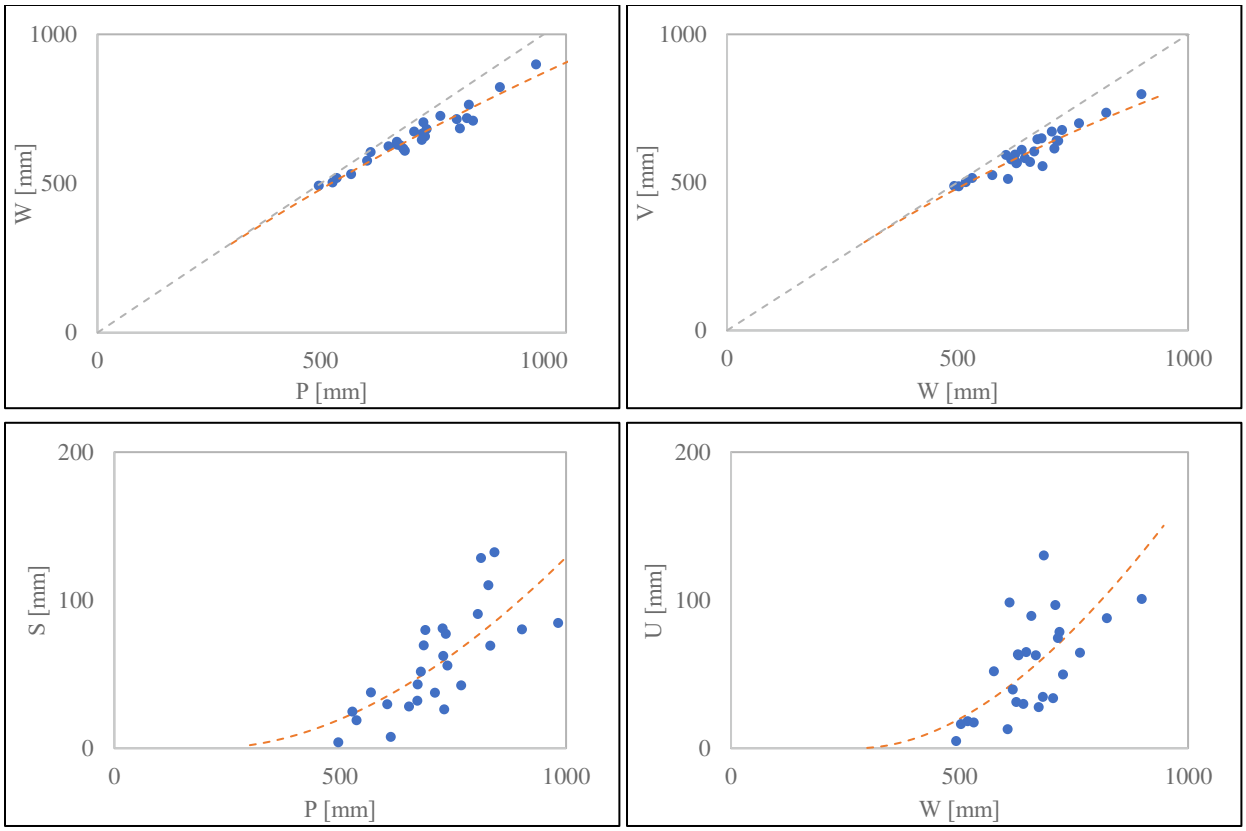

*Figure D3 - 77 : L'Vovich water balance relationships extracted for **Cervaro, Italy**; Wetting W= f(P), Vaporization V=f(W), Quick flow S=f(P) and slow flow U = f(W); Points represent data (equations 14,15,16 and 17), and the dashed lines are Ponce and Shetty mathematical formulations (equations 18b and 19b)*

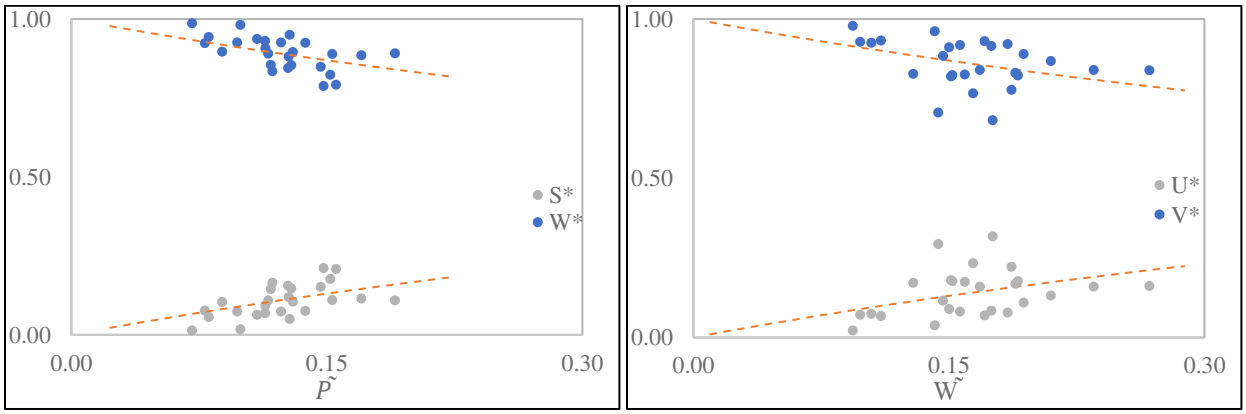

Figure D3 - 78 : Interannual variability of nondimensional annual estimates of (left) W and S* and (right) U* and V* versus annual climatic drivers $\tilde{P}$ and $\tilde{W}$ for **Cervaro, Italy**; Points represent data (equations 22 and 23), and the dashed lines are theoretical (equations 25 and 26).*

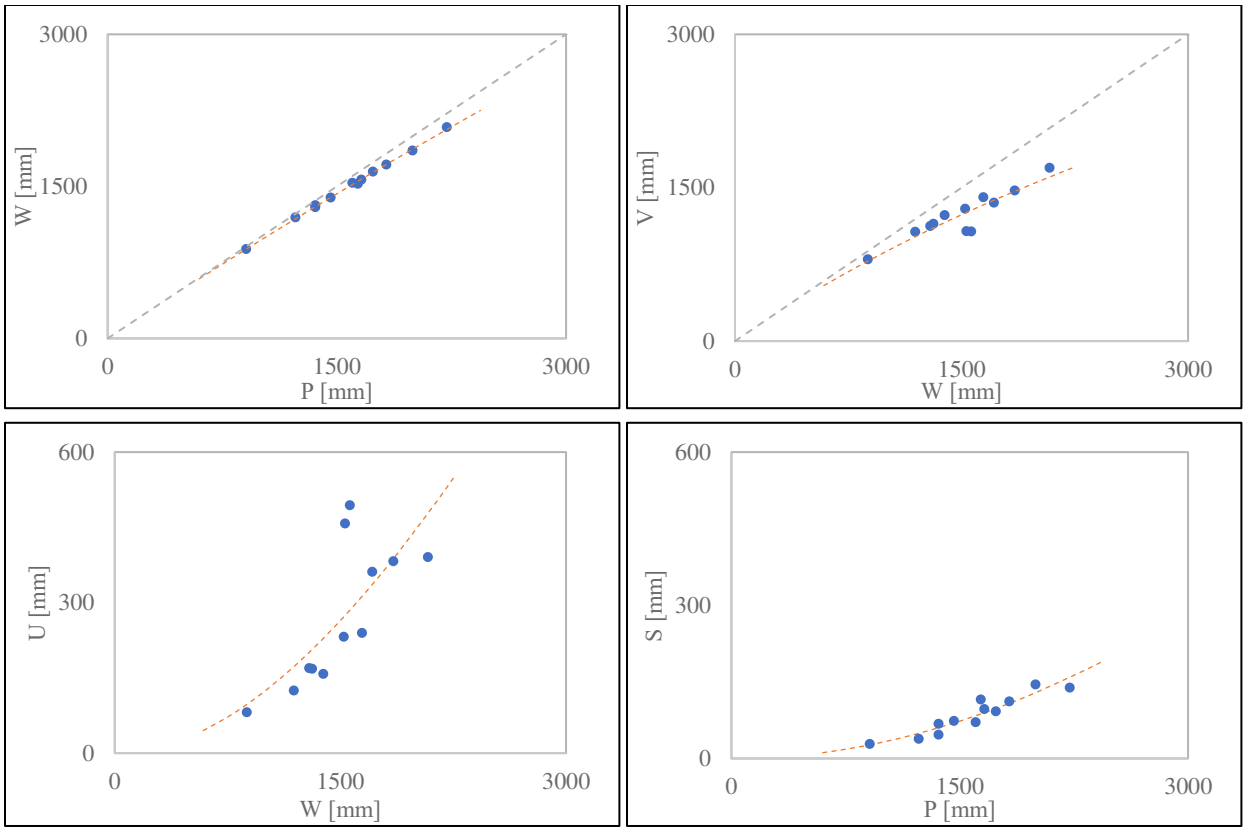

*Figure D3 - 79 : L'Vovich water balance relationships extracted for **Nahr el Jaouz, Lebanon**; Wetting W= f(P), Vaporization V=f(W), Quick flow S=f(P) and slow flow U = f(W); Points represent data (equations 14,15,16 and 17), and the dashed lines are Ponce and Shetty mathematical formulations (equations 18b and 19b)*

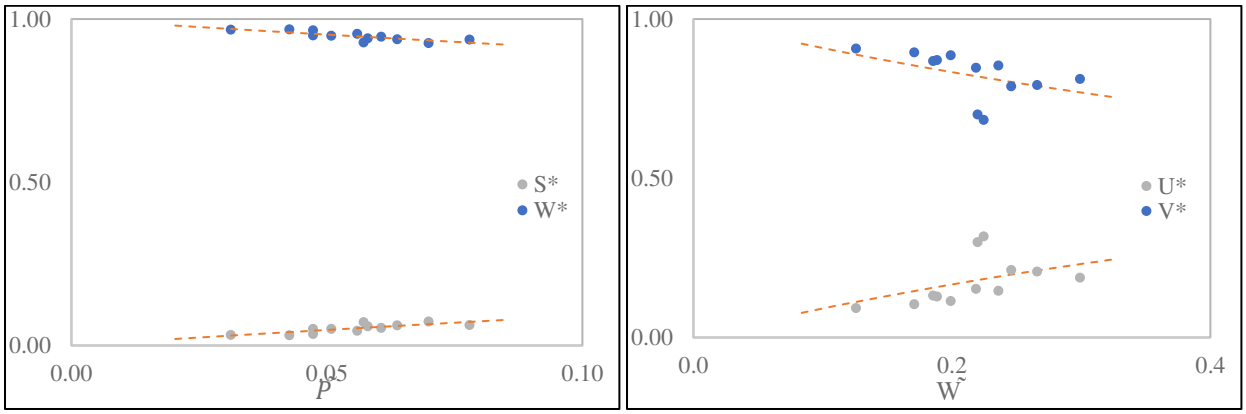

Figure D3 - 80 : Interannual variability of nondimensional annual estimates of (left) W and S* and (right) U* and V* versus annual climatic drivers $\tilde{P}$ and $\tilde{W}$ for **Nahr el Jaouz, Lebanon**; Points represent data (equations 22 and 23), and the dashed lines are theoretical (equations 25 and 26).*

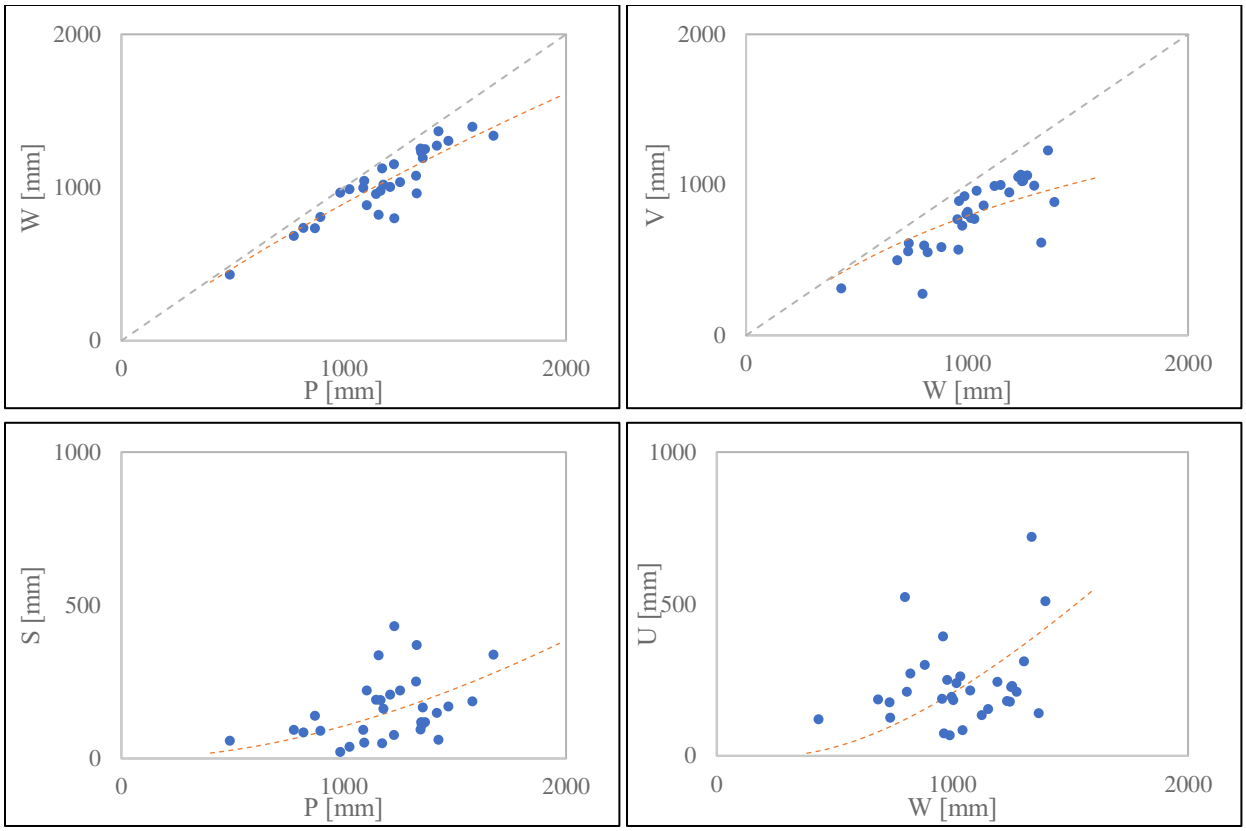

*Figure D3 - 81 : L'Vovich water balance relationships extracted for **Nahr Beyrouth, Lebanon**; Wetting W= f(P), Vaporization V=f(W), Quick flow S=f(P) and slow flow U = f(W); Points represent data (equations 14,15,16 and 17), and the dashed lines are Ponce and Shetty mathematical formulations (equations 18b and 19b)*

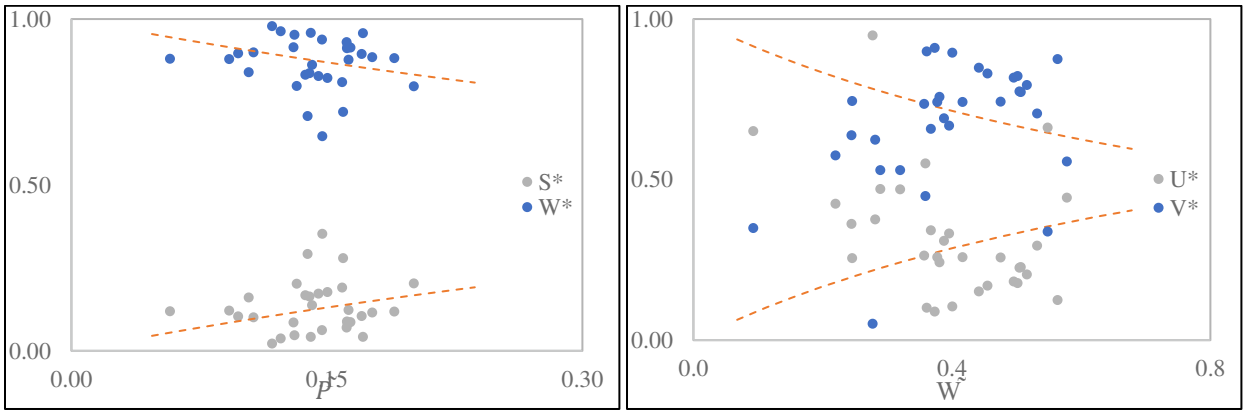

Figure D3 - 82 : Interannual variability of nondimensional annual estimates of (left) W and S* and (right) U* and V* versus annual climatic drivers $\tilde{P}$ and $\tilde{W}$ for **Nahr Beyrouth, Lebanon**; Points represent data (equations 22 and 23), and the dashed lines are theoretical (equations 25 and 26).*

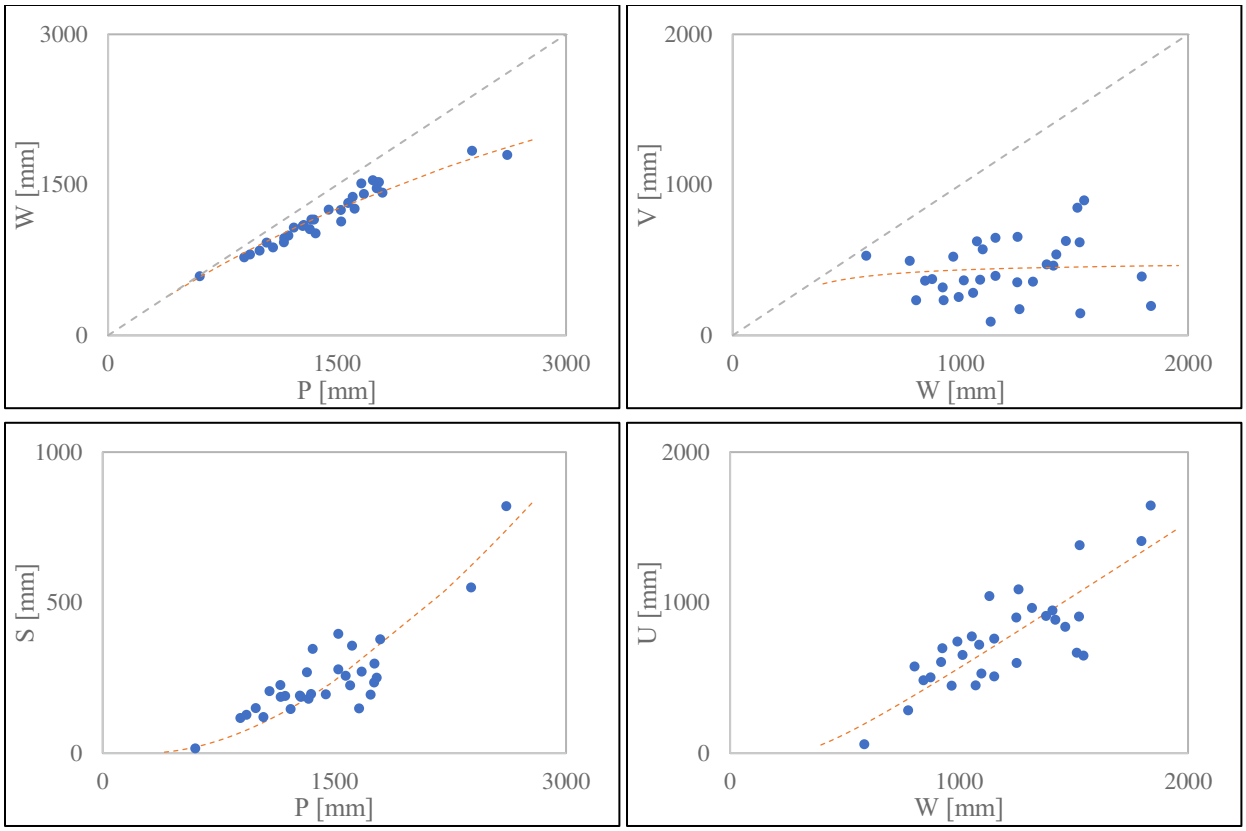

*Figure D3 - 83 : L'Vovich water balance relationships extracted for **Nahr El Kalb, Lebanon**; Wetting W= f(P), Vaporization V=f(W), Quick flow S=f(P) and slow flow U = f(W); Points represent data (equations 14,15,16 and 17), and the dashed lines are Ponce and Shetty mathematical formulations (equations 18b and 19b)*

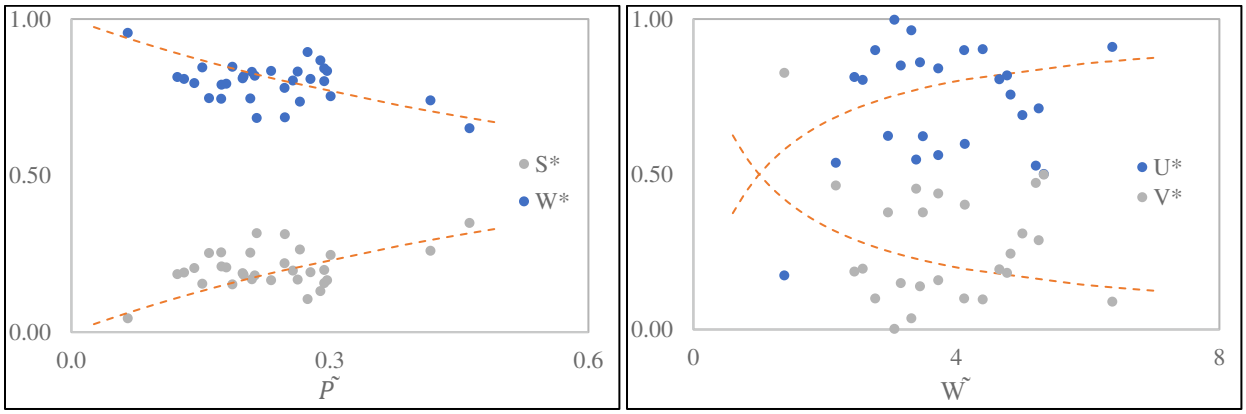

Figure D3 - 84 : Interannual variability of nondimensional annual estimates of (left) W and S* and (right) U* and V* versus annual climatic drivers $\tilde{P}$ and $\tilde{W}$ for **Nahr El Kalb, Lebanon**; Points represent data (equations 22 and 23), and the dashed lines are theoretical (equations 25 and 26).*

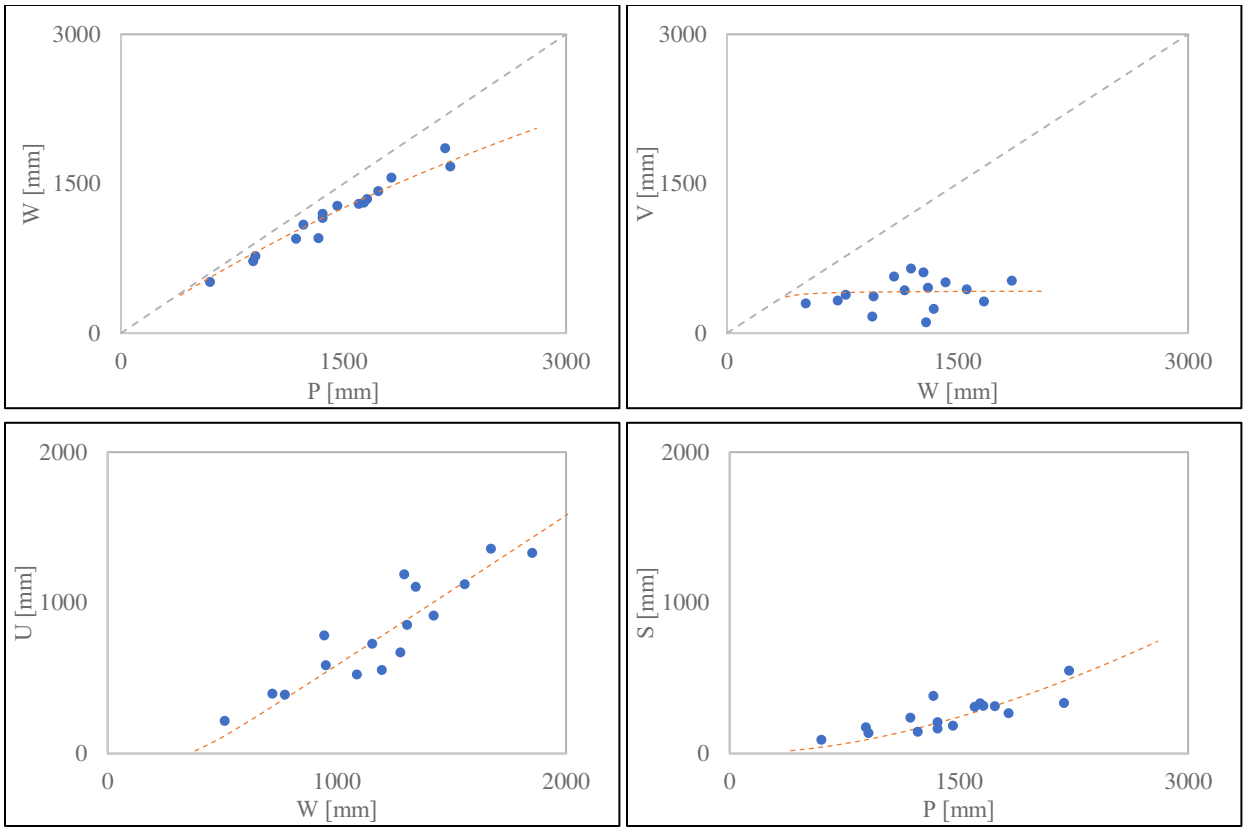

*Figure D3 - 85 : L'Vovich water balance relationships extracted for **Nahr Ibrahim, Lebanon**; Wetting W= f(P), Vaporization V=f(W), Quick flow S=f(P) and slow flow U = f(W); Points represent data (equations 14,15,16 and 17), and the dashed lines are Ponce and Shetty mathematical formulations (equations 18b and 19b)*

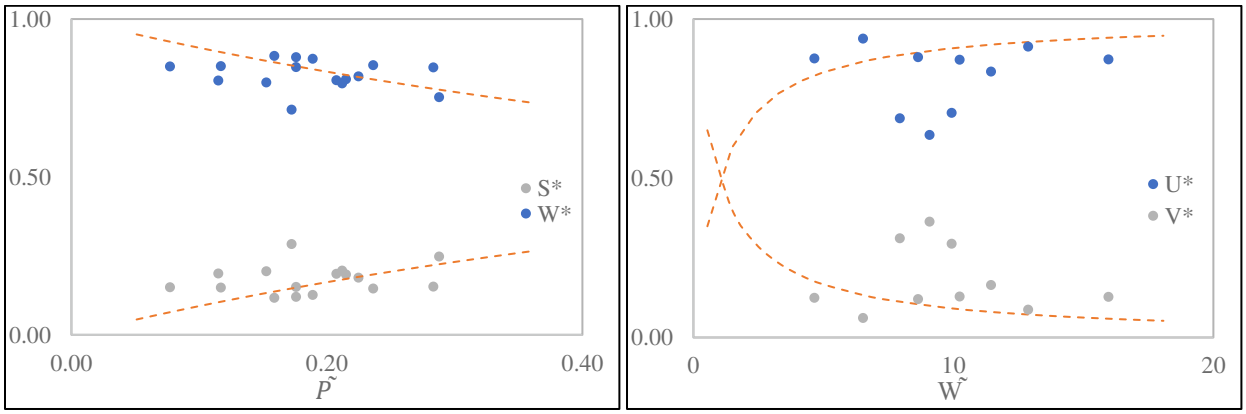

Figure D3 - 86 : Interannual variability of nondimensional annual estimates of (left) W and S* and (right) U* and V* versus annual climatic drivers $\tilde{P}$ and $\tilde{W}$ for **Nahr Ibrahim, Lebanon**; Points represent data (equations 22 and 23), and the dashed lines are theoretical (equations 25 and 26).*

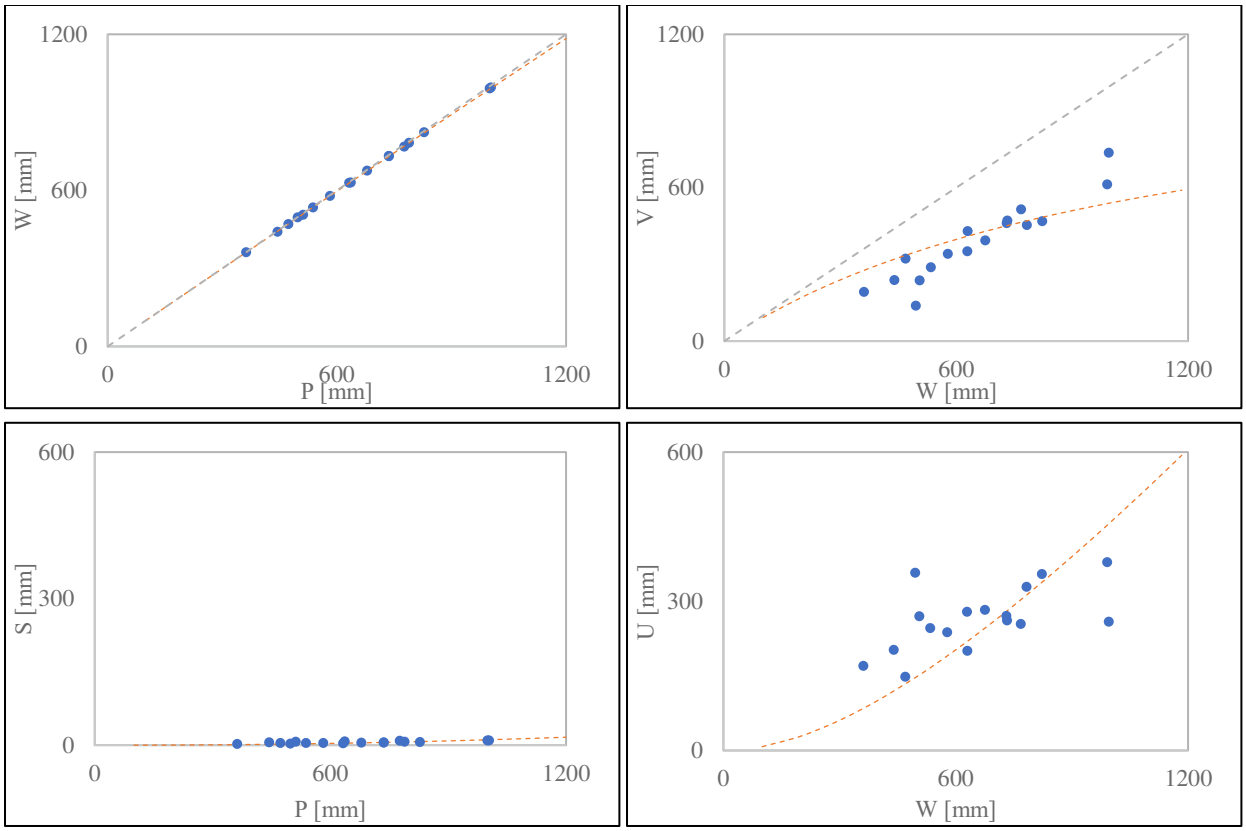

*Figure D3 - 87 : L'Vovich water balance relationships extracted for **Nahr Assi, Lebanon**; Wetting W= f(P), Vaporization V=f(W), Quick flow S=f(P) and slow flow U = f(W); Points represent data (equations 14,15,16 and 17), and the dashed lines are Ponce and Shetty mathematical formulations (equations 18b and 19b)*

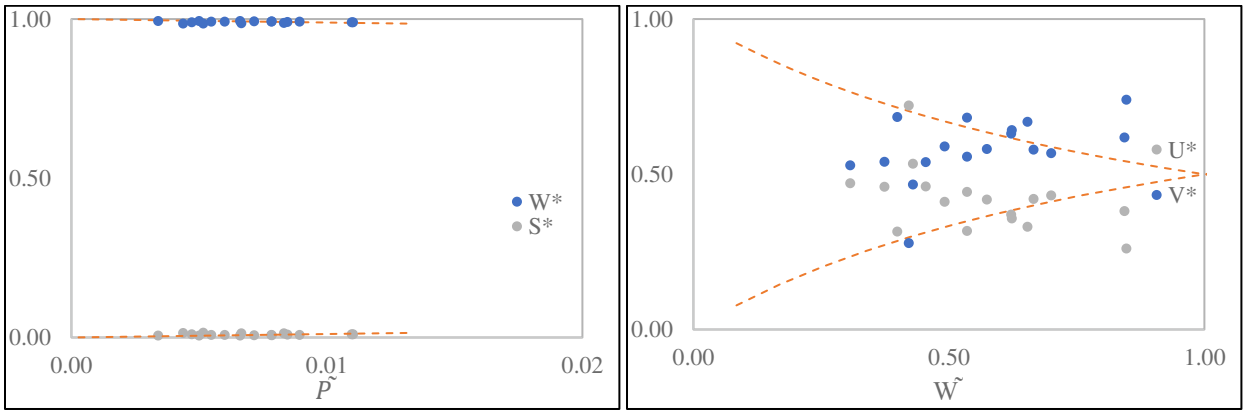

Figure D3 - 88 : Interannual variability of nondimensional annual estimates of (left) W and S* and (right) U* and V* versus annual climatic drivers $\tilde{P}$ and $\tilde{W}$ for **Nahr Assi, Lebanon**; Points represent data (equations 22 and 23), and the dashed lines are theoretical (equations 25 and 26).*

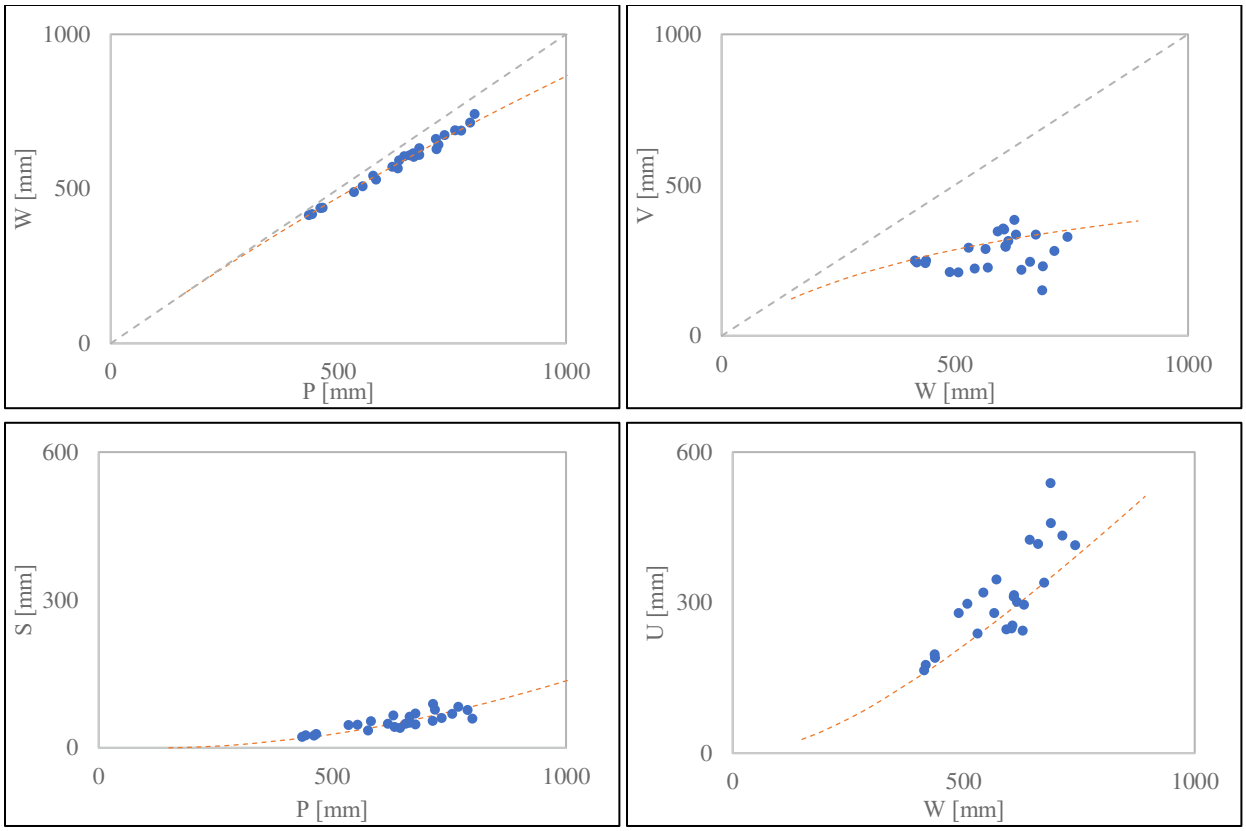

*Figure D3 - 89 : L'Vovich water balance relationships extracted for **Nahr Litani, Lebanon**; Wetting W= f(P), Vaporization V=f(W), Quick flow S=f(P) and slow flow U = f(W); Points represent data (equations 14,15,16 and 17), and the dashed lines are Ponce and Shetty mathematical formulations (equations 18b and 19b)*

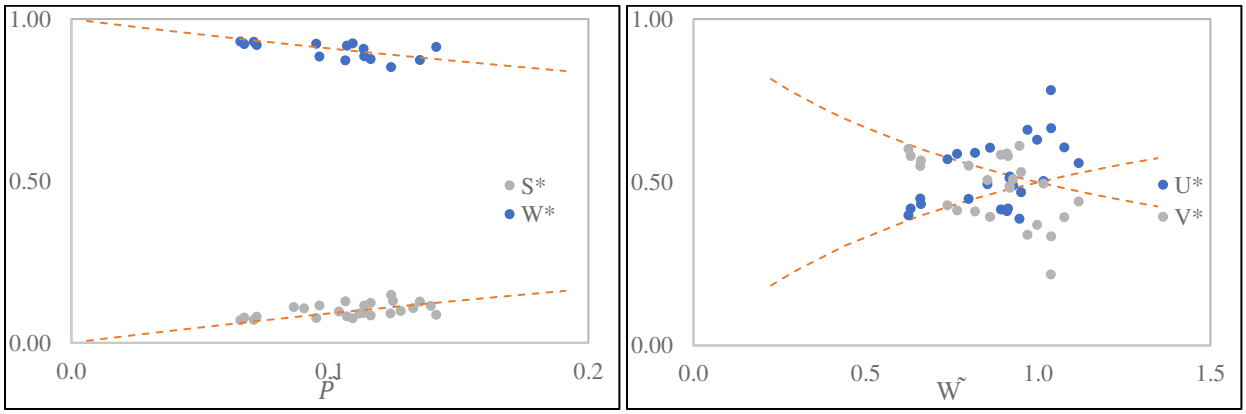

Figure D3 - 90 : Interannual variability of nondimensional annual estimates of (left) W and S* and (right) U* and V* versus annual climatic drivers $\tilde{P}$ and $\tilde{W}$ for **Nahr Litani, Lebanon**; Points represent data (equations 22 and 23), and the dashed lines are theoretical (equations 25 and 26).*

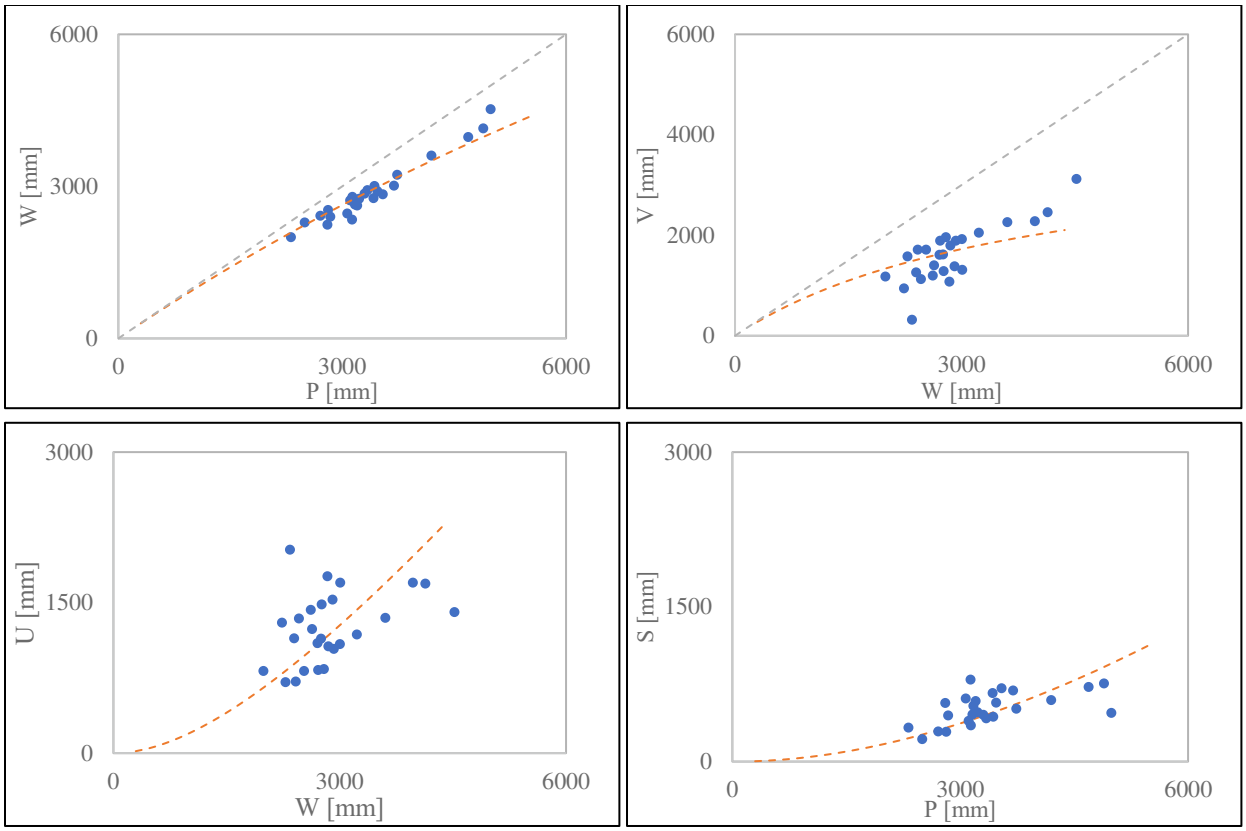

*Figure D3 - 91 : L'Vovich water balance relationships extracted for **Moraca, Montenegro**; Wetting W= f(P), Vaporization V=f(W), Quick flow S=f(P) and slow flow U = f(W); Points represent data (equations 14,15,16 and 17), and the dashed lines are Ponce and Shetty mathematical formulations (equations 18b and 19b)*

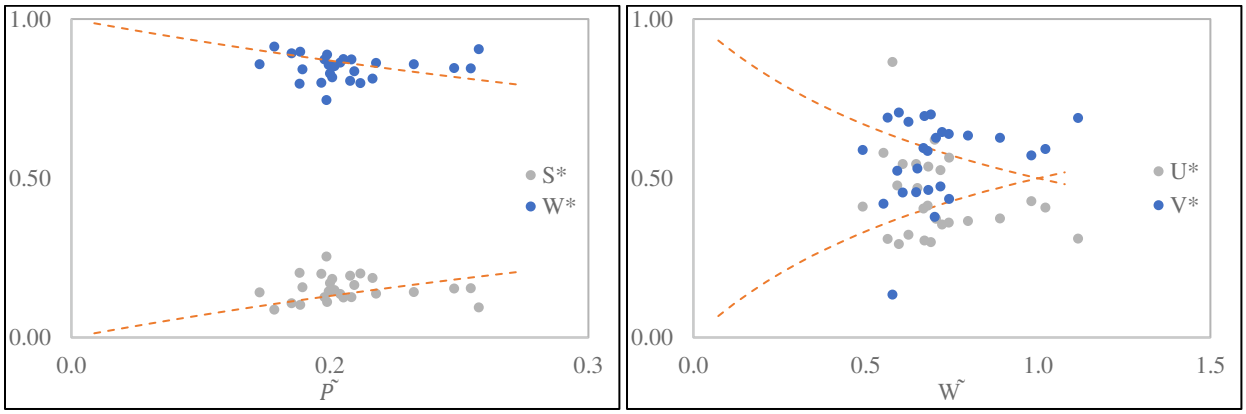

Figure D3 - 92 : Interannual variability of nondimensional annual estimates of (left) W and S* and (right) U* and V* versus annual climatic drivers $\tilde{P}$ and $\tilde{W}$ for **Moraca, Montenegro**; Points represent data (equations 22 and 23), and the dashed lines are theoretical (equations 25 and 26).*

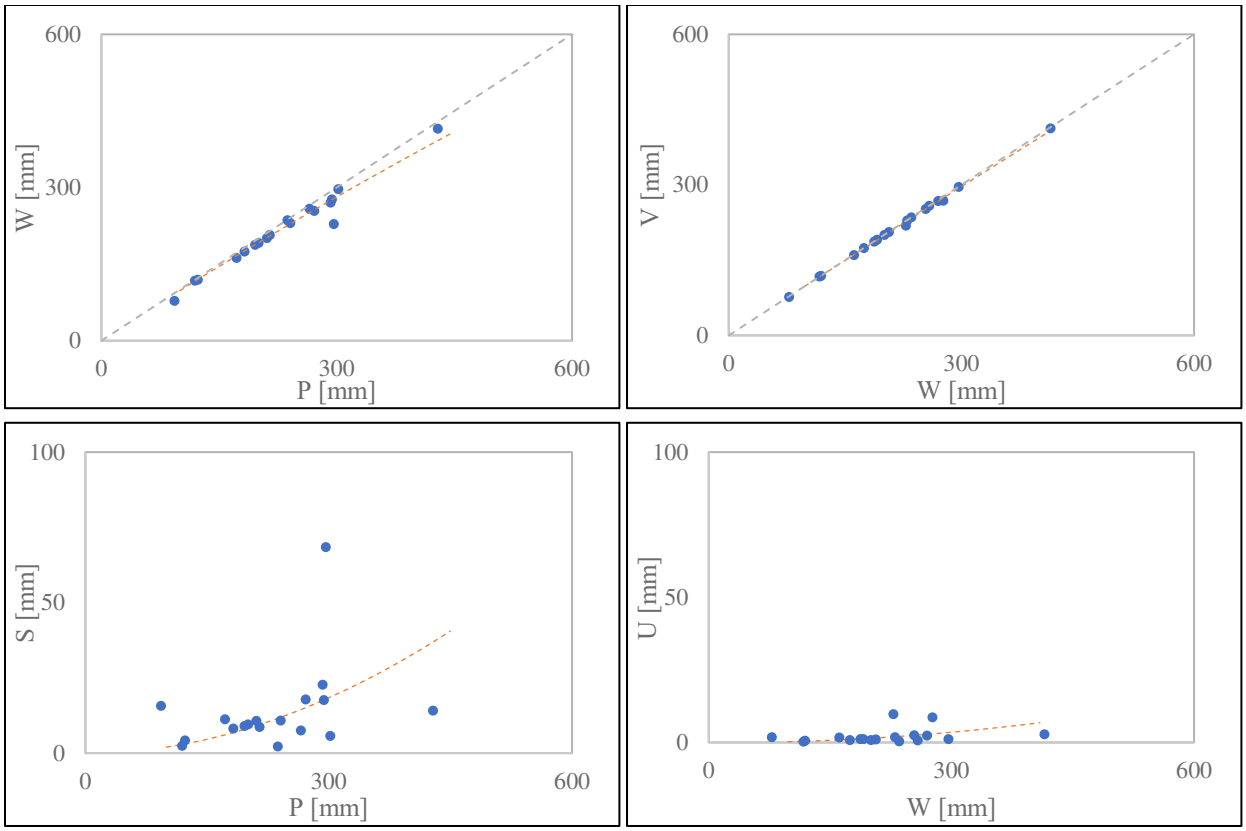

*Figure D3 - 93 : L'Vovich water balance relationships extracted for **Kert, Morocco**; Wetting W= f(P), Vaporization V=f(W), Quick flow S=f(P) and slow flow U = f(W); Points represent data (equations 14,15,16 and 17), and the dashed lines are Ponce and Shetty mathematical formulations (equations 18b and 19b)*

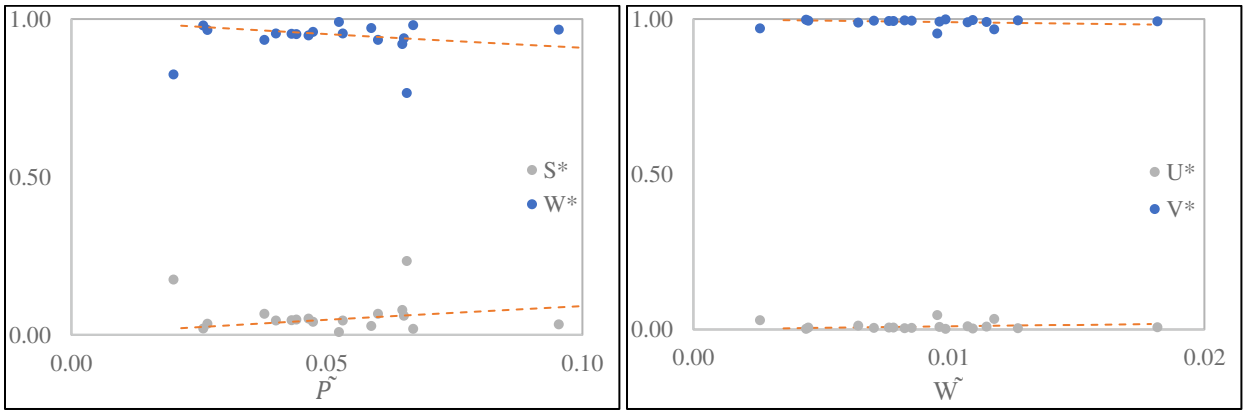

Figure D3 - 94 : Interannual variability of nondimensional annual estimates of (left) W and S* and (right) U* and V* versus annual climatic drivers $\tilde{P}$ and $\tilde{W}$ for **Kert, Morocco**; Points represent data (equations 22 and 23), and the dashed lines are theoretical (equations 25 and 26).*

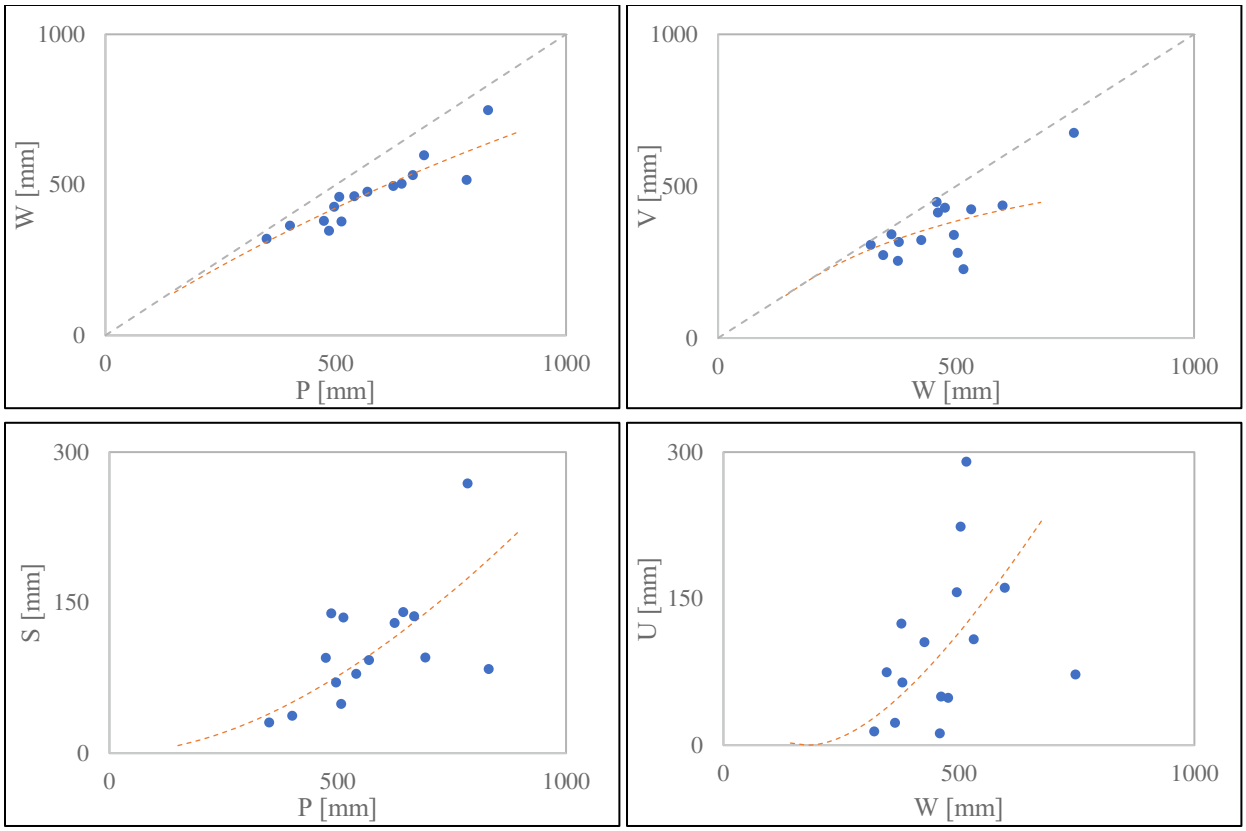

*Figure D3 - 95 : L'Vovich water balance relationships extracted for **Emsa, Morocco**; Wetting W= f(P), Vaporization V=f(W), Quick flow S=f(P) and slow flow U = f(W); Points represent data (equations 14,15,16 and 17), and the dashed lines are Ponce and Shetty mathematical formulations (equations 18b and 19b)*

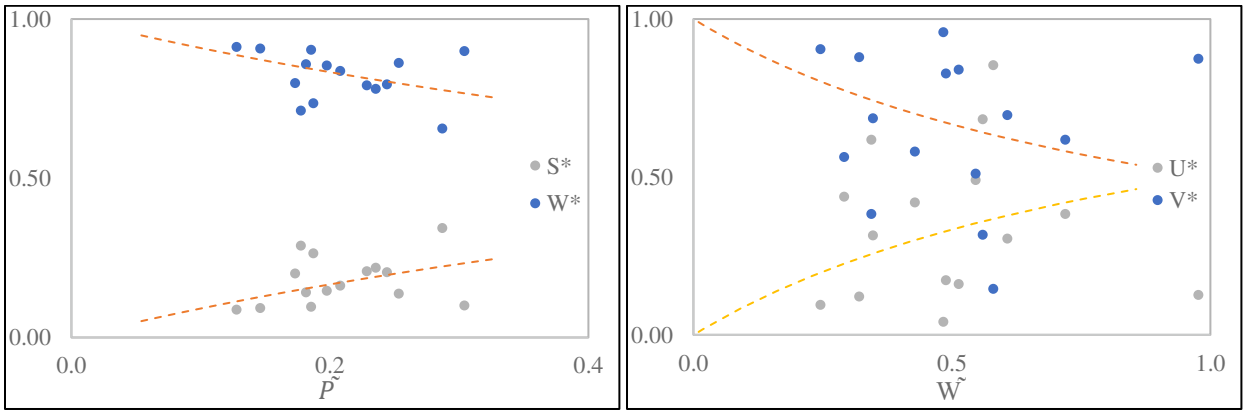

Figure D3 - 96 : Interannual variability of nondimensional annual estimates of (left) W and S* and (right) U* and V* versus annual climatic drivers $\tilde{P}$ and $\tilde{W}$ for **Emsa, Morocco**; Points represent data (equations 22 and 23), and the dashed lines are theoretical (equations 25 and 26).*

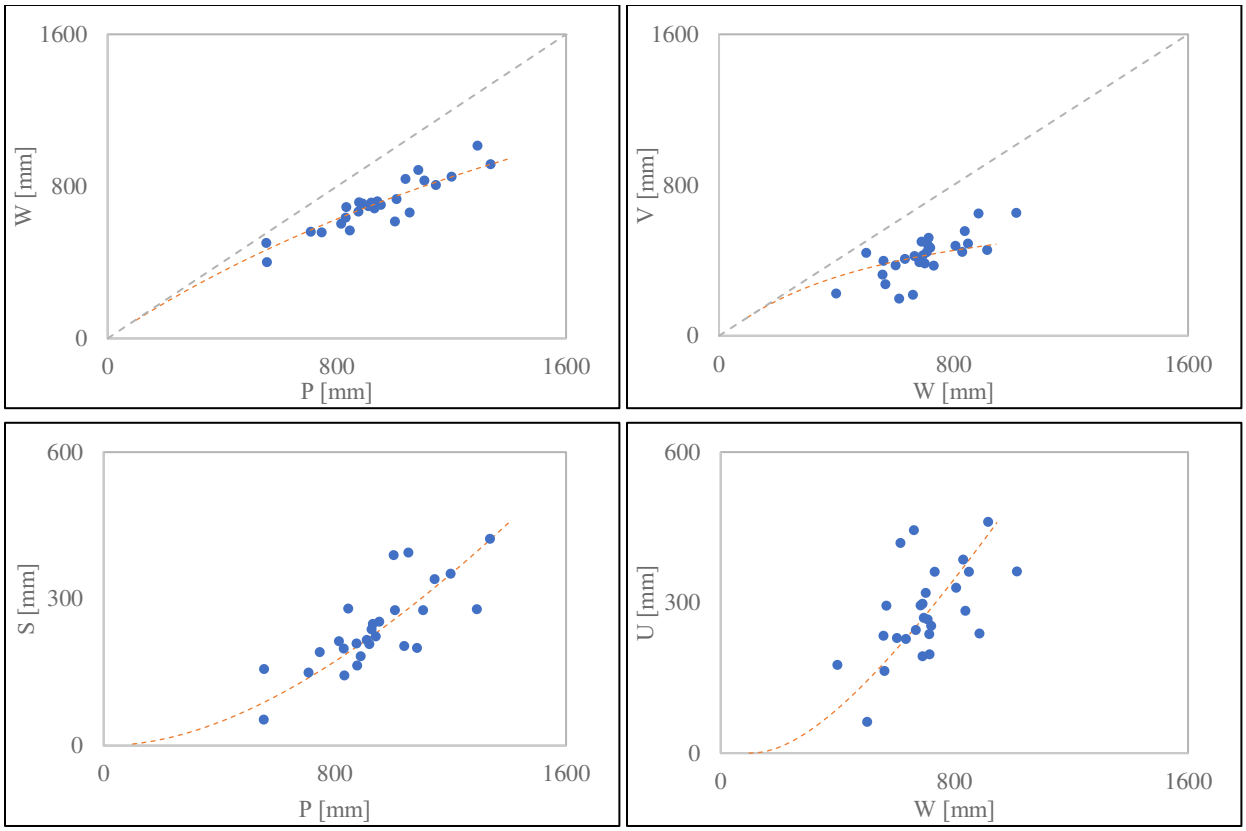

*Figure D3 - 97 : L'Vovich water balance relationships extracted for **Rižana, Slovenia**; Wetting W= f(P), Vaporization V=f(W), Quick flow S=f(P) and slow flow U = f(W); Points represent data (equations 14,15,16 and 17), and the dashed lines are Ponce and Shetty mathematical formulations (equations 18b and 19b)*

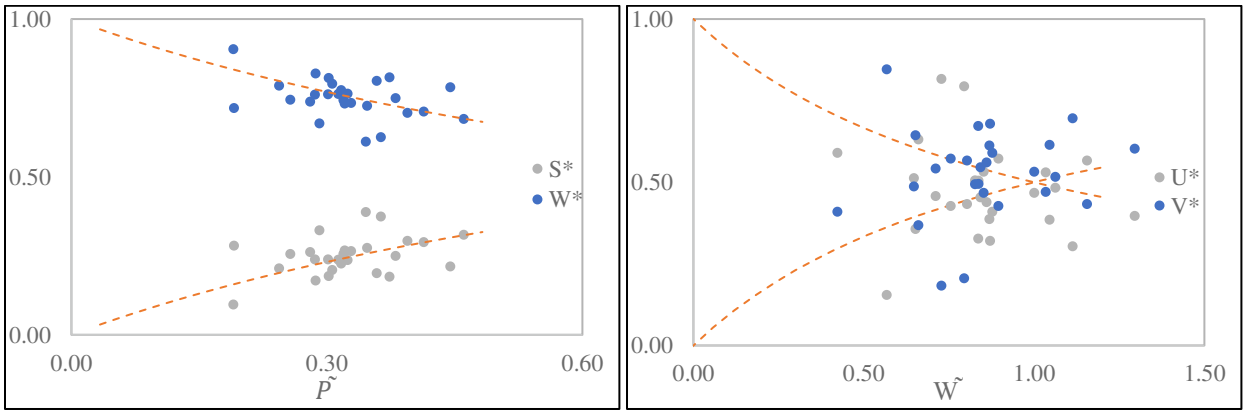

Figure D3 - 98 : Interannual variability of nondimensional annual estimates of (left) W and S* and (right) U* and V* versus annual climatic drivers $\tilde{P}$ and $\tilde{W}$ for **Rižana, Slovenia**; Points represent data (equations 22 and 23), and the dashed lines are theoretical (equations 25 and 26).*

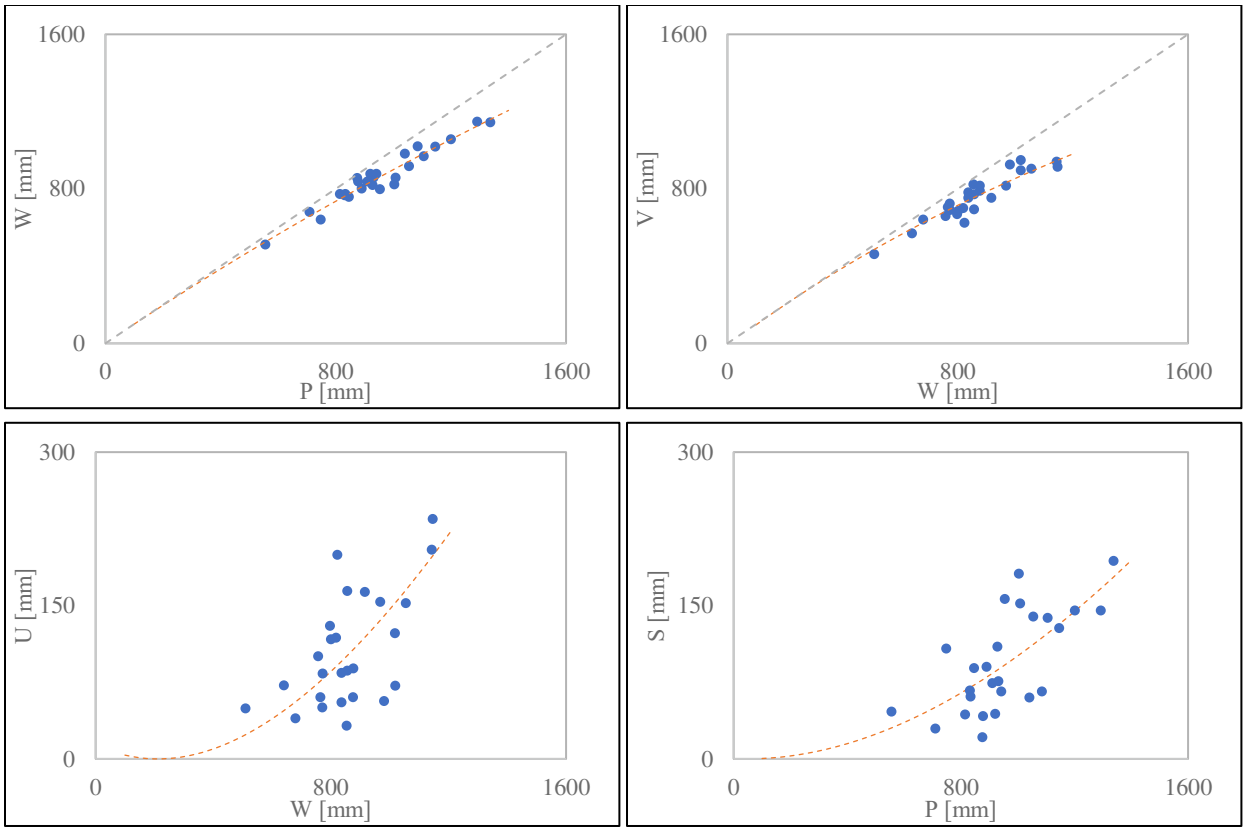

*Figure D3 - 99 : L'Vovich water balance relationships extracted for **Dragonja, Slovenia**; Wetting W= f(P), Vaporization V=f(W), Quick flow S=f(P) and slow flow U = f(W); Points represent data (equations 14,15,16 and 17), and the dashed lines are Ponce and Shetty mathematical formulations (equations 18b and 19b)*

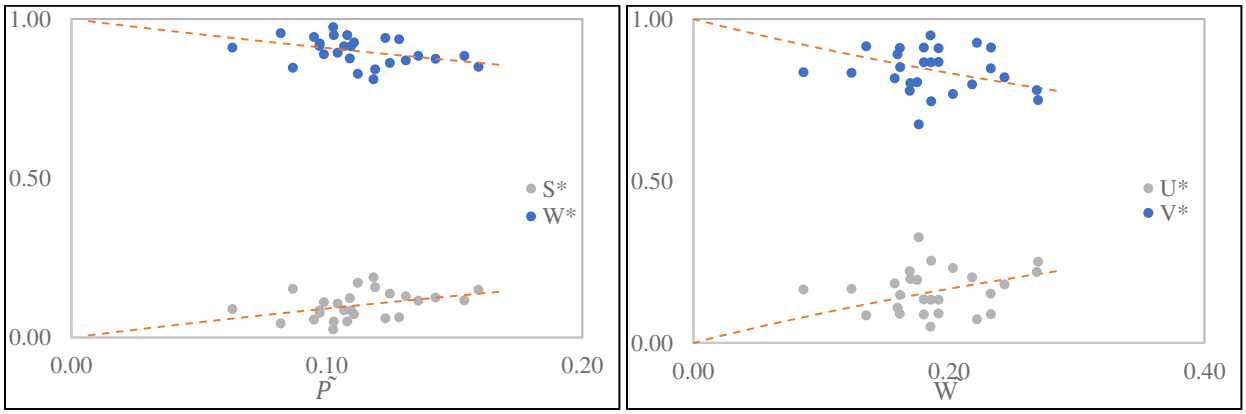

Figure D3 - 100 : Interannual variability of nondimensional annual estimates of (left) W and S* and (right) U* and V* versus annual climatic drivers $\tilde{P}$ and $\tilde{W}$ for **Dragonja, Slovenia**; Points represent data (equations 22 and 23), and the dashed lines are theoretical (equations 25 and 26).*

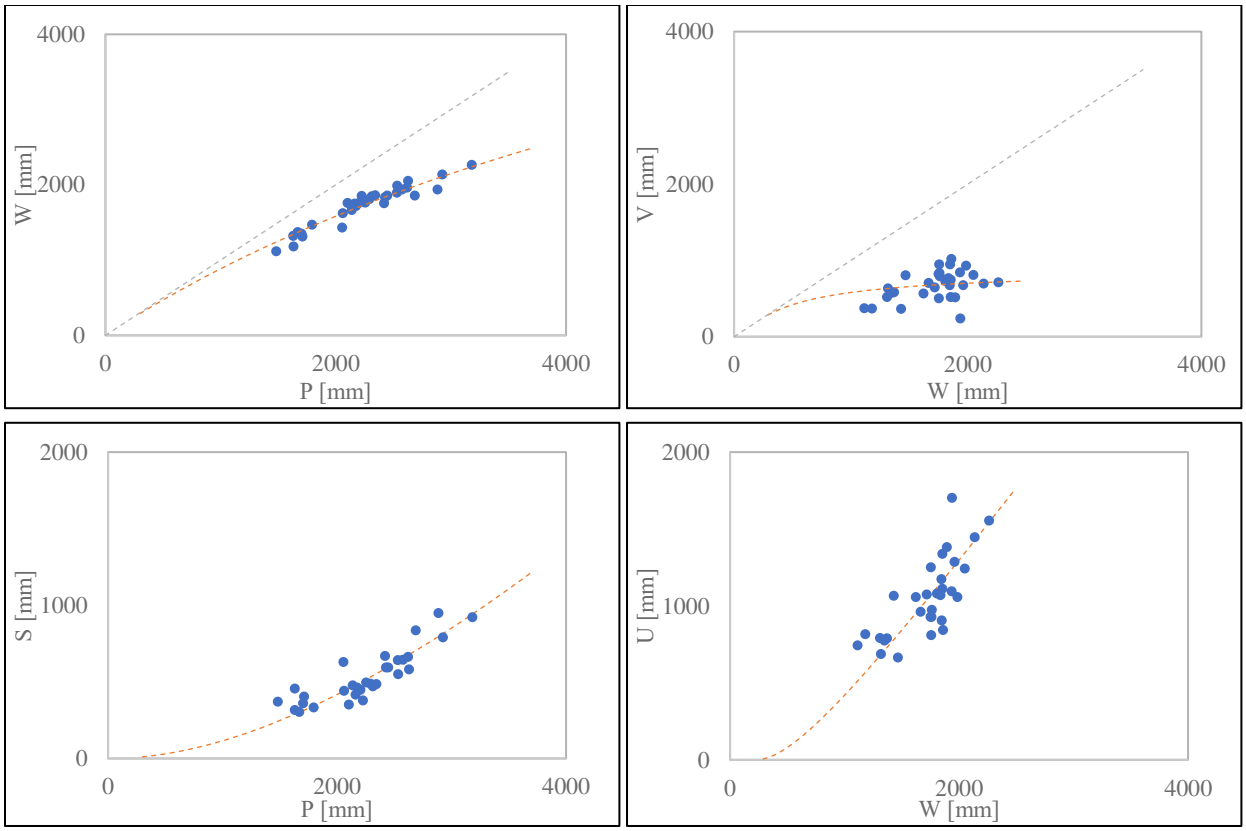

*Figure D3 - 101 : L'Vovich water balance relationships extracted for **Isonzo, Slovenia**; Wetting W= f(P), Vaporization V=f(W), Quick flow S=f(P) and slow flow U = f(W); Points represent data (equations 14,15,16 and 17), and the dashed lines are Ponce and Shetty mathematical formulations (equations 18b and 19b)*

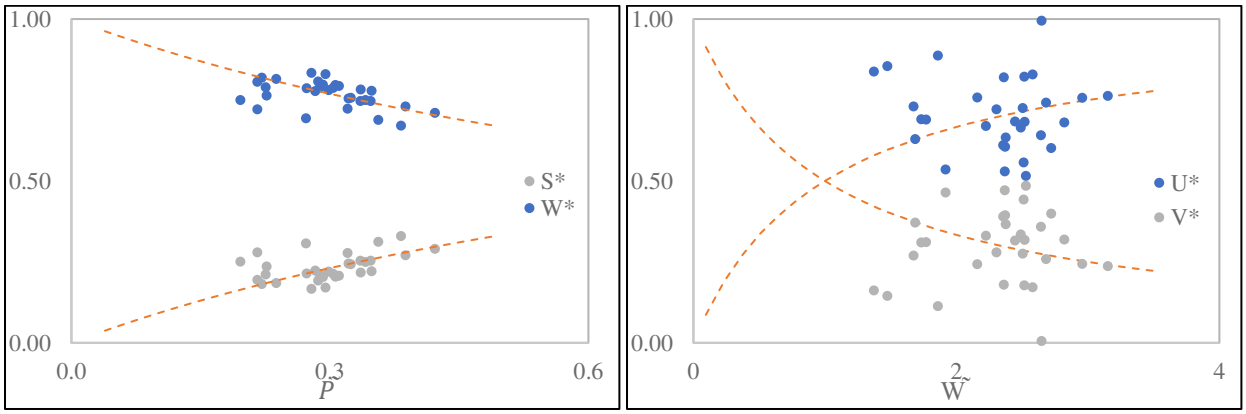

Figure D3 - 102 : Interannual variability of nondimensional annual estimates of (left) W and S* and (right) U* and V* versus annual climatic drivers $\tilde{P}$ and $\tilde{W}$ for **Isonzo, Slovenia**; Points represent data (equations 22 and 23), and the dashed lines are theoretical (equations 25 and 26).*

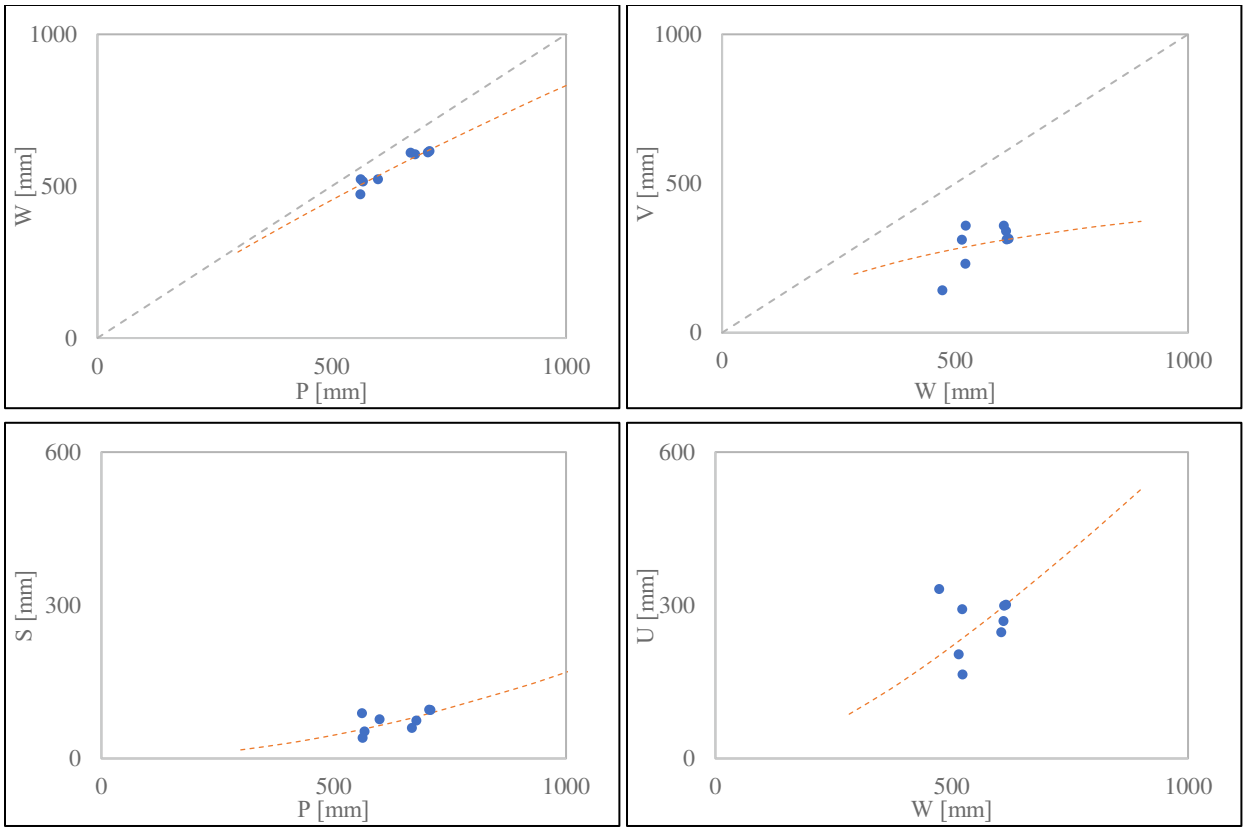

*Figure D3 - 103 : L'Vovich water balance relationships extracted for **Koeprue, Turkey**; Wetting W= f(P), Vaporization V=f(W), Quick flow S=f(P) and slow flow U = f(W); Points represent data (equations 14,15,16 and 17), and the dashed lines are Ponce and Shetty mathematical formulations (equations 18b and 19b)*

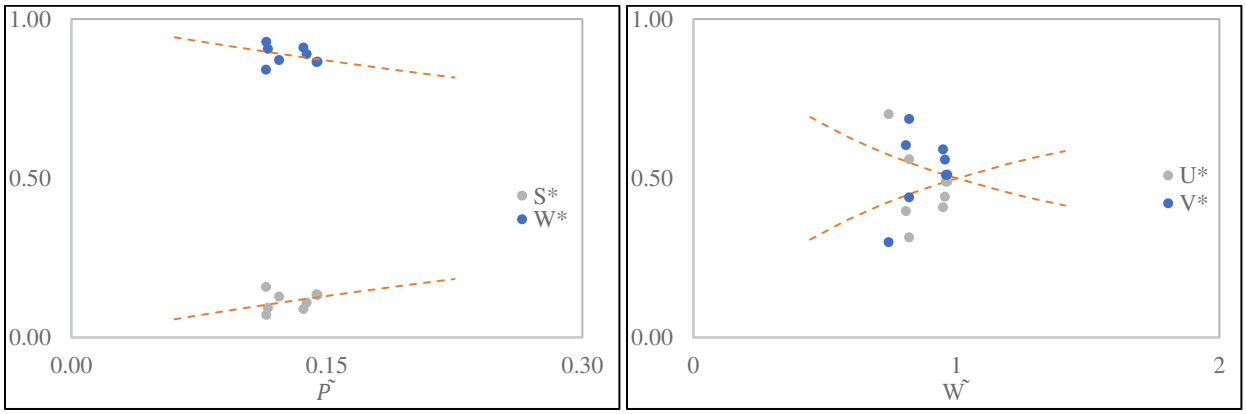

Figure D3 - 104 : Interannual variability of nondimensional annual estimates of (left) W and S* and (right) U* and V* versus annual climatic drivers $\tilde{P}$ and $\tilde{W}$ for **Koeprue, Turkey**; Points represent data (equations 22 and 23), and the dashed lines are theoretical (equations 25 and 26).*

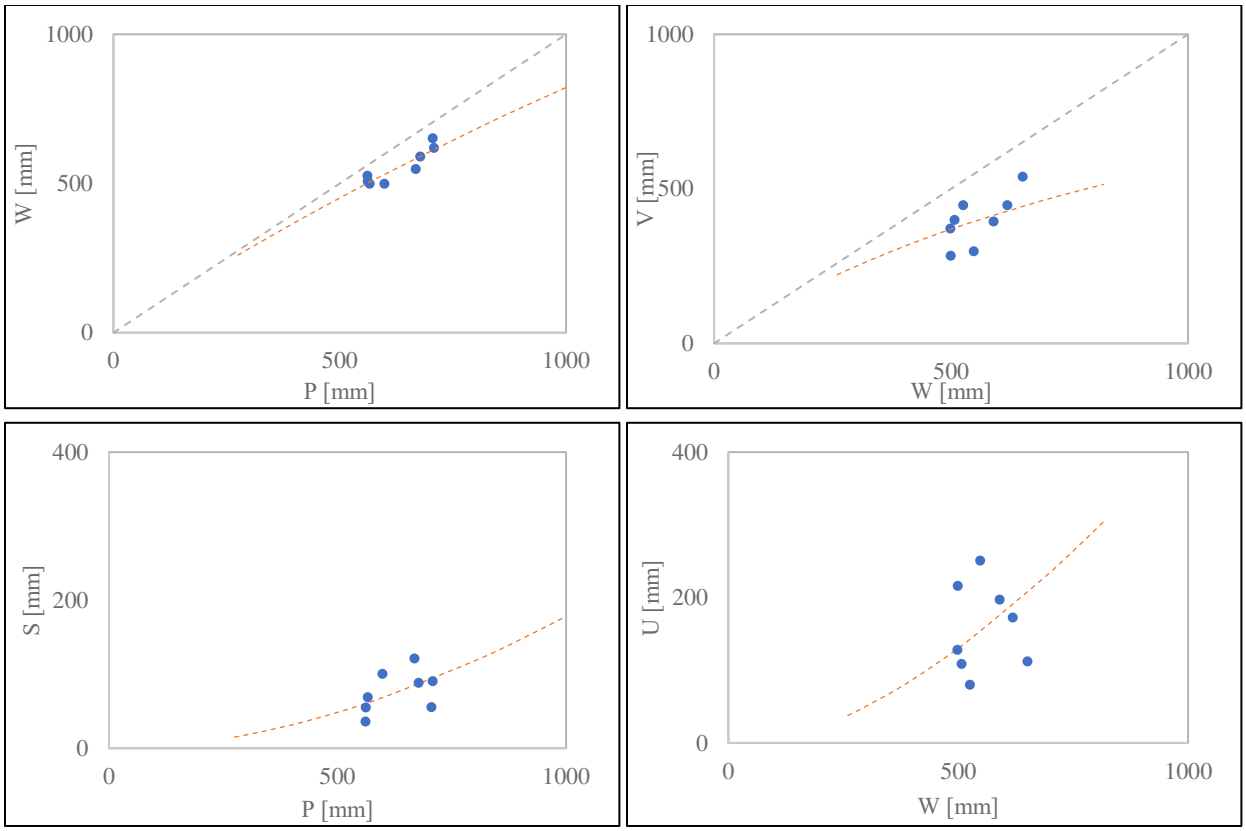

*Figure D3 - 105 : L'Vovich water balance relationships extracted for **Cine Cayi, Turkey**; Wetting W= f(P), Vaporization V=f(W), Quick flow S=f(P) and slow flow U = f(W); Points represent data (equations 14,15,16 and 17), and the dashed lines are Ponce and Shetty mathematical formulations (equations 18b and 19b)*

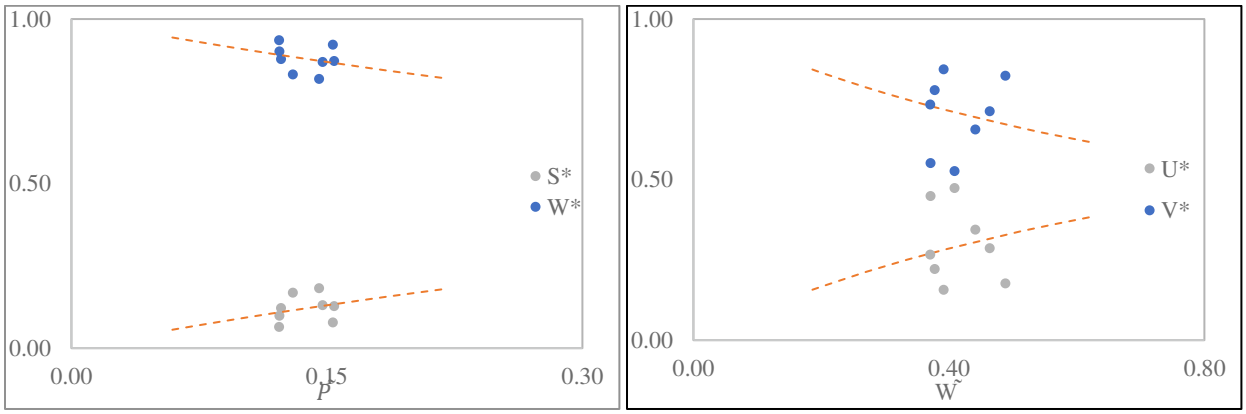

Figure D3 - 106 : Interannual variability of nondimensional annual estimates of (left) W and S* and (right) U* and V* versus annual climatic drivers $\tilde{P}$ and $\tilde{W}$ for **Cine Cayi, Turkey**; Points represent data (equations 22 and 23), and the dashed lines are theoretical (equations 25 and 26).*

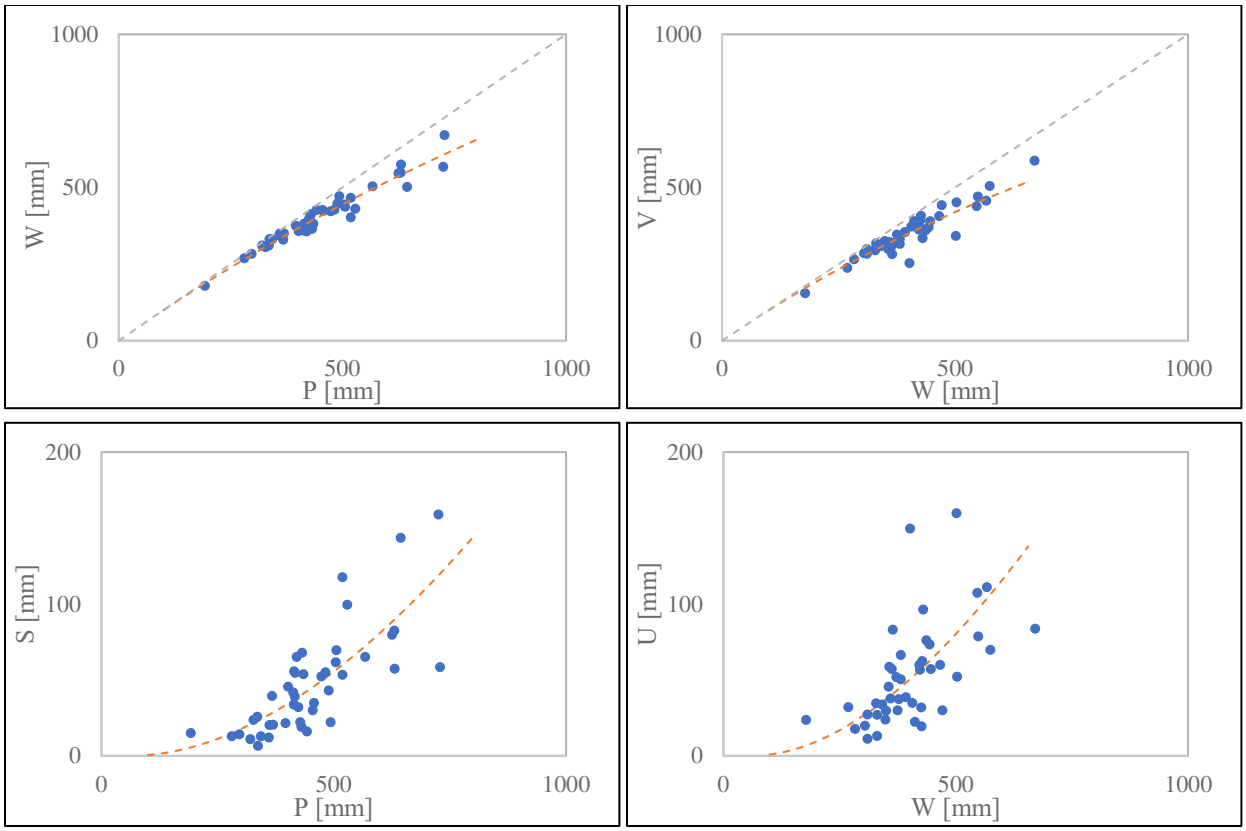

*Figure D3 - 107 : L'Vovich water balance relationships extracted for **Mejerda, Tunis**; Wetting W= f(P), Vaporization V=f(W), Quick flow S=f(P) and slow flow U = f(W); Points represent data (equations 14,15,16 and 17), and the dashed lines are Ponce and Shetty mathematical formulations (equations 18b and 19b)*

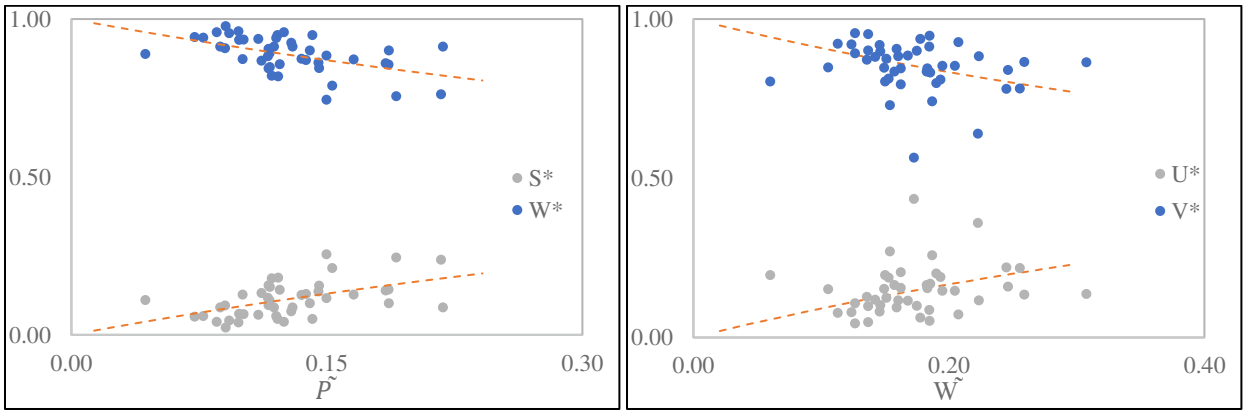

Figure D3 - 108 : Interannual variability of nondimensional annual estimates of (left) W and S* and (right) U* and V* versus annual climatic drivers $\tilde{P}$ and $\tilde{W}$ for **Mejerda, Tunis**; Points represent data (equations 22 and 23), and the dashed lines are theoretical (equations 25 and 26).*

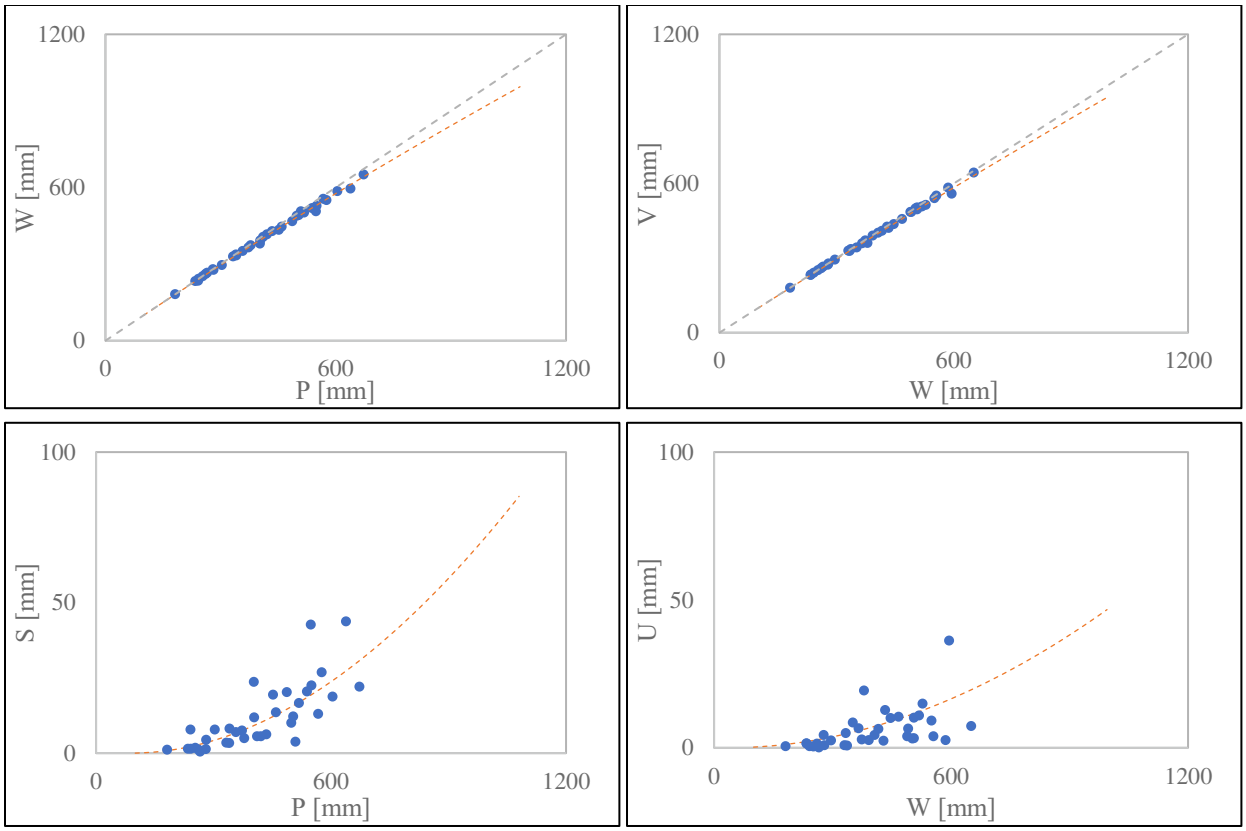

*Figure D3 - 109 : L'Vovich water balance relationships extracted for **Miliane, Tunis**; Wetting W= f(P), Vaporization V=f(W), Quick flow S=f(P) and slow flow U = f(W); Points represent data (equations 14,15,16 and 17), and the dashed lines are Ponce and Shetty mathematical formulations (equations 18b and 19b)*

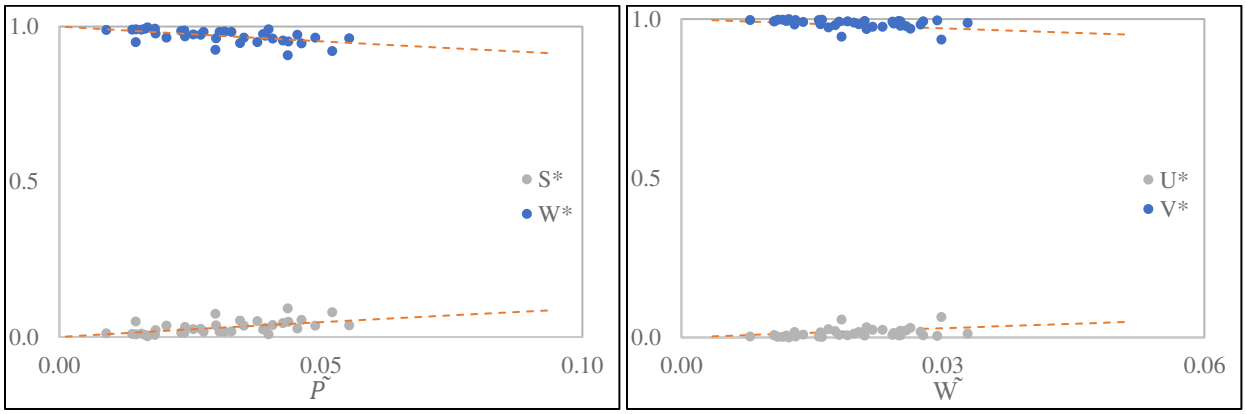

Figure D3 - 110 : Interannual variability of nondimensional annual estimates of (left) W and S* and (right) U* and V* versus annual climatic drivers $\tilde{P}$ and $\tilde{W}$ for **Miliane, Tunis**; Points represent data (equations 22 and 23), and the dashed lines are theoretical (equations 25 and 26).*

APPENDIX D4

The nondimensional water balance curves of Sivapalan

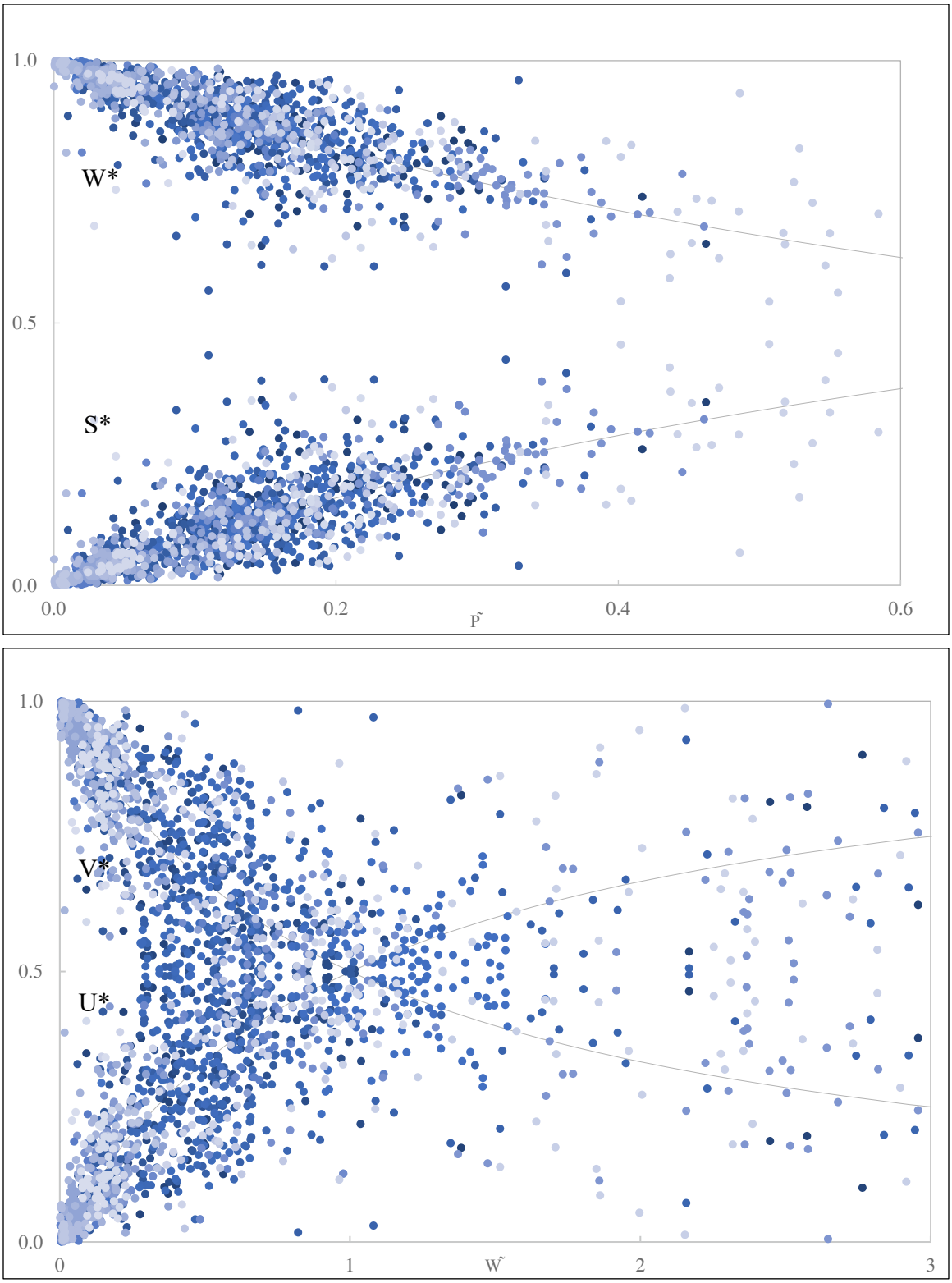

Figure D4 - 1 : Inter-annual variability of water balance nondimensional estimates of W and S* versus annual climatic driver $\tilde{P}$ (up) and U* and V* versus annual climatic driver $\tilde{W}$ (down) for all 55 catchments. Points represent data (equations 22 and 23), and dashed lines are theoretical (equations 25 and 26).*

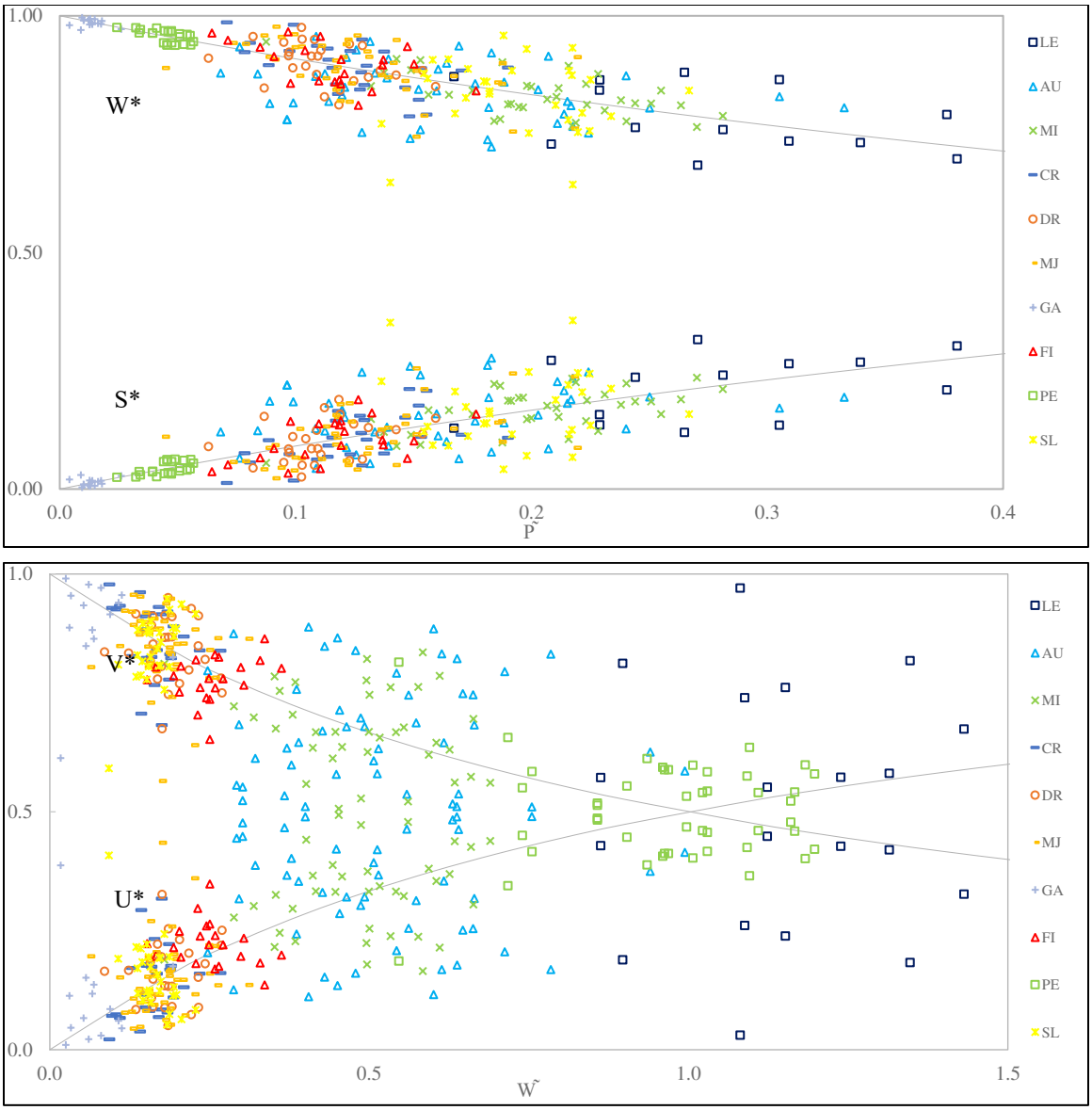

Figure D4 - 2 : PC1 inter-annual variability of water balance nondimensional estimates of W and S* versus annual climatic driver $\tilde{P}$ (up) and U* and V* versus annual climatic driver $\tilde{W}$ (down).*

OID	*NAME*	*Code*	*Country Code*	*PC*	*CC*	*Area (km^2)*	*MAP (mm)*	*MAQ (mm)*	*MEp (mm)*	*CE*
175	*GAIA*	*GA*	*ES7*	*1*	*5*	*424*	*462*	*17*	*881*	*0.04*
297	*LEZ*	*LE*	*FR3*	*1*	*4*	*150*	*629*	*382*	*840*	*0.61*
541	*AUDE*	*AU*	*FR6*	*1*	*5*	*1754*	*557*	*342*	*775*	*0.61*
677	*MIRNA*	*MI*	*HR1*	*1*	*5*	*579*	*1164*	*384*	*727*	*0.33*
710	*FIORA*	*FI*	*IT2*	*1*	*4*	*818*	*959*	*287*	*699*	*0.30*
845	*PESCARA*	*PE*	*IT9*	*1*	*5*	*3125*	*783*	*487*	*811*	*0.62*
903	*S. LEONARDO*	*SL*	*IT11*	*1*	*3*	*522*	*660*	*195*	*820*	*0.30*
913	*CERVARO*	*CR*	*IT13*	*1*	*4*	*657*	*713*	*103*	*566*	*0.14*
960	*DRAGONJA*	*DR*	*SI2*	*1*	*5*	*147*	*956*	*216*	*801*	*0.23*
1048	*MEJERDA*	*MJ*	*TS1*	*1*	*4*	*1490*	*450*	*99*	*923*	*0.22*

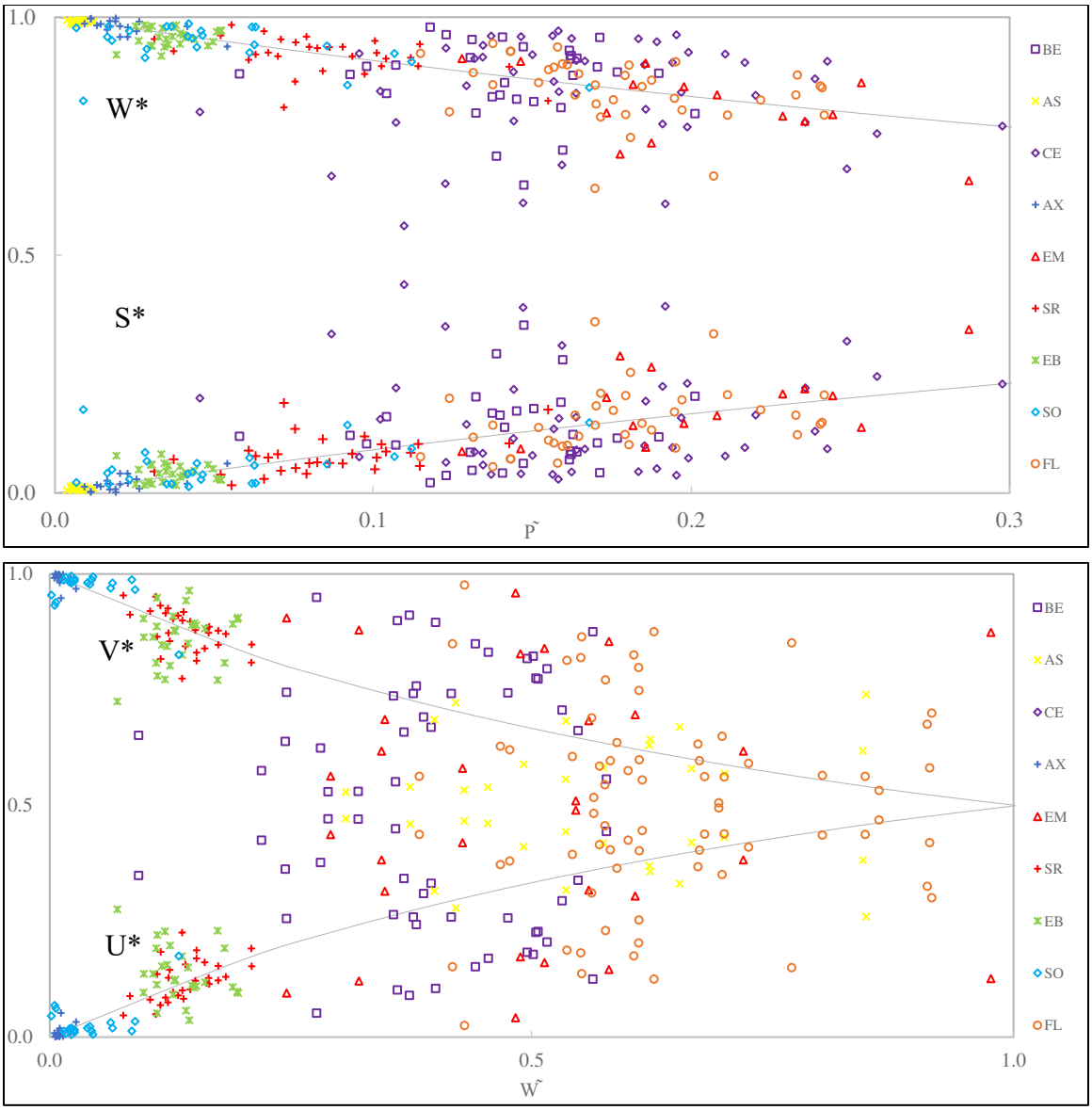

Figure D4 - 3 : PC3 catchments inter-annual variability of water balance nondimensional estimates of W and S* versus annual climatic driver P̃ (up) and U* and V* versus annual climatic driver W̃ (down).*

OID	*NAME*	*Code*	*Country Code*	*PC*	*CC*	*Area (km²)*	*MAP (mm)*	*MAQ (mm)*	*Mean Ep*	*CE*
47	*SERRAKHIS*	*SR*	*CY1*	*3*	*3*	*77*	*1006*	*188*	*950*	*0.19*
88	*CENIA*	*CE*	*ES1*	*3*	*4*	*97*	*529*	*281*	*830*	*0.53*
174	*EL BESÒS*	*EB*	*ES6*	*3*	*5*	*1036*	*644*	*126*	*807*	*0.20*
692	*ALEXANDER*	*AX*	*IS1*	*3*	*2*	*953*	*603*	*11*	*888*	*0.02*
693	*SOREQ*	*SO*	*IS2*	*3*	*2*	*492*	*543*	*18*	*949*	*0.03*
725	*FLUMINIMAGGIORE*	*FL*	*IT4*	*3*	*4*	*83*	*747*	*320*	*867*	*0.43*
929	*BEYROUTH*	*BE*	*LB2*	*3*	*3*	*217*	*1032*	*454*	*935*	*0.44*
936	*ASSI*	*AS*	*LB6*	*3*	*3*	*1507*	*1141*	*266*	*815*	*0.23*
951	*EMSA*	*EM*	*MO2*	*3*	*3*	*110*	*572*	*203*	*887*	*0.35*
1035	*KOEPRUE*	*KO*	*TR1*	*3*	*3*	*1942*	*632*	*336*	*703*	*0.53*

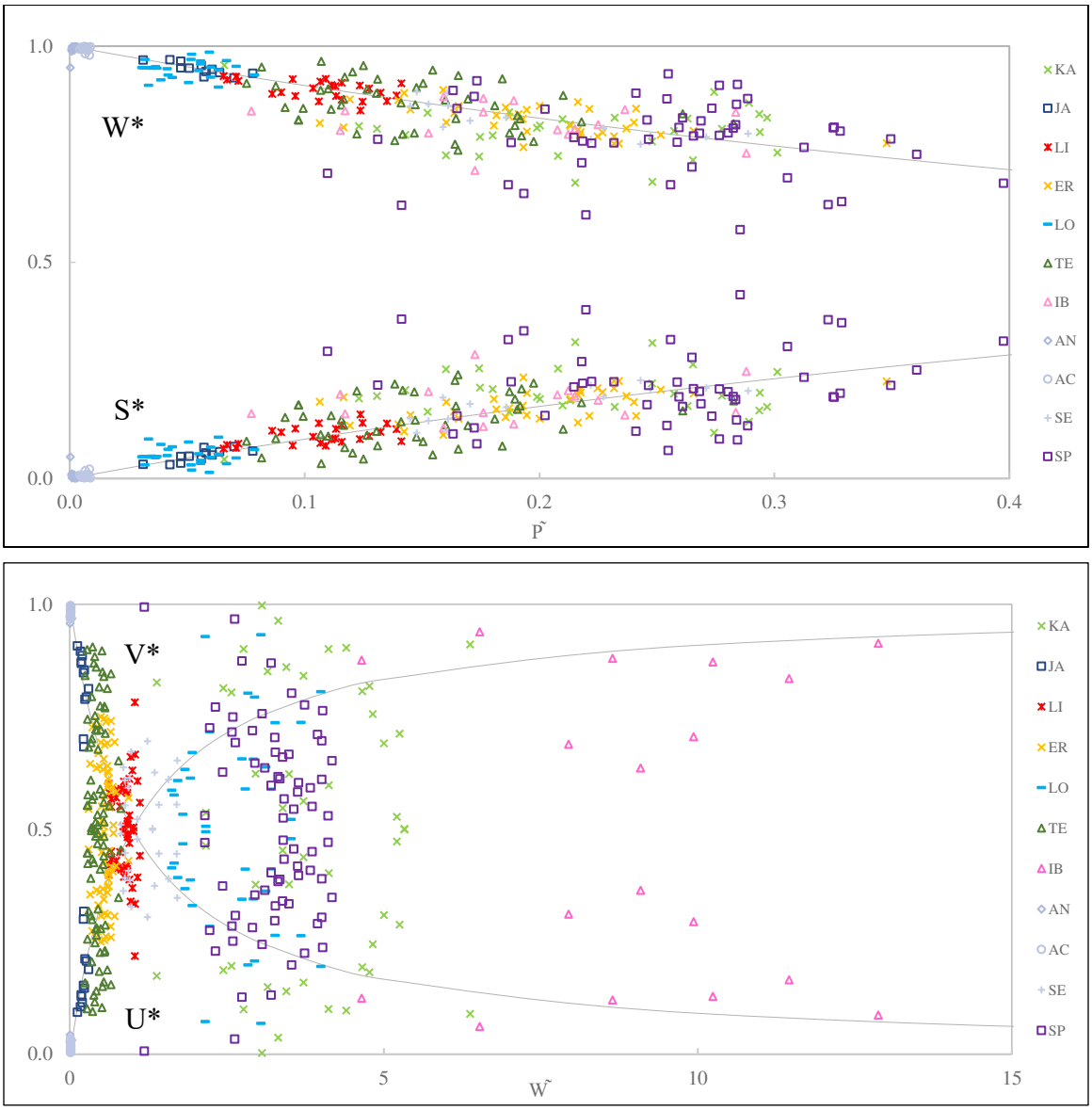

Figure D4 - 4 : PC1 CC4 inter-annual variability of water balance nondimensional estimates of W and S* versus annual climatic driver $\tilde{P}$ (up) and U* and V* versus annual climatic driver $\tilde{W}$ (down).*

OID	*NAME*	*Code*	*Country Code*	*PC*	*CC*	*Area (km^2)*	*MAP (mm)*	*MAQ (mm)*	*MEp (mm)*	*CE*
15	*ERZENIT*	*ER*	*AL1*	*4*	*4*	*760*	*1202*	*553*	*841*	*0.46*
194	*ANDARAX*	*AN*	*ES8*	*4*	*4*	*490*	*242*	*2*	*988*	*0.01*
319	*LOUP*	*LO*	*FR4*	*4*	*5*	*264*	*755*	*541*	*835*	*0.72*
561	*TET*	*TE*	*FR9*	*4*	*5*	*1371*	*557*	*244*	*848*	*0.44*
634	*SPERCHIOS*	*SP*	*GR1*	*4*	*4*	*1282*	*701*	*575*	*890*	*0.82*
722	*ALCANTARA*	*AC*	*IT3*	*4*	*3*	*475*	*658*	*14*	*1000*	*0.02*
800	*SERCHIO*	*SE*	*IT6*	*4*	*5*	*1525*	*1831*	*997*	*571*	*0.54*
928	*JAOUZ*	*JA*	*LB1*	*4*	*3*	*189*	*1413*	*304*	*812*	*0.21*
930	*KALB*	*KA*	*LB3*	*4*	*3*	*249*	*1440*	*904*	*812*	*0.63*
934	*IBRAHIM*	*IB*	*LB5*	*4*	*3*	*326*	*1450*	*1005*	*812*	*0.69*
937	*LITANI*	*LI*	*LB7*	*4*	*3*	*1808*	*637*	*289*	*825*	*0.45*

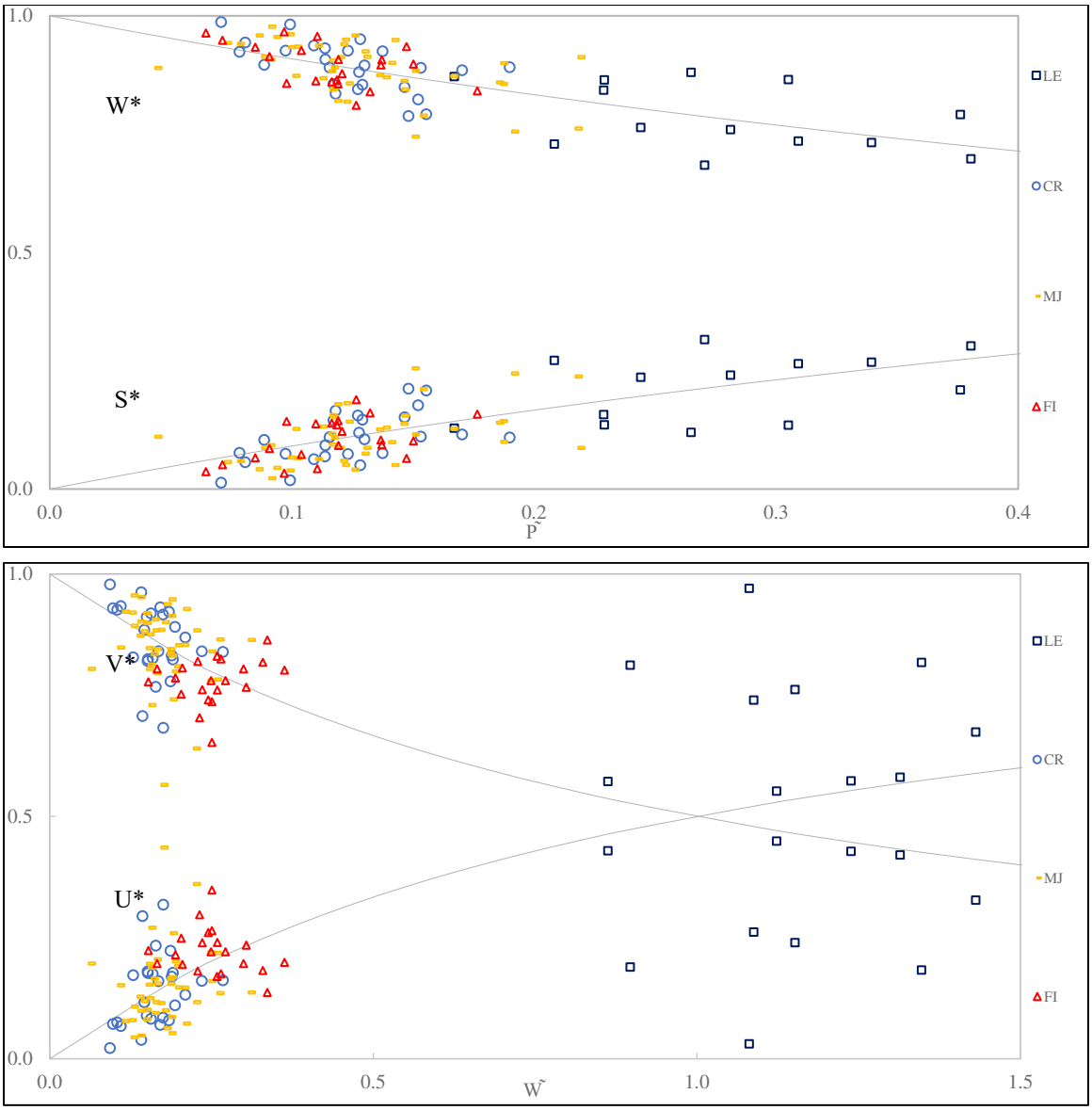

Figure D4 - 5 : PC1 CC4 inter-annual variability of water balance nondimensional estimates of W and S* versus annual climatic driver $\tilde{P}$ (up) and U* and V* versus annual climatic driver $\tilde{W}$ (down).*

OID	*NAME*	*Code*	*Country Code*	*PC*	*CC*	*Area (km^2)*	*MAP (mm)*	*MAQ (mm)*	*MEp (mm)*	*CE*
297	*LEZ*	*LE*	*FR3*	*1*	*4*	*150*	*629*	*382*	*840*	*0.61*
710	*FIORA*	*FI*	*IT2*	*1*	*4*	*818*	*959*	*287*	*699*	*0.30*
913	*CERVARO*	*CR*	*IT13*	*1*	*4*	*657*	*713*	*103*	*566*	*0.14*
1048	*MEJERDA*	*MJ*	*TS1*	*1*	*4*	*1490*	*450*	*99*	*923*	*0.22*

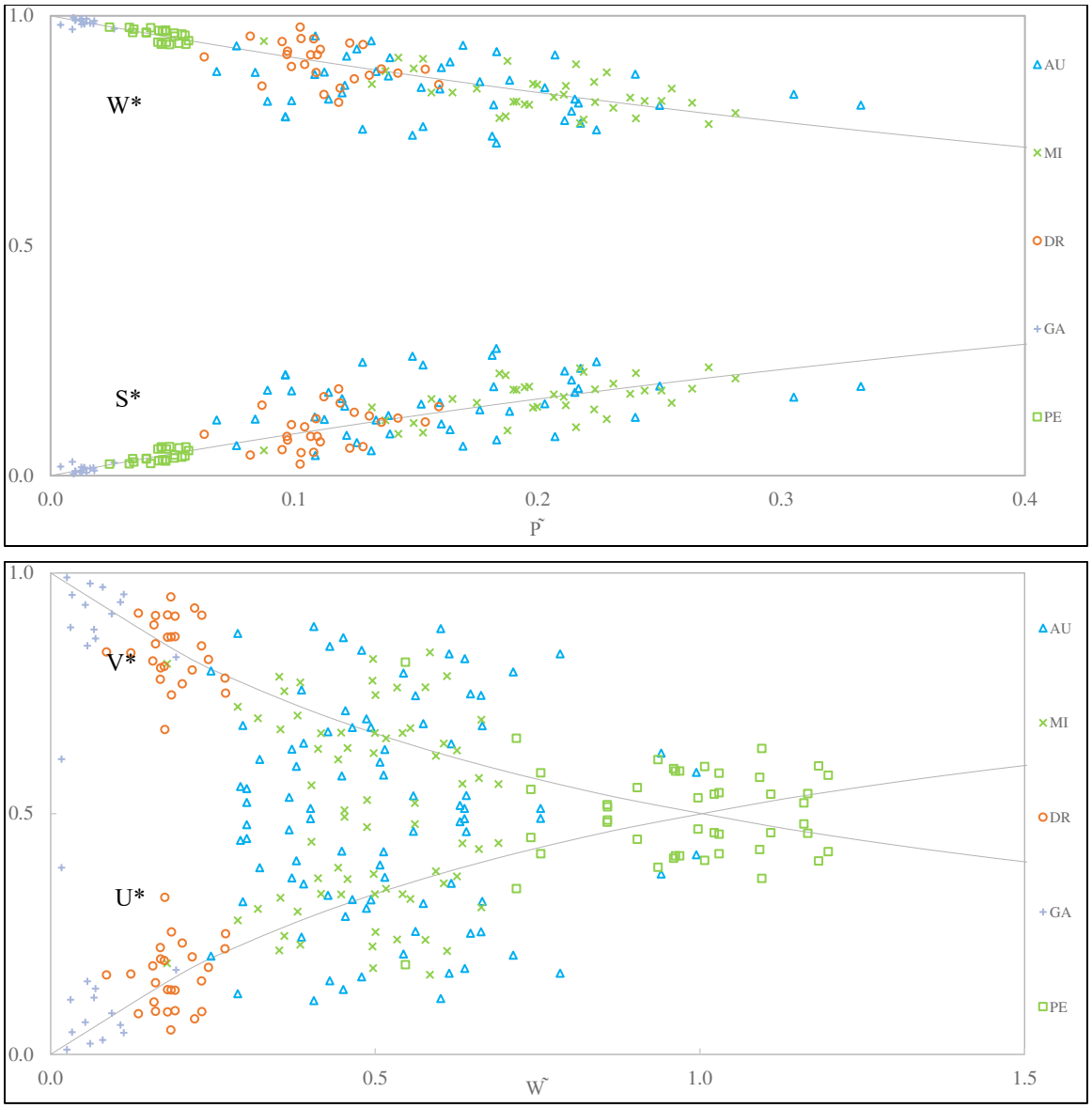

Figure D4 - 6 : PC1 CC5 inter-annual variability of water balance nondimensional estimates of W and S* versus annual climatic driver $\tilde{P}$ (up) and U* and V* versus annual climatic driver $\tilde{W}$ (down)*

OID	*NAME*	*Code*	*Country Code*	*PC*	*CC*	*Area (km^2)*	*MAP (mm)*	*MAQ (mm)*	*MEp (mm)*	*CE*
175	*GAIA*	*GA*	*ES7*	*1*	*5*	*424*	*462*	*17*	*881*	*0.04*
541	*AUDE*	*AU*	*FR6*	*1*	*5*	*1754*	*557*	*342*	*775*	*0.61*
677	*MIRNA*	*MI*	*HR1*	*1*	*5*	*579*	*1164*	*384*	*727*	*0.33*
845	*PESCARA*	*PE*	*IT9*	*1*	*5*	*3125*	*783*	*487*	*811*	*0.62*
960	*DRAGONJA*	*DR*	*SI2*	*1*	*5*	*147*	*956*	*216*	*801*	*0.23*

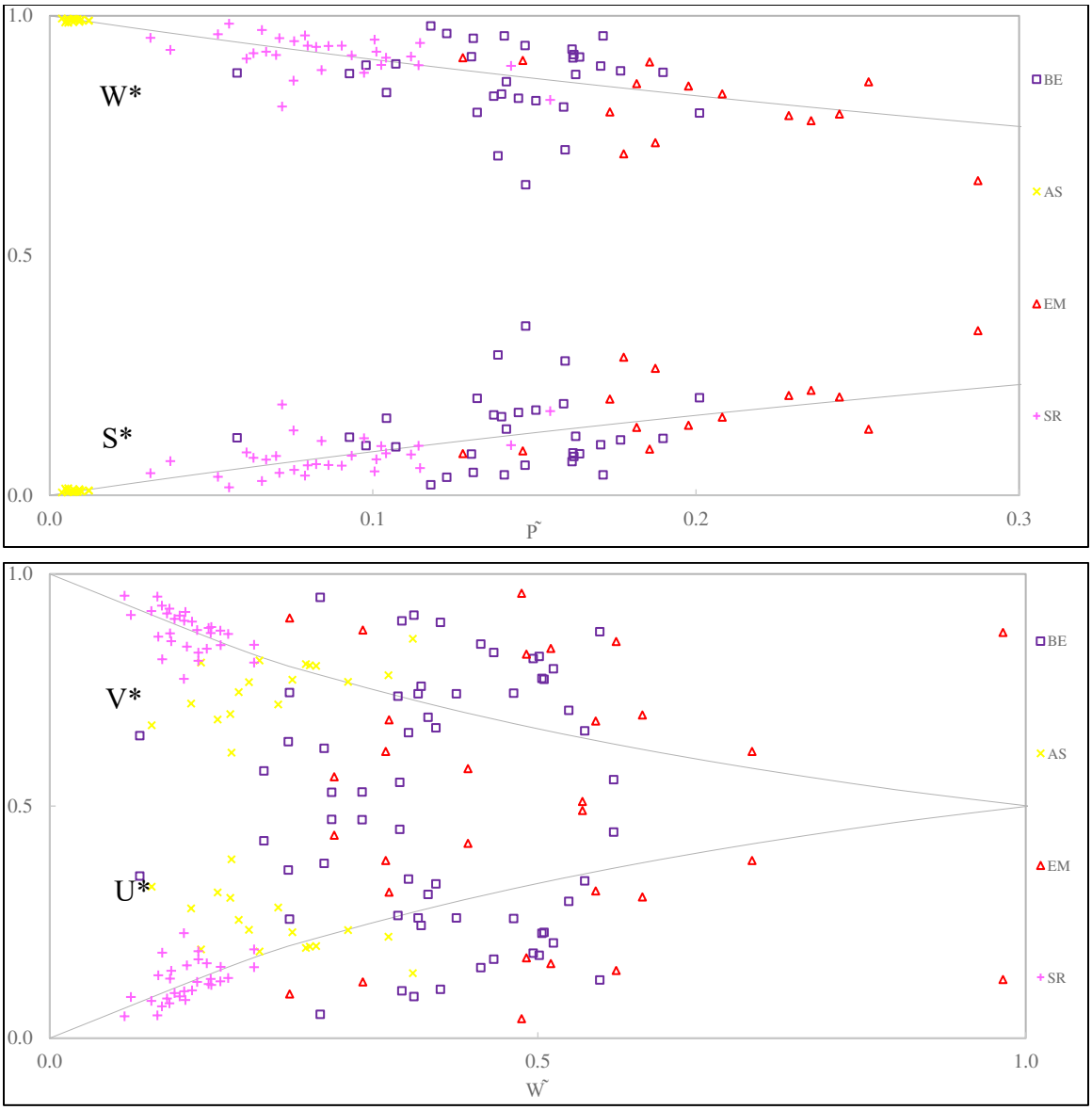

Figure D4 - 7 : PC3 CC3 inter-annual variability of water balance nondimensional estimates of W and S* versus annual climatic driver $\tilde{P}$ (up) and U* and V* versus annual climatic driver $\tilde{W}$ (down) for all 55 catchments.*

OID	*NAME*	*Code*	*Country Code*	*PC*	*CC*	*Area (km²)*	*MAP (mm)*	*MAQ (mm)*	*Mean Ep*	*CE*
47	*SERRAKHIS*	*SR*	*CY1*	*3*	*3*	*77*	*1006*	*188*	*950*	*0.19*
929	*BEYROUTH*	*BE*	*LB2*	*3*	*3*	*217*	*1032*	*454*	*935*	*0.44*
936	*ASSI*	*AS*	*LB6*	*3*	*3*	*1507*	*1141*	*266*	*815*	*0.23*
951	*EMSA*	*EM*	*MO2*	*3*	*3*	*110*	*572*	*203*	*887*	*0.35*
1035	*KOEPRUE*	*KO*	*TR1*	*3*	*3*	*1942*	*632*	*336*	*703*	*0.53*

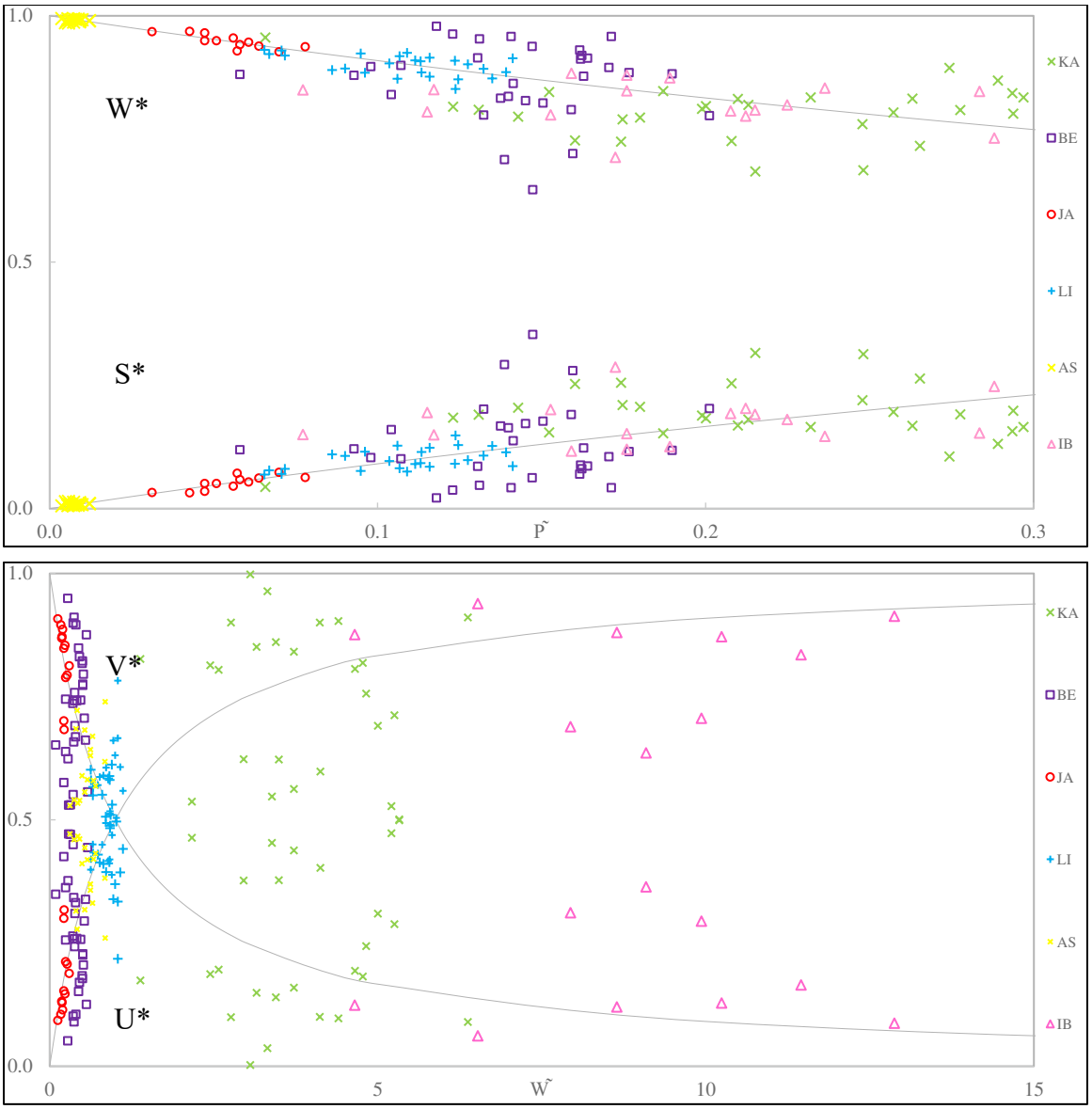

Figure D4 - 8 : ***Lebanese catchments*** *inter-annual variability of water balance nondimensional estimates of W* and S* versus annual climatic driver P̃ (up) and U* and V* versus annual climatic driver W̃ (down)*

OID	*NAME*	*Code*	*Country Code*	*PC*	*CC*	*Area (km²)*	*MAP (mm)*	*MAQ (mm)*	*Mean Ep*	*CE*
928	*JAOUZ*	*JA*	*LB1*	*4*	*3*	*189*	*1413*	*304*	*812*	*0.21*
929	*BEYROUTH*	*BE*	*LB2*	*3*	*3*	*217*	*1032*	*454*	*935*	*0.44*
930	*KALB*	*KA*	*LB3*	*4*	*3*	*249*	*1440*	*904*	*812*	*0.63*
934	*IBRAHIM*	*IB*	*LB5*	*4*	*3*	*326*	*1450*	*1005*	*812*	*0.69*
936	*ASSI*	*AS*	*LB6*	*3*	*3*	*1507*	*661*	*266*	*815*	*0.40*
937	*LITANI*	*LI*	*LB7*	*4*	*3*	*1808*	*637*	*289*	*825*	*0.45*

APPENDIX E1

Baseflow and Runoff coefficients under MED-CORDEX RCM climate change scenario

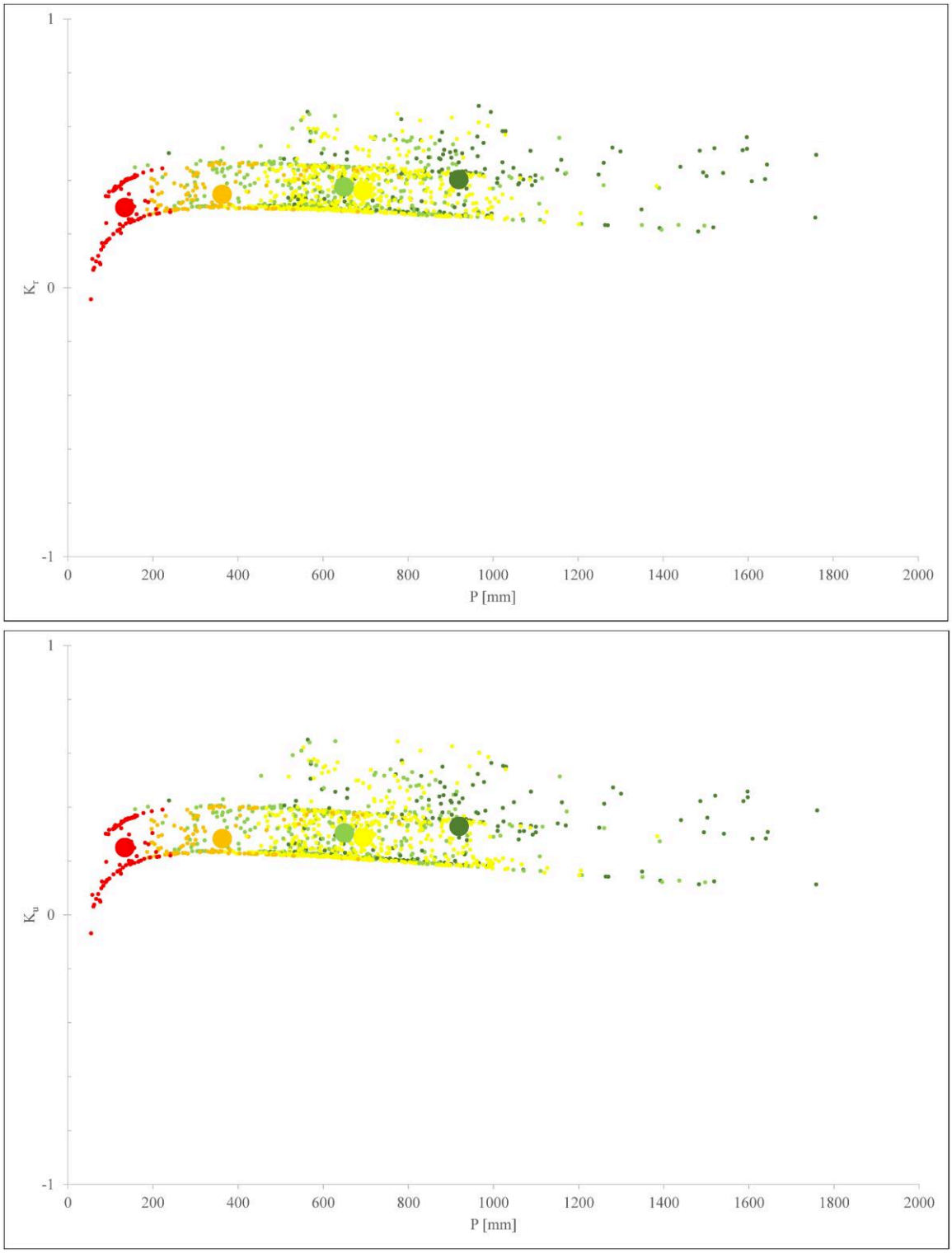

Figure E1 - 1 : Projected regionalised runoff and baseflow coefficient K_r, and K_u with average values coloured according to climatic classes based on projected climatic indices under Aladin RCP 4.5 scenario for 2070-2100.

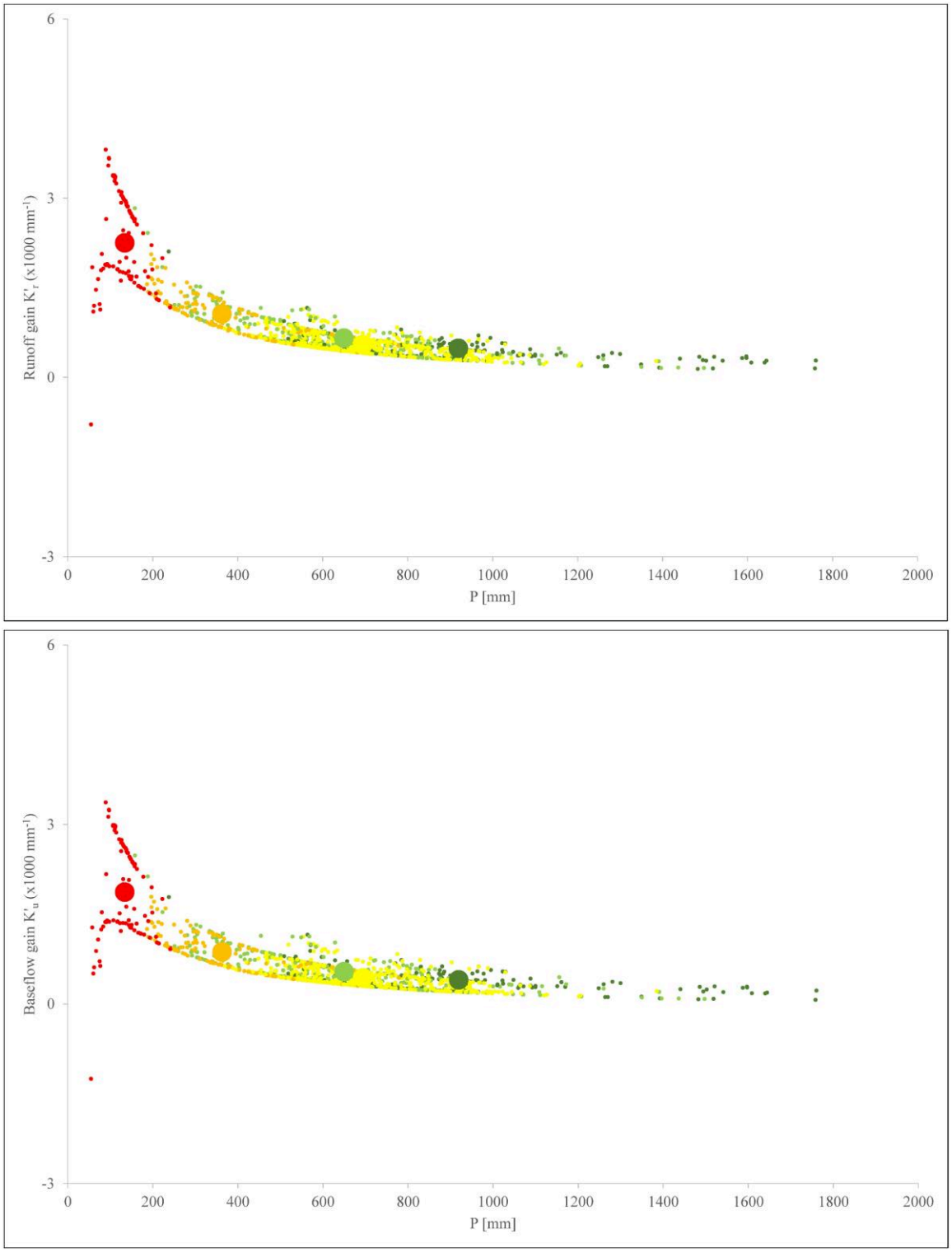

Figure E1 - 2 : Projected regionalised runoff and baseflow gains K'r, and K'u with average values coloured according to climatic classes based on projected climatic indices under Aladin RCP 4.5 scenario for 2070-2100.

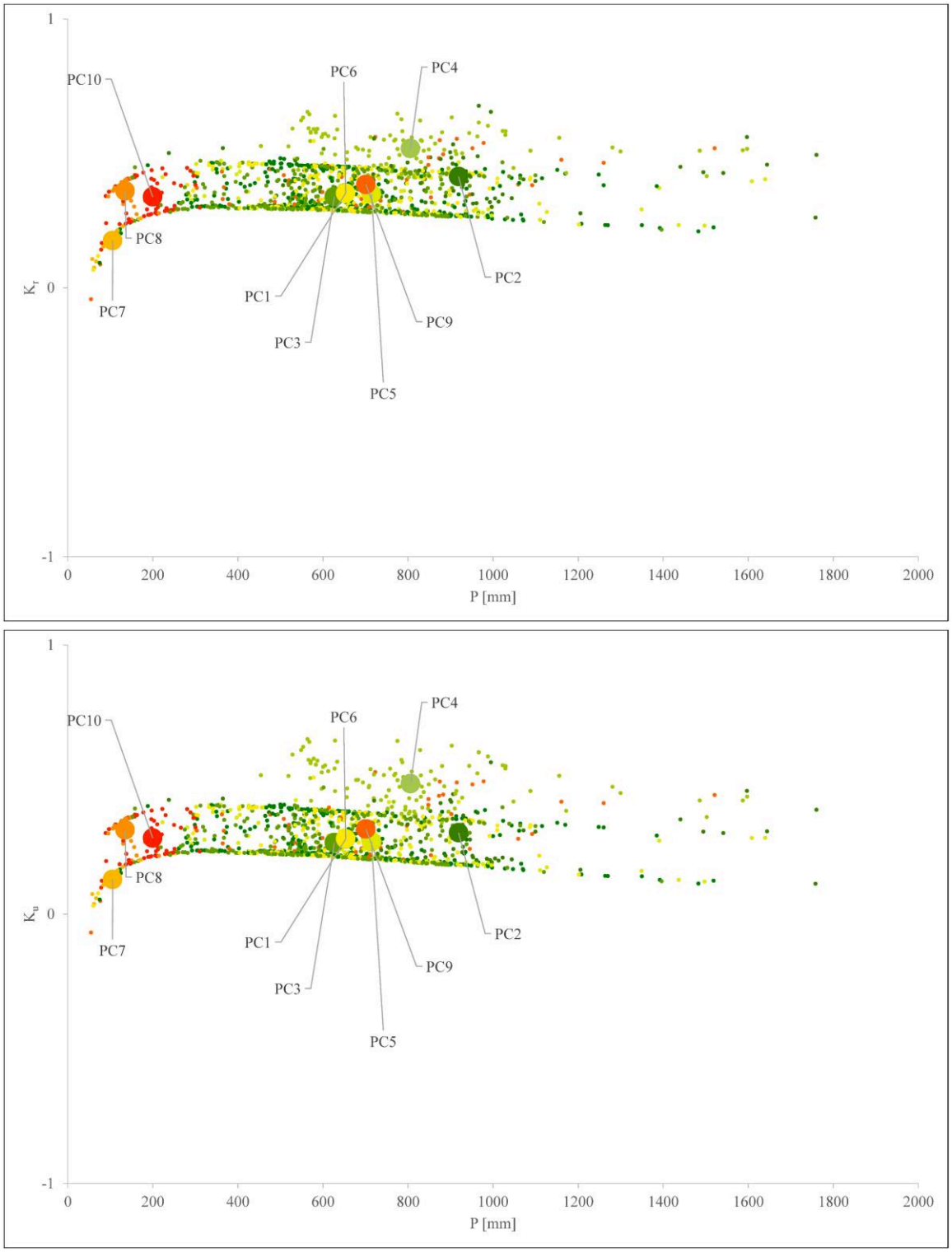

Figure E1 - 3 : Projected regionalised runoff and baseflow coefficient K_r, and K_u with average values coloured according to physiographic classes based on projected climatic indices under Aladin RCP 4.5 scenario for 2070-2100.

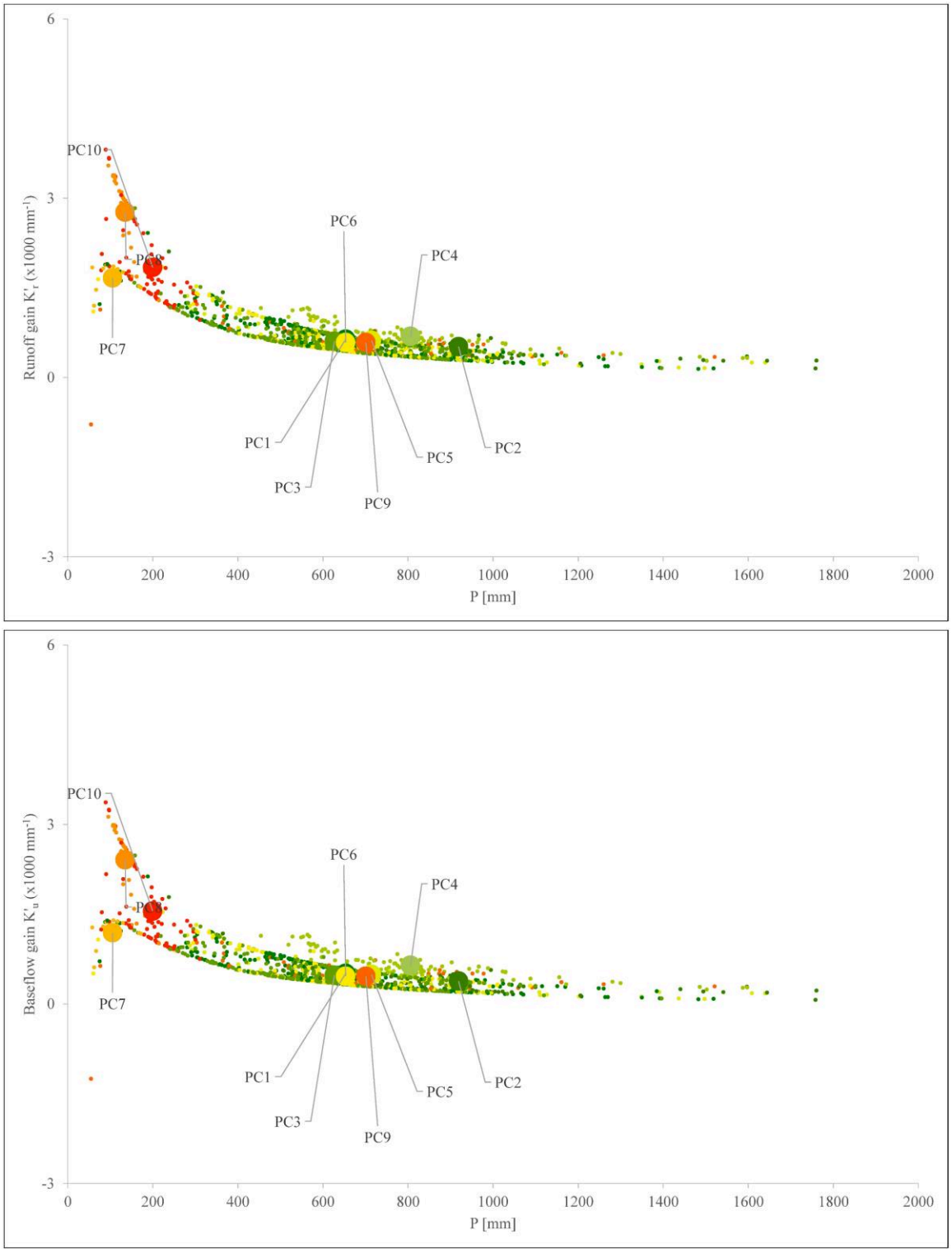

Figure E1 - 4 : Projected regionalised runoff and baseflow gains K'r, and K'u with average values coloured according to physiographic classes based on projected climatic indices under Aladin RCP 4.5 scenario for 2070-2100.

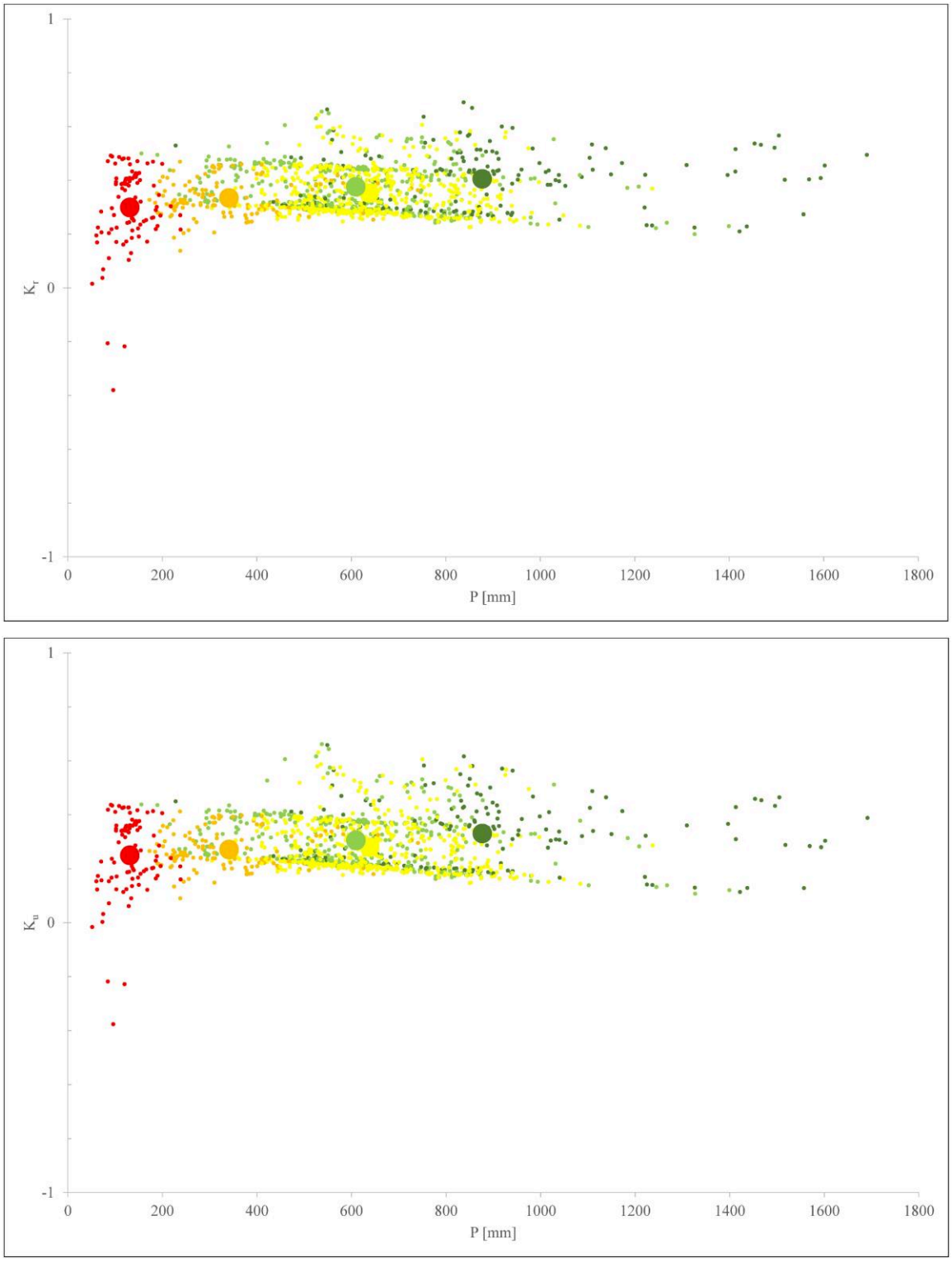

Figure E1 - 5 : Projected regionalised runoff and baseflow coefficient K_r, and K_u with average values coloured according to climatic classes based on projected climatic indices under Aladin RCP 8.5 scenario for 2070-2100.

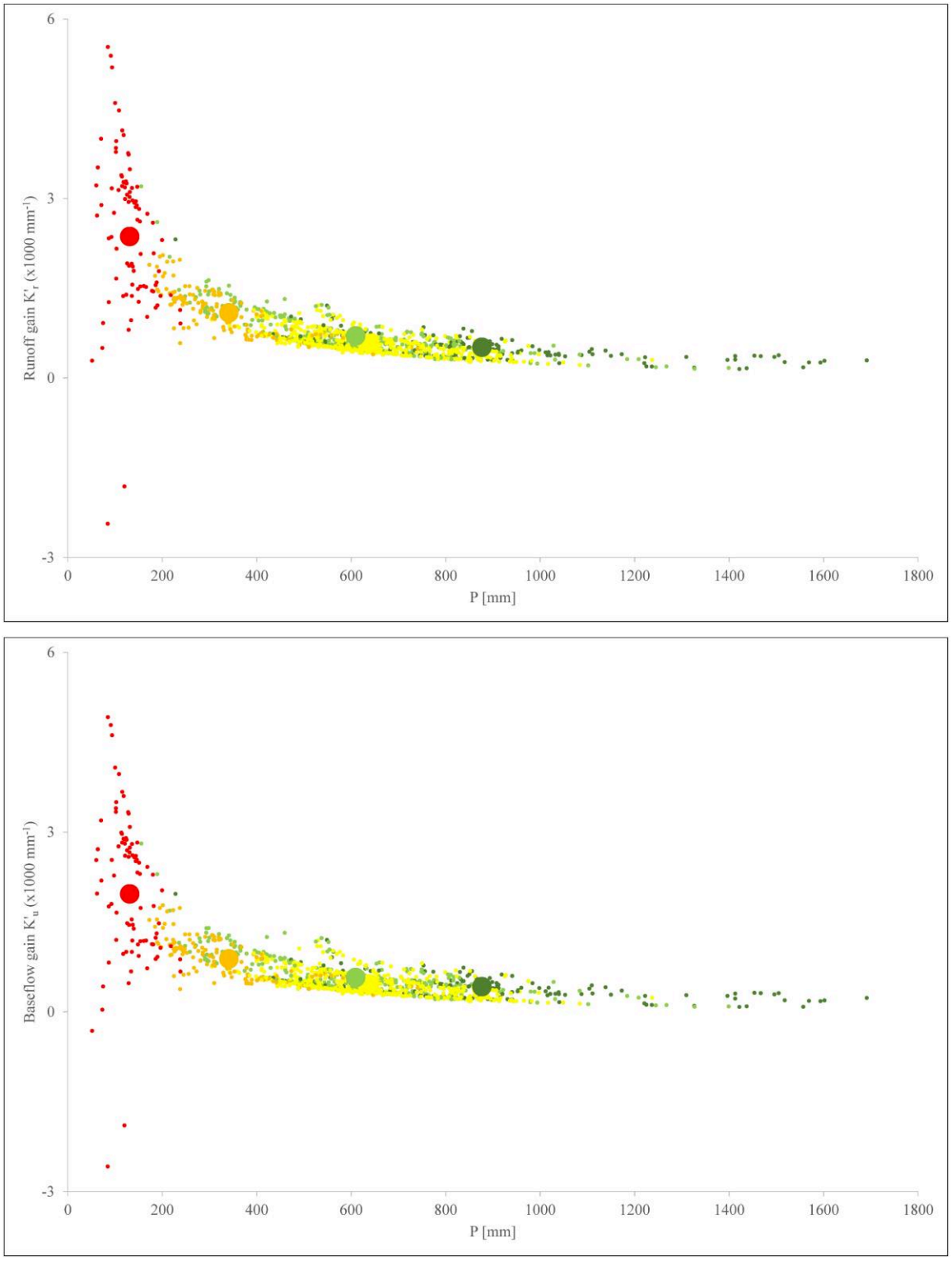

Figure E1 - 6 : Projected regionalised runoff and baseflow gains K'$_r$, and K'$_u$ with average values coloured according to climatic classes based on projected climatic indices under Aladin RCP 8.5 scenario for 2070-2100.

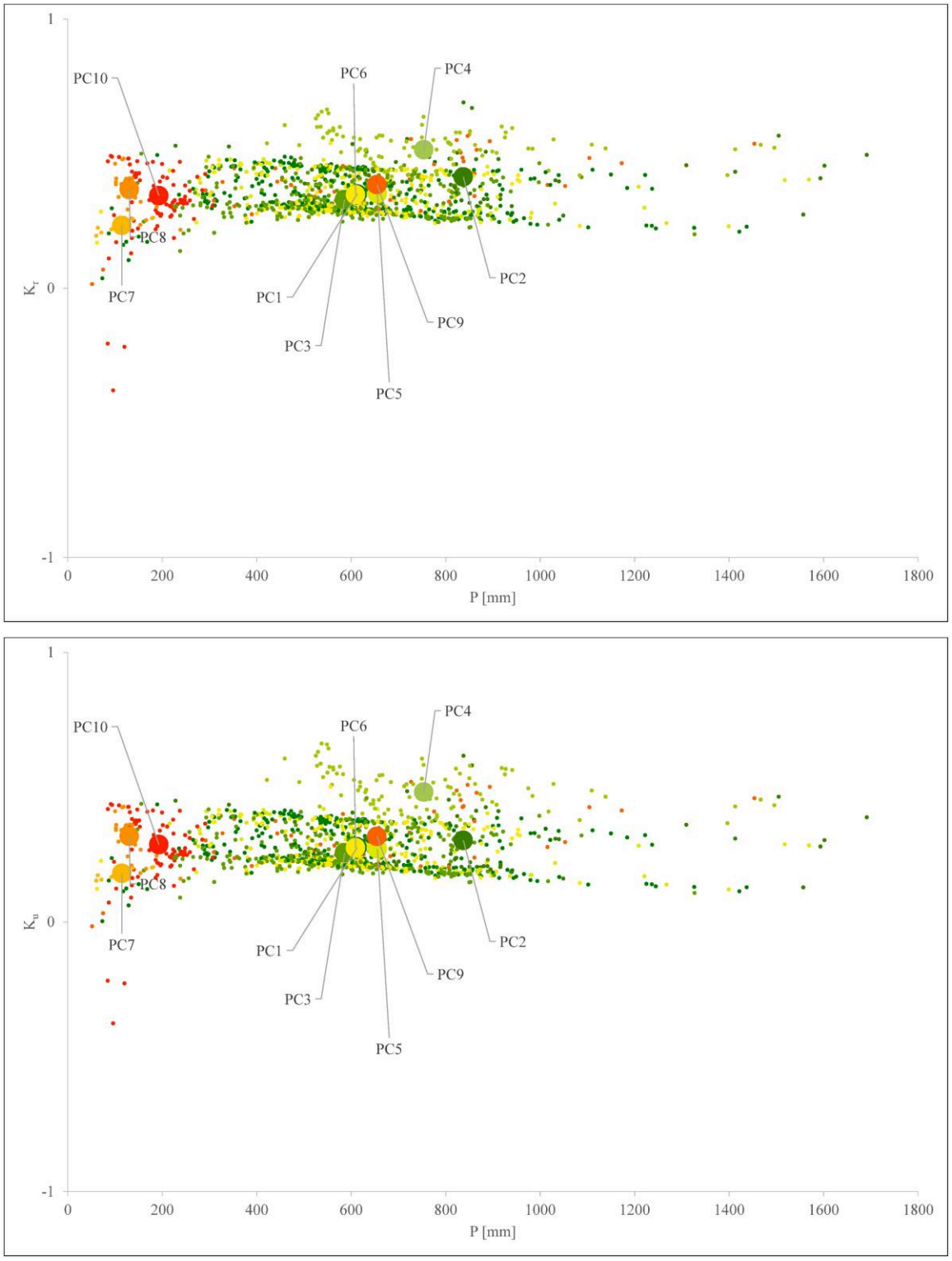

Figure E1 - 7 : Projected regionalised runoff and baseflow coefficient K_r, and K_u with average values coloured according to physiographic classes based on projected climatic indices under Aladin RCP 8.5 scenario for 2070-2100.

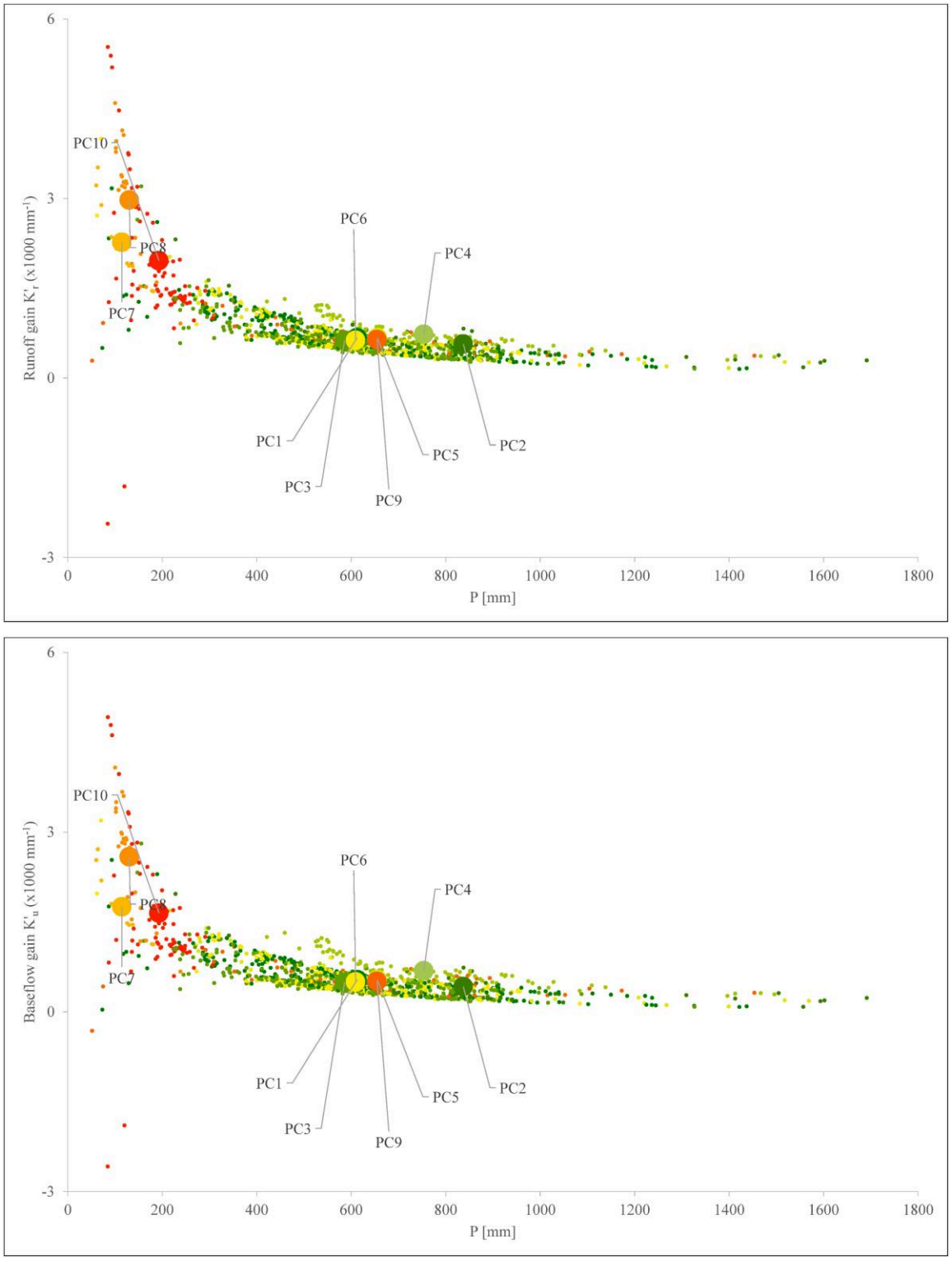

Figure E1 - 8 : Projected regionalised runoff and baseflow gains K'r, and K'u with average values coloured according to physiographic classes based on projected climatic indices under Aladin RCP 8.5 scenario for 2070-2100.

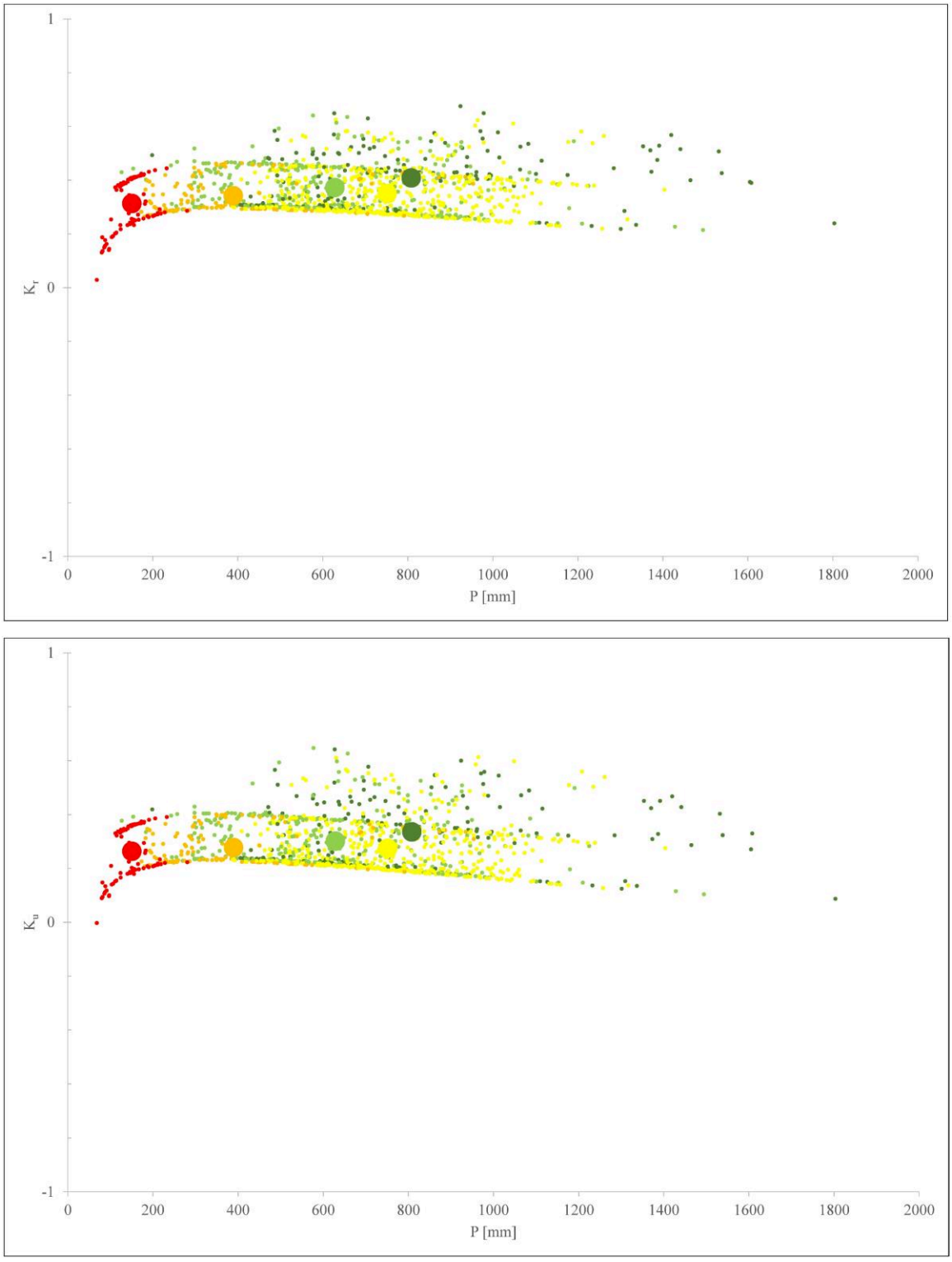

Figure E1 - 9 : Projected regionalised runoff and baseflow coefficient K_r, and K_u with average values coloured according to climatic classes based on projected climatic indices under CCLM RCP 4.5 scenario for 2070-2100.

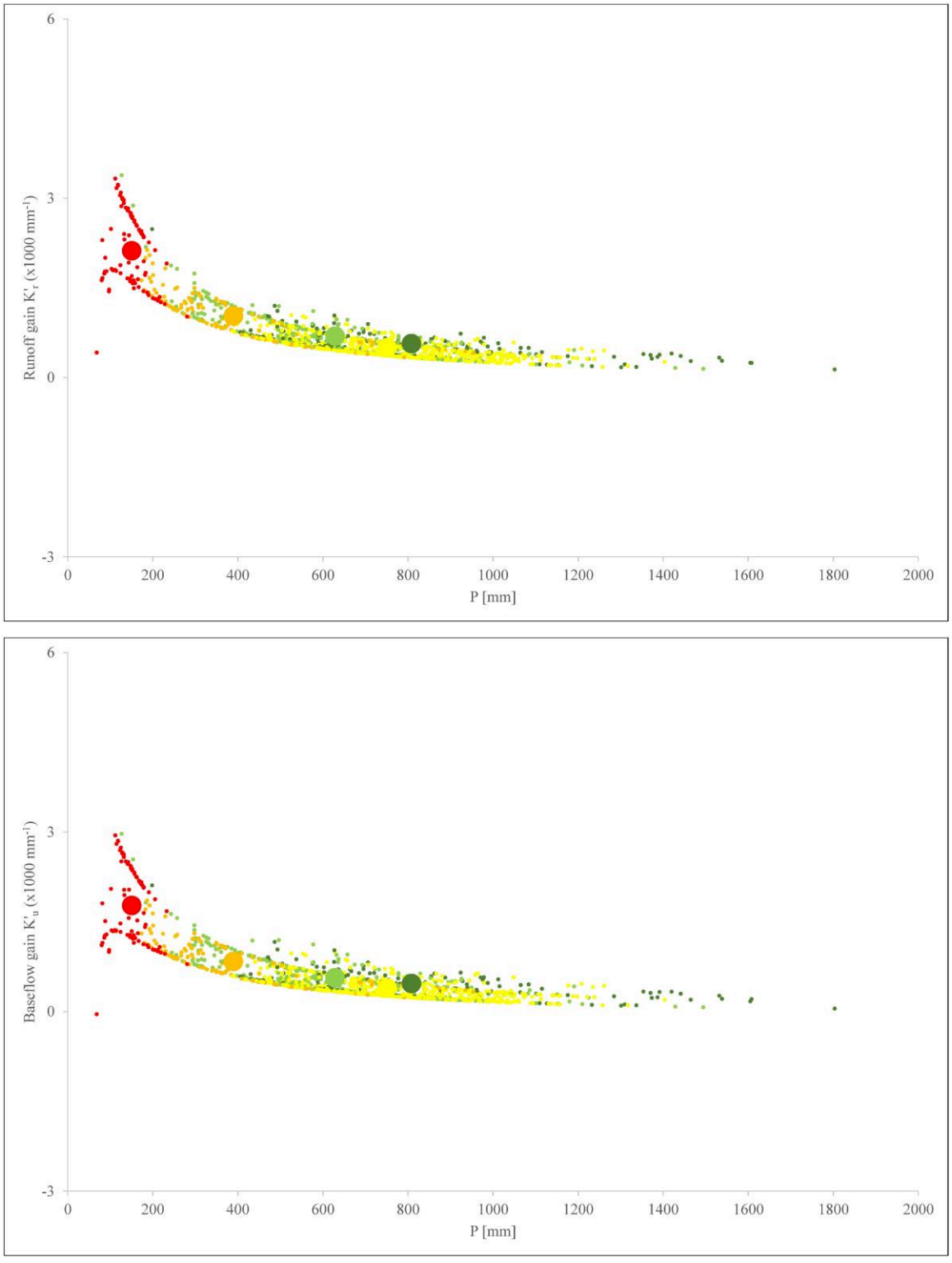

Figure E1 - 10 : Projected regionalised runoff and baseflow and gains K'r, and K'u with average values coloured according to climatic classes based on projected climatic indices under CCLM RCP 4.5 scenario for 2070-2100.

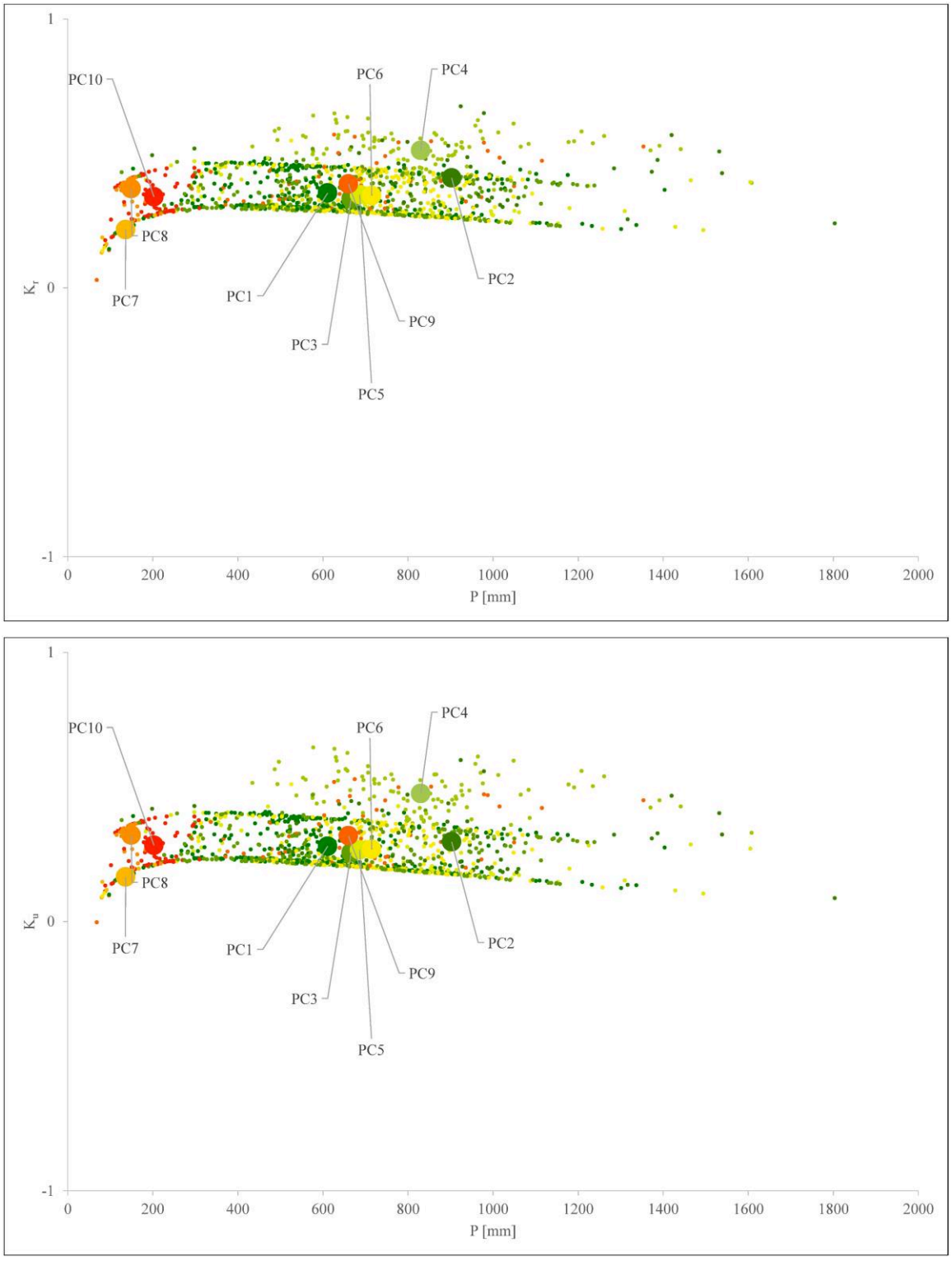

Figure E1 - 11 : Projected regionalised runoff and baseflow coefficient K_r, and K_u with average values coloured according to physiographic classes based on projected climatic indices under CCLM RCP 4.5 scenario for 2070-2100.

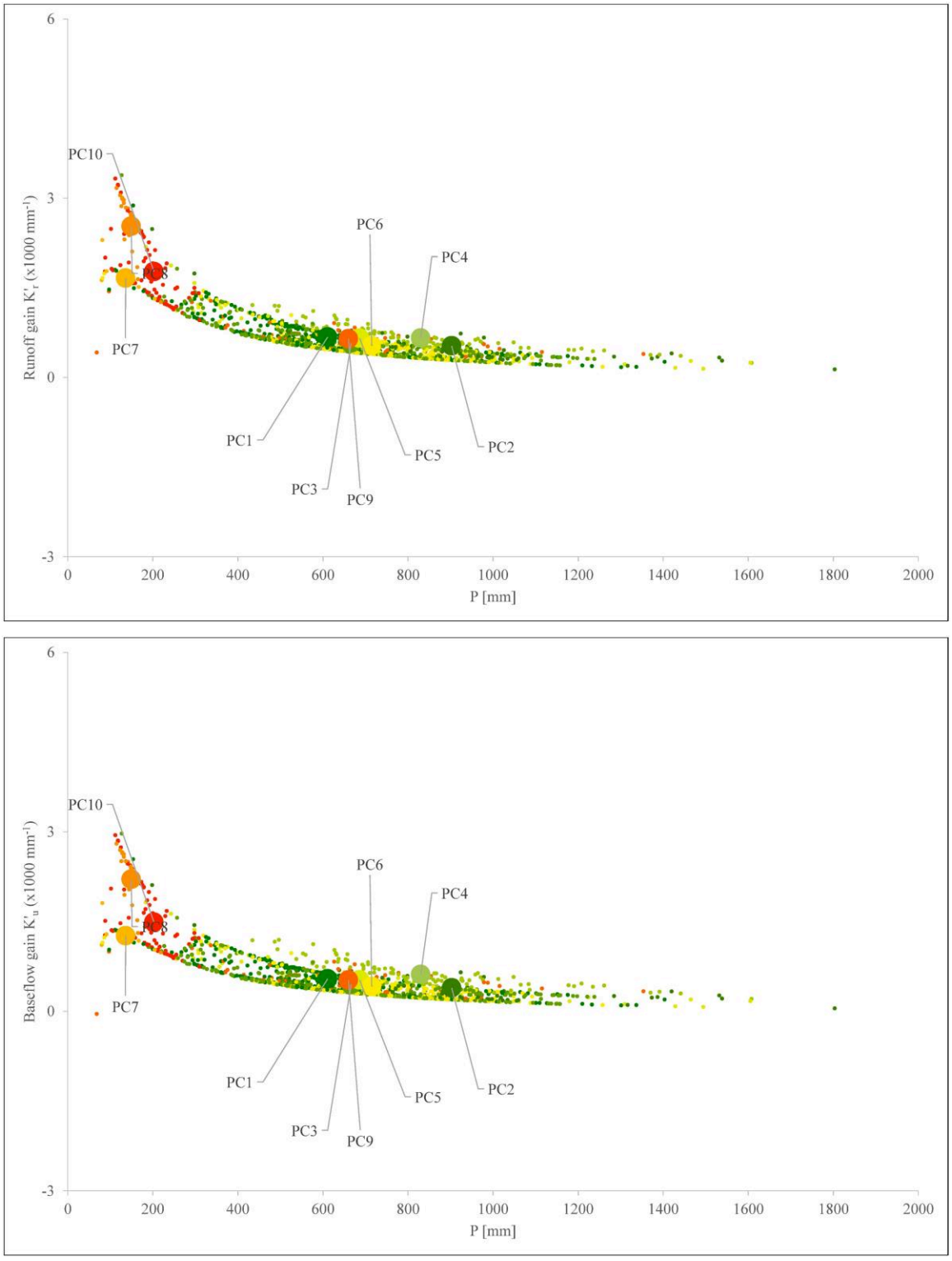

Figure E1 - 12 : Projected regionalised runoff and baseflow gains K'r, and K'u with average values coloured according to physiographic classes based on projected climatic indices under CCLM RCP 4.5 scenario for 2070-2100.

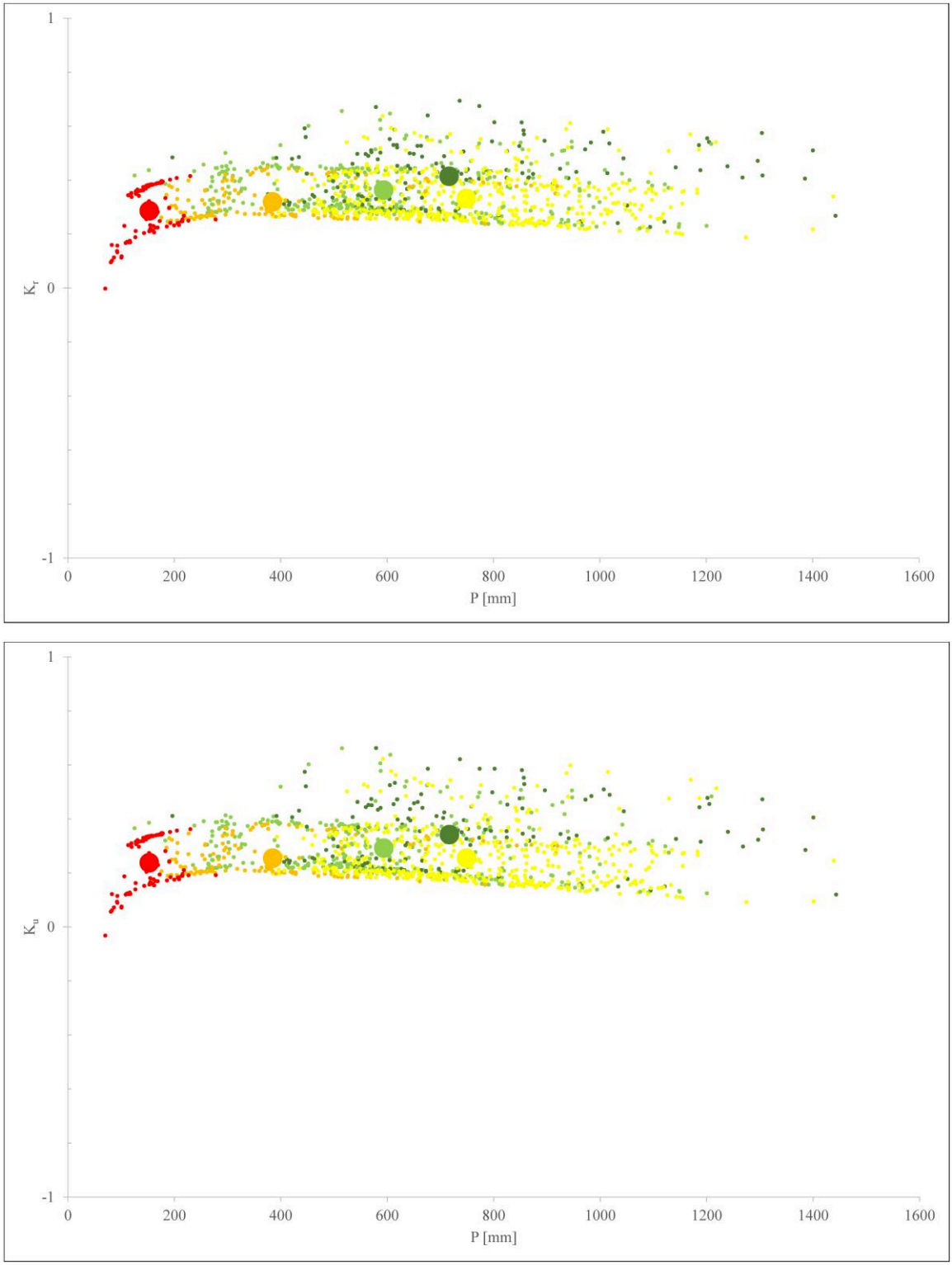

Figure E1 - 13 : Projected regionalised runoff and baseflow coefficient K_r, and K_u with average values coloured according to climatic classes based on projected climatic indices under CCLM RCP 8.5 scenario for 2070-2100.

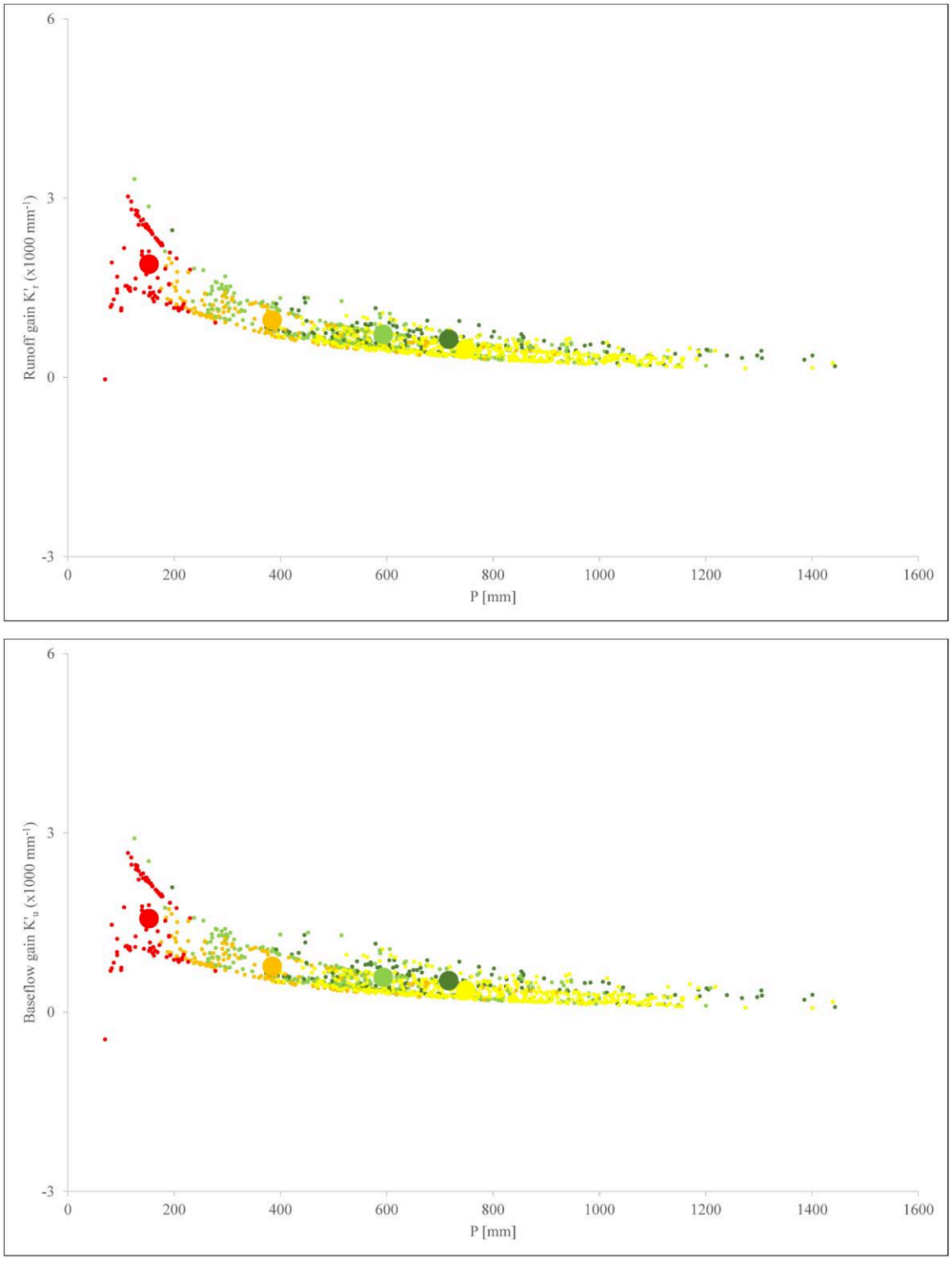

Figure E1 - 14 : Projected regionalised runoff and baseflow gains K'r, and K'u with average values coloured according to climatic classes based on projected climatic indices under CCLM RCP 8.5 scenario for 2070-2100.

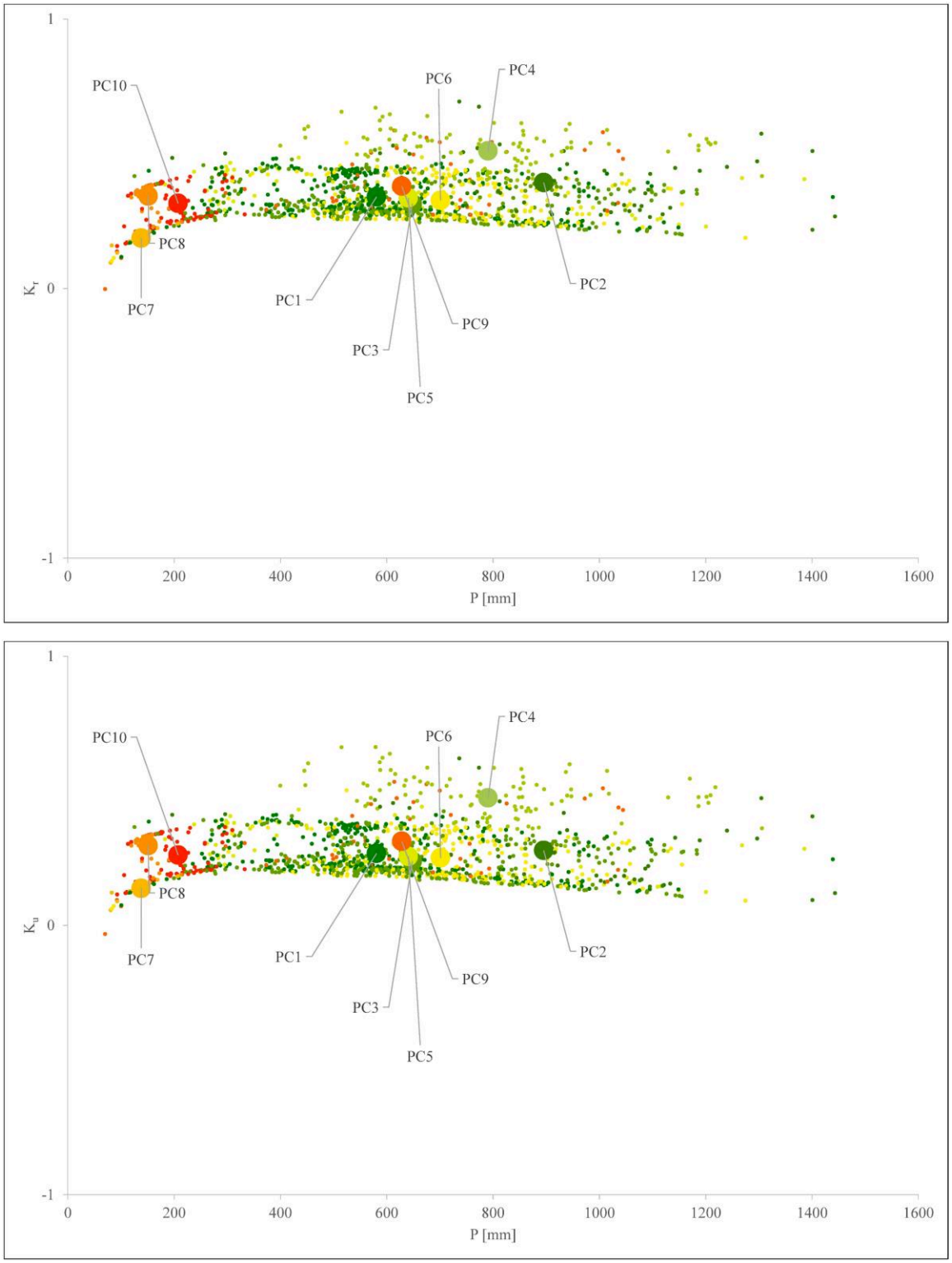

Figure E1 - 15 : Projected regionalised runoff and baseflow coefficient K_r, and K_u with average values coloured according to physiographic classes based on projected climatic indices under CCLM RCP 8.5 scenario for 2070-2100.

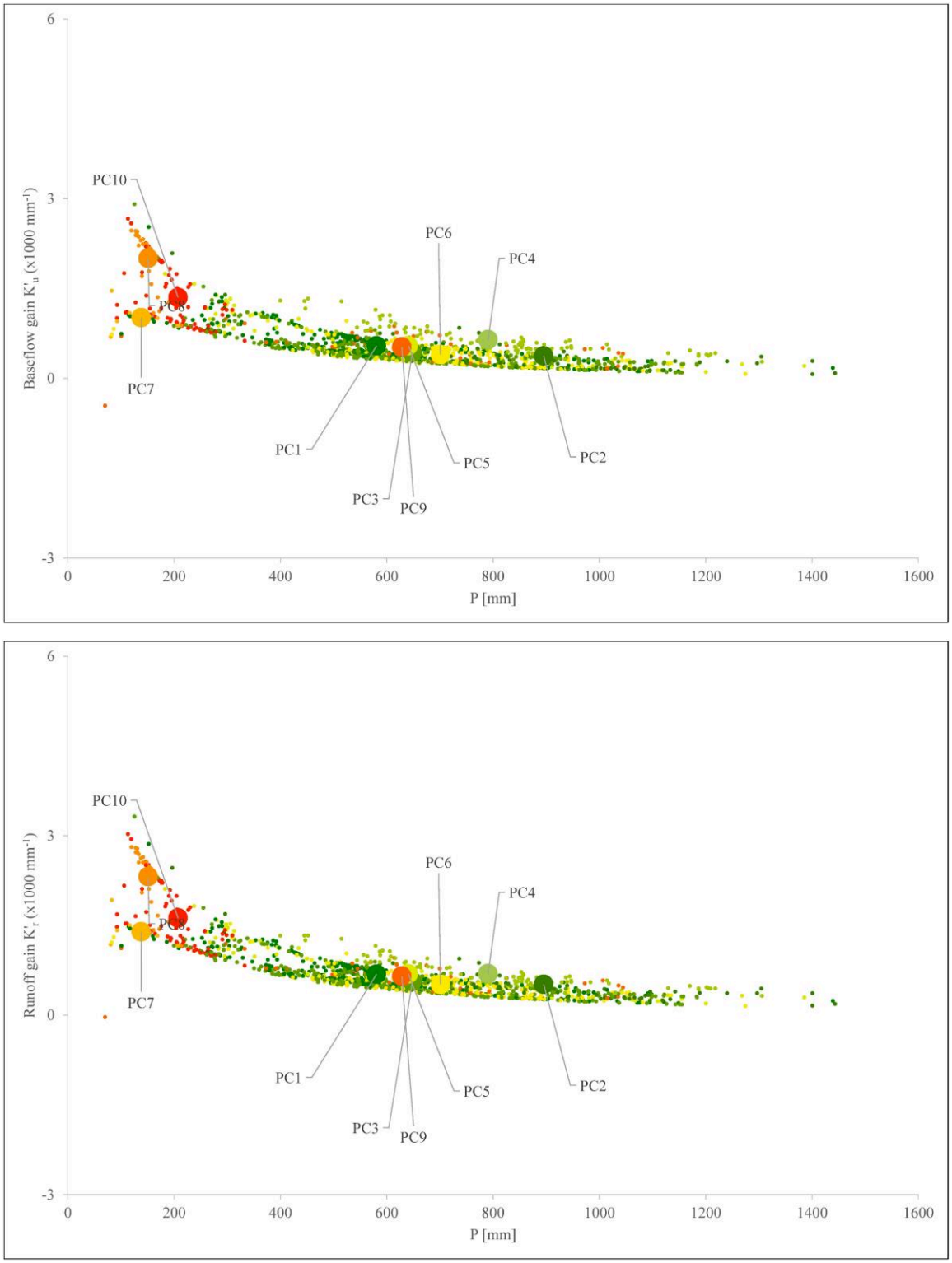

Figure E1 - 16 : Projected regionalised runoff and baseflow gains K'r, and K'u with average values coloured according to physiographic classes based on projected climatic indices under CCLM RCP 8.5 scenario for 2070-2100.

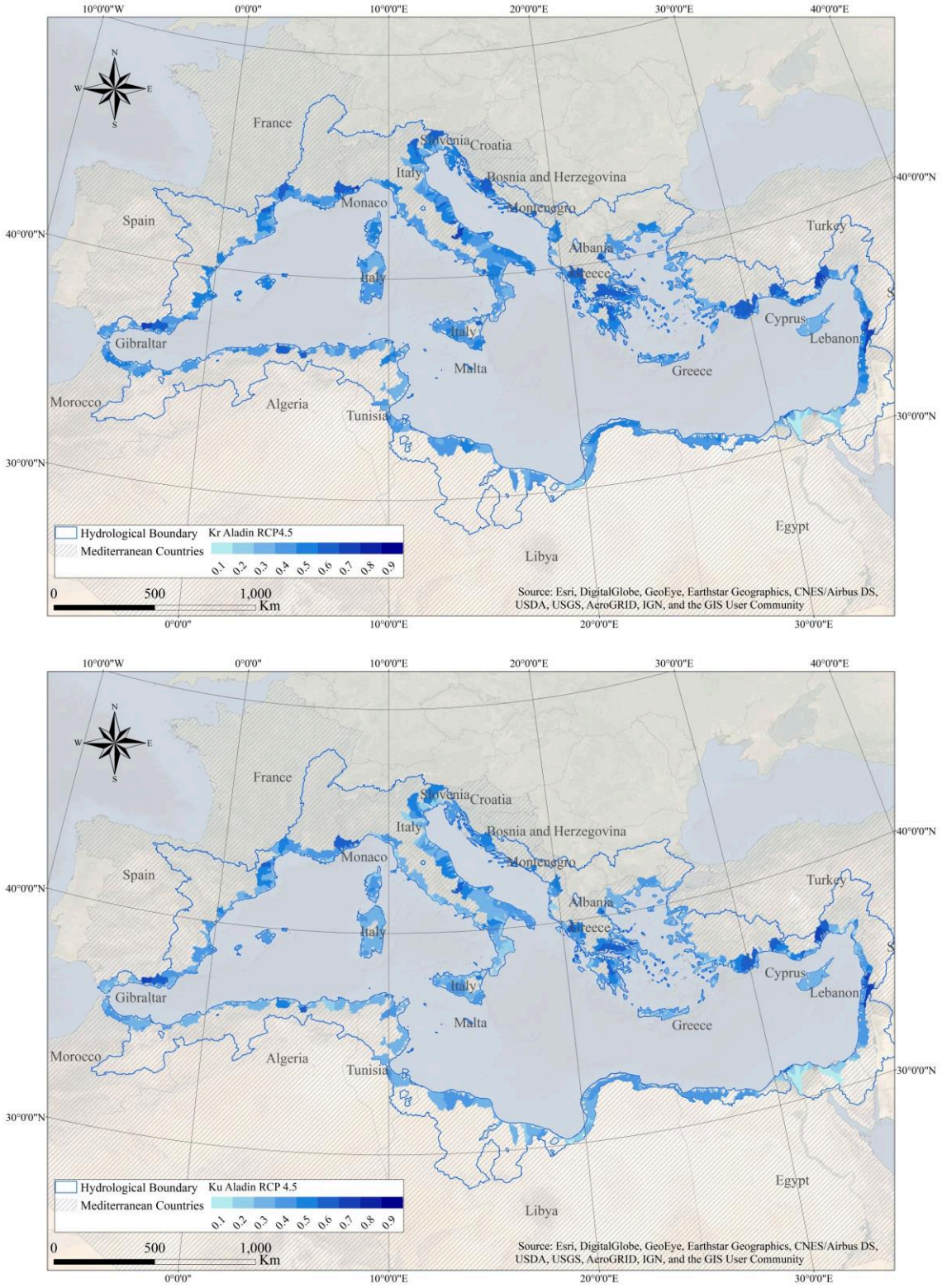

Figure E1 - 17 : Spatial distribution of the projected regionalised runoff and baseflow coefficients K_r and K_u based on projected climatic indices under ALADIN RCP4.5 scenarios for 2070-2100.

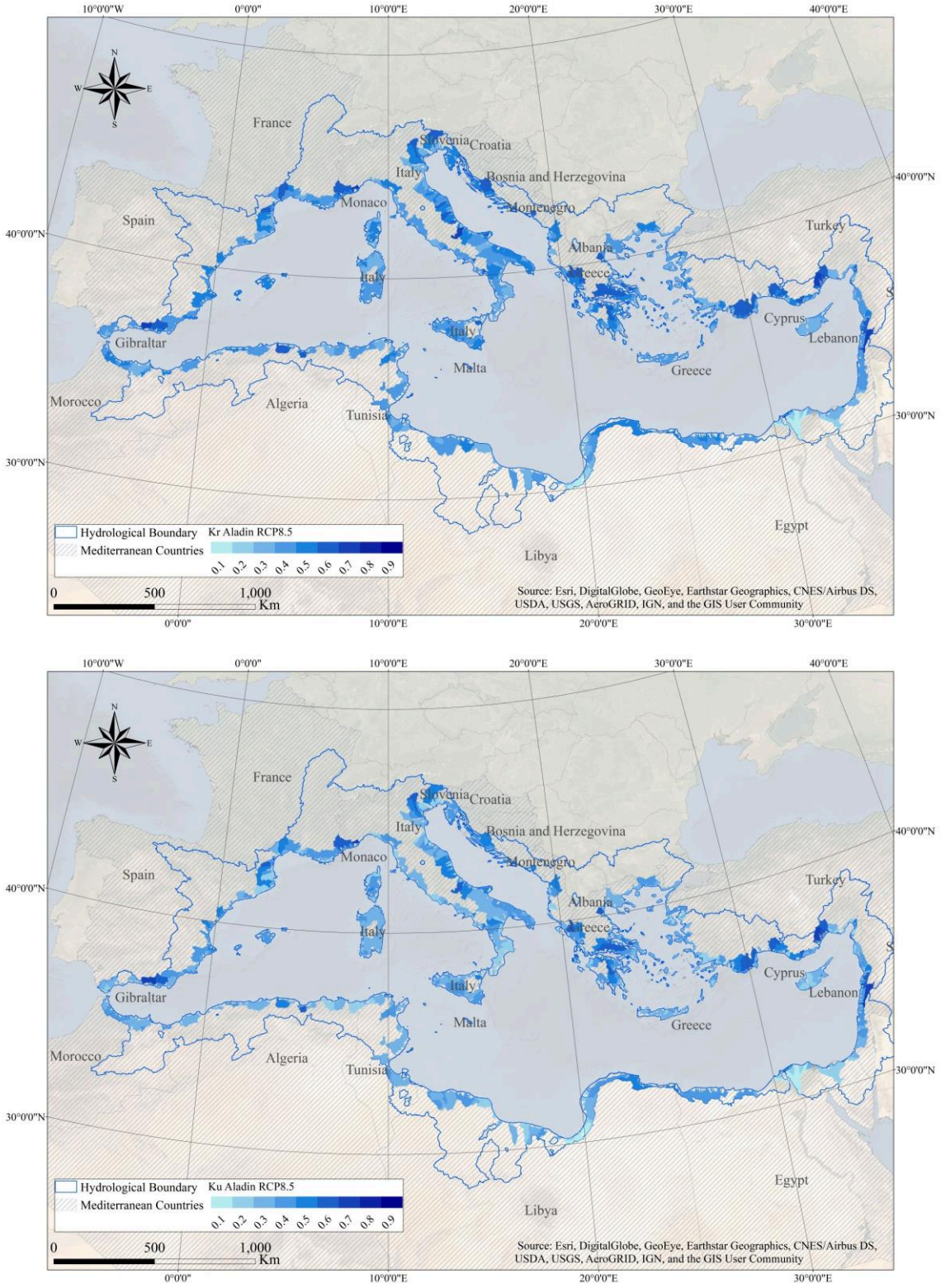

Figure E1 - 18 : Spatial distribution of the projected regionalised runoff and baseflow coefficients K_r and K_u based on projected climatic indices under ALADIN RCP8.5 scenarios for 2070-2100.

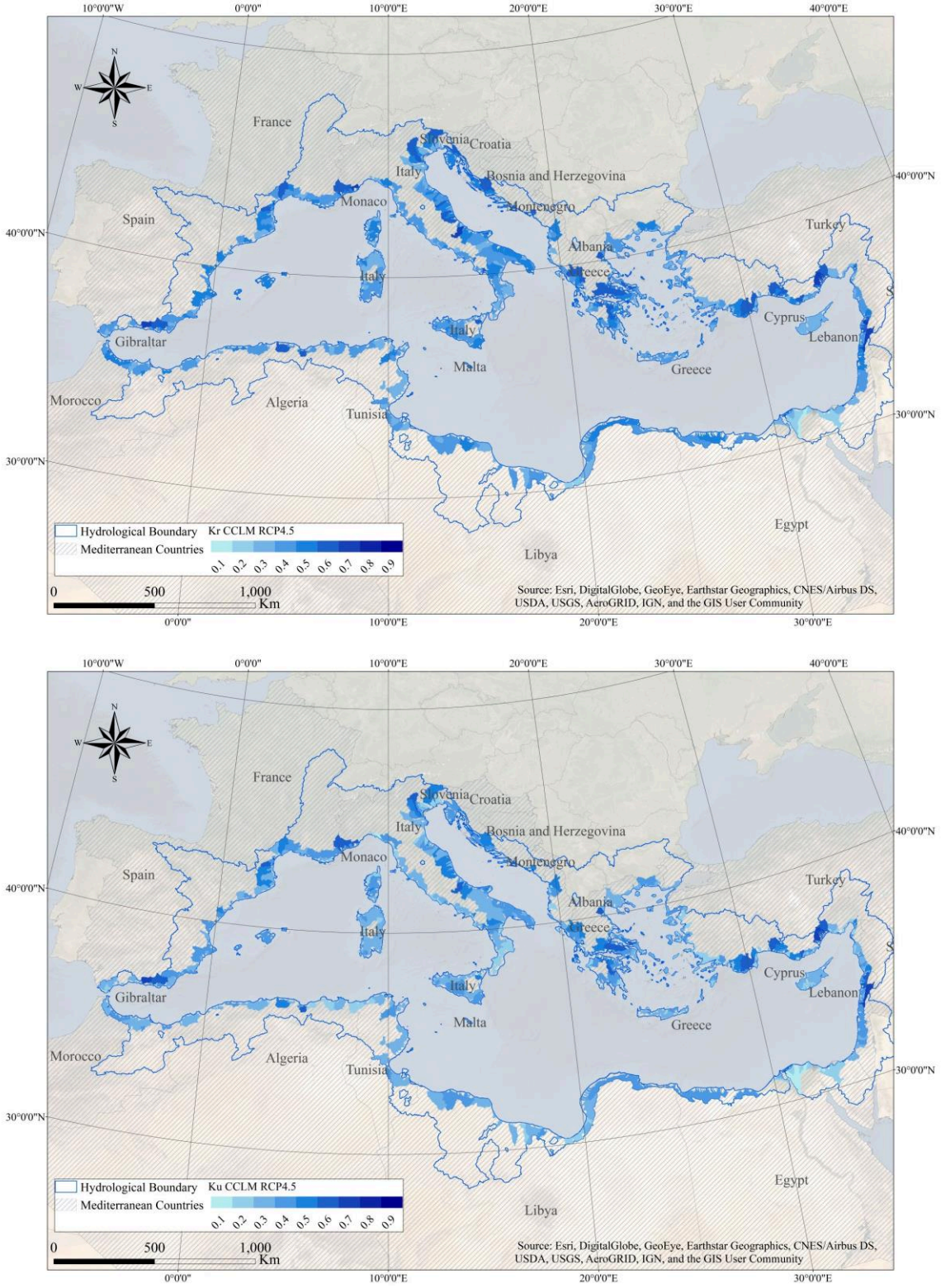

Figure E1 - 19 : Spatial distribution of the projected regionalised runoff and baseflow coefficients K_r and K_u based on projected climatic indices under CCLM RCP4.5 scenarios for 2070-2100.

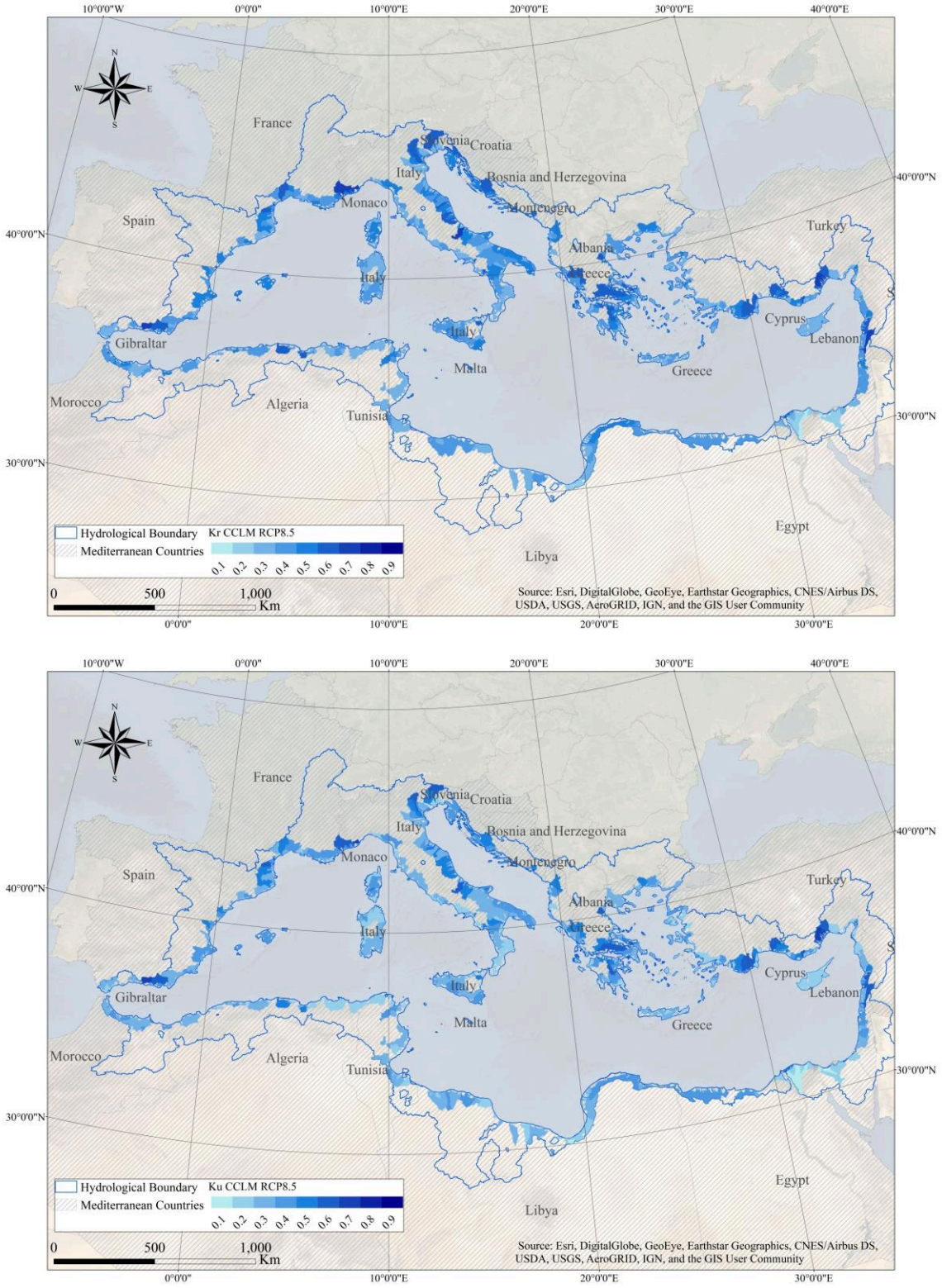

Figure E1 - 20 : Spatial distribution of the projected regionalised runoff and baseflow coefficients K_r and K_u based on projected climatic indices under CCLM RCP4.5 scenarios for 2070-2100.

Table E1 - 1: Climatic classes water balance runoff coefficients and gains projection under RCM ALADIN and CCLM RCP scenarios with evolution ratio in italic blue

	CLASS	K_r		K_u		K'_r		K'_u	
BASELINE 1970-2000	CC1	0.03		0.01		-0.00016		-0.00029	
	CC2	0.26		0.21		0.00080		0.00063	
	CC3	0.35		0.28		0.00053		0.00042	
	CC4	0.38		0.31		0.00068		0.00056	
	CC5	0.49		0.41		0.00064		0.00054	
ALADIN RCP 4.5 2070-2100	CC1	0.30	895%	0.25	2403%	0.00225	1507%	0.00187	744%
	CC2	0.35	33%	0.28	35%	0.00106	33%	0.00087	37%
	CC3	0.36	3%	0.29	2%	0.00054	3%	0.00043	3%
	CC4	0.37	-1%	0.30	-2%	0.00066	-3%	0.00054	-4%
	CC5	0.40	-18%	0.33	-20%	0.00049	-24%	0.00040	-26%
ALADIN RCP 8.5 2070-2100	CC1	0.30	896%	0.25	2397%	0.00237	1578%	0.00197	778%
	CC2	0.33	28%	0.27	29%	0.00109	36%	0.00088	40%
	CC3	0.35	0%	0.28	0%	0.00058	9%	0.00046	10%
	CC4	0.38	-1%	0.30	-2%	0.00070	3%	0.00057	2%
	CC5	0.40	-17%	0.33	-20%	0.00051	-20%	0.00042	-22%
CCLM RCP 4.5 2070-2100	CC1	0.31	944%	0.26	2534%	0.00212	1424%	0.00177	711%
	CC2	0.34	31%	0.28	32%	0.00103	29%	0.00084	33%
	CC3	0.35	0%	0.27	-2%	0.00050	-6%	0.00039	-7%
	CC4	0.37	-2%	0.30	-3%	0.00069	1%	0.00056	1%
	CC5	0.41	-17%	0.34	-18%	0.00057	-12%	0.00047	-14%
CCLM RCP 8.5 2070-2100	CC1	0.29	854%	0.24	2277%	0.00189	1283%	0.00156	639%
	CC2	0.32	22%	0.25	21%	0.00096	20%	0.00077	22%
	CC3	0.33	-5%	0.25	-9%	0.00047	-11%	0.00037	-13%
	CC4	0.36	-5%	0.29	-6%	0.00072	5%	0.00058	4%
	CC5	0.41	-15%	0.34	-17%	0.00063	-1%	0.00053	-3%

Table E1 - 2: Physiographic classes water balance runoff coefficients and gains projection under RCM ALADIN and CCLM RCP scenarios with evolution ratio in italic blue

	CLASS	K_r		K_u		K'_r (mm^{-1})		K'_u (mm^{-1})	
BASELINE 1970-2000	PC1	0.35		0.28		0.00059		0.00046	
	PC2	0.43		0.32		0.00057		0.00043	
	PC3	0.32		0.25		0.00056		0.00044	
	PC4	0.58		0.54		0.00077		0.00073	
	PC5	0.35		0.27		0.00063		0.00050	
	PC6	0.34		0.27		0.00050		0.00039	
	PC7	-0.13		-0.15		-0.00189		-0.00199	
	PC8	0.11		0.09		0.00086		0.00070	
	PC9	0.40		0.34		0.00033		0.00024	
	PC10	0.17		0.13		0.00089		0.00069	
ALADIN RCP 4.5 2070-2100	PC1	0.35	*1%*	0.28	*0%*	0.00064	*8%*	0.00051	*10%*
	PC2	0.41	*-4%*	0.30	*-5%*	0.00051	*-10%*	0.00038	*-12%*
	PC3	0.34	*6%*	0.27	*6%*	0.00061	*8%*	0.00048	*9%*
	PC4	0.52	*-11%*	0.48	*-10%*	0.00069	*-11%*	0.00065	*-11%*
	PC5	0.35	*0%*	0.27	*0%*	0.00062	*-2%*	0.00049	*-2%*
	PC6	0.35	*4%*	0.28	*3%*	0.00058	*17%*	0.00046	*18%*
	PC7	0.18	*235%*	0.13	*186%*	0.00167	*188%*	0.00119	*160%*
	PC8	0.36	*228%*	0.31	*248%*	0.00277	*222%*	0.00241	*244%*
	PC9	0.38	*-4%*	0.32	*-7%*	0.00058	*77%*	0.00046	*92%*
	PC10	0.34	*99%*	0.28	*118%*	0.00184	*107%*	0.00155	*125%*
ALADIN RCP 8.5 2070-2100	PC1	0.35	*0%*	0.28	*-1%*	0.00067	*14%*	0.00054	*16%*
	PC2	0.41	*-4%*	0.30	*-5%*	0.00057	*-1%*	0.00042	*-2%*
	PC3	0.33	*3%*	0.26	*3%*	0.00063	*12%*	0.00049	*12%*
	PC4	0.51	*-11%*	0.48	*-11%*	0.00073	*-5%*	0.00069	*-6%*
	PC5	0.35	*0%*	0.27	*0%*	0.00067	*7%*	0.00053	*7%*
	PC6	0.35	*2%*	0.27	*2%*	0.00063	*26%*	0.00050	*28%*
	PC7	0.23	*279%*	0.18	*220%*	0.00227	*220%*	0.00175	*188%*
	PC8	0.37	*233%*	0.32	*253%*	0.00297	*245%*	0.00259	*270%*
	PC9	0.38	*-4%*	0.32	*-7%*	0.00064	*95%*	0.00051	*113%*
	PC10	0.34	*102%*	0.29	*120%*	0.00196	*120%*	0.00165	*139%*
CCLM RCP 4.5 2070-2100	PC1	0.35	*1%*	0.28	*0%*	0.00068	*15%*	0.00054	*18%*
	PC2	0.41	*-5%*	0.30	*-7%*	0.00053	*-7%*	0.00039	*-9%*
	PC3	0.33	*4%*	0.26	*2%*	0.00057	*3%*	0.00045	*2%*
	PC4	0.51	*-12%*	0.48	*-12%*	0.00066	*-15%*	0.00061	*-16%*
	PC5	0.35	*-1%*	0.27	*-2%*	0.00066	*4%*	0.00052	*5%*
	PC6	0.34	*1%*	0.27	*-1%*	0.00053	*6%*	0.00042	*7%*
	PC7	0.22	*266%*	0.17	*210%*	0.00166	*188%*	0.00126	*163%*
	PC8	0.37	*236%*	0.32	*257%*	0.00253	*194%*	0.00220	*215%*
	PC9	0.39	*-3%*	0.32	*-6%*	0.00065	*96%*	0.00052	*117%*
	PC10	0.34	*99%*	0.28	*118%*	0.00177	*99%*	0.00149	*116%*
CCLM RCP 8.5 2070-2100	PC1	0.34	*-3%*	0.27	*-5%*	0.00068	*16%*	0.00054	*18%*
	PC2	0.39	*-9%*	0.28	*-13%*	0.00051	*-10%*	0.00037	*-13%*
	PC3	0.31	*-2%*	0.24	*-5%*	0.00056	*0%*	0.00043	*-2%*
	PC4	0.51	*-12%*	0.47	*-12%*	0.00069	*-10%*	0.00064	*-12%*
	PC5	0.34	*-4%*	0.26	*-5%*	0.00069	*9%*	0.00054	*9%*
	PC6	0.33	*-4%*	0.25	*-7%*	0.00051	*3%*	0.00040	*1%*
	PC7	0.19	*244%*	0.14	*192%*	0.00139	*174%*	0.00101	*151%*
	PC8	0.34	*212%*	0.30	*229%*	0.00232	*169%*	0.00200	*186%*
	PC9	0.38	*-5%*	0.31	*-8%*	0.00065	*97%*	0.00052	*118%*
	PC10	0.32	*86%*	0.26	*101%*	0.00162	*82%*	0.00135	*96%*

APPENDIX E2

EGU General Assembly 2019 Conference Poster

Determination of Hydrologically Homogeneous Mediterranean Catchments based on Multivariate Analysis

Geophysical Research Abstracts
Vol. 21, EGU2019-**PREVIEW**, 2019
EGU General Assembly 2019

Regionalisation of Mediterranean catchments flow characteristics based on Canonical Correlation Analysis

Antoine Allam (1,2), Roger Moussa (1), and Wajdi Najem (2)

(1) Saint Jospeh University, Faculty of Engineering, CREEN, Lebanon (antoine.allam@net.usj.edu.lb), (2) UMR LISAH, Univ. Montpellier, INRA, Montpellier, France (roger.moussa@inra.fr)

Regional analysis is an essential step to improve water management plans and transpose flow characteristics on ungauged catchments. The Mediterranean region limited by the topographical boundary is a highly fragmented area with 1270 catchments ranging between 100 and 3000 km2 and draining towards the Mediterranean Sea. Qualified as one of the most sensitive and challenging regions to climatic and anthropogenic variations and lacking flow measurements, mostly in its southern side, this region stands as a good candidate for regional analysis.
Despite all the research at the regional scale, a specific Mediterranean hydrology is long to be defined yet and require additional research related to the relation between hydrological processes and their climate and physiographic descriptors. This paper seeks to define these relations relying on multivariate analysis approach.
The proposed methodology consists of (1) defining the most contributing climatic and physiographic indices, (2) classifying the catchments using k-means clustering and (3) regionalising flow characteristics based on the physio-climatic similarity issued from a canonical correlation analysis. The main characteristics were uniformly collected across the Mediterranean and a representative data set of catchments covering 15 countries was considered for the regionalisation.
The canonical correlation analysis highlighted homogeneous sub-regions, similar catchments and resulted with a new cartography for Mediterranean catchments hydrological characteristics.

Key words: Canonical Correlation Analysis, Regionalisation, Mediterranean hydrology, physio-climatic similarity

Determination of Hydrologically Homogeneous Mediterranean Catchments Based on Multivariate Analysis

Antoine ALLAM [1, 2], Roger MOUSSA [2], Wajdi NAJEM [1]
[1] CREEN, Saint-Joseph University, Faculty of Engineering, Beirut, Lebanon (antoine.allam@net.usj.edu.lb)
[2] LISAH, University of Montpellier, INRA, IRD, SupAgro, Montpellier, France (roger.moussa@inra.fr)

EGU General Assembly 2019
This presentation participates in OSPP
Outstanding Student Poster & PICO Contest

MOTIVATION

Mediterranean is one of the most sensitive regions to climatic variations and anthropogenic pressures.

- Socio-economically, the demographic evolution is causing critical water stress periods.
- Climatically, the trend towards warming and aridification of the Mediterranean is becoming a fact. Each of the last three decades, the surface of the Earth has been successively warmer than any previous decade since 1850 (IPCC, 2014).
- Hydrologically, the increase of water management challenges facing small administrative divisions require better management plans for medium scale catchments.

The objective is to identify similar Mediterranean catchments through the regionalization of hydrologic indices of a set of donor catchments based on a CCA with their physio-climatic indices.

The mapping of hydrologically homogeneous Mediterranean regions is one of the basic studies to be used by researchers, engineers, governments and international organizations which Mediterranean region form their target study areas. These results could help in catchment scale studies like PUB or regional scale studies like climate, landuse or demographic evolution impact prediction on Mediterranean hydrology.

STUDY AREA & DATABASE

HOW WOULD THE MEDITERRANEAN BOUNDARY BE DEFINED?

- Climatic boundary, defined according to Köppen's classification where a set of regions share similar temperature and precipitation characteristics known for their warm and dry summers and cold and humid winters (Köppen, 1936).
- Topographic boundary, defined by the set of catchments discharging into the Mediterranean Sea (Milano, 2013). This definition neglects some climatic regions like Portugal, part of Spain and give advantage to geographically adjacent regions like Egypt and Libya.
- Agricultural-bioclimatic boundary, defined by the set of regions sharing the same types of vegetation considered as indicators of the Mediterranean region such as olives (Moreno, 2014).
- Administrative boundary, defined by the set of countries adjacent to Mediterranean Sea but has a problematic definition independent of a natural base (Wainwright & Thornes, 2004). This boundary includes several climatic classes and cover larger areas then the topographical limits.

The **Topographic boundary** was adopted as a study area with a set of catchments mostly within the climatic boundary as shown in Figure 1.

HOW MANY CATCHMENTS ARE THERE?

The European Commission's Joint Research Centre (JRC) has done extensive and elaborate work on the delimitation of catchments in Europe and some adjacent countries as part of the "Catchment Characterization and Modelling" (CMM) project (De Jager & Vogt, 2010). HydroSHEDS catchments from World Wildlife Fund project was adopted for Middle East and Northern Africa, (Lehner & Grill, 2013).

According to these databases, there are **3682 catchments** that discharge into the Mediterranean from which **1270 range between 100 and 3000 km² forming 28%** of total area without the Nile.

WHERE DID ALL THIS DATA COME FROM?

Climatic data used for this study has two types,

- WorldClim-2, 1-km resolution climate surface data averaged for each catchment (Fick and Hijmans 2017)
- At sites data collected from several National and International database.

Physiographic data were derived from global databases using GIS.

- Digital Elevation Map (SRTM)
- CLC 2012 map at a scale of 1:1 M from the EAE and GLC 2000 for North African catchments.
- Geologic and lithologic map at a scale of 1:5M (Ian Jackson, 2002; Hartmann, 2012)
- World Karstic Aquifer Map WHYMAP (Chen et al, 2017)
- Soil map at 1:1 M from ESDAC (Panagos & al, 2012)

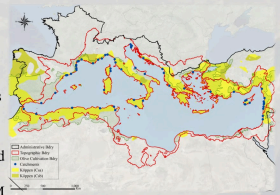

Figure 1. Mediterranean Boundary

Hydrologic set of 55 catchments covering 16 Mediterranean countries was collected from ACA, SAIH, HYDRO, ISPRA, ARSO, DHMZ, YPEKA, ONL, SIEREM, GRDC & MedHycos based on data availability at their outlet and respecting the following criteria

- Hydroclimatic timeseries at a daily timestep, climatic stations located within or at catchment vicinity
- Continuous daily data with at least uninterrupted 10 years mostly between 1950 and present;
- Limited influence of hydraulic structures and management projects.

CLIMATIC CLASSIFICATION

The objective of this section is to establish a fine climate classification of the Mediterranean that highlights climatic continuity and could evaluate change trends from one catchment to another. The proposed approach for both climatic and physiographic classification consists of

(a) PCA to reduce the number of climate indices and consider only the most contributory.

(b) K-Means Classification distributing into 5 catchment classes.

(c) Decision tree construction based on the distances to classes kernels to determine whether a place belongs to a Mediterranean climate or not and to which type it belongs to if so.

The PCA of 18 Climatic Indices showed that I_A, $P_{25\%}$, $S_{P1.5}$, S_{PTm}, I_{Arid}, S_{ETP} and $T_{25\%}$ were the most contributing for the first two components with 70% total variance explained.

The K-Means classification showed that a distribution into 5 classes coincided with a geographical distribution.

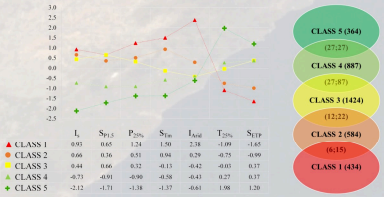

	I_A	$S_{P1.5}$	$P_{25\%}$	S_{PTm}	I_{Arid}	$T_{25\%}$	S_{ETP}
CLASS 1	0.93	0.65	1.24	1.50	2.38	-1.09	-1.65
CLASS 2	0.66	0.36	0.51	0.94	0.29	-0.75	-0.99
CLASS 3	0.44	0.66	0.32	-0.13	-0.42	-0.03	0.37
CLASS 4	-0.73	-0.91	-0.90	-0.58	-0.43	0.27	0.37
CLASS 5	-2.12	-1.71	-1.38	-1.37	-0.61	1.98	1.20

Table 1. Climatic Classes Kernels

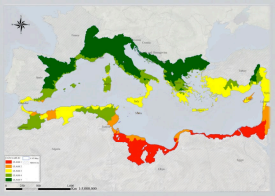
Figure 2. Climatic Classification

Climatic classification is a fuzzy classification with several arbitrary classes. The analysis of interclass connectivity showed that climate is continuous from one place to another, since some catchments can meet the membership criteria of adjacent classes.

The Mediterranean climatic characteristics and specifically precipitation seasonality, main contributor to the PCA climatic classification, plays a key role in the hydrological mechanisms of Mediterranean catchments and flow intermittence. The climatic classification carried out in this study will be analysed within the framework of a hydrological regionalization hereafter along with hydrological and physiographic characteristics.

PHYSIOGRAPHIC CLASSIFICATION

Physiographic Indices described catchments shapes, landform, geology & karst, Available Water Capacity, soil types, landuse, etc…. PCA/K-Means classification was then applied on the 1270 catchments dataset and reduced the number of PIs to 13 with A, Z_{Mean}, ZS_{Mean}, T_AWC, Leptosols and CLC2&3 subtypes as the most contributing in the first 5 components and 64% of total variance explained.

K-Means clustering into 10 classes showed a widespread diversity all over the Mediterranean with kernels' indices showing mixed distribution.

Average area A ranges between 180 and 838 km2 except for Class 9 representing wide cultivated catchment of 2146 km2. Average altitude Z_{Mean}, ZS_{Mean} and I_{Hypso} indicate morphological contribution with high landforms provoking orographic precipitations if exposed to cold fronts case of Class 4 with a snow cover lasting over 1 month/year and low landforms dissipate any possible precipitation and permit desertic influence in North Africa through low corridors case of Class 7, 8 and 10 preventing any vegetation except for sparse shrubs or herbaceous covers.

T_AWC conditions catchments natural landcover, accordingly, it was deduced that only shrubs and needle leaved trees grow in leptosols, low T_AWC and high seasonality, case of Class 6 dominant in East Mediterranean region. Highly cultivated and managed catchments are dominant in North Mediterranean countries and Italy where low lands and wide fields are suitable for agricultural activities Class 1 and 9. Mixed leaved tree forests dominant in North West Mediterranean Class 5, while broadleaved trees preferred North Eastern Mediterranean where high T_AWC and low seasonality reigns case of Class 2.

KNOW YOUR CATCHMENT? CLASSIFY IT!!!

CLASS	NO	REGION	DESCRIPTION	A (km²)	ZMean (m)	ZSMean (m)	T_AWC (mm)	Leptosols (%)	BA (%)	CMA (%)	SC-COD (%)	SHC (%)	TC-BCD (%)
1	304	North West	Small, Highly Cultivated and Managed at 70%	286	184	-	50.8	11%	1%	71%	7%	1%	2%
2	62	South West & Italy	Broadleaved Tree Covered at 60%	415	497	224	51.3	12%	0%	10%	7%	0%	60%
3	351	Mediterranean	No specific overwhelming influence	221	289	-	49.6	13%	1%	12%	34%	3%	2%
4	105	North and East	High altitude with Snow and Karst influence	662	871	1462	38.6	51%	1%	16%	30%	4%	8%
5	88	North West	Mixed leaf Tree Covered 26 %	266	398	-	50.8	17%	0%	19%	8%	2%	12%
6	190	East & Libya	Shrub Covered at 50 %, low T_AWC and Leptosols at 78%	181	341	-	27.4	79%	0%	13%	52%	1%	1%
7	10	Sinai	Desertic	730	107	-	0.8	0%	87%	0%	0%	8%	0%
8	29	Egypt, Libya	Desertic	838	124	-	51.6	16%	70%	0%	0%	25%	0%
9	49	Mediterranean	Wide and Highly Cultivated & Managed at 50% with Snow Influence	2146	411	428	50.3	26%	0%	49%	11%	4%	12%
10	75	Egypt Libya Tunisia	Semi Desertic, Sparse Herbaceous or Shrub Covered at 87%	537	133	-	49.5	19%	5%	1%	3%	87%	0%

Table 2. Physiographic Classes Kernels

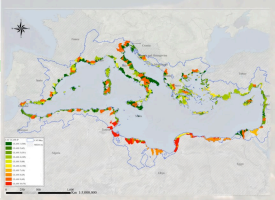
Figure 3. Physiographic Classification

HYDROLOGIC HOMOGENEITY

A Canonical Correlation Analysis was performed between the most contributing PCIs obtained previously and 90-days HIgh-flow & Low-flows magnitude and frequency indices to determine hydrologically homogeneous Mediterranean catchments. CCA results for both HF and LF, illustrated in correlation circles (figure 4), highlight a relationship between the two groups of indices with a correlation of 0.83 for the first canonical variable and zero value for Wilks significance test. The most significant P-CIs were found to be A, $T_{25\%}$, MAP and T_AWC.

Another valuable illustration is the sample dataset representation on the canonical space of the P-CIs and HIs based on the regression equations from raw coefficients shown in figure 5. Scatter diagrams didn't show any organized distribution at first but once coloured according to classes, homogeneous clusters were well identified with limited overlapping between class.
The similarity of catchments distribution between diagrams is observable, where catchments of same class are evenly positioned vis-a-vis other catchments in both physio-climatic and hydrological canonical variables charts.

	HIGH FLOWS				LOW FLOWS			
Canonical Variable	Eigenvalue	Pct. %	Canon Cor.	Sig. of F	Eigenvalue	Pct. %	Canon Cor.	Sig. of F
1	2.17	88.21	0.83	0.00	2.43	92.12	0.84	0.00
2	0.29	11.79	0.47	0.01	0.21	7.9	0.41	0.02
	Correlation		Coefficients		Correlation		Coefficients	
PCIs	1	2	1	2	1	2	1	2
T_AWC	0.23	-0.74	-0.14	-0.80	0.00	-0.73	0.10	-0.75
A	-0.76	0.38	0.77	0.29	0.58	0.15	-0.55	0.52
MAP	-0.75	-0.44	0.75	-0.42	0.44	-0.83	-0.46	-0.21
$T_{25\%}$	-0.83	-0.32	0.83	0.06	0.28	0.49	-0.26	-0.49
HIs	1	2	1	2	1	2	1	2
DH_V/DL_V	-0.95	0.31	0.91	0.42	0.78	0.69	-0.87	0.57
FH_V/FL_V	-0.55	-0.83	0.66	-0.75	0.44	-0.94	-0.32	-1.00

Table 3. CCA Results

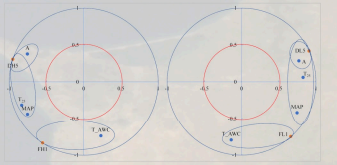

Figure 4. Correlation Circles

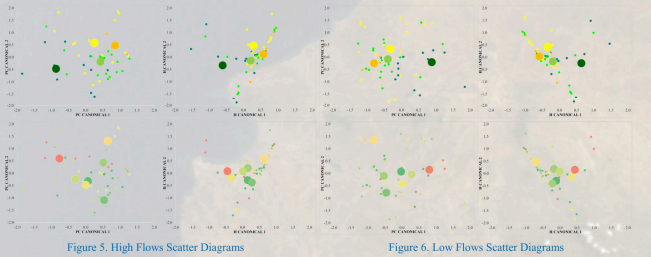
Figure 5. High Flows Scatter Diagrams

Figure 6. Low Flows Scatter Diagrams

DISCUSSION

A hydrological database was developed for the Mediterranean region including climatic, physiographic and hydrologic data with the focus on 1270 catchments ranging between 100 and 3000 km² and outflowing towards Mediterranean Sea. The main challenge consisted of the spatial spread and the work on a very wide and diversified area.

Relying on multivariate analysis methods, PCA and K-Means were performed and catchments were clustered into 5 climatic and 10 physiographic classes. CCA helped identifying hydrological homogeneity out from physio-climatic indices. The illustration of canonical diagrams according to their climatic and physiographic clusters helped identifying the homogeneous clusters in the canonical spaces. The climatic indices might have forced some spatial clustering due to their uniform distribution despite that physiographic indices are very variable across the Mediterranean.

This homogeneity will serve for regionalizing flow indices and water balance metrics across the Mediterranean, emphasizing the assumption that if catchments attributes are similar, one would expect a hydrologic similarity. This could be validated by also applying CCA and multiple regression separately for each of the physiographic classes.

Mediterranean hydrological sensitivity to climatic and anthropogenic variations could now be tested for

- Socio-economic trends of cultivation and demographic change
- Climate change trends
- Water management optimisation
- Discovery of similar or exceptional catchments

SUMMARIES SUBMITTED TO ADUM

RESUME DE LA THESE EN FRANÇAIS

En Méditerranée, les ressources en eau sont plus que jamais exposées à de grands défis; les besoins croissants de l'agriculture, l'industrie, le tourisme, le développement urbain, démographique et l'évolution climatique.

Cette thèse vise à caractériser les bassins versants méditerranéens avec quatre objectifs motivés par la recherche d'une hydrologie méditerranéenne spécifique.

- Le premier consiste à rassembler une base de données hydrologique complète avec comme zone d'étude la limite hydrologique des bassins qui s'écoulent vers la Méditerranée.
- Le deuxième, à établir une nouvelle classification climatique pour l'hydrologie basée sur des indices climatiques spécifiques à la Méditerranée tels que la saisonnalité des précipitations et l'aridité.
- Le troisième, à effectuer une classification physiographique de tous les bassins en fonction des indices de relief, d'occupation du sol, etc. pour mettre en évidence la variabilité méditerranéenne.
- Le quatrième, à effectuer une analyse approfondie du bilan hydrologique de 55 bassins versants méditerranéens selon les différents modèles fonctionnels tels avancés par Budyko (1974), L'vovich (1979), élaborés par Ponce & Shetty (1995) et Sivapalan (2011), pour vérifier la variabilité hydrologique et la similarité entre tous les bassins versants et entre les mêmes classes climatiques et / ou physiographiques.

La classification climatique en 5 classes coïncide avec une distribution géographique allant du climat le plus sec et saisonnier au Sud vers le moins saisonnier et plus humide au Nord. L'impact du changement climatique sur cette classification, suivant les scénarios RCP 4.5 et 8.5, évalué pour la période 2070-2100 avec les modèles climatiques régionaux ALADIN et CCLM développés dans le cadre du projet MED-CORDEX, a indiqué une évolution de la région méditerranéenne vers le climat aride. Les classes situées au Nord évolueront lentement vers des classes côtières modérées ce qui pourrait affecter les régimes hydrologiques en raison des saisons humides plus courtes et des fontes précoces des neiges.

La classification et l’analyse des caractéristiques physiographiques, principalement le relief a révélé l’existence d'une variabilité microclimatique masquée par l'homogénéité macro-climatique. Cette variabilité microclimatique est la cause principale de la variabilité naturelle de la couverture végétale.

L'analyse du bilan hydrologique selon la modélisation fonctionnelle, a mis en évidence une tendance méditerranéenne alignée avec le contexte climatique général. En effet, le climat est le principal déterminant de l'hydrologie méditerranéenne, mais n’est pas unique, puisque l’homogénéité hydrologique a été identifiée pour la classe physiographique des bassins versants montagneux karstiques et influencés par la neige malgré les différents climats, avec les débits de base et coefficients de ruissellement les plus élevés.

La régionalisation a permis aussi de prévoir l'impact du changement climatique sur les coefficients de ruissellement et d’écoulement souterrain, selon les mêmes scénarios du MED-CORDEX. Dans l'ensemble, l'évolution projetée a principalement affecté les extrêmes, minimisant ainsi la variabilité interclasse et augmentant l'homogénéité des bassins versants. Les bassins versants se sont rapprochés des classes les plus méditerranéennes sans changer leurs tendances avec toujours les bassins karstiques et sous influence de la neige les plus productifs.

L'alerte climatique et les effets anthropiques appellent à des mesures d'adaptation et d'atténuation urgentes qui devraient être incluses dans les futures stratégies nationales et plans de gestion des ressources en eau et qui devraient être davantage basées sur la recherche régionale en approfondissant les connaissances sur la variabilité spatiale et temporelle des ressources hydrologiques partout dans la Méditerranée.

RESUME DE LA THESE EN ANGLAIS

Mediterranean water resources usually available in this region are now, more than ever, exposed to continuous increasing demand for agriculture, industry, tourism, urban and demographic development, and climate evolution.

This PhD aims to characterise Mediterranean catchments, for that we have four objectives motivated by the quest for a specific Mediterranean hydrology.

- The first consists of collecting an inclusive hydrological database including with the hydrological boundary as the project area.
- The second to establish a new high-resolution climatic classification for hydrology purposes based on Mediterranean specific climate indices like precipitation seasonality and aridity.
- The third, to carry out a physiographic classification of all Mediterranean catchments based on landform, landcover and soil indices to highlight Mediterranean variability.
- The fourth, to carry out an extensive water balance analysis of 55 Mediterranean catchments based on different water balance functional models as advanced by L'vovich (1979) and elaborated by Ponce & Shetty (1995a, 1995b) and Sivapalan et al., (2011) to check the hydrological variability and similarity between all catchments and between same climatic and/or physiographic classes catchments.

The climatic classification into 5 classes coincided with a geographical distribution in the Mediterranean ranging from the most seasonal and dry CC1 in the south to the least seasonal and most humid CC5 in the North. The MED-CORDEX ALADIN and CCLM historical and projected data simulated under RCP 4.5 and 8.5 scenarios for the 2070-2100 period served to assess the climate change impact on this classification and have demonstrated an evolution of the Mediterranean region towards arid climate. The classes located to the north are slowly evolving towards moderate coastal classes which might affect hydrological regimes due to shorter humid seasons and earlier snowmelts.

The physiographic classification and analysis provided a unique overview of Mediterranean catchments, mainly landform which revealed the existence of a micro-climatic variability, shadowed by the macro climate homogeneity. This micro-climatic variability is the main reason behind natural landcover variability like different tree cover.

The water balance analysis highlighted the Mediterranean trend aligned with the general climatic setting. In fact, the climate is the main driving force of the Mediterranean hydrology, however, it is not the only one as the hydrological homogeneity was identified, under different climates, for the mountainous karstic and snow influenced catchments which yield the highest baseflows and runoff coefficients.

The regionalisation has permitted the prediction of the MED-CORDEX climate change scenarios impact on runoff and baseflow coefficients. The projected evolution has mainly impacted the extremes, hence minimising the interclass variability and increasing catchments homogeneity. Catchments scatter and classes have drawn closer to the moderate Mediterranean catchments, with karstic and snow influenced catchments staying as the highest yielding catchments.

The alerting climatic and anthropogenic impacts call for urgent adaptation and mitigation measures that should be included in future national strategies and water resources management plans and that should be more based on regional research by deepening the knowledge on the spatial and temporal variability of hydrological resources all over the Mediterranean.

RESUME DE THESE VULGARISE POUR LE GRAND PUBLIC EN FRANCAIS

En Méditerranée, les ressources en eau sont exposées aux évolutions démographiques et climatiques. Pour mieux saisir ces défis, l'objectif de cette thèse est de rassembler une base de données hydrologique, d'établir une nouvelle classification climatique méditerranéenne pour l'hydrologie, identifier la variabilité physiographique, et analyser le bilan hydrologique de 55 bassins versants selon les différents modèles fonctionnels. Nous avons établi 5 classes climatiques, 10 classes physiographiques et identifié l'homogénéité hydrologique générale intra climats et inter climats surtout dans le cas des bassins karstiques montagneux influencés par la neige. L'impact du changement climatique indique une évolution de la région méditerranéenne vers le climat aride avec les bassins Nord en translation lente vers les bassins modérés Sud ce qui pourrait affecter les régimes hydrologiques et les pratiques agricoles, en raison des saisons humides plus courtes et des fontes précoces des neiges.

RESUME DE THESE VULGARISE POUR LE GRAND PUBLIC EN ANGLAIS

Mediterranean water resources are more than ever exposed to the increasing demand of demographic and climatic evolution. To better understand these challenges, this thesis aimed to collect a Mediterranean hydrological database, establish a new climatic classification for hydrology purposes, identify the physiographic variability, and analyze the hydrological balance of 55 catchments according to different functional models. We have established 5 climatic classes, 10 physiographic classes and identified the general intra-climate hydrological homogeneity and inter-climate homogeneity, especially in the case of mountainous karstic catchments under snow influence. The impact of climate change, indicated an evolution of the Mediterranean region towards the arid climate with the northern catchments in slow translation towards the moderate southern catchments which could affect hydrological regimes and agricultural practices, due to the shorter wet seasons and early snowmelt.